Proceedings of The 2010 NASA Laboratory Astrophysics Workshop

"… a forum within which the scientific community can review the current state of knowledge in the field of Laboratory Astrophysics …"

Workshop sponsors

NASA

OAK RIDGE National Laboratory

SELAC SouthEast Laboratory Astrophysics Community

Proceedings of
The 2010 NASA Laboratory Astrophysics Workshop

October 25-28, 2010
Gatlinburg, Tennessee, U.S.A.

Workshop sponsors:

The National Aeronautics and Space Administration
Oak Ridge National Laboratory
The Southeast Laboratory Astrophysics Community

Proceedings editor:

David R. Schultz, Oak Ridge National Laboratory

May 2011

Preface

The fourth NASA Laboratory Astrophysics Workshop (LAW) was held October 25-28, 2010 in Gatlinburg, Tennessee and organized by staff members of the Oak Ridge National Laboratory in close partnership with the LAW Scientific Organizing Committee. This workshop follows those held at the Harvard-Smithsonian Center for Astrophysics (1998), the NASA Ames Research Center (2002), and the University of Nevada, Las Vegas (2006). LAW has been envisioned, and has indeed become, an important forum in which the scientific community can review the current state of knowledge of laboratory astrophysics and help assess the priorities for work to support NASA space astrophysics missions.

Pursuant to the charge given to the SOC and all participants of the LAW by NASA, the present proceedings compiles papers written by the invited speakers which review (i) the decadal survey, "New Worlds, New Horizons in Astronomy and Astrophysics" (Astro2010), with a particular emphasis on roles played by laboratory astrophysics, (ii) the principal NASA missions and their needs for laboratory astrophysics, and (iii) ongoing laboratory astrophysics from the perspective of its practitioners. In addition, authors of the contributed posters at the workshop were given the opportunity to include here brief summaries of their presentations to give a broad view of the community's activities.

In addition, following the charge from NASA, the SOC has produced a "White Paper" identifying key accomplishments and needs for future work in laboratory astrophysics to support and enrich the return from NASA astrophysics missions, which is reproduced here and available on-line from both the workshop website (www-cfadc.phy.ornl.gov/nasa_law) and the NASA ADS. Input for the White Paper was received through working group sessions at the LAW from all the participants. On behalf of the SOC, we thank all of the 105 participants of the workshop, and its sponsors (NASA, Oak Ridge National Laboratory, and the Southeast Laboratory Astrophysics Community), for contributing to the success of the meeting and its output.

Special thanks also go to the workshop secretaries, Ms. Fay Ownby and Ms. Lynda Saddiq who, along with the Oak Ridge National Laboratory and Park Vista Hotel conference staff, worked tirelessly to plan and carry out the workshop. We note with great sadness the unexpected and tragic loss of Fay Ownby shortly after the workshop and we dedicate this proceedings to her memory.

David R. Schultz

May 2011

Table of Contents

Preface ……. iii

Table of Contents ……. v

Organizing Committees ……..……... vii

Laboratory Astrophysics White Paper ……..... W-1

Annex A. Charter for the 2010 NASA LAW ……. W-19
Annex B. Workshop Format ……... W-22
Annex C. Recent Successes ……W-23

Invited Papers …….. I-1

Contributed Papers ……. C-1

Appendix …… A-1

Workshop Agenda ……. A-1
List of Participants ……...…… A-5
Index of authors ……..… A-12

Organizing Committees

Scientific Organizing Committee

Daniel Wolf Savin, Chair (Columbia Astrophysics Laboratory)
Lou Allamandola (NASA Ames Research Center)
Steve Federman (University of Toledo)
Paul Goldsmith (NASA Jet Propulsion Laboratory)
Hashima Hasan, *ex officio* (NASA)
Douglas Hudgins, *ex officio* (NASA)
Caroline Kilbourne (NASA Goddard Space Flight Center)
Martin Laming (Naval Research Laboratory)
Karin Oberg (Harvard-Smithsonian Center for Astrophysics)
Wilt Sanders, *ex officio* (NASA)
David Schultz (Oak Ridge National Laboratory)
Ted Snow (University of Colorado)
Susanna Widicus Weaver (Emory University)

Local organizers

David Schultz, Local Chair (Oak Ridge National Laboratory)
Fay Ownby, Workshop Secretary (Oak Ridge National Laboratory)
Lynda Saddiq, Workshop Secretary (Oak Ridge National Laboratory)

NASA LAW, October 25-28, 2010, Gatlinburg

Laboratory Astrophysics White Paper (Based on the 2011 NASA Laboratory Astrophyiscs Workshop in Gatlinburg, Tennessee, 25-28 October 2010)

Daniel Wolf Savin, *Columbia University*

Lou Allamandola, *NASA Ames Research Center*

Steve Federman, *University of Toledo*

Paul Goldsmith, *NASA Jet Propulsion Laboratory*

Caroline Kilbourne, *NASA Goddard Space Flight Center*

Karin Öberg, *Harvard-Smithsonian Center for Astrophysics*

David Schultz, *Oak Ridge National Laboratory*

Susanna Widicus Weaver, *Emory University*

Additional contributions on plasma laboratory astrophysics by:

Hantao Ji, *Princeton Plasma Physics Laboratory*

Bruce Remington, *Lawrence Livermore National Laboratory*

Reviewers:

Nancy Brickhouse, *Harvard-Smithsonian Center for Astrophysics*

Farid Salama, *NASA Ames Reseach Center*

Lucy Ziurys, *University of Arizona*

Executive Summary

Our understanding of the cosmos rests on knowledge of the underlying physical processes that generate the spectra, composition, and structure of the observed astronomical objects. Laboratory astrophysics is the Rosetta Stone that enables us to translate these observations into knowledge. Astrophysical discoveries such as the accelerating expansion of the universe, the atmospheric composition of exoplanets, and the organic nature of interstellar chemistry rely upon advances in laboratory astrophysics. This importance of laboratory astrophysics was noted by the National Research Council 2010 Decadal Survey of Astronomy and Astrophysics (Astro2010), which called out laboratory astrophysics as one of the NASA's core research programs "fundamental to mission development and essential for scientific progress".

The purpose of the 2010 NASA Laboratory Astrophysics Workshop (LAW) was, as given in the Charter from NASA, "to provide a forum within which the scientific community can review the current state of knowledge in the field of Laboratory Astrophysics, assess the critical data needs of NASA's current and future Space Astrophysics missions, and identify the challenges and opportunities facing the field as we begin a new decade". LAW 2010 was the fourth in a roughly quadrennial series of such workshops sponsored by the Astrophysics Division of the NASA Science Mission Directorate.

The findings of the 2010 LAW are that

- Astrophysical discovery continues to be propelled forward by advances in laboratory astrophysics leading, for example, to new insights into Type Ia supernovae, the role of water and complex organic molecules in interstellar chemistry, exo-planet formation, and accretion disk physics.
- Maximizing the scientific return of NASA's Space Astrophysics missions requires a vibrant laboratory astrophysics program to generate the needed data and ongoing support for databases to archive the data generated.
- Astro2010 recommended growing the Astrophysical Research and Analysis (APRA) program for laboratory astrophysics by $2 million over the baseline funding level.
- Astro2010 recommended that missions requiring significant amounts of new laboratory astrophysics data to reach their science goals should include within their program budgets adequate funding for the necessary experimental and theoretical investigations.
- NASA SMD Astrophysics Division support for laboratory astrophysics has fallen sharply. Since 2005, the number of awards has dropped by a factor of two. Funding has de-

creased by 32% since the 2006 LAW. Declining support is a prime candidate to explain the corresponding decrease in the number of submitted proposals.

- In order to maintain the basic laboratory astrophysics support required by current NASA Space Astrophysics missions, will require a restoration of funding levels to their previous levels. Additional funding to supplement this basic level of support is needed to enable the laboratory astrophysics community to develop the new techniques required to provide critical support for the next generation of NASA Space Astrophysics missions.

The required laboratory astrophysics science for current and future NASA Space Astrophysics missions span from the sub-mm to the X-ray and include every bandpass in between. The needed information includes data for spectra and structure; electron driven collisions; heavy particle collisions; photon driven processes; chemical reactions in the gas phase, on grain surfaces, and in ices; formation and destruction mechanisms for molecules, dust, and ices; and radiatively driven, magnetically driven, and kinetically driven plasma processes Addressing a number of these needs will require the development of new technologies and instrumentation and, in some cases, interagency collaboration involving various combinations of NASA, NSF, and the Departments of Commerce, Defense, and Energy.

In order to realize the recommended scientific goals of the 2010 Decadal Survey, the 2010 LAW found that there were a number of possible concrete actions which NASA could take. These include:

- **Restoring APRA funding to the baseline funding level of FY 2006.**
- **Implementing the Astro2010 recommendations to grow the APRA program support and to provide mission support for laboratory astrophysics.**
- **Establishing a series of new initiatives in order to revitalize, grow and ensure the future of laboratory astrophysics.**
- **Developing an appropriate mechanism to ensure the long-term viability of laboratory astrophysics databases.**
- **Continuing to sponsor this quadrennial series of Laboratory Astrophysics Workshops, the next meeting of which should take place in the 2014-2015 period.**

1. Preface

"Laboratory astrophysics and complementary theoretical calculations are the foundations of astronomical and planetary research and will remain so for many generations to come. From the level of scientific conception to that of the scientific return, it is our understanding of the underlying processes that allows us to address fundamental questions regarding the origins and evolution of galaxies, stars, planetary systems, and life in the cosmos. In this regard, laboratory astrophysics is much like detector and instrument development at [NASA]; these efforts are necessary for the astronomical research being funded by [NASA]." This opening paragraph from the White Paper generated by the 2006 NASA Laboratory Astrophysics Workshop (LAW) remains as valid now as it was then.

The 2010 NASA LAW was held in Gatlinburg, Tennessee, from 26-28 October 2010. It was sponsored by the Astrophysics Division of the NASA Science Mission Directorate (SMD). The Charter from NASA is given in Annex A and the format of the workshop is described in Annex B. As was done in the past, laboratory astrophysics is taken to encompass both laboratory and theoretical work and no distinction is made between the two unless necessary.

The Workshop was timed to take place shortly after the National Research Council 2010 Decadal Survey on Astronomy and Astrophysics (Astro2010) issued their report. In this way, LAW 2010 would be able to respond to and amplify upon the Astro2010 recommendations.

The Astro2010 Decadal Survey stressed the critical importance of laboratory astrophysics for advancements in astronomy and in the science return from space missions. The survey issued strong recommendations to augment the funding of the APRA program by $2M/year and that missions which "require significant amounts of new laboratory data to reach their science goals should include within their program budgets adequate funding for the necessary experimental and theoretical investigations."

Throughout this White Paper, as requested in the Charter, we "outline specific opportunities and threats facing NASAs Laboratory Astrophysics Program, and articulate concrete actions by which the Agency can capitalize on the opportunities and mitigate the challenges."

2. General Findings

- Astrophysical discovery continues to be propelled forward by advances in laboratory astrophysics.
- Maximizing the scientific return of NASA's Space Astrophysics missions requires a vibrant laboratory astrophysics program to generate the needed data and ongoing

support for databases to archive the data generated.

- Astro2010 recommended growing the Astrophysical Research and Analysis (APRA) program for laboratory astrophysics by $2 million over the baseline funding level.
- Astro2010 recommended that missions requiring significant amounts of new laboratory astrophysics data to reach their science goals should include within their program budgets adequate funding for the necessary experimental and theoretical investigations.
- NASA SMD Astrophysics Division support for laboratory astrophysics has fallen sharply. Since 2005, the number of awards has dropped by a factor of two. Funding has decreased by 32% since the 2006 LAW. Declining support is a prime candidate to explain the corresponding decrease in the number of submitted proposals.
- In order to maintain the basic laboratory astrophysics support required by current NASA Space Astrophysics missions, will require a restoration of funding levels to their previous levels. Additional funding to supplement this basic level of support is needed to enable the laboratory astrophysics community to develop the new techniques required to provide critical support for the next generation of NASA Space Astrophysics missions.

3. Recent Success

Astrophysical discovery continues to be driven in part by experimental and theoretical work in laboratory astrophysics. For example, atomic astrophysics data have been critical for studying supernovae over a wide wavelength range. They have also played a key role in observations of O stars, and are having an impact on wavelength standards used for exoplanet searches employing wobble-induced Doppler shifts. Molecular astrophysics has been essential for interpreting data from the Herschel Space Observatory on a number of key species, notably water. Molecular data have underlain impressive results on recently detected fullerene molecules, and on the spectroscopy of hot-Jupiter exoplanets. Dust and ices play many important roles in the interstellar medium, and study of them requires data on broadband opacities and spectral features, as well as laboratory data on different types of surfaces that impact chemistry in dense regions. Plasma astrophysics looks at diverse regions of high energy density, studies of which require a broad range of laboratory results. These address problems ranging from planet formation to accretion disks. Annex C elaborates on these examples of the richness of astrophysical discovery arising from laboratory astrophysics.

4. Current and Future Needs

Current and future space astrophysics missions span from the sub-millimeter to the X-ray and include every bandpass in between. Laboratory astrophysics capabilities need to cover all of these bandpasses. As highlighted below, other common needs for laboratory astrophysics are accurate line intensities, useful databases, and high-performance computing capabilities (to study complex systems and to provide benchmarks). Addressing a number of the needs listed below will require the development of new technologies and instrumentation. Some will also require interagency collaboration involving various combinations of NASA, NSF, and the Departments of Commerce, Defense, and Energy. Examples of areas for which such cooperation is needed include databases (as is discussed in Section 5.2) and plasma astrophysics (which often require experimental facilities only available at DOE laboratories).

The rest of this section is largely in bullet format and not in any order of priority. Space limitations prevent us from providing more than a general listing of the required data. This section is also likely incomplete because of our inability to fully anticipate the future. Proposers seeking NASA Astrophysics funding for laboratory astrophysics can use the points below as a guide, but they will need to make a clear connection between the astrophysical science problem(s), the relevant NASA Space Astrophysics mission(s), and how the specific proposed laboratory astrophysics research will help to achieve the desired astrophysical understanding.

4.1. Atomic Astrophysics

4.1.1. Spectra and Structure

- Obtain better wavelengths, line identifications, oscillator strengths, hyperfine structure, and isotope shifts for the first 3 spectra of iron group elements and beyond.
- Improve wavelengths and oscillator strengths for fine structure lines above 1 μm.
- Measure X-ray wavelengths accurate to better than 1 mÅ for Fe and Ni L- and M-shell spectra, including inner-shell transitions.
- Determine wavelengths for satellite lines generated through dielectronic recombination.
- Improve accuracy of line diagnostics in the X-ray region.

4.1.2. Electron-Impact Collisions

- Improve electron impaction excitation data for Fe and Ni L-shell ions, H- and He-like ions for high excitation to high Rydberg levels, temperature and density sensitive lines, low charge states of Fe group elements, and forbidden transitions.
- Improve electron impact ionization data for valence and inner-shell electrons, especially benchmark laboratory measurements using ion beams either free of metastable contamination or with well characterized initial populations.
- Generate reliable dielectronic recombination data for low temperature plasmas and in high temperature plasmas for satellite line strengths and wavelengths.
- Develop modern data for Auger yields resulting from innershell ionization or excitation.
- Continually update ionization equilibrium calculations including sensitivity studies of how uncertainties in the ionization and recombination data propagate through to the predicted fractional abundances.

4.1.3. Heavy Particle Collisions

- Generate state-of-the-art charge exchange data for ions with neutrals such as H, He, H_2, CO_2, H_2O, etc.
- Improved fine structure excitation cross sections due to ion collisions with H, He, and H_2.
- Improve electronic excitations data for neutral-neutral collisions with H, He, and H_2.
- Calculate modern proton impact excitation and ionization data.
- Determine reaction rates between H, N, O, and S for PAHs containing between 50 and 200 carbon atoms in the neutral, cation, and anion states.
- Determine H_2 formation rates on PAHs containing between 50 and 200 carbon atoms as a function of PAH size and charge.

4.1.4. Photon Driven Processes

- Obtain better photoionization data of innershell K and L electrons including details around the K-shell threshold.

- Generate reliable Auger and fluorescence yields due to innershell photo-excitation or ionization and provide data as a function of both initial and final state.
- Perform experiments at synchrotron light sources and free electron lasers on highly charged ions to benchmark theory.
- Obtain probability distributions for the number of electrons emitted following the creation and then relaxation of an innershell hole.

4.2. Molecular Astrophysics

4.2.1. Instrument and Technology Development

- Develop broadband measurement techniques to enable rapid data acquisition over large ranges in frequency.
- Develop new techniques to address the challenge of generating, processing, monitoring and measuring in the laboratory the spectra and the structure of large complex molecules under conditions analogous to space conditions.
- Increase sensitivity (especially in the far-IR) to enable characterization of unstable species.
- Increase wavelength coverage to match NASA mission capabilities.
- Develop new methods for reaction kinetics and dynamics measurements.

4.2.2. Spectal Complexity

- Expand lab efforts beyond the current focus on interstellar "weeds" (commonly observed molecules with many lines in a frequency interval) to also include interstellar "flowers" (species of particular importance).
- Increase spectral coverage for all molecules, especially above 2 THz through mid-IR.
- Develop better theoretical models that couple rotation and vibration.
- Generate more complete sets of data on hot band lines.

4.2.3. Molecular Complexity

- Bridge gap between molecular astrophysics (small molecules with up to $\sim$ tens of atoms) and solid-state astrophysics (large molecules such as PAHs with $\gg 100$ atoms).
- Develop new approaches for interpreting spectra and excitation of complex molecules.
- Identify wavelength ranges for measurements of signatures of complex molecules.
- Extend chemical models to include large species.
- Determine electron affinities and electron-ejection energies for PAHs containing between 50 and 200 carbon atoms.

4.2.4. Spectral and Kinetic Databases

- Streamline.
- Maintain.
- Critically review.
- Extend.

4.2.5. Science Interpretation

- Conduct kinetics measurements for key reactions.
- Develop new methods and extend existing methods to study reaction dynamics.
- Measure collisional excitation rates.
- Quantify line intensities.
- Extend chemical models.

4.2.6. Computer and Theory

- Complete work on small molecules.
- Extend methods to large molecules.

- Determine reaction rates.
- Develop high performance computing contributions to spectroscopy and interpretation.
- Provide laboratory and computational benchmarks.

4.3. Dust and Ices Astrophysics

4.3.1. Ice, Dust, and PAH Identification at IR Wavelengths

- Prepare and characterize, spectroscopically and structurally, standard (terrestrial) and astronomically realistic silicatious, carbonaceous, ice (containing PAHs), and dust analogs to understand the differences between terrestrial "standard" and extraterrestrial materials. Characterize these materials both before and after in-situ energetic processing with UV and high energy particles (simulating cosmic rays). Measure the UV, optical, mid- and far-IR spectra of these materials from 0.1 to 1000 μm and determine optical constants as a function of composition and temperature.
- Measure the UV, optical, mid-and far-IR spectra of PAHs from 0.1 to 1000 μm with a focus on PAHs containing between 60 and 200 carbon atoms. Spectra are needed for neutral, cation, and anion forms. Investigations into the effects of oxygen and nitrogen incorporation into PAHs are also important.
- Measure the UV, optical, mid- and far-IR spectra of homo- and hetero-geneous PAH clusters as a function of cluster size and charge.
- Establish the protocol and standards for the creation of an UV to sub-millimeter spectroscopic database of refractory dust materials, pure ices and ice mixtures, and develop the database.

4.3.2. Diagnostics of Surface Formation Pathways

- Measure reactions comprising the most abundant, reactive elements H, C, N, O, S, and P on different types of dust surfaces at different temperatures and determine isotopic fractionation, new radical and molecule formation and destruction routes, and their branching ratios.
- Determine the rotational temperatures of the various ice species as they are ejected into the gas phase from realistic ice/dust surfaces at different temperatures.

4.3.3. Ice Formation and Destruction

- Develop a comprehensive experimental program to measure the yields of various reaction pathways, including dissociation channels and desorption mechanisms, as a function of input energy.
- Create models of the chemical evolution during star and planet formation with a sufficient level of detail to interpret current observations.
- Measure ice and carbonaceous dust formation and destruction processes (including shock and sputtering pathways) under realistic protoplanetary disk conditions to determine the amount of volatiles and carbon generated.

4.3.4. PAH and Amorphous Carbon Particle Formation and Destruction

- Delineate PAH formation pathways under circumstellar conditions as a function of C/H ratios.
- Delineate carbonaceous particle formation routes from molecular precursors in circumstellar shells and determine the factors that determine their final H/C ratio and aromatic to aliphatic C ratio.
- Determine PAH destruction mechanisms and kinetics in various astronomical environments (HII regions, PNe, PDRs, etc.) as a function of molecular size.

4.4. Plasma Astrophysics

4.4.1. Radiatively Driven Laboratory Experiments

- Develop scaled, radiatively driven, nonlinear hydrodynamics experiments suitable to test astrophysical models of molecular cloud dynamics and star formation dynamics.
- Extend precision opacity measurements into stellar core conditions.
- Extend equation of state measurements to higher pressures and off-Hugoniot conditions more relevant to star and planet formation.
- Develop non-relativistic and relativistic collisionless shocks to test our fundamental understanding of shocks in the universe.

- Extend scaled supernova explosion dynamics into the turbulent regime in relevant geometries to test astrophysical modeling of natures most powerful explosions.
- Develop experiments of shock and radiation processing of the environment (dust, ice, molecules) to improve our understanding of the formation of stars, planets, and life.

4.4.2. Magnetically Driven Laboratory Experiments

- Build next generation experiments to study reconnection in larger and more collisionless plasmas to be directly relevant to space and astrophysical plasmas, as well as the associated particle acceleration.
- Explore reconnection processes in high energy density (HED) conditions where plasma kinetic energy substantially exceeds magnetic energy.
- Investigate the effects of plasma processes and magnetic fields on the dynamics of dust particles, including charging, growth, breakup, and collective processes.
- Provide EUV spectroscopic data of metal inner-shell lines at high density and well-confined fusion plasmas.

4.4.3. Kinetically Driven Laboratory Experiments

- Develop experimental capabilities to access and understand nonlinear dynamos at larger magnetic Reynolds numbers in liquid metal and plasmas.
- Detect and study magnetorotational instability and the associated angular momentum transport scaling with respect to magnetic Reynolds number in liquid metal, gas, and plasmas.
- Extend experiments of flow driven and jet driven shocks to higher Mach number and larger size (Reynolds number) to test modeling of star formation dynamics.
- Develop experiments to test our understanding of the role of magnetic fields in instabilities, mixing, and evolution of turbulence.

5. Specific Issues/Questions for Consideration

5.1. What steps should be taken to increase collaboration, cooperation, and communication within the NASA Laboratory Astrophysics Program?

One suggestion at the workshop included the establishment of a database listing data needed by the space mission astrophysics community. One form that this could take would be a listserv or wiki to which people could post requests. Other suggestions included establishing a quarterly newsletter and/or using social networking tools such as facebook and twitter. The importance of venues where people could come together was noted.

To a certain extent, some of these suggestions are already in place. This is a direct outgrowth of the 2006 LAW which recommended that the American Astronomical Society (AAS) establish a Working Group on Laboratory Astrophysics (WGLA). The WGLA was established in May 2007 and now sponsors a yearly meeting on laboratory astrophysics which is held during the AAS summer meeting. To date the WGLA has sponsored 4 such meetings, the first on laboratory astrophysics as a whole, the second on dust and ices, the third on plasmas, and the upcoming one on nuclear and particles astrophysics. Their listserv currently has over 300 members. Building upon the successes of the WGLA would go a long way toward increasing collaboration, cooperation, and communication within the NASA Laboratory Astrophysics Program.

Databases and the required collaborations needed to maintain them also provide an opportunity to achieve this goal. So would large collaborative programs which are instrument heavy. However, each of these requires sufficient levels of funding to be viable. Another suggestion involved having close ties between laboratory astrophysics, observational programs, and mission user groups. This could be done, in part, though the creation of mission-specific laboratory astrophysics programs which would receive their support from the missions.

5.2. How should laboratory astrophysics databases be organized to minimize redundancy and cost, validated to ensure data consistency and quality, and curated to guarantee easy, widespread access by the community of data users?

The ultimate answer to this question will likely involve participation by the relevant domestic, foreign, and international agencies, departments, and organizations. To achieve this will likely require a NASA-sponsored workshop involving all relevant parties in order to determine how best to proceed.

Databases need to be maintained over periods of decades. Appropriate funding strategies are needed to ensure their survival. Mission support can help in part, but the databases clearly have lifetimes far longer than any NASA astrophysics space mission and their applications span multiple missions. Funding from the Astrophysics Data Curation and Archiving (ADCAR) program would be a more stable source of long term support. The databases also need to stay current and of relevance to the astrophysics users. Databases should strive to be compatible with one another and with the principles of the Virtual Observatory (e.g., easy public access with sufficient metadata to enhance portability, track version number, and proper data source attribution). While the data do need to be critically evaluated before inclusion in the database, often unevaluated data are better than no data and the databases should be structured to accommodate such data. Previous versions of databases also need to be available so that researchers can readily determine how astrophysical interpretations have changed between the old and new data.

Laboratory astrophysics databases which are commonly used by astrophysicists are maintained in the U.S. by NASA, the Department of Commerce, the Department of Energy, and the Department of Defense. A number of foreign and international organizations also maintain relevant databases. All together, the various databases in this country and abroad overlap to varying degrees with the NASA space astrophysics needs, but the overlap is rarely perfect. Additionally there is no standard format used across databases for the archived information. Organizing all these databases so as to minimize redundancy and cost, validate the data to ensure consistency and quality, and curate the data to guarantee easy, widespread access by the community of data users represents a grand challenge which is going to require a significant amount of continued study. A model for consideration is that established by the NASA ADCAR program or by the Department of Energy for nuclear data (U.S. Nuclear Data Program USNDP), involving national laboratories, universities, and NIST. However, the budget for USNDP exceeds the current APRA budget by nearly a factor of two

5.3. How might a new initiative in supporting laboratory astrophysics research (e.g. group/team awards, centers of excellence, NASA Laboratory Astrophysics Institute) be structured and implemented so as to augment the current program?

The emphasis here is on how such an initiative could *augment* the current laboratory astrophysics research. The LAW community felt very strongly that such an initiative should not come at the expense of the APRA program which, through its support of individual

Principal Investigators (PIs), helps to maintain the core competency of the laboratory astrophysics community.

That said, the community recognized that there are some scientific questions which are too big for a single PI to solve and which require a multi-expertise approach. To that end, NASA could establish a program of group/team awards in laboratory astrophysics to address well-defined grand astrophysical challenges. The questions posed by Astro2010 provide examples of such challenges. This program should be of limited term. It was felt that five years was a reasonable length. Proposals to the program would have to lay out a specific set of goals to be accomplished in that time. Any renewals would have to compete in an open call for proposals to ensure that the supported research remains relevant to NASA space astrophysics missions. Concern was also expressed that such a program would have to be structured to prevent there being too many group members on a proposal, thereby resulting in none of the research groups getting sufficient funding to carry out the proposed research.

5.4. What is the role of NASAs field centers and scientists in pursuing the Agencys critical Laboratory Astrophysics data needs?

While there was not a lot of discussion of this question at the meeting, some points were raised on the many possible roles for NASA's field centers and scientists in pursuing the critically needed laboratory astrophysics data. These include identifying and articulating NASA's needs for various missions, generating the needed data, making their unique research facilities available to the broader community for collaboration, and technology transfer of state-of-the-art instrumentation (particularly detectors) to non-NASA scientists. Although, to varying degrees, some of this is already largely occurring, there is clearly room for expansion.

5.5. What steps can NASA take to attract new talent (e.g., graduate student/postdoctoral fellowships, targeted proposal opportunities for junior faculty)?

Bringing new talent to laboratory astrophysics will require providing funding opportunities at all career levels. Establishing both graduate student and postdoctoral research fellowships in the field will help to direct the recipients into careers in laboratory astrophysics. The transition from postdoctoral researcher to either a research or faculty track

position would be aided by targeted proposal opportunities in laboratory astrophysics for outstanding young investigators who have completed their postdoc and are less than 10 years from having received their Ph.D. or equivalent. A robust APRA program coupled with a robust technology development and instrumentation program that also funds the required personnel will then enable these researchers to build and maintain their research programs and thereby continue their careers in laboratory astrophysics. Mission supported programs in laboratory astrophysics would augment this. These last three programs will also provide opportunities for researchers and faculty in other related areas to redirect their research into laboratory astrophysics and focus on issues important to NASA's Space Astrophysics missions. In short, if sufficient funding is provided for the field, that will attract new talent at all career levels.

6. LAW 2010 Conclusions

In order to realize the recommended scientific goals of the 2010 Decadal Survey, the 2010 LAW found that there were a number of possible concrete actions which NASA could take. These include:

1) Restoring APRA funding to the baseline funding level of FY 2006. The core competency of laboratory astrophysics needed to maximize the scientific return from NASA space astrophysics missions has eroded significantly over the past 4 years. If the current funding trend is not reversed, the field will die within the decade. Returning the baseline funding level to that of FY 2006 will reverse the trend and repair the damage.

2) Implementing the Astro2010 recommendations to grow the APRA program support and to provide mission support for laboratory astrophysics. These recommendations are critical to maintaining a core competency in laboratory astrophysics combined with enabling the field to respond on a "rapid" time scale to specific NASA space mission needs. The Astro2010 recommended $2M growth of the APRA program should be in addition to the restoration of the program to its baseline funding level of FY 2006. The Astro2010 recommendations echo two of the findings from the 2006 LAW White Paper. The WGLA, another product of the 2006 LAW, emphasized these points in the White Papers they submitted to each of the Astro2010 Science Frontier Panels (SFPs) as well as to the Astro2010 Infrastructure Working Group on Facilities, Funding, and Programs. That these 2006 LAW findings made it into the final Astro2010 recommendation testifies to the importance of their implementation.

3) Establishing a series of new initiatives in order to revitalize, grow, and ensure the future of laboratory astrophysics:

- Graduate student and postdoctoral research fellowships in laboratory astrophysics are needed to train the next generation in the field. These fellowships should be tenable at any U.S. host institution of the fellows' choice.
- A technology development and instrumentation program that also supports the required personnel is needed to enable vital research which cannot be performed with current facilities. This program should be open to both experimentalists and theorists.
- Targeted proposal opportunities in laboratory astrophysics are needed for outstanding young investigators who have completed their postdoc but are less than 10 years from having received their Ph.D. or equivalent. Such a program should be open to young investigators in either a research or faculty track at their host institution.
- As part of Phase B plans for future missions, laboratory data requirements to achieve the scientific goals described in the mission proposal need to be addressed, with sufficient funding in the budget to acquire the necessary data.
- A program of group/team awards in laboratory astrophysics is needed to address grand astrophysical challenges. This program should be of limited term and proposals would have to lay out specific goals to be accomplished in that time. Renewals would have to compete in an open call for proposals to ensure that the supported research remains relevant to NASA Space Astrophysics missions.
- None of these new initiatives should come at the expense of the APRA program which supports the core competency of the field.

4) Developing an appropriate mechanism to ensure the long-term viability of laboratory astrophysics databases. Databases are vital archives for the vast quantities of laboratory astrophysics data which have been and are being generated. If these data are not properly archived, they will be lost to future generations as the producers of the data retire and the corresponding facilities are decommissioned. Regenerating the needed data often requires years of development at a cost vastly exceeding that of the original work. Laboratory astrophysics databases, which are commonly used by astrophysicists, are maintained by a variety of domestic, foreign, and international organizations, agencies, and departments, the needs of which overlap to varying degrees with the NASA space astrophysics needs. The ultimate solution to ensuring the long-term viability of the laboratory astrophysics data is likely to involve cooperation between the various domestic, foreign, and international

agencies, departments, and organizations who currently maintain the relevant databases. Possible models include NASA's ADCAR program or the USNDP. To address this issue will likely require a NASA-sponsored workshop involving all relevant parties in order to determine how best to proceed.

5) Continuing to sponsor this quadrennial series of Laboratory Astrophysics Workshops, the next meeting of which should take place around 2014-2015. Astro2010 laid out three grand science objectives for the coming decade and emphasized the importance of laboratory astrophysics to enable the successful accomplishment of these goals. The various SFPs each laid out four questions for the coming decade and one discovery area. Four of the five SFPs emphasized the importance of laboratory astrophysics in pursuing these goals. As NASA Space Astrophysics missions work to achieve the objectives laid out by Astro2010 and the associated SFPs, it is clear that laboratory astrophysics will play a critical role. For this reason, it is vital that regular LAWs be held throughout the coming decade to monitor the health of the field and to ensure NASA's Space Astrophysics missions can meet the objectives laid out in the Astro2010 Decadal Survey.

Annex A. Charter for the 2010 NASA LAW

Purpose of workshop: The purpose of the Laboratory Astrophysics Workshop (LAW) 2010 is to provide a forum within which the scientific community can review the current state of knowledge in the field of Laboratory Astrophysics, assess the critical data needs of NASA's current and future space astrophysics missions, and identify the challenges and opportunities facing the field as we begin a new decade. LAW 2010 is sponsored by the Astrophysics Division of NASA's Science Mission Directorate (SMD).

Target audience: Laboratory Astrophysicists and Astrochemists (experimentalists, theorists, and modelers), Astronomers and Astrophysicists (observers, theorists, and modelers), Space Mission Scientists, Instrument Developers and other interested researchers.

Specific Goals: LAW 2010 will:

1. Review the current state-of-the art in laboratory astrophysics;
2. Review the recommendations of previous LAWs and assess progress toward meeting those recommendations.
3. Identify the critical data needs of NASA's current and future planned space astrophysics missions, and assess the degree to which NASA-supported research efforts currently address those data needs;
4. Assess the strengths, weaknesses, opportunities, and threats facing NASA's Laboratory Astrophysics program in the context of the Astro2010 Decadal Survey report;
5. Formulate a White Paper summarizing the key findings from the workshop for submission to the NAC Astrophysics Subcommittee and the Astrophysics Division (draft to be submitted by 25 Jan 2011; final report to be submitted by 25 Feb 2011);
6. Generate a volume of science proceedings from the workshop that will serve as a reference to NASA and the community, and distribute that volume through the NASA Astrophysics Data System (ADS).

Overview: LAW 2010 is the fourth in a series of NASA-sponsored Laboratory Astrophysics Workshops. Held approximately quadrennially, previous LAWs were held in 1998 (Harvard-Smithsonian Center for Astrophysics), 2002 (NASA Ames Research Center), 2006 (U. Nevada, Las Vegas). The strength of these workshops lies in bringing together producers and users of laboratory astrophysics data so that they can understand each other's needs and limitations in the context of NASA's mission needs. The workshops also serve to increase

collaboration and cross fertilization of ideas thereby ensuring that the priorities of NASA's Laboratory Astrophysics Program are aligned with the critical data needs of NASA's space astrophysics missions, and that the products of NASA-sponsored Laboratory Astrophysics research feeds back to the user community in a timely way.

The single most important and valuable deliverable from LAW 2010 will be the White Paper summarizing the proceedings and outcomes of the workshop. That White Paper should provide detailed findings on the critical laboratory astrophysics data that are required to maximize the scientific return on NASA's past, current, and future planned space astrophysics missions. The White paper should also outline specific opportunities and threats facing NASA's Laboratory Astrophysics Program, and articulate concrete actions by which the Agency can capitalize on the opportunities and mitigate the challenges.

Another important item in the White Paper should be a tabulation of recent significant astronomical results where the input from laboratory astrophysics was of critical importance (although the laboratory astrophysics contribution may not have received the credit due it, as is so often the case). The current funding environment, including the very difficult years ahead, will require a certain amount of salesmanship.

Lastly, with an eye on the future, a discussion should also be given as to what can be done in order to help foster the creation of new faculty positions and the education and production of future generations of laboratory astrophysics scientists.

Specific Issues/Questions for Consideration:

- What steps could be taken to increase collaboration, cooperation, and communication within the NASA Laboratory Astrophysics Program?
- How should laboratory astrophysics databases be organized to minimize redundancy and cost, validated to ensure data consistency and quality, and curated to guarantee easy, widespread access by the community of data users?
- How might a new initiative in supporting laboratory astrophysics research (e.g. group/team awards, centers of excellence, NASA Laboratory Astrophysics Institute) be structured and implemented so as to augment the current program?
- What is the role of NASA's field centers and scientists in pursuing the Agency's critical Laboratory Astrophysics data needs?
- What steps can NASA take to attract new talent (e.g. graduate student/post doctoral fellowships, targeted proposal opportunities for junior faculty).

Agenda: The workshop will feature invited talks by members of the scientific community representing data users. The invited speakers will provide a broad overview of the needs in the field. The workshop will also feature shorter talks and posters by data producers (NASA Laboratory Astrophysics Program grantees and others). Breakout sessions chaired by the Scientific Organizing Committee members will be held to promote discussion of focused issues of importance to meeting the critical data needs of NASA space astrophysics missions.

Annex B. Workshop Format

The Workshop began with a report from a Survey Committee member, followed by presentations given by one member from each of the five Astro2010 Science Frontier Panels (SFPs). In addition there were four invited review talks on current and future NASA Space Astrophysics Missions as well as 13 on various areas in laboratory astrophysics. These 23 speakers represented both users and producers of laboratory astrophysics data. Sessions for contributed posters were held on the first two days of the Workshop, highlighting exciting new developments in laboratory astrophysics. The number of laboratory astrophysics grants awarded by the Astrophysics Division over the 5 funding cycles preceding LAW 2010 is roughly 47% atoms, 38% molecules, 12% solids, and 4% plasma. The number of the poster presentations closely reflected this distribution. On the third day, breakout sessions in each of these four areas provided an opportunity for users and producers to discuss current and future laboratory astrophysics needs for NASA space astrophysics missions. The meeting concluded with reports given by each of the breakout groups followed by a plenary discussion of the findings.

Annex C. Recent Successes

Astrophysical discovery continues to be driven in part by experimental and theoretical work in laboratory astrophysics. Here we present selected examples of significant astrophysical advances arising from recent laboratory astrophysics studies. These examples demonstrate the richness of astrophysical discovery arising from laboratory astrophysics but are not meant to be exhaustive; space limitations prevent us from being complete.

6.1. Atomic Astrophysics

Type Ia supernovae (SNe) are used as standard candles to study dark energy and the expansion of the universe. Chandra and XMM-Newton X-ray studies of young supernova remnants (SNRs) have deepened our understanding of these standard candles. X-ray spectra of young SNRs in the Milky Way and the Magellanic Clouds offer the most detailed view of Type Ia SN ejecta available at any wavelength and provide invaluable constraints on the physics of these explosions and the identity of their progenitor systems. Utilizing public domain atomic data, it is now possible to model the X-ray emission and distinguish SNRs resulting from bright and dim Type Ia SNe. This has been validated by the detection and spectroscopy of SN light echoes for the Tycho SNR (Badenes et al. 2006, ApJ, 645, 1373; Krause et al. 2008, Nature, 456, 617) and SNR 0509-67.5 in the LMC (Badenes et al. 2008, ApJ, 680, 1149; Rest et al. 2008, ApJ, 680, 1137). Key advantages of these X-ray studies of nearby SNRs over optical studies of extragalactic SNe are that the SNRs are close enough to examine the circumstellar medium sculpted by the progenitor systems (e.g., the Kepler SNR, Reynolds et al. 2007, ApJ, 668, L135) and also to study the resolved stellar populations associated with them (Badenes et al. 2009, ApJ, 700, 727). Recent X-ray observations have also discovered emission from Mn and Cr in young Type Ia SNRs. This can be used to measure the metallicity of the progenitor system (Badenes et al. 2008, ApJ, 680, L33), one of the key variables that might affect the cosmological use of Type Ia SNe and which cannot be determined for extragalactic SNe.

Advances in our understanding of the elemental evolution of the cosmos has come about from spectroscopic observations carried out using HST, Chandra, and XMM-Newton coupled with new laboratory astrophysics data. For example, a clearer distinction between the main r-process and the "weak" r-process has resulted from new transition probabilities for many neutron capture elements. This finding rests on detailed abundance studies of the neutron capture elements in old metal-poor halo stars carried out using both HST-STIS and ground-based observations including Keck I HIRES (e.g., Sneden et al. 2009, ApJS, 182, 80) coupled with the measurement of new transition probabilities for many neutron capture elements

(e.g., Lawler et al. 2009, ApJS, 182, 51). The r-process neutron capture elemental abundance pattern which has emerged from this effort constrains nucleosynthesis modeling and provides a clearer distinction between the main r-process and the weak r-process (Kratz et al. 2007, ApJ, 662, 39).

Another example involves X-ray observations of O stars. Their powerful radiatively driven winds are important sources of chemical enrichment in the universe. Recent analyses of UV P Cygni profiles and X-ray emission line profiles have been used to determine mass loss rates (Fullerton et al. 2006, ApJ, 637, 1025; Cohen et al. 2010, MNRAS, 405, 2391). These studies used state-of-the-art wavelengths (accurate to a few m), and a relatively complete database of important X-ray emission lines, together with data on relative line strengths in coronal plasmas, in order to accurately account for blended complexes of Doppler broadened emission lines. These works found that the mass loss rate from O-stars is a factor of a few less than previously thought, a finding resulting from recent improvements in atomic data from laboratory and theoretical calculations. This changes our understanding of chemical enrichment of galaxies, especially during their early starburst phase.

Exoplanet discovery from planetary-induced stellar line Doppler shifts rests on precisely calibrated wavelength standards. These discoveries depend on the measurement of small changes in the wavelengths of the stellar lines due to the Doppler shift caused by the wobble of thestar as the planet moves around it. A velocity change of 10 m s^{-1} requires the measurement of Doppler shifts to 3 parts in 10^8. To achieve this precision, an accurate wavelength reference is needed that is stable over decades of time (Marcy & Butler 1992, PASP, 104, 270). The HIRES spectrograph on the Keck telescope, used in the recent discovery of a planet in the habitable zone of a star (Vogt et al. 2010, ApJ, 723, 954), uses a carefully calibrated iodine reference cell placed in the beam from the telescope. The calibration of this cell is made in the laboratory using high-resolution Fourier transform spectroscopy. Similar discoveries using the HARPS spectrograph in Chile use thorium-argon hollow cathode lamps that have been calibrated in the laboratory.

6.2. Molecular Astrophysics

Water plays a key role in interstellar chemistry. It is the dominant molecular carrier of oxygen in interstellar clouds, and it is important in biological systems on Earth. Far-infrared observations using Herschel now open the possibility for direct observations of water and related molecules. First results from the Herschel Key Programs indicate the exciting possibilities in store for advancing our understanding of the water budget during star and planet formation. O-related chemistry has challenged interstellar cloud chemical

models. Odin Satellite observations of water in dense clouds gave strict upper limits on the fractional abundance relative to H_2 (Klotz et al. 2008, A&A, 488, 559), which stood in stark contrast to model predictions (Lee et al. 1996, A&AS, 119, 111). The abundance of water in cold clouds and its formation and destruction remained a mystery until recent Herschel observations. They provided the first direct detection of water in starless cores, such as in L1544 (Caselli et al. 2010, A&A, 521, L29). Surprisingly, water was not detected in the DM Tau protoplanetary disk (Bergin et al. 2010, A&A, 521, L33). However, Herschel results reveal a rich water-related chemistry in other types of interstellar environments. Ionized water, H_2O^+, and the related ion OH^+ were detected in numerous sources ranging from massive star-forming cores (Schilke et al. 2010, A&A, 521, L11; Gupta et al. 2010, A&A, 521, L47 2010) to diffuse clouds (Neufeld et al. 2010, A&A, 521, L10). Far-IR observations of water using Herschel also enabled the first determination of the water production rate from a comet (Val-Borro et al. 2010, A&A, 521, L50). Likewise, the isotopic fractionation of water in massive star-forming regions was traced through Herschel observations (Comito et al. 2010, A&A, 521, L38). These advances in the understanding of the water budget during star and planet formation were based on laboratory studies of water and related species in the submillimeter range. The spectral catalog for water was extended to include transitions across the frequency range covered by the HIFI instrument on Herschel (Pickett et al. 2005, JMS, 233, 174). A similar analysis provided a global spectral fit of OH^+ (Müller et al. 2005, J. Mol. Struct., 742, 215). The analysis leading to the detection of H_2O^+ occurred in the reverse order its rotational spectral feature, including a distinctive hyperfine splitting pattern, was first detected in absorption in HIFI spectra (Ossenkopf et al. 2010, A&A 518, L111). The distinctive hyperfine splitting led to this ion being recognized as a likely carrier, and detailed analysis of its high-resolution infrared spectrum led to the confirmation that this feature arose from H_2O^+.

Additional observations have explored the extent of molecular complexity in interstellar and circumstellar environments. Fullerene molecules such as C_{60} and C_{70} have been prime targets ever since their discovery in laboratory experiments designed to simulate the chemistry of carbon star outflows (Kroto et al. 1985, Nature, 318, 162). Recent Spitzer Space Telescope observations revealed for the first time the spectroscopic signatures of C_{60} and C_{70} in a variety of astronomical environments. The molecules were first detected in a hydrogen-poor planetary nebula (Cami et al. 2010, Science, 329, 1180). The hydrogen-poor conditions were thought to be necessary in light of laboratory measurements on fullerene production (De Vries et al. 1993, Geochim. Cosmochim. Acta, 57, 933; Wang et al. 1995, J. Mater. Res., 10, 1977). Other Spitzer spectra reveal the presence of C_{60} in the reflection nebulae NGC 7023 and NGC 2023 (Sellgren et al. 2010, ApJ, 722, L54) and in planetary nebulae in our Galaxy and the Small Magellanic Cloud (García-Hernández et al. 2010, ApJ, 724,

L39). The latter work shows that the fullerenes are present in a variety of environments, including hydrogen-rich ones; García-Hernández et al. suggest that the photochemistry of hydrogenated amorphous carbon plays a key role. These detections would not have been possible without spectroscopic laboratory data (Krätschmer et al. 1990, Nature, 347, 354; Frum et al. 1991, Chem. Phys. Lett., 176, 504; Martin et al. 1993, Phys. Rev., B47, 14607; Nemes et al. 1994, Chem. Phys. Lett., 218, 295; Fabian 1996, Phys. Rev., B53, 13864; Sogoshi et al. 2000, J. Phys. Chem. A, 104, 3733). These measurements provided the wavelengths and line strengths to confirm the astronomical detections.

In addition to the advances in understanding interstellar and circumstellar chemistry, molecular laboratory studies have led to great improvements in our understanding of the chemistry occurring in the atmospheres of hot-Jupiter exoplanets. HD 189733b and HD 209458b are two of the most observed hot-Jupiter exoplanets, and recent observations with the NICMOS instrument on the Hubble Space Telescope reveal the presence of molecular features attributed to water, methane, and carbon dioxide in their atmospheres (e.g., Swain et al. 2008, Nature, 452, 329; Swain et al. 2009a, ApJ, 690, L114; Swain et al. 2009b, ApJ, 704, 1616). Transmission spectra acquired during primary eclipse and dayside emission spectra were the basis for the detections. Analysis of these spectra provides important constraints on the physical conditions and relevant processes in exoplanet atmospheres. In order to model the observed spectra, molecular data relevant to high temperatures are required. Swain et al. (2009b) used data of Barber et al. (2006, MNRAS, 368, 1087) and Zobov et al. (2008, MNRAS, 387, 1093) for the hot water lines. The results of Nassar & Bernath (2003, J. Quan. Spectrosc. Rad. Transf., 82, 279) and Rothman et al. (2005, J. Quan. Spectrosc. Rad. Transf., 96, 139) were used for CH4 lines. The compilation of Rothman et al. is known as the HITRAN database. The data on hot CO2 lines came from Tashkun et al. (2003, J. Quan. Spectrosc. Rad. Transf., 82, 165).

6.3. Dust and Ices Astrophysics

During the past few years, observations with the Spitzer Space Telescope have transformed our understanding of dust, polycyclic aromatic hydrocarbons (PAHs), and ices in a wide range of environments, from protoplanetary disks to high-redshift galaxies and even galactic halos. This transformation is a direct result of laboratory studies of dust, PAH, and ice spectroscopy, ice and surface chemistry experiments, and dust coagulation studies.

Spitzer observations of silicate features at 10-30 μm in protoplanetary disks have been crucial to constrain the dust composition, heating history, and coagulation as well as how dust changes radially in the planet-forming zone (e.g., Bouwman et al. 2008, ApJ, 683,

479). These studies used laboratory dust optical constants (e.g., Koike et al. 2003, A&A, 399, 1101). Laboratory dust opacities have been instrumental in quantifying the properties of transition and pre-transition disks among the Spitzer observed disk sample (Calvet et al. 2005, ApJ, 630, L185; Espaillat et al. 2007, ApJ, 670, L135). These disks have large holes or gaps, potentially cleared out by Solar System analogs. Together the dust processing observations and the frequency of these transition objects as well as the sizes of their holes and gaps are among the best constraints available on different (exo)-planet formation models.

Spitzer observed the many mid-infrared spectral features from PAHs toward an unprecedented number of extra-galactic sources across the Universe. These PAH bands, identified and analyzed based on laboratory and computational spectra, have become a standard tool to measure the spectroscopic red-shift, to measure the star formation rate, and to classify the galaxies as either starburst or active galactic nuclei (AGNs) out to redshifts $z > 4$ (e.g., Smith et al. 2007, ApJ, 656, 770; Draine et al. 2007, ApJ, 663, 866; Pope et al. 2008, ApJ, 675, 1171; Riechers et al. 2010, BAAS, 42, 238). Spitzer also discovered a family of new emission features between 15 and 20 μm which, again thanks to the extensive database of PAH spectra produced with support of the Laboratory Astrophysics program, were readily attributed to PAHs. These new features fall in the transition region between nearest neighbor vibrations to full-skeleton modes, giving the first glimpse into the size, geometry, and charge of the largest members of the astronomical PAH family (Bauschlicher et al. 2008, ApJ, 678, 316; Bauschlicher et al, 2009. ApJ, 697, 311; Boersma et al. 2010, A&A, 511, A32). In addition to being critical for understanding mid-IR observations made by JWST, these large PAHs will impact the upcoming far-IR observations made with SOFIA and Herschel.

The importance of different types of interstellar grain surface chemical pathways for the formation of molecules other than H_2 has been a topic of debate for decades. The high sensitivity of Spitzer allowed for observations of icy grain mantles toward previously inaccessible astronomical objects such as solar-type protostars, protoplanetary disks, starless and star-forming clouds, and a range of extra-galactic sources (e.g., Bergin et al. 2005, ApJ, 627, L33; Boogert et al. 2008, ApJ, 678, 985; Oliveira et al. 2009, ApJ, 707, 1269). The ices and ice structures were identified and quantified with laboratory ice spectroscopy (e.g., Hudgins et al. 1993, ApJ, 86, 713; White et al. 2009, ApJS, 180, 182). Together with surface astrochemistry studies on hydrogenation (e.g., Hidaka et al. 2004, ApJ, 614, 1124) these observations have explored the formation efficiencies and pathways of the small molecules commonly associated with the origin of life, especially water, methane, ammonia, and methanol (for a review see Herbst & van Dishoeck 2009, ARAA, 47, 427).

Other laboratory work has established the formation yields and pathways of more complex molecules such as methyl formate and dimethyl ether through UV photolysis and ion

bombardment (Bennet et al. 2007, ApJ, 660, 1588; Öberg et al. 2009, A&A, 504, 891). These experiments are being used to interpret the wealth of data on complex organic molecules obtained with Herschel, where enough lines are detected to use these molecules as probes of the physical conditions in hot molecular cores (e.g., Kama et al. 2010, A&A, 521, L39).

6.4. Plasma Astrophysics

The most efficient energy sources known in the universe are accretion disks. Those around black holes convert 5-40% of rest mass energy to radiation. Like water circling a drain, inflowing mass must lose angular momentum, presumably by vigorous turbulence in disks, which are essentially inviscid (Shakura & Sunyaev 1973, A&A, 24, 337). The origin of the turbulence is conjectural. Hot disks of electrically conducting plasma inferred from observations of Chandra and XMM (Rappaport et al. 2010, ApJ, 721, 1348) can become turbulent via the linear magnetorotational instability (MRI; Balbus & Hawley 1998, Rev. Mod. Phys., 70, 1). Cool disks, such as the planet-forming disks of protostars inferred from observations with the Hubble Space Telescope and Spitzer (De Marchi et al. 2010, ApJ, 715, 1), may be too poorly ionized for MRI, hence essentially unmagnetized and linearly stable. Nonlinear hydrodynamic instability often occurs in linearly stable flows (e.g., pipe flows) at sufficiently large Reynolds numbers. Although disks have extreme Reynolds numbers, Keplerian rotation enhances their linear hydrodynamic stability, so whether nonmagnetic disks can be turbulent and thereby transport angular momentum effectively is controversial (Richard & Zahn 1999, A&A, 347, 734; Lesur & Longaretti 2005, A&A, 444, 25). Based on a well-controlled and diagnosed laboratory experiment, it was shown (Ji et al. 2006, Nature, 444, 343) that nonmagnetic quasi-Keplerian flows at Reynolds numbers up to millions are essentially steady. Scaled to accretion disks, rates of angular momentum transport lie far below astrophysical requirements. By ruling out purely hydrodynamic turbulence, these results indirectly support MRI as the likely cause of turbulence even in cool disks (Balbus 2009, arXiv:0906.0854).

Laboratory experiments have played an important role in our quest to understand planet formation and planetary interiors. Experiments using different facilities and techniques have unambiguously demonstrated that the transition from non-conducting molecular hydrogen to atomic metallic hydrogen at high pressures is a continuous transition, and not a discontinuous first order phase transition (Nellis 2000, Planet. Space Sci., 48, 671; Celliers et al. 2000, Phys. Rev. Lett., 84, 5564). This suggests that the metallic region of Jupiter's interior extends out to 90% of the radius of the planet, and may explain why the magnetic field of Jupiter is so much stronger than that of the other planets of our solar system. Additionally, connections

have recently been established between high-pressure laboratory tests of equation of state (EOS) models of H and He and predictions of the interior structure of Jupiter, from surface to core (Saumon & Guillot 2004, ApJ, 609, 1170; Fortney et al. 2009, Phys. Plasmas, 16, 041003).

NASA LAW, October 25-28, 2010, Gatlinburg

The Astro2010 decadal survey: What does it say about laboratory astrophysics?

D. McCammon

Physics Department, University of Wisconsin, Madison, WI 53706

mccammon@physics.wisc.edu

ABSTRACT

I will discuss the charge to the Astro2010 decadal survey committee, differences from previous decadal reports, the overall approach, and recommendations for support of laboratory astrophysics at NSF, NASA, and DOE.

"...Once limited to studying only visible light, astronomers and astrophysicists now observe the universe using the entire electromagnetic spectrum, from radio waves to gamma rays. Using these and other methods of investigation, the astronomy and astrophysics communities are able to answer profound questions about the origins of the universe and Earth's place within it. A compelling program of research that includes complementary space-based and ground-based facilities and foundational research efforts is needed to maximize scientific progress. New Worlds, New Horizons presents just such a program, ..."

"...This report, the result of a survey of astronomy and astrophysics for the decade of the 2010's, lays out a plan for sustaining the current progress in research over the coming decade and beyond. The proposed plan focuses on three science objectives: the exploration of the origins of the universe, the search for habitable planets outside our solar system, and the use of astronomical observations to investigate fundamental physics. The sixth in a series of decadal surveys, this study differs from its predecessors by reconsidering past unrealized priorities in addition to suggesting new research activities. The study also includes a detailed analysis of technical readiness and cost risks of projects and activities, resulting in a coherent program that fits within the survey's projected funding profiles for the three sponsoring agencies: the National Aeronautics and Space Administration (NASA), the National Science Foundation (NSF), and the Department of Energy (DOE). ..."

(from **NWNH, Astro 2010 Report in Brief**, The National Academy of Sciences)

1. Organization of the 2010 Decadal Survey

1.1. Community Input

Community input has been an increasingly important part of all decadal surveys, but the response this time was unprecedented: 324 science white papers (a unique snapshot of the field), 69 state of the profession position papers, 70 white papers on technology development, theory, computation, and laboratory astrophysics, and 108 community responses to a request for information on research activity proposals, plus email inputs to the committee and community-organized Town Halls.

These contributions included eight specifically on laboratory astrophysics, listed in Fig. 1.

Laboratory Astrophysics and the State of Astronomy and Astrophysics
Submitted by the
American Astronomical Society Working Group on Laboratory Astrophysics
http://www.aas.org/labastro/

Laboratory Astrophysics in the U.S.
J. Lawler et al.

Roles, Current Status, Opportunities, Future Trends, and Funding Issues for Laboratory Plasma Astrophysics
A State of the Profession Position Paper Submitted to the Astro2010 Decadal Survey
Hantao Ji et al.

A Novel Instrument to Study the Cosmic Origins of Organic Chemistry
Daniel Wolf Savin - Columbia University

From Molecular to Highly-Charged Ions: Expansion of Laboratory Astrophysics Through the Use of the Electrostatic Storage Ring and Electron Beam Ion Trap
Ara Chutjian et al.

Laboratory Astrochemistry Facility to underpin the next Decade of Astronomy and Astrophysics
David R. Schultz

Study of Magnetic Reconnection in Collisional (MHD) and Collionless (Kinetic) Plasmas by Upgrading Magnetic Reconnection Experiment (MRX) Device
Masaaki Yamada

The Need for Plasma Astrophysics in Understanding Life Cycles of Active Galaxies
H. Li et. al

Fig. 1.— Community contributions on laboratory astrophysics. The submitted papers can be found respectively at http://sites.nationalacademies.org/BPA/BPA_049492, papers 68, 29 and 25; http://sites.nationalacademies.org/BPA/BPA_051118, papers 2, 3, 4 and 8; and http://sites.nationalacademies.org/BPA/BPA_050603, paper 60.

1.2. Science Frontier Panels

The organization of this survey was strongly "science first," and the first panels to meet were the five Science Frontier Panels: Planetary Systems and Star Formation (PSF), chaired by Lee Hartmann, Stars and Stellar Evolution (SSE) - Roger Chevalier, The Galactic Neighborhood (GAN) - Mike Shull, Galaxies across Cosmic Time (GCT) - Meg Urry, and Cosmology and Fundamental Physics (CFP), chaired by David Spergel.

These panels worked to identify the science themes that should define the research frontiers for the 2010-2020 decade, taking into considerations those areas where the technical means and the theoretical foundations are in place for major steps forward. In many cases, contributions from laboratory astrophysics were identified as a necessary ingredient for the desired process.

1.3. Infrastructure Study Groups

Six infrastructure study groups collected background data on various aspects of the astrophysics enterprise. Much material on laboratory astrophysics came from the hardworking Facilities, Funding, and Programs (FFP) group chaired by J. Craig Wheeler of the University of Texas at Austin. Other members were Rebecca A. Bernstein, University of California, Santa Cruz; David Burrows, Pennsylvania State University; Webster Cash, University of Colorado; R. Paul Drake, University of Michigan; Jeremy Goodman, Princeton University; W. Miller Goss, National Radio Astronomy Observatory; Kate Kirby, Harvard-Smithsonian Center for Astrophysics; Anthony Mezzacappa, Oak Ridge National Laboratory; Robert Millis, Lowell Observatory; Catherine Pilachowski, Indiana University; Farid Salama, NASA Ames Research Center; and Ellen Zweibel, University of Wisconsin.

This group attempted to make a systematic assessment of current mission needs as a basis for future planning. Figure 2 shows an attempt to make a matrix of lab astro needs for each of the current major facilities. This was abandoned as not useful because there were too many checkmarks.

At the same time that laboratory astrophysics needs to ramp up studies to match the demands of new observations, the funding for laboratory astrophysics has evolved and declined over the past fifteen years. The White Paper submitted by the AAS Working Group on Laboratory Astrophysics points out that the priorities of the lab atomic and molecular physics communities, once a large component of NSF and DoE funding, have shifted away from programs of astrophysical interest. Traditional support for atomic physics now is more focused on Bose-Einstein condensates, molecular physics has shifted to biological

wavelength	mission	collision cross-sec.	rate coeff.	nuclear masses	nuclear decays	nuc. Matter equation of state	line transitions	grain properties (opacities, etc.)	grain photoelectric yields	x-ray absorption	photoionization and recombination rates	magnetzed and high energy density plasmas	HCI cross-sections
OIR	HST	✔	✔	✔	✔	✔	✔	✔	✔		✔	✔	
	ground-based	✔	✔	✔	✔	✔	✔	✔	✔		✔	✔	
	(VLT, Keck, Subaru)	✔	✔	✔	✔	✔	✔	✔	✔		✔	✔	
	JSWT	✔	✔	✔	✔	✔	✔	✔	✔		✔	✔	
	Spitzer	✔	✔	✔	✔	✔	✔	✔	✔		✔	✔	
	Sofia	✔	✔	✔	✔	✔	✔	✔	✔		✔	✔	
radio, submm	ALMA, etc.	✔	✔	✔	✔		✔	✔	✔		✔	✔	
x-ray	Chandra	✔	✔	✔	✔		✔			✔	✔	✔	✔
	XMM	✔	✔	✔	✔		✔			✔	✔	✔	✔
uv	HST	✔	✔	✔	✔		✔	✔	✔		✔	✔	✔

Fig. 2.— An abandoned attempt to make a systematic matrix of laboratory astrophysics requirements by science mission.

applications, and solid matter is applied to nano-science technologies. Similarly, university support has declined as the focus has changed. As shown in table 1, NSF Physics support for lab astro has declined to less than one-third of the level of two decades ago. Although there has been an increase in the number of NSF AST AMO lab astro awards (table 2), the combined Physics plus Astronomy lab astro support is down by more than one-third.

Table 1: AMOLA(atomic and molecular lab astro) grants from the NSF Divisions of Physics and Chemistry.

Original Award Date	Total Awards	AMOLA Awards	AMOLA/Total	AMOLA/year %
1989-1993	186	29	16	5.8
1994-1998	255	26	10	5.2
1999-2003	251	11	4.4	2.2
2004-2008	264	8	3.0	1.6

Table 2: AMOLA grants from the NSF Division of Astronomical Sciences.

Original Award Date	Total Awards	AMOLA Awards	AMOLA/Total	AMOLA/year %
1989-1993	701	12	1.7	3.2
1994-1998	686	12	1.7	2.4
1999-2003	906	11	1.2	2.2
2004-2008	1038	19	1.7	3.8

1.4. Program Prioritization Panels

Four Program Prioritization Panels (PPPs), Radio, Millimeter and Submillimeter from the Ground (RMS), chaired by Neal Evans, Optical and Infrared Astronomy from the Ground (OIR) - Pat Osmer, Electromagnetic Observations from Space (EOS) - Alan Dressler, and Particle Astrophysics and Gravitation (PAG), chaired by Jackie Hewitt, were charged with developing a ranked program of major research projects in their respective areas. Each program was developed to most efficiently address the major science areas identified by the Science Frontier Panels. Although they were not required to address the supporting needs of their recommended projects, most of them did. And laboratory astrophysics was often identified as a high-priority requirement.

2. Recommendations of the Survey

This survey was tasked with recommending a program that would fit entirely within a defined budget. The budget scenarios adopted are shown in Figure 3.

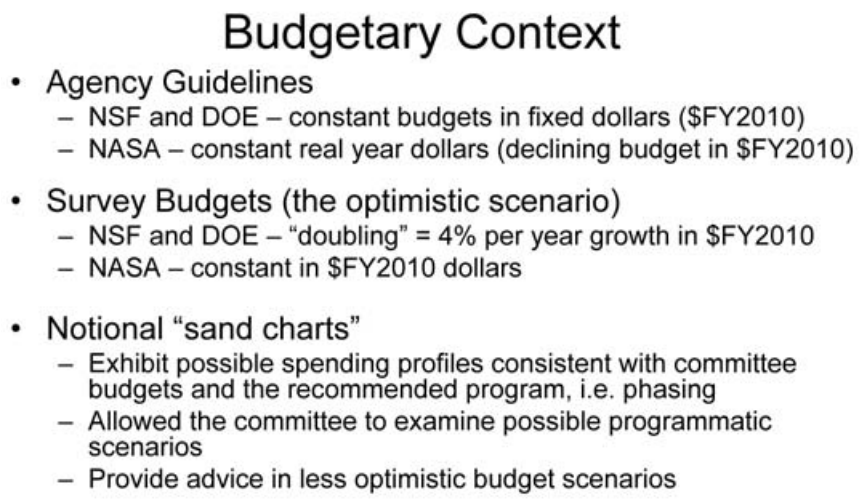

Fig. 3.— Budgetary context of the decadal survey. The recommended program was required to fit within a specified budget. The committee chose to use both the budget scenario provided by the agencies and a slightly more optimistic one.

Given the constrained budgets and the large commitments already in place, the program recommended by this decadal survey was necessarily quite modest compared with previous decades. A particularly large fraction of the available resources were aimed at

building infrastructure: the technology, theory, science pathfinding, laboratory astrophysics, and workforce development that the major projects of future decades will be based on. This was particularly true for NASA, where cost overruns on major missions over much of the past decade resulted in major cutbacks in these supporting programs. Heroic efforts by NASA astrophysics managers over the past two years have restored many of these cuts, but the programs are still functioning at well below their early-decade levels, and more resources are needed for a healthy program. Figure 4 shows a graphical presentation of "balance" in the NASA program as represented in 1998 expenditures.

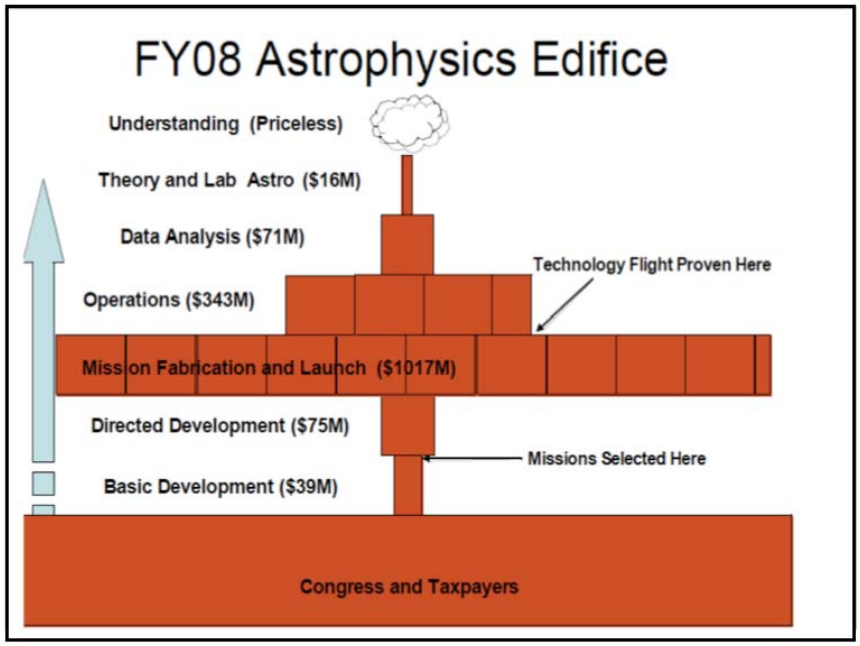

Fig. 4.— Graphical view of breakdown of NASA Astrophysics Division funding for 2008. Division of the $39M "basic development" between mission-specific and long-range technology development is not shown.

3. Laboratory Astrophysics in the Survey Report

"Laboratory astrophysics" is called out on 21 different pages. It is referenced in all chapters and sections except chapter 2, and there are a total of 44 references.

Where to the major discussions and recommendations:
Ch 1: summary of recommendations
Ch 4: Demographics

Ch 5: Core program description
Ch 7: Budget plans

Specific recommendations are shown below. The page references refer to the prepublication version of the full survey report available at: http://www.nap.edu/catalog.php?record_id=12951

3.1. NASA

NASA Laboratory Astrophysics:

Herschel, JWST, SPICA, and IXO, with their fine spectral capabilities, will place new demands on basic nuclear, ionic, plasma, atomic, and molecular astrophysics. Care should be taken to ensure that these needs are met. ***An increase by $2 million per year*** in the funding of the present program is recommended (p1-9).

It is recommended that *NASA, in coordination with DOE, assess the level of funding available for laboratory astrophysics through the APRA program relative to the requirements* of its current and future spectroscopic missions. Funding through APRA that is aimed at mission-enabling laboratory astrophysics should be augmented at a level recommended by this scientific assessment. While the costs of obtaining the data that will be needed in the coming decade are difficult to estimate, an increase of 25 percent over the current budget, or a notional *budget increment of $20 million over the decade,* may be required (p7-27).

3.2. NSF

Astronomy and Astrophysics Grants Program (AAG):

Individual investigator grants provide critical support for astronomers to conduct the research for which the observatories and instruments are built. The current funding level has fluctuated, especially due to the welcome injection of ARRA5 funding, but the rough baseline is $46 million. An increase of $8 million to bring the baseline to $54 million is recommended. *This increase should include the support of new opportunities in Laboratory Astrophysics*(p1-12).

Astronomy and Astrophysics Grants Program:

Competed individual investigator grants, as described in Chapter 5, provide critical support for astronomers to conduct the research for which the observatories and instruments are built. The current funding level has fluctuated, especially because of the welcome injection

of ARRA funding, but the rough baseline is $46 million per year. An increase of $8 million to $54 million per year is recommended. *This increment should include the support of new opportunities in Laboratory Astrophysics* (p7-39).

3.3. DOE

CONCLUSION: DOE national laboratories, including those funded by the Office of Science and the National Nuclear Security Administration, have many unique facilities that can provide basic astrophysical data. The committee believes that NASA, NSF, and DOE will need to include funding for laboratory astrophysics in support of new missions and facilities and supports this conclusion in its proposed program. Other funding models should be considered if it is deemed necessary and cost-effective.

RECOMMENDATION: NASA and NSF support for laboratory astrophysics under the Astronomy and Physics Research and Analysis and the Astronomy and Astrophysics Research Grants programs, respectively, should continue at current or higher levels over the coming decade because these programs are vital for optimizing the scientific return from current and planned facilities. Missions and facilities, including DOE projects, that will require significant amounts of new laboratory data to reach their science goals should include within their program budgets adequate funding for the necessary experimental and theoretical investigations (pp 1-17; 5-23,24).

4. Conclusion

This is an extraordinary time in the study of the cosmos, but also a time of serious constraints on federal discretionary budgets. The recommended program is science-driven and will enable progress across a large swath of research and open up more discovery space. A balanced program should be maintained throughout the decade. Effective international, public-private and inter-agency collaboration is required for success of the program.

Astro2010 has had unprecedented involvement and support by the astronomical community and immense effort by the committee, panels and consultants, as well as the strong cooperation of the agencies and professional societies.

NASA LAW, October 25-28, 2010, Gatlinburg

Cosmology and Fundamental Physics and their Laboratory Astrophysics Connections

W. C. Haxton

Department of Physics, MC 7300, University of California, Berkeley, CA 94720-7300 and Lawrence Berkeley National Laboratory, MS 70R0319, Berkeley, CA 94720-8169

haxton@berkeley.edu

ABSTRACT

The Decadal Survey of Astronomy and Astrophysics created five panels to identify the science themes that would define the field's research frontiers in the coming decade. I will describe the conclusions of one of these, the Panel on Cosmology and Fundamental Physics, and comment on their relevance to the discussions at this meeting of the NASA Laboratory Astrophysics community.

1. Introduction

The Committee for the Decadal Survey of Astronomy and Astrophysics (2010) convened five panels to consider the science themes that would define the field's research frontiers in the next decade. One of these, the Panel on Cosmology and Astrophysics, had a particularly broad mandate that included topics of interdisciplinary interest. The panel was chaired by David Spergel and included David Weinberg (vice chair), Rachel Bean, Neil Cornish, Jonathan Feng, Alex Filippenko, Marc Kamionkowski, Lisa Randall, Eun-Suk Seo, David Tytler, Cliff Will, and myself. The organizers of this Laboratory Astrophysics Workshop have asked me to summarize the Panel's conclusions and comment on their relevance to laboratory astrophysics and future NASA missions.

The context for Panel discussions was established by a set of recent discoveries that have strengthened the links between astrophysics/cosmology and fundamental physics conducted in terrestrial laboratories. These include

- The development of a relatively simple cosmological model fitting astronomical data, Lambda Cold Dark Matter, with parameters known to better than 10% and with immediate implications for beyond-the-standard-model physics.

- Cosmic microwave background (CMB) and large-scale structure (LSS) studies that appear consistent with the predictions of inflation: a nearly flat universe with a matter distribution that is Gaussian with nearly scale-invariant initial fluctuations.
- CMB confirmation of the Big Bang nucleosynthesis (BBN) conclusion that baryons comprise about 4% of the closure density Ω_c, so that dark matter must be primarily nonbaryonic.
- Supernova data indicating that the expansion of the universe is accelerating, consistent with dark energy dominance of the universe's present energy density.
- Astrophysical ν discoveries, from the Sun and from cosmic rays (CRs) impinging on Earth, that show neutrinos have mass and undergo flavor oscillations, providing the first direct evidence of physics beyond the standard model (and the first identification of a component of the dark matter).
- The identification of a cutoff in ultra-high-energy (UHE) CRs consistent with the expected GZK scattering off the CMB. Thus the universe may be opaque to us at cosmological distances and asymptotic energies, apart from UHE νs.

The Panel considered community input, generally provided as white papers, on a wide range of topics: the early universe; the CMB; probes of LSS through observations of galaxies, intergalactic gas, or their associated gravitational distortions; determinations of cosmological parameters; dark matter; dark energy; tests of gravity; astrophysical measurements of physical constants; and the fundamental physics that might be derived from astronomical messengers (νs, γs, CRs). Among the white papers considered, several addressed either laboratory astrophysics or theory and computation.

The Panel's response was formulated around four "big questions:" 1) How did the universe begin (the mechanism behind inflation)? 2) Why is the universe accelerating (the nature of the dark energy)? 3) What is dark matter? 4) What are the properties of neutrinos? Gravitational wave astronomy was designated as the discovery area.

This meeting's organizers have asked me to summarize the Panel's conclusions, commenting on their connections to laboratory astrophysics and NASA missions. In this written version of my talk I will focus the last two of the four questions, in part because I know these areas best, but also because they may have substantial connections to laboratory astrophysics. Here "laboratory astrophysics" is defined quite broadly, given that the Panel's charge included the intersection of astrophysics and astronomy with the particle and nuclear physics programs of major accelerator facilities, and with a broad array of ground-based detectors for dark matter, νs, CRs, and related studies.

2. What is Dark Matter?

The majority of matter in the universe is dark, invisible to us apart from its gravitational effects on the structure we do see. In addition to its deep roots in cosmology and astrophysics, the dark matter (DM) problem is central to high-energy physics, where DM particles may be discovered in the debris from collisions between ordinary particles, and in underground science, where the recoil of detector nuclei may indicate interactions with dark matter particles. (For a recent review of the topics summarized here, see Feng (2010).)

DM was first postulated to account for the anomalous velocity rotation curves of galaxies. DM particles must be stable or long-lived, cold or warm (sufficiently slow that they can seed structure formation), gravitationally active, but without strong couplings to themselves or to baryons. The DM/dark energy contributions to the universe's total energy density evolves with redshift, with the former dominant early and the latter dominant today. Two leading DM candidates are Weakly Interacting Massive Particles (WIMPs) and axions. WIMPS are intriguing because the properties necessary for astrophysics match expectations that new particles will be found at the mass generation scale of the standard model of 10 GeV - 10 TeV. The WIMP "miracle" is the observation that the annihilation cross section for massive, weakly interacting particles natural leads to the expectation that $\Omega_{\rm WIMP} \sim 0.1$.

Figure 1 illustrates three avenues of attack on the DM problem: direct detection where a DM particle $\chi_{\rm DM}$ scatters off a standard-model particle $\rm f_{SM}$, causing recoil; indirect detection, where DM particles annihilate or decay into ordinary particles that can then be detected; and particle collider experiments, where DM particles are produced from the scattering of ordinary particles and identified from the missing energy. DM particle interactions can be either independent (SI) or dependent (SD) on target spin, depending on parameter choices in the underlying model, and while their predicted cross sections span a wide range, $\sigma_{SI} \sim 10^{-45}$ cm^2 is a representative value. Current detectors in the $\sim$ 10-100 kg range are probing DM particle-nucleon cross sections well below 10^{-43} cm^2 for DM particle masses of $\sim$ 100 GeV. The international program is focused on developing new detectors in the 1-10 ton range, using media such as ultra-clean nobel-gas liquids, with sensitivities of a few events per year, or $\sigma_{SI} \sim 10^{-47}$ cm^2. There have been claims of detection, interpreted as low-mass WIMPs, but no consensus has been reached.

This field has a number of laboratory and theory needs, including:

- support for direct searches, including detector R&D and the development of deep underground locations for detectors, as energetic neutrons produced by penetrating CR muons are an important background;

- clean-room facilities to control environmental activities, as trace radionuclides within detectors or in surrounding materials are a second major background source;
- nuclear theory for estimates of WIMP SI form factors and SD cross sections;
- for direct production experiments, facilities like the LHC that can reach the energies necessary for $\chi_{\rm DM}$ creation; and
- for indirect detection searches, astrophysical modeling that will allow observers to distinguish WIMP annihilation signals from other high-energy astrophysics phenomena.

Ideally, multiple lines of investigation will lead to DM detection. An attractive scenario is the discovery of supersymmetry at the LHC and the identification of a lightest stable SUSY particle; direct detection of cosmic WIMPS with consistent properties; and consequently, improved constraints on the local DM density and its effects on structure at subgalactic scales, testing the paradigm of cold, collisionless, stable DM.

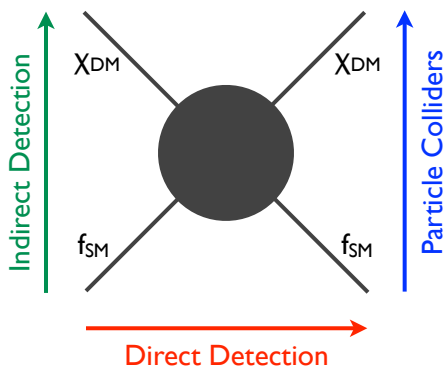

Fig. 1.— Three strategies for detecting dark matter particles $\chi_{\rm DM}$ via their interactions with standard-model particles $f_{\rm SM}$.

3. What are the Properties of Neutrinos?

[For a review of topics discussed in this section, see the APS Multi-Divisional Neutrino Study Group (2004).] Neutrino astrophysics has rich intersections with laboratory nuclear and particle astrophysics. A 1958 measurement showing that the cross section for ^{3}He+^{4}He is a 1000 times larger than then expected was crucial to the first solar ν experiment: this reaction leads to pp chain branches producing higher energy ^{7}Be and ^{8}B νs, which the Cl experiment could detect. The discrepancies that emerged from the Cl experiment stimulated

30 years of careful laboratory cross section measurements and the development of a standard solar model (SSM) capable of predicting the Sun's core temperature to $\sim 1\%$. When the pattern of solar ν fluxes did not match that predicted by the model nor by any plausible variation in that model, expectations grew that a more fundamental problem must exist. Finally the atmospheric ν measurements of Super-Kamiokande and the solar ν measurements made by SNO demonstrated that neutrinos have mass and that two distinct oscillations occur, governed by the mass splittings $\Delta m^2_{\rm sol}$ and $\Delta m^2_{\rm atm}$ (see Fig. 2).

Unsettled issues in ν physics with important implications for astrophysics include the absolute scale of neutrino mass; the origin of matter in the cosmos; ν properties affecting energy transport and nucleosynthesis in extreme astronomical environments; and the high-energy limits of astrophysical accelerators. The associated laboratory astrophysics is very "high end," predicated on next generation ν experiments requiring new beamlines and massive underground detectors.

The ν differs from other fermions of the standard model because it has no charge or other additively conserved quantum number. Consequently it can have two kinds of mass terms, Dirac and Majorana, while other particles must be Dirac fermions. This provides a natural explanation for an otherwise mysterious fact, that νs are much less massive than other standard-model particles. The ν mass matrix can be written schematically as

$$\begin{pmatrix} M_L \sim 0 & M_D \\ M_D^\dagger & M_R \end{pmatrix} \Rightarrow m_\nu^{\rm light} \sim M_D \left(\frac{M_D}{M_R}\right), \tag{1}$$

yielding a light ν mass that is proportional to the Dirac mass, multiplied by M_D/M_R, the ratio of the Dirac mass to the right-handed Majorana mass. If $M_R \gg M_D$, one has a natural explanation for the smallness of the ν mass, relative to the Dirac mass M_D of other fermions. Indeed, based on what we have learned from ν oscillations, the necessary $M_R \sim 0.5 \cdot 10^{15}$ GeV, close to the $\sim 10^{16}$ GeV grand unified mass scale. Thus νs not only involve an entirely distinct mass generation mechanism, but that mechanism could depend on UHE physics that otherwise is far beyond experimental reach. There is great interest in determining the absolute ν mass and whether Majorana masses exist. (The latter question involves the process of neutrinoless $\beta\beta$ decay, which I will not discuss here.)

Neutrino oscillation mass differences tell us that the ν mass could be as small of 0.05 eV. The most promising test we have of such small ν masses is cosmology: LSS is influenced by νs, because they are relativistic and free-streaming, and thus suppress the growth of LSS. The smaller the mass, the longer they remain relativistic, and the larger the scale at which they suppress the growth of structure. The critical wave number is related to the mass by

$$k_{\rm free\ streaming} \sim 0.004\sqrt{m_\nu/0.05\ {\rm eV}}\ {\rm Mpc}^{-1}. \tag{2}$$

Neutrinos are a unique DM component because they transition from relativistic to nonrelativistic matter with expansion. Thus their effects are both scale and red-shift dependent. To see effects due to $m_\nu \sim 0.05$ eV, a sensitivity to DM at 0.1% of Ω_c must be achieved. (However, their effects in suppressing power at large scales and low Z can be several per cent.) The current best limits correspond to 1.3% of Ω_c. Future analyses that combine large data sets with different sensitivities to scale and redshift will clearly have the most impact on improving sensitivity to ν mass – assuming systematic uncertainties of multiple data sets are under control. As the sensitivity of LSS surveys typically scales as $\sqrt{N}$, where N is the number of modes, one needs new LLS surveys that exceed past ones by a factor ~ 100. The Panel discussed a variety of planned surveys of high-redshift galaxies, QSOs, and the CMB that might achieve such improvements. Some combination of such surveys, data from 21-cm radio telescopes with large collecting areas (~ 0.1 km), and weak lensing studies could reach the sensitivity to detect ν mass at the 0.05 eV lower bound.

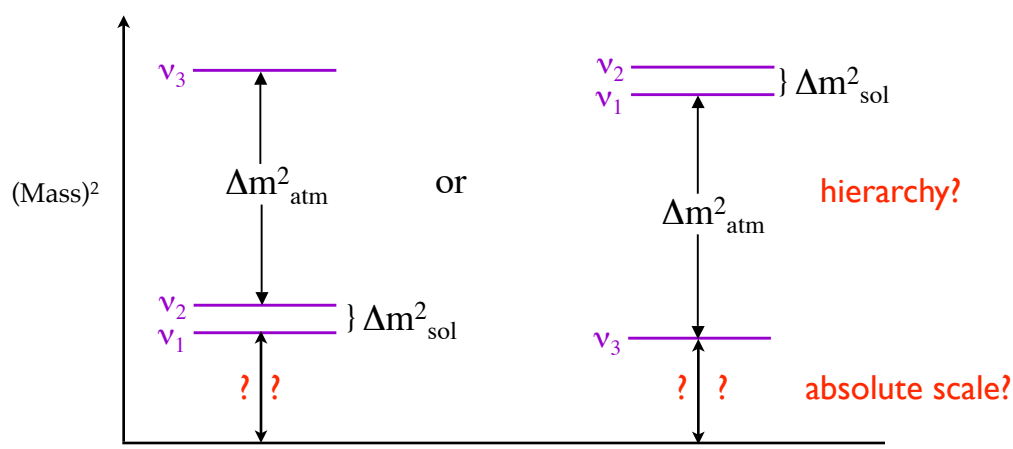

Fig. 2.— The normal (left) and inverted (right) ν mass hierarchies are both consistent with existing oscillation data.

Other open ν questions affect astrophysical phenomena such as Type II supernova explosions. Figure 2 illustrates an ambiguity in the ν mass pattern: both the normal and inverted hierarchies are compatible with existing oscillation data. In solar ν measurements, the MSW effect alters oscillation results: the ν_e becomes heavier in matter, generating a level crossing at some critical density where the effective mass generated by ν_e interactions with solar matter just cancels the vacuum mass difference. The imprint of matter effects on the solar ν spectrum is how we know the sign of $\Delta m_{\rm sol}$. But for the atmospheric ν oscillations, $\Delta m_{\rm atm}$ is too large for terrestrial matter effects to enter. Consequently, we do not know the sign of $\Delta m_{\rm atm}$, leading to the ambiguity illustrated in Fig. 2.

However, in core collapse supernovae, νs decouple from the matter at very high density, $\sim 10^{11}$ g/cm^3. As they free-stream through the carbon zone, at a density of about 10^4 g/cm^3, they encounter the critical density where a crossing occurs for $\Delta m_{\rm atm}$. For the normal hierarchy, the crossing is between the ν_e and its heavy-flavor counterpart. But for the inverted hierarchy, the crossing is between the corresponding $\bar{\nu}$s. That is, the sign of the density-dependent effective mass is opposite for ν_es (which become heavier in matter) and $\bar{\nu}_e$s (which become lighter). As the ν_es and $\bar{\nu}_e$s from a supernova are expected to be less energetic that the heavy-flavor ν_xs, the flavor swap will lead to either anomalously hot ν_es or anomalously hot $\bar{\nu}_e$s – depending on the hierarchy.

This crossing also depends on a third mixing angle θ_{13} that is currently unknown, bounded only by reactor $\bar{\nu}_e$ disappearance experiments. The phenomena described above require $\theta_{13} \gtrsim 10^{-4}$. As next-generation terrestrial ν experiments have a more modest sensitivity goal of $\theta_{13} \gtrsim 10^{-2}$, it is quite possible that high precision measurements of the ν flux and flavors from the next galactic supernova could also be important in probing θ_{13}.

This issue is important to another cosmological puzzle, the origin of matter (baryons) in the universe. We know some process broke the symmetry between matter and antimatter in the Big Bang: an excess of matter over antimatter led to incomplete annihilation, so that today baryons comprise 4% of Ω_c. One of several requirements for baryogenesis in the early universe is CP violation – yet the known CP violation in the standard model is too weak to drive this process. Thus there likely is some undiscovered source of CP violation. One consequence of nonzero ν masses is that a Dirac CP phase δ now appears in the ν mass matrix. This phase could be responsible for the generation of baryons through the process of leptogenesis: the CP violation originates with νs, but is communicated to the baryons through interactions. Given what we know about other mixing angles, the condition for CP violation to be large among the νs (in contrast to quarks, where other small mixing angles suppress the effects of CP violation) is that neither δ nor θ_{13} is small. Thus, if we detect the effects of θ_{13} on supernova ν oscillations, this would be a major step forward, ensuring that $\theta_{13} \gtrsim 10^{-4}$.

4. Conclusion

The laboratory astrophysics $\leftrightarrow$ astrophysics/cosmology intersection described in this talk is sometimes conventional – e.g., the nuclear cross section measurements done in support of solar ν experiments or BBN modeling – but more often unconventional. For example, in determining the overall scale of neutrino mass, the experiments done in the laboratory (tritium β decay, $\beta\beta$ decay, reactor and accelerator ν oscillation searches) complement what

can be done in cosmology. Each probes an important quantity – tritium β decay probes the masses of νs in proportion to their coupling probability to the electron, $\beta\beta$ decay probes the Majorana mass, oscillations test m_ν^2 differences, and cosmology responds to the sum of the ν masses – but the quantities are different. So the traditional relationship has given way to one where the universe has be viewed as another laboratory, one that is playing a very important role in pushing back the frontiers of precision particle physics. This is a theme that may have been best expressed in another NRC study, From Quarks to the Cosmos.

In the coming decade the community hopes to build new ν beamlines and underground detectors on the $10^2 - 10^3$ kiloton scale to determine the hierarchy through matter effects, measure ν CP violation, and fix all mixing angles and mass differences to high precision. Cosmology could be an equal partner in this effort: if the effects of ν mass on LLS can be determined to sufficient accuracy, both the absolute scale and hierarchy questions might be resolved in this way.

In DM the situation is similar. One of the goals of the LHC is to find the new particles that are expected to accompany TeV-scale physics. We also have a new generation of massive DM detectors that will be mounted on Earth (or more precisely, within the Earth) that will be probing the cosmological flux of DM particles. One hopes that both endeavors succeed, and that we will be able to reconcile the cosmological properties of DM with those determined from collider experiments.

I thank the organizers for the opportunity to attend this workshop, and my colleagues on the Cosmology and Fundamental Physics Panel for sharing their perspectives on this field. This work was supported by the US Department of Energy, Office of Nuclear Physics.

REFERENCES

Committee for the Decadal Survey of Astronomy and Astrophysics. 2010. New Worlds, New Horizons in Astronomy and Astrophysics, National Research Council

Feng, J. L., 2010, Ann. Rev. Astron. Astrophys. 48, 495

APS Multi-Divisional Neutrino Study Group. 2004. http://www.aps.org/policy/reports/multidivisional/neutrino/

This preprint was prepared with the AAS LaTeX macros v5.2.

NASA LAW, October 25-28, 2010, Gatlinburg

Laboratory Astrophysics in the Astro2010 Science Frontier Panel on Planetary Systems and Star Formation

Héctor G. Arce

Department of Astronomy, Yale University, New Haven, CT 06511

hector.arce@yale.edu

ABSTRACT

The recent report of the Astro2010 Science Frontier Panel (SFP) on planetary systems and star formation identified several general research questions that should drive the field in the coming decade. In the report, laboratory work was recognized to be essential for interpreting the data needed to answer the questions that will advance the field; from studies of how stars form and how circumstellar disks evolve and form planetary systems to research on exoplanet diversity and the search for habitable planets. Here I discuss the findings of the Astro2010 SFP on planetary systems and star formation and the relevant laboratory astrophysics needs to carry out the exciting research and interpret the data from current and future NASA Astrophysics missions and other important ground-based observatories in the coming decade.

1. Introduction

The Astro2010 Science Frontier Panel on planetary systems and star formation was asked to consider science opportunities that would define the frontier research for the coming decade in a range of of topics, including studies of molecular clouds, protoplanetary and debris disks and extrasolar planets, as well as ground-based studies of solar system bodies, astrochemistry and exobiology. From these range of topics the panel recognized several areas that offer the most promising progress in research in the next decade and will also serve as scientific drivers of the field. The panel identified four central questions that should be answered (or that will see major advances) over the next ten years, and one area of unusual discovery potential. These areas can be summarized with the title "The Birth of Stars and Planetary Systems, and the Search for Habitable Worlds." The four questions and the area

of unusual discovery are:

- How do stars form?
- How do circumstellar disks evolve and form planetary disks?
- How diverse are planetary systems?
- Do habitable worlds exist around other stars, and can we identify the telltale signs of line on an exoplanet?
- Area of unusual discovery: Identification and characterization of a nearby habitable exoplanet.

Whithin each of these questions, there are one or more sub-topics in which advances and further development in laboratory astrophysics and chemical modeling were identified as essential for helping interpret the wealth of data that will soon be available, and to answer the questions listed above.

2. Star Formation and Laboratory Astrophysics

The panel identified three key aspects of star formation that can be addressed in the next 10 years with existing and new facilities. These include: 1) understanding what determines star formation rates and efficiencies in molecular clouds; 2) understanding what determines the properties of pre-stellar cloud cores; and 3) determining the origin of the stellar mass function (also known as the initial mass function or IMF). Out of these, laboratory astrophysics will play a crucial role in the last two.

Star formation takes place in the densest regions of molecular clouds, typically refereed as cores. Protostars form as a consequence of the gravitational contraction of dense gas in cores, and once the process of star formation begins, the dense core will act as the primary mass reservoir of the forming star. Pre-stellar cores —dense condensations in molecular clouds with infall motions, but no obvious stellar source— thus represent the initial conditions of star formation. In order to understand how stars form we need to know how cores form and evolve, as well as how core properties depend on environment, and in turn how these affect the mass distribution of the stars that form in them.

Studies of cores rely on observations of dust continuum emission (to trace the density structure) and molecular line emission (to probe the core kinematics and chemistry). The

Atacama Large Millimeter Array (ALMA) will provide high-resolution line and continuum observations of cores that will help us characterize the properties of pre-stellar cores and help us understand the origin of the IMF. In particular high-density molecular line tracers are needed to explore how non-spherical, asymmetric core geometries may produce further fragmentation into multiple star systems, and how fragmentation affects the IMF.

Most importantly for the laboratory astrophysics community is the fact that different molecular lines are used to probe different density regimes in the circumstellar environment. This is in part due to the varying excitation conditions and physical and chemical processes that take place in different regions of the circumstellar environment (at distinct densities and distances from the protostars), which produce different abundances of various molecules (e.g., Herbst & van Dishoeck 2009). This results in a rich chemistry in regions close to the protostar. Understanding these chemical processes and recognizing the lines that can best probe the different circumstellar environments will be essential for future high-resoltion studies with ALMA. In regions where high-mass stars form, the inner core may exhibit temperatures exceeding 1000 K (e.g., Doty et al. 2002), and these regions are best traced by high excitation lines in the far-infrared (FIR) and ro-vibrational molecular lines in the mid-infrared. These wavelength ranges are observable by the Herschel Space Observatory and the Stratospheric Observatory For Infrared Astronomy (SOFIA), yet it is a poorly studied region of the spectrum where there are many unidentified lines.

Recommendations by the panel, of interest to the laboratory astrophysics community, that will help answer the questions regarding the studies of how stars form include:

- Expand laboratory work in the poorly studied far-infrared and sub-millimeter regions of the spectrum.
- Improve understanding of surface reaction rates and mechanisms on small particles through laboratory and theoretical work.
- Improve models of chemical evolution so that they include effects of the cloud dynamical evolution, in order to make detail comparisons with observations.

3. Circumstellar Disks and Laboratory Astrophysics

During the collapse process, the infalling material in the core does not simply collapse to a single point to form a star. Instead, as a consequence of angular momentum conservation, it mostly falls onto a rotationally supported disk. The forming star acquires most of its mass from material in the inner core that is channel through the circumstellar disk and accreted

onto the protostar. Disks around young stars also provide the reservoir of material for planet formation. Disks are therefore essential to both the formation of stars and planetary systems.

Two important specific questions in the study of circumstellar disks in which laboratory astrophysics will help and are important to future NASA missions are:

- What is the Nature of the Planet-Forming Environment?
- How do Giant Planets Accrete and Interact with Disks?

Up to date only approximately 150 disks have been imaged either with scattered light, continuum emission or molecular line emission.[1] Dust continuum emission emission is typically used to detect disks and estimate their masses, while molecular line observations (typically using CO) probe the gas content, kinematics and chemistry of the disk. We have a general idea of the different processes that take place in the disk (e.g., optical through X-ray irradiation from central star, ionization by cosmic rays and from interstellar UV, infall shocks from envelope, etc.). However, how disks evolve and form planets is still not fully understood. Studying the detailed chemical structure and evolution of disks is crucial, as the chemical composition may affect planet formation as well as the accretion process. Knowing the distribution and abundance of water as well as that of complex organic and pre-biotic molecules in disks is of particular interest to the study of life.

Little is known about disk chemistry and only recently some studies have tackled this problem by observing disks using different molecular lines (Jørgensen & van Dishoeck 2010; Öberg et al. 2010). These limited studies show what we can expect in the next decade with much better instruments, in terms of studies needed to characterize the planet-forming environment. ALMA will be able to map the distribution (and abundance) of water and complex molecules in disks with a resolution of a few AU. Although SOFIA will not have the angular resolution to map disks, it will have sufficient spectral resolution to resolve molecular vibrational lines that arise from different velocity regimes in the disk. Studying the velocity distribution of different lines that probe different excitation and density regimes using instruments onboard SOFIA will provide an estimate of the chemical stratification in disks. Observations of ions and ionized molecules with SOFIA will also allow estimates of the disk ionization fraction, essential for understanding the role of magnetic fields in the dynamics of the disk material.

In the coming decade new facilities will allow, for the first time, the direct detection and imaging of a forming protoplanet. Models indicate that ALMA will be able to detect

[1] see http://circumstellardisks.org/

protoplanets using both line and continuum emission in certain nearby systems, at distances of about 100-150 pc (Wolf & D'Angelo 2005; Narayanan et al. 2006; Semenov et al. 2009). Even in cases where the protoplanet is not detectable, effects of the disk (e.g., gaps) could still be detected. The Hubble Space Telescope (HST) has recently imaged planets in a system with a debris disk, where both the stars and planets are fully formed, but are still relatively young at a few hundred million years of age (Kalas et al. 2008). The James Webb Space Telescope (JWST) will be able to make similar coronographic observations of similar systems with much better sensitivity. Observations of disks around different types of stars and at different evolutionary stages will allow a better understanding of how giant planets accrete and interact with disks.

In order to take full advantage of the data that will be collected to study the aspects of circumstellar disks described above, major efforts in chemical modeling and laboratory astrophysics should take place. The same recommendations given above in Section 2 apply to the research related to disks. That is, improvement in chemical models and a better understanding of surface reaction rates is needed to understand molecule formation in disks. These models should guide us in deciding which molecules are the best for tracing different processes that take place in the disk. Also, laboratory work is needed to identify more molecular spectra in the infrared regime that will probe the inner regions of the disk, and will help interpret SOFIA and Herschel data. In addition, further laboratory experiments that study angular momentum transport (e.g., Ji et al. 2006) should include magnetic fields so they resemble the processes taking place in circumstellar disks.

4. Exoplanet Studies and Laboratory Astrophysics

Although we now know of the existence of more than 500 exoplanets[2], we know very little of their properties. In most cases, only an estimate of the minimum mass and the semi-major axis of the planet are known. Sound measurements of an exopanet's mass and size allow an estimate of the planet's density, which then permit to estimate the planet's bulk composition. This can be done when the planet is detected via both the radial velocity and the photometric transit methods —but which has been done only for a fraction of all the known exoplanets. Detection and modeling of exoplanet atmospheres has only been done for even fewer sources (a few tens) as this is much more time consuming than merely detecting the planet. To learn how diverse planetary systems are we need to extend the exoplanet census to investigate the range of planet masses, their bulk composition and atmospheres. A

[2]see http://exoplanet.eu/

thorough census of exoplanets will allow the comparison of observed properties with models of planet formation and provide us with a better understanding of their origin.

Of particular interest to laboratory astrophysics is the study of exoplanet atmospheres. Most studies of exoplanet atmospheres are conducted using observations of transiting planets where measurements during primary eclipse (i.e., when the planet is in front of the star) will include absorption by the exoplanet's atmosphere. In addition, comparing between observations during secondary eclipse (i.e., when the planet is behind the star) and observations before or after provide estimates of the exoplanet's thermal radiation (for more details see Seager & Deming 2010). Most exoplanet atmosphere studies use observations of broad-band photometry (and in some cases narrow-band photometry and low-resolution spectra as well) to compare it with an atmosphere model. A reliable result not only depends in obtaining high signal-to-noise data at a range of wavelengths, but also relies on having accurate atmosphere models. Instruments onboard JWST will allow observations over a wider wavelength range (and with higher spectral resolution) compared to what has been possible with the Spitzer Space Telescope. Atmosphere models should therefore improve to be able to interpret the wealth of new (and better) data that will be available in the next decade. For this reason the panel recommended the following (taken directly from the report):

- Development of models of exoplanet atmospheres of varying composition under differing levels of radiation, including the study of clouds and photochemistry.
- Tabulation of molecular line data supported by laboratory astrophysics as needed in support of atmosphere modeling efforts.

The area of unusual discovery potential identified by the panel is the detection and characterization of a population of nearby super-Earths (planets with about 1 to 10 Earth masses). For this to be successful, the same recommendations shown above apply. Of particular interest is the vast diversity that atmospheres of super-Earths are expected to exhibit (Seager & Deming 2010). Detection of nearby super-Earth atmospheres will be possible with JWST. Thus, model atmospheres for these interesting objects should be in place in order to successfully interpret the unprecedented spectroscopic data that will be available once JWST is launched.

4.1. Habitable Worlds

The fourth question that the panel thought would be important to consider over the next decade deals with the search and discovery of a habitable Earth-like planet orbiting

around a Sun-like star at a distance of about 1 AU. The Kepler Mission should find these kinds of planets, if they exist. Follow-up radial-velocity observations will be needed to get a handle on the mass, and density of Earth-like exoplanets. Even then, very little will be known about the planets composition, surface, and atmosphere. One does not have to go far to see why knowing these properties are important to determine whether the planet is potentially habitable. In our own Solar System, Venus, Earth and Mars orbit around the Sun at about 1 AU distance, yet they differ drastically in their atmospheres, surface and habitability. It is therefore extremely important to know an exoplanet's atmosphere and composition to study its potential to harbor life.

The panel recognized that the facilities and space missions that will finally take an image and a spectrum of an Earth-like planet will not be available in the next decade. However, the panel though this was a topic of extreme importance and that it should be included in the Astro2010 report. The panel proposed that this coming decade should be used to lay the necessary ground-work for a successful terrestrial planet finder mission in the future.

Of particular interest to the laboratory astrophysics community is research on the measurable characteristics that define habitability. The panel supports further investigation of biosignatures in order to understand their limitations and to know which spectral features would give us the most reliable indication of the existence of life on an exoplanet. For example, it should be investigated whether the detection of liquid water and a non-equilibrium chemistry is enough to declare that a planet harbors life, as well as the uncertainties in these assumptions. Research on other possible spectral signatures of life should also expand. Advances in planetary atmosphere models as described in the recommendations listed above will be essential for the reliable identification of biomarkers.

5. Summary

The Astro2010 Science Frontier Panel on planetary systems and star formation identified four questions that should be ripe for answering over the next decade and one area of unusual discovery potential. The topics include understanding how stars form, investigating how circumstellar disks evolve and form planets, extend the exoplanet census, work towards fulfilling a successful planet finder mission, and the discovery and characterization of a population of Super-Earths. For studies of star formation and circumstellar disks molecular line observations play an important role, and expanding laboratory work on the identification of molecular lines in the millimeter/sub-millimeter/FIR regions of the spectrum will be needed to fully interpret the spectral line data from ALMA, Herschel and SOFIA. In addition, improvements in our understanding of dust surface reaction rates and more sophis-

ticated chemical evolution models are essential to know how (and which) molecules form in the core and disk around protostars —key for deciding which are the best tracers to probe the different regimes in the circumstellar environment. For studies of exoplanets, further development of improvements in atmospheric models and tabulation of molecular line data in support of modeling efforts will be needed to construct detailed and reliable exoplanet atmosphere models to compare with future space-based telescope data. In summary, laboratory astrophysics work in combination with chemical models will be essential to interpret the wealth of data that will be available from upcoming ground-based telescopes and NASA missions.

The panel report was a group effort and I would like to acknowledge all the members for their contributions. The SFP panel on planetary systems and star formation was composed of thirteen members: Lee Hartmann (chair), Héctor Arce, Claire Chandler, Eugene Chiang, David Charbonneau, Suzan Edwards, Eric Herbst, David Jewitt, James Lloyd, Eve Ostriker, David Stevenson, Jonathan Tan, and Dan Watson.

REFERENCES

Doty, S. D., van Dishoeck, E. F., van der Tak, F. F. S., Boonman, A. M. S., A&A, 389, 446

Herbst, E. & van Dishoeck, E. F. 2009, ARAA, 47, 427

Ji, H., Burin, M., Schartman, E., Goodman, J. 2006, Nature, 444, 343

Jørgensen, J. K. & van Dishoeck, E. F. 2010, ApJ, 710, L72

Kalas, P., Graham, J. R., Chiang, E., Fitzgerald, M. P., Clampin, M., Kite, E. S., Stapelfeldt, K., Marois, C., Krist, J. 2008, Science, 322, 1345

Öberg, K. I., Qi, C., Fogel, J. K. J., Bergin, E. A., Andrews, S. M., Espaillat, C., van Kempen, T. A., Wilner, D. J., Pascucci, I. 2010, ApJ, 720, 480

Wolf, S. & D'Angelo, G. 2005, ApJ, 619, 1114

Narayanan, D., Kulesa, C. A., Boss, A., Walker, C. K. 2006, ApJ, 647, 1426

Seager, S. & Deming, D. 2010, ARAA, 48, 631

Semenov, D., Pavlyuchenkov, Y., Henning, T., Wolf, S., Launhardt, R. 2009, ApJ, 673, L195

This preprint was prepared with the AAS LaTeX macros v5.2.

NASA LAW, October 25-28, 2010, Gatlinburg

Laboratory Astrophysics in the Stars and Stellar Evolution 2010 Panel

M. H. Pinsonneault

Department of Astronomy, Ohio State University, Columbus, OH 43210

pinsonneault.1@osu.edu

ABSTRACT

The role of laboratory astrophysics in the Stars and Stellar Evolution (SSE) panel of the Astro 2010 Decadal Survey is reviewed. The four main science questions of the panel were

1) How Do Rotation and Magnetic Fields Affect Stars?

2) What Are the Progenitors of Type Ia Supernovae, And How Do They Explode?

3) How Do The Lives Of Massive Stars End?

4) What Controls The Mass, Radius, And Spin of Compact Remnants?

Laboratory astrophysics has a key role in deciphering these complex phenomena, and sample cases related to the basic panel question are reviewed. Two distinct classes of applications emerge: experimental measures of complex physical phenomena, and a transition to experimentally based models for precision stellar astrophysics. I will use two cases (opacity measurements and solar neutrinos) to illustrate the important role of the latter class of experimental data.

1. Introduction

These are exciting times for stellar astrophysics. A series of technical breakthroughs have provided both large surveys of previously rare objects and exquisitely precise studies of individual objects. The most promising areas of study identified by the 2010 Stars and Stellar Evolution (SSE) panel emphasize two broad themes: precision stellar astrophysics and the very real prospect of progress in subjects which were historically too complex to understand well. Laboratory astrophysics will play a key role in advancing our knowledge, and important contributions can be made in both areas.

On the precision astrophysics front we require better input physics to detect subtle clues about the structure and evolution of stars. A specific example may be enlightening. Interiors models rely on theoretical calculations of the equation of state and opacity (photon mean free path), for example. Sophisticated diagnostics of internal structure, such as the pattern frequencies of nonradial oscillations in the Sun, permit the measurement of the depth of the solar surface convection zone and the abundances of oxygen and helium (Basu & Antia 2008) inferred from the impact of their ionization on the solar internal thermal structure. The surface solar abundances inferred from may have uncovered discrepancies between the solar abundance predicted by interiors theory (Delahaye & Pinsonneault 2006) and those preferred by some (Asplund et al. 2009) but not all (Caffau et al. 2011) recent stellar atmospheres calculations. Laboratory measurements of opacities for solar interiors conditions (Bailey et al. 2009) may provide a crucial experimental test of the theory used in the interiors models. A transition to models grounded in experimental data, such as in this case, could have broad implications. The same interiors models are used to infer stellar ages, inform chemical evolution models, and are used for near-field cosmology reconstructions of the formation of the Milky Way galaxy.

There are also aspects of stellar evolution where our understanding of the relevant physics is sorely lacking; the physics of supernova explosions is perhaps the most dramatic example. Laboratory astrophysics can play an important, but different, role in such subjects: providing physical insights into the underlying causes of complex and poorly understood processes. With these two underlying themes in mind, I now turn to the science frontiers and discovery area called out in specific by the SSE Panel.

2. Key Questions

Numerous white papers were submittted to the Decadal Review panel on the subject of stars and stellar evolution. The SSE panel converged on four science frontiers; two were related to the physics of supernovae and will be discussed together here. We also called out time-domain astronomy as an important discovery area for the study of stars. I will briefly introduce the topics and then highlight their connection to the study of laboratory astrophysics.

2.1. How Do Rotation and Magnetic Fields Affect Stars?

Theoretical stellar models are traditionally one dimensional and neglect rotation and magnetic fields. We now have both the observational and theoretical tools to discard these assumptions. At one level we now recognize that rotation can have a powerful impact on the structure and evolution of stars, especially massive ones; however, there is still no consensus on the relative importance of hydrodynamic instabilities, waves, and magnetic fields for internal angular momentum transport in stars. Large new surveys are producing a wealth of observational constraints on stellar rotation, and nonradial stellar oscillations can also yield important clues about internal stellar rotation.

Magnetic fields are important both in their own right and as a powerful influence on stellar angular momentum evolution. Basic questions, such as the origin of stellar magnetic fields and the heating of the extended outer chromospheres and coronae, are still open. But advances in numerical simulations and spectacular new data, especially for the Sun, are leading to substantive improvements in our understanding of these basic issues.

We will not be able to reconstruct the underlying physics without experimental data. In particular, laboratory studies of magnetic reconnection, angular momentum transport, and hydrodynamic instabilities related to rotation will be needed to translate the powerful emerging observational constraints into a coherent theoretical framework.

2.2. Supernovae

There are two major channels which produce supernovae: the core collapse of a massive star (Sn II) and thermonuclear explosions of white dwarfs (Sn Ia). Both processes have major open questions and provide distinct opportunities for contributions from the laboratory astrophysics community.

In the case of Sn Ia, all of the proposed formation channels involve the evolution of close binary systems. The study of the precursors would be substantially improved with laboratory measurements of X-ray transition probabilities and improved knowledge of accretion disk physics, such as the magneto-rotational instability or MRI. We are now in a position to obtain time-resolved spectra of explosions and trace out the detailed yields in the ejecta; again, laboratory measurements will be required to interpret the spectra. Nuclear physics can also play a role; the measurement of both electron capture rates and the cross-sections for important reactions such as C12+C12 are important for our understanding of the ignition conditions. Experiments related to combustion will also be valuable in the context of understanding the explosion mechanism and the chemical yields; observations require that

the ejecta from exploding white dwarfs is not fully burned.

Our understanding of the end stages of massive star evolution is complicated both by difficulties in simulating supernova explosions and by our limited understanding of the properties of supernova progenitors. Radiation pressure is important for the most massive stars, especially as a driver for mass loss. Experiments on plasma physics in a radiation pressure dominated regime could contribute to our knowledge of supernova progenitors. Rotation is clearly important for at least some core-collapse explosions, such as gamma-ray bursts in the collapsar model. As already noted in the previous topic, experimental data on internal angular momentum transport will be crucial for establishing the core rotation of supernova progenitors.

Finally, laboratory measurements of neutron-rich species (related to the r-process), explosive nucleosynthesis cross-sections, and studies of the nuclear equation of state will all be needed to improve our understanding of core-collapse supernovae. Facilities such as FRIB and DUSEL will be especially important for these problems.

2.3. What Controls the Mass, Radius, and Spin of Compact Remnants?

Our fourth science frontier is related to the end states of stellar evolution. The radii of neutron stars are closely related to the equation of state of ultra-dense matter. Large samples of pulsars will be obtained by next-generation surveys, and both the masses and radii of neutron stars can be inferred. Laboratory nuclear physics experiments will provide complementary constraints on the equation of state of nuclear matter.

White dwarfs emerge after a red giant star has shed its envelope. The physics of this stage sets the boundary between stars which explode and those which do not. Molecular opacity and transition probabalities for very cool stars would be extremely helpful in advancing our understanding of this phase of evolution.

2.4. Discovery Area: Time Domain Astronomy

As an important final note, many advances in the field are arising from time domain studies of stars. The Kepler and CoRoT missions, for example, have detected nonradial oscillations in thousands of sunlike stars and red giants. Large upcoming surveys, such as the LSST, will provide novel insights into the transient sky. Such surveys will open up completely new fields of inquiry, and astronomers of all kinds should be open to the need for new ideas and new experiments to understand the new classes of problems that will likely

emerge from these new capabilities.

3. Conclusion

The promise of fundamental insights from laboratory astrophysics is strong, The key ingredient for realizing this promise is to nurture close linkages between the experiments and the astrophysical communities that will be using their results.

I am summarizing the work of the entire NASA LAW SSE panel, which includes Roger Chevalier (chair), Bob Kirshner (vice-chair), Deepto Chakrabarty, Suzanne Hawley, Jeff Kuhn, Stan Owocki, Elliot Quateret, Scott Ransom, Hendrik Schatz, Lee Anne Willson, Stan Woosley, and myself.

REFERENCES

Asplund, M. et al. 2009, A.R.A.A. 47, 481

Basu, S. & Antia, H.M. 2008, Phys.Rep., 457, 217

Bailey et al. 2009, Phys.Pl.,16,e8101b

Caffau, E. et al. 2011, Sol. Phys. 268, 255

Delahaye, F. & Pinsonneault, M.H. 2006, ApJ, 649, 529

This preprint was prepared with the AAS LaTeX macros v5.2.

NASA LAW, October 25-28, 2010, Gatlinburg

Galactic Neighborhood and Laboratory Astrophysics

Q. Daniel Wang

Astronomy Department, University of Massachusetts, Amherst, MA 01003

wqd@astro.umass.edu

ABSTRACT

The galactic neighborhood, extending from the Milky Way to redshifts of about 0.1, is our unique local laboratory for detailed study of galaxies and their interplay with the environment. Such study provides a foundation of knowledge for interpreting observations of more distant galaxies and their environment. The Astro 2010 Science Frontier Galactic Neighborhood Panel identified four key scientific questions: 1) What are the flows of matter and energy in the circumgalactic medium? 2) What controls the mass-energy-chemical cycles within galaxies? 3) What is the fossil record of galaxy assembly from first stars to present? 4) What are the connections between dark and luminous matter? These questions, essential to the understanding of galaxies as interconnected complexes, can be addressed most effectively and/or uniquely in the galactic neighborhood. The panel also highlighted the discovery potential of time-domain astronomy and astrometry with powerful new techniques and facilities to greatly advance our understanding of the precise connections among stars, galaxies, and newly discovered transient events. The relevant needs for laboratory astrophysics will be emphasized, especially in the context of supporting NASA missions.

1. Introduction

The Galactic Neighborhood (GAN) Panel was charged to identify key scientific questions (as well as a potential major discovery area), which could be effectively addressed in the upcoming decade, regarding galaxies and their surroundings out to redshifts $z \approx 0.1$. This local volume of the universe contains a diverse array of objects (e.g., galaxies of vastly different masses, morphologies, and star formation rates). But the basic constituents of the GAN objects may be divided into three classes: 1) stars (including their remnants);

2) gaseous systems [the interstellar medium (ISM), circumgalactic medium (CGM), and intergalactic medium (IGM)]; 3) dark components [massive black holes (MBHs), typically seen at centers of galaxies, and dark matter]. The study of the interconnection among these constituents is a key part of the GAN science.

Why is the GAN science important in astronomy and astrophysics? The GAN is where astronomical phenomena can be examined in great detail. Because of their proximity, objects can be observed with unparalleled sensitivities, on small physical scales, across the electromagnetic spectrum, and within a relatively well-determined galactic or intergalactic environment. For example, stellar populations can be resolved into individual stars only in the GAN. Such observations are often necessary in order to firmly identify underlying astrophysical processes and, occasionally, even new physics (e.g., the discovery of dark matter around galaxies). The understanding of astronomical phenomena and astrophysical processes in the GAN thus represents the cornerstone for properly interpreting observations of distant universe. The GAN further provides a test bed to check the validity of various assumptions, approximations, or recipes that are often needed in modeling/simulating the structure formation and evolution of the universe. Locally calibrated empirical relations (such as the peak to width relation of Type Ia SN light-curves and star formation laws) are also very useful tools for studying distant galaxies. Moreover, local measurements (e.g., star formation rates and total stellar masses of galaxies) provide important anchors in determining how the universe has evolved.

The panel strived to identify key science questions that the GAN can potentially offer the most powerful and unique constraints to. In doing so, a broad range of questions were synthesized and ranked without regard for cost, current agency plan, or specific proposed instrumentation, although the panel was mindful of various limitations, both technical and financial. The four embraced questions, as well as the two identified potential discovery areas, exploit the use of the GAN as a venue for studying interconnected astrophysical systems, for constraining complex physical processes, and for probing small scales.

High signal-to-noise observations, which can often be obtained for GAN objects, need to be interpreted with correspondingly accurate physical data. They are sometimes best obtained by experiment, and sometimes by theoretical calculation, jointly referred to as "laboratory astrophysics". Its importance is highlighted in the summary of the GAN Panel Report (2010): "The prospects for advances in the coming decade are especially exciting in these four areas, particularly if supported by a comprehensive program of theory and numerical calculation, together with laboratory astrophysical measurements or calculations." In the following, I briefly describe my interpretation of the laboratory astrophysics needs as well as the questions/discovery areas, particularly with consideration of the observing

capabilities likely available from existing and upcoming NASA missions.

2. Questions, Discovery Areas, and Laboratory Astrophysics Needs

Q1: What are the flows of matter and energy in the circumgalactic medium?

How a galaxy evolves depends largely on how it interacts with its environment. Cosmological simulations have hinted that the accretion of matter onto a galaxy can have various different modes: "hot", "cold", or "recycled wind", depending primarily on galaxy mass. The biggest uncertainty in this emerging picture of galaxy formation and evolution is our poor understanding of galactic feedback. A number of feedback mechanisms have been proposed, ranging from pre-heating by the extragalactic UV background generated collectively by early star formation and AGN activities, to *in situ* momentum- and/or energy-driven superwinds from starbursts and/or AGNs, and to long-lasting gentle outflows powered by Type Ia supernovae in galactic spheroids (e.g., Wang (2010) and references therein). However, none of these mechanisms are well understood. While observations have shown strong evidence for infall (accretion) and outflow (feedback) of matter around galaxies, little is yet known about how mass, energy, and chemical elements actually circulate between galaxies and the environment. The CGM — the galaxy/IGM interface where this circulation occurs — thus needs to be carefully studied in order to answer such fundamental questions as: where is the "missing" baryon matter in galaxies? how are they fed? and how does galactic feedback work?

In the GAN, it is possible to directly observe the working of the CGM, which may extend from a few kpc up to about 1 Mpc around galaxies (e.g., Fig. 1a). Two effective observational strategies: UV/X-ray absorption-line tomography and spectral imaging, have been demonstrated, primarily in the study of gas in and around the Milky Way (for a review, see Wang (2010)). To obtain transformative gains, however, these techniques need to be applied to more targets at better velocity resolution and over a broad temperature range. Such observations at wavelengths most sensitive to the mass, energy, and key element flows will help to remove uncertainties in simulations of galaxy formation and evolution, which currently lack the resolution required for direct modeling of all physical processes.

Q2: What controls the mass-energy-chemical cycles within galaxies?

To understand such cycles, we need to study the ISM and its interplay with stars inside galaxies. The scale considered here ranges from kpc (spiral structure), to parsecs (giant molecular clouds, starbursts, and star clusters), and down to the sub-pc level where individual stars form. First, we need to measure ISM conditions that control the molecular cloud

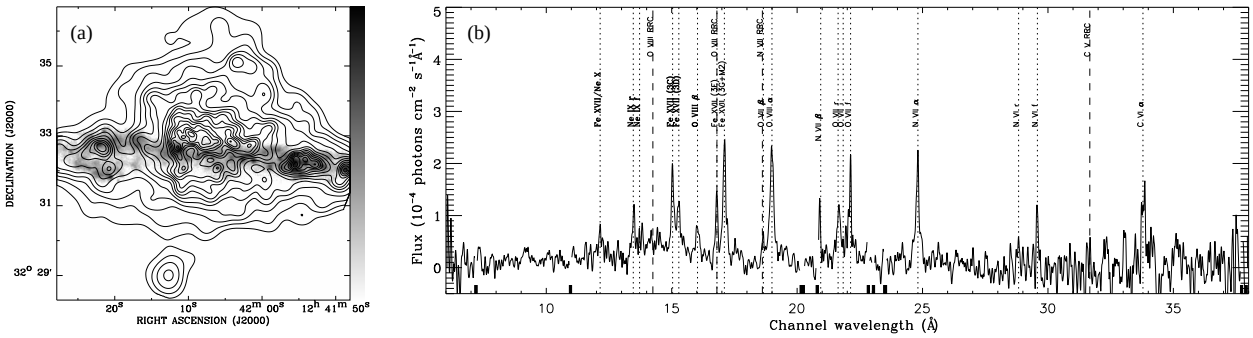

Fig. 1.— (a) NGC 4631 seen in diffuse soft X-ray (intensity contours) and in far-ultraviolet (gray-scale image; see Wang et al. (2001) for details), illustrating strong disk/halo interaction of this nearby edge-on spiral galaxy. (b) XMM-Newton grating spectrum of the central starforming region of M51. Notice the strong "forbidden" component of the OVII Kα triplet, which cannot be accounted for by emission from a plasma in a collisional ionization equilibrium and needs to be explained [similar X-ray spectra are also observed in central regions of several other nearby galaxies, including M31; Liu et al. (2010)].

formation, the rate of star formation, and the stellar initial mass function (IMF) in various environments, ranging from massive starbursts to ultra-faint, low-mass, low-metallicity, dwarf galaxies, and from outer regions of spiral galaxies to the close proximity of the MBH at the center of the Milky Way. Such measurements, which can be made with existing observing facilities such as Herschel and with upcoming ones such as JWST, ALMA, and large single-dish millimeter/submillimeter-wave telescopes, will allow us to calibrate our understanding of how galaxies build up their stellar component over cosmic time.

Second, we need to examine the effects of stellar energy/chemical feedback on the structure and physical state of the ISM and on gas-to-star conversion efficiency in the Milky Way and nearby star-forming galaxies. The ISM spans a huge range of densities and temperatures and includes magnetic fields and cosmic rays, both of which can be dynamically important. The statistical properties of this complex system remain poorly determined, including even the geometry and topology of the density field, as well as the thermal phase distribution. The application of the UV/X-ray spectroscopy and imaging techniques similar to those described in Q1 will greatly improve this situation, particularly for the understanding of the ISM in the Milky Way. Sensitive surveys in other wavelength bands will further allow us to characterize various components of the ISM in galaxies out to $z = 0.1$, and hence their complex galactic ecosystem.

Laboratory Astrophysics Needs for Q1 and Q2:

These two questions, dealing with the so-called gastrophysics, have some common laboratory astrophysics needs, which may be met with reasonable efforts in the near future. Particularly important are accurate physical data required to provide the diagnostics of

heating and cooling processes in the ISM and CGM, especially in (sub)millimeter/infrared and X-ray, which upcoming observing facilities with high spectral resolution capabilities (e.g., ALMA, JWST and Astro-H) will be sensitive to. To make full use of the UV/X-ray spectroscopic data, for example, it is important to complete the measurements of radiative rates, electron-impact excitation rates, ionization rates, and dielectronic recombination rates as well as the listing of importtant emission and absorption lines of collisional plasma (e.g., Fe XVII). At present, many lines (even Fe L-shell) are still not identified. Line energies from theories are typically only good to ~ 700 km s^{-1}, which is not sufficient for accurate velocity measurements of starburst-driven outflows. For such measurements, we also need better identifications of satellite lines, which could otherwise lead to confusion with Doppler broadening. Moreover, it is essential to investigate processes involved in the interaction between plasma and cool gas, such as charge exchange, which may be responsible for much of diffuse soft X-ray emission observed in galaxies (e.g., Fig. 1b). In addition, data on cosmic-ray heating of the ISM and CGM (e.g., the proton impact excitation cross sections) need to be substantially improved. It is reasonable to suspect that PAHs might account for the diffuse interstellar bands, but only careful measurement of PAH absorption cross sections in the gas phase in the laboratory can confirm this. Laboratory measurements are also needed of photoelectric yields from dust grains over a range of sizes, including PAHs. Various other examples for the required improvements in understanding the important "microphysics" (e.g., on MHD, plasma, and shock waves) are given in the panel report.

Q3: What is the fossil record of galaxy assembly from first stars to present?

One way to probe how galaxies actually come to be is to study the evolution of their properties by looking back in time. However, inevitably limited by the angular resolution and sensitivity of observing distant universe, this look-back approach relies on the measurements of globally-averaged properties (such as luminosity and color of galaxies). The approach can be complemented by examining stellar fossil record in local galaxies. One can read in the color-magnitude diagrams (CMD) of resolved stellar populations to determine star formation histories, which can be associated with such galaxy properties as gas content, environment, and morphology. Even internal patterns can be examined, such as the relationship of stellar populations with spiral arms or as a function of galactocentric distance. One can further spatially and kinematically probe substructures in the galactic halos of the Milky Way and other local galaxies, unraveling stellar streams and dwarf satellite galaxies. Such studies can provide critical information about how gas collapses and forms stars down to these small physical scales and faint luminosities, as well as about the merger histories of the galaxies, illuminating the process of galaxy formation more generally. In addition, one can measure metallicity of individual stars, particularly interesting for tracing extremely metal-poor stars formed in earliest epochs. All these fossil record studies can only be done in the GAN!

With the expected improvements in optical and near-IR imaging/spectroscopy capabilities over the next decade, substantial progress can be made in this field. One will be able to determine the star-formation histories of galaxies across the Hubble sequence, to detect a significant sample of the smallest galaxies, and to measure precise abundances for elements from all the important nucleosynthetic processes that act in stars, from which much information can be obtained about the population of stars that produced the metals. With these measurements, one can potentially address such questions as: How old are the oldest stars in the Milky Way? Where are the lowest metallicity stars in the Milky Way and when did they form? Did the IMF vary with metallicity and galactic conditions? Can chemical tagging of metal-poor stars be used to identify coeval populations, later dispersed around the galaxy? The enormous potential of the fossil record to probe galaxy assembly from first stars to present will then be realized in the next decade or so.

Q4: What are the connections between dark and luminous matter?

While the cold dark matter (ΛCDM) paradigm has passed many serious tests, there are still apparent conflicts between the predictions and observations on scales of kpc or smaller. Potential resolution of these conflicts has been complicated by the uncertain interplay between dark and baryon matters. This confusion should be minimal in lower-mass galaxies, which appear to be increasingly dominated by dark matter. Such galaxies, observable in the local universe, can readily be identified from future large-scale, deep, multi-color, photometric surveys of stars, together with follow-up spectroscopy. A substantially increased local inventory of small galaxies will enable us to confront the well-known "missing satellites" problem. The best place to look for the signature of weakly interacting dark matter (via possible γ-ray and/or X-ray radiation from annihilation) is the heart of ultra-faint dwarf galaxies, because of the high central densities and minimum astrophysical confusion from proportionally fewer stars. Dark matter distributions on galaxy scales can also be explored in multiple ways, ranging from studying kinematics of stars and gas to mapping properties of diffuse hot gas in hydrostatic equilibrium. Particularly interesting are the distribution and kinematics of dark matter within the Milky Way at the solar circle, providing constraints useful to the *direct* detection experiments.

MBHs play an increasingly important position in astronomy and astrophysics. However, how MBHs form and evolve is still a question that remains to be answered; we are stil very uncertain about their seeds ($\sim 10^2 M_\odot$ stellar remnants, $10^4 M_\odot$ "intermediate-mass" BHs from Pop III stars, or $10^5 M_\odot$ MBHs from direct collapses of matter), about their merger history, and about the accretion process. The formation and evolution of MBHs are intimately related to their interplay with host galaxies. The most apparent manifestation of this interplay is the mass relation between MBHs and surrounding stellar spheroids. Large

uncertainties in the relation remain, however, especially at the low-mass end, where the presence of nuclear stellar clusters may play a central role. MBHs are also known to be an important source of galaxy feedback, although the efficiency remains very uncertain at low-accretion rates. The coupling between this feedback and surrounding matter is also poorly understood. The local universe offers the most promising avenues to advance our understanding of MBHs and their interplay with galaxies. Advances in spatial resolution (adaptive optics systems) and sensitivity (larger telescopes) will enhance the most used techniques for measuring MBH masses and for studying stellar properties. The nuclei of the Milky Way galaxy and several other nearby galaxies provide our best opportunity to observe the interaction of MBHs with their immediate environments. Many fascinating questions remain to be fully addressed, regarding the formation and dynamics of stars under extreme hostile condition. X-ray observations with large collecting areas and good spectral resolutions will be essential to the study of the accretion process. Interesting new constraints on the process can also be obtained from the spins of MBHs, which can be measured over a wide mass range for local galaxies. Furthermore, one may find potential seed black holes through dynamical studies of nearby systems and through the possibility of measuring gravitational waves of black-hole inspiral events. Detection of gravitational waves will in general open up a new avenue for characterizing the demographics and merger rate of black holes.

Laboratory Needs for Q3 and Q4:

The star formation history and metal abundance measurements clearly depend on our knowledge about stellar evolution, which in turn relies on the accuracy of laboratory astrophysics data on nucleosynthesis, opacity, etc. There remain significant rooms for improvements in the quality of such data (e.g., $^{12}\mathrm{C}(\alpha,\gamma)^{16}\mathrm{O}$ reaction rate and β-decay lifetime for many r-process isotopes). A true comprehension of dark matter ultimately requires a direct detection in laboratory, while the modeling of the accretion and feedback of BHs demands a good understanding of important plasma astrophysical processes, particularly the magneto-rotational instability and magnetic reconnection.

Discovery Areas

The time-domain astronomy is identified as a major GAN discovery area, chiefly because enormous swaths of parameter space remain to be explored. Large-scale, multiple-epoch surveys, together with ever increasing computational capability and algorithm development, make the transient sky an area particularly ripe for discoveries of new objects and/or physical processes. The GAN is particularly suited for such discoveries, because measurements of the distance, energetics, rates, and demographics of newly observed phenomena, as well as their associations with stellar populations and galactic structure, is the first essential step in understanding the underlying physics.

Astrometry is considered to be another area with exceptional discovery potential. A variety of powerful astrometric techniques [radio, (sub)mm VLBI, time-resolved large optical surveys] are now reaching maturity to open a new window for the discovery of vast numbers of extrasolar planets, Kuiper Belt objects, asteroids, and comets; to test the weak-field limit of general relativity with unprecedented precision (for the MBH at the Milky Way center); to measure the aberration of quasars from the centripetal acceleration of the Sun by the galaxy; to provide a complete inventory of stars near the Sun; to measure orbits of the globular clusters and satellite galaxies of the Milky Way and galaxies of the Local Group; and to fix properties of the major stellar components of the Milky Way.

3. Summary

While progress in addressing the four science questions and in the areas of discovery potential can be made with existing and upcoming facilities, reaching the full science goals will require powerful new observing capabilities: Imaging/spectroscopy abilities in UV and X-ray will be essential to the understanding of the interconnected, multiphase nature of galaxies and their surroundings, while enhanced capability at longer wavelengths from ratio to optical will be particularly important to probing the processes that transform accreted gas into stars, to measuring the fossil record, and to finding the connections between dark and luminous matter. In many of these efforts, the laboratory astrophysics can play a significant or even essential role!

Astro2010 Frontier Science Galactic Neighborhood Panel consisted of Leo Blitz, Julianne Dalcanton, Bruce Draine, Rob Fesen, Karl Gebhardt, Juna Kollmeier, Crystal Martin, Michael Shull, Jason Tumlinson, Q. Daniel Wang, Dennis Zaritsky, and Steve Zepf, plus Astro2010 Survey Science Liaison, Scott Tremaine. I thank Mike Shull, the chair of the panel, for various inputs and comments on this write-up.

REFERENCES

Astro2010 Panel Reports – New Worlds, New Horizons in Astronomy and Astrophysics, 2010, http://sites.nationalacademies.org/BPA/BPA_048094

Liu, J., Wang, Q. D., Li, Z.-Y., & Peterson, J. R. 2010, MNRAS, 404, 1879

Wang, Q. D., et al. 2001, ApJL, 555, 99

Wang, Q. D. 2010, PNAS, 107, 7168

NASA LAW, October 25-28, 2010, Gatlinburg

Galaxies Across Cosmic Time

A. J. Baker

Department of Physics & Astronomy, Rutgers, the State University of New Jersey, Piscataway, NJ 08854-8019

ajbaker@physics.rutgers.edu

ABSTRACT

As part of the Astro2010 Decadal Survey, the Galaxies across Cosmic Time (GCT) Science Frontier Panel was asked to identify the main scientific themes that between now and 2020 will drive research on the formation, evolution, and global properties of galaxies and galaxy clusters, as well as on supermassive black holes and active galactic nuclei. In its report, released in late August 2010, the panel articulated four central questions: (1) How do cosmic structures form and evolve? (2) How do baryons cycle in and out of galaxies, and what do they do while they are there? (3) How do black holes grow, radiate, and influence their surroundings? (4) What were the first objects to light up the universe, and when did they do it? The last of the four overlaps with what the panel identified as a prime area of unusual discovery potential: the Epoch of Reionization. This contribution reviews the panel's findings about the space-based observational programs deemed important for making progress in addressing these questions, as well the valuable role to be played by "critical work in... intellectual infrastructure, such as laboratory astrophysics." Separately, it provides the author's personal perspective on the most important contributions that can be made by laboratory work to GCT science via NASA missions over the next decade.

1. Introduction

Since the turn of the millenium, astronomers have made tremendous strides in understanding how the properties of galaxies and their central black holes have evolved over cosmic time. Observers have detected individual galaxies out to redshifts $z > 8$ and charted an extremely tight relation between the velocity dispersions of galactic spheroids and the masses

of the central black holes those spheroids host. Theorists have inferred an important role for feedback from active galactic nuclei (AGN) and supernovae in shaping this relation, as well as the observed properties of $z = 0$ galaxy samples and the predicted properties (phase, metallicity, redshift evolution, etc.) of the intergalactic medium. These and other discoveries have taken on greater significance with the emergence of a consensus ΛCDM cosmology and structure formation paradigm. Against this backdrop of major advances, the Galaxies across Cosmic Time (GCT) Science Frontier Panel (SFP) of the Astro2010 Decadal Survey was charged in early 2009 with identifying the main scientific themes that in the 2010–2020 window would drive research on the formation and evolution of galaxies and galaxy clusters, as well as on supermassive black holes and AGN. The panel's findings, as expressed in a peer-reviewed report released in late August 2010, have important implications for the prioritization of NASA missions and the laboratory astrophysics efforts that support them. This writeup describes how the GCT panel went about its work, reviews its findings insofar as they are relevant to NASA activities, and discusses the author's personal views about where laboratory astrophysics will have the greatest scientific impact over the next decade.

2. Creation of the GCT report

To understand some aspects of the GCT report's content, it is important to consider the external constraints under which the panel was operating, as well as the decisions it made on how to respond to those constraints. The official statement of task from the National Research Council defined the scope of the panel's work as addressing the "formation, evolution, and global properties of galaxies and galaxy clusters, as well as active galactic nuclei and QSOs, mergers, star formation rate, gas accretion, and supermassive black holes." Because two other SFPs were asked to consider slightly overlapping science areas, the SFP chairs early in the process negotiated informal boundaries in terms of redshift. The GCT panel thus claimed the range $0.1 \leq z \leq z_{\rm reionization}$, leaving lower redshifts to the Galactic Neighborhood (GAN) panel and higher redshifts (as well as observations of galaxies and clusters for strictly cosmological purposes) to the Cosmology and Fundamental Physics (CFP) panel. Each of the five SFPs was charged with identifying four central science questions and one area of "unusual discovery potential" within its scope. They were also instructed not to refer in their reports to specific new missions or facilities, apart from those (like *JWST* and ALMA) for which construction was already underway, although they were asked to provide quantitative guidance about general technical capabilities to the four Program Prioritization Panels (PPPs) that were a major audience for the reports. The GCT report was sent out for external peer review in September 2009, so does not reflect all major scientific advances made in the eleven additional months that elapsed before its public release.

Subject to the above boundary conditions, the GCT panel was given complete independence in determining its four central questions and one discovery area, and in structuring its report. In the end, for each question, the panel formulated a series of sub-questions to clarify the full range of science it encompassed; assessed progress to date and identified the critical observational steps for the next decade that *could* lead to the greatest additional progress absent major budget limitations[1] and without regard to stated agency plans; and ranked these scientific programs as "important," "very important," and "most important" for addressing the question. The decision to focus on observational programs was motivated by the panel's sense that astronomy is a data-driven field; however, given that observations alone do not a complete scientific program make, the panel also chose to make a separate, strong endorsement of the key connective tissue represented by theory and laboratory astrophysics.

3. NASA-related findings of the GCT report

The GCT panel report has as its epigraph a couplet from the St. Paul Irish Codex as translated by Robin Flower: "I get wisdom day and night / Turning darkness into light." While nominally describing a monk (and his cat), this line also captures both the practice and the subject matter of astronomers doing forefront GCT science through NASA missions. The first key question articulated by the panel– *How do cosmic structures form and evolve?*– asks how luminous galaxies, groups, and clusters emerge from the underlying dark matter distribution. The two associated sub-questions are (a) What is the structure of dark matter haloes on galaxy, group, and cluster scales? (b) What is the origin of the observed correlations among the fundamental properties of galaxies and of clusters, and how do they evolve with time? The panel placed two related space-based observational programs in the "most important" category: *HST*-resolution lensing surveys of very large samples, allowing the determination of halo mass profiles and mass functions, and X-ray spectroscopy of groups and clusters, allowing study of the intracluster medium's dynamics, its ionization, temperature, and metallicity structure, and the development of cluster scaling relations.

The second key question articulated in the GCT panel report– *How do baryons cycle in and out of galaxies, and what do they do while they are there?*– highlights the complex physics of ordinary (non-dark) matter that forms bright new stars from interstellar gas and is released from old stars into interstellar (if not intergalactic) gas. The four associated

[1]Observational programs were considered for inclusion if they were viewed as technologically ready and not so expensive individually that they would exceed decadal budgetary constraints. However, detailed cost/benefit analyses and balancing across all science areas were left to the PPPs.

sub-questions are (a) How do galaxies acquire gas across cosmic time? (b) What processes regulate the conversion of gas to stars as galaxies evolve? (c) How are the chemical elements created? (d) Where are the baryons as a function of redshift? The panel rated two related space-based programs as "very important" for addressing these questions: spectral mapping and high-resolution spectroscopy in the ultraviolet (with the sensitivity of a 4 m telescope), to study the physics of circumgalactic gas and warm intergalactic gas at $z < 1.5$, and far-IR spectroscopy of luminous dusty galaxies, to disentangle their rates of obscured star formation and accretion. In addition, two more space-based programs were placed in the "important" category: *JWST* integral field spectroscopy of $z \sim 2$ galaxies, to study their dynamics, inflows, feedback, and enrichment, and moderate-resolution soft X-ray spectroscopy along $\sim$ 100 quasar sightlines, enabling an accurate inventory of the warm-hot intergalactic medium.

The third key question articulated in the GCT panel report– *How do black holes grow, radiate, and influence their surroundings?*– unites the extreme physics that manifests on the small scale of a black hole's Schwarzschild radius with its effects on luminous matter over vastly larger scales. The three associated sub-questions are (a) How do black holes grow over cosmic time? (b) How do the quantity and form of energy production in accreting systems depend on black hole mass, accretion rate, and spin? (c) How does black hole feedback shape the evolution of cosmic structures? Two related space-based programs were deemed "most important" for tackling these questions in the next decade: high-S/N X-ray spectroscopy of $\sim$ 100 nearby AGN to determine the black hole spin distribution (and examine accretion and jet physics for the brightest objects), and X-ray imaging spectroscopy of the nearest galaxy groups and clusters, to examine the physics of turbulence and/or bulk flow feedback in the intracluster medium. "Very important" priorities in space were obtaining time-resolved UV (with *HST*/COS) and X-ray spectroscopy of AGN, to assess the role of quasar winds in galaxy-scale feedback; conducting a wide-field hard X-ray survey to obtain a complete AGN census as a function of redshift; and searching for gravitational radiation at sub-LIGO frequencies, to constrain the cosmic history of black hole merging. Studies of blazars and radio galaxies in X-ray polarization, along with multiwavelength observations of the former extending to the gamma-ray regime, were judged to be "important" for understanding the compositions, formation mechanisms, and magnetic field geometries of jets.

The final key question articulated in the GCT panel report– *What were the first objects to light up the universe, and when did they do it?*– quite clearly illustrates the report's "darkness into light" theme and is closely linked with the panel's choice of an area of unusual discovery potential, namely the Epoch of Reionization. The three associated sub-questions are (a) Where and when did the first objects form? (b) When did the first galaxies emerge, and what were they like? (c) How did these first objects reionize the universe? The boundary between "science question" and "discovery area" is inexact, but qualitatively, there will

be a difference between observations that apply familiar techniques to higher-redshift extensions of familiar galaxy samples, and observations that probe such new regions of parameter (and discovery) space that it is difficult to predict the results in detail. From space, the "most important" program was judged to be deep (possibly lensing-assisted) *JWST* surveys to detect He II and Ly α emission from the first H II regions. Fast infrared spectroscopic followup of large gamma-ray burst (GRB) samples, which would deliver a sample of several dozen $z > 8$ GRBs, and near-IR absorption-line spectroscopy with *JWST* to probe the physical conditions of the intergalactic medium at the end of reionization, were both rated "very important." The independent probe of the reionization epoch afforded by measuring the E-mode polarization of the cosmic microwave background was a final "important" recommendation.

In addition to the four science questions and the prioritized set of observational programs they motivate, the GCT panel report includes the following broad language about laboratory astrophysics: "Underlying all of astronomy and astrophysics is critical work in theory and other intellectual infrastructure, such as laboratory astrophysics... Laboratory astrophysics is clearly important to understanding galaxies, black holes, and clusters across cosmic time... Although the lack of laboratory measurements may not today be a limiting factor in the studies outlines earlier in this report, it may well become the limiting factor as the data improve." The report also explicitly lays out a (non-exclusive) list of priority laboratory measurements that will facilitate the next decade of GCT science: the details of absorption by dust grains, cross sections for hot gas cooler than 4×10^6 K, recombination rates that determine ionization equilibria, and catalogs of spectral features at infrared through millimeter wavelengths. Somewhat less obviously, recalling that the Working Group on Laboratory Astrophysics (WGLA) white paper submitted to the Astro2010 panels states that the field "comprises both theoretical and experimental studies of the underlying physics," a number of "sub-grid physics" areas called out by the GCT panel as theory priorities are also closely connected to laboratory astrophysics. These include the physics of two-phase interfaces/instabilities due to gas flows moving through ambient media with very different physical conditions; simulations of MHD turbulence that correctly treat viscosity and conduction in describing feedback; magnetic reconnection, particle acceleration, and cosmic ray transport in plasmas; the interaction of radiation with clumpy gas distributions; and the inclusion of nonthermal and hydrodynamic elements in jet/disk models.

4. Personal perspective

With the benefit of hindsight on how the findings of the GCT panel report were processed by the PPP reports and the main Astro2010 survey report, it is clear that some space-based observational programs are better positioned than others to provide strong justification for laboratory astrophysics work in the next decade. GCT-recommended science programs that did not match up with PPP and survey-recommended missions include the *HST*-resolution lensing studies of large samples, spectral mapping and high-resolution spectroscopy with a 4 m-class ultraviolet space telesope (although this capability was tagged for technology development), and the wide-field hard X-ray survey. Among GCT science programs that did survive to later stages of the Astro2010 process, those with a stronger spectroscopic component will be the ones with greater laboratory astrophysics relevance; however, this relevance is not uniformly distributed with respect to mission. The key spectroscopic science with *JWST* (related to the "first light" question/discovery area) will be driven by detection S/N rather than precision, and therefore will have limited connections to laboratory work. For the *SPICA* mission, in which NASA may become involved through support of the BLISS instrument, the situation will likely be the same as for *Herschel* now: science in the GCT redshift range will be largely driven by empirical comparisons with template objects in the GAN redshift range, and will only indirectly depend on precise laboratory measurements. There is no obvious laboratory relevance for *LISA* or an alternative space-based gravitational wave mission. The great exception here is *IXO* (or an alternative X-ray mission), which is highly relevant to the first three of the GCT panel report's four key science questions, and for which precision laboratory measurements will be essential. A useful way to frame laboratory work in support of X-ray (and to a lesser extent, UV) space missions over the next decade may be to stress the need for the astronomical community to "retire risk" on interpretation in parallel with its efforts to do so on technology. Relatively modest investments to ensure that missing or inadequate laboratory measurements do not limit the scientific output of ambitious and expensive new missions would appear to be wise strategy indeed.

I thank my colleagues on the GCT panel– Meg Urry (chair), Mitch Begelman (vice-chair), Neta Bahcall, Romeel Davé, Tiziana Di Matteo, Henric Krawczynski, Joe Mohr, Rich Mushotzky, Chris Reynolds, Alice Shapley, Tommaso Treu, Jacqueline van Gorkom, and Eric Wilcots– for the many stimulating discussions that fed into our final report, and the NASA LAW organizers for inviting me to attend the meeting at which this material was originally presented.

NASA LAW, October 25-28, 2010, Gatlinburg

Herschel, SOFIA, and Laboratory Data

J. C. Pearson

Jet Propulsion Laboratory, California Institute of Technology, Mail Stop 264-782, 4800 Oak Grove Dr., Pasadena, CA 91009

John.C.Pearson@jpl.nasa.gov

ABSTRACT

Thermal dust emission typically peaks in the far infrared and is often becomes optically thin at wavelengths longer than the peak. This allows atomic and molecular emission features to be observed in either emission or absorption on the dust continuum. The reduced optical opacity means that heavily obscured objects such as the early phases of star formation and early dusty galaxies can be directly observed. Unfortunately, far infrared astronomy is greatly hampered by atmospheric absorption of water vapor. Two major missions, the Herschel Space Observatory and the Stratospheric Observatory for Infrared Astronomy (SOFIA), have been designed to access the far infrared spectral region. Far infrared astronomy is critically dependent on high quality laboratory data for planning and interpretation of observations. The line shape of observed features is almost entirely due to Doppler motions. Sufficient spectral resolution provides line of sight information on the local dynamics. The lines of atoms and molecules provide enormous insight into the local density, chemistry, radiation environment and energy balance. Full interpretation of lines requires accurate frequencies, transition moments, excitation cross sections and chemical reaction rates in the gas phase and solid phase. Interpretation of photometric observations is often critically dependent on dust parameters and estimates of the molecular contributions to the continuum. Initial Herschel observations underscore the criticality of high spectral resolution in interpreting far infrared atomic and molecular lines and the necessity of high quality laboratory data for molecular species. The Herschel and SOFIA beams are too large to fully resolve the richest molecular sources or the finest scale dust structure, but they do feature high frequencies that are challenging for laboratory studies. The higher spatial resolution, that will ultimately be required to beat far infrared source confusion limits, will also resolve the richest molecular regions and the small scale dust structure. Herschel and SOFIA

already present an enormous challenge to laboratory astrophysicists, which will only be compounded as more capable future systems come on line.

1. Introduction

Far infrared astronomy relies on the detection of heat radiated by cool or cold gas and dust. This radiation must be detected against the background heat of the observing system and the atmosphere unless the telescope is space based. Terrestrial telescopes are generally close to 300 Kelvin and are quite bright compared to many astronomical objects. Atmospheric absorption by molecules especially water limit terresterial observations in the far-infrared to a few narrow windows at the highest and driest sites. As a result, access to most of the far infrared sky requires being above most or all the atmosphere, ideally with a cold telescope. NASA is directly involved in two major new facilities to exploit the far infrared. The first is the space based Herschel Space Observatory (Pilbratt et al. 2010) and the second is a high altitude aircraft the Stratospheric Observatory for Far Infrared Astronomy (Gehrz et al. 2009).

Far infrared instruments can be successfully constructed with either direct or heterodyne detection. Direct detection systems have the potential to achieve local background limited sensitivity even at high spectral resolution. This sensitivity is only useful if the detector is more sensitive than the background and the light can be dispursed. However, in the long wavelength limit the dispersive elements required for high spectral resolution become impractically large. The result is direct detection systems are effectively limited to resolutions of a few thousand in the far infrared increasing linearly with frequency. As a result, the high resolution needed to velocity resolve transitions requires heterodyne technology at wavelengths shorter than about 25μm.

2. Herschel

The Herschel Space Observatory was launched on the 14th of May 2009 by the European Space Agency with NASA participation. The observatory resides at the second Earth/Sun system Legrange point, L2, allowing its 3.5 meter telescope to be passively cooled to approximately 80 Kelvin. Three instruments are contained in a 2500 liter cryostat of superfluid Helium. The mission is expected to have a 3 year operational life time and three calls for proposals open to all observers are anticipated. The first two of these calls have been awareded including the key project call (large programs) and the first open time call (smaller

programs). The final open time call is anticipated in the summer of 2011. The three Herschel instruments are the Photodetector Array Camera and Spectrometer (PACS) (Poglitsch et al. 2010), the Spectral and Photometric Imaging Receiver (SPIRE) (Griffin et al. 2010; Swinyard et al. 2010) and the Heterodyne Instrument for Far Infrared (HIFI) (de Graauw et al. 2010). Figure 1 shows the Herschel Space Observatory during ground test in the Netherlands.

The PACS instrument can operate in either photometry or spectroscopy mode. The photometry mode utilizes two filled silicon bolometer arrays at 0.3 K with 16×32 pixels and 32×64 pixels for the red and blue arrays, respectively. The red array observes $125 - 210\mu$m while a filter is used to select either $60 - 85\mu$m or $85 - 125\mu$m for the blue array. Both arrays simultaneously observe a $\sim 1.75' \times 3.5'$ field of view with near Nyquist beam sampling. The spectroscopy mode uses two Ge:Ga photoconductor arrays stressed for the red array and unstressed for the blue array with 16×25 pixels each. The spectrometer is an integral field design which utilizes an image slicer to image a $47' \times 47'$ field on a 5×5 array each pixel having a ~ 1500 kms^{-1} spectral coverage and a resolution of $\sim$ 175 kms^{-1} (Poglitsch et al. 2010). The spectrometer was designed with the determining spectral energy distributions and extra galactic spectroscopy as the primary objectives.

The SPIRE instrument also has a photometry and a spectroscopy mode. The photometry mode is a simultaneous three band imager utilizing $2f\lambda$ feed horn coupled bolometer arrays cooled to 0.3 K centered at 250μm, 350μm and 500μm. The arrays simultaneously cover a $4' \times 8'$ field of view and are limited by extra galactic confusion in modest integration times (Nguyen et al. 2010). The spectroscopy mode utilizes an imaging Fourier Transform Spectrometer with an adjustable scan length so that the resolution can be varied from 1.2 GHz to 25 GHz. Two arrays cover an approximately circular $2.6'$ field of view over the $194 - 671\mu$m wavelength range (Griffin et al. 2010; Swinyard et al. 2010). The spectrometer was designed with determining spectral energy distributions and extra galactic spectroscopy as the primary objectives.

The HIFI instrument is a high resolution heterodyne spectrometer. Five superconductor-insulator-superconductor bands cover 480 to 1280 GHz with one pixel for each vertical and horizontal polarization each providing 4 GHz of IF. Two hot electron bolometer bands cover 1440 to 1910 GHz also with one pixel for each polarization each providing 2.4 GHz of IF. A total of 14 local oscillators, two for each receiver band, are utilized to achieve the frequency coverage. Two spectrometers analyze each polarization. The wide band acousto-optical spectrometer provides 4 GHz of instantaneous IF band analysis with ~ 8000 channels resulting in a Nyquist resolution of 1.1 MHz while the high resolution autocorrelation spectrometer has adjustable Nyquist resolution of approximately 134, 268, 536 and 1072 kHz. The high resolution spectrometer can be configured as two separate sub-bands within the IF de Graauw

et al. (2010). The HIFI instrument was designed with local interstellar medium chemistry and physics as the primary objectives.

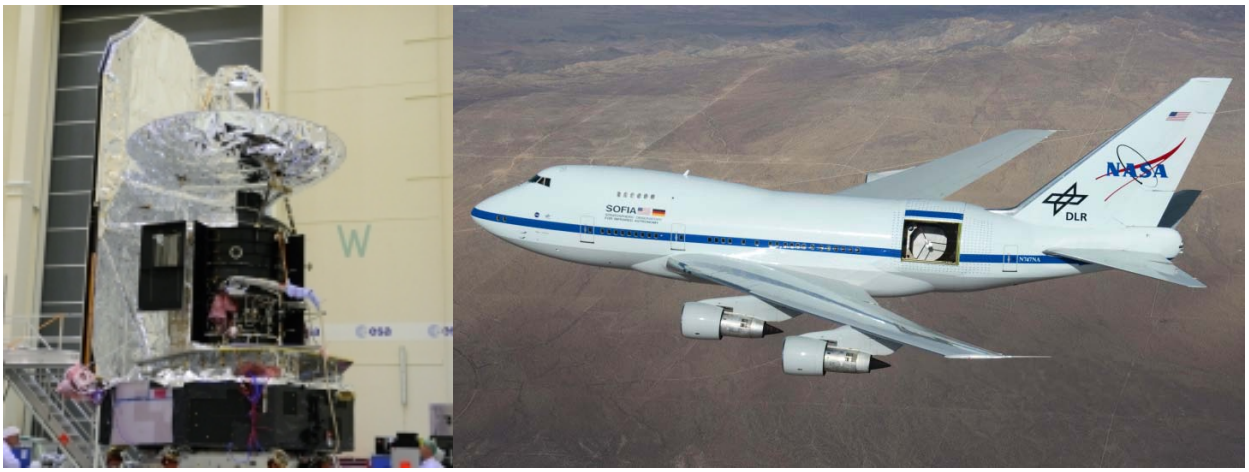

Fig. 1.— Photos of the Herschel Space Observatory (*left*) during ground testing and the Stratospheric Observatory for FarInfrared Astronomy (*right*).

3. SOFIA

SOFIA is a Boeing 747-SP based observatory built by NASA with significant contributions from the German space agency DLR. It includes a 2.7 meter telescope designed to operate in flight to 45,000 feet of altitude. First light was achieved in the middle of 2010 and initial science operations are expected to begin in early 2011. SOFIA is expected to make approximately 120 flights per year each of about 8-10 hours duration for the next 20 years. The full operational schedule should begin by 2014. The SOFIA observatory will be periodically updated with new instruments significantly adding to the initial capability. Initial operations will utilize a suite of 8 instruments covering 0.3 to 655μm. The first call for science proposals has already been awarded, and many more are expected over the 20 year operational life. The SOFIA payload consist of three facility class instruments including the High-resolution Airborne Wideband Camera (HAWC), the Faint Object Infrared Camera for the SOFIA Telescope (FORECAST) and First Light Test Experiment Camera (FLITECAM) and five principle investigator instruments including the German Receiver for Astronomy at Terahertz Frequencies (GREAT), the Field Imaging Far-Infrared Line Spectrometer (FIFI-LS), the High-speed Imaging Photometer for Occultation (HIPO), the Echelon-Cross-Echelle Spectrograph (EXES), and Sub-millimeter and Far-Infrared Experiment (SAFIRE). Figure 1 on the right shows SOFIA flying with the telescope door open during validation of the flight

system.

FORECAST is a mid-infrared camera with selectable filters for two $4-25\mu$m and one $25-40\mu$m bands. It also incorporates low resolution ($R = 200-800$) Grism spectroscopy in the $4-8$, $16-25$ and/or the $25-40\mu$m regions. FORECAST is one of the two first light instruments. GREAT is a heterodyne instrument with three bands $1.25-1.92$ THz, $2.4-2.7$ THz and the 63μm transition of OI. Maximum resolution is 45 kHz or $R > 10^7$. First light configuration includes $1.25-1.5$ THz, $1.8-1.925$ THz and $2.4-2.7$ THz. GREAT is the other of the two first light instruments. FIFI-LS is an imaging spectrometer of similar design to the spectrometer on the Herschel PACS instrument with two bands covering $42-110\mu$m and $110-210\mu$m. The resolution is approximately 1700. FLITECAM provides imaging from $1-3\mu$m and $3-5.2\mu$m. It also provides moderate resolution ($R \sim 2000$) grism spectroscopy. HIPO is a special purpose instrument that provides two simultaneous channels of high-speed time resolved imaging photometry at optical wavelengths. HIPO was designed to take advantage of SOFIA's mobility to capture transient events. HAWC in a far infrared camera covering $50-240\mu$m with a spectral resolution, $R = 5-10$. HAWC bands include 53, 88, 155 and 215μm. EXES is an imaging spectrometer that utilizes Si:As BIB detectors and a large echelon grating to cross-disperse the spectrum. Resolution of $10^5, 10^4$ or 3000 can be selected over the $5-28\mu$m band. SAFIRE is an imaging spectrometer covering 145 to 655μm with a spectral resolving power of about 1000.

4. Laboratory Data

The kind and nature of laboratory data needed to interpret observations varies greatly depending on the instrument system utilized. In general, photometers require the least laboratory support; however, interpretation does require a number of assumptions be made about the nature of the dust. Many of these assumptions are poorly supported observationally and are not on that solid of a laboratory basis. Ices, carbonaceous dust and silicate dust have received quite a bit of laboratory attention, but significant observational questions remain about the physical details of the observed material. Sorting out the details of solid state features cannot be achieved with photometry and will require at least modest resolution spectroscopy.

Spectrometers with resolutions of a few thousand or less actually require the most laboratory data. They are ideally suited for solid state spectroscopy, can easily see stronger gas phase features and match the spatially unresolved velocity distributions of distant galaxies. As such they require good line catalogs for line identification and assessment of line confusion. They also need temperature dependent data on solid state features including dust

(carbonaceous and silicate) and ices. High resolution spectrometers require line resolved catalogs with precise velocity knowledge, collisional excitation rates, line strengths, energies, and chemical reaction rates. Additionally data are required on the physical structure of the object from other wavelengths. The laboratory data are critical inputs in the modeling of observations often even at modest resolution. A very important point is that few astronomical sources are in thermal equilibrium so that interpertation always requires line resolved input data for models.

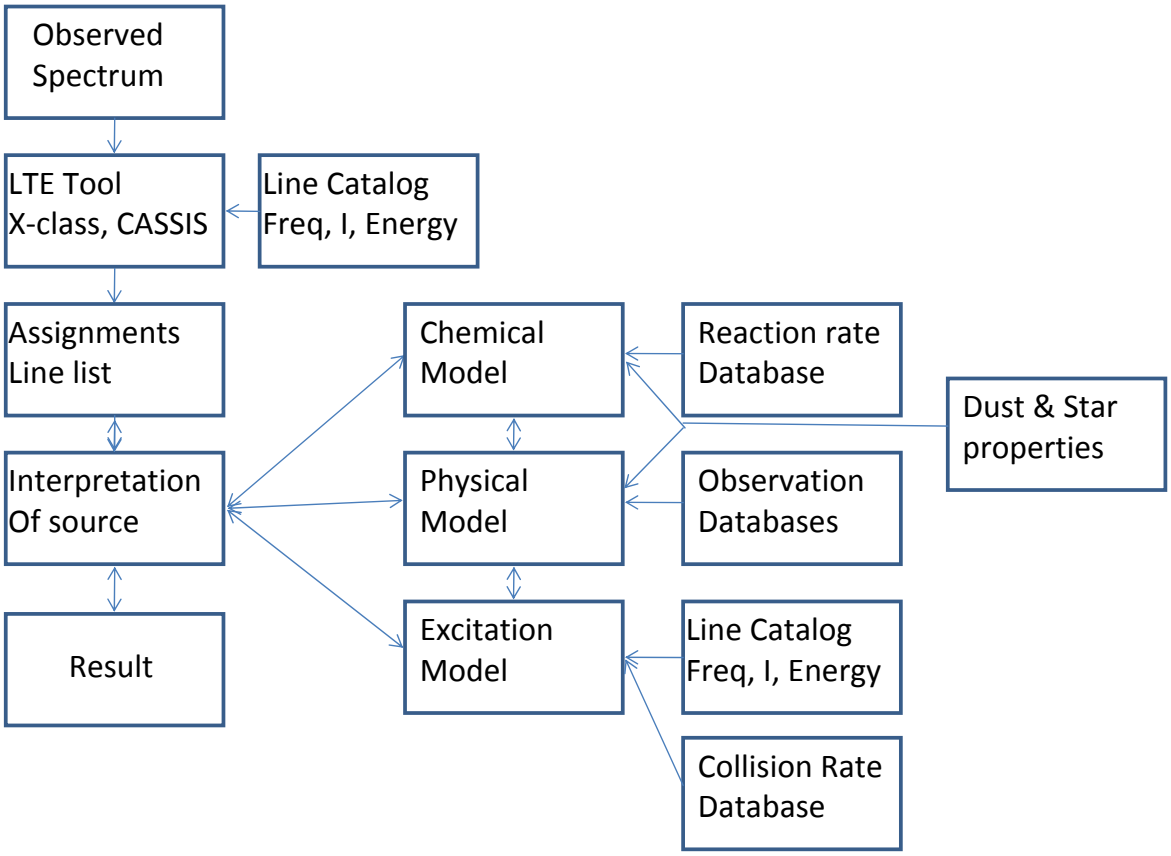

Fig. 2.— Flow chart showing the general process of interpreting spectoscopic astronomical observations.

The rotational bands of many astronomical molecules are well known and in most cases have been cataloged in great detail. However there are still a number of highly prevalent interstellar molecules where significant data is still missing. An excellent example is ^{13}C methanol where the currently available molecular models end at 1 THz or below all SOFIA observations and many Herschel observations. Higher frequency, larger quantum number studies especially of isotologues of common species are the most urgent spectroscopic need.

Additionally, there are some major holes in our understanding of interstellar molecules with the most prominent Herschel example being a large unidentified absorption line at 617.8 GHz that appears in all the line of sight components towards Sgr B2 and in several SPIRE extra galactic spectra. At infrared or shorter wavelengths there are no astrophysical line catalogs for molecules. This will be a huge problem for EXES on SOFIA. Another significant challenge is a good way to calculate collsional rates not requiring a full quantum mechanical potentials. This is especially important for larger molecules observed primarily in hot cores needs to be developed. Lastly there are a number of rather fundamental chemical reactions where the rates remain to be measured and are only guessed in the chemical networks. Figure 2 is a flow chart for analyzing astronomical spectra showing where and how the laboratory data is utilized. The single most pressing need is to have integrated machine readable line catalogs including rotation, vibration, and electronic bands. The interstellar radiation field does interact with all molecular bands so a complete understanding requires complete data.

5. Conclusion

Herschel and SOFIA have opened up the far infrared region of the spectrum to photometery and spectroscopy. Additionally, SOFIA will provide velocity resolved infrared spectroscopy. These missions will require laboratory data on the spectral properties of dust as a function of both physical and chemical composition, ices as a function of physical and chemical conditions and the properties of dust grains with ice mantels. Gas phase observations require precise rest frequencies, energies and transition moments of molecules from the submillimeter through the near infrared. Interpretation of the observations requires collisional rates, chemical rates, and models of the physical, dynamical, and chemical conditions. The molecular data must be in a machine readable format for easy ingestion into modeling codes. Presently, there is no infrared or shorter wavelength database targeting the needs of astronomers. Advances are also needed in calculating rates for larger molecules and in many chemical reactions. These laboratory studies will find immediate utility in the interpretation of Herschel and SOFIA results and will be essential for the success of shorter wavelength instruments abord SOFIA.

This work was performed at the Jet Propulsion Laboratory, California Institute of Technology, under contract with the National Aeronautics and Space Adminsitration. Copyright 2010© California Institute of Technology. All rights reserved.

REFERENCES

de Graauw, Th., et al., 2010, Astron. & Astrophys., 518, L6

Gehrz, R. D., Becklin, E. E., de Pater, I., Lester, D. F., Roellig, T. L., & Woodward C. E., 2009, Adv. Space Research, 44, 413

Griffin, M. J., et al., 2010, Astron. & Astrophys., 518, L3

Nguyen, H. T., et al., 2010, Astron. & Astrophys., 518, L5

Pilbratt, G. L., Riedinger, J. R., Passvogle, T., Crone, G., Doyle, D., Gageur, U., Heras, A. M., Jewell, C., Metcalfe, L., Ott, S., & Schmidt, M., 2010, Astron. & Astrophys., 518, L1

Poglitsch, A., et al., 2010, Astron. & Astrophys., 518, L2

Swinyard, B. M., et al., 2010, Astron. & Astrophys., 518, L4

This preprint was prepared with the AAS LaTeX macros v5.2.

NASA LAW, October 25-28, 2010, Gatlinburg

The James Webb Space Telescope: Mission Overview and Status

M. Greenhouse & the JWST Science Working Group[1]

Laboratory for Astronomy & Solar Physics, NASA/GSFC, Code 685, Infrared Astrophysics Branch, Greenbelt, MD 20771

Matthew.A.Greenhouse@nasa.gov

ABSTRACT

The James Webb Space Telescope (JWST) is the infrared successor to the Hubble Space Telescope. It is a cryogenic infrared space observatory with a 25 m^2 aperture (6 m class) telescope yielding diffraction limited angular resolution at a wavelength of 2μm. The science instrument payload includes three passively cooled near-infrared instruments providing broad- and narrow-band imagery, coronagraphy, as well as multi-object and integral-field spectroscopy over the 0.6$< \lambda <$ 5.0 μm spectrum. An actively cooled mid-infrared instrument provides broad-band imagery, coronagraphy, and integral-field spectroscopy over the 5.0$< \lambda <$ 29 μm spectrum. The JWST is being developed by NASA, in partnership with the European and Canadian Space Agencies, as a general user facility with science observations to be proposed by the international astronomical community in a manner similar to the Hubble Space Telescope. Technology development and mission design are complete, and construction is underway in all areas of the program.

1. Designing for Discovery

The science motivation for the JWST mission was developed by a succession of international science working groups and is described by Gardner et al. 2006, with updates maintained by the JWST flight science working group at: http://www.stsci.edu/jwst/science/

[1]John C. Mather, Mark Clampin, Rene Doyon, Kathryn A. Flanagan, Marijn Franx, Matthew A. Greenhouse, Heidi B. Hammel, John B. Hutchings, Peter Jakobsen, Simon J. Lilly, Jonathan I. Lunine, Mark J. McCaughrean, Matt Mountain, George H. Rieke, Marcia J. Rieke, George Sonneborn, Massi-mo Stiavelli, Rogier Windhorst and Gillian S. Wright.

whitepapers/. This science case forms the basis from which detailed science and mission requirements were derived to guide engineering design and development of the JWST as a research tool. The science observations that are actually implemented by the JWST will be proposed by the international astronomical community in response to annual peer reviewed proposal opportunities. The discovery potential of the JWST relative to other concurrent facilities is discussed in Thronson et al. 2009.

The emergence of the first sources of light in the universe (after decoupling) marks the end of the "Dark Ages" in cosmic history (Rees 1997). The ultraviolet radiation field produced by these sources created the ionization that is observed in the local intergalactic medium (IGM). The JWST design provides unique capability to address key questions about this era in cosmic evolution including: what is the nature of the first galaxies; how and when did ionization of the space between them occur; and what sources caused the ionization?

The JWST architecture is primarily shaped by requirements associated with answering the above questions. In contrast to the Hubble Space Telescope (HST), the JWST is designed as an infrared optimized telescope to observe the redshifted ultraviolet radiation from the first galaxies and supernovae of the first stars. To achieve the nJy sensitivity needed to observe this era ($z \sim 6 - 20$), the observatory must have a telescope aperture that is larger in diameter than the largest rocket faring, and the entire optical system must be cooled to $\sim$40 – 50K. Finally, the resulting large deployable cryogenic telescope must achieve HST-like angular resolution across the SWIR spectrum. The major observatory design features seen in Figure 1 trace directly from these requirements and differ markedly from those of the HST (Table 1).

Performance Parameter	HST	JWST
OTE Diameter (meters)	2.4	6.1 by 6.6
Mass (kg)	11600	6330
Output Power at Load Input (watts)	2400	2079
Unobscured Aperture (Sq meters)	4.5	25
Overall Optical Transmission	45 to 25%	62% to 43%
Telescope Field of View (Arcmin)	14.6 (Radius)	18 by 9
Wavelength of Diffraction Limited Performance (Microns)	0.5	2
Rayliegh Radius (Arcsec)	0.043	0.069
Telescope Strehl Ratio	80%	80%
Pointing Accuracywithout Fine Guidance (Arcsec)	22	7
Pointing Stability with Fine Guidance (Arcsec)	0.007	0.007
Total Pixels (Megapixels)	25	60
Data Throughput (Gbits/day)	27	471
Observing Efficiency	50%	70%

Table 1: Key design parameters of the JWST and HST.

Fig. 1.— Full scale display model of the JWST space vehicle.

The JWST science instrument payload is designed to probe the first galaxies with high angular resolution near-infrared image surveys in broadband filters. This capability enables identification of primeval galaxies by searching their Lyman continuum break with multi-filter photometry. This prominent feature occurs in the near-infrared (1.3 – 2.6 μm) for galaxies with redshifts in the range of 10 – 20. This broadband technique exploits the maximum sensitivity of the observatory, such that the space density of galaxies can be probed to z $\sim$ 20. JWST high angular resolution imagery across the 0.6 – 29 μm spectrum will probe the assembly and evolution of galaxy morphologies to enable observation of when and how the Hubble sequence formed.

The JWST is designed to enable near-infrared multi-object spectroscopy of thousands of galaxies at several spectral resolutions ($\sim 10^2$, $\sim 10^3$). This capability will probe the chemical evolution and metallicity of galaxies, and the ionization state of the IGM across cosmic time. Low resolution multi-object spectroscopy will enable calibration of photometric redshifts for primeval galaxy studies. The JWST spectrometers include integral field capability over the 0.6 – 29 μm spectrum that will enable detailed spectral, morphological, and kinematic studies of high redshift galaxies and local galaxy nuclei. JWST spectroscopy includes wide

field scanning Fabry-Perot and narrowband filter imagery at low ($\sim 1\%$) spectral resolution and high angular resolution to enable both wide field emission line imagery and high redshift surveys of emission line galaxies.

The JWST observatory design enables wide discovery potential beyond cosmology and galaxy studies. The JWST high angular resolution imagery and imaging spectroscopy across the $0.6 - 29$ μm spectrum will open a new window on observation of star formation in our own galaxy to reveal: how molecular clouds collapse; how environment effects star formation and vice-versa; the mass distribution of low mass stars; and the relationship between stellar debris disks and the formation of terrestrial planets.

The JWST instruments include coronagraphic imagery and spectroscopy capability that will enable a wide range of stellar debris disk studies and extra-solar planet observations at high angular resolution. High dynamic range modes of the JWST instruments will enable extra-solar planet transit photometry and spectroscopy across the above wavelength range. The JWST observatory enables non-sidereal tracking so that the full observatory capability can be used observe the outer solar system to enable comparative studies between stellar debris disks and our own solar system.

2. Architecting for success

The large primary mirror area and cryogenic operating temperature are key drivers on the JWST mission architecture. The telescope is the largest space telescope ever constructed. Liquid cryogen cooling techniques used by prior infrared space observatories (IRAS, ISO, Spitzer) cannot be practically scaled to meet JWST requirements, and existing cryo-cooler technology could not meet the heat lift requirements of this large system. As a consequence, a passively cooled architecture was adopted for the majority of the system. A libration point orbit about the Sun-Earth L2 point (Figure 2) was selected to meet this requirement. In this orbit, the observatory follows the earth around the sun such that the sun and earth always appear in the same direction. Hence, it is possible to continuously shield portions of the observatory from the sun and earth to enable passive cryogenic cooling. The orbit about the L2 point itself is sized to avoid eclipse; thus enabling continuous generation of power with solar arrays. This orbit has a period of approximately 6 months and is unstable, requiring use of station-keeping thrusters. Propellant for orbit maintenance and momentum management ultimately limits the lifetime of the observatory to approximately twice the duration of its required 5 year science mission.

The JWST can observe the whole sky while remaining continuously in the shadow of its

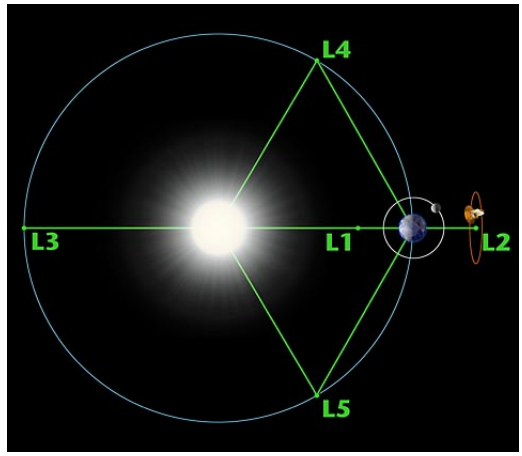

Fig. 2.— The JWST will orbit the Sun-Earth L2 point.

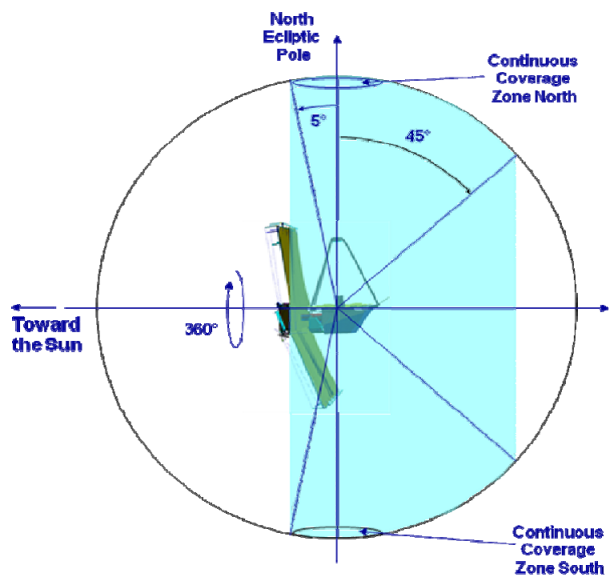

Fig. 3.— The JWST can observe the whole sky while remaining in the shadow of its sun-shield.

sun shield. As shown in Figure 3, the space vehicle can pitch through an angle of 50 degrees and rotate completely about the earth-sun line to observe sources within an annulus that covers approximately 39% of the sky. As the observatory orbits the sun, this annulus sweeps over the whole sky each year with small continuous viewing zones at the ecliptic poles.

The JWST can reach this orbit in approximately 100 days after launch from Kourou Launch Center in French Guiana using an Arian 5 ECA launch vehicle via a direct transfer trajectory. This class of launch vehicle provides adequate fairing volume and mass capability

to enable an observatory design that meets the above science requirements.

The 6.5 m diameter telescope and its tennis-court sized sunshield, are designed to be stowed within the Ariane 5 m diameter fairing along with the science instrument payload and spacecraft (Figures 4, 5) such that the observatory can deploy into the operational

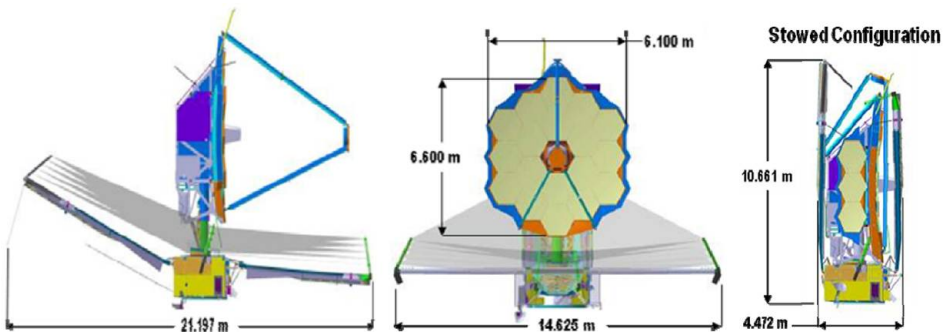

Fig. 4.— The JWST is the largest cryogenic optical system ever constructed.

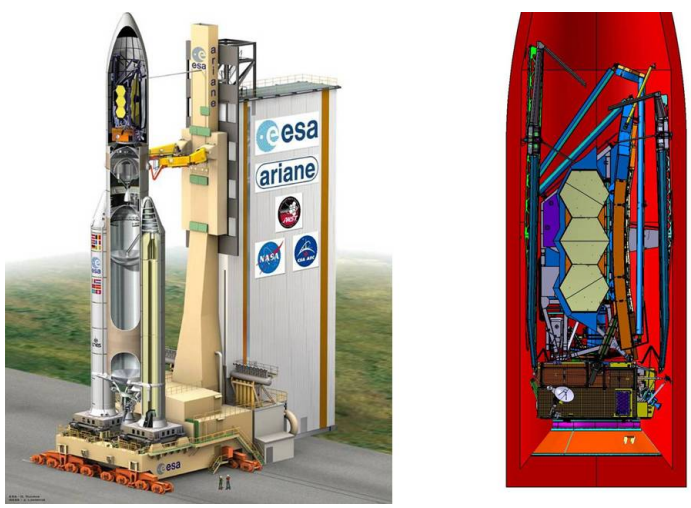

Fig. 5.— The JWST is designed to integrate with an Ariane 5m diameter fairing.

configuration shown in Figure 1 (see animation at: www.jwst.nasa.gov/videos_deploy.html). The observatory is launched warm and cooling begins after sunshield deployment en route to the L2 point.

The resulting mission architecture is shown in Figure 6. During operations, the NASA Deep Space Network is used to support two 4 hr communications contacts each day during which approximately 470 Gbits of science and engineering data are downloaded. Both mission and science operations are supported by the Space Telescope Science Institute. Overall

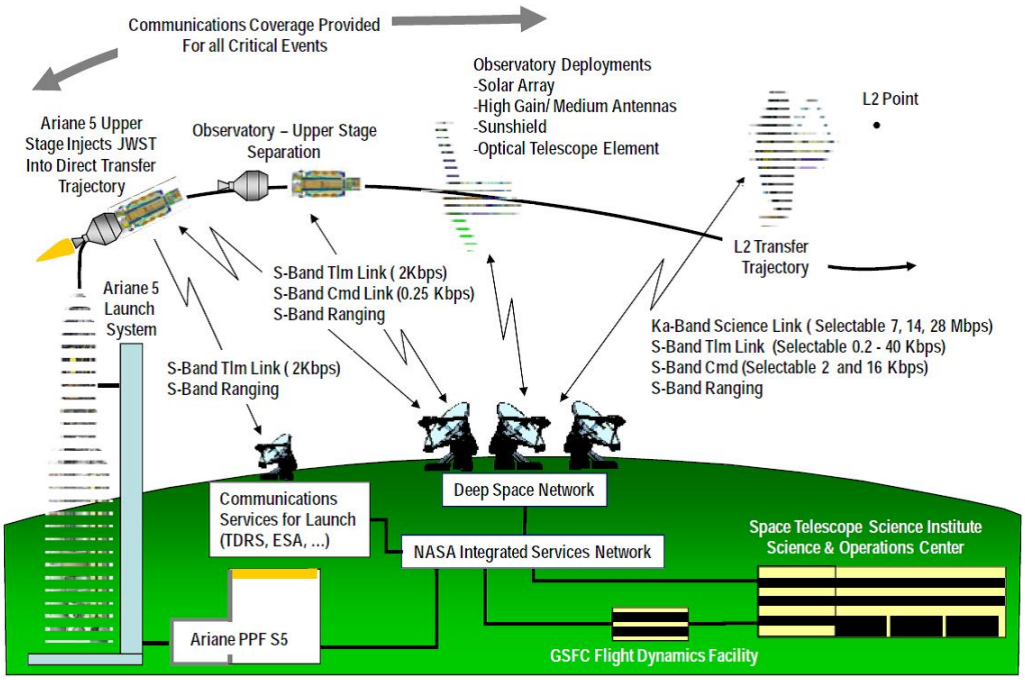

Fig. 6.— The JWST mission architecture.

mission management, as well as guidance, navigation, and control, are provided by Goddard Space Flight Center.

3. Collecting the first light

A three mirror anastigmat (TMA) telescope design was selected to enable high image quality over a wide field of view. In contrast to ground-based telescopes, minimizing mass is a key design driver on the JWST telescope. Beryllium was selected as a material for the three TMA mirrors due to its high thermal conductivity, high stiffness to mass ratio, and low expansion coefficient at the $\sim$ 50K operating temperature. A segmented primary mirror design was chosen to enable fold-up stowage as shown in Figure 7. The deployed aperture is tricontagon in shape with a collecting area of 25 m^2. The primary mirror is composed of 18 hexagonal segments (1.32 m flat-to-flat) of three optical prescriptions. Each primary mirror segment and the secondary mirror are mechanized to provide in-flight position adjustment in 6 degrees of freedom (Figure 8). The primary mirror segments also have in-flight radius of curvature adjustment. A fine steering mirror is located near a pupil position (Figure 7). This mirror is servo controlled using an image-based fine guidance sensor located in the science instrument focal plane to enable 7 mas rms pointing stability. The mirrors are polished to

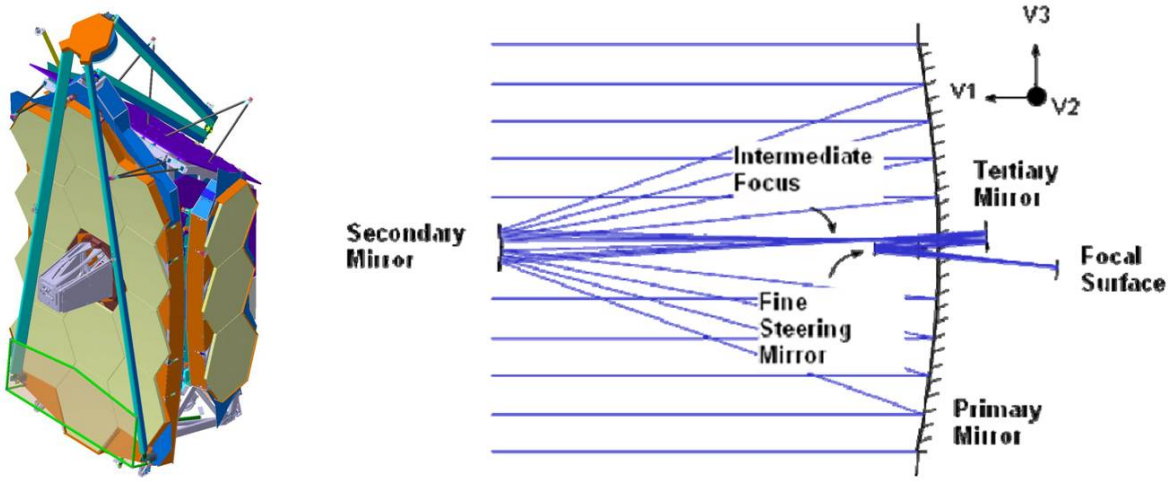

Fig. 7.— Left – The telescope in it stowed configuration; Right – The telescope deploys into a three mirror anastigmat configuration.

Fig. 8.— A primary mirror segment entering cryogenic testing (left), mechanized segment mount assembly provides 6 DOF and radius of curvature adjustment (right).

a cryogenic figure error of approximately 20 nm rms via an iterative cryo-test and polishing process. Gold was selected as a mirror coating to provide high throughput over the 0.6 – 29 μm spectrum. This coating choice limits the JWST to wavelengths > 0.6 μm. The 29 μm long wavelength limit results from detector technology and cooling constraints. The telescope structure consists of a M55J-954-6 cynate ester composite material that affords a high stiffness to mass ratio and a low cryogenic expansion coefficient to yield high optical alignment stability.

The mirror segment actuators are periodically adjusted in flight to ensure diffraction limited image quality throughout the mission. The observatorys main near-infrared science

camera (Section 4) is used as the wavefront error sensor for this process. Initial coarse phasing of the segments is accomplished using dispersed Hartman sensing optics in this camera (Figure 9). The subsequent fine phasing is performed on defocused images using

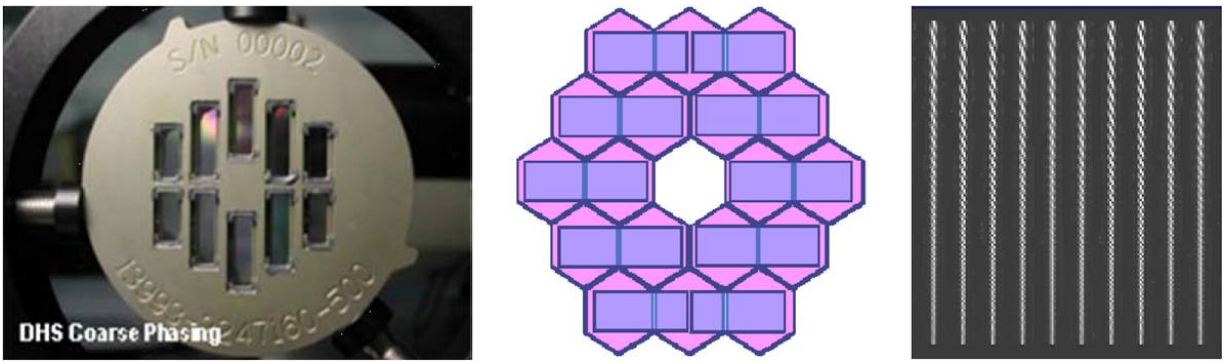

Fig. 9.— Dispersed Hartman sensing is used to perform coarse phasing of the mirror segments.

a modified Gerchberg-Saxton algorithm (Acton et al. 2004). This process is designed to achieve a telescope Strehl ratio of 0.8 at a wavelength of 2 μm. The dispersed Hartman coarse phasing process was demonstrated on the Keck telescope (Albanese et al. 2006). The overall flight wavefront sensing and control process has been demonstrated on a 1/6 scale fully functional model (Figure 10) of the JWST telescope (Feinberg et al. 2007; Contos et al. 2008).

4. Extracting information from starlight

The JWST science instrument payload contains four science instruments, a fine guidance sensor, and supporting systems for instrument control, command and data handling, cryogenic thermal control, and other functions (Greenhouse et al. 2006, 2010). Near-infrared imagery is provided by the NIRCam instrument (Rieke 2005, 2008) shown in Figure 11. This camera provides high angular resolution wide-field imagery over the 0.6-5 μm spectrum. The detector pixel scale is chosen to optimally sample the telescope point spread function across this wavelength range by use of a dichroic beam splitter (Table 2). Two identical optical modules image adjacent fields of approximately 4 square arcminutes to provide full redundancy for telescope wavefront sensing. Occulting coronagraphy, yielding a rejection ratio of $\sim$104, is provided in both long and short wavelength channels. All focal plane arrays support high cadence sub-array exposures to provide a high dynamic range capability for exoplanet transit observations.

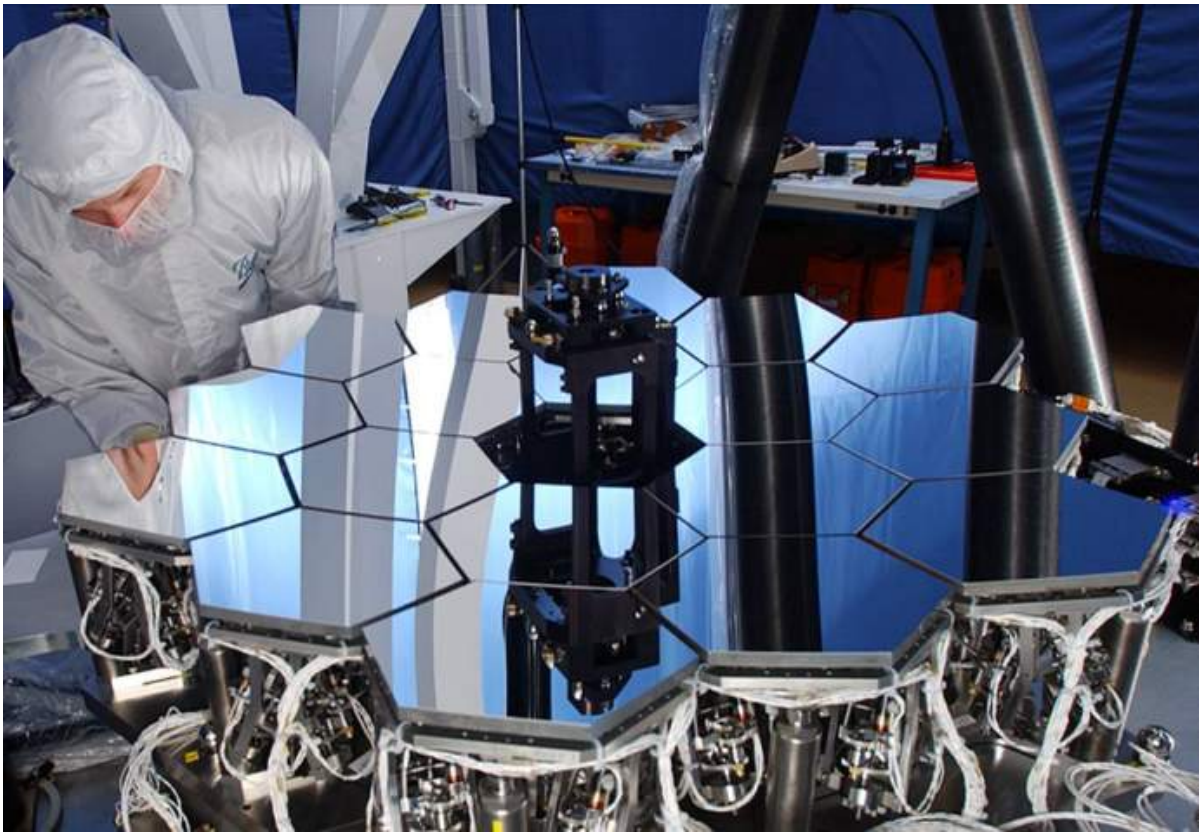

Fig. 10.— A 1/6 scale fully functional model of the JWST telescope was used to develop the overall wavefront sensing and control process.

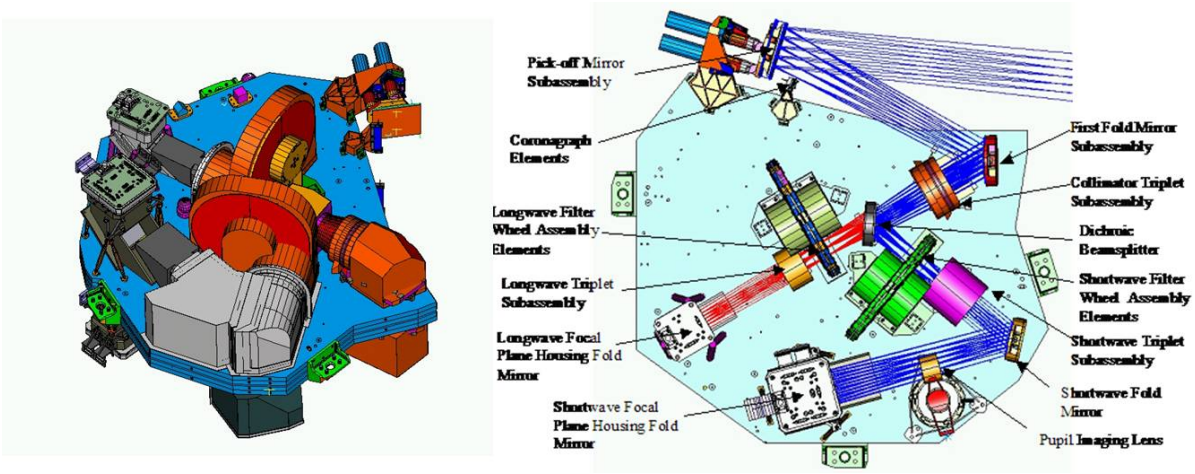

Fig. 11.— The NIRCam provides high angular resolution imagery.

Key Instrument Characteristics (as of Mar 06)									
Instrument	Channel/Mode	Wavelength (microns)	Typical Spectral Resolution ($\bar{\lambda}/\Delta\lambda$)	FOV	Angular Resolution (arc sec)	Number of Sensor Chip Arrays	Mega Pixels	Detector Type / Format NIR=18 um pixels MIR=25 um pixels	Detector Temp (K)
NIRCam	Shortwave	0.6 - 2.3	4,10,100	2.2' x 2.2' each of 2 modules	0.032 / pixel	8	34	HgCdTe / 2048 x 2048	40
	Longwave	2.4 - 5.0	4,10,100	2.2' x 2.2' each of 2 modules	0.065 / pixel	2	8	HgCdTe / 2048 x 2048	40
NIRSpec	Multi-Object Spec	1.0 - 5.0	1000	203 x 463 mas clear shutter aperture, 267 x 528 mas pitch, 4 x 171 x 365 shutter array format, 9.7 sq arcmin multi-object targetable solid angle	see FOV	2	8	HgCdTe / 2048 x 2048	37
		0.6 - 5.0	100						
	Long Slits (5)	1.0 - 5.0	100, 1000, 2700	200 x 3500 mas x 3, 400 x 4000 mas, 100 x 2000 mas					
	IFU	0.7 - 5.0	2700	3 x 3 arc-sec	0.10 slice width				
MIRI	Imager	5 - 27	4-6	1.9' x 1.4'	0.11 / pixel	1	1	Si:As / 1024 x 1024	7
	Low Res Slit	5 - 11	100	5" x 0.6"	see FOV	1	1	Si:As / 1024 x 1024	7
	Med Res IFU	4.87 - 7.76	3000	3.7" x 3.7"	0.18 slice width	1	1	Si:As / 1024 x 1024	7
		7.45 - 11.87	3000	4.7" x 4.5"	0.28 slice width				
		11.47 - 18.24	3000	6.2" x 6.1"	0.39 slice width				
		17.54 - 28.82	2250	7.1" x 7.7"	0.65 slice width				
FGS-TF		1.6 - 2.5, 3.2 - 4.9	100	2.2' x 2.2'	0.065 / pixel	1	4	HgCdTe / 2048 x 2048	40
FGS-Guider		0.8 - 5.0	0.7	2.3' x 2.3' each of 2 modules	0.068 / pixel	2	8	HgCdTe / 2048 x 2048	40

Table 2: JWST science instrument characteristics (coronagraphic modes not shown).

Near-infrared scanning Fabry-Perot imagery is provided by the FGS-TF instrument (Doyon et al. 2008). This instrument (Figure 12) provides a narrow-band imaging capability

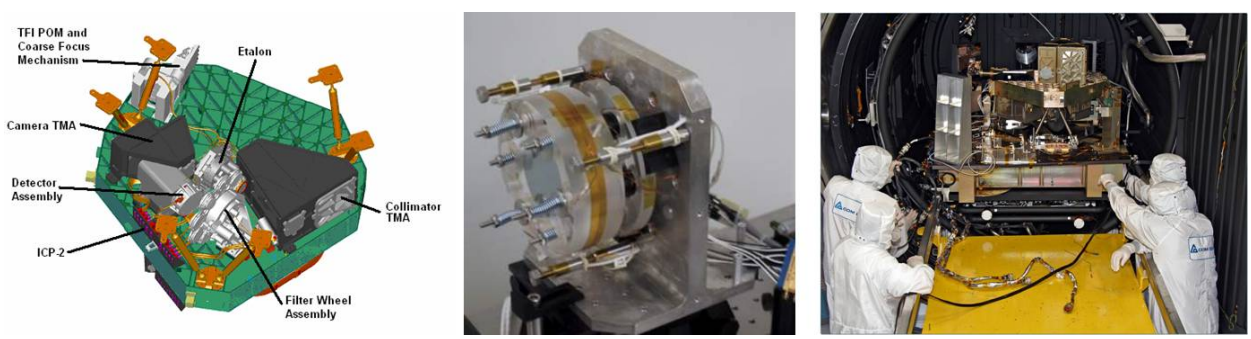

Fig. 12.— The FGS-TF instrument layout (left), test unit in space simulation chamber (center), and prototype Fabry-Perot etalon (right).

with the same size field of view as the NIRCam and over a similar wavelength range (Table 1). Its applications include deep surveys for emission line objects over a flexible range of redshifts. The instrument includes occulting coronagraphy that can achieve a contrast ratio of $\sim 10^4$ using a speckle suppression technique that is enabled by the scanning capability of the etalon.

The FGS-TF shares an optical bench with the FGS-Guider. The latter is a fully redundant very broad-band camera (Table 1) that functions as the fine guidance sensor for the telescope fine steering mirror system (Figure 7). It delivers guide star centroid measurements with a noise equivalent angle of 3 mas at a rate of 16 Hz. Its wide field of view enables 95% probability of guide star acquisition over the whole sky and autonomous pattern recognition

for guide star identification.

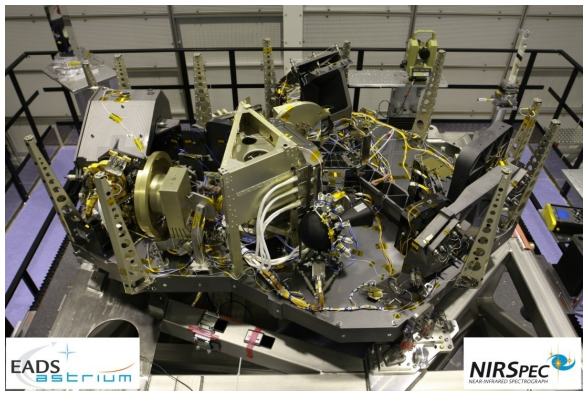

Fig. 13.— The NIRSpec instrument engineering test unit.

Spectroscopy over the 0.6 – 5 μm spectrum is provided by the NIRSpec instrument (Bagnasco et al. 2007). The NIRSpec affords a range of spectral resolutions shown in Table 1 that can be used with long slit, multi-object, and integral field aperture control modes. This instrument (Figure 13) is the first multi-object spectrometer developed for space flight. It is designed to target 100 compact sources simultaneously within a 9 square arcminute field.

Aperture control for multi-object spectroscopy is provided by a 0.25 Mpixel array of micro-shutters (of dimensions shown in Table 1) that are configured for the desired target

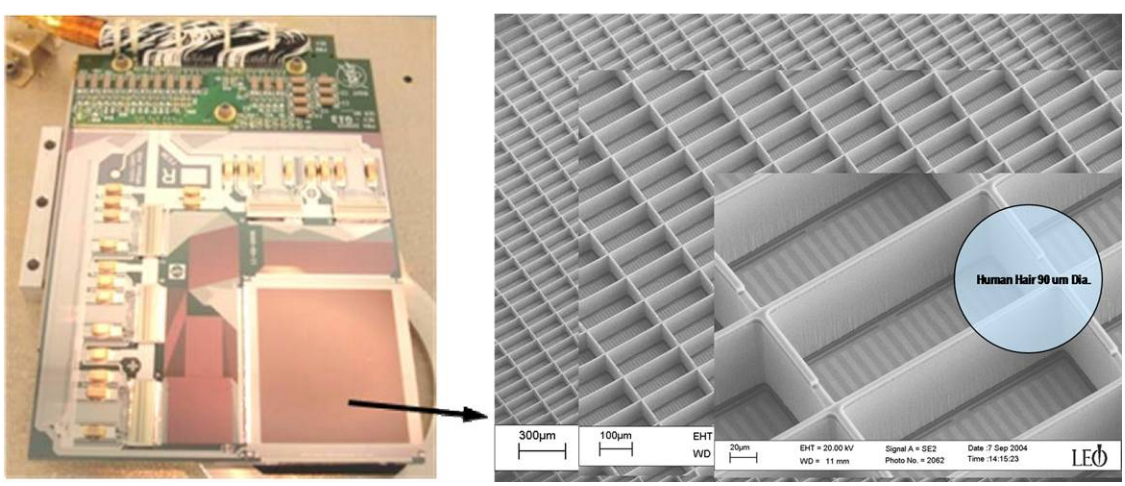

Fig. 14.— A quadrant of the NIRSpec micro-shutter array for multi-object spectroscopy is shown (left) along with a micrograph of its optical area (right).

field based on prior NIRCam imagery (Figure 14). A variety of fixed long slits are provided

to enable high contrast and exoplanet transit spectroscopy. Integral field spectroscopy is provided over a 9 square arcsecond field via a conventional image slicer.

Imagery and spectroscopy over the 5-29 μm spectrum is provided by the MIRI instrument (Wright et al. 2008). This instrument (Figure 15) provides broad-band imagery, low

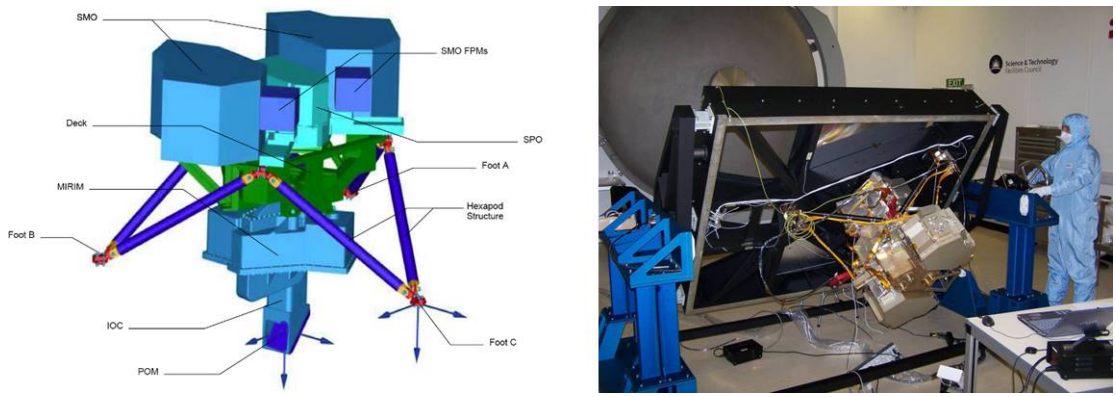

Fig. 15.— The MIRI instrument configuration (left) and verification model (right).

spectral resolution (1%) long slit spectroscopy, and medium spectral resolution ($\sim 10^3$) integral field spectroscopy (Table 1). The imaging mode includes both occulting and quadrant phase mask coronagraphy. The latter type enables very small inner working angle observations of stellar debris disks and exoplanet systems. When used in combination with the NIRSpec instrument, an optimally sampled integral field spectrum covering the whole 0.6 – 29 μm JWST wavelength range can be obtained at medium spectral resolution.

The detectors for the JWST instruments define the state of art for high performance space flight infrared imaging arrays. The near-infrared instruments utilize HgCdTe 4 Mpixel sensor chip arrays (SCA) operated at $\sim$ 40 K. Zodiacal background limited sensitivity is achieved in all broad-band instrument modes (Table 3). The MIRI instrument utilizes Si:As

JWST Sensitivity							
Wavelength (microns)	Instrument/Mode	Bandwidth ($\lambda/\Delta\lambda$)	SNR	Wall Clock Time (s)	Continuum Flux Density (nJy)	Continuum Flux Density (10^{-33} W m^{-2} Hz^{-1})	Unresolved Line Flux (10^{-21} W m^{-2})
2	NIRCam	4	10	10,000	11.40	0.11	NA
3.5	FGS-TF	100	10	10,000	126.00	1.26	NA
3	NIRSpec/Low Res	100	10	10,000	132.00	1.32	NA
2	NIRSpec/ Med Res	NA	10	100,000	NA	NA	0.57
10	MIRI/ Broadband	5	10	10,000	700.00	7.00	NA
21	MIRI/Broadband	4.2	10	10,000	8700.00	87.00	NA
9.2	MIRI/Spectrometer	2400	10	10,000	NA	NA	10
22.5	MIRI/Spectrtometer	1200	10	10,000	NA	NA	56.00

Table 3: JWST sensitivity benchmarks.

1 Mpixel SCAs operated at $\sim$ 7 K. Significant gains in noise performance and SCA format

were achieved during the JWST technology development phase to enable the above mission science goals (Figures 16, 17). The near-infrared SCAs are designed to be edge-butted

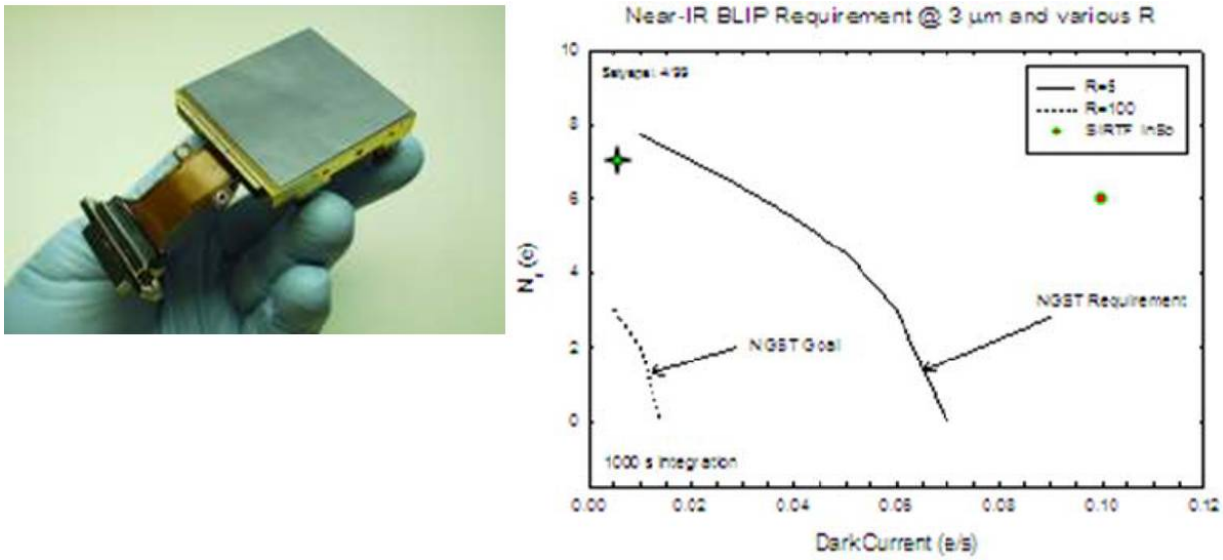

Fig. 16.— Left – A Teledyne H2RG 4 Mpixel sensor chip array; Right – noise performance of this technology (green cross) compared to that of 0.07 Mpixel InSb sensors used on the Spitzer space telescope (red dot). The lines shown are the original (circa 1999) requirement and goal for back-ground limited performance (BLIP) for the JWST (then called NGST).

on three sides to from larger format focal plane array (FPA) assemblies. For example, the NIRCam short wavelength channel utilizes a 16 Mpixel FPA consisting of 4 of these SCAs, and the NIRSpec utilizes an 8 Mpixel FPA consisting of 2 SCAs. The mid-infrared SCAs are used individually in 1 Mpixel FPA assemblies.

5. Making sure it all works

Testing at the scale and operating temperature of the JWST requires the largest deep cryogenic ($\sim$ 30K) space simulation facilities in the world. The system is built up and tested in incremental steps in which each subunit is tested before it is integrated into the next higher level of assembly. As integration proceeds, larger and larger facilities are needed. The fully integrated instrument payload will be tested at Goddard Space Flight Center using a telescope simulator (Hagopian et al. 2007; Ohl et al. 2009). After integration with the actual telescope, the whole system is tested in a larger facility at Johnson Space Center (Figure 18) (Atkinson et al. 2008). Unlike the Hubble Space telescope, which resides in low

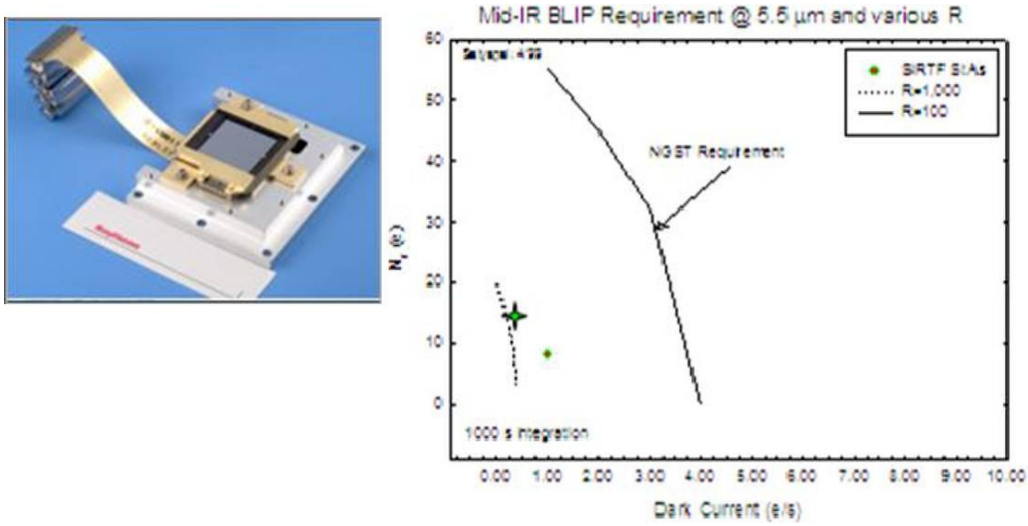

Fig. 17.— Left – A Raytheon Si:As 1 Mpixel sensor chip array; Right – noise performance of this technology (green cross) compared to that of 0.07 Mpixel Si:As sensors used on the Spitzer space telescope (red dot). The lines shown are the original (circa 1999) requirement and goal for background limited performance (BLIP) for the JWST (then called NGST).

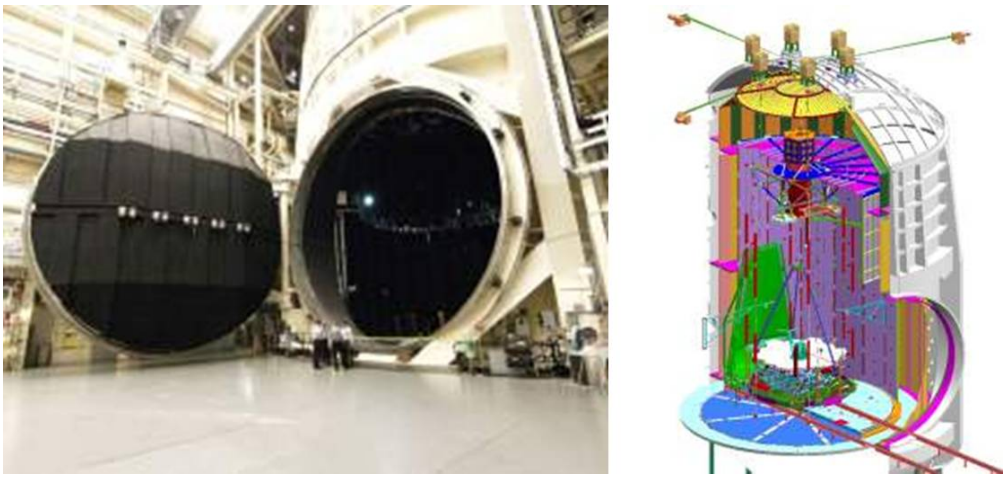

Fig. 18.— The JWST will be tested in JSC chamber A (120 feet tall, 60 feet diameter).

earth orbit, the JWST cannot be serviced by astronauts due to its more distant SE-L2 point orbit. However, in contrast to prior space observatories, the JWST telescope and instrument optical systems employ a high degree of freedom for in-flight adjustment (Barto et al. 2008), and lessons learned from prior observatory test programs are carefully taken into account in design of the JWST test program (Feinberg et al. 2008).

REFERENCES

Acton, D. S., et al., 2004, James Webb Space Telescope Wavefront Sensing and Control Algorithms, Proc. SPIE, 5487, 877

Albanese, M. A., et al., 2006, Verification of the James Webb Space Telescope coarse phase sensor using the Keck Telescope, Proc. SPIE, 6265, 62650Z

Atkinson, C., et al., 2008, Architecting a revised optical test approach for JWST, Proc. SPIE, 7010, 24

Bagnasco, G., et al. 2007, Overview of the near-infrared spectrograph instrument on-board the James Webb Space Telescope, Proc. SPIE, 6692, 17

Barto, A., et al., 2008, Optical performance verification of the James Webb Space Telescope, Proc. SPIE, 7010, 23

Contos, A., et al., 2008, Verification of the James Webb Space Telescope (JWST) wavefront sensing and control system, Proc. SPIE, 7010, 26

Doyon, R., et al., 2008, The JWST tunable filter imager (TFI), Proc. SPIE, 7010, 70100

Feinberg, L., et al., 2007, TRL-6 for the JWST wavefront sensing and control, Proc. SPIE 6687, 668708

Feinberg, L., et al., 2008, Applying HST lessons learned to JWST, Proc. SPIE, 7010, 13

Gardner, J. P., et al., 2006, Space Sci. Rev., 123, 485

Greenhouse, M. A., et al., 2006, The James Webb Space Telescope Integrated Science Instrument Module, Proc. SPIE 6265, 33

Greenhouse, M. A., et al., 2010, Status of the James Webb Space Telescope Integrated Science Instrument Module, Proc. SPIE 7731, 773108

Hagopian, J., et al., 2007, Optical alignment and test of the James Webb Space Telescope Integrated Science Instrument Module, IEEE Aerospace Conference, 3-10 Mar 2007, Big Sky, Montana

Ohl, R., et al., 2009, Updates to the optical alignment and test plan for the James Webb Space Telescope Integrated Science Instrument Module, Proc. SPIE, 7433, 743305

Rees, M. J., 1997, The Hubble Space Telescope and the High Redshift Universe, N. R. Tanvir, A. Aragon-Salamanca, & J. V. Wall eds., World Scientific: Singapore, 115

Rieke, M., 2005, Overview of James Webb Space Telescope and NIRCam's Role, Proc. SPIE, 5904, 1

Rieke, M., 2008, see: http://ircamera.as.arizona.edu/nircam/AAS_June08.pdf

Thronson, H. A., et al., 2009, Astrophysics in the Next Decade: the James Webb Space Telescope and Concurrent Facilities, H. A., Thronson, M., Stiavell & A. G. G. M., Tielens eds, Springer Verlag

Wright, et al., 2008, Design and development of MIRI, the mid-IR instrument for JWST, Proc. SPIE, 7010, 27

This preprint was prepared with the AAS LaTeX macros v5.2.

NASA LAW, October 25-28, 2010, Gatlinburg

The Hubble Space Telescope and Laboratory Astrophysics

Jennifer J. Wiseman[1]

NASA Goddard Space Flight Center, Greenbelt, MD 20771

jennifer.wiseman@nasa.gov

ABSTRACT

The Hubble Space Telescope (HST) continues to push the limits on world-class astrophysics. Cameras including the Advanced Camera for Surveys and the new panchromatic Wide Field Camera 3, which was installed on the recent successful servicing mission SM4, offer imaging from near-infrared through ultraviolet wavelengths. Spectroscopic studies of sources from black holes to exoplanet atmospheres are making great advances through the versatile use of STIS, the Space Telescope Imaging Spectrograph. The new Cosmic Origins Spectrograph, also installed last year, is the most sensitive UV spectrograph to fly in space and is uniquely suited to address particular scientific questions on galaxy halos, the intergalactic medium, and the cosmic web. With these outstanding capabilities on HST come complex needs for laboratory astrophysics support including atomic and line identification data. This paper provides an overview of Hubble′s current capabilities and the scientific programs and goals that particularly benefit from the studies of laboratory astrophysics. With no current plans for further servicing of Hubble (and thus limited further observations), and no future major optical/UV space observatory currently planned for at least the next decade, it is essential to maximize the critical laboratory astrophysics support needed for Hubble observations in the near-term.

1. Introduction

Starting with the Copernicus observatory in the early 1970's, the astronomical community has had nearly continuous access to spectroscopy at ultraviolet wavelengths for nearly four decades. In addition to Copernicus there were the International Ultraviolet Explorer (IUE), the Goddard High Resolution Spectrograph (HST/GHRS), the Faint Object Spectrograph (HST/FOS), the Space Telescope Imaging Spectrograph (HST/STIS), the

Far-Ultaviolet Spectroscopic Explorer (FUSE), and most recently the Cosmic Origins Spectrograph (HST/COS). This long and distinguished series of instruments has revealed in great detail the resonance and low-excitation line spectra of numerous atomic/ionic species in astronomical sources. It also revealed serious deficiencies in the existing database of atomic parameters that characterize many of these transitions (see, e.g., Leckrone et al. (1990)). Over the years the community of experimental and theoretical atomic physicists has risen admirably to the challenges posed by the astrophysical observations. However, as we push farther into the vacuum ultraviolet we encounter higher ionization states in stars, the interstellar medium, and the hot intergalactic medium. The challenges to our knowledge of atomic/ionic structure and the parameters that characterize line spectra, thus, continue. Laboratory studies are also being extended to model the dynamics and composition of other astrophysical systems, such as jets from protostars and the atmospheres of exoplanets. Such modeling is critical not only for interpreting Hubble observations but also for setting the stage for data from future observatories such as the James Webb Space Telescope.

2. Servicing Mission 4 and the Cosmic Origins Spectrograph

May of 2009 heralded perhaps the most complicated, and ultimately successful, servicing mission ever in Hubble's two-decade history. Though the mission had been cancelled a few years prior due to Shuttle safety concerns, careful study and planning brought a reinstatement of the mission. With it came a rebirth of hope for science from the observatory, with the goal, now realized, that after this servicing mission Hubble would be more scientifically powerful than ever before.

Astronauts installed two new cutting edge scientific instruments: The panchromatic Wide Field Camera 3 (WFC3), providing sensitive imaging from the near UV through visible and into near-IR wavelengths, and the Cosmic Origins Spectrograph (COS), providing extremely high spectroscopic sensitivity in the ultraviolet. Astronomers were also delighted with the repair and restoration of two other highly successful instruments, the Advanced Camera for Surveys (ACS) and the Space Telescope Imaging Spectrograph (STIS).

For spectroscopy and related laboratory astrophysics, the restoration of STIS and the capabilities of COS are of particular interest. Put simply, COS is the most sensitive ultraviolet spectrograph ever to fly in space. It contains a minimum number of optical elements that reflect or disperse the light, since with each bounce of a light beam off an optical surface there is some loss, thus reducing the throughput of an instrument. The ultraviolet light-sensing detectors on COS are especially sensitive and efficient. COS has two channels, the Far Ultraviolet (FUV) channel covering wavelengths from 115 to 177 nm, and the Near

Ultraviolet (NUV) channel, covering 175-300 nm (Figure 1).

Key goals for COS include the study of the intergalactic medium (IGM) and the interstellar medium (ISM). The sensitivity of COS is allowing the detection of weak absorption features, and thus the composition of the IGM, along the line of sight to bright quasars, amplifying the need for accurate line identification. For the ISM, UV spectra are particularly capable of distinguishing specific molecules, and laboratory studies of organic molecules including PAHs are critical for COS data interpretation. COS spectra are also being used to anayze the atmospheric characteristics of transiting exoplanets.

COS characteristic	FUV channel	NUV channel
Spectral range (nm)	115-205	170-320
Spectral resolution	16000-24000 med. 2000-3000 low	16000-24000 med. 2000-3000 low
Detector type	cross-delay line	NUV MAMA
Detector array (pixels)	32768 x 1024	1024 x 1024
Pixel size (microns)	6 x 24	25 x 25
Gratings	3	4
Enhancement factor over previous spectrograph	Detection of objects more than 30x fainter than with STIS	Detection of objects more than 2x fainter than with STIS

Fig. 1.— Characteristics of the Cosmic Origins Spectrograph. The STIS and COS spectrographs on HST are complementary. While STIS has spatial imaging and wavelength coverage that COS does not have, COS is more sensitive for faint UV spectroscopy.

3. Stellar Atmospheres

The ultraviolet spectra produced in the photospheres of stars covering an enormous range in effective temperature (less than 9000 K up to over 70,000 K) are dominated by the line opacities of iron group atoms and ions, with progressively higher ionization states showing up at progressively hotter effective temperatures. What is at work here is the nexus of the relatively high cosmic abundances of the iron group and the great complexity of their energy level structures, resulting in extremely rich observed and calculated spectra. Accurately calculating the line strengths of all of these transitions with model stellar atmospheres

is both important and extremely challenging. It is important for accurately modeling the effects of line blanketing on the temperature-pressure structure of the stellar atmospheres and for accurately modeling the effects of line blending in those cases where one is attempting to derive accurate abundances from ultraviolet lines of other elements. These line opacities also play a significant role in models of stellar evolution that account for dynamical processes below the photosphere radiatively-driven diffusion, convection, turbulence and mass loss in winds (see e.g. Richer et al. (2000), Vick et al. (2010)).

Progressively higher ionization states of all elements exhibit their strongest transitions at progressively shorter wavelengths, as the upper level of transitions from a ground or low-excitation state is found at progressively higher excitation potentials. So, for example, the ground state Multiplet 1 of neutral iron occurs around 5200 Å, UV Multiplet 1 of Fe II is found around 2600 Å, while UV Multiplet 1 of Fe III occurs near 1130 Å. It is probably reasonable to generalize that more is known about the energy levels and term structures (and corresponding wavelengths and transition probabilities) of lower ionization states than of higher states of any particular iron group element and transitions to progressively higher and higher excitation states, occurring at shorter and shorter wavelengths, are characterized by a diminishing quantity and quality of atomic data.

A specific example of this state of affairs afflicting observational and computational astrophysics can be seen in Figure 2, which is a reproduction of a table from Leckrone et al. (1999). The table gives line identification statistics for four wavelength intervals in the ultra-sharp-lined chemically peculiar B-type star, chi Lupi (Teff = 10,650 K), observed at very high spectral resolution ($\sim 90,000$) with the Goddard High Resolution Spectrograph on HST. In this case the percentage of unidentified lines, including relatively strong and well-resolved features, increases substantially as one goes to progressively shorter wavelengths. Over one quarter of the lines in the shortest wavelength interval, 1317 - 1543 Å, while moderately strong are unidentified. Only 3% fall into this category in the longest wavelength interval, 2334 - 2688 Å. A short segment of the chi Lupi spectrum around 1323 Åis plotted and compared to a model synthetic spectrum in Figure 3. The numerous unidentified lines and incompletely characterized line blends are very clear.

Figure 4 illustrates similar problems in the case of an extremely hot star, the white dwarf REJ0503-289 (Teff = 70,000 K), observed with FUSE (Barstow et al. (2007)). In this case one expects to see lines arising from much higher ionization states, e.g. C IV, S V, S VI, Ni V, etc. Although the match between observed (black line) and synthetic (blue line) spectra was improved with the inclusion of the Kentucky line database (www.pa.uky.edu/peter/atomic/), the fit is still quite poor with numerous examples of unidentified features and inaccurate transition probabilities.

STATISTICS OF LINE IDENTIFICATIONS VERSUS WAVELENGTH

λ Range (Å)	$\langle\delta\lambda\rangle$[a] (Å)	⟨Number of Lines⟩[b]	Firm ID[c]	Probable ID[d]	Total Unidentified[e]	Stronger Unidentified[f]
2334–2688..... ⟨29, 34, 36⟩[g]	14	105	57%	36%	7%	3%
1904–2160..... ⟨17, 18, 24⟩	11	112	44%	36%	20%	7%
1644–1873..... ⟨13, 14, 16⟩	10	112	36%	42%	22%	13%
1317–1543..... ⟨3, 9, 11⟩	8	133	30%	31%	39%	28%

[a] Average width of observed intervals.
[b] Average number of spectral features counted per interval.
[c] Observed feature closely matched by spectrum synthesis.
[d] Discrepancies between spectrum synthesis and observations probably reflect uncertainties of atomic data or issues with abundances as discussed in the text. Unmodeled features plausibly identified by wavelength from laboratory spectra.
[e] Substantial line opacity missing in spectrum synthesis; no plausible identification.
[f] Subset of unidentified features that are moderately strong and (in most cases) well resolved.

Fig. 2.— Table from Leckrone et al. (1999), showing the significant number of unidentified lines in star chi Lupi spectra, especially toward shorter wavelengths.

4. Protostars, Exoplanets, and Laboratory Simulations

Protostars and exoplanets are currently of high astrophysical interest, and spectroscopy is essential for analyzing exoplanet atmospheres and star formation environments. Spectroscopy from the Hubble NICMOS instrument (not currently in operation) is being used for first preliminary identifications of molecules in exoplanet atmospheres. But clearly the modeling of observed absorption spectra shows the need for significant improvement in identifying the infrared lines involved (Swain, Vasisht, & Tinetti (2008)). Laboratory studies also include actual physical simulations of dynamical astrophysical systems. Protostellar jets observed with HST, for example, are being effectively modeled with both computer simulations and actual jet production in the laboratory. Studies include the effects of jet deflection which is likely common in astrophysical environments (see Figure 5), and are also revealing that some protostellar jet features are most likely due to a pulsed driving source (Hartigan et al. (2009)).

5. Conclusion

Thanks to the fantastic success of Servicing Mission 4, the Hubble Space Telescope is currently more scientifically powerful than ever before, with precision tools for spectroscopy including the repaired Space Telescope Imaging Spectrograph (STIS) and the new Cosmic

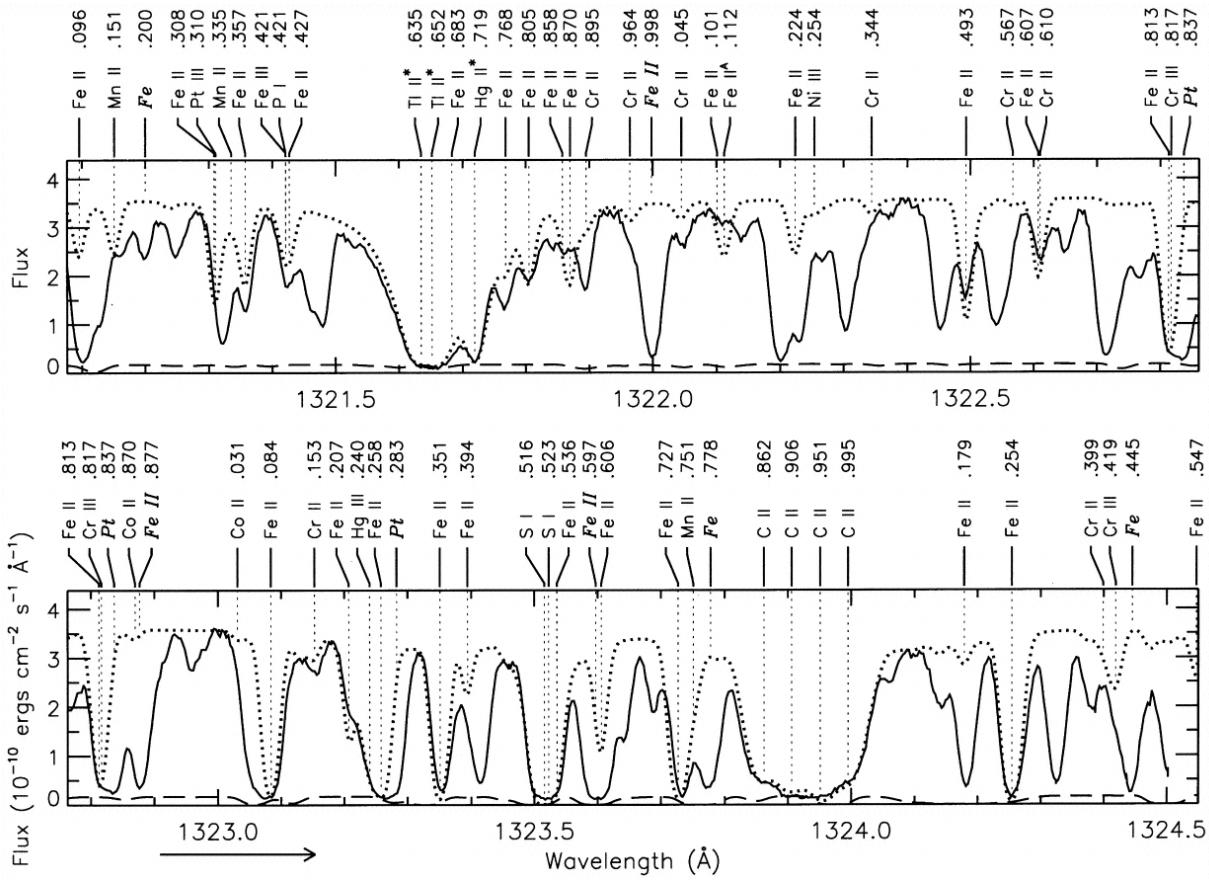

Fig. 3.— HST GHRS chi Lupi spectrum from Brandt et al. (1999), showing the observed (solid line) data as compared to synthetic (dotted line) spectra. .

Origins Spectrograph (COS). The sensitivity of COS is breaking new ground for exploring weak lines in the intergalactic and interstellar medium. Spectroscopy and related laboratory astrophysics are supporting HST studies of diverse sources including stellar atmospheres, supernova remnants, the IGM and Cosmic Web, astrophysical jets, and exoplanets. With no more servicing missions planned, and no new flagship UV/optical mission in the near future, it is critical that needed laboratory and theoretical be conducted in the near-term, such as to aid not only interpretation of data taken but also to inform choices on highest priority observations in the few remaining HST cycles left. Of particular need for laboratory astrophysics studies are the identification of higher ionization level atomic lines and their transition probabilities for study of, e.g., stellar and white dwarf atmospheres. Also needed are better models for transiting exoplanet molecular atmosphere spectra, as observed in the infrared.

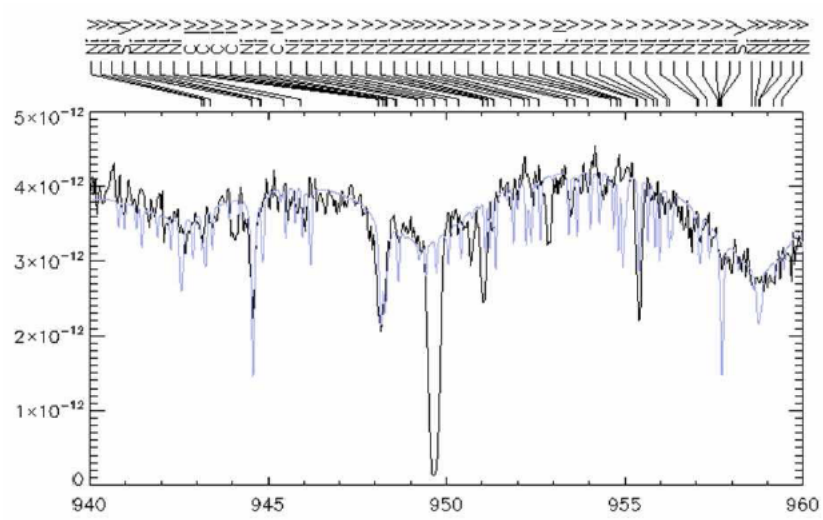

Fig. 4.— White Dwarf REJ0503-289 spectrum, from Barstow et al. (2007), showing FUSE observations (black line) as compared to the model (purple/grey). Clearly there are still poor matches in some regions of the spectrum, with unidentified lines and inaccurate f-values, even with "Kentucky database" lines added. .

The research discussed here is made possible by Hubble Space Telescope scientific observers and the HST support community around the world, and it is gratefully acknowledged. The work and input of emeritus HST senior project scientist David Leckrone for this and related papers is also much appreciated.

REFERENCES

Brandt, J., Heap, S., Boggess, A., et al. 1999, A. J. 117, 1505

Barstow, M., Dobbie, P., Forbes, A. & Boyce, D. 2007, ASP Conference Series, 372, ed. R. Napiwotzki, R. & M. Burleigh, 243.

Hartigan, P., Foster, J. M., Wilde, B. H., et al. 2009, Ap.J. 705, 1073

Leckrone, D., Johansson, S., Kurucz, R., & Adelman, S. 1990, in Atomic Spectra and Oscillator Strengths for Astrophysical and Fusion Research, ed. J. Hansen, Amsterdam: Royal Netherlands Academy of Arts and Sciences, 3

Leckrone, D., Proffitt, C., Wahlgren, G., Johansson, S., & Brage, T. 1999, A.J. 117, 1454

Richer, J., Michaud, G. & Turcotte, S. 2000, Ap.J. 529, 338

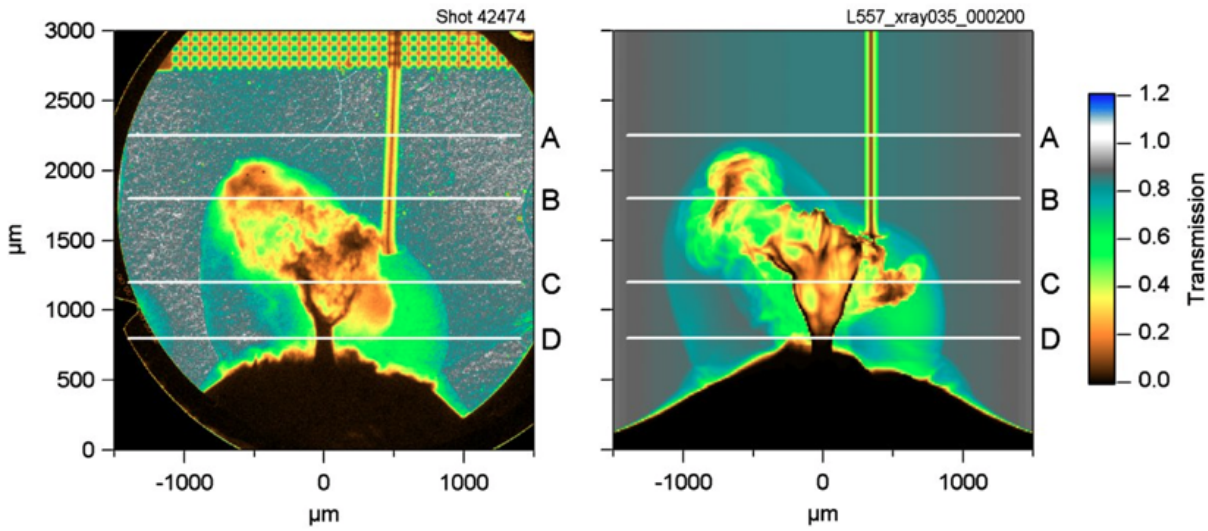

Fig. 5.— Observation (left) and simulation (right) of a deflected supersonic jet created in the laboratory (Hartigan et al. (2009)).

Swain, M., Vasisht, G., & Tinetti, G. 2008, Nature, 452, 329

Vick, M., Michaud, G., Richer, J. & Richard, O., 2010, A. & A. 521, A62

This preprint was prepared with the AAS LaTeX macros v5.2.

NASA LAW, October 25-28, 2010, Gatlinburg

Laboratory Astrophysics Needs for Current and Future X-ray Missions

R. K. Smith, A. R. Foster, L. Ji, N. S. Brickhouse

Smithsonian Astrophysical Observatory, Cambridge, MA 02138

rsmith@cfa.harvard.edu, afoster@cfa.harvard.edu, lji@cfa.harvard.edu, nbrickhouse@cfa.harvard.edu

ABSTRACT

Although the analysis of moderate-resolution X-ray spectra benefits from good-quality atomic data, the emergence of high-resolution X-ray data from current X-ray satellites has shown the need for high-quality atomic data of all stripes: wavelengths, absorption cross sections, and collisional and radiative rates. This process will continue with upcoming missions such as Astro-H and IXO. We describe the successes of both theoretical calculations and laboratory measurements, as well as the many remaining needs and the science that hinges upon them. These include, amongst other issues, accurate wavelength measurements in the soft X-ray band, calibrated line ratios of selected strong lines, and high-resolution absorption cross sections for abundant ions.

1. Introduction

Although astronomical X-ray spectroscopy has many similarities to other bandpasses, there are a few aspects of fundamental physics that impact the X-rays far more than other wavebands. We restrict ourselves here to thermal plasmas, as non-thermal X-ray emitting plasmas (typically synchrotron-dominated) do not require atomic data and photoionized plasmas will be discussed elsewhere (Kallman et al. 2010). Most importantly, a thermal X-ray spectrum contains significant fractions of both line and continuum emission, so neither can be safely ignored. In a few situations (*e.g.* the surfaces of neutron stars) the continuum takes the shape of a blackbody, but the majority of thermal astronomical plasmas are optically-thin and the continuum is primarily from bremsstrahlung radiation. The resulting broad-band temperature-dependent emission means that even detectors with low spectral resolution can

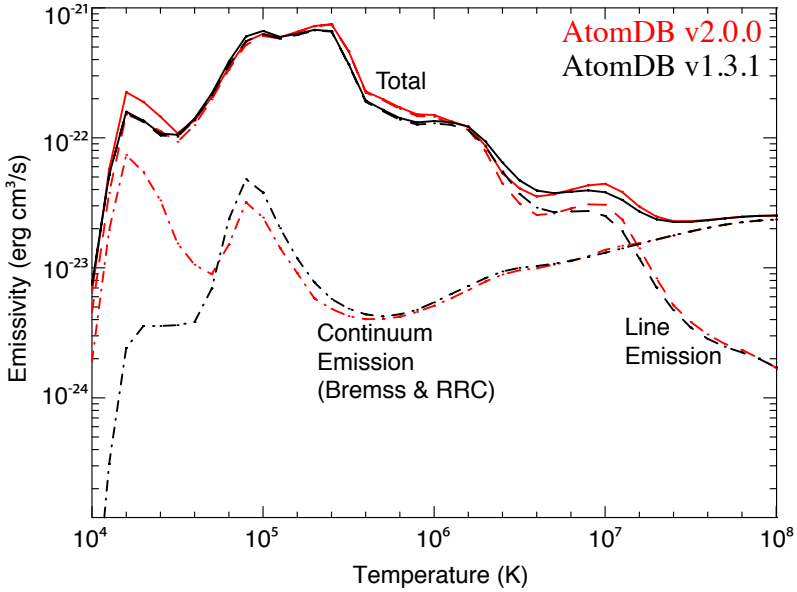

Fig. 1.— The cooling curve from AtomDB v2.0.0 and v1.3.1, separated into line and continuum components. The continuum emission includes both bremsstrahlung radiation due primarily to electron-proton interaction as well as radiative recombination (RRC) created when electrons recombine with ions; this is responsible for the peaks at 2×10^4 K and 10^5 K.

accurately measure the temperature of the plasma – enabling, for example, the *Einstein* observatory's discovery that clusters of galaxies are filled with hot gas.

Figure 1 shows the most recent calculation of the total cooling power from a hot plasma, using data from AtomDB v2.0.0[1] and comparing to v1.3.1. The total cooling has been separated into line and continuum components. Although line emission dominates below 2×10^7 K, continuum emission dominates above that temperature. Therefore, for sufficiently high temperatures, the most important atomic data requirement is to determine the bremsstrahlung free-free gaunt factor accurately (which is by now well-known!).

However, at lower temperatures, emission from lines dominates the spectrum. Fortunately, a relatively small set of ions themselves dominate the line emission. These are the hydrogen-like, the helium-like, and the iron L-shell (Fe XVII – Fe XXIV) ions. This can be seen clearly in the recent Chandra HETG spectrum of TW Hya (Brickhouse et al. 2010). Their strength makes these emission lines the easiest to detect and, therefore, the most important first step for any atomic physics compilation. It should be noted that these lines

[1]Available at http://www.atomdb.org

are not necessarily the most powerful diagnostics. Dielectronic satellite lines, for example, are unambiguous diagnostics of both temperature and equilibrium state, but as they are relatively faint and require high (> 500) spectral resolution to detect, their importance in practical X-ray spectroscopy to date has been limited.

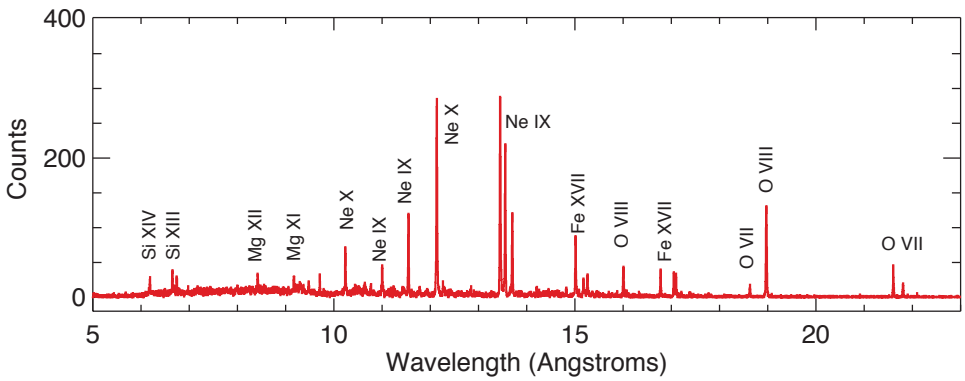

Fig. 2.— Chandra HETG spectrum of the T Tauri star TW Hya showing strong emission lines from hydrogen-like and helium-like ions as well as Fe XVII. From Brickhouse et al. (2010).

1.1. Newly-available atomic data

The issues discussed above are not new, and atomic physicists around the world have been working on improving the atomic data for these ions over the past decade. These efforts are nearly concluded, and the new data has recently been incorporated into the atomic database AtomDB and released as v2.0.0. We withhold further discussion of the new data here as details can be found in Foster et al. (2010). New atomic data have also been included in the recently released CHIANTI v6.0 (Dere et al. 2009) and SPEX v2.0 (Kaastra et al. 1996).

2. Future Atomic Data Needs

The long-standing efforts of a large number of atomic physicists, both theoretical and laboratory, have hopefully addressed the most significant outstanding problems with the atomic calculations, such as those identified by Testa et al. (2004) regarding He-like line ratios or the long-standing Fe XVII problem (Beiersdorfer 2003). Of course, this can only be confirmed by observers using the new codes, so more work may remain. However, there are a

number of newly-identified issues particularly relevant to high-resolution X-ray spectroscopy that should be addressed by the NASA lab astrophysics program; we discuss a selection of these problems briefly here. However, this list is far from exhaustive – for example, we omit issues regarding the shapes of fluorescent emission lines used for calibration or how to include systematic errors in theoretical atomic rates, amongst other topics.

2.1. Emission lines with wavelength between 50-150Å

Figure 3, taken from Raassen & Kaastra (2007), shows the kind of spectral data that can be obtained from a bright source (such as Capella) using the Chandra gratings, covering a huge bandpass ranging from 1-180Å. However, Desai et al. (2005) showed that the atomic data for these transitions are woefully inadequate, with errors in relative flux of 100% or more in many cases. In addition, many lines in the longer bandpass from 50-150Å remain unidentified and so cannot be used spectroscopically at all. Although calculations by Gu (2003) improve the accuracy, flux ratio errors of more than 30% remain for many transitions. Improving the quality of data in this bandpass is a difficult problem that requires both theoretical and laboratory work. Many of the ions involved in this bandpass are only moderately-ionized, making theoretical models significantly more challenging. Laboratory work is needed to identify lines and provide a baseline to test models; this work is in progress (*e.g.* Lepson et al. 2008) but more remains.

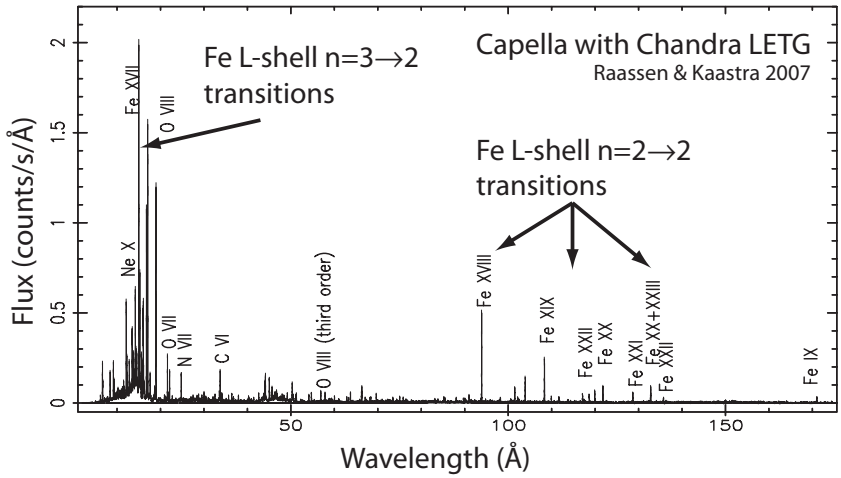

Fig. 3.— Chandra LETG spectrum of Capella from Raassen & Kaastra (2007) showing a broad range of significant emission lines; the atomic data for lines with $\lambda > 50$ Åare in general poor.

2.2. Interstellar absorption cross sections

In addition to occupying the bandpass where the continuum and line emission power crosses, the 0.1-10 keV X-ray bandpass also happens to be extremely sensitive to interstellar absorption. At low ($\sim 0.25\,$keV) energies, an $A_V \sim 0.1$ (or $\mathrm{N_H} = 1.9\times10^{20}\,\mathrm{cm}^{-2}$) corresponds to optical depth $\tau \sim 1$, while 3 keV X-rays do not reach $\tau \sim 1$ until $A_V \sim 20$ ($\mathrm{N_H} = 4 \times 10^{22}\,\mathrm{cm}^{-2}$). As a result, nearly all sources are impacted to some degree by absorption. When modeling low- or moderate-resolution spectral data, a simple model based on the Henke et al. (1993) tables weighted by cosmic abundances adequately describes the absorption. However, high-resolution spectroscopy requires significantly better data, as absorption lines and edge structures can then be resolved (Paerels et al. 2001). A number of efforts are underway to generate the necessary data (*e.g.* McLaughlin & Kirby 1998; García et al. 2005; Hasoglu et al. 2010), but a systematic effort will be needed to create and store this data in a format that can be accessed by X-ray astrophysicists. An additional complication arises as molecules and dust also have diagnostically-useful absorption features (Kaastra et al. 2009) – but they must be adequately calibrated (Lee et al. 2009).

2.3. Charge Exchange

The importance of charge exchange in X-ray astronomy was only realized after ROSAT observations of the comet Hyakutake (Lisse et al. 1996) showed that the comet was, against expectations, a strong X-ray emitter. This was eventually explained as resulting from solar wind ions exchanging electrons with neutral cometary material, leaving the ions in a highly-excited state that rapidly stabilizes via X-ray and UV emission. Even without a comet to provide the necessary neutral material, solar wind charge exchange (SWCX) creates a low-level diffuse X-ray background of line emission due to interactions with exospheric or heliospheric neutral atoms (see, *e.g.,* Lallement 2004). Since the solar wind tends to have an ionization balance typical of a $\sim 10^6 - 10^7\,$K plasma, the resulting recombined ions tend to emit at low (0.1-1 keV) energies with the majority of lines expected in the 0.1-0.3 keV bandpass. Although only observed at CCD resolution to date, the launch of a microcalorimeter on Astro-H will finally enable high-resolution spectral studies. Although both theoretical (Pepino et al. 2004; Ali et al. 2010) and laboratory (Frankel et al. 2009) efforts are ongoing, more work will be needed both to use the SWCX to diagnose the solar wind *in situ* (a long-standing desire of the heliophysics community) or to remove the SWCX "background" from distant astrophysical sources.

2.4. Accurate wavelengths

Theoretical calculations can relatively easily determine wavelengths that are 1% accurate, but this unfortunately inadequate for high-resolution X-ray spectroscopy. For many years the only solution was to obtain laboratory measurements for each wavelength, such as was done by Brown et al. (2002) for many strong Fe L-shell lines. Recently Kotochigova et al. (2010) showed that detailed theoretical calculations (informed by laboratory measurements of selected strong lines) could achieve the necessary accuracy, as shown in Figure 4. However, more data are needed for other ions, such as the Ni L-shell series in the 0.8-2 keV bandpass and other abundant L-shell ions, primarily in the 0.1-0.3 keV bandpass.

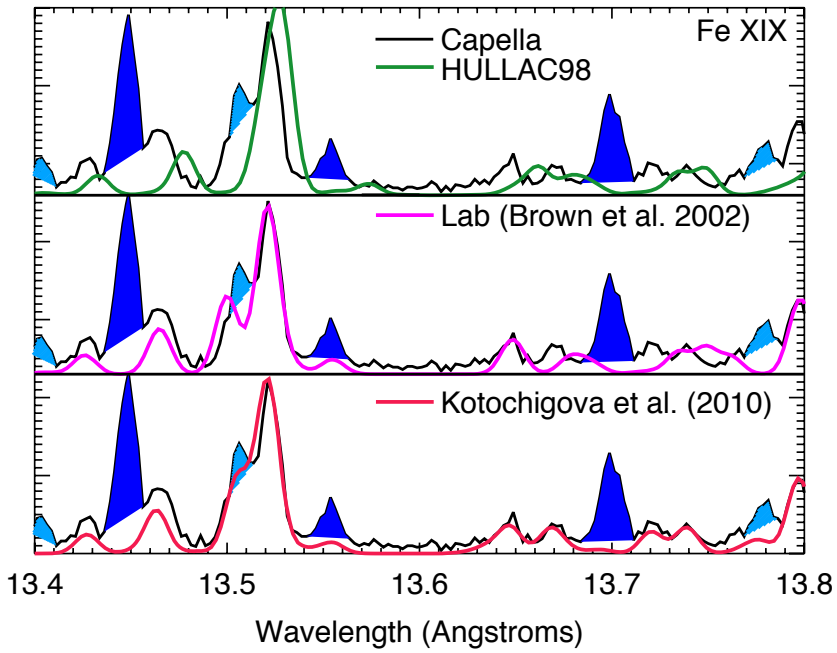

Fig. 4.— HETG Spectrum of Capella showing a number of Fe XIX lines (plus Ne IX lines, shown in blue) fit with data from [Top] uncorrected distorted wave calculation, [Middle] laboratory wavelengths, and [Bottom] detailed atomic calculations. Based on figure in Kotochigova et al. (2010).

3. Conclusion

Before the launch of Chandra and XMM-Newton, there was great concern that the available atomic data were inadequate to the task of analyzing the high-resolution data

expected from these missions. Fortunately, after substantial work, many of the problems identified in 2000 have now largely been addressed. However this statement is in part true because the gratings on Chandra and XMM-Newton are only useful when observing bright point or slightly-extended sources. With the upcoming launch of Astro-H, X-ray astronomers will have high-resolution spectroscopic data on all sources, combined with significantly more effective area than the existing gratings. This will open up new possibilities, but will also require a new push to ensure that the atomic data needed to analyze these spectra are available.

This work was supported in part by NASA grant NNX09AC71G.

REFERENCES

Ali, R., Neill, P. A., Beiersdorfer, P., Harris, C. L., Schultz, D. R., & Stancil, P. C. 2010, ApJL, 716, L95

Beiersdorfer, P. 2003, ARA&A, 41, 343

Brickhouse, N. S., Cranmer, S. R., Dupree, A. K., Luna, G. J. M., & Wolk, S. 2010, ApJ, 710, 1835

Brown, G. V., Beiersdorfer, P., Liedahl, D. A., Widmann, K., Kahn, S. M., & Clothiaux, E. J. 2002, ApJS, 140, 589

Dere, K. et al. 2009, A&A, 498, 915

Desai, P., et al. 2005, ApJL, 625, L59

Foster, A. R., Smith, R. K., Li, J. & Brickhouse, N. S. 2010, this proceedings

Frankel, M. et al. 2009, ApJ, 702, 171

García, J., Mendoza, C., Bautista, M. A., Gorczyca, T. W., Kallman, T. R., & Palmeri, P. 2005, ApJS, 158, 68

Gu, M. F. 2003, ApJ, 582, 1241

Hasoglu, M. F., Abdel-Naby, S. A., Gorczyca, T. W., Drake, J. J., & McLaughlin, B. M. 2010, ApJ, 724, 1296

Henke, B. L., Gullikson, E. M., & Davis, J. C. 1993, ADNDT, 54, 181

Kaastra, J. S., Mewe, R., Nieuwenhuijzen, H. 1996, UV and X-ray Spectroscopy of Astrophysical and Laboratory Plasmas, Editor K. Yamashita, & T. Watanabe (Univ. Ac. Press:Tokyo), 411

Kaastra, J. S., de Vries, C. P., Costantini, E., & den Herder, J. W. A. 2009, A&A, 497, 291

Kallman, T. et al. 2010, this proceedings

Kotochigova, S., Linnik, M., Kirby, K. P., & Brickhouse, N. S. 2010, ApJS, 186, 85

Lallement, R. 2004, A&A, 418, 143

Lee, J. C., et al. 2009, astro2010: The Astronomy and Astrophysics Decadal Survey, 2010, 178

Lepson, J. K., Beiersdorfer, P., Bitter, M., & Kahn, S. M. 2008, Can. J. of Phys, 86, 175

Lisse, C. M., et al. 1996, Science, 274, 205

McLaughlin, B. M., & Kirby, K. P. 1998, J Phys. B, 31, 4991

Paerels, F., et al. 2001, ApJ, 546, 338

Pepino, R., Kharchenko, V., Dalgarno, A., & Lallement, R. 2004, ApJ, 617, 1347

Raassen, A. J. J., & Kaastra, J. S. 2007, A&A, 461, 679

Testa, P., Drake, J. J., & Peres, G. 2004, ApJ, 617, 508

This preprint was prepared with the AAS LaTeX macros v5.2.

NASA LAW, October 25-28, 2010, Gatlinburg

Atomic data from the UV to the IR: With consideration to NASA missions

G. M. Wahlgren[1]

Department of Physics, The Catholic University of America, Washington, DC, 20064

glenn.m.wahlgren@nasa.gov, wahlgren@cua.edu

ABSTRACT

Current NASA mission spectroscopic capabilities for wavelengths ranging from the ultraviolet to the near-infrared reside in the instruments on-board the *Hubble Space Telescope*. Future missions (*JWST, SOFIA*), replacing and extending recent capabilities, will allow spectral observations at mid-infrared wavelengths. Coupled with an archive system from past missions and ground-based observatories, a robust network of multi-wavelength spectral data is available for astronomical targets from the solar system to cosmological distances. However, the analysis of this trove of spectral data continues to be dependent upon, among other things, the accuracy and completeness of atomic data. The atomic data needs of current and future NASA mission science is considered.

1. Introduction

High-resolution ultraviolet (UV) spectroscopy was ushered into a new era on 4 October 1990, when the first *HST*/GHRS observation of the sharp-lined chemically peculiar star χ Lupi was taken as part of the GHRS SMOV program. A single, previous GHRS spectrum had been obtained for R Dor on 21 September, but that low-resolution, low-S/N observation of C IV λ1554Å resembled its *IUE* spectrum. High-resolution *Copernicus* spectra were of a similar quality as the spectrum taken on that October night, but the anticipation of things to come was palpable, since this was not the échelle format being tested. The laboratory astrophysics community had previously been made aware of the potential distress that could

[1]NASA GSFC, Code 667, Greenbelt, MD, 20771

befall UV spectral analysis, once high-resolution *HST* data accentuated the unsatisfactory nature of the atomic line database (Leckrone et al. 1990). Laboratory spectroscopists and theoreticians, rallied by the first observations of χ Lupi, especially the exquisite échelle spectra, provided the atomic data needed to begin analyzing these and other *HST* spectra. Their efforts lead to dozens of publications on atomic data, as recounted in a summary of the first 10 years of analysis (Leckrone et al. 1999) and subsequent studies. Atomic data that will be utilized to explore these early spectra are still being created.

2. Atomic Data and its Availability

Accurate atomic data are needed to perform simple spectrum analysis tasks, such as to identify spectral features and empirically determine plasma parameters, as well as detailed line profile analysis. Absorption lines are characterized by their absorption coefficient, which in an LTE analysis requires knowledge of the wavelength, oscillator strength (f-value), ionization potential, energy levels and their statistical weights, and the related partition function, along with damping parameters that quantifies the line shape. A non-LTE analysis requires additional parameters, collision strengths for excitation and ionization and photo-ionization cross-sections. For emission line sources, such as gaseous nebulae, AGN, and stellar coronae, the line emissivity is described by the frequency, transition probability (A), and energy level populations. These environments cool through the radiative decay of excited states, and the level populations are therefore the result of particle collisions. Photoionization cross sections and collision strengths are required to describe the processes of electron impact excitation and ionization, along with radiative and dielectronic recombinations. (The treatment of these latter parameters is discussed by others at this conference.)

Atomic data are created through experiment and calculation, which for the purposes of this discussion both fall under the moniker of 'laboratory astrophysics.' As a general statement, one can say that experiments provide data that may be more accurate than *ab initio* calculations. Atomic structure calculations have their strength in providing large amounts of data that would otherwise be prohibitive to produce in a laboratory, whether it be due to instrument limitations or light sources. Such parameters include collisional data and oscillator strengths.

Current experimental techniques typically measure the lifetime of an excited atomic state and combine it with the measured intensity of lines emanating from that excited state to produce A values, which are then transformed into the f-values through an analytical expression (Wahlgren 2010a, 2010b). For many atomic systems, there is a need to use a broad wavelength range to determine A because transitions from a given upper level can

be spread over wavelength from the UV to the IR. Laboratory experiments would then either need to be conducted over this entire range or any missing regions would need to be accounted for by calculations or constraints from stellar spectra.

For the UV to IR, atomic data availability is subject to the misconception that a century of laboratory spectroscopy has provided all of the data that are needed, at least for optical wavelengths. The periodic table has not been equitably treated by spectroscopists, even for the optical region. The atomic data gathered over the past century have been influenced by its purported impact and the ease with which it can be obtained. Thus, elements lighter than the iron group have useful data across this wavelength range because of relatively few lines, simpler systems to be calculated, importance to critical nuclear-burning scenarios, and relatively high cosmic abundance. Iron-group elements have been relatively well studied at optical wavelengths, and much work is even now being dedicated to them at all wavelengths because of their impact on opacity and line blending through their many transitions. Work on iron-group elements at all wavelength regions remains a critical task and should continue to be supported. A number of post-iron group element (Sr, Y, Zr, Ba, Eu) are recognized for their importance in identifying neutron capture nucleosynthesis processes and they are therefore better studied than many other trace elements. However, understanding nucleosynthesis processes and the impact of individual elements on planet formation and astrobiology requires that other elements be equally well studied. The availability of atomic data for other heavy elements, in particular among the lanthanides and platinum group elements, has been improved during the last twenty years, although much work remains to be done to improve the completeness and accuracy of the atomic data for UV and IR wavelengths.

Atomic data are most useful to astronomers when they are collected into data bases. Among the most cited on-line data bases for UV to IR atomic data are the: a) NIST spectral data base (www.nist.gov/pml/data/asd.cfm), comprised mostly of compilations of experimentally determined atomic data for a growing number of elements; b) atomic spectral line database of R. Kurucz (kurucz.harcard.edu), comprised of his calculated oscillator strengths along with values determined from published experiments for most atoms and some ions; c) VALD (Vienna Atomic Line Database) (vald.astro.univie.ac.at/ $\sim$ vald/php/vald.php), expands upon the data base of R. Kurucz; and d) the Atomic Line List v2.04 (www.pa.uky.edu/ $\sim$ peter/atomic, not updated this century), computes wavelengths from the energy levels presented in the NIST data base. None of these data bases are close to being complete in terms of the number of transitions, and therefore, the researcher must check the literature for new data. Starting points for such a search include the bibliographic data bases at NIST (www.nist.gov/pml/data/asbib/index.cfm) and Troitsk (das101.isan.troitsk.ru/bibl.htm), as well as the triennial report of Commission 14 (Atomic and Molecular Data) of the International Astronomical Union. Several atomic structure codes are utilized to calculate

atomic data, and a laudable effort would be to identify their strengths and weaknesses as applied to applications in astrophysics. One data base of note for calculated A-values is the MCHF/MCDHF Database of C. Froese Fischer and G. Tackiev (nlte.nist.gov/MCHF/).

Parsed by wavelength, attention must be given to acquiring atomic data for the UV and IR regions. The UV spectral region, which is effectively defined by the space missions, provides access to both high and low energy phenomena. Added importance to UV line data comes from knowing that at cosmological distances ($z > 2$) wavelengths in the range 200 - 300 nm are redshifted into the near-IR, a prime motivation for *JWST* science programs. Aside from strong features of abundant elements, the VUV ($\lambda < 200$ nm) requires much work for accurate wavelengths and transition probabilities for most elements.

Infrared spectroscopy from space has been limited to low spectral resolution at near-IR (*HST*) and mid-IR (*ISO, Spitzer, AKARI*). The identification and analysis of individual atomic lines has been limited to strong lines and relatively narrow fine-structure emission lines. The scientific promise of instrumentation onboard future missions, *JWST* (low spectral resolution) and the *SOFIA* airplane observatory (low to high spectral resolution), will benefit from improvements in ground-based astronomical spectroscopy for their interpretation. New directions in laboratory spectroscopy will need to prioritize IR experiments for lines of many elements. Few experimentally determined f-values (~ 120) are found in the NIST database for wavelengths longer than 1 μm. An extensive amount of work for line identifications must also be undertaken to interpret spectra emitted at IR rest wavelengths.

3. Data Needs - Realities

Focusing on NASA missions, we first direct our attention to their archives, where it is evident that the UV domain presents a dilemma for obtaining new atomic data. Archived spectra exist for many missions. The archives of the *HST* and *FUSE* missions alone would keep laboratory spectroscopists busy for years, at the rate in which atomic data are currently generated. But a look through the archives reveals that many spectral observations have received no attention beyond their initial purpose, and many have never been analyzed for publication. One reason is that many astronomical spectra await atomic data before being further exploited. The combination of limited funding and personnel for atomic data studies insures that the most recent missions receive the greatest attention, but may quickly be abandoned in favor of more lucrative funding opportunities. A healthy archive data analysis program should continue to be supported to extract science results from costly space missions and encourage atomic data studies to facilitate archive research. Archived spectra for optical and IR wavelengths are more limited in number and generally of a low spectral resolution

(IR data), but are nonetheless useful.

An indication of atomic data needs might also be gleamed from the *HST* proposals to be executed during the current cycle. The statistics for cycle 18 show there to be 155 GO proposals and 41 archival proposals accepted. Approximately half of the GO programs (75) utilize a spectroscopic mode. The STIS (37) and COS (35) instruments are nearly equally requested by number of proposals, with the low-resolution optical and IR capabilities of the STIS (18) and WFC3 (10) being modestly represented. The vast majority of the spectroscopy proposals request low and moderate spectral resolutions, for which one would not anticipate new atomic line data being a necessity. One surprise in the statistics is that the unprecedented high spectral resolution of the STIS échelle mode is part of so few accepted proposals (6). In addition, of the accepted archive proposals, only two may consider new atomic data. Today's *HST* observing agenda does not appear to support large investments in atomic data, if judged solely by proposal statistics.

The near-term plans for NASA missions exclude UV and optical spectroscopy after the present suite of *HST* instruments is retired. The IR, from 1 to 200 μm, will be the domain of the *JWST* and *SOFIA* (and ESA *Herschel*) missions. The low spectral resolution of the *JWST* instruments will likely preclude the study of individual absorption lines. *SOFIA* will eventually have high resolution capabilities longward of 5 μm, where atomic transitions tend to be ground-state, fine-structure transitions. The situation for these lines is currently unsatisfactory, in terms of the completeness and accuracy of wavelength and transition probability data.

4. Resources

Data: It needs to be stressed that for the purpose of creating new atomic data for astrophysics, a symbiotic relationship exists between astronomical and laboratory spectroscopy. Both are needed to efficiently determine accurate atomic data that will be used in the analysis of astronomical spectra. High-resolution stellar spectra are needed over the entire wavelength interval from the UV to the IR for stars of various spectral classifications ($T_{\rm eff}$ and luminosity) in order to test gf-values and identify useful spectral features to be prioritized for laboratory analysis. Stellar spectra that are useful for these purposes exist for optical wavelengths in the ESO VLT archives. For UV wavelengths there are very few stars in the *HST* archive that would be suitable. (The *Copernicus* and *IUE* observatories did provide extensive wavelength coverage at UV wavelengths, but the resolution and S/N ratio of the data are not suitable for providing guidance for laboratory spectroscopy.) New high-resolution spectra for cool stars are to be obtained with the *HST*/STIS instrument during

the current cycle, but for hot stars and non-solar chemical compositions (for trace elements) additional stars will need to be observed. One legacy of *HST* could therefore be a library of high resolution spectra over the full range of stellar conditions, a resource that would be used for a variety of studies.

At near-IR wavelengths (1 - 5 μm) ground-based high-resolution spectra are being obtained using the ESO/CRIRES instrument for stars across the H-R diagram through the CRIRES-POP program (Lebzelter et al. 2010). High-resolution spectra also exist for the Sun (ATMOS - Geller 1992; ACE - Hase et al. 2010, KPNO atlases) and the cool giant star Arcturus (Hinkle et al. 1995) at these wavelengths. Taken together, these resources are suitable for interpreting the lower resolution near-IR spectra taken from space if the sharp-line spectral features can be identified.

A similar argument can be forwarded regarding laboratory spectra, to establish a library of high-resolution, high-S/N spectra for wavelengths ranging from far-UV to IR (90 - 5300 nm). With this resource astronomers would be able to identify spectral features, measure accurate wavelengths, determine branching fractions, construct transition probabilities and oscillator strengths if appropriate atomic lifetimes exist, and interpret line structure. Theoreticians would have a resource for testing calculations for atomic data. The only such data available to astronomers is the archive of the KPNO/NSO FTS (staging.noao.edu/newnso/nso_kp/nso-kp.html). Interferograms and transformed spectra can be found for many elements. These data are very incomplete in terms of their wavelength coverage, number of elements observed, excitation conditions, and calibration for serving as reference data to astronomical spectrum interpretation. They were not obtained for the purposes being proposed here, but instead to address particular problems in atomic spectroscopy. It is somewhat surprising that for the limited number of elements ($\sim$90) and ionization stages (I, II, III) relevant to stellar photospheres studies, that high-quality laboratory spectra are not readily available. Creating a library of laboratory spectra can be accomplished using current facilities, and is, therefore, a project that should receive immediate attention.

Laboratory facilities: There are very few laboratory facilities being used for the acquisition of atomic data for astronomical purposes. In the US, laboratories making regular contributions to the literature of atomic data consist of NIST, the University of Wisconsin (spectra of neutral and some single-ions), and the University of Toledo (beam-foil spectroscopy for lifetimes). (The KPNO/NSO FTS has not been operational for years.) A limited number of universities and facilities around the world also contribute to creating atomic data, although with few exceptions these efforts are not a primary line of research. However, there are laboratory facilities at US educational institutions that are capable of performing the necessary experiments to acquire atomic data for astrophysics. Involving these facilities will

require that they receive direction in identifying worthwhile projects. Providing incentive and instigating collaborations to perform laboratory atomic spectroscopy experiments would result in an increase in the number of facilities.

People and Funding: It may seem to be a glib statement, but the atomic data needs of astronomy at UV to IR wavelengths can be tackled by an increase in the number of laboratory spectroscopists and funding. The atomic data that astronomers require does not await technological breakthroughs. The technology exists, even if the number of facilities are few.

Funding opportunities for laboratory astrophysics exist in the current framework of NASA and NSF programs. However, typically, few such proposals are funded through these sources. Industrial resources have been used in recent times for funding university research in atomic spectroscopy but can not be considered a continuing resource. The bulk of laboratory experiments are conducted as unfunded or indirectly funded research by universities and government facilities through student research projects and individual efforts.

5. Summary remarks

Despite the continuing efforts by the laboratory astrophysics community in providing fundamental atomic data for astrophysics, there remains a need for additional data to address the challenges of NASA mission science.

At all wavelengths, but particularly for the UV and IR regions, the analysis and interpretation of astronomical spectra require more complete and accurate data sets to address gross spectral structure and discrete features. Both the UV and IR harbor numerous unidentified features in astronomical spectra. Specific and immediate data needs include: 1) the thorough analysis of iron-group elements for wavelengths and oscillator strengths, from the UV to the IR, 2) A-values for high-excitation states of low-charge ions (Fe II, for example), 3) wavelengths and f-values for transitions at UV and IR wavelengths for post-iron-group elements, and all elements at IR wavelengths, 4) atomic data for ground-state fine-structure lines at IR wavelengths

Certain areas related to resources and infrastructure should also receive attention. In this discussion mention was made to: 1) maintain or increase support for research utilizing NASA mission archives, since atomic spectroscopy studies can be conducted with these data in anticipation of new mission data, 2) encourage additional US laboratory facilities in NASA-related research through funding and collaborative partnerships, and 3) create libraries of high quality laboratory and stellar spectra.

This work was supported by NASA grant NNG06GJ29G.

REFERENCES

Geller, M. 1992, NASA Ref. Publ. 1224, vol III

Hase, F. et al. 2010, JQSRT, 111, 521

Hinkle, K., Wallace, L. Livingston, W., 1995, PASP, 107, 1042

Lebzelter, T. et al. 2010, The Messenger, 139, 33

Leckrone, D. S., Johansson, S., Kurucz, R. L. & Adelman, S. J. 1990, in Atomic Spectra and Oscillator Strengths for Astrophysics and Fusion Research (ASOS3), ed. J. E. Hansen, (North-Holland: Amsterdam), 3.

Leckrone, D. S. et al. 1999, AJ, 117, 1454

Wahlgren, G.M. 2010a, in Non-LTE Formation for Trace Elements in Stellar Astrophysics, eds. R. Monier, B. Smalley, G. Wahlgren, and Ph. Stee, EAS Publ. Ser. 43, (EDP Services), 91

Wahlgren, G.M. 2010b, in Atomic Spectra and Oscillator Strengths for Astrophysics and Fusion Research (ASOS10), eds. P. Beiersdorfer, W. Wiese, and E. Biemont, Canadian J. Physics, in press

This preprint was prepared with the AAS LaTeX macros v5.2.

NASA LAW, October 25-28, 2010, Gatlinburg

Atomic Physics Measurements in Support of X-Ray Astronomy

P. Beiersdorfer

Physics Division, Lawerence Livermore National Laboratory, Livermore, CA 94550

beiersdorfer@llnl.gov

ABSTRACT

Here we give a brief review of the recent atomic physics measurements of interest to X-ray astronomy as well as of current and future needs.

1. Introduction

The high-resolution spectral instrumentation of current and future X-ray astronomy missions (e.g.,*Chandra*, *XMM-Newton*, *Astro-H*, *IXO*) has driven a strong need for laboratory astrophysics data. An important issue has been to understand the Fe L-shell emission, and the Fe XVII spectrum in particular (Beiersdorfer 2003). A lot of progress has been made. In addition, new laboratory techniques have provided calibrations of spectral electron-density density diagnostics (Lepson et al. 2010, 2011) as well as wavelengths and cross sections for lines important for understanding absorption features (Simon et al. 2009). Measurements of dielectronic recombination and ionization rates have improved the quality of charge balance calculations (Bryans et al. 2006, 2009), and measurements of X-ray production by charge exchange have emboldened the search for such processes in the heliosphere, the ISM, and other stellar systems. In the following we will discuss some of the recent laboratory X-ray astrophysics measurements and point out areas in need of further measurements.

2. Emission Spectroscopy

Despite many years – one may argue centuries – of effort, there is still a large need for for emission spectroscopy experiments to identify lines and measure their wavelength. A recent measurement of the Fe XVI L-shell emission lines on the Livermore electron beam ion trap device (Graf et al. 2009) between 15 and 18 Å illustrates this need.

The position of the collisional Fe XVI L-shell lines were known from several calculations, as shown in Fig. 1(a,b). The measurement by Graf et al. (2009) identified lines and assigned wavelengths that were quite different from those calculated earlier, as shown in Fig. 1(c). New calculations, which managed to more closely reproduce the measured wavelengths, then confirmed the identifications (cf. Fig. 1(d)).

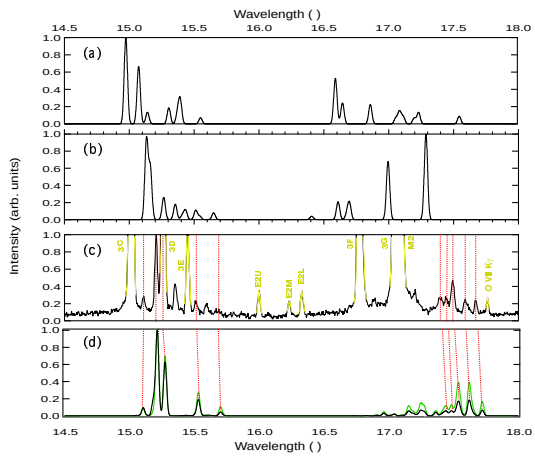

Fig. 1.— Measured and calculated L-shell emission from Fe XVI. Calculations are from (a) Cornille et al. (1994), (b) Phillips et al. (1997), and (d) Graf et al. (2009). The measured spectrum in (c) is from Graf et al. (2009). Known lines from Fe XVII and O VII are marked.

Similarly, the spectra from many astrophysically important ions in the 30–180 Å region are still not well known. Recent measurements of the L-shell emission lines of aluminum were presented by Gu et al. (2011), and almost none of the lines had been tabulated before.

3. Absoprtion Spectroscopy

Spectra from AGNs, which show a plethora of absorption features, have demonstrated the need for accurate atomic energy levels of complex ions with an innershell hole and a partially filled outer shell. For example, photoabsorption by an L-shell electron in an M-shell iron ion produces distinct absoprtion lines in the 15 – 17 Å region, which cannot be readily be calculated with spectroscopic accuracy. The resultant excited level typically does not de-excite by X-ray emission, and thus emission spectroscopy cannot be used to measure the energy level. The level decays instead by emisison of an Auger electron.

To make progress in measuring photoionization processes, efforts have been started to study photoexcitation and photoionization by probing complex ions from an EBIT with a

monoenergetic sychrotron or free-electron laser beam (Simon et al. 2009). The method has produced the first photoionization measurements of complex ions, including those of L-shell ionization of the M-shell Fe^{14+} ion Simon et al. (2010a,b). Highly accurate measurements of Fe XVI spectra are being carried out at the Berlin BESSY-II synchrotron and the Stanford LCLS X-ray laser (cf. Fig. 2).

Fig. 2.— Installation of the Heidelberg EBIT at the BESSY-II sychrotron. The EBIT is rolled to the beam line and connected within a few hours.

4. Ionization Equilibrium Measurements

The collisional ionization equilibrium is a key astrophysical parameter, which still needs much experimental data to check the theoretical data used by equilibrium codes. Atomic data are needed both for ionization and recombination. Such measurements are currently performed on the Test Storage Ring in Heidelberg (Lestinsky et al. 2009; Schmidt et al. 2008). Measurements include rates of recombination of neonlike Fe^{16+} ions forming Fe^{15+} (Schmidt et al. 2009) and electron-impact ionization cross sections of Mg^{7+} forming Mg^{8+} (Hahn et al. 2010). The measured rates are fed back into ionization equilibrium calculations, which are adjusted to provide updated ionization fractions for a given electron temperature. The most recent updates for iron have yielded considerable changes in the ionization fractions (Bryans et al. 2006, 2009).

5. The Fe XVII Problem

Historically, the line intensities of the Fe XVII L-shell spectrum produced by theoretical predictions do not match laboratory measurement at the level needed for analyzing *Chandra* or *XMM-Newton* observations (e.g., confer Beiersdorfer et al. (2004)). In particular, theory overestimated the ratio of line $3C$ to line $3D$ and underestimated the intensity of the $2p-3s$ transitions, i.e. lines $3F$, $3G$, and $M2$. For over a decade there was the additional controversy that the laboratory measurements performed on the NIST EBIT (Laming et al. 2000) did

not agree with those performed on the two Livermore EBITs (Beiersdorfer et al. 2002).

Much progress has been made. Very recently, the NIST EBIT line ratio measurements were repeated and now agree with those performed at Livermore (Gillaspy et al. 2011). This result is not surprising, as a similar measurement of the corresponding ratios in Ni XIX by the NIST EBIT group (Chen et al. 2006, 2007) also reproduced the ratios observed earlier by the Livermore EBIT group (Gu et al. 2004).

The ratio of lines $3C$ and $3D$ is now experimentally well established, and differences between this value and astrophysical observations are now known in most cases to be due to blending of line $3D$ with a line from Fe XVI, as first demonstrated by Brown et al. (2001) in laboratory measurements. The search for other Fe XVI lines in the iron L-shell spectra that confirms such blending is helped by the line list published recently by Graf et al. (2009).

Many theoretical approaches have been published to reproduce the laboratory data (e.g. Chen & Pradhan (2002); Fournier & Hansen (2005)). The R-matrix value by Chen & Pradhan (2002) gives a $3C/3D$ ratio of 3.27, which compares to an earlier calculation of 3.78 (Zhang & Sampson 1989) using the distorted-wave (DW) method and favorably to the measured ratio of 3.0 ± 0.1 (Brown et al. 1998). However, ratios can be deceiving, as errors in the numerator and denominator often cancel out. Indeed, when comparing the calculated absolute cross sections for $3D$ and $3C$ to those measured four years later Brown et al. (2006), the old DW calculations (Zhang & Sampson 1989) do a better job in reproducing the measurement than the R-matrix result of Chen & Pradhan (2002).

R-matrix calculations published subsequently by Chen (2007) revised the value for $3C$ and attained much better agreement with the cross section measurements. A disagreement of 25%, however, remained between the measured and calculated values. A year later, Chen (2008) reaffirmed his most recent results and suggested the difference with experiment was caused by an experimental error. In a seperate paper Chen (2008) argued that the theoretical values used for normalization of the experimental data were incorrect by 24%, i.e., by the amount needed to produce agreement between theory and measurement.

More recently, Chen et al. (2009) has argued that the theoretical X-ray line polarization adjustment used in the experiment is incorrect. He argued that the polarization may differ as much as 30% from the values given by the theory of Zhang et al. (1990). This assertion has now been refuted by Zhang et al. (2010).

While a 24% error in the theoretical values used for normalization of the experimental data would bring excellent agreement with the absolute cross sections, as mentioned by Chen (2008) and more recently by Gillaspy et al. (2011), there is doubt that this is the full or correct answer. First, the ratio of $3C/3D$ predicted by the most recent R-matrix calculations

is 2.74, which is 10% too small (while the earlier ratio was 10% too big). Second, the issue of calculating the correct cross section is less a matter of including all the many resonances, as is attempted by the R-matrix method, than a matter of correctly mixing the two upper levels of lines $3C$ and $3D$. An attempt to do this correctly was outlined by Gu (2009). Publication of this paper was unfortunately stopped by a referee who favored the R-matrix approach.

Progress has also been made concerning the $2p - 3s$ transitions. A recent measurement at Livermore concentrated on the radiative rate of the $M2$ transition. Predictions varied between 4.0 and 7.2 μs. The measurement narrowed this to 4.9 μs (Crepo López-Urrutia & Beiersdorfer 2010).

A recent effort has noted that Fe XVII dielectronic recombination satellites can be observed in *Chandra* spectra (Beiersdorfer et al. 2011). These can be used to determine the electron temperature experienced by the Fe^{16+} ions. Investigations will be needed to fully explore this diagnostic.

6. Charge Exchange

Historically, charge exchange has been considered relevant mostly as a recombination mechanism that reduces the average ionization fraction of a given plasma. In the past decade, charge exchange has been recognized as an X-ray line formation mechanism, which can add significant flux to the soft X-ray background (e.g., Wargelin et al. (2009)).

A variety of measurements of charge exchange cross sections of astrophysical ions colliding with neutral molecules have been carried out in recent years (Mawhorter et al. 2007; Djurić et al. 2008; Simcic et al. 2010a,b). These measurements employed the electron cyclotron resonance ion source at the Jet Propolusion Laboratory.

X-ray spectra produced by charge exchange have also been reported (Beiersdorfer et al. 2008; Frankel et al. 2009; Ali et al. 2010). In most cases, the theoretical description does not match the experimental data. The observed discrepancies are much worse than those afflicting the "Fe XVII problem" discussed above. An X-ray measurement of the Lyman transitions of argon and phosphor produced by charge exchange and reported by Leutenegger et al. (2010) demonstrated that even for such simple systems, there is no theoretical description that can match measurements: Theory predicts that the Lyman series emission for the two hydrogenlike ions should look similar, but the measurements showed unexpectedly that the two spectra look strikingly different. This means that X-ray production by charge exchange needs a lot more laboratory investigations before a satisfactory X-ray production model can be put together.

7. Conclusion

The need for accurate laboratory X-ray data persists unabatedly. However, specific needs have changed, as astronomers have shifted their sights to different objects. Photoionization spectra and line formation by charge exchange are two important new areas with many needs.

Work at LLNL was performed under the auspices of DOE under contract DE-AC53-07NA27344 and supported by NASA's APRA program under contracts NNH07AF81I and NNG06WF08I.

REFERENCES

Ali, R., Neill, P. A., Beiersdorfer, P., Harris, C. L., Schultz, D. R., & Stancil, P. C. 2010, ApJ, 716, L95

Beiersdorfer, P. 2003, Ann. Rev. Astron. Astrophys., 41, 343

Beiersdorfer, P., Behar, E., Boyce, K. R., Brown, G. V., Chen, H., et al. 2002, ApJ (Lett.), 576, L169

Beiersdorfer, P., Bitter, M., von Goeler, S., & Hill, K. W. 2004, ApJ, 610, 616

Beiersdorfer, P., Gu, M. F., Lepson, J. K., & Desai, P. 2011, Astr. Soc. Pac., in press

Beiersdorfer, P., Schweikhard, L., Liebisch, P., & Brown, G. V. 2008, ApJ, 672, 726

Brown, G. V., Beiersdorfer, P., Chen, H., Chen, M. H., & Reed, K. J. 2001, ApJ, 557, L75

Brown, G. V., Beiersdorfer, P., Chen, H., Scofield, J. H., Boyce, K. R., et al. 2006, Phys. Rev. Lett., 96, 253201

Brown, G. V., Beiersdorfer, P., Kahn, S. M., Liedahl, D. A., & Widmann, K. 1998, ApJ, 502, 1015

Bryans, P., Badnell, N. R., Gorczyca, T. W., Laming, J. M., Mitthumsiri, W., & Savin, D. W. 2006, ApJ (Suppl.), 167, 343

Bryans, P., Landi, E., & Savin, D. W. 2009, ApJ, 691, 1540

Chen, G.-X. 2007, Phys. Rev. A, 76, 062708

—. 2008, Phys. Rev. A, 77, 022701

—. 2008, Phys. Rev. A, 77, 022703

Chen, G. X., Kirby, K., Brickhouse, N. S., Lin, T., & Silver, E. 2009, Phys. Rev. A, 79, 062715

Chen, G. X., Kirby, K., Silver, E., Brickhouse, N. S., Gillaspy, J. D., Tan, J. N., Pomeroy, J. M., & Laming, J. M. 2006, Phys. Rev. Lett., 97, 143201

—. 2007, Phys. Rev. Lett., 99, 109902

Chen, G. X. & Pradhan, A. K. 2002, Phys. Rev. Lett., 89, 013202

Cornille, M., Dubau, J., Faucher, P., Bely-Duabu, F., & Blanchard, C. 1994, Astron. Astrophys. Suppl., 105, 77

Crepo López-Urrutia, J. R. & Beiersdorfer, P. 2010, ApJ, 721, 576

Djurić, N., Smith, S. J., Simcic, J., & Chutjian, A. 2008, ApJ, 679, 1661

Fournier, K. B. & Hansen, S. B. 2005, Phys. Rev. A, 71, 012717

Frankel, M., Beiersdorfer, P., Brown, G. V., Gu, M. F., Kelley, R. L., Kilbourne, C. A., & Porter, F. S. 2009, ApJ, 702, 171

Gillaspy, J. D., Lin, T., Tedesco, L., Tan, J. N., Pomeroy, J. M., Laming, J. M., Brickhouse, N., Chen, G., & Silver, E. 2011, ApJ, 728, 132

Graf, A., Beiersdorfer, P., Brown, G. V., & Gu, M. F. 2009, ApJ, 695, 818

Gu, M. F. 2009, ArXiv e-prints, 0905.0519

Gu, M.-F., Beiersdorfer, P., Brown, G. V., Chen, H., Boyce, K. R., Kelley, R. L., Kilbourne, C. A., Porter, F. S., & Kahn, S. M. 2004, ApJ (Lett.), 607, L143

Gu, M. F., Beiersdorfer, P., & Lepson, J. K. 2011, ApJ, 732, 91

Hahn, M., Bernhardt, D., Lestinsky, M., Müller, A., Novotný, O., Schippers, S., Wolf, A., & Savin, D. W. 2010, ApJ, 712, 1166

Laming, J. M., Kink, I., Takacs, E., Porto, J. V., Gillaspy, J. D., et al. 2000, ApJ, 545, L161

Lepson, J., Beiersdorfer, P., Clementson, J., Gu, M. F., Bitter, M., Roquemore, L., Kaita, R., Cox, P. G., & Safronova, A. S. 2010, J. Phys. B, 43, 144018

Lepson, J. K., Beiersdorfer, P., Gu, M. F., & Desai, P. 2011, these Proceedings

Lestinsky, M., Badnell, N. R., Bernhardt, D., Grieser, M., Hoffmann, J., et al. D. 2009, ApJ, 698, 648

Leutenegger, M. A., Beiersdorfer, P., Brown, G. V., Kelley, R. L., Kilbourne, C. A., & Porter, F. S. 2010, Phys. Rev. Lett., 105, 063201

Mawhorter, R. J., Chutjian, A., Cravens, T. E., Djurić, N., Hossain, et al. 2007, Phys. Rev. A, 75, 032704

Phillips, K. J. H., Greer, C. J., Bhatia, A. K., Coffey, I. H., Barnsley, R., & Keenan, F. P. 1997, Astron. Astrophys., 324, 381

Schmidt, E. W., Bernhardt, D., Hoffmann, J., Lestinsky, M., Lukić, D. V., Müller, A., Orlov, D. A., Savin, D. W., Schippers, S., & Wolf, A. 2009, J. Phys. Conf. Ser., 163, 012028

Schmidt, E. W., Schippers, S., Bernhardt, D., Müller, A., Hoffmann, J., et al. 2008, Astron. Astrophys., 492, 265

Simcic, J., Schultz, D. R., Mawhorter, R. J., Čadež, I., Greenwood, J. B., Chutjian, A., Lisse, C. M., & Smith, S. J. 2010a, Phys. Rev. A, 81, 062715

Simcic, J., Schultz, D. R., Mawhorter, R. J., Greenwood, J. B., Winstead, C., McKoy, B. V., Smith, S. J., & Chutjian, A. 2010b, ApJ, 722, 435

Simon, M. C., Crespo López-Urrutia, J. R., Beilmann, C., Schwarz, M., Harman, Z., et al. 2010b, Phys. Rev. Lett., 105, 183001

Simon, M. C., Schwarz, M., Schmitt, B. L., Beilmann, C., Epp, S. W., et al. 2009, J. Phys. Conf. Ser., 194, 012009

Simon, M. C., Schwarz, M., Epp, S. W., Beilmann, C., Schmitt, B. L., et al. 2010a, J. Phys. B, 43, 065003

Wargelin, B. J., Juda, M., & Slavin, J. D. 2009, in Aip Conf. Series, Vol. 1156, AIP, ed. R. K. Smith, S. L. Snowden, & K. D. Kuntz, 85

Zhang, H. L., Fontes, C. J., & Ballance, C. P. 2010, Phys. Rev. A, 82, 036701

Zhang, H. L. & Sampson, D. H. 1989, At. Data Nucl. Data Tables, 43, 1

Zhang, H., Sampson, D., & Clark, R. 1990, Phys. Rev. A, 41, 198

This preprint was prepared with the AAS LaTeX macros v5.2.

NASA LAW, October 25-28, 2010, Gatlinburg

Low-Energy electron-ion and ion-atom collisions: progress and needs for modeling of future NASA astrophysics observations

P. C. Stancil[1]

Department of Physics and Astronomy and Center for Simulational Physics, University of Georgia, Athens, GA 30602-2451

stancil@physast.uga.edu

ABSTRACT

Nearly every class of astrophysical environment is characterized by some physical property residing out of equilibrium and in many cases, far from equilibrium. In such environments, collisions play a vital role in establishing the ionization balance, thermal balance, and specie internal level populations. Detailed modeling of astrophysical environments, required to interpret and to extract the maximum scientific information from NASA space-based observations, rely on the availability and accuracy of collisional data. A review of recent progress, needs, and challenges in the experimental and theoretical determination of low-energy collisional processes involving electrons, atomic ions, and neutrals is given, though far from comprehensive. The focus is limited to excitation by low-energy electron and atom collisions and charge exchange, with the former addressing both electronic and fine-structure excitation.

1. Introduction

In the analysis of astronomical spectra, the first consideration is the identification of the individual absorption or emission features by matching to wavelength tabulations of atomic, molecular, and/or solid-state data obtained in the laboratory. Typically, such analyses give an indication of the elements and species present in the observed source, but far more information can be gleamed from detailed models of the environment, which attempt to include as much physics and chemistry as possible and appropriate. Such models require as (one type of) input, collisional data describing various interactions between the constituents present in the environment. In certain regimes, some properties may approach an equilibrium

limit in which collisional data are not needed, but this is generally not the case for most astrophysical environments.

In this review, the focus is primarily on low-temperature environments such as interstellar clouds, protoplanetary disks, photodissociation regions, X-ray dominated regions, and related photoionized gaseous nebulae, which typically have temperatures less than 50,000 K. Here we consider primarily inelastic collisions. which change the internal level of the target atom or ion, but charge exchange is also addressed. The latter is a reactive process which changes the ionization state of both reactants. To remain within the low-temperature regime, we restrict consideration of ion charge q to less than 6.

The review is also constrained to advances that have occurred following the previous NASA LAW meeting (Weck, Kwong, & Salama 2006). The status of the field through the summer of 2008 was reviewed by Peach, Dimitrijevic, & Stancil (2008) for processes relevant to astrophysics. As this survey is necessarily far from comprehensive, references to additional work can be found in the bibliographic database at the Oak Ridge National Laboratory Controlled Fusion Atomic Data Center (CFADC, www-cfadc.phys.ornl.gov).

2. Electron Collisions with Atoms and Ions

Of all inelastic collisional processes, the one recognized as the most important to the vast majority of astrophysical environments is electron impact excitation (EIE). It plays a role in both photoionized- and collisionally-ionized gas and is important as a diagnostic of electron density, electron temperature, and elemental abundances (see, for example, Osterbrock & Ferland 2006). EIE is important in determining the internal level populations of atoms and molecules and therefore contributes to the emission spectrum and radiative cooling. Results are generally given in the form of collision strengths or effective collision strengths, but tabulations are generally not very comprehensive. Some sources for EIE data include the Atomic Data for Astrophysics webpage (www.pa.uky.edu/ṽerner/atom.html) and the CFADC webpage (www-cfadc.phy.ornl.gov/data_and_codes/aurost/aurost_excit/home.html).

2.1. Electronic Excitation due to Electron Impact

Primarily, work on EIE has focused on electronic level excitation which is readily amendable to both experimental and theoretical investigations. Experiments are typically performed for electron-ion collisions using either the merged electron-ion beam energy loss approach or the electron beam ion trap (EBIT), though other methods have been developed.

A review of experimental EIE approaches was given by Bannister et al. (1998).

A variety of theoretical approaches have been developed to treat EIE. Earlier work involved perturbation methods, but for the past two decades, the preferred method has been some variant of the R-matrix approach, using either the LS or intermediate couplings schemes.

As a typical example, the EIE process

$$\mathrm{S}^{5+}(^2\mathrm{S}) + \mathrm{e}^- \rightarrow \mathrm{S}^{5+}(^2\mathrm{P_J}) \tag{1}$$

was measured with the merged electron-ion beam approach at ORNL for electron energies from 12 to 20 eV (Wallbank et al. 2007) and found to be in reasonable agreement with R-matrix calculations.

Work with R-matrix calculations are making tremendous strides in terms of both problem size and sophistication. EIE calculations for the complicated $\mathrm{Fe}^{4+}(3d\,^5D)$ into a number of excited states involved 2400 channels on a supercomputer and found significant enhancements in collision strengths compared to previous work done with smaller bases (Ballance, Griffin, & McLaughlin 2007). Work on Fe^{2+} showed that non-relativistic treatments for both collision strengths and radiative transition probabilities were insufficient. Dirac R-matrix calculation were need to improve agreement between observed and modeled Fe III lines in the Orion Nebula (Bautista et al. 2010).

R-matrix calculations have also been performed for neutrals. An example is the work of Barklem (2007) for EIE of oxygen from its three lowest electron configurations $(2p^4, 3s, 3p)$. Rate coefficients were presented for transitions between the seven lowest LS states between 1000 and 50,000 K and found to be in good agreement with the sparsely available experimental and prior theoretical results. The results are relevant to a range of environments where non-LTE modeling of OI is vital.

While much progress continues to be made, there is a continual need for experimental benchmarks particularly for lowly-charged Fe ions and neutrals. It has been pointed out by Sterling et al. (2010) that EIE data for so-called neutron-capture elements, which include Se, Kr, Xe, Br, Rb, ..., are lacking. Emission lines from these species have been detected in planetary nebulae and could be used to explore neutron-capture nucleosynthesis in AGB and post-AGB stars when their photospheres are enshrouded.

2.2. Fine-Structure Excitation due to Electron Impact

Electron collisions are also important for exciting the fine-structure levels within the ground electronic term of atoms and atomic ions. The process is typically important in relatively cool and/or molecular environments and often results in very intense infrared emission. As such, it plays an important, if not dominating role, as a cooling mechanism, but also may provide important temperature, density, and ambient radiation diagnostics.

Measurements of fine-structure excitation are rare and few calculations have been performed over the past four years. However, computations of the collision strengths for C^+ and Si^+ with the R-matrix method were completed by Tayal (2008a,b).

3. Heavy-Particle Collisions of Atoms and Ions

In most astrophysical environments the dominant species are typically H, He, and H_2, though H^+ may also be abundant. These will interact with metal atoms and ions through a variety of processes. At the low energies typical of most environments, a molecular wave function description of the scattering complex is usually the most appropriate. At higher energies, semiclassical and atomic-orbital approaches become valid.

3.1. Electron Capture due to Ion-Neutral Collisions

One of the primary heavy-particle collisional processes is that of charge exchange (or charge transfer or electron capture) which may involve the collision of an ion with an atom and an exchange of an electron, so-called single electron capture (SEC). A variety of experimental approaches have developed that can measure a variety of parameters from the total charge transfer cross section to the relative photon yield following capture to a particular internal level. For a review of experimental approaches, see Havener (2001). As mentioned above, a variety of theoretical approaches have also been developed to treat charge exchange. Brief reviews are given in Stancil (2001) and Krasnopolsky, Greenwood, & Stancil (2004).

Traditionally, charge exchange has primarily been studied for collisions of ions with atomic H and some activity has occurred since the last NASA LAW. As an example, Bruhns et al. (2008) measured the total charge transfer cross section for the process

$$Si^{3+} + H \rightarrow Si^{2+} + H^+ \tag{2}$$

using the merged-beam approach between 40 and 3000 eV/u. Excellent agreement was found

with earlier molecular orbital calculations. Work has also occurred for He targets with the molecular calculation by Wu et al. (2009) for O^{3+} + He, as a recent example.

On the other hand, very little work has occurred for proton collisions with neutral atoms. It is very difficult to estimate rate coefficients in such cases (see Stancil 2001) and the often adopted Langevin limit may be a poor approximation. As an example, it was found that models of Fe I features in damped Lyman α clouds could not reproduce the observations suggesting that the Fe + H^+ charge exchange rate estimate adopted in the model was too large (Jones et al. 2010). Similar to the case of EIE, Sterling et al. (2010) have pointed out that charge exchange measurements and calculations are practically non-existent for neutron-capture elements. As a minimum, for modeling of planetary nebulae spectra, charge transfer rate coefficients are needed for Se, Kr, and Xe ions with $q = 1 - 5$ colliding with H.

3.2. Fine-Structure and Electronic Excitation

While electron collisions (EIE) are typically the primary population mechanism for excited atoms and ions, in many environments neutral colliders may be competitive or even dominate. This is particularly true for fine-structure excitation.

As for the case of electron fine-structure excitation, measurements for neutral atom excitation are rare so that calculations are adopted. Recent work appears to be limited to the excitation of C and O fine-structure levels by H impact (Abrahamsson et al. 2007). Adopting state-of-the-art molecular structure calculations with a molecular scattering approach, they obtained rate coefficients which were larger by a factors of 2-4 compared to earlier work.

Recent activity in the modeling of protoplanetary disks (see, for example, Meijerink et al. 2008) have focused on a number of IR diagnostics which were observed by *Spitzer* and potentially be observed by *Herschel*: [SI], [NeII], and [NeIII]. These lines result from transitions between fine-structure levels which are excited by both electrons and H. Unfortunately, rate coefficients due to H collisions are not available.

Neutral atoms can also contribute to electronic state excitation and become particularly important when the electron abundance is small. Recent calculations have been performed for the O $^3P \rightarrow ^1D$ excitation due H (Krems et al. 2006) and Na $^2S \rightarrow ^2P$ excitation due to He (Lin et al. 2008).

4. Conclusion

In summary, collisions due to electron and neutral atom impact play a variety of important roles in low-temperature astrophysical gases. Progress has been made in measuring and/or computing cross sections and rate coefficients for a number of collision systems and processes. However, as the sensitivity of detectors from the submm to the x-ray improve, as the variety of astronomical objects grows, and as the breath of interest of astronomers expands, the need for collisional data on unstudied species and the need for the reduction in the uncertainty of available collisional data will remain constant.

This work was supported in part by NASA grants NNX09AC46G and NNX10AD56G from the Astronomy and Physics Research and Analysis Program and the Astrophysics Data Program, respectively.

REFERENCES

Abrahamsson, E., Krems, R. V., & Dalgarno, A. 2007, ApJ, 654, 1171

Ballance, C. P., Griffin, D. C., & McLaughlin, B. M. 2007, J. Phys. B, 40, F327

Bannister, M. E., et al. 1998, in *Atomic Processes in Plasmas*, M. S. Pindzola and E. Oks, AIP Press: New York, 149

Barklem, P. S. 2007, A&A, 462, 781

Bautista, M. A., et al. 2010, ApJ, 718, 189

Bruhns, H. et al. 2008, Phys. Rev. A, 77, 064702

Havener, C. C. 2001, in *Spectroscopic Challenges of Photoionized Plasmas*, ASP Conf. Ser. 247, p. 17

Jones, T. M. et al. 2010, ApJ, 715, 1497

Krasnopolsky, V. A., Greenwood, J. B., & Stancil, P. C. 2004, Space Sci. Rev., 113, 271

Krems, R. V., Jamieson, M. J., & Dalgarno A. 2006, ApJ, 647, 1531

Lin, C.Y. et al. 2008, Phys. Rev. A, 78, 052706

Meijerink, R. et al 2008, ApJ, 676, 518

Osterbrock, D. E. & Ferland, G. J. 2006, *Astrophysics of Gaseous Nebulae and Active Galactic Nuclei*, Univ. Science Book: Sausalito

Peach, G., Dimitrijevic, M. S., & Stancil, P. C. 2008, *Division XII, Commission 14, Working Group, Collision Processes,* Proc, Intern. Astron. Union, 4, 385

Stancil, P. C. 2001, in *Spectroscopic Challenges of Photoionized Plasmas*, ASP Conf. Ser. 247, p. 3

Sterling, N. C., et al. 2010, Can. J. Phys., in press

Tayal, S. S. 2008a, A&A, 486, 629

Tayal, S. S. 2008b, ApJS, 179, 534

Wallbank, B., et al. 2007, Phys. Rev. A, 75, 052703

Weck, P. F., Kwong, V. H. S., & Salama, F. 2006, *Proc. NASA Laboratory Astrophysics Workshop*, NASA-CP 2006-214549.

Wu, Y. et al. 2009, Phys. Rev. A, 79, 062711

This preprint was prepared with the AAS LaTeX macros v5.2.

NASA LAW, October 25-28, 2010, Gatlinburg

High-energy Electron-ion and Photon-ion Collisions: Current Status and Future Prospects

T. Kallman and M. C. Witthoeft

NASA Goddard Space Flight Center, Greenbelt, MD 20771

1. Introduction

We review the current status of laboratory astrophysics work on collisions relevant to high energy astrophysics. This includes collisions between electrons and ions, and between photons and ions, in which the energy of either particle is greater than 0.1 keV. This is limited to consideration of astrophysically abundant ions, and covers techniques which are applicable outside of the high energy domain. We also neglect truly high energy processes, those which might be considered important in the treatment of cosmic ray interactions, for example, in which the energies exceed $\sim 10^5$ eV.

It should be emphasized that many of these topics were covered in more detail by others at this workshop, and more thorough reviews of many of these topics exist (Kallman & Palmeri 2007; Kjeldsen 2006). Thus, the emphasis will be on recent work, since the previous workshop in this series. Some of these developments are as follows. For theoretical calculations, there has been continued progress in the efficiency and scalability of codes such as the R-matrix package (Berrington et al. 1995). This allows treatment of larger problems than previously, and allows wider exploration of physical processes such as Dirac effects. Progress in experiment includes continued use of storage rings and traps to prepare targets in desired states, and also progress in light sources which facilitate studies of photoionization. The review is divided by process, beginning with electrons interactions.

2. Electron impact excitation (EIE)

X-ray astronomy often proceeds by fitting the ensemble of observed line emission. Given the number of lines which are needed for this, calculations are generally needed. Experiments provide key checks on the calculations, but the quantity of available experimental data is generally not sufficient to be used for many lines. Calculations are generally divided into two parts: first the structure of the electronic states of the initial ion is optimized, then these

wave functions are used in the scattering calculation. Calculations of structure are common to many of the topics in this review. Current calculations are all based on the treatment of the many electron system as an anti-symmetrized product of one electron basis function, with the electron correlation effects being treated via the configuration interaction (CI) formalism (Cowan 1981). Calculations are distinguished by their treatments of relativistic effects (full Dirac vs. non-relativistic with corrections) along with their treatments of electron coupling. Key questions at this time include: the number of configurations needed in the CI expansion and the importance of relativistic effects on the resonance structure.

The two methods most widely used for scattering calculations are distorted wave and R-matrix. Distorted wave (DW) remains workhorse for many purposes (Bhatia 2000), though implementation of parallel versions of the R-matrix codes has recently greatly expanded the range of problems which can be addressed.

An example showing the importance that the size of the configuration interaction expansion can have on electron impact excitation cross sections is shown in figure 1. These are Dirac R-matrix (DARC) calculation of EIE in Fe^{5+}. The ground level configuration is $3p^6\ 3d^4$. Shown are two calculations: 328 levels (dashed) includes 4s configurations plus one $3p^5$ configuration and 1728 levels (solid) including two $3p^4$ configurations. The increase in numbers of levels results in a $\sim$10% effect on the upsilons for the many transitions in this ion. This indicates both the scale of calculations which are now possible, and the magnitude of the improvement when the CI expansion is increased.

2.1. Relativistic effects in EIE

Relativistic effects can be important for accurately determining the positions of resonances in heavy systems. Berrington et al. (2005) have shown a comparison of a Dirac R-matrix calculation with a semi-relativistic, Breit-Pauli R-matrix calculation (BPRM) for Fe^{14+}. This demonstrates the degree of uncertainty associated with BPRM which is largest at low temperatures where resonant enhancement is most important, and is $\simeq$20%. Beyond $T = 4 \times 10^6$ K, the agreement between the two methods is quite good (as is assumed in the bulk of the literature for similar ion stages of Fe). This comparison demonstrates, however, the caution that must be taken when using any excitation data, regardless of the source, at low temperatures where the precise position of near-threshold resonances are vital for obtaining the correct effective collision strengths.

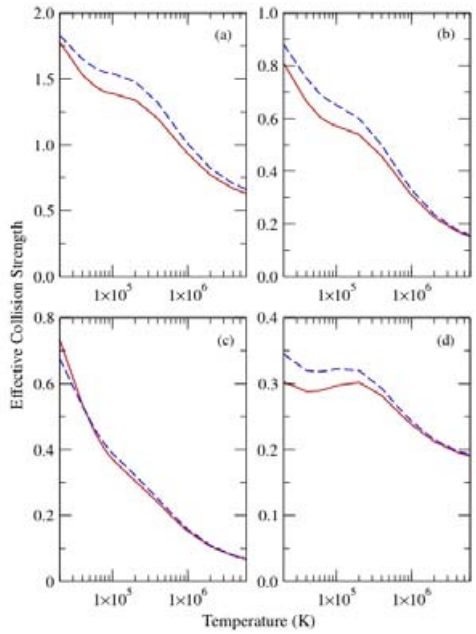

Fig. 1.— Effect on upsilons for EIE of increase in CI expansion size (Ballance and Griffin 2008).

2.2. Absolute Measurements of EIE

A key challenge for experimental methods is the measurment of absolute cross sections, since this requires knowledge of the number of target ions in addition to the final state yield. A recent example in which this was done is the energy loss measurement carried out a merged beam experiment at JPL (Hossain et al. 2007). Results are shown in figure 2 for the fine-structure transition in Fe^{13+} and compared with an 18-state (dashed) and a 135-state, BPRM (solid) R-matrix calculations.

3. Electron impact ionization (EII)

Electron-impact ionization is important for many astrophysical problems associated with coronal plasmas. Unlike EIE, with EII only a few cross sections are important, namely those connecting the ground and metastable states of the initial ion with those of the final ion. Therefore, experiment plays a large role in supplying EII data instead of merely benchmarking theory. This is particularly true for near-neutral ions where continuum coupling effects make accurate calculations difficult. There have been many measurements of EII, see the

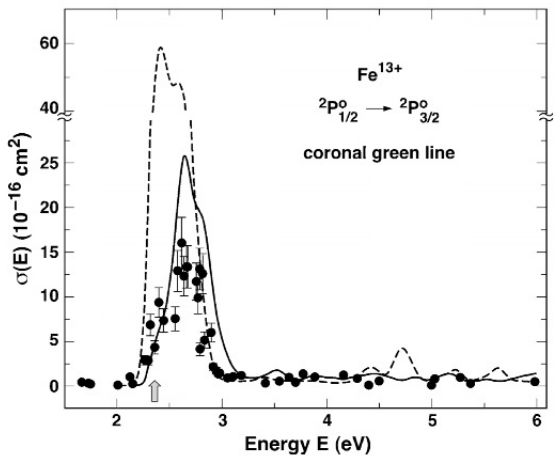

Fig. 2.— Absolute measurements of electron impact excitation of Fe^{13+} (Hossain et al. 2007).

compilations of Bryans et al. (2009) and others. Much astrophysical modeling now uses fits to experiment using formalism motivated by distorted wave calculations.

3.1. Measurements of EII with Heidelberg storage ring (TSR)

Figure 3 shows the results of measurements of the absolute cross sections using the Heidelberg storage ring. This apparatus has the advantage that the ions remain in the beam for long enough before reacting that the metastable levels decay. Shown are the cross sections for Mg^{7+} Mg^{8+}. This is part of a campaign to benchmark theory for all isoelectronic sequences. Shown is a comparison with DW calculations.

4. Dielectronic recombination (DR)

Traditional calculations of this process are adequate for high temperature plasmas. These are inadequate at low temperature, since they do not include the autoionizing states very close to threshold. Accurate rates require knowledge of the energies of these states, which is challenging for calculations. Experiments have proven to be crucial as benchmarks and guides for calculations. Measurements using the Heidelberg storage ring (TSR) provide key validation for calculations. This apparatus provides beams of ions and electrons with low relative speed which allows measurements of near-threshold cross section. A campaign to calculate DR rate coefficients has been carried out by the ADAS collaboration (Badnell et

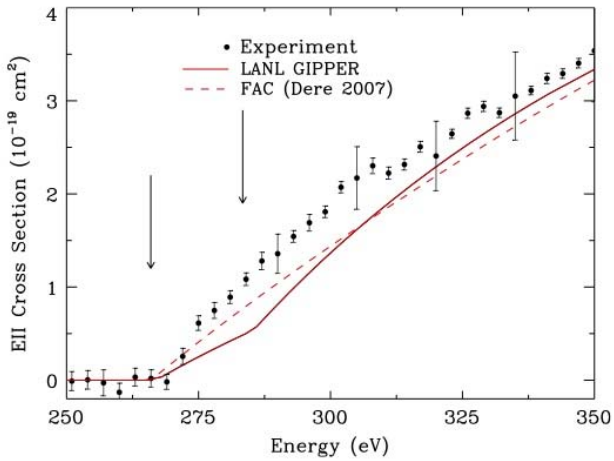

Fig. 3.— Near threshold blowup of measurement of EII from Heidelberg storage ring (Hahn et al. 2008).

al. 2003). Badnell (2006) demonstrated that the rate coefficients which had previously been in use for the third row iron ions were too low by large factors. The results of these changes to temperature DR rate coefficients have been discussed by Kallman (2010). Recent work has included the measurement of DR in Fe at low charge. DR has now been measured for Fe^{7+} – Fe^{10+} using TSR. This work has been reviewed by Schippers et al. (2010).

5. Photoionization (PI)

In astrophysics, photoionization is important in situations where there is a strong source of continuum radiation, such as close to an accreting black hole or neutron star. It also is the inverse to radiative recombination, which is universal. Photoionization is simpler to treat computationally than electron collisions, since it does not involve multiple partial waves in the final state. On the other hand, since non-thermal spectra are common in astrophysical sources, cross sections are needed which span a large range in energy. Since all astrophysical X-rays must traverse the interstellar medium, all are affected by photoabsorption by interstellar ions and neutrals, and knowledge of cross sections is key to interpreting this effect.

5.1. Calculation of PI

Calculations of photoionization based on a central potential have been available since Reilman & Manson (1979). These include both valence and inner shells. The use of R-matrix for accurate calculation of the resonance structure associated with photoionization was begun by the opacity project. It has culminated in the treatments of inner shells by Palmeri et al. (2002, 2003b); García et al. (2005); García et al. (2009); Witthoeft et al. (2009, 2011).

K-shell photoionization is affected by the spectator Auger process. This involves photoexcitation to np levels, which then decay via Auger involving L shell electrons. This leads to a series of broad resonances converging onto the K edge. An example is shown in figure 4. This shows a calculation of the cross section for Ca^{3+} near the K edge. The significance of Auger damping is apparent in the large difference between the photoabsorption (red) and photoionization (blue) cross sections.

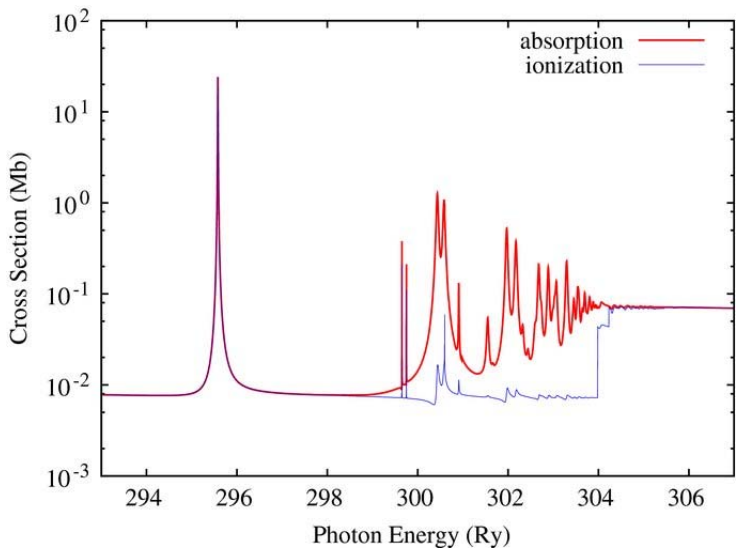

Fig. 4.— Calculations of K shell photoionization (blue) and photoabsorption (red) cross section from Ca^{3+} (Witthoeft et al. 2011)

Experimentally, these can be benchmarked using light sources and traps or beams. An example is the measurements of Ar^{8+} photoionization using an electron beam ion trap (EBIT) together with the Hamburg light source. The cross section is shown in figure 5 together with a comparison with a multi-configuration Dirac-Fock (MCDF) calculation. More such measurements will be made using this light source and the one at ICSLS.

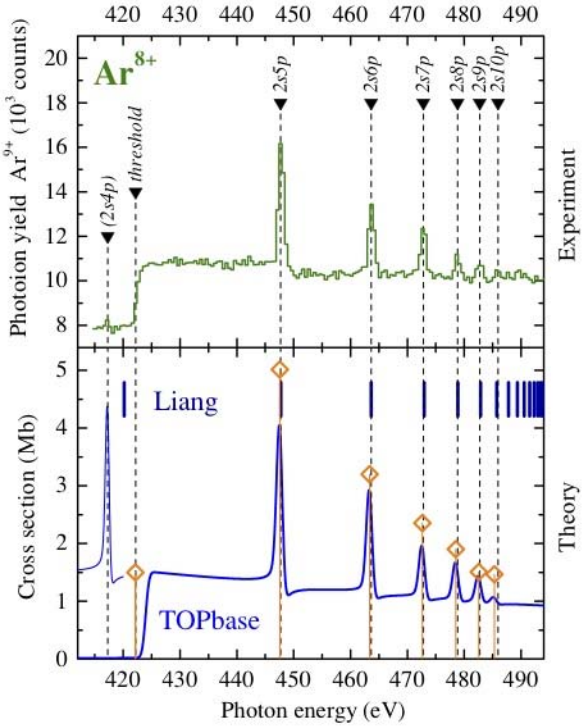

Fig. 5.— EBIT + FLASH measurement of Ar^{8+} photoionization (Simon et al. 2010)

6. Summary

Future challenges to the study of high energy electron and photon collisions in this context include: the need for accurate data for more elements, i.e. the iron peak and the low abundance odd-Z elements; rates which are appropriate to non-equilibrium situations; inner shell absorption cross sections for molecules; rates for interactions with protons, in order to obtain accurate diagnostics of the potential importance of these particles.

We thank our collaborators: M. Bautista, J. Garcia, C. Mendoza, P. Palmeri, P. Quinet. Funding for this work was provided by grant NASA 07-APRA07-0089.

REFERENCES

Badnell, N. R., et al. 2003, A&A, 406, 1151

Badnell, N., 2006 Ap. J. Lett. 651 L73

Ballance, C., and Griffin, D., 2008 JPB 41 195205

Berrington et al. 1995 Comput. Phys. Commun. 92 290

Berrington et al.2005 JPB 38 1667

Bhatia, A. K. 2000, Atomic Data Needs for X-ray Astronomy , 41

Bryans, P., Landi, E., & Savin, D. W. 2009, ApJ, 691, 1540

Cowan, R. D. 1981, Los Alamos Series in Basic and Applied Sciences, Berkeley: University of California Press, 1981,

García, J., et al. 2005, Ap. J. Supp., 158, 68

García, J., et al. 2009, Ap. J. Supp., 185, 477

Griffin, D., and Ballance, C., 2009 JPB 42 235201

Hahn et al. 2008 Ap J. 712 1166

Hossain et al., 2007 Phys Rev A 75 22709

Kallman, T. R. 2010, Sp. Sci. Rev., 157, 177

Kallman, T. R., & Palmeri, P. 2007, Reviews of Modern Physics, 79, 79

Kjeldsen, H. 2006, Journal of Physics B Atomic Molecular Physics, 39, 325

Palmeri, P., Mendoza, C., Kallman, T. R., & Bautista, M. A. 2002, Ap. J. Lett., 577, L119

Palmeri, P., Mendoza, C., Kallman, T. R., Bautista, M. A., & Meléndez, M. 2003b, Ast. Ap.,410, 359

Reilman, R. F., & Manson, S. T. 1979, ApJS, 40, 815

Schippers, S., et al. 2010 Archiv:1002.35678

Simon et al. 2010 JPB 43 065003)

Witthoeft, M. C., Bautista, M. A., Mendoza, C., Kallman, T. R., Palmeri, P., & Quinet, P. 2009, Ap. J. Supp., 182, 127

Witthoeft, M. C., García, J., Kallman, T. R., Bautista, M. A., Mendoza, C., Palmeri, P., & Quinet, P. 2011, Ap. J. Supp., 192, 7

This preprint was prepared with the AAS LaTeX macros v5.2.

NASA LAW, October 25-28, 2010, Gatlinburg

Vibrations and High-frequency Rotations: Supporting Current and Future Space Missions in the Laboratory

Michael C. McCarthy

Atomic and Molecular Physics Division, Harvard-Smithsonian Center for Astrophysics, Cambridge, Massachusetts, 02138, USA

mccarthy@cfa.harvard.edu

ABSTRACT

With the *Herschel* Space Observatory now in full operation, and the launch of SOFIA and JWST expected in the next few years, it seems likely that the paradigm which has historically characterized laboratory astrophysics will gradually shift from 'one line, one molecule at a time' to one more geared towards rapid data acquisition, wide frequency bandwidth, and high detection sensitivity at high frequency. As the recent detection of the fullerenes C_{60} and C_{70} with NASA's Spitzer Space Telescope vividly demonstrates, molecules of considerably complexity are known or thought to possess strong spectral features in the frequency bands that will soon be accessible to many of these new frontier space observatories — a general indication that highly accurate rotation-vibrational data will be needed for organic molecules over a wide range of sizes and structures. This paper highlights some of the most critical spectroscopic data that will be required to support these space missions, and laboratory approaches that might be used to provide this information.

1. Recent Successes: H_2O^+ and Fullerenes

2010 has been a remarkably successful year for laboratory astrophysics, highlighted by two significant astronomical discoveries which have only been possible owing to high-quality laboratory measurements: detection of radio lines of H_2O^+ (Ossenkopf et al. 2010, Gerin et al. 2010) with the HIFI instrument on board *Herschel*, and detection of the infrared spectrum of buckministerfullerene C_{60} and the related fullerene C_{70} (Cami et al. 2010) with the Spitzer

Space Telescope. Following the initial discovery of H_2O^+ toward star forming regions, astronomical work on this fundamental ion has proceeded quickly, with its subsequent detection along many different lines of sight, mainly diffuse clouds and massive star forming regions such as Sgr B2(M) (Schilke et al. 2010) and Orion KL (Gupta et al. 2010), but extragalactic sources as well. The derived *ortho/para* ratio or spin temperature of 21±2 K towards Sgr B2(M) is unexpected; it can not be explained by any known formation mechanism, implying instead that a process exists which produces both spin states in equal amounts.

Cami and co-workers recently reported the infrared spectrum of Tc 1, an unusual planetary nebula, which exhibits strong emission at wavelengths that coincide with laboratory measurements of neutral C_{60} and C_{70} (Krätschmer et al. 1990). On the basis of the relative strength of three C_{60} emission bands they concluded that the excitation temperature of the fullerenes is approximately 330 K and thermal, and that the two molecules amount to a few percent of the available cosmic carbon. Separately, Sellgren et al. (2010) reported evidence for C_{60} in the reflection nebula NGC 7023, and on the basis of extensive analysis of archived Spitzer data, García-Hernández et al. (2010) recently reported evidence for C_{60} in four other sources. Several of these sources are also characterized by strong emission features due to polycyclic aromatic hydrocarbons (PAHs), suggesting that further work is needed to understand the chemical pathways by which large organic molecules — either those completely devoid or rich in hydrogen – are synthesized.

There are a number of other recent examples in which laboratory astrophysics has played an important role in identifying and interpreting data from NASA space missions. The recent detection of H_2Cl^+ (Lis et al. 2010), for example, was based on the laboratory work of Araki et al. (2001), and new astronomical observations in the THz band of other light hydrides such as OH^+, HF, and commonly observed interstellar molecules such as methanol, HCN, SiC_2, etc. have only been possible because precise rest frequencies for many of these species have been measured in the laboratory. The large body of experimental work on the infrared spectra of PAHs has been invaluable in interpreting numerous Spitzer and ISO studies of local and extragalactic environments.

2. Data Needs at THz and far-IR wavelengths

Because *Herschel*, SOFIA, and JWST will cover such a wide spectral range, from 650 to about 0.5 μm, with unprecedented sensitivity, angular resolution, and modest to very high spectral resolution (ranging from 10^3 to 10^7), the laboratory astrophysics requirements are many and highly varied, encompassing, but not limited to rotational and vibrational spectroscopy of many entirely new species to improved line measurements for a wide range

of well-studied interstellar molecules. To properly support current and future missions, such studies will need to be undertaken over a wide range of abundance (e.g. isotopic species), and excitation temperature, since as a general rule, objects with small angular scale, such as circumstellar shells, protoplanetary disks, and planetary atmospheres are often quite warm (i.e. 300 to several 1000 K). In this context, a number of complementary experimental and theoretical studies will be needed. In light of the high quality of new astronomical data which will become routinely available, commensurate advances in sensitivity and frequency agility of laboratory techniques, analysis methods, and improved theoretical tools for analyzing complex molecules systems will likely be required.

2.1. Light (Ionic) Hydrides

Although the spectroscopy of radicals and ions derived from water is fairly complete, with the exception of H_2O^+ for which the fundamental transition is uncertain to approximately ±50-100 MHz (see Neufeld et al. 2010), no positive ions of NH_3 and only CH^+ in the ion network of CH_4 have been adequately characterized by high-resolution spectroscopy. For many there is simply no spectroscopic data, while for a few others, such as CH_5^+, their highly fluxional nature is a major impediment to spectral analysis and assignment. Many of these light ionic hydrides are thought to be intermediates in the chemistry of interstellar clouds, and can likely be identified in space provided that precise laboratory data is available to guide an astronomical search. Analogous ions containing second-row elements such as sulfur and phosphorus may also be of laboratory and astronomical interest.

In circumstellar shells of certain evolved carbon stars and other rich astronomical sources, the spectra of metal hydrides such as SiH^+, HSO^+, etc. are probably good candidates for astronomical detection. Here too, the laboratory measurements are either incomplete or entirely unknown. Absorption spectroscopy of these and related species up to about 2 THz may be feasible using fairly standard commercial components in which the target species is produced in an extended negative glow by magnetically confining the discharge plasma.

2.2. Broad Program in Rotational Spectroscopy

As expected, unbiased line surveys with *Herschel*/HIFI such as the HEXOS survey of the chemically rich Orion Nebula have identified a large number of molecular lines (e.g., Crockett et al. 2010). Many of these arise from common interstellar molecules such as water, methanol, and SO, but a significant fraction have not yet been unassigned. Spectral line

surveys of other sources such as IRC+10216 and Sgr B2 are equally rich in the THz band. The open question at this point is: do these lines arise from entirely new interstellar molecules, or are they simply unassigned transitions of "interstellar" weeds? To best answer this question a broad, long-term program in laboratory astrophysical rotational spectroscopy is required. One of the more intriguing unidentified features is an absorption line near 617.8 GHz; its complex velocity structure, reminiscent of c-C_3H_2, indicates that the carrier is present in all spiral arm clouds between us and the galactic center (Matthew & Irvine 1985).

To effectively combat this deluge of new, high-quality astronomical data, a dual-pronged attack in laboratory astrophysics emphasizing the spectra of commonly observed molecules and exotic new species is needed. As is often the case, new astronomical observations in a previously inaccessible wavelength band expose the inadequacies of laboratory astrophysics measurements that, at an earlier time, were sufficient to support radioastronomical observations. With respect to known molecules, continued emphasis of a wide range of frequency, abundance (e.g.,isotopic species), and temperature (e.g. low-lying vibrational excited states) is needed. In hot core sources, for example, work on methanol and many so-called "class 2" interstellar weeds (i.e. ethyl cyanide) is incomplete. Unstable species, such as radicals and ions, and prebiotic/biogenic intermediates, such as protonated derivates methanol, methyl formate, etc., should receive high priority, because of their importance in chemical networks, and because studies of highly reactive species often drive experimental innovation.

The far-IR ($\lambda > 30$ μm) is also prime territory to detect the bending and other lower frequency vibrational modes of PAHs and other large organic molecules. Observations of strong emission features in the mid-IR (e.g., 15-21 μm region) by Spitzer and ISO have resulting in the assignments of PAHs families, and estimates of relative size and ionization state (neutral versus positively-charged) along different lines of sight using databases such as NUV-NIR and MIR-FIR (see Salama 2008, and references therein) which combine matrix and gas-phase infrared spectra and theoretical estimates. Although no assignments of individual PAHs have yet been made, the FIR region may provide such an opportunity. Recent calculations by Boersma *et al.* (2010) conclude that the FIR/sub-mm spectra of PAHs are molecule dependent, with the spectral complexity depending both on overall size and shape. Low-frequency bending modes of long carbon chains and other organic molecules are also predicted to fall in the FIR/sub-mm. Many of the characteristic bands are predicted in the 100-200 μm range, which is prime SOFIA territory using high-spectral resolution instruments such as GREAT ($R \sim 10^6 - 10^8$ between 60-200 μm).

2.3. The Need for New Laboratory Tools

New laboratory capabilities, most acutely high sensitivity in the THz band and beyond, will likely be required to detect the rotational spectra of highly reactive molecules, such as protonated species and radical ions which are difficult to produce in high abundance in the laboratory. The lack of adequate radiation sources in the 2-30 THz region is an area of particularly concern as SOFIA prepares to resume flight operations in next few years.

One promising technique now under development by the Widicus Weaver group is to improve current detection sensitivities by extending cavity ringdown spectroscopy (CRDS) into the THz band. CRDS is a highly sensitive absorption spectroscopy technique routinely used at shorter wavelengths, in which pathlengths of 1 km or more can be achieved, resulting in a commensurate increase in detection sensitivity of $10^2 - 10^4$ compared to that of conventional absorption spectrometers. There are several technical obstacles which need to be overcome, including the lack of mirrors to couple THz radiation into the cavity while maintaining high-reflectivity. A cavity design utilizing wire-grid polarizers as the reflectors holds great promise to overcome this difficulty, and a prototype instrument based on this design is reported in these proceedings (Carroll et al.). When fully-implemented, the sensitivity of a CRDS-THz instrument should rival that of Fourier transform microwave and infrared CRDS spectrometers.

2.4. Complementary Studies

In addition to a variety of new laboratory studies, a large number of complementary investigations, either experimental or theoretical, are needed to properly support new or anticipated astronomical observations. These include significant effort to improve the completeness of databases and catalogs, while developing standard and streamlined protocols by which new laboratory measurements can be efficiently incorporated into databases; robust methodologies are also needed so that the laboratory data are readily available to the astronomical community in a wide range of possible formats. Additional effort in collisional studies of many fundamental molecules are urgently needed, along with highly accurate *ab initio* studies of molecular properties, such as rotation-vibrational energy levels and transition moments (IR intensities and dipole moments). Measurements of reaction rates for many species is lacking, as are photodissociation cross-section of important species such as H_3O^+ — to highlight just a few of the more crucial needs.

3. Data Needs in the mid-IR

Because SOFIA possesses higher spectral and angular resolution compared to either Spitzer or ISO, and because JWST will have exquisite sensitivity at modest resolution (MIRI, with $R \sim 5000$), there will be a need for high-resolution data in the mid-IR, particularly in the 5-28 μm region.

3.1. H_2O, CH_4, and NH_3, and Other Abundant Species

Water, methane, and ammonia represent perhaps three of the most important molecules in the study of protoplanetary and planetary systems and of their evolution whose infrared spectra are blocked by the Earth's atmosphere. Because the inner disks of many protoplanetary systems are moderately warm (500-1500 K), it is essential that high-resolution laboratory measurements are made at these temperatures or higher, so that atmospheric models and derived atmospheric opacities are based on accurate and comprehensive spectroscopic parameters which fully account for contributions from low-lying vibrational states. Possible synergies with predictions made with highly accurate *ab initio* potentials may be significant in this regard. Other species such as CO_2 may also warrant additional laboratory work. The spectra of late-type stars are also often quite rich, with many line blends and unidentified lines, which likely require high-quality spectroscopic data of metal containing hydrides and other small molecules.

3.2. Nonpolar Molecules or Those with Unfavorable Rotational Partition Functions

There are a large number of carbon molecules for which gas-phase infrared spectra are needed, including ionic species such as $C_3H_3^+$ (Ricks et al. 2010), H_5^+ (Cheng et al. 2010), CH_5^+, etc., symmetric hydrocarbon chains such as $HC_{2n}H$ and C_n, and larger organic molecules over a wide range of structure and sizes, including (positively) charged species. The astronomical identification of C_{60}, for example, is not based on gas-phase measurements, but rather solid state data (Krätschmer et al. 1990). Now that it has been found, a sensitive search for C_{60}^+ is probably worth undertaking, provided that precise laboratory data are available.

In light of the high resolution provided by instruments such as TEXES on the IRFT ($R \sim 5 \times 10^5$) and EXES on SOFIA, the mid-IR spectra of many well-studied molecules such as HCCH will need to be systematically measurement at higher resolution. A similar limitation exists for HCN and its isotopic species, and undoubtably other species.

3.3. Molecules Containing Main Functional Groups

Systematic studies of molecules containing ten or so of the most important functional groups are also needed in the mid IR. A strong motivation for this effort is the empirical correlation between interstellar conditions approaching those required for star and planet formation, and the similarity of that chemistry to the chemistry on Earth. Organic (prebiotic) molecules possess many distinctive mid-IR spectral features which are diagnostic of their composition, structure, and functional groups. Exact wavelength positions, widths, and relative intensities for many organics are needed so that JWST MIRI spectra can be used to help determine the chemical pathways by which prebiotic molecules are assembled in interstellar environments.

3.4. Related Studies

A number of related or follow-up studies will be needed to better understand the emission processes in the IR, mid IR, and far IR. Electronic spectroscopy in the optical and UV of the same species that give rise to strong IR emission, for example, is highly desirable in this regard, and because studies at these wavelengths often provide clearer evidence for specific carriers. Owing to the very high sensitivity of JWST, strong IR emitters may be detectable at z=1 and beyond, suggesting that strong features in the near IR and optical in other galaxies may be detectible with NIRSpec and MIRI. Theoretical calculations and chemical modeling are clearly needed as part of this general effort.

3.5. New Laboratory Tools

One of the more promising techniques that might be used to detect and identify a wide range of molecules of astronomical interest in the IR has been developed by Duncan and co-workers (see Cheng et al. 2010, and references therein). By performing photodissociation spectroscopy in a reflectron time-of-flight mass spectrometer, his group has recently investigated the infrared spectroscopy of a number of protonated organic molecules, including protonated acetylene, ethylene, benzene, naphthalene, using rare gas "tags". New methods now under development by his group may eliminate the need for the rare gas atoms altogether, thus providing spectra of the free ion which can then be directly compared with astronomical spectra. Because of its intrinsically high sensitivity, high spectral resolution, and wide spectral coverage, this method might be applied with good success to organic molecules over a wide range of size and structure.

I am indebted to a number of colleagues for helpful discussions and for providing support materials for this review, including Edwin Bergin, Karin Oberg, Jose Cernicharo, Ewine van Dishoeck, Susanna Widicus Weaver, Harshal Gupta, John Pearson, Darek Lis, Frank DeLucia, Ben McCall, Farid Salama, Louis Allamandola, Michael Duncan, Eric Herbst, and Holger Müller, among others. This work was supported in part by NASA grant NNX08AE05G.

REFERENCES

Araki, M., Furuya, T., & Saito, S. 2001, J. Mol. Spec., 210, 132

Boersma, C., et al. 2010, ApJ, submitted.

Cami, J, Bernard-Salas, J., Peeters, E., & Malek, S. E. 2010, Science, 329, 1180

Cheng, T. C., et al. 2010, J. Phys. Chem. Lett. 2010, 1, 758

Crockett, N. R, et al. 2010, A&A, 521, L21

Gerin, H., et al. 2010, A&A, 518, L110

García-Hernández, D. A., et al. 2010, ApJ, 724, L39

Gupta, H., et al. 2010, A&A, 521, L47

Krätschmer, W., Lamb, L. D., Fostiropoulos, K., & Huffman, D. R. 1990, Nature, 347, 354

Lis, D. C., et al. 2010, A&A, 521, L9

Matthews, H. E., & Irvine, W. M. 1985, ApJ, 298, L61

Neufeld, D. A., et al. 2010, A&A, 521, L10,

Ossenkopf, V., et al. 2010, A&A, 518, L111

Ricks, A. M., et al. 2010, J. Chem. Phys., 132, 051101

Schilke, P., et al. 2010, A&A, 521, L11

Sellgren, K., et al. 2010, ApJ, 722, L54

Salama, F. 2008, in *Organic Matter in Space*, eds. S. Kwok & S. Sandford, Proceedings IAU Symposium No. 251, International Astronomical Union

---

This preprint was prepared with the AAS LaTeX macros v5.2.

NASA LAW, October 25-28, 2010, Gatlinburg

Spectroscopic Databases for Astronomical Applications

Linda R. Brown

Jet Propulsion Laboratory, California Institute of Technology,
4800 Oak Grove Drive, Pasadena, CA 91109, USA

Linda.R.Brown@jpl.nasa.gov

ABSTRACT

Astronomers detect new species (atoms, molecules, ions, radicals present in gas, liquid and solid phase) and determine their abundances, temperatures, pressures, velocities etc. through spectroscopic remote sensing. Nearly every physical phenomenon that influences the radiative transfer of an astronomical body can be detected and quantified using specific spectral features, provided sufficient spectroscopic knowledge is available. Collections of spectroscopic information are formed and then revised as new objectives and techniques evolve. The resulting spectroscopic databases should be complete, accurate and organized in convenient forms. Much is accessible for far- and mid-IR applications, but the available compilations are often deficient at shorter wavelengths. In this presentation, the current status of these molecular spectroscopic databases will be reviewed.

1. Introduction

Remote sensing of the universe requires extensive knowledge of molecular spectroscopy throughout the full range of the electromagnetic spectrum. With each decade, improved technologies are applied to obtain observations of gaseous features associated with the interstellar medium, stars, planets, moons, comets, etc. using space-, aircraft- and ground-based platforms. This in turn necessitates better characterization of the basic molecular spectroscopy.

The essential molecular line parameters required to quantify the spectral characteristics of vibration-rotation transitions are shown in Fig. 1. These include the line center frequency, the line intensity, the energy value of the transition lower state (to provide the temperature

dependence of the intensity) and the identity of the upper and lower states (i.e. the quantum assignment) of the transition. Parameters for the shape of spectral lines are also required. The simplest case, Doppler-limited profiles, require only knowledge of the gas temperature and molecular weight, but with environments at higher pressure, additional pressure broadening effects and their temperature dependence must be considered. The additional line parameters needed are the Lorentz widths, and pressure induced shifts in frequency. More subtle effects include line mixing, narrowing of the Doppler width, line mixing between specific transitions, and at very high pressures, collision-induced absorptions (Hartmann et al. 2008). The numerical values of the parameters can be obtained through the methods list in Fig. 1. In the ideal case, quantum mechanical models are applied to interpret laboratory measurements of each parameter set, which in turn provide model constants to calculate all the transitions needed. In practice, this approach often falls short, and the community must rely on less than perfect predictions for the essential parameters. If correct theoretical models are intractable, observers often must resort to faulty empirical line-by-line lists directly measured from laboratory spectra. For some species and some wavelength, the spectra are so crowded that individual transitions are unresolved, in which case laboratory spectra are formatted into 'absorption coefficients' or cross sections. In the worst case raw lab spectra are used directly.

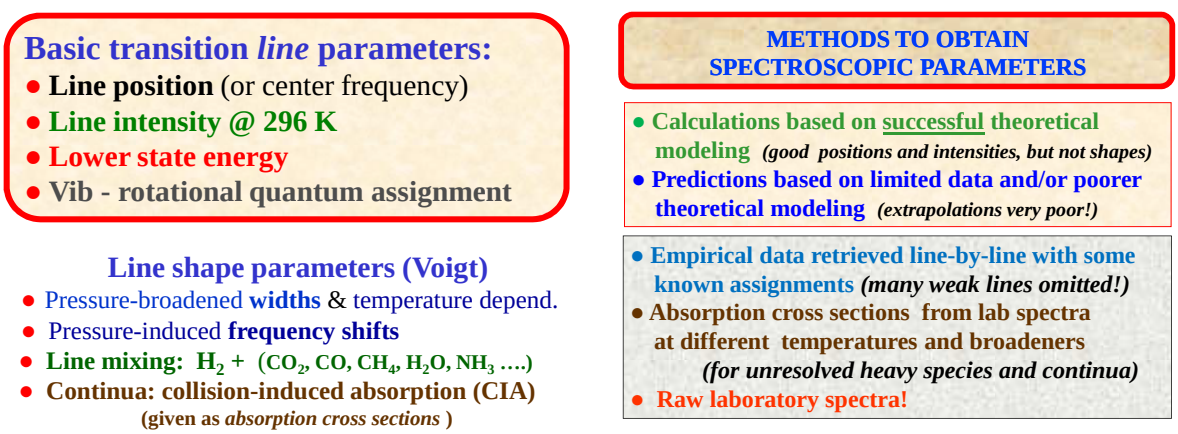

Fig. 1.— Line parameters (left) and methods to obtain them (right).

2. Spectroscopic Databases

Organized collections of spectroscopic line parameters began in the early 1970's (McClatchey et al. 1973), to respond to the needs of the remote sensing community. Currently, the main 'public' databases are **HITRAN** (Rothman et al. 2009), **GEISA** (Jacquinet-Husson et al. 2011), and the **JPL** (Pickett et al. 2010) and **CDMS** (Müller et al. 2005)

catalogs. Examples of their content are shown in Figs. 2 and 3.

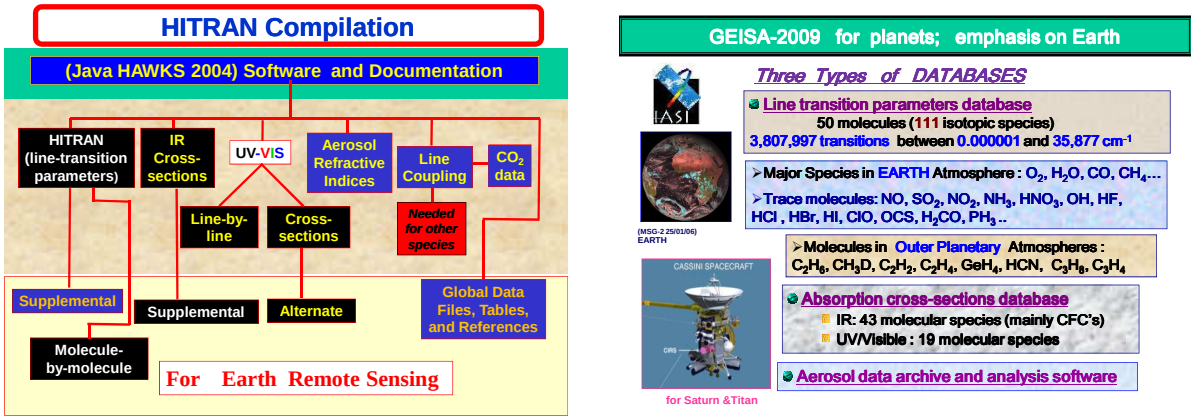

Fig. 2.— Examples of information provided by **HITRAN** and **GEISA**.

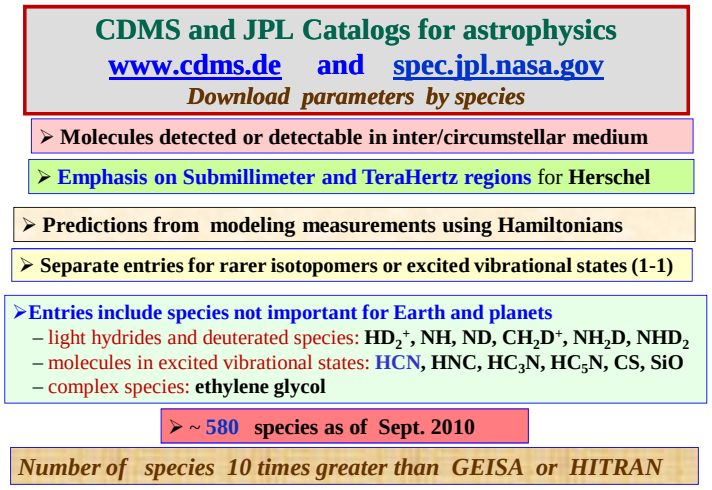

Fig. 3.— Examples of information provided by the **CDMS** and **JPL** catalogs.

HITRAN primarily serves the Earth-observing community and emphasizes the infrared wavelengths; **GEISA** was initiated to support planetary studies, but later focused on the needs of European Earth studies (because the planetary financial support was not maintained). **HITRAN** has an advisory board and holds bi-annual meetings to bring together laboratory spectroscopists and the remote sensing users in an effort to meet the evolving remote sensing needs. **HITRAN** also provides a separate collection of five molecules **HITEMP** (Rothman, et al. 2010) intended for hot gas applications. The **JPL** and **CDMS** catalogs are tailored specifically for astrophysical observations of the interstellar medium and

cover the microwave into the far-IR; these contain several hundred species, including atomic and ionic transitions.

An overview of the four compilations is shown in Fig. 4.

Current Public Databases (from Web)

Standardized formats, documentation, Quality control and FUNDED!!

Database	Websites (http://)	cm^{-1}	#Species	#Transitions
HITRAN 2008 HITEMP 2010	cfa - www.harvard.edu (/hitran) H_2O, CO_2, CO, OH, NO	0.0 to 26000 *(385 nm)*	39 + 32 xsec	2,713,968 ~ 114 million
GEISA 2009	ara.lmd.polytechnique.fr molecules planetary → terrestrial	0.0 to 35877 *(279 nm)*	50 (111 with iso)	3,807,997
JPL 2010 CMSD (Cologne)	spec.jpl.nasa.gov www.ph1.uni-koeln.de molecules, radicals, atoms for astrophysics	0. to ~500. ++ (one species up to 5600 cm^{-1})	~580	1,530,000 *at long wavelengths*

Fig. 4.— Overview of public databases of molecular line parameters.

All these databases periodically update their entries to provide the best available information and publish detailed descriptions of their contents in peer-reviewed papers. All provide some indication of the accuracies of the parameters. **HITRAN** and **GEISA** often have similar content, but the databases have different formats. They maintain websites for which users can be given permission to download the complete compilations.

It should be noted that the information at shorter wavelengths is usually incomplete or missing altogether. Then other sources of spectroscopy must be used. For the UV-VIS wavelengths, there is a wealth of information is available at the sites shown in Fig. 5, but users needing to take parameters from the different sources may encounter slightly different values for the same molecule and must evaluate for themselves which is the better set for their purposes.

If users cannot locate needed parameters in the organized databases, then there is some potentially useful information available at sites listed in Fig. 6.

The **UCL** site has a component specifically devoted to astrophysical studies, and current efforts include generating ab initio calculations for H_3^+, H_2D^+, H_2O, HDO, HCN, HeH^+, C_2H_2, C_3 and NH_3; see Tennyson et al. 2010 as an example. For CH_4 spectroscopy, there is an ongoing project in Dijon, France to map the dominate transitions up to 7000 cm^{-1}. Lower resolution cross sections are available at the Oxford site (for NH_3 and CH_4), while at

UV-VUV info (via Web) examples?

Lists?	Websites (http://)	Data
MPI-Mainz *(Oct 2010)*	www.atmosphere.mpg.de/enid/2295 *Easy to use*	840 species (atlas, cross sections)
CFA → *'other lists' on HITRAN*	www.cfa.harvard.edu/amp *VUV cross sections, energy levels and wavelengths (ASCII files)*	O_2, H_2O, O_3, C_2H_2, CO_2, CO, SO_2, N_2 NO, NO_2,N_2O
MOLAT *(2006?)*	molat.obspm.fr/index.php?page=pages/menuSpectreMol.php	VUV H_2, D_2, CO, N_2
Individual research	www.wellesley.edu/Physics/gstark/N2_ANU_cross_sections/	N_2

Fig. 5.— Websites for spectral information at short wavelengths (Visible & UltraViolet).

the **PNNL** site, 336 species related to air pollution in the Earth's atmosphere are given as cross sections obtained with dilute mixtures of each molecule in 1 bar of N_2; see Sharpe et al. 2004. The **VPL** site offers a user-friendly guide for planetary observers about what is available in **HITRAN**, **PNNL** and some other sources.

NEED *MORE*? Try specialized collections

for near-IR: *(Follow 'other lists' links on HITRAN site)*
UCL (Tennyson) www.tampa.phys.ucl.ac.uk/ftp/astrodata/
(Ab initio methods for almost possible transitions)
Oxford, UK (Irwin) www.atm.ox.ac.uk/user/irwin/band.html
(cross sections for NH_3, CH_4)
PNNL nwir.pnl.gov 336 species
(600-6000 cm^{-1} cross sections: *no funding now*)
Dijon (V. Boudon) icb.u-bourgogne.fr/titan
(linelists for CH_4 up to 6300 cm^{-1})
Virtual Planet Lab vpl.astro.washington.edu/sci/
(plots of spectra/ 0.0 –22000 cm^{-1} : PNNL+ HITRAN +)

Fig. 6.— Websites for specialized lists of spectroscopic parameters.

The above sites can be accessed openly, but in fact most astronomers gather spectroscopic results (published and unpublished) which are kept as 'privately held.' One recent example is that from Sharp and Burrows 2007. The collected parameters themselves are not openly available, but the paper provides a detailed description in which these authors do

document the sources of the spectroscopic information used for their various astronomical studies of brown dwarf and planets (solar and exosolar). Most collectors do not provide such detailed descriptions.

In the ideal case, astrophysicists would have 'one-stop' shopping for spectroscopic information at all required wavelengths. One important aspect for this is to develop 'common parameter sets' with standardized database formats. This is made difficult because different spectral wavelengths are described using different units (MHz, cm^{-1}, microns, nm, etc.) and there are different expressions in use for the transition probabilities (line strengths, line intensities, Einstein coefficients, branching ratios, etc.). However, with some major effort, this obstacle can be overcome.

The most serious problem for spectroscopic databases is the lack of 'longevity' because financial support is not sustained. Researching websites revealed a number of entries which had not been updated for several years. Worse, some links failed altogether. It seems that major efforts had been started but could not continue in operation. When the site is removed, the easy access to the information (and perhaps even the information itself) is simply gone.

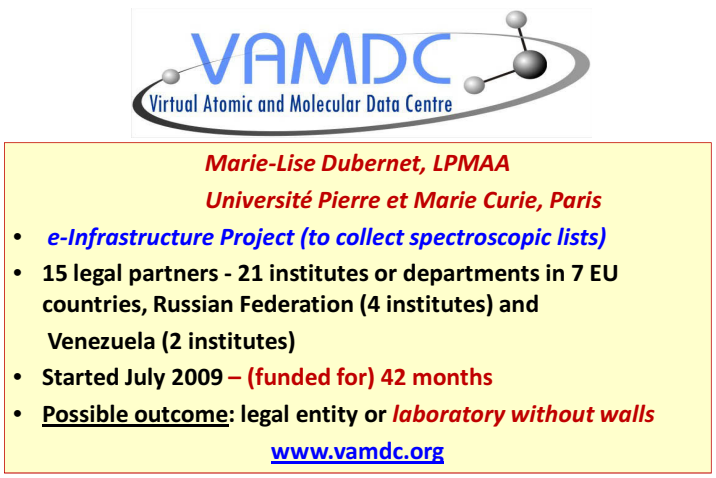

Fig. 7.— An ongoing effort to create a distribution system for spectroscopic information.

What is needed is long term commitment of funding to maintain the collective spectroscopic information for astrophysics. It can be patterned after the systems in place for earth remote sensing (i.e. **HITRAN** and **GEISA**), but it must be expanded to include all the atomic, ionic and molecular species through all the important wavelengths. Currently there is an effort in Europe to develop a system to collect, document and then openly distribute such information; see Fig. 7.

3. Conclusions

As indicated in Fig. 8, there is a serious shortfall in available spectroscopic information in databases for astrophysics. This can be remedied by a sustained effort supported over the long term.

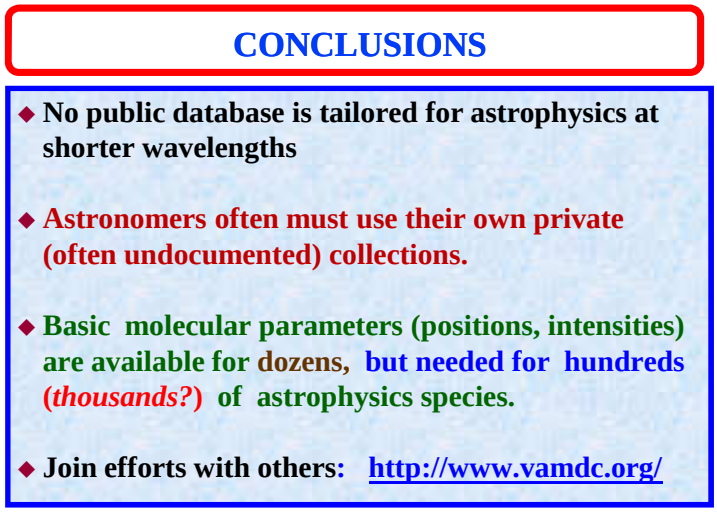

Fig. 8.— Overview of database problems to be remedied.

Part of the research described in this paper was performed at the Jet Propulsion Laboratory, California Institute of Technology, under contract with The National Aeronautics and Space Administration.

REFERENCES

Hartmann, J.-M., Boulet, C., & Robert, D. 2008, Collisional Effects on Molecular Spectra, Amsterdam, Elsevier, 1

Jacquinet-Husson N., Crepeau, L. et al., J. Quant. Spectrosc. Radiat. Transfer (accepted)

McClatchey, R. A., Benedict, W. S., Clough, S. A., Burch, D. E., Calfee, R. F. et al. AFCRL-TR-7300096, Jan. 26, 1973, Envion. Res. Papers #434

Müller, H. M. P., Schloder, F., Stutzki, J., & Winnewisser, G. 2005, J. Mol. Struct., 742, 215

Pickett H. M., Poynter, R. L., Cohen, E. A., Delitsky, M. L., Pearson, J. C., & Müller, H. S. P. 2010, J. Quant. Spectrosc. Radiat. Transfer, 111, 1617

Rothman, L. S., Gordon, I. E., Barbe, A., Benner, D. C., Bernath, P. F. et al. 2009, J. Quant. Spectrosc. Radiat. Transfer, 110, 573

Rothman, L. S., Gordon, I., Barber, R. J., Dothe, H., Gamache, R. R. et al. 2010, J. Quant. Spectrosc. Radiat. Transfer, 111, 2139

Sharp C. M., & Burrows, A. 2007, Ap. J. Sup. Ser., 168, 140

Sharp S. W., Johnson, T. J., Sams, R. L. et al. 2007, Appl. Opt., 158, 1452

Tennyson, J., Bernath, P. F., Brown, L. R., Campargue, A., Fally, S. et al. 2010, J. Quant. Spectrosc. Radiat. Transfer, 111, 2160

NASA LAW, October 25-28, 2010, Gatlinburg

Molecular Processes in the Gas Phase and on Dust Particles

E. Herbst

Departments of Physics, Astronomy and Chemistry, The Ohio State University, Columbus, OH 43210

herbst.6@osu.edu

ABSTRACT

The current state of chemical simulations of interstellar sources is discussed in the context of necessary additional work in the laboratory study of both gas-phase and grain-surface rate processes.

1. Introduction

Although spectroscopic information obtained for diverse regions of the interstellar medium (ISM) can be used to determine the molecular inventory as well as the current physical conditions, the use of chemical simulations adds additional information such as the lifetime and detailed history of the sources. The rates of chemical reactions are functions of temperature, density, and lifetime, and their use in chemical simulations results in predictions of abundances as functions of time for a given set of physical conditions. These conditions can range from simple homogeneous ones without any time dependence to heterogeneous ones that can be time-varying. Moreover, the outputs of chemical simulations need not be simple abundances. In more complex regions, it can be more advantageous to calculate total columns or even to calculate spectral lines. Whatever the output of the chemical simulation, the results must be compared with observational results so that variation of parameters can lead to their best values. For example, in cold dense cores of larger dark clouds in the interstellar medium, observed abundances of many gas-phase carbon-chain species are best reproduced at lifetimes of $10^5 - 10^6$ yr, if one starts from atoms, except for molecular hydrogen, and uses homogeneous physical conditions of $n = 10^4$ cm^{-3} and $T = 10$ K. At shorter times, the organic species have not yet had enough time to be synthesized, while at longer times they both accrete onto dust particles and react in the gas to form CO.

Chemical models, based on networks of purely gas-phase or gas-phase and grain-surface reactions, have been used to study many different sources in the ISM, among which are diffuse clouds, both nearby and in galactic spiral arms, and assorted objects in large dense clouds, some of which trace the evolutionary stages to low-mass and high-mass star formation, as well as the formation of planets. The dense interstellar medium, especially, is very diverse, and some larger regions, known as giant molecular clouds, contain many stars as well as protostars, and collapsing objects such as cold pre-stellar cores and hot cores. The best-known and nearest such region is the Orion Molecular Cloud, while Sagittarius B2, near the Galactic Center, is another large and diverse source, with many complex molecules.

Although the use of chemical simulations for regions in the ISM is widespread, their accuracy is limited by the robustness of the laboratory astrophysics-based information used as input. Although laboratory astrophysicists have helped immeasurably in increasing our knowledge of chemical reactions, there are still many processes, especially those occurring on surfaces, that have not been studied in sufficient detail. As observations become far more detailed, thanks to NASA-supported missions such as the HIFI instrument on the *Herschel Space Observatory*, which is currently operational, the *Stratospheric Observatory for Infrared Astronomy (SOFIA)*, which is soon to be operational, and the *James Webb Space Telescope (JWST)*, chemical simulations will require even more information from laboratory astrophysicists. In this paper, we discuss chemical models, and specific future needs to improve them.

2. Gas-Phase Models

There are a number of gas-phase networks available from web pages, including the two best-known: the UMIST Database for Astrochemistry (http://www.udfa.net/) and the Ohio State University network (osu; http://www.physics.ohio-state.edu/ eric/) , both of which contain thousands of reactions and hundreds of reactants. The networks are updated at semi-regular scheduled intervals, so as to take advantage of new laboratory and theoretical results. Although labeled as gas-phase networks, these collections of reactions do contain a few processes that occur on grain surfaces, most notably the formation of molecular hydrogen from two atoms of hydrogen. The networks and their forbear, the network of Prasad & Huntress (1979), started with the special purpose of simulating cold interstellar regions. As warmer regions, such as hot cores, became known, some reactions were added to the networks, especially to udfa, to make them useful up to 300 K or so. Recently, a high-temperature version of the osu network has been reported; in this network the gas-phase chemistry should be relatively reliable through temperatures of 800 K, although the amount of information

concerning the surface formation of H_2 at temperatures above 400 K is uncertain (Harada et al. 2010). This high-temperature version should be especially useful for the inner portions of protoplanetary disks and the larger disks surrounding black holes in so-called Active Galactic Nuclei (AGNs). Even higher temperature networks exist to study the chemistry that occurs after the passage of a shock wave through a portion of a cloud; here the temperature can reach 4000 K, but the time scale for cooling is short. Networks in which isotopic fractionation is included also exist. Here, the reaction network is expanded to include isotopologues including deuterium, ^{13}C, or ^{15}N. Isotopic fractionation, which can be a very large effect, as occurs with deuterated isotopologues at low temperatures, yields much information concerning physical conditions and time scales, and much work has been done to understand and utilize it. Other networks extend the maximum size of molecules up through the size of fullerenes, which have recently been detected in the ISM (Bettens & Herbst 1995). Yet another large network contains reactions involving polycyclic aromatic hydrocarbons (PAH's) to ascertain how they affect the abundances of smaller species. Finally, based on new studies from Herschel concerning ortho-para ratiios for exotic species such as H_2O^+, work has begun to incorporate these spin modifications into model networks (Herbst & Roueff 2010). The need to simulate diverse sources that lie over a wide range of temperatures means that there is a continuing need for new studies in the laboratory astrophysics of gas-phase rate processes.

At present, the major gas-phase networks are dominated in number by ion-molecule reactions, although radical-neutral and dissociative recombination reactions also play important roles. Although the last decade has seen a vast increase in our knowledge of the latter two (hitherto exotic) processes, there are still individual unstudied systems of importance. Other classes of exotic reactions are very poorly understood, and much work will be needed to improve our knowledge of them. These classes include the following: radiative association and radiative attachment, positive ion- negative ion recombination, and dissociative attachment. The current state of knowledge of the chemical processes used in chemical simulations is contained in a large review article (Wakelam et al. 2010). In addition, detailed information on important reactions, as compiled by experts in the field, is now being assembled on a new web site known as KIDA, which is short for *Kinetic Database for Astrochemistry*, and can be found at http://kida.obs.u-bordeaux1.fr/.

Of the poorly understood classes of reactions, there is most hope for near term improvement in positive ion-negative ion recombination reactions because several large-scale experiments are being assembled to study this process. The radiative processes present a longer-term challenge because they occur only at very low densities, so that they need to be studied in the laboratory in sources such as ion traps. Only a few systems have been studied (Gerlich & Horning 1992) and, in my view, there is some doubt about the results since no photons have ever been detected. In these processes, two species combine to form

one stable product by emitting sufficient energy in the form of a photon. One can imagine an intermediate species, known as a complex, which can either re-dissociate, or emit the radiation. One important process in diffuse interstellar clouds is the radiative association between C^+ and H_2:

$$C^+ + H_2 \rightleftharpoons (CH_2^+)* \rightarrow CH_2^+ + h\nu, \tag{1}$$

where the asterisk refers to an unstable complex. This reaction has been studied in the laboratory, and a data sheet prepared for it in KIDA, but the reaction rate coefficient is determined by a long extrapolation and no photons actually detected. Another system that has been studied in the laboratory is the radiative association between $CH_3^+ + H_2$, although once again, no photons have been detected. A third system, $CH_3^+ + H_2O$, is the most troubling of all, because the measured laboratory rate is highly uncertain, and, if correct, rules out the interstellar gas-phase production of methanol, a wide-spread neutral, which can then be formed only on dust particle surfaces. Corresponding radiative association processes involving neutral species are even more difficult to study, and at the current stage of knowledge, simple statistical theories for the rate coefficients must be utilized. As for radiative attachment, this process is critical for the formation of negative ions from precursor neutrals, such as occurs in the reaction

$$C_6H + e^- \rightleftharpoons (C_6H^-)* \rightarrow C_6H^- + h\nu, \tag{2}$$

which leads to the most widespread interstellar anion. At present, only a simple statistical theory, known as the phase space theory, has been utilized to treat these reactions, although higher-level quantum scattering calculations have been promised by several investigators (Herbst & Osamura 2008). Laboratory work is also urgently needed.

To determine the importance of individual reactions, one can make use of sensitivity studies. In these studies, the rate coefficients of individual reactions are varied, typically randomly within their measured or estimated errors, and the effect on the chemical simulation determined (Wakelam et al. 2010). One can focus on either the number of molecules changed in abundance by more than a certain amount or one can focus on the change regarding individual species. For example, Table 3 of Wakelam et al. (2010) shows the most important reactions in cold cores by virtue of the number of species affected strongly. Here, the radiative association reaction

$$C + H_2 \rightarrow CH_2 + h\nu \tag{3}$$

influences the most species - 73 - at so-called early times ($10^5 - 10^6$ yr). A Monte Carlo method can also be used to determine the *overall* uncertainty of a molecular abundance as a function of uncertainties in rate coefficients as well as in parameters such as density and temperature (Wakelam et al. 2010).

3. Gas-grain Models and Experiments

It is now well-known that surface chemistry is primarily responsible for the ices that form as mantles on interstellar dust grains during the long lifetimes of cold dense interstellar clouds. These ices consist mainly of water, CO_2, CO, and methanol, as observed by infrared absorption measurements, both against field stars and young stellar objects as sources of continuum radiation. In addition, in the warming layers surrounding star-forming regions, the ice mantles, before sublimating, provide the milieu in which surface chemical processes can produce more complex species, following the formation of reactive intermediates known as radicals by photodissociation processes on surfaces. Gas-grain models with corresponding surface networks have been around for some time (Pickles & Williams 1977), although they have become more popular within the last two decades (Hasegawa et al. 1992). In addition to gas-phase chemistry and grain-surface chemistry, these models must couple the two sets of reactions by accretion from the gas onto dust particles, and desorption from ice mantles back into the gas. Desorption can be thermal, as occurs as the mantles are heated, or can be non-thermal, as must occur to some extent in cold sources, since there are many observations of gas-phase material in these sources.

Within the last decade to decade-and-a-half, a number of laboratory astrophysics groups in assorted places, including Syracuse, New York; NASA-Ames; London, UK; Leiden, Holland; Aarhus, Denmark; and Paris, France have been actively pursuing the study of surface reactions and other processes of importance to interstellar chemistry. Theoretical work has also been prominent, especially concerning effects caused by the small sizes of dust particles and the resulting small number of reactive species on each dust particle. The laboratory studies have been performed to study a number of different topics, including (Katz et al. 1999; Watanabe & Kouichi 2002; Oberg et al. 2009a,b; Thrower et al. 2008):

- H_2 formation on bare and icy surfaces
- Ice build-up leading to simple water, CO_2, and methanol at low temperatures
- Radical-radical photochemistry leading to complex molecules as the mantles heat up
- Thermal desorption of mixed ices as well as photodesorption from cold ices.

With additional information from such studies, current gas-grain models are able to simulate the growth of ice mantles in cold cores, and the radical-radical chemistry that occurs as the core warms due to star formation, with at least semi-quantitative agreement with observation. Although these types of measurements have led to much improvement

in chemical simulations, there are still two major problems with them. First, they are not performed on tiny dust particles but on cold larger surfaces. Secondly, it is not facile to convert the results of laboratory measurements to useful input for simulations because the laboratory information is rarely sufficiently quantitative. Let us give an example. For diffusive reactions on a granular surface, rate coefficients are normally expressed as sums of diffusion rates over entire grains, which are given by the equation (Hasegawa et al. 1992)

$$k = \nu / N_{\rm s} \exp(-E_{\rm d}/kT), \tag{4}$$

where $N_{\rm s}$ is the number of surface binding sites, ν is the frequency of motion within a potential well for an adsorbate, and $E_{\rm d}$ is the barrier against diffusion from site to site. In the best of all worlds, experiments should be able to determine all three parameters, but this is quite unusual. Moreover, for a number of processes studied in the laboratory, it is not even clear that the diffusive (Langmuir-Hinshelwood) mechanism is the appropriate one either in the laboratory or in space. Other mechanisms, such as the Eley-Rideal and the hot-atom processes, may be indicated. So, there is still much more to learn about rates and mechanisms in surface chemistry (Wakelam et al. 2010). What would be ideal is the detailed simulation of laboratory data to determine parameters that could be used to simulate interstellar processes, even though they occur under vastly different conditions.

4. Stochastic Theories of Surface Chemistry

Our final topic concerns the need for stochastic treatment of surface rate processes, especially for smaller and warmer grains than the norm. The basic problem is that rate equations, in which the rate of formation or disappearance of a reactant/product is written in terms of a rate coefficient multiplied by the product of the abundances of reactants, constitute a mean field theory where average abundances are used which do not necessarily pertain to single grains. If the average abundance of a reactive species, such as H, is less than unity, then it is unlikely that a mean field theory can be accurate. Instead, one should use stochastic methods, in which the discrete aspects of the problem and its fluctuations can be treated.

Stochastic theories of rate processes stem from the so-called master equation, in which probabilities for discrete numbers of a given species on a grain are propagated forward in time via deterministic differential equations. In a system with different species on a grain, the probabilities for given numbers of the different species are coupled, so that many more differential equations are needed than would be the case for rate equations. Approximations are needed to limit the number of equations; those in use include a mixed use of master

equation and rate equation techniques depending on whether or not the population of a species is less than or greater than unity, and an expansion in terms of moments (Barzel & Biham 2007). Neither has yet been perfected to work on a complex system of equations.

The second approach is to use a Monte Carlo realization of the master equation, such as pioneered by Gillespie (1976). The major problem with this approach is that it is very difficult to couple with the rate equations used for the gas-phase chemistry. Recently, this secondary problem was solved by Vasyunin et al. (2009), who used a Monte Carlo procedure to solve the gas-phase chemistry as well as the surface chemistry. So far, this approach is the best that can be done, although it is very difficult to run it for times longer than 10^5 yr under dense cloud conditions because of the computer time needed. A reasonable approximation, which is much more efficient computationally, can be obtained by modifying rate equations for surface reactions to approach the results of stochastic treatments.

The stochastic methods discussed above can be labeled macroscopic methods, because their solution yields only the average number of atoms or molecules of each species on a grain. Suppose we wished more detailed information, such as where on a grain and in which monolayers the species are located. Then, a more detailed stochastic approach is required, now known simply as the kinetic Monte Carlo technique, or more historically, as the continuous-time random-walk approach (Cuppen et al. 2009). In this approach, one approximates the grain as a lattice with sites, each equivalent to a binding site for an adsorbate. The process of diffusion from site to site, reaction when two adsorbates lie in the same site, accretion onto the lattice, and desorption from the lattice are all treated by a Monte Carlo technique in which the probabilities of each of these processes happening in a random time period are computed. Moreover, different mechanisms for surface chemistry can be included, as can the chemistry occurring in pores inside a porous ice mantle, the development of which can also be determined. Given its high degree of complexity, the kinetic Monte Carlo method cannot easily be coupled with either a rate equation or a macroscopic Monte Carlo treatment of the gas-phase chemistry. Its main use up to now has been to study specific granular processes, such as ice mantle growth (Cuppen et al. 2009).

5. Conclusions

Many more experiments are needed in gas-phase dynamics and kinetics to study exotic classes of reactions at temperatures in the range 10 K - 800 K, and to refine our knowledge of specific reactions in better understood classes but judged to be especially important by sensitivity studies. Also, much more work needs to be done in the analysis of experimental results in surface chemistry.

This work was supported in part by grants from NASA through the Herschel program and for studies in laboratory astrophysics.

REFERENCES

Barzel, B., & Biham, O. 2007, ApJ, 658, L37
Bettens, R.P.A., & Herbst, E. 1995, Int. J. Mass Spectrom. Ion Proc., 149/150, 321
Cuppen, H.M., van Dishoeck, E.F., Herbst, E., & Tielens, A.G.G.M. 20009, A&A, 508, 275
Gerlich, D., & Horning, S. 1992, Chem. Rev., 92, 1509
Gillespie, D.T. 1976, J. Comp. Phys., 22, 403
Harada, N., Herbst, E., & Wakelam, V. 2010, ApJ, 721, 1570
Hasegawa, T.I., Herbst, E., & Leung, C.M. 1992, ApJS, 82, 167
Herbst, E., & Osamura, Y. 2008, ApJ, 679, 1670
Herbst, E., & Roueff, E. 2010, J. Phys. Conf. Ser., in press
Katz, N., Furman I., Biham, O., Pirronello, V., & Vidali, G. 1999, ApJ, 522, 305
Öberg, K.I., Garrod, R.T., van Dishoeck, E.F., & Linnarstz, H. 2009a, A&A, 504, 891
Öberg, K.I., Linnartz, H., Visser, R., & van Dishoeck, E.F. 2009b, ApJ, 693, 1209
Pickles, J.B., & Williams, D.A. 1977, Ap&SS, 52, 443
Prasad, S.S., & Huntress, Jr., W.T. 1980, ApJS, 43, 1
Thrower, J.D. et al. 2008, ApJ, 673, 1233
Vasyunin, A.I., Semenov, D.A., Wiebe, D.S., & Henning, Th. 2009, ApJ, 691, 1459
Wakelam, V. et al. 2010, Sp. Sci. Rev., in press
Watanabe, N., & Kouchi, A. 2002, ApJ, 571, L173

NASA LAW, October 25-28, 2010, Gatlinburg

Laboratory Astrophysics of Astrophysically-Relevant Materials: Developing Dust as a Diagnostic

S. A. Rinehart

NASA Goddard, Code 665, Observational Cosmology Laboratory, Greenbelt, MD 20771

Stephen.A.Rinehart@nasa.gov

ABSTRACT

Over forty years ago, observations in the new field of infrared astronomy showed a broad spectral feature at 10 microns; the feature was quickly associated with the presence of silicate-rich dust. Since that time, improvements in infrared astronomy have led to the discovery of a plethora of additional spectral features attributable to dust. By combining these observations with spectroscopic data acquired in the laboratory, astronomers have a diagnostic tool that can be used to explore underlying astronomical phenomena. As the laboratory data improves, so does our ability to interpret the astronomical observations. Here, we discuss some recent progress in laboratory spectroscopy and attempt to identify future research directions.

1. Introduction

Even before the observational discovery of dust within astronomical environments, theorists had anticipated its existence. For instance, Gaustad (1963) discussed the role of refractory dust grains and ices in formation of stars. Optical observations had also implied the presence of materials with high opacity, but it took infrared observations to provide the key data to identify the source of the opacity. Gillett, Low, & Stein (1968) found an anomalous broad emission feature at 10 μm in several late-type stars (Figure 1); shortly thereafter Woolf & Ney (1969) identified the source of this emission as due to silicate-rich minerals. Thanks to infrared observatories, we now know that dust is ubiquitous, and that there is a wide range of spectral features. Future facilities such as JWST and SOFIA will lead to further discoveries.

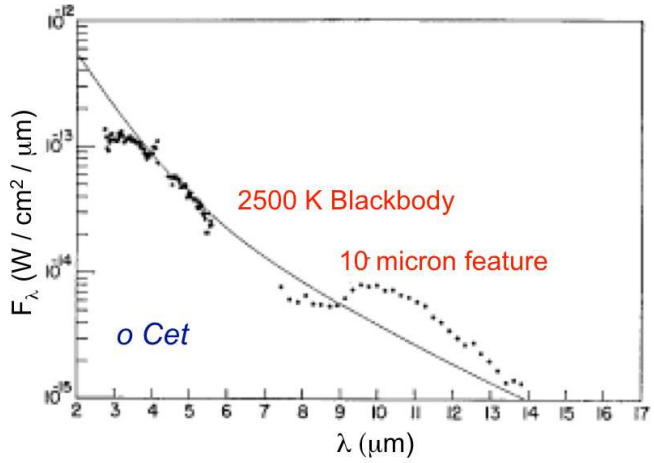

Fig. 1.— Infrared spectroscopy led to the first direct detection of dust. Since that time, improvements in infrared spectroscopy have led to the discovery of dust in a wide range of different astrophysical environments and to the discovery of a wide variety in broad mineralogical features. Figure taken from Gillett, Low, & Stein (1968).

Studying dust materials in the laboratory is a natural companion to infrared astronomical observations. Modern infrared astronomical spectroscopy often produces rich data sets, with a wide array of spectroscopic features. To understand the origins of these features, laboratory data is needed for comparison. This is an active and exciting field of current research, and in this paper we will review some of the recent progress in the study of astronomically-relevant silicate-rich materials, as well as discuss a few areas which require future research effort. We do not discuss recent progress made in the study of polyaromatic hydrocarbons (PAHs), but good reviews of this area can be found in Tielens (2008) and Salama (2008).

2. Recent Progress

2.1. Methods

Given the typical absorption constants of dust materials in the mid-infrared, the most common method used for laboratory measurements involve embedding the material in a matrix. The individual particles are well-mixed into another material, such as KBr, CsI, or polypropylene. This substance is then pressed into the form of pellets or thin disks. The relatively small amount of material within the matrix makes it optically thin, allowing measurement of transmission and absorption within the sample in the near- and mid-infrared. This method, however, does have a few disadvantages. The biggest problem with such

measurements is that embedding medium causes changes in the observed spectral profiles (Figure 2). This is caused by the electromagnetic polarization of the embedding material (Fabian et al. 2001). The second disadvantage is that post-measurement analysis, such as TEM measurements, cannot be made, as the sample cannot be extracted from the matrix.

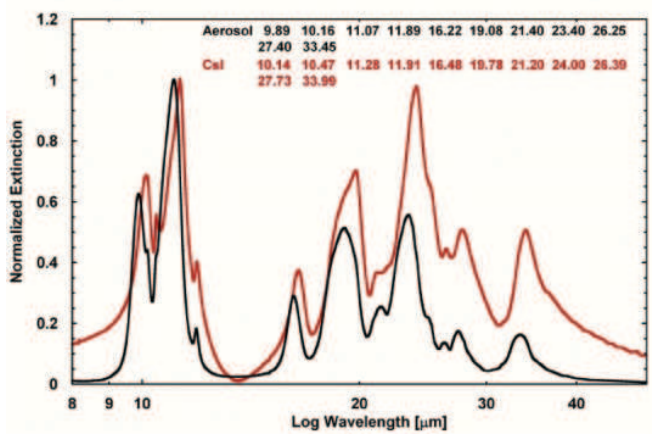

Fig. 2.— In the past few years, the aerosol method has begun to be used for characterization of dust. The aerosol method allows for measurement of a spectrum uncontaminated by the effects of the embedding material. Figure taken from *http : //www.astro.uni − jena.de/Laboratory/Speclab/databases.html*, Tamanai, et al. 2006.

It is also possible to conduct bulk measurements to obtain optical characterization data of samples. A variety of different approaches can be taken in preparing bulk samples, but in each case, the primary difficulty is that the quantity of sample material is relatively large, leading to high optical depths ($\tau > 1$) in the near- and mid-infrared, making accurate transmission and absorption measurements impossible. However, in the far-infared, where the grain opacity drops, the sample can remain optically thin, but with sufficient depth to allow measurement (Figure 3).

In recent years, however, the aerosol measurement technique has come into use within the laboratory (Tamanai et al. 2006). In this method, a powdered sample is injected into a nitrogen gas stream. Filters remove large particles from the stream before it is densified to 10^6 particles / cm^3. The aerosolized particles are then trapped in a long cell, where particles less than about 1μm in size couple well to the gas, remaining in suspension for up to several hours. The cell is attached to a Fourier Transform Spectrometer; the infrared light from the FTS enters the cell and makes multiple passes through the cell via mirrors at each end of the cell, increasing the effective optical depth of the suspended sample and providing high signal-to-noise measurements in the mid-infrared. The aerosol method provides several distinct

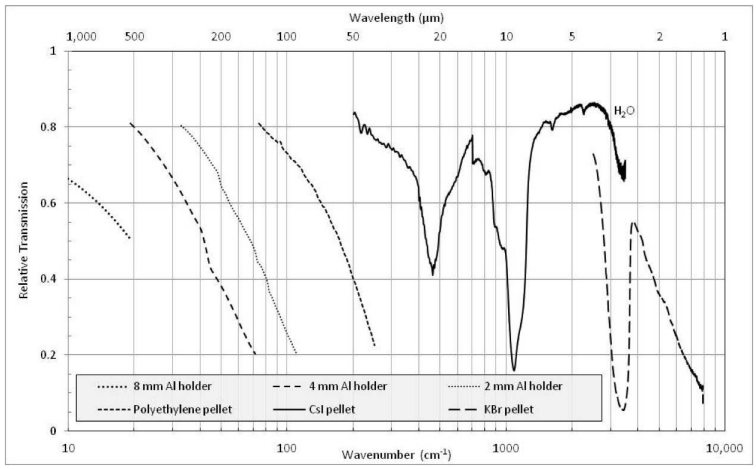

Fig. 3.— To properly interpret data from modern infrared observatories, we need high-quality laboratory data covering a wide range of wavelengths. However, covering such a large spectral range requires the combination of different methodologies. Here, the matrix method is used at short wavelengths, while bulk methods are used at long wavelengths (Kinzer, et al. 2010).

advantages: (1) it provides some flexibility in the amount of material in the beam, allowing measurements at short wavelengths; (2) a filter in the aerosol stream can capture a fraction of the silicate particles for post-measurement analysis; and (3) the measured spectrum is free of the effects of the embedding material. This technique, therefore, provides a more accurate spectrum of the sample material than corresponding matrix methods. However, the aerosol method does have several disadvantages. First, the method itself does not lend itself to precise knowledge of the amount of material in the column, and since the material slowly settles out of the gas over time, the amount of material drops with time. This complicates the determination of the absorption constant. Secondly, this method is not suited for measurements at low temperatures. This limits the methods utility in the far-infrared, and does not allow for exploration of the effects of temperature on the spectra of the sample material.

2.2. Materials

The identification of silicates as the source of mid-infrared spectral features arose from laboratory spectroscopy of terrestrial minerals, and much of the laboratory work that has been done (and that is still done) is based upon additional measurements of such materials. One of the drawbacks of this, however, is that the terrestrial materials are typically in

either crystalline or melt form, and are therefore not analagous to amorphous silicates that have been observed in astronomical environments. The sol-gel technique produces amorphous samples, but the sample grains tend to be small and relatively uniform; microscopy of captured interplanetary dust grains, however, shows that such grains have complicated structure. Laser ablation, arc-discharge ablation, and smoke condensation methods (Rietmeijer, Nuth, & Karner 1999) are newer methods which can both reproduce both the amorphous chemistry and the complicated morphology of grains (although the two ablation methods can lead to a wide range of particle sizes). Grain shape can have a significant impact on the measured spectrum (Figure 4).

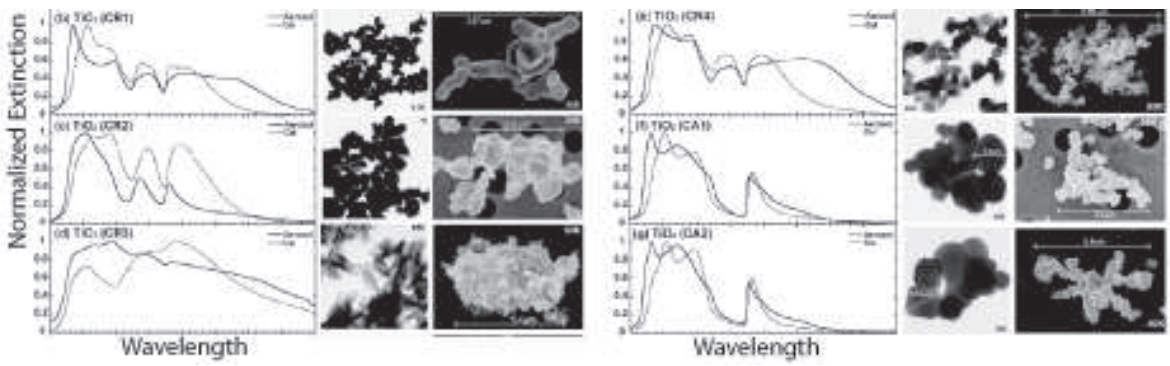

Fig. 4.— Grain shape plays an important role in the spectra of silicates. Samples of TiO_2 prepared by different methods have different grain shapes (images on the right, above), and these different grain shapes produce different spectra both when measured in matrix and with the aerosol method (Tamanai, et al. 2009).

One of the most interesting developments in recent years, however, has come from the attempt to characterize how the spectra of silicate rich materials change as a function of temperature. It has been known for over 30 years that the infrared optical properties of dust grains are different at low temperatures than at room temperature (Day 1976), but recent work has shown that the spectral changes are more significant than perhaps previously thought, with changes in both position and shape of spectral features and in the underlying continuum opacity (Figure 5). This raises the possibility that astronomical spectra of dust could be used as a direct temperature diagnostic.

2.3. Modeling

It has long been known that grain morphology plays an important role in the observed spectra of dust grains. Simple spherical models (Mie theory) have proven inadequate for

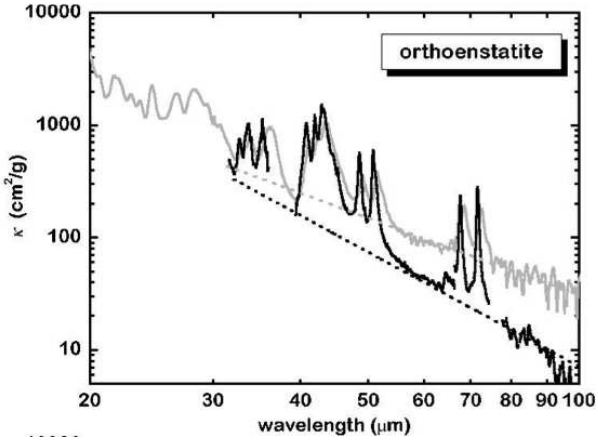

Fig. 5.— Recent experiments have shown that the spetral features of some silicate-rich samples can change significantly with temperature (Chihara et al. 2001).

reproducing observed spectra, and while more sophisticated models such as the continuous distribution of ellipsoids (CDE, Bohren & Hufman 1983) have been more effective, they have still fallen short of reproducing observations. Recently, however, new models such as the distribution of form factors (DFF, Min et al. 2005) have been used to reproduce laboratory measurements acquired via the aerosol and matrix methods (Figure 6). The results of these models are encouraging; while significant work remains, further development of the model may allow reconciliation of measurements obtained with different methods.

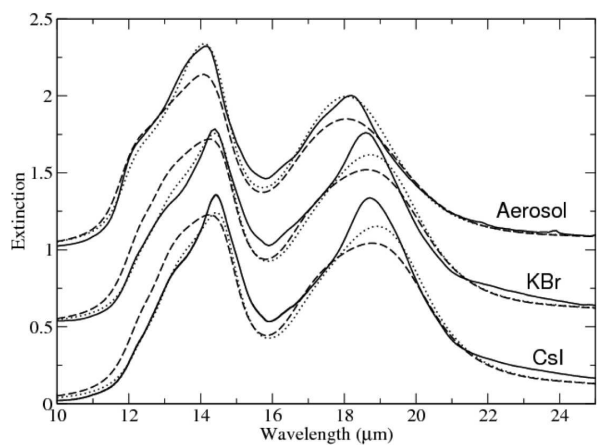

Fig. 6.— Since a the variety of different sample production and measurement methods each have advantages and disadvantages, we rely on theoretical models to reconcile the different measurements. Recent modeling efforts have been more successful, but more work is needed (Mutschke, Min, & Tamanai 2009)

3. What needs to be done?

With sufficient understanding of the properties of astronomical dust, it is possible that spectroscopic observations could serve as a powerful diagnostic tool. At the current state of knowledge, astronomers already use the broad spectral features from dust to infer the composition of the material and as an archaeological tool to understand how the dust has been processed. However, these efforts are still hampered by some fundamental limitations of laboratory measurements. How can we overcome these limitations and make dust spectroscopy an even more powerful astronomical tool?

First, we must continue to refine methodologies. The aerosol method has significant potential, but has some serious limitations, as do the more established methods of bulk and matrix measurements. A significant improvement will be made in the coming years by carefully comparing the results from the different methodologies. Aerosol measurements will provide an unbiased room-temperature measurement that can be used to understand how spectral features shift due to the presence of a matrix material, and will ideally lead to an ability to calibrate matrix spectra to account for the medium. Further, if the complementary measurements could be used to develop a theoretical understanding of the observed shifts, it would be possible to extract the "real" spectra from matrix measurements over a wide range of temperatures.

Second, measurements have already shown how the spectral features of silicates can change signficantly at low temperatures. What is lacking, however, is a detailed series of measurements to show how the transition occurs as a function of temperature. By acquiring data in the laboratory at a number of temperatures ranging from room temperature down to 4 K, it should be possible to map how the spectral features change with temperature. This will provide a solid footing for using observed spectra to estimate dust temperature.

Third, the wavelength coverage explored within the laboratory needs to be expanded. While, as a rule, the majority of spectral features produced by dust are in the near- to mid-infrared, features are known as far out as 90 μm, and it is possible that some very low energy modes could produce features at even longer wavelengths. SOFIA is going to provide some very powerful new measurement capabilities in the far-infrared, but understanding those observations is going to require complementary laboratory data.

Fourth, as has been known for some time, simple spherical models of dust grains using derived optical constants do a relatively poor job of matching observed spectra. However, recent models using aggregates of ellipsoidal grains have been much more successful. In the near future, continued development of such models will be important for understanding the sensitivity of spectra on grain shape, and for understanding if there is a degeneracy in the

solution space of dust material and dust shape. It will also be important to compare these models of dust grains to TEM observations of captured dust grains from Stardust and future sample retrieval missions.

Finally, we must continue to experiment with different materials and amalgams of materials. Most astrophysical dust is likely a combination of a range of materials. For instance, in many environments, dust is likely mixed with icy materials, and there may be icy mantles on dust grains. Laboratory measurements of ices and of ice/dust mixtures will be important, particularly as additional long-wavelength capabilities (e.g. SOFIA) become available.

The author would like to thank the members of the Optical Properties of Astronomical Silicates with Infrared Techniques (OPASI-T) team at Goddard; D. Benford, E. Dwek, R. Henry, R. Kinzer, J. Nuth, R. Silverberg, and E. Wollack. This work was supported in part by grants from NASA.

REFERENCES

Fabian, D., Henning, T., Jäger, C., Mutschke, H., Dorschner, J., & Wehrhan, O. 2001, Astron. & Astrophys. 378, 228.

Gaustad, J. 1963, ApJ, 138, 1050.

Gillett, F., Low, F., & Stein, W. 1968, ApJ, 154, 677

Kinzer, R., Rinehart, S., Benford, D., Dwek, E., Henry, R., Nuth, J., Wheeler, C., & Wollack, E. 2010, Proc. SPIE, 7741, 62.

Rietmeijer, F, Nuth, J., & Karner, J. 1999, ApJ, 527, 395.

Salama, F. 2008, *Organic Matter in Space*, Proc. IAU, 251, 357.

Tamanai, A., Mutschke, H., Blum, J., & Meeus, G. 2006, ApJ, 648, L147.

Tamanai, A., Mutschke, H., Blum, J., Posch, T., Koike, C. & Ferguson, J.. 2009, A&A, 501, 251.

Tielens,A. 2008, ARAA, 46, 289.

Woolf, N. & Ney, E. 1969, ApJ, 155, L181.

This preprint was prepared with the AAS LaTeX macros v5.2.

NASA LAW, October 25-28, 2010, Gatlinburg

Molecule Formation on Interstellar Grains

G. Vidali

Physics Department, Syracuse University, Syracuse, NY 13244-1130 (USA)

gvidali@syr.edu

ABSTRACT

The first experiments that were expressively designed to be applicable to hydrogen formation reactions in the ISM measured the efficiency of formation of molecular hydrogen on a polycrystalline olivine (Pirronello et al. (1997a)). It soon turned out that more was needed, and research began on the mechanism of reaction, on the influence of the surface morphology, and on the excitation of the just-formed molecule. In this review, I summarize what we learned from these and other experiments, and where more work is needed: in the elementary steps of reaction, in the bridging of the laboratory-ISM gap (large flux/large surface - small flux/small grain) using simulations, and in using realistic samples of dust grains. Understanding what experiments can and cannot deliver will help in designing and targeting observations, and vice-versa.

1. Introduction

There are a handful of molecules, the simplest being hydrogen, water and methanol, that are believed to be made on interstellar dust grains, since no gas-phase reactions can explain the densities observed in interstellar medium (ISM) environments. These molecules are also vital to important astrophysics/astrochemistry processes, such as star formation, catalytic production of other molecules, and pathways in origin-of-life scenarios (Herbst & van Dishoeck (2009)).

The formation of molecules such as CO_2, CH_3OH, and HCO on/in ices coating dust grains has been studied in the laboratory for many years since the pioneering work of Mayo Greenberg in the late 1970s. Most of the laboratory work was done by studying the formation of molecules following the impact of uv light and cosmic rays analogs (Sivaraman et al. (2008); molecule formation in ices is covered elsewhere in this volume). Recently, the pace

of experimentation of hydrogenation and oxidation reactions using low energy neutral H and O atoms has picked up (Roser et al. (2001), Ioppolo et al. (2008), Miyauchi et al. (2008), Dulieu et al. (2010)).

Of the molecules for which formation routes in the gas-phase are not sufficient to justify their abundances, molecular hydrogen deserves special consideration for the following reasons. Molecular hydrogen, detected through transitions from an excited state or via a proxy, such as through transitions in CO following H_2-CO collisions, is ubiquitous in the interstellar medium, from diffuse clouds to dense clouds. Because its destruction rate via photodissociation is known, to maintain a steady state a comparable formation rate is needed. The rate coefficient of molecular hydrogen formation R (cm^3 sec^{-1}) is related to the total number density of hydrogen atoms (both in atomic and molecular forms) $n = n_{\rm H} + 2n_{\rm H_2}$ and the photodissociation rate $\beta = 5 \times 10^{-10}$ (sec^{-1}) by: $Rn_{\rm H}n = 0.11\beta n_{\rm H_2}$ Duley & Williams (1984). Jura (1975) calculated, based on an analysis of Copernicus observations in the local diffuse cloud medium, that the formation rate coefficient on grains is $10^{-17} < R < 3 \times 10^{-17}$ (cm^3 sec^{-1}). Since then, R has been measured in several different ISM environments. Remarkably, these analyses give a value of R very similar to the one estimated by Jura for local diffuse clouds. Gry et al. (2002) looked at the formation rate of H_2 in the diffuse ISM, using FUSE data, Habart et al. (2004) examined this rate in photodissociation regions, using SWS-ISO data.

The importance of knowing how molecular hydrogen forms is clear. It intervenes in most chemical schemes to make more complex molecules. For example, oxygen chemistry follows from: $H_2 + cr \rightarrow H_2^+ + e, H_2^+ + H_2 \rightarrow H_3 + +H, H_2^+ + O \rightarrow H^+ + H_2$ and hydrocarbon chemistry from: $H_2 + C^+ \rightarrow CH^+ + H$, where cr is a cosmic ray. It plays a role in aiding the initial gravitational collapse of a cloud by absorbing photons and re-radiating energy in the infrared through which the cloud is transparent, thus allowing to collapse further (Herbst (2005)).

The formation of molecular hydrogen cannot occur in the gas-phase in space environments because the protomolecule would have to make a spin forbidden transition in order to get rid of the energy gained in making the bond. Salpeter and collaborators (Hollenbach & Salpeter (1971a), Hollenbach et al. (1971b)) proposed that H_2 formation occurs on interstellar dust grains by the association of two H atoms that happen to be on the grain surface. They considered the grain as made of polycrystalline water and calculated the sticking and diffusion of H atoms and the desorption of H_2. By assuming fast tunneling of H on the surface of ice at 10K, they found that if two atoms happen to be on a grain of typical size of 0.1 micron, the two atoms diffuse fast enough that they meet before desorbing. Under these conditions, molecular hydrogen is formed with an efficiency that is in agreement with

observations. But Smoluchowski (1981) and (1983) found a much reduced formation rate when he considered a more realistic model of ice, i.e., an amorphous ice.

In recent times, chemical evolution models of ISM environments began to incorporate reactions that take place on surfaces (Herbst & Cuppen (2006)). Ideally, given the macroscopic condition of a cloud and the distribution of size and composition of grains, the efficiency of molecular hydrogen formation can be calculated. But we know little of the composition of grains, and also about the efficiency of H_2 formation on a given surface. Initially, such as in the experiments of Pirronello and Vidali of H_2 formation on a telluric sample of olivine (Pirronello et al. (1997a), Pirronello et al. (1997b)) or on a sample of amorphous carbon (Pirronello et al. (1999)), the focus of the investigations was on the efficiency of the reaction. Soon it became clear that, to obtain rates in different temperature ranges and on different surfaces, a deeper understanding of how H_2 is formed was needed, as discussed below.

Atom-surface interactions can be classified in two types. The physical adsorption interaction is dominated by long-range weak van der Waals forces, while the short range is due to the Pauli exclusion of electrons of the atom and the solid. Typical interaction strengths, measured for a variety of light gases on well characterized surfaces, usually single crystals, are of the order of a few tens of meV. In contrast, the chemical adsorption, or chemisorption, involves localized bonding and has strengths of the order of 1 eV and more. The residence time of an atom on a surface depends on the strength of this interaction, $t = \tau e^{-E_{des}/k_B T}$, where $\tau \sim 10^{12}$ sec. is a characteristic time related to the vibrational frequency of an atom in the potential well of a surface site and E_{des} is the energy needed to desorb. For a desorption energy of $\sim$ 500K, a typical value obtained from the analysis of experiments of H interaction with dust grain analogs and ices (see the Section 4), the residence time is of the order of the time between arrivals of H on a surface of a dust grain in an ISM cloud (n=100 atoms/cm^3) (Vidali et al. (2005)). Thus, while this is sufficient to get recombination reactions going in diffuse and dense cloud environments, obviously stronger binding is necessary to hold atoms down in environments where the dust is considerably hotter, such as PDRs; there have been a few experiments on carbonaceous materials that have addressed this question (Mennella (2008), Hornekaer et al. (2006)). However, experiments on dust grain analogs have shown that in most cases, in the grain temperature range of 10-20 K, the physical adsorption interaction dominates the formation of H_2. Because the interaction is long-range, its strength is not as sensitive to different surface sites as strong adsorption (chemisorption). Indeed, it is possible to draw some general conclusion on the strength of the interaction based on easily found parameters, such as the polarizability of the atom and the dielectric function of the solid, see Vidali et al. (1991).

Broadly speaking, there are three mechanisms of reaction: Langmuir-Hinshelwood (L-

H), Eley-Rideal (E-R) and the Hot-Atom (H-A). In the first, the atom becomes thermally accommodated with the surface (sticking) with a certain probability; then it might diffuse. If it encounters another atom it might make a bond. The resulting molecule remains on the surface or is ejected from it depending on how the excess energy is distributed among the different degrees of freedom. Obviously, if the atom-surface interaction is weak, diffusion is easy and so is desorption from the surface. In the E-R reaction, the incoming atom strikes an atom on the surface and makes a bond without becoming accommodated with the surface. The departing molecule carries a lot of the excess energy. The H-A reaction is similar to the E-R reaction and it differs in the fact that the incoming atom when it strikes the surface maintains a good portion of its energy, thus traveling considerably because of the excess kinetic energy. Eventually it finds another atom and reacts with it. Evidence of the E-R reaction has been found in H-covered surfaces of single crystal metals and semiconductors (Rettner & Auerbach (1995), Koleske et al. (1994)). The hot-atom reaction has been found in H covered metal surfaces as well, and to operationally distinguish one from the other is not simple. As the study of H_2 formation on grain analogs at low temperature is concerned, these two mechanisms have been invoked in interpreting data of HD formation on hydrogen loaded amorphous carbon (Mennella (2008)), and in D_2 formation on an amorphous silicate (Lemaire et al. (2010)).

2. Experimental Methods

In this section we illustrate an experiment designed to obtain information on the formation of molecular hydrogen. In doing so, we introduce the typical measuring methods, and how the measured quantities are interpreted.

We use the apparatus at Syracuse University as an example (Vidali et al. (2009)). It consists of two atomic/molecular beam lines, each with a dissociation source and three differentially pumped stages. The base pressure in the third stage, the closest to the main chamber, is 10^{-8} torr. The strength and dissociation rate are measured by a quadrupole mass spectrometer located in the main chamber. Dissociation rates in the 70-80% range are typically achieved using radio-frequency sources. The maximum of dissociation occurs at source pressure of a few tenth of a torr. The calculated flux entering the main chamber is of the order of $F_0 = 10^{12}$ (atoms cm^{-2}s^{-1}). The main chamber has a base pressure of 10^{-10} torr and houses the sample holder and the quadrupole mass spectrometer. The latter is mounted on a doubly differentially pumped rotatable platform so the detector can be placed in front of the surface or in front of the beams.

A typical experiment is done as follows. The surface of the sample is exposed to the

beams for a given amount of time (the irradiation phase). During this time the detector collects molecules that come out from the surface. For example, if a good fraction of the energy released in making the bond is not transferred to the substrate, the molecule can use that energy to desorb. However, since the first experiments done on a polycrystalline olivine sample (Pirronello et al. (1997a)), it is clear that few molecules desorb from the surface at this time. Therefore, on the surface there remain atoms and/or molecules that formed during the irradiation. To induce more reactions the temperature of the sample is raised quickly. This is the Temperature Programmed Desorption (TPD) part of the experiment. In the ISM, a similar result can be achieved by the sudden rise of the dust temperature because of the absorption of a photon/ cosmic ray, or by simply waiting a long time for stochastic diffusion of atoms to bring them together for an associative reaction. As Pirronello et al. (1997b) have shown, the study of the kinetics of desorption in the case of polycrystalline olivine reveals the role of thermal activation in H diffusion. However, this was disputed in the case of H formation on water ice (Hornekaer et al. (2003)). But Watanabe et al. (2010) showed that there are low and high energy sites for H, and the latter form traps that can be overcome only by thermal activation.

3. From the Laboratory to the ISM

In the study of the ISM we are interested most often in steady-state processes; however, experiments give data obtained kinetically. Furthermore, the flux of atoms impinging on a surface in the laboratory is several orders of magnitude higher than in the interstellar medium. Therefore, the raw data coming out of laboratories might be of limited value to astronomers/astrochemists without further elaboration.

For example, rate equations can be used to fit the experimental data, as it has been done in Katz et al. (1999), Perets et al. (2007),Vidali & Li (2010):

$$\frac{dn_H}{dt} = f(1 - n_H) - W_H n_H - 2D_H n^2 \tag{1}$$

$$\frac{dn_{H_2,i}}{dt} = \frac{\rho_i - n_{H_2,i}}{\Sigma_j(\rho_j n_{H_2,j})} D_H n_H^2 - W_{H_2}, i n_{H_2,i} \tag{2}$$

and the total desorption rate is $R = \Sigma_i W_i n_i$. Here f is the flux of atoms sticking on the surface, n_H is the number density of H atoms on the surface, ρ_i is the density of sites of type i, $W = \nu e^{-\frac{E_{des}}{k_B T}}$ is the desorption rate, E_{des} is the desorption energy, ν a characteristic frequency of vibration of the atom/molecule in the potential well of the adsorption site , $D = \nu e^{-\frac{E_{diff}}{k_B T}}$, D is the diffusion rate if thermally activated, and E_{diff} is the energy barrier

for diffusion. A more complete model in which there is diffusion of molecules from site to site is given in Li et al. (2010). From fitting TPD data, one obtains the energy barriers for the various processes and the order of kinetics. For example, the diffusion energy and the desorption energy barriers for hydrogen atoms are obtained which cannot be easily measured directly. The next step is to use these values in a simulation of the formation of molecular hydrogen in actual ISM conditions. Biham and co-workers (Katz et al. (1999), Biham et al. (2001), Lipshtat & Biham (2005)), developed methods to extract from the experiments quantities that can then be used in codes of the chemical evolution of ISM environments (Herbst & Cuppen (2006), LePetit et al. (2009)). The data from the experiments are entered in a model of a cloud; this is coupled to a gas-surface interaction model that has a certain distribution of grain sizes; the master equation or the moment equation approach are used to take into account the stochastic nature of infrequent processes, such as the ones of sticking and diffusion of atoms on a small grain. For example, LePetit et al. (2009) coupled the gas-surface interaction model into a code of the evolution of a PDR. In such a case, one obtains the efficiency of formation of molecular hydrogen as a function of A_v, the visual extinction. As more detailed experimental data become available, more of these types of simulations will be possible.

4. Summary of Results

After the first experiments of Pirronello et al. of H_2 formation on a polycrystalline olivine sample, better analogs of ISM grains have been used; for example, amorphous materials were considered. Broadly speaking, the following quantities were measured: the efficiency of H_2 formation, the desorption energy of molecules, the sticking coefficient of atoms/molecules on the surface, the ro-vibrational and translation energies of the just-formed molecule, and the influence on the above of the morphology of the surface. As detailed in another section, further insight can be gained by studying the efficiency of formation under various conditions and by fitting the data with theoretical models, such as rate equations. Because any of these measurements are time consuming and require highly specialized equipment, all these measurements are usually not done in one apparatus or sample. Nonetheless, useful information can be obtained by collating data and using computer models. In the following table, the type of information obtained for different types of grain analogs is summarized. The picture that emerges is: 1. At low grain temperature, H-grain interaction is weak; 2. Rough and/or amorphous surfaces give a high H recombination efficiency over a larger grain temperature range than flat surfaces (Cuppen & Herbst (2005), Perets et al. (2007)); 3. Ro-vibrational excitations of H_2 from amorphous water are quenched (Congiu et al. (2009)); 4. Competing reaction mechanisms might operate at the same time (Lemaire et al. (2010)).

Table 1: Sample of experimental results of H_2 (or HD, D_2) formation on dust grain analogs. 0<R< 1 is the formation efficiency, T is the sample temperature range investigated, E_{des} is the desorption energy of H_2 (see references for specifics), L-H, E-R, H-A refer to Langmuir-Hinshelwood, Ealy-Rideal and Hot-Atom, respectively, K.E. is the kinetic energy of the departing H_2. Ro-vibr. describes the degree of ro-vibrational excitation.

Dust analog	R	T (K)	$E_{des}(meV)$	Mechanism	Ro-vibr.	K.E.	Ref.
olivine (polycrys.)	low	5-20	27	L-H	-	-	a
amorphous carbon	high	5-20	47	L-H			b
amorphous water ice	high	5-30	40-70	L-H, H-A	low	thermal	c
amorphous silicate	high	5- 30	35-53-75	L-H			d
amorphous silicate	high	5- 70		L-H, H-A	high		e
H-loaded amorph.carbon		300K		E-R			f
graphite		>15K		E-R	high		g
tholin	5-30K	5-30	30-55	L-H			h

Note. — Some of the references report the diffusion energy of H atoms (usually in the 25-55 meV range). [a] Pirronello et al. (1997a). Analysis of data in Katz et al. (1999). [b] Pirronello et al. (1999). Analysis of data in Katz et al. (1999). [c] Results depend on the type of water ice: Manico et al. (2001), Roser et al. (2002). Analysis in Perets et al. (2005). Kinetic or ro-vibrational data in Roser et al. (2003), Hornekaer et al. (2003), Congiu et al. (2009). [d] Vidali et al. (2009). Analysis of data in: Perets et al. (2007) [e] Lemaire et al. (2010) [f] Mennella (2008) [g] Latimer et al. (2008) [h]Li et al. (2010)

5. Conclusion

In this review, I highlighted the tremendous advancement in the comprehension of H_2 formation catalyzed by ISM grains that took place in the last decade and a half. While the first studies concentrated on obtaining the H_2 formation efficiency, soon research moved to the study of the mechanisms of reaction, the influence of the surface conditions, and the detection of the ro-vibrational energy of the nascent molecule. It became clear that data from most of the systems studied could be explained by the weak physical adsorption interaction between H and a grain analog. However, more experiments are necessary to understand how H_2 forms in ISM environments, such as PDRs and post shocked regions, where, because of the higher grain and/or gas temperature, other mechanisms must play a role. It is also important to underscore the necessity of a theoretical underpinning that takes the laboratory data and makes predictions of H_2 formation in actual ISM conditions. Similar considerations

can be made about the formation of larger molecules, where work on step-wise reactions of addition of H and O has just begun.

I would like to acknowledge my collaborators Dr. P.Frank, J.He, L.Li, J.Roser, Profs. Biham, Lemaire and Pirronello and their collaborators, and Dr. J.Brucato. This work was supported in part by a grant from the NSF Astronomy and Astrophysics Division (0908108). Support for prior research from NASA APRA Program is also acknowledged.

REFERENCES

Biham, O., Furman, I., Pirronello, V., & Vidali, G. 2011, Astrophys. J., 553, 595

Congiu, E., et al. 2009, Mon. Not. R. Astron. Soc. 397, L96

Cuppen, H.M., & Herbst, E. 2005, Mon. Not. R. Astron. Soc., 361, 565

Duley , W. & Williams, W.A. 1984, Interstellar Chemistry (New York: Academic Press)

Dulieu, F., et al. 2010, Astron. & Astrophys., 512, A30

Gry, C., et al. 2002, Astron. Astrophys., 391, 675

Habart, E., et al. 2004 Astron. Astrophys, 414, 531

Hagen, W., Allamandola, L. J., & Greenberg, J. M. 1979, Astrophys. & Space Sci., 65, 215

Harris, J., & Kasemo, B. 1981, Surf. Sci., 105, L281

Herbst, E. 2005, J. Chem. Phys. A, 109, 362

Herbst, E., & Cuppen, H.M. 2006, Proc. Nat. Acad. Sci., 103, 12257

Herbst, E., & van Dishoeck, E.F. 2009, Anu.Rev.Astron & Astrophys. 47, 427

Hollenbach, D. & Salpeter, E. E. 1971, Astrphys. J., 163, 155

Hollenbach, D., Werner, M. W. & Salpeter, E. E. 1971, Astrphys. J., 163, 165

Hornekaer, L., et al. 2006, Phys. Rev. Lett., 96, 6104

Hornekaer, L., Baurichter A ., Petrunin, V. V., Field. D. & Luntz, A, C, 2003 Science, 302, 1943

Ioppolo, S., et al. 2008, ApJ, 686, 1474

Jura, M. 1975, Astrphys. J., 197 575

Katz, N., Furman, I., Biham, O., Pirronello, V. & Vidali, G. 1999, Astrophys. J., 522, 305

Koleske, D.D., Gates, S.M., & Jackson, B. 1994, J. Chem. Phys., 101, 3301

Latimer, E.R., Islam, F., & Price, S.D. 2008, Chem. Phys. Letters 455, 174

Lemaire, J.L., Vidali, et al. 2010, Astrophys. J., 725, L1

Le Petit. F., et al. 2009, Astron. & Astrophys., 505, 1153

Li, L. et al. 2010, J. Phys. Chem A, 114, 10575

Lipshtat, Az., & Biham, O. 2005, Mon. Not. Royal Astron. Soc. 362, 666

Manicò, G., Raguni, G., Pirronello, V., Roser, J. E., & Vidali, G. 2001, Astrphys. J., 548, L253

Mennella, V. 2008, Astrophys. J. Lett., 684, L25

Miyauchi, N., et al.. 2008, Chem.Phys.Lett., 456, 27

Perets, H.B., et al. 2005, Astrophys.J. 627, 850

Perets, H., et al. 2007, Astrophys. J., 661, L163

Pirronello, V., Liu, C., Roser, J. E., & Vidali, G., 1999 Astron. Astrophys., 344, 681

Pirronello, V., Liu, C., Shen, L., & Vidali, G., 1997, Astrphys. J., 475, L69

Pirronello, V., Biham, O., Liu, C., Shen, L. & Vidali, G. 1997 Astrphys. J., 483, L131

Rettner, C.T., & Auerbach, D.J., Phys. Rev. Lett., 74, 4551

Roser, J.E., Vidali, G., Manicò, G., & Pirronello, V. 2001, Astrophys. J., 555, L61

Roser, J. E., Manicò, G., Pirronello, V. & Vidali, G. 2002, Astrophys. J., 581, 276

Roser, J. E., Swords, S., Vidali, G., Manicò, G. & Pirronello, V. 2003, Astrphys. J., 596, L55

Sivaraman, B. et al. 2008, Organic Matter in Space, IAU Symposium, 251, 451

Smoluchowski, R. 1981, Astrophys. & Space Sci., 75, 353

Smoluchowski, R. 1983, J. Phys. Chem., 87, 4229

Vidali, G., Ihm, G., Kim, Y. S., & Cole, M.W. 1991, Surf. Sci. Rep., 12, 133

Vidali, G. et al. 2005, J. Phys.: Conf. Ser., 6, 36

Vidali, G., Li, L., Roser, J.E., & Badman 2009, Adv. Space Research, 43, 1291

Vidali, G. & Li, L. 2010, J. Phys.: Condens. Matter 22, 304012

Watanabe, N., et al. 2010, Astrophys. J., 714, L233

This preprint was prepared with the AAS LaTeX macros v5.2.

NASA LAW, October 25-28, 2010, Gatlinburg

Laboratory Spectroscopy of Ices of Astrophysical Interest

Marla H. Moore & Reggie L. Hudson

NASA Goddard Space Flight Center, Greenbelt, MD 20771

marla.h.moore@nasa.gov, reggie.l.hudson@nasa.gov

ABSTRACT

Ongoing and future NASA astronomy missions need detailed information on the spectra of ices of a variety of species to help establish the identity and abundances of molecules observed in astronomical data. Examples of condensed phase molecules already detected in cold cloud regions include: H_2O, CO, CO_2, OCS, OCN^-, NH_3, CH_4, and CH_3OH. In addition there is the ongoing search for signatures of more complex carbon-containing species. Existing and future observations often impose special requirements on the information that comes from the laboratory. For example, the measurement of spectra, determination of integrated band strengths, and extraction of complex refractive indices of ices (and icy mixtures) in both the amorphous and crystalline phase at relevant temperatures are an important data set. Similarly the measurement of spectra of species embedded in astrophysically relevant ice matrices is important. One of the newer requirements is for laboratory studies of ices in the far-infrared wavelength region and at temperatures as low as 7 K. This laboratory astrophysics review will look at some of the existing experimental work and capabilities in this area along with what more may be needed to meet current and future NASA Astrophysics mission needs.

1. Introduction

Laboratory spectra of ices have been applied to observations of objects located in a variety of space environments enabling the identification of icy species. In cometary and planetary environments, H_2O ice has been identified in the spectrum of, e.g. Comet Hale-Bopp and the rings of Saturn. Nitrile ices have been identified in the atmosphere of Titan. On the surfaces of many of the outer satellites and TNOs a variety of icy mixtures dominated

either by H_2O, sulfur, or N_2 ices are known. The wavelength region over which these identifications have been made is roughly from 2 to 55 μm. This brief review will focus on the application of laboratory spectra to the identification of icy species in interstellar regions. Currently, a conservative list of identified ices includes H_2O, CO, CO_2, $^{13}CO_2$, OCN^-, OCS, CH_3OH, and CH_4.

2. Applications of Laboratory Spectra to Observational Data

Relevant laboratory spectral data that provides band positions, shapes, intensities and optical constants have been used and continue to be needed for the interpretation of observations. Listed below are three illustrations of how observed vibrational bands have been interpreted using laboratory data leading to the identification of icy species:

- The identification of H_2O at 3 μm in several sources is discussed by Smith et al. (1989). Optical constants for H_2O were available for amorphous-phase ice at 10, 23, and 77 K, and for crystalline phase at 150 K (see references in Smith et al. 1989). These optical constants together with models for the radii of the underlying interstellar grains were used to generate fits to the observations.

- The identification of CH_3OH at 3.53 μm is described in a paper by Allamandola et al. (1992). The laboratory absorption spectrum of CH_3OH formed at 10 K was a good match for the distinctive absorption feature found on the low-frequency wing of the H_2O band for several sources.

- The identification of the 4.62 μm band with that of the ion, OCN^-, is discussed by Hudson et al. (2001). Before systematic laboratory studies were available, the label for this feature was "XCN" and candidate ice species such as HNCO or CH_3NC were suggested absorbers. After many laboratory experiments involving a variety of ices, isotopes, and thermal and radiation studies it was demonstrated that the OCN^- ion was the carrier for the absorption feature that formed at 4.62 μm in processed laboratory ices. It is a marker of energetic processing of ices in interstellar environments.

- Through comparisons to laboratory data, the 15 μm bending mode features of CO_2 observed in interstellar ices were shown to indicate the that this molecule exists in at least two phases of ice: one rich in H_2O and one rich in nonpolar ice species (de Graauw et al. 1996; Gerakines et al. 1999). The profile of the CO_2 interstellar ice feature also indicates that CH_3OH exists in many of the CO_2-bearing ice mantles toward young stellar objects.

Using existing laboratory spectra, all of the main absorption features seen in the *ISO*-LWS spectrum of W33 A (see, e.g., Gibb et al. 2000) from 2.4 to 25 μm have been identified. The identification of ice absorption features overlapping with the 10 μm silicate band are less secure as are those that overlap in the 6-6.8 μm region. The identifications of weaker features with absorptions of, e.g., $HCOO^-$, HCOOH, or NH_4^+ are also less secure and will require additional observations.

Water is the dominant ice in W33 A and other interstellar ice environments, as it is in cometary nuclei and in many planetary environments. Solar system exceptions are the sulfur-dominated ice environment on Io and the nitrogen-ice dominance on Triton, Pluto, and some TNOs. It is not surprising that H_2O ice has had its optical constants determined over a very wide wavelength region. A survey of these measurements was originally compiled by Warren (1984), and more recently updated by Warren & Brandt (2008). These papers include references to both amorphous and crystalline-phase H_2O ice studies at several different temperatures, and studies in both the mid- and far-IR to 1000 μm. In addition to H_2O, the ubiquitous CO_2 ice feature at 4.2 μm is found in both planetary and interstellar environments. Its optical constants have also been determined over a wide wavelength region (see survey by Warren 1986 and references to more recent work in Table 1). Although the optical properties of H_2O and CO_2 have been studied, future observations by *Herschel*, *SOFIA* and *SPICA* will generate needs for optical constants, band positions, band shapes, and FWHMs for other known and suspected interstellar ices in the far-IR.

3. Parameters Influencing Spectra

Factors affecting the precise peak position, band shape, and FWHM of IR vibrational absorption features for pure ices are: (1) ice phase, (2) temperature, and (3) crystalline quality. A few examples from the literature are listed below where these factors are studied or discussed for far-IR spectra:

- Far-IR spectra of both the amorphous and crystalline-phase of H_2O, CH_3OH, CO_2, H_2CO and NH_3 ices are compared in Moore & Hudson (1994).
- Hudgins et al. (1993) show figures where the changes in the far-IR spectra of H_2O and CH_3OH can be followed as the ice converts from the amorphous to the crystalline phase with warming.
- Far-IR spectra of amorphous and crystalline-phase nitrile ices (HCN, C_2N_2, CH_3CN, C_2H_5CN, and HC_3N) show differences in band shape, FWHM, and peak position (Dello Russo & Khanna 1996; Moore et al. 2010).

- Moore & Hudson (1994) show that there are reversible changes in peak frequencies for crystalline ices as a function of temperature.

In the laboratory and in space, the exact position of an observed absorption feature can be used to determine the formation temperature or thermal history of the ices. However, in the case of crystalline-phase ice, the quality of the crystalline structure needs to be considered. Moore et al. (2010) showed clear evidence that amorphous-phase ice that has been converted to the crystalline phase by warming to and holding at the ice's annealing temperature is a less-ordered ice than that attained through quenching the gas at the annealing temperature. The peak position and FWHM for some bands were found to be different in the two cases. In some environments, such as in Titan's atmosphere, ices are formed as descending gases are quenched in the stratosphere forming crystalline-phase ice. Similarly, in complex nebular environments warm gas could be quenched as it moves into colder regions, producing crystalline phase ice. For these environments, spectra of quenched laboratory ices, rather than annealed ices, may be the correct spectral model.

The peak positions, band shapes, and FWHMs of absorption features in the spectra of icy mixtures are affected by the nature of the matrix material, concentration of components, temperature, phase, and crystalline quality of the mixture. A few examples from the literature that illustrate the effects of these factors are:

- Mid-IR spectra of CO mixed in both polar and non-polar ice matrices were studied by Ehrenfreund et al. (1996). These data were used to help fit the 4.67 μm band of CO ice observed in several dense cloud regions (Chiar et al. 1998). Some fraction of CO in both polar and non-polar matrices was needed to produce the best fit to the observations, suggesting that both ice types existed within the line of sight.

- Sandford & Allamandola (1990) discuss the band position, shape, and FWHM of the 4.2 μm CO_2 absorption feature for different concentrations of CO_2 in H_2O + CO_2 icy mixtures. White et al. (2009) present mid-IR spectra, peak positions, and FWHM for the 15 μm bending mode of CO_2 both in the pure ice and in a variety of mixtures with H_2O and/or CH_3OH. Subsequent warming of these ices showed that each evolves differently producing a variety of band shapes. New mid-IR spectra by Knez et al. (2009) using different concentrations of C_2H_2 in polar and non-polar matrices show peak position and band shape changes as a function of temperature.

- The influence of crystalline quality on absorption spectral bands was discussed by Sandford & Allamandola (1990). An H_2O + CO_2 ice mixture formed at 10 K was slowly warmed to near 100 K. The same gas mixture was quenched at 100 K and its

spectrum showed a narrower 4.2 μm CO_2 absorption feature. The crystalline quality of icy mixtures is also discussed by Schmitt et al. (1998).

4. Determining Optical Properties of Ices

Calculated parameters from laboratory data of value to astronomers include (1) the intrinsic band strength (A-value), (2) absorption coefficient (α), and (3) optical constants, the real, n, and imaginary, k, values. The intrinsic band strength is of interest to observers since knowing the A-value (in cm molec^{-1}) and the area under an observed feature allows one to calculate the column density of that material in the line of sight. However, a potentially unsafe laboratory assumption is the value of the ice density that is required to determine an A-value. The absorption coefficient, α (in cm^{-1}) in many papers, is used to estimate the extinction coefficient using the relationship $k = \alpha/4\pi\nu$ (where ν is the wavenumber). Because multiple reflection losses are not accounted for, this calculation is an approximation. The most correct method for calculating k is by extracting the optical constants, both the real (n) and imaginary (k) refractive indices. Only by determining the optical constants is the entire optical transfer of light considered, including all reflection losses.

Optical constants are needed for the quantitative analysis of observational data. Knowing the complex refractive indices (the real and imaginary parts, n and k, respectively), observational data can be treated quantitatively using a radiative transfer approach. Combined with scattering theory and particle size distributions, one can calculate synthetic spectra for fitting purposes. Potentially unsafe assumptions required for the optical constants are the values of the ice density and the index of refraction at visible wavelengths (e.g., see Moore et al. 2010). Table 1 is a summary of far-IR (beginning at 500 cm^{-1}, 20 μm) optical constants currently available in the literature.

5. Conclusion - Future Needs

Some of the current and future laboratory needs related to laboratory spectroscopy of relevant ice species are listed:

- Measurements of laboratory IR spectra of ices/icy mixtures at relevant temperatures and phase are needed especially for the far-IR region. Characterization of known interstellar ice species in the far-IR, and both mid- and far-IR characterization of likely minor condensates (e.g., C_2H_2, C_2H_6, and HCN) will be valuable as higher quality observations become available.

- Extraction of optical constants from well characterized mid- and far-IR spectra will be of value to the observational community for fits to data.
- Determination of the visible index of refraction of ice films in both the amorphous and crystalline phase is essential in support of the extraction of optical constants.
- Quantification of ice density for well determined laboratory conditions is necessary in support of calculations of optical constants and determination of A-values.

This work was supported by the following NASA programs: Astronomy and Physics Research and Analysis, Planetary Geology and Geophysics, Planetary Atmospheres, Outer Planets Research, Cassini Data Analysis, Mars Fundamental Research, and Exobiology. The support of the NASA Astrobiology Institute's Goddard Center for Astrobiology is acknowledged.

REFERENCES

Allamandola, L. J., Sandford, S. A., Tielens, A. G. G. M., & Herbst, T. M., 1992, Ap. J. 399, L34

Bertie, J. E., Labbe, H. J., & Whalley, E., 1996, J. Chem. Phys. 50, 4101

Chiar, J. E., Gerakines, P. A., Whittet, D. C. B., Pendleton, Y. J., Tielens, A. G. G. M., Adamson, A. J., & Boogert, A. C. A., 1998, Ap. J. 498, 716

Curtis, D. B., Rajaram, B., Toon, O. B., & Tolbert, M. A., 2005, Applied Optics, 44, 4102

de Graauw, T., et al. 1996, A&A 315, L345

Dello Russo, N., & Khanna, R. K., 1996, Icarus, 123, 366

Ehrenfreund, P. Boogert, A. C. A., Gerakines, P. A., Jansen, D. J., Schutte, W. A., Tielens, A. G. G. M., & van Dishoeck, E. F., 1996, A&A, 315, 341

Gerakines, P. A., et al. 1999, Ap. J. 522, 357

Gibb, E. L., Whittet, D. C. B., Schutte, W. A., Boogert, A. C. A., Chiar, J. E., Ehrenfreund, P., Gerakines, P. A., Keane, J. V., Tielens, A. G. G. M., van Dishoeck, E. F., & Kerkhof, O., 2000, Ap. J. 536, 347

Hudson, R. L., Moore, M. H., & Gerakines, P. A., 2001, Ap. J. 550, 1140

Hudgins, D. M., Sandford, S. A., Allamandola, L. J., & Tielens, A. G. G. M., 1993, Ap. J. Suppl Series, 86, 713

Johnson, B. R. & Attreya, S. K.,1996, Icarus 119, 405

Knez, C. Moore, M., Ferrante, R. & Hudson, R., 2009, BAAS 214, 663

Martonchik, J. V., Orton, G. S., & Appleby, J. F., 1984, Applied Optics, 23, 542

Moore, M. H. & Hudson, R. L., 1994, Astron. & Astrophys. Supp. Ser. 103, 45

Moore, M. H., Ferrante, R. F. Moore, W. J., & Hudson, R. L., 2010, Ap. J. Supp. Ser. 191, 96

Khanna, R. K., Ospina, M. J., & Zhao, G., 1988, Icarus, 73, 527

Ospina, M., Zhao, G., & Khanna, R. K., 1988, Spectrochimica Acta, 44A, 23

Sandford, S. A. & Allamandola, L. J.,1990, Ap. J. 355, 357

Schmitt, G., Quirico, E., Trotta, F., & Grundy, W. M. 1998. In Solar System Ices (Schmitt et al. eds) Kluwer Academic Publishers, pp. 199-240

Sill, G. Fink, U., & Ferraro, J. R., 1980, J. Opt. Soc. Am., 70, 724

Smith, R. G., Sellgren, K., & Tokunage, A. T., 1989, Ap. J. 344, 473

Warren, S. G., & Brandt, R. E., 2008, J. Geophys. Rev. 113, D14220

Warren, S. G., 1984, Applied Optics 23, 1206

Warren, S. G.,1986, Applied Optics 25, 2650

White, D. W., Gerakines, P. A., Cook, A. M., & Whittet, D. C. B., 2009, Ap. J. Supp. Ser. 180, 182

This preprint was prepared with the AAS LaTeX macros v5.2.

Table 1: A summary of current published far-IR optical constant data.

Molecule	Spectral Range		Phase	Temperature	Reference
	[cm^{-1}]	[μm]		[K]	
H_2O	500-30	20-233	Crystalline	100	Bertie et al. (1996)
H_2O	500-100	20-100	Amorphous Crystalline	77 100, 150	Johnson & Attreya (1996)
H_2O	500-50	20-200	Amorphous Crystalline	10-100 150	Hudgins et al. (1993)
H_2O	500-50	20-200	Amorphous & Crystalline	106-176	Curtis et al. (2005)
CO_2	500-100	20-100	Crystalline	80, 100, 120	Johnson & Attreya (1996)
NH_3	500-50	20-200	Crystalline	77-88	Martonchik et al. (1984)
CH_3OH	500-50	20-200	Amorphous Crystalline	10-100 120	Hudgins et al. (1993)
Nitriles: HCN, C_2N_2, CH_3CN, C_2H5CN, HC_3N	500-30	20-333	Amorphous & Crystalline	Temps including 50, 75, 95, 110, 120, 135	Moore et al. (2010)
Nitriles: HCN, C_2N_2, CH_3CN, C_2H5CN, HC_3N, CH_2CHCN, C_4N_2, CH_3C_3N	500-80	20-125	Crystalline	35, 95	Dello Russo & Khanna (1996)
C_2N_2	500-200	20-50	Crystalline	70	Ospina et al. (1988)
C_2H_2, C_4N_2	500-200	20-50	Crystalline	70	Khanna et al. (1988)

NASA LAW, October 25-28, 2010, Gatlinburg

The Origins and Evolution of Molecules in Icy Solids

R. L. Hudson & M. H. Moore

Astrochemistry Laboratory, NASA Goddard Space Flight Center, Greenbelt, MD 20771

reggie.hudson@nasa.gov, marla.h.moore@nasa.gov

ABSTRACT

It is now well established that molecular ices exist in the interstellar medium, on cometary surfaces, and on the satellites and other bodies of the outer solar system. Such ices, despite temperatures on the order of 10 - 100 K, are certainly not inert, but rather change in response to cosmic rays, far-UV photons, and magnetospheric radiation. Laboratory studies of the chemistry thus initiated in these ices is briefly reviewed in this paper and some needs and challenges for the future are listed.

1. Introduction

Astronomical observations of the past few decades have revealed the existence of a variety of molecules in extraterrestrial ices. These molecules include H_2O, CO, and CO_2, OCS, and organics such as CH_4, CH_3OH, and C_2H_6. Some ices are dominated by polar molecules, while non-polar N_2 and hydrocarbons appear to dominate others. Observations, mainly in the infrared (IR) and radio regions, have allowed the inference of other solid-phase molecules whose formation remains difficult to understand by gas-phase chemistry alone.

Several laboratory research groups have reported extensive and elaborate experiments on the reaction chemistry of icy materials, generally as initiated by either ionizing radiation or by vacuum-UV photons. These experiments not only permit molecular identifications to be made from astronomical observations, but also allow for predictions. The 10 - 100 K temperature range has received the most interest, with appropriate radiation and photon doses being applied to ice analogs of interstellar, cometary, and icy-satellite molecules.

This laboratory approach has evolved over more than 30 years with much of the earliest work focusing on complex mixtures thought to represent either cometary or interstellar

ices. Although those early experiments documented a rich solid-state photo- and radiation chemistry, they revealed few details of reactions for particular solid-phase molecules, partly due to the multi-component nature of the samples (Hagen et al. 1979; Moore et al. 1983). Since then, model systems have been examined that allow the chemistry of individual species and specific reactions to be probed. Reactions involving most of the smaller astronomical molecules have been studied, and specific processes identified. The current state of laboratory ice chemistry suggests that a variety of reactions can occur, including atom additions, reductions, oxidations, acid-base processes, dimerization of radicals, proton transfers, and isomerizations.

2. Goals and Methods

Two important goals of the laboratory study of the chemistry of extraterrestrial ices are (i) to explain the presence of molecules observed in extraterrestrial environments and (ii) to predict as yet unobserved species. For the first goal one hopes for an understanding of both the sequence of chemical reactions leading to an observed molecule and, when possible, reaction yields, rates, and equilibrium abundances. Abundances also require knowledge of a molecule's destruction rate and the relevant reaction paths. For predictions of new molecules, uncertainties in what is known of astronomical environments (e.g., temperature, radiation) can limit quantitative statements, but the problem is not so severe as to prevent verifiable predictions from being made.

The primary analytical tools used for the laboratory study of astronomical ices are infrared spectroscopy and mass spectrometry (MS). Ices of interest are prepared under vacuum at a specific temperature, usually near 10 K for interstellar and cometary applications, but closer to 100 K for many planetary studies (e.g., Jovian satellites, Titan). Changes in an ice are initiated by warming, by exposure to vacuum-UV photons, by ionizing radiation (e.g., keV electrons or MeV ions), or with some combination of all of these. Sputtered material, or material released on warming, can be detected mass spectrometerically, and IR spectroscopy can be used for *in-situ* detection of chemical changes. Other techniques have been applied, but none has achieved either the popularity or the success of IR and MS methods. Among these other techniques are Raman spectroscopy, electron spin resonance spectroscopy, and various forms of photoelectron spectroscopy. Measurements in the UV and visible regions have been reported in some cases, but the lack of characteristic spectral features for specific ice molecules is problematic. Studies of ice chemistry using far-IR and longer wavelengths are still rare, although needed for understanding observations with Herschel, Spitzer, Cassini-CIRS, and other instruments.

It is at first surprising to discover that the IR-observed chemical changes in H_2O-dominated ices caused by ions, electrons, and far-UV photons depend but slightly on the initial energy in each case. Photons and particles in the keV and MeV regions cause ionizations of frozen H_2O molecules to produce H_2O^+ and energetic electrons, which initiate much of the observed chemistry (Swallow 1973). It is not as well known that condensed-phase molecules, such as H_2O (Boyle et al. 1969) and PAHs (Gudipati & Allamandola 2004), can experience a substantial lowering of their first ionization energy from its gas-phase value, to the degree that far-UV photolysis can produce a chemistry similar to that of radiolysis. This suggests that the oft-presented competition of photo- and radiation chemical changes in astronomical ices may be difficult, if not impossible, to unravel. In other words, both photochemistry and radiation chemistry give rise to similar final reaction products. (See Hudson & Moore (2002) for a rare exception.)

3. Examples and Case Histories

One example of how laboratory studies have contributed to our understanding of ice chemistry is in the study of triply-bonded molecules, such as CO and C_2H_2 (acetylene) in H_2O-rich ices. Each triple bond is resistant to cleavage by vacuum-UV photons, while higher-energy photons and ions tend to give complex, refractory carbon-oxide and hydrocarbon products. However, in an ice dominated by H_2O, both ionizing radiation and far-UV photons will produce H atoms and OH radicals from H_2O, with sufficient energy to combine with both CO and C_2H_2. The resulting reaction paths are as follows:

$$C{\equiv}O \rightarrow H_2CO \rightarrow CH_3OH$$

$$HC{\equiv}CH \rightarrow C_2H_4 \rightarrow C_2H_6$$

In each case the bond-order between the non-hydrogen atoms is reduced from 3 to 2 to 1. The spectra in Fig. 1 show an example of this transformation for the proton irradiation of H_2O + CO near 15 K. Before the irradiation (0.8 MeV p^+) the spectrum in this region is essentially featureless. After irradiation, the uppermost trace shows multiple absorbances, shoulders, and inflections, which can be assigned with the aid of reference spectra of unirradiated ices, as shown in the four lower traces. A reaction sequence is given in Fig. 2, and quantification of the products has been published by Hudson & Moore (1999). Note that the asterisks in the figure are for two bands of the formate ion ($HCOO^-$). When NH_3 was present initially, to form a three-component H_2O + CO + NH_3 ice, then OCN^- and NH_4^+ were detected in the final products (Hudson et al. 2001).

Essentially the same reaction scheme applies to H_2O-rich ices containing C_2H_2, as shown

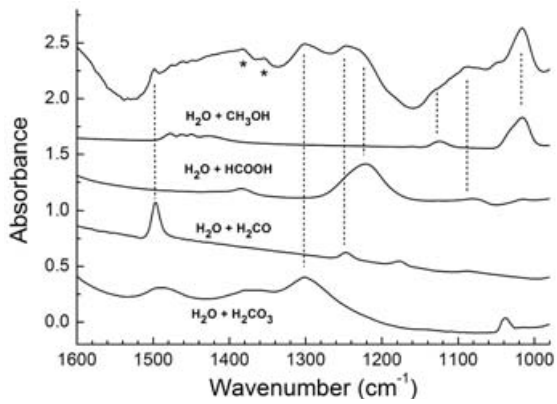

Fig. 1.— IR spectrum of a proton-irradiated H_2O + CO (∼10:1) ice near 15 K. The dose was about 5 eV per molecule.

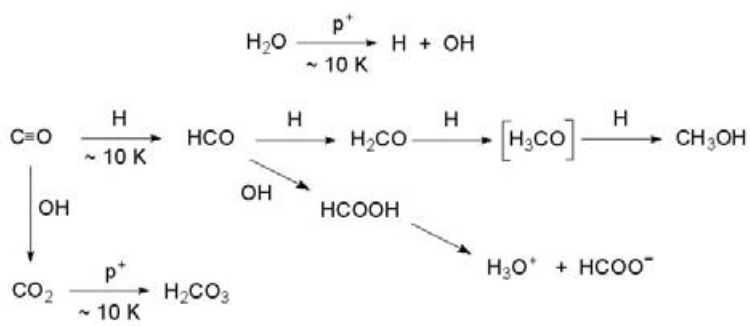

Fig. 2.— Reaction scheme for a proton-irradiated H_2O + CO (∼10:1) ice near 15 K.

in Fig. 3 of Moore & Hudson (1998). That the same scheme fits these two cases is not surprising given the isoelectronic relationship between CO and C_2H_2. For both molecules, the addition of H and OH to an unsaturated system is clearly demonstrated. These results bear on the problems of CH_3OH (methanol) formation in interstellar environments and the unexpectedly high C_2H_6 abundance in some comets (Mumma et al. 1996).

As a bonus, these experiments led to two predictions of extraterrestrial molecules that were subsequently confirmed. The vinyl alcohol, $CH_2CH(OH)$, of Fig. 3 later was discovered in the ISM by Turner & Apponi (2001). Our subsequent studies of methanol (Hudson & Moore 2000) led to the conclusion that $(CH_2OH)_2$, ethylene glycol, should be both interstellar and cometary, and observations agree, such as the cometary work of Crovisier et al. (2004). Multiple synthetic pathways can be envisioned for ethylene glycol, with the dimerization of hydroxymethyl radicals (H_2COH) being perhaps the most straightforward.

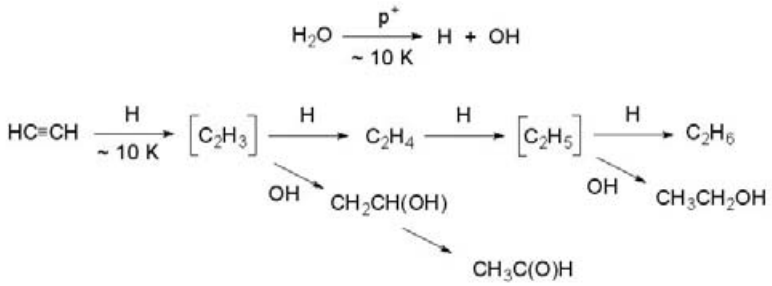

Fig. 3.— Reaction scheme for a proton-irradiated H_2O + C_2H_2 (∼10:1) ice near 15 K.

The examples given so far are for molecules formed from a precursor by free-radical chemistry, but intramolecular changes also are known from laboratory experiments. In a 2004 paper we described rearrangements of CH_3CN in various ices (Hudson & Moore 2004), both polar and non-polar. In all cases we detected the $H_2C{=}C{=}NH$ isomer, known as ketenimine. The latter was subsequently discovered in the ISM in 2006 (Lovas et al. 2006).

Using just these three types of reactions (reduction, dimerization, isomerization), one can make predictions of other interstellar and cometary molecules. For example, since CH_3CN rearranges to $H_2C{=}C{=}NH$, then the isoelectronic NH_2CN is expected to isomerize to HCNCH, which has a published high-resolution IR spectrum (Birk & Winnewisser 1986), but has not yet been observed in an extraterrestrial environment. As another example, since H_2COH radicals from CH_3OH are known to dimerize to give $(CH_2OH)_2$ in ices, then it is safe to predict that H_2CCN radicals from CH_3CN also will dimerize to give $(CH_2CN)_2$, the succinonitrile molecule.

Many additional laboratory-based examples of molecular evolution in ices are available in the literature, both work from our own group and others. Both oxidations and reductions have been reported, along with atom capture (e.g., $CO_2 \rightarrow CO_3$), molecular eliminations (e.g., $CH_3OH \rightarrow H_2CO$), and insertion reactions, among many others. Our compilation in Hudson et al. (2008) was published for the planetary-science community, but the same results apply to interstellar ice chemistry.

4. Difficulties and Needs

The study of molecular evolution in extraterrestrial ices has reached a certain state of maturity after several decades of activity. Almost all classes of small organics, and numerous inorganics, have been examined to the degree that few surprises are expected. Nevertheless, much laboratory work remains, and so we end with a list of needs and challenges.

1. Large molecules - The icy chemistry of small organic molecules (under about 10 atoms) has received substantial attention by laboratory astrochemists. However, some of the more-exciting discoveries in recent years have involved larger systems, such as C_{60}, PAHs, and long-chain unsaturated nitriles. See, for example, Cami et al. (2010). Although reactions of such molecules have been studied in the solid state, little success has been reported on their *syntheses* in ices. Success would likely shed light on the formation of complex molecules in meteorites.

2. Better quantification - Much of the laboratory work to date on astronomical ices has focused on the identification of reaction products and pathways. A much-needed next step will involve greater quantification of reaction rates and product abundances.

3. Many experiments now have been reported on one-component ices, complementing earlier work with ice mixtures. Although experiments with single-component samples are relatively easy to conduct, and constitute important baseline studies (e.g., Kim et al. 2010), a new examination is needed of selected multi-components ices, especially including competition studies.

4. Molecular destructions also are rather easy to study and numerous experiments are in print (e.g., Peeters et al. 2005). What is needed next are results that quantify branching ratios among reaction channels for, as an example, photo- and radiolytic destructions in ices.

5. It already has been stated that to a first approximation photolysis and radiolysis of ices give similar products. However, in only a few cases have the yields of those products been compared quantitatively (e.g., Baratta et al. 2002).

6. Most of the experiments cited in this paper have been conducted on ice samples of micrometer thickness. However, results are starting to appear on sub-micrometer-size samples that, to avoid substantial contamination, must be studied under ultra-high vacuum conditions (e.g., Öberg et al. 2010). The degree to which these experiments will reveal new chemistry is unknown, but their relevance to the study of interstellar ices is substantial.

7. Molecules in astronomical ices can be observed in the IR, but much of the motivation for the laboratory work described here results from the ejection of molecules from ices into the gas phase, for subsequent radio detection. While multiple mechanisms have been proposed for solid-to-gas ejections, few lab-based tests and quantitative comparisons exist.

8. Several research groups studying the chemistry of extraterrestrial ices are now well established in the US and abroad (e.g., Italy, France, Japan, and the Netherlands). Nevertheless, the impression of some veteran researchers is that relatively few new workers are entering the field, despite a substantial need for additional data for Spitzer, SOFIA, Herschel,

and other observatories.

9. Finally, there is the issue of instrumentation and techniques. New laboratory methods are needed for the examination of the chemistry and physics of astronomical ices. The past and present heavy reliance on IR methods should be supplemented with exploratory work involving, among other approaches, ESCA and fluorescence methods. For NASA purposes, some of the techniques used by laboratory astrochemists could more readily be adapted to flight missions than others.

5. Conclusion

Although laboratory investigations of astronomical ices have been conducted for several decades, there is an on-going need for new work. Neither computational methods nor theoretical modeling are sufficiently advanced to either explain or predict the complexities of ice chemistry, such as equilibrium abundances, product ratios, and reaction efficiencies. NASA missions, such as Spitzer, Sofia, Galileo, and SOFIA, have returned results that cannot be interpreted without the aid of laboratory data.

The authors' work was supported by the following NASA programs: Astronomy and Physics Research and Analysis, Planetary Geology and Geophysics, Planetary Atmospheres, Outer Planets Research, Cassini Data Analysis, Mars Fundamental Research, and Exobiology. The support of the NASA Astrobiology Institute's Goddard Center for Astrobiology also is acknowledged.

REFERENCES

Baratta, G. A., Leto, G. & Palumbo, M. E., 2002, Astronomy & Astrophysics, 384, 343

Birk, M., & Winnewisser, M, 1986, Chem. Phys. Letters, 123, 386

Boyle, J. W., Ghormley, J. A., Hochanadel, C. J., & Riley, J. F., 1969, J. Phys. Chem., 73, 2886

Cami, J., Bernard-Salas, J., Peeters, E., & Malek, S. E., 2010, Science, 329, 1180

Crovisier, J., Bockelée-Morvan, D., Biver, N., Colom, P., Despois, D., & Lis, D. C., 2004, Astronomy & Astrophysics, 418, L35

Gudipati, M., & Allamandola, L., 2004, Astrophysical Journal, 615, L177

Hagen, W., Allamandola, L. J., & Greenberg, J. M., 1979, Astrophysics and Space Science, 65, 215

Hudson, R. L., & Moore, M. H., 1999, Icarus, 140, 451

Hudson, R. L., & Moore, M. H., 2000, Icarus, 145, 661

Hudson, R. L., Moore, M. H., & Gerakines, P. A., 2001, Astrophysical Journal, 550, 114

Hudson, R. L., & Moore, M. H., 2002, Astrophysical Journal, 568, 1095

Hudson, R. L. & Moore, M. H., 2004, Icarus, 172

Hudson, R. L., Palumbo, M. E, Strazzulla, G., Moore, M. H., Cooper, J., & Sturmer, S. J., 2008, The Solar System Beyond Neptune, M. A. Barucci, H. Boehnhardt, D. P. Cruikshank, & A. Morbidelli, Tucson: University of Arizona Press, 507

Kim, Y. S., Bennett, C. J., Chen, L., O'Brien, K., & Kaiser, R. I., 2010, Astrophysical Journal, 711, 744

Lovas, F. J., Hollis, J. M., Remijan, A. J., & Jewell, P. R., 2006, Astrophysical Journal, 645, L137

Moore, M. H., Donn, B., Khanna, R., & A'Hearn, M. F., 1983, Icarus, 54, 388

Moore, M. H., & Hudson, R. L., 1998, Icarus, 135, 518

Mumma, M. J., DiSanti, M. A., Dello Russo, N., Fomenkova, M., Magee-Sauer, K. Kaminski, C. D., & Xie, X., 1996, Science, 272, 1310

Öberg, K. I., van Dishoeck, E. F., Linnartz, H., & Andersson, S., 2010, Astrophysical Journal, 718, 832

Peeters, Z., Botta, O., Charnley, S. B., Kisiel, Z., Kuan, Y.-J., & Ehrenfreund, P., 2005, Astronomy & Astrophysics, 433, 583

Turner, B. E., & Apponi, A. J., 2001, Astrophysical Journal, 561, L207

Swallow, A. J., 1973, Radiation Chemistry, New York: John Wiley

---

This preprint was prepared with the AAS LaTeX macros v5.2.

NASA LAW, October 25-28, 2010, Gatlinburg

Magnetic Reconnection and Angular Momentum Transport

Hantao Ji

Princeton Plasma Physics Laboratory, Princeton University, Princeton, NJ 08543

hji@pppl.gov

ABSTRACT

Significant progress has been made in the past decade in laboratory studies of magnetic reconnection and angular momentum transport; both of which are important plasma processes in astrophysics. In the area of magnetic reconnection, Hall effects were confirmed and an electron diffusion region with associated wave activity were identified near the reconnection site. Next generation reconnection experiments will access new phases in large-sized and high-S plasmas, as well as reconnection in partially ionized plasmas. In the area of angular momentum transport, hydrodynamic turbulence was shown to be insufficient to explain the angular momentum transport required for fast accretion. The first demonstration of the Magnetorotational Instability (MRI) is in progress on a liquid metal experiment. Gas and plasma experiments are being developed to explore new regimes for the MRI.

1. Introduction to Plasma Astrophysics

The visible universe is dominated by matter in the plasma form. Example range from extremely weakly ionized plasmas in molecular clouds to fully ionized relativistic plasmas around neutron stars; from usual electron-ion plasmas to exotic electron-positron plasmas; from extremely tenuous plasmas in clusters to superdense degenerated plasmas in stellar interiors. The physics of these extremely diverse plasmas is of critical importance for understanding the observed astrophysical phenomena.

In order to assess major opportunities in this relatively young field of plasma astrophysics, a grass root activity, called the Workshop on Opportunities in Plasma Astrophysics or WOPA (http://www.pppl.gov/conferences/2010/WOPA/), was initiated. More than 70 experts participated through ten topical groups from three communities: laboratory plasma

physics, space and solar physics, and astrophysics, roughly equally distributed between observers/experimentalists and theorists/modelers. A workshop report titled "Research Opportunities in Plasma Astrophysics", highlighting ten major plasma astrophysics questions, was generated. The ten major plasma astrophysics questions are

1. How do magnetic explosions work?
2. How are cosmic rays accelerated to ultrahigh energies?
3. What is the origin of coronae and winds in virtually all stars, including Sun?
4. How are magnetic fields generated in stars, galaxies, and clusters?
5. What powers the most luminous sources in the universe?
6. How is star and planet formation impacted by plasma dynamics?
7. How do magnetic field, radiation and turbulence impact supernova explosions?
8. How are jets launched and collimated?
9. How is the plasma state altered by ultra-strong magnetic field?
10. Can magnetic fields affect cosmological structure formation?

To answer these questions, a sufficient understanding of the ten plasma processes is required, and each of them is discussed in a chapter. Among them are magnetic reconnection and angular momentum transport. Both these processes deal with effects related to magnetic fields. In this short article, a concise overview of laboratory studies of each of these processes is given, emphasizing the most recent achievements and near future prospects.

2. Roles of Laboratory Experiments in Understanding Astrophysical Plasmas

Before proceeding, some brief comments on the roles of laboratory experiments in plasma astrophysics are warranted since the field is quite different from other parts of laboratory astrophysics. Plasma experiments are made possible by significant advances over the past decades in laboratory plasma physics in terms of physical understanding, production and control technologies, and plasma diagnostics, with help from theory and modeling. Compared to observation of space and astrophysical plasmas, laboratory experiments can more easily allow for both *in situ* and remote sensing measurements of crucial physical quantities. Such

laboratory experiments can verify or confront theory, benchmark or challenge simulations, and provide unique opportunities to validate numerical codes. The latter can be a difficult task without quality data from well-controlled and well-diagnosed experiments. Results from laboratory experiments can also be directly compared with observations and therefore support space and astrophysical missions. Sometime, new physics can be discovered in the laboratory before being applied to explain observations. In short, laboratory plasma experiments can support space and astrophysical missions by helping achieve their science goals.

3. Magnetic Reconnection

Magnetic reconnection, the efficient release of magnetic energy by topological rearrangement of field lines, is one of the most important and fundamental plasma processes in space and astrophysical plasmas. It plays key roles in phenomena including solar and stellar flares, coronal mass ejections, solar wind propagation and dissipation, interaction of interplanetary plasma with Earth and other planets' magnetospheres, and energetic phenomena associated with magnetized neutron star and accretion disk coronae. Magnetic reconnection is also thought to regulate angular momentum transport (Sec. 4) by saturating the magnetorotational instability (MRI) in accretion disks and to be a necessary part of dynamo processes that maintain magnetic fields in the stars and in galaxies.

Important initial progress was made in understanding reconnection in 1950s and early 1960s as represented by the classical Sweet-Parker model, but its predicted reconnection rates are too slow to be consistent with observations. The Pestchek model predicts faster rates, but the required shock structures are unrealistic. Since then essentially no new progress was made until the 1990s when the significance of two-fluid physics to fast reconnection was demonstrated in numerical results. Major advances since then, including significant contributions from the laboratory, are summarized by two recent reviews (Zweibel and Yamada 2009; Yamada et al. 2010). Listed below are a few major contributions from the laboratory:

- Quantitative tests of the Sweet-Parker model (Ji et al. 1998). This classical reconnection model proposed in 1950s was not tested experimentally until late 1990s. Significant modifications were required for quantitative agreements with experiment.
- Two-fluid effects for fast reconnection (Ren et al. 2005; Brown et al. 2006). Existence of a quadrupolar out-of-plane magnetic field was predicted numerically (Birn et al. 2001), consistent with space data (e.g. Mozer et al. 2002), but definite confirmation by 2D measurements was done.

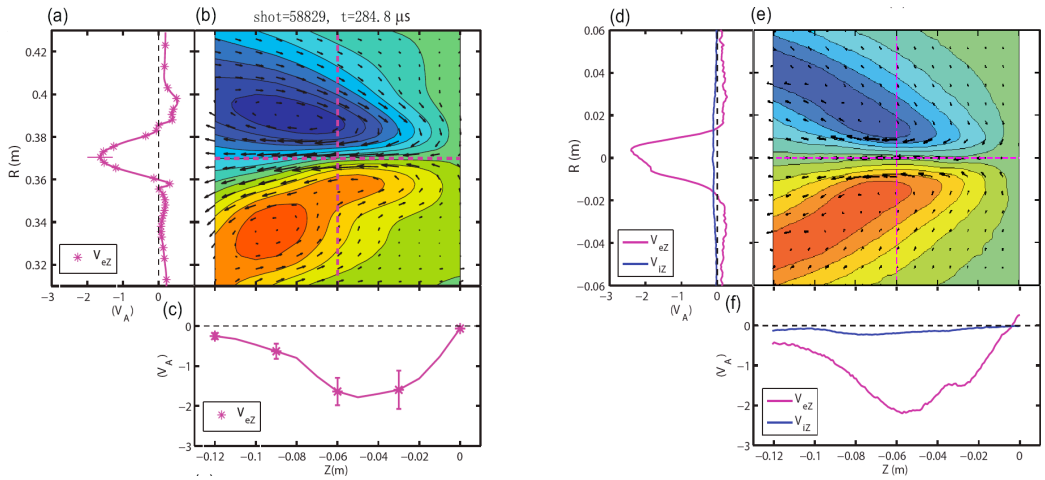

Fig. 1.— Comparisons between experiment and simulation Panels (a-c) show an experimental example taken from a hydrogen plasma. Results from a corresponding 2D simulation are shown in the same format in the lower three panels (d-f). Taken from Ji et al. (2008).

- Detection of the electron diffusion region (Ren et al. 2008). Its thickness was measured accurately and compared directly with state-of-the-art 2D PIC simulations as shown in Fig. 1. The comparisons challenged modeling and implied that 3D physics might be important in explaining the remaining disagreements with data (Ji et al. 2008). Detecting and studying the electron diffusion region is a goal of the MMS (Magnetospheric Multi Scale) mission scheduled for launch in 2014.

- Microturbulence in current sheets (Carter et al. 2002; Ji et al. 2004; Fox et al. 2008). Predicted theoretically, electrostatic fluctuations were detected for lower-hybrid drift waves or electron phase space holes, but electromagnetic fluctuations were surprises.

- Potential well and electron kinetics (Egedal et al. 2005). With measurements and physical understanding of the electrostatic potential around the X-line, one can quantitatively explain the measured electron distribution function near the Earth's magnetotail.

There exist two major opportunities for future reconnection experiments. The first is a next generation experiment based on the Magnetic Reconnection Experiment (MRX; http://mrx.pppl.gov) for reconnection study in plasmas of normalized size on the order of 10^3 and Lundquist number on the order of 10^5. The physics of reconnection in the new regime has more direct relevance with space and astrophysical plasmas than those already accessible by the existing experiments as indicated in a reconnection phase diagram (Ji and Daughton 2011). With the capabilities to access new regimes with multiple X-lines

reconnection, the critical issues on particle acceleration, global impulsive relaxation, and non-periodic boundary conditions in a large system can be studied.

The second opportunity involves reconnection in partially ionized plasmas which are also ubiquitous in astrophysics. A nearby example is reconnection in solar chromosphere where magnetic energetic activity has been observed by many existing solar observatories as well as a planned new mission called Interface Region Imaging Spectrograph (IRIS; http://iris.lmsal.com) scheduled for 2012 launch. However, the reconnection physics is still largely unexplored and in principle can be studied in the laboratory in detail. Various spectral lines sensitive to a wide range of plasma temperature will be used in the IRIS mission; comparable scoping experiments in partially ionized plasmas are underway in MRX.

4. Angular Momentum Transport

Accretions disks consist of gas, dust, and plasma rotating around and gradually falling onto a central object. Many important phenomena take place in accretion disks including formation of stars and planets in proto-star systems, the mass transfer and energetic activity in binary star systems, and efficient energy releases in quasars and active galactic nuclei. A common puzzle across all these kinds of accretion disks is why accretion occurs many orders of magnitude faster than predictions based on classical viscosity. This is equivalent to the question of how angular momentum is rapidly transported radially outwards. This rapid transport is generally attributed to the presence of rigorous turbulence in the accretion disk.

The difficulty of the problem, however, originates from the fact that there exist no known robust linear hydrodynamic instabilities in Keplerian disks where angular velocity, Ω, scales as radius, $R^{-3/2}$. Therefore, there exist only two main mechanisms to generate turbulence in accretion disks: (1) nonlinear hydrodynamic instabilities and (2) linear magnetohydrodynamic instabilities, more specifically the Magnetorotational Instability or MRI. The possibility of nonlinear hydrodynamic instabilities was discussed by Richard and Zahn (1999) based on experiments in the 1930s on Taylor-Couette flows. Their idea is similar to the subcritical transition shown to generate turbulence in pipe flows despite linear stability. They argue that in cool, star-forming disks where the ionization fraction is too low for the magnetic field to have an effect on disk dynamics, these non-magnetic, nonlinear hydrodynamic instabilities may be the only available mechanisms to generate the required turbulence. However, these nonlinear instabilities have not been demonstrated conclusively under astrophysically relevant conditions either theoretically, numerically, or experimentally.

In hot, sufficiently ionized accretion disks such as those found in binaries, magnetic

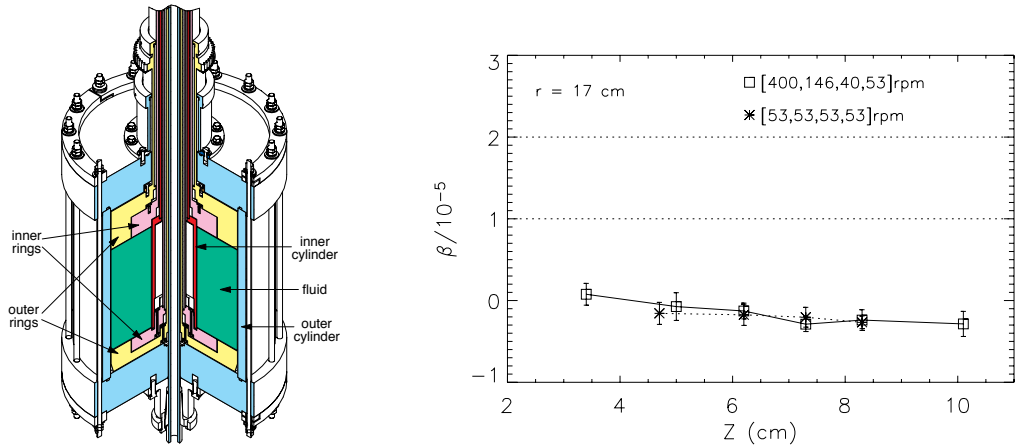

Fig. 2.— (left) End caps are divided into two rings in the Princeton MRI experiment; each of them are driven at the different speed to minimize the Ekman effect. (right) Measured angular momentum transport in quasi-Keplerian flows is indistinguishable from that in solid body flow with proper boundary controls, indicating no signs of turbulence.

field effects are widely expected to generate turbulence (Shakura and Sunyaev 1973). The well-accepted mechanism for the turbulence is the Magnetorotational Instability (MRI), originally discovered in 1950s and re-discovered for astrophysical applications by Balbus and Hawley (1991). The MRI is a linear ideal MHD instability which grows locally on the orbital timescale of Keplerian disks in a weak magnetic field. Because of the robustness of the MRI in numerical simulations, there is little doubt of the existence of MRI, but it has not been positively confirmed either observationally or experimentally in the laboratory. The key problem being hotly debated is how much turbulent viscosity the MRI can generate to transport angular momentum.

There are three kinds of laboratory experiments where angular momentum transport relevant to astrophysical disks can be studied. Hydrodynamic experiments on the quasi-Keplerian flow (where $d(R^2\Omega)/dR > 0$ and $d\Omega/dR < 0$) in Taylor-Couette geometry began only recently. It was found that such flows are extremely sensitive to axial boundary conditions due to the Ekman circulation (Kageyama et al. 2004), which is minimized by active controls as shown in Fig.2(left)(Schartman et al. 2009). Local Reynolds stress for angular momentum transport was determined through correlating radial and azimuthal velocity components. It was found that there are no signs of turbulence in quasi-Keplerian flows with boundary controls at Reynolds numbers up to 2×10^6 (Ji et al. 2006; Schartman et al. 2010), as shown in Fig.2(right). The measured transport efficiency is significantly below the

requirements set by the observed accretion rates. Scaling these results to accretion disks, it seems highly unlikely that hydrodynamic turbulence is responsible for fast accretion even for cool disks. Future tasks for hydrodynamic experiments should address questions including why quasi-Keplerian flows are so nonlinearly stable and whether coherent waves such as Rossby waves (Rossby et al. 1939) can efficiently transport angular momentum.

Modern MHD Taylor-Couette flow experiments using liquid metal were not proposed (Ji et al. 2001; Rüdiger and Zhang 2001) until a decade after the rediscovery of the MRI. The standard setup for such an experimental realization is to apply a sufficiently strong axial magnetic field to destabilize an otherwise stable, quasi-Keplerian flow. To date, however, a definitely positive identification of the MRI in the standard setup has not been realized due to technical difficulties in achieving sufficiently fast speeds while maintaining mechanical integrity of the device. Currently, the highest speeds achieved in the Princeton MRI experiment are right on the edge of the required speeds to destabilize the MRI. In the meanwhile, two other relevant experiments were reported. The first one is based on a spherical Couette flow (Sisan et al. 2004) where the MRI-like signatures were reported but are subject to the interpretation as Schercliff layer instabilities (Gissinger et al. 2011). Interestingly, coherent oscillations in the external magnetic field (Nornberg et al. 2010) and in the internal flow (Roach et al. 2010) were also identified in the Princeton MRI experiment. These oscillations resemble the predicted Schercliff layer instabilities. The second relevant experiment reported a variation of the MRI, called the Helical MRI (HMRI), which is destabilized at much lower Reynolds numbers by imposing an additional azimuthal magnetic field (Hollerbach and Rüdiger 2005; Stefani et al. 2006). The nature of the HMRI was identified as a weakly destabilized inertial oscillation, which is unfortunately stable for Keplerian flows (Liu et al. 2006). Future tasks for MHD experiments should include a scaling study of angular momentum transport so that laboratory results can be extrapolated to astrophysically relevant parameters.

A number of physical effects, such as Hall effects, ambipolar diffusion, and kinetic effects, can be studied in gas and plasma experiments. Although there existed quite a few rotating plasma experiments, few of them were specifically relevant to astrophysical disks. Currently, there are two active lines of approach to study the MRI in plasmas. The approach under development at Wisconsin uses the multipolar magnetic configuration to confine plasma spun by electrode biasing (Collins et al. 2010). The second approach, proposed at Princeton (Ji 2011), is based on a prototype experiment using helicon wave plasmas (Ji et al. 2007). The idea is to set up a swirling gas flow with the desired profiles by utilizing a gas injection-pumping system. Spiral antennas will be used to transmit RF power into the experiment to achieve the desirable degree of ionization. A wide range of outstanding issues can be studied in such a device, including: nonlinear hydrodynamic instability, baroclinic instability with

axial or azimuthal temperature gradient, MRI in weakly ionized plasmas with Hall effect and ambipolar diffusion.

5. Conclusion

Significant progress has been achieved in studying magnetic reconnection and angular momentum transport relevant to space and astrophysics in the laboratory. Well-controlled and well-diagnosed experiments have become a necessity rather than a luxury especially for theory and modeling, directly supporting missions' science goals. There exist near-future major opportunities to critically impact current understanding of the observed plasma phenomena in both of these areas as well as in all other areas identified in the WOPA report. Thus, laboratory plasma astrophysics is expected to continue to grow in significance and excitement.

This work was supported in part by NASA Grants No. APRA04-0152, No. ATP06-0035, and No. APRA08-0066.

REFERENCES

S.A. Balbus and J.F. Hawley. *Astrophys. J.*, 376:214–222, 1991.

J. Birn et al. *J. Geophys. Res.*, 106(A3):3715, March 2001.

M. R. Brown, C. D. Cothran, and J. Fung. *Phys. Plasmas*, 13(5):056503, 2006.

T.A. Carter et al. *Phys. Rev. Lett.*, 88:015001, 2002.

C. Collins et al. *Bull. Am. Phys. Soc.*, 55:BAPS.2010.DPP.NP9.68, 2010.

J. Egedal et al. *Phys. Rev. Lett.*, 94(2):025006, 2005.

W. Fox et al. *Phys. Rev. Lett.*, 101:255003, 2008.

C. Gissinger, H. Ji, and J. Goodman. to be submitted, 2011.

R. Hollerbach and G. Rüdiger. *Phys. Rev. Lett.*, 95(12):124501, 2005.

H. Ji. to be submitted, 2011.

H. Ji and W. Daughton, 2011. to be submitted to Phys. Plasmas.

H. Ji et al. *Phys. Rev. Lett.*, 80:3256, 1998.

H. Ji, J. Goodman, and A. Kageyama. *Mon. Not. Astron. Soc.*, 325:L1–L5, 2001.

H. Ji et al. *Phys. Rev. Lett.*, 92:115001, 2004.

H. Ji et al. *Nature.*, 444:343–346, 2006.

H. Ji et al. *Bull. Am. Phys. Soc.*, 52:BAPS.2007.DPP.BP8.86, 2007.

H. Ji et al. *Geophys. Res. Lett.*, 35:L13106, July 2008.

A. Kageyama et al. *J. Phys. Soc. Jpn.*, 73:2424–2437, 2004.

W. Liu et al. *Phys. Rev. E*, 74:056302, 2006.

F. S. Mozer, S.D. Bale, and T. D. Phan. *Phys. Rev. Lett.*, 89:015002, 2002.

M. Nornberg et al. *Phys. Rev. Lett.*, 104:074501, 2010.

Y. Ren et al. *Phys. Rev. Lett.*, 95(5):055003, July 2005.

Y. Ren et al. *Phys. Rev. Lett.*, 101:085003, 2008.

D. Richard and J.-P. Zahn. *Astron. Astrophys.*, 347:734–738, 1999.

A. Roach et al. *Bull. Am. Phys. Soc.*, 55:BAPS.2010.DPP.NP9.75, 2010.

C.G. Rossby et al. *J. Mar. Res*, 2(1):38–55, 1939.

G. Rüdiger and Y. Zhang. *Astron. Astrophys.*, 378:302–308, 2001.

E. Schartman, H. Ji, and M. Burin. *Rev. Sci, Instrum.*, 80:024501, 2009.

E. Schartman et al. submitted to Astron. Astrophys., 2010.

N.I. Shakura and R.A. Sunyaev. *Astron. Astrophys.*, 24:337–355, 1973.

D. R. Sisan et al. *Phys. Rev. Lett.*, 93(11):114502, 2004.

F. Stefani et al. *Phys. Rev. Lett.*, 97:184502, 2006.

M. Yamada, R. Kulsrud, and H. Ji. *Rev. Mod. Phys.*, 82:603, 2010.

E.G. Zweibel and M. Yamada. *A&A*, 47(1):291, 2009.

This preprint was prepared with the AAS LaTeX macros v5.2.

NASA LAW, October 25-28, 2010, Gatlinburg

High Energy Density Laboratory Astrophysics: Shocks, Jets, and Other Extreme Dynamics

Bruce A. Remington & Hye-Sook Park

Lawrence Livermore National Laboratory, 7000 East Ave, Livermore, CA 94550

remington2@llnl.gov, park1@llnl.gov

ABSTRACT

The James Webb Space Telescope (JWST) is the infrared successor to the Hubble Space Telescope. It is a cryogenic infrared space observatory with a 25 m^2 aperture (6 m class) telescope yielding diffraction limited angular resolution at a wavelength of 2μm. The science instrument payload includes three passively cooled near-infrared instruments providing broad- and narrow-band imagery, coronagraphy, as well as multi-object and integral-field spectroscopy over the $0.6< \lambda < 5.0$ μm spectrum. An actively cooled mid-infrared instrument provides broad-band imagery, coronagraphy, and integral-field spectroscopy over the $5.0< \lambda < 29$ μm spectrum. The JWST is being developed by NASA, in partnership with the European and Canadian Space Agencies, as a general user facility with science observations to be proposed by the international astronomical community in a manner similar to the Hubble Space Telescope. Technology development and mission design are complete, and construction is underway in all areas of the program.

1. Introduction

We provide here a brief review of high energy density laboratory astrophysics (HEDLA), focusing on shocks, shock driven systems, and jets. Previous reviews can be found in Remington 1999, 2000, 2005; Remington et al. 2006; Drake 1999. For full details of these types of experiments, the reader is referred to the compendium of proceedings from the HEDLA conference series (HEDLA 2000, 2005, 2007, 2009, 2011) In Sec. 2 we describe shocks and shock driven systems in astrophysics and in the laboratory. Jets in all their varieties are described in Sec. 3. We conclude, and provide some thoughts about future prospects in Sec. 4.

2. Shocks

2.1. Shocks in astrophysics

Shocks and shock driven systems are ubiquitous in the universe. One dramatic example of shocks in astrophysics is given by supernova (SN) explosions. Shown in Fig. 1 are images from Supernova 1987A (Fig. 1a), a core-collapse SN that exploded 24 yrs ago (Arnett et

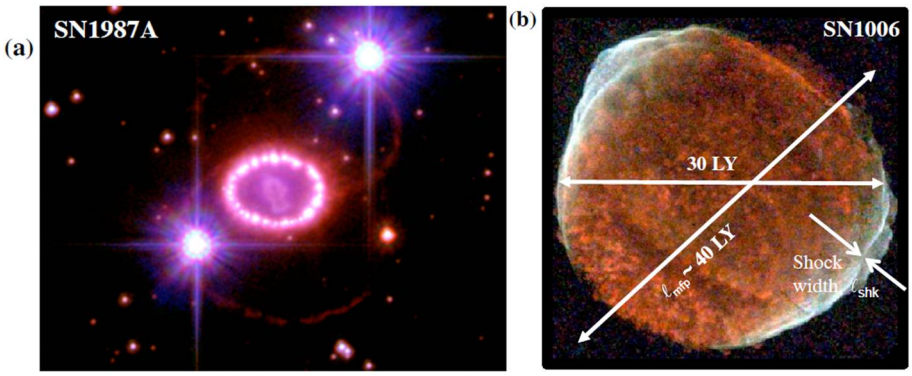

Fig. 1.— (a) HST image of SN1987A taken 20 yrs after its explosion in Feb. 1987 (http://www.weizmann.ac.il/home/galyam/SNF20070406-008.html). (b) X-ray image of SN1006, taken with the Chandra x-ray satellite (http://en.wikipedia.org/wiki/SN_1006).

al. 1989; McCray 1993, 2007; France 2010) and SN 1006 (Fig. 1b), a Type-1a SN that exploded over 1000 yrs ago (Winkler et al. 2003; Gardner et al. 1965; Acero et al. 2010). There continues to be great interest in the SN explosion mechanisms, the strong shock driven dynamics that occurs during and after the explosion, and the dynamics right at the (collisionless) shock front in the supernova remnant (SNR) phase. We describe a few examples of experiments being done on high energy density (HED) facilities to investigate these interesting and challenging dynamics.

2.2. Shock driven laboratory systems

We show in Fig. 2 a selection of examples of strong shock driven hydrodynamics experiments done on high energy, high power laser facilities to investigate these strong shock driven, nonlinear dynamics and test our ability to model and understand their evolution in time. Multi-dimensional simulations of SN explosions have established that there are strong shock driven, deep nonlinear hydrodynamic instabilities involved in the explosion and subsequent

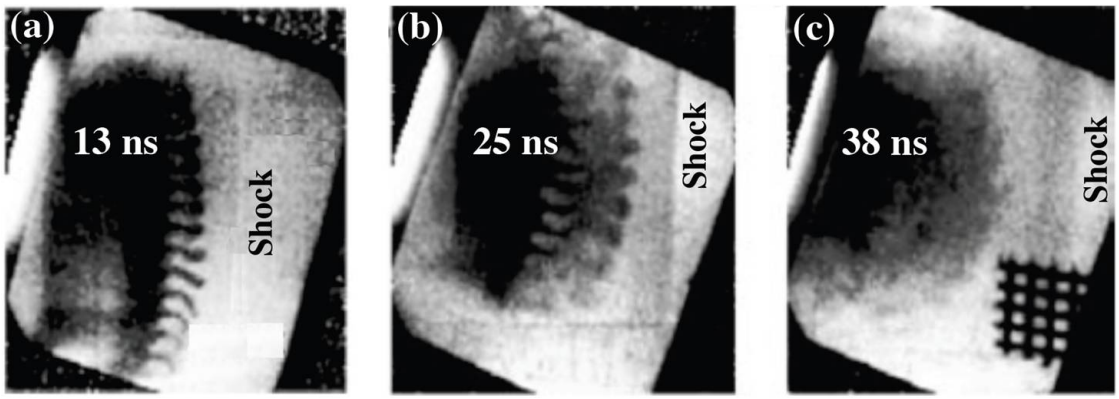

Fig. 2.— Scaled supernova Rayleigh-Taylor experiments done on the Omega laser, with side-on x-ray radiographs taken at (a) 13 ns, (b) 25 ns, and (c) 38 ns. The imposed 2D perturbation at the CH-foam interface corresponds to a superposed two-mode sinusoidal pattern of wavelengths λ_1=50 μm and λ_2=5 μm (Kuranz et al. 2005; Kuranz 2007).

SNR evolution (Kifonidis 2003, 2006; Borkowski et al. 1997; Chevalier et al. 1992; Klein et al. 1994). The micro-physics of such deep nonlinear, turbulent hydrodynamics is very uncertain, and a need for scalable laboratory experiments to test such thinking and simulations has long been desired but only recently become possible. With the advent of modern high energy, high power lasers and magnetic pinch facilities (Z-pinches), developed as part of the international effort in inertial confinement fusion (ICF), it has become possible for the first time to carry out scaled, strong shock driven experiments relevant to SN dynamics. The first such experimental demonstration of scaled experiments simulating the Rayleigh-Taylor (RT) instability evolution at the He-H interface in systems such as SN1987A was done on the Nova laser in 1997 (Kane 1997; Remington 1997, 1999). The Euler scale transformations relating the laboratory experiments to SN1987A were also worked out at that time (Ryutov et al. 1999). Since then, a lengthy series of RT experiments relevant to SN1987A has been carried out on the Omega Laser, an example of which is shown in Figs. 2a-c (Robey et al. 2001; Kuranz et al. 2005; Kuranz 2007; Miles et al. 2005). The experimental results shown correspond to 2D, two-mode experiments (λ=50 μm superposed with λ=5 μm), showing the evolution of the perturbations at three different times in a laboratory setting that reproduces in a scaled sense the strong shock driven dynamics at the He-H interface of SN1987A. The instability evolution spans the weakly nonlinear to deeply nonlinear stages, and finally transitions into what appears to be a turbulent phase. The simulations generally agree well with the experimental data in the weakly nonlinear regime, start to have more difficulty in the deep nonlinear regimes, and generally do not enter the fully turbulent regime at all, due to limitations in numerical Reynolds number possible on current computers (Miles et

al. 2005). The frontier over the next 5 – 10 yrs is to get simulations to fully transition into the turbulent regime, and compare against well characterized experiments in the same turbulent regime, where the full time sequence has been measured and modeled. At stake is our understanding of how core-collapse SNe explode, invert inside-out, and eject their core material rapidly and efficiently.

Given that the most uncertain part of the hydrodynamics simulations and our understanding of the ensuing dynamics appears to be the transition into the turbulent regime, two more experiments were developed that emphasized this aspect of the flows. Figure 3

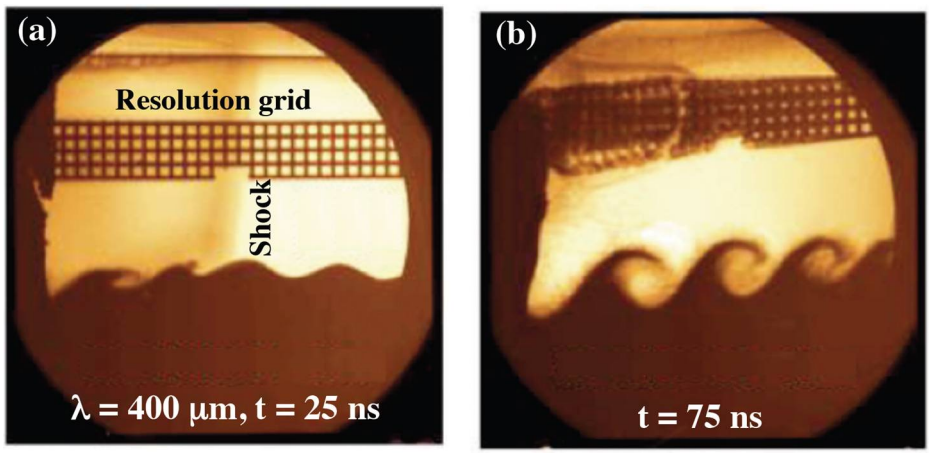

Fig. 3.— Laser driven HED Kelvin-Helmholtz experiments. Side-on radiography, 2D time resolved x-ray images taken at (a) 25 ns and (b) 75 ns. The imposed 2D perturbation at the CH-foam interface corresponded to a single model sinusoidal pattern of wavelength 400 μm and peak-to-valley amplitude of 60 μm (Harding et al. 2009; Hurricane et al. 2009).

shows two side-on x-ray radiographs taken at two different times from a single-mode Kelvin-Helmholtz (KH) experiment done on the Omega laser, where a strong shock is driven transversely along a rippled interface between foam and doped plastic (Hurricane et al. 2008, 2009; Harding et al. 2009). The shock passage, shown in Fig. 3a, causes a shear flow along the rippled interface, which in turn drives up the KH instability (Fig. 3b). The experiment shows what appears to be a transition to the turbulent regime inside the vortex roll-ups late in time, which at the moment cannot be reproduced in the simulations. A related experiment was developed on the Nike laser (Harding et al. 2010).

Another experiment, shown in Fig. 4, drives a strong shock past an embedded higher density clump, as might occur when a SNR shock encounters a molecular cloud. In this case the higher density localized clump in the scaled experiment is a 120 μm diameter solid Al sphere embedded in an ambient medium of lower density foam (Hansen et al. 2007; Robey

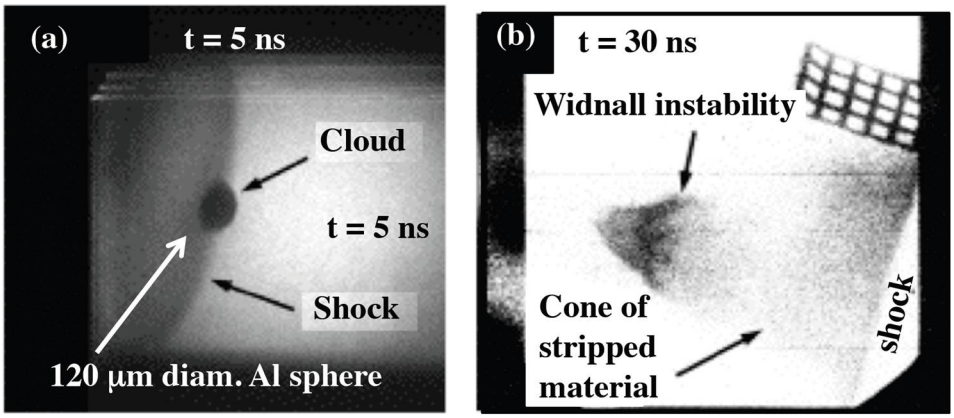

Fig. 4.— Scaled shock-cloud interaction experiments done on the Omega laser. Side-on x-ray radiographs taken at (a) 5 ns, and (b) 30 ns (Hansen et al. 2007).

2002; Klein et al. 2003). The shock passage across this sphere deposits vorticity which cases the formation of a vortex ring, much like a smoke ring, which breaks up via an azimuthal instability called the Widnall instability. Turbulent mass stripping is inferred to occur from this shear flow across the Al sphere interface. Eventually the localized clump (Al sphere) is completely eaten away and mixed into the ambient medium downstream from its original location. The 3D hydrodynamics simulations show the onset of the Widnall instability, but at present do not capture the turbulent mass stripping and total destruction of the clump (Robey 2002). Both this experiment and the KH experiment provide high quality experimental data that will challenge the next generation 3D hydrodynamics codes and simulations, as the numerical Reynolds number is increased above $\sim 10^4$ so that a transition to turbulence in the simulations can or should occur.

2.3. Radiative shocks

Experiments have been developed to look at the dynamics of strong shocks and blast waves in otherwise homogenous, semi-infinite media. Examples of a set of blast wave experiments that are purely hydrodynamic (non-radiative), Fig. 5a, and highly radiative (Fig. 5b) have been demonstrated on the Janus laser at the Jupiter Laser Facility, by varying the gas into which the strong blast wave was launched. The shock in low density nitrogen, N_2, yields a purely hydrodynamic, Sedov-Taylor blast wave, as shown in Fig. 5a. The blast wave in low density Xe gas, however, produces a strong shock with a very strong radiative precursor, as shown in Fig. 5b. The radiative precursor depletes the strength of the original blast wave by heating and increasing the pressure in the plasma ahead of the shock. A new shock is

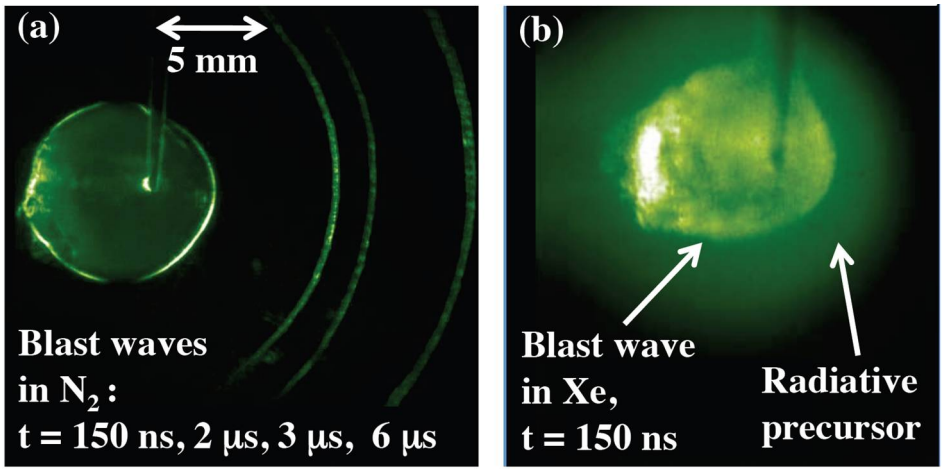

Fig. 5.— Scaled shock-cloud interaction experiments done on the Omega laser. Side-on x-ray radiographs taken at (a) 5 ns, and (b) 30 ns (Hansen et al. 2007).

launched ahead of the original shock, by the heating due to the radiative precursor (Hansen et al. 2006a,b). To create a strongly radiative blast wave in planar geometry, the Omega laser was used to launch a strong shock down a shock tube filled with Xe gas, as shown in Fig. 6 (Doss et al. 2009). By side-on x-ray radiography, it was inferred that the compression behind the shock front was ρ/ρ_0 =30 due to the radiative collapse of the shocked gas. The beginning stages of a Vishniac-like instability were observed, as has been postulated to occur in SNR shocks (Vishniac 1983; Ryu & Vishniac 1987, 1991).

2.4. Collisionless shocks

The most recent series of laser driven shock experiments are being developed to try to observe and study how collisionless shocks are formed, evolve, and ultimately accelerate particles. In an experiment developed on the Gekko laser, two low density, high velocity plasma flows intersect, start to interpenetrate, and then eventually lead to the initial stages of formation of a collisionless, electrostatic shock, as shown with optical images in Fig. 7a (1D streaked interferogram) and Fig. 7b (streaked optical 1D image in emission) (Kuramitsu et al. 2009, 2011; Morita et al. 2010). The streaked interferogram shows that plasma ablated from the CH foil driven by intense laser irradiation at an intensity of a few x 10^{14} W/cm^2 is moving as fast as 1000 km/s or more, whereas the plasma from the facing foil driven by the radiation from the driven foil is denser and moving at a few x 100 km/s. Typical electron densities were $10^{18} - 10^{19}$ cm^{-3}. The streaked optical pyrometer (SOP) image shows a diffuse boundary early in time as the two intersecting plasmas first start to interact (interpenetrate).

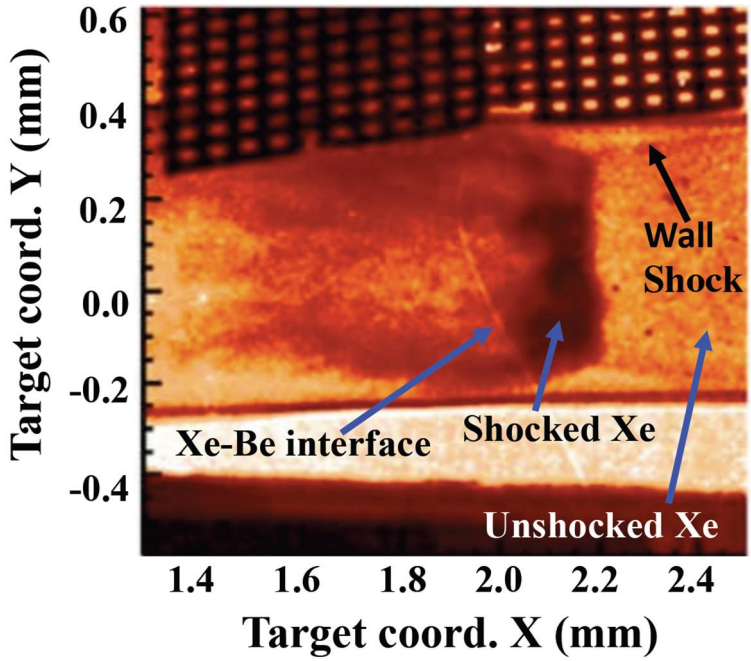

Fig. 6.— Scaled shock-cloud interaction experiments done on the Omega laser. Side-on x-ray radiographs taken at (a) 5 ns, and (b) 30 ns (Hansen et al. 2007).

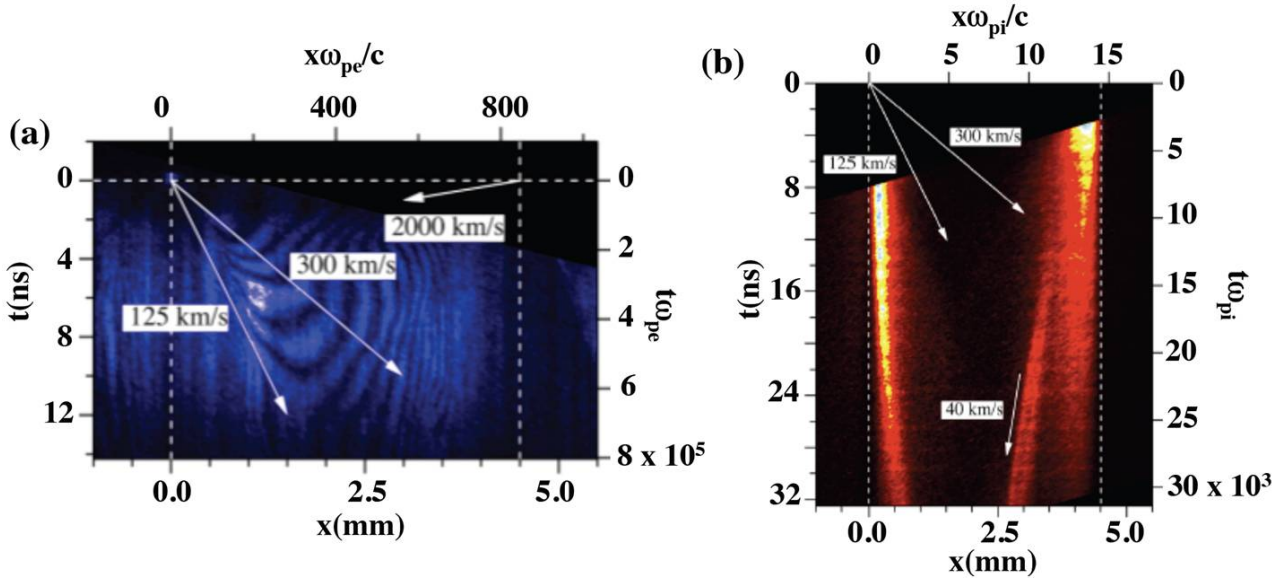

Fig. 7.— Scaled shock-cloud interaction experiments done on the Omega laser. Side-on x-ray radiographs taken at (a) 5 ns, and (b) 30 ns (Hansen et al. 2007).

Later in time, t > 15 ns, the intersecting region steepens into a shock moving at ∼40 km/s. Since the densities are low and initial flow velocities are high, the ion-ion Coulomb collision mean free path is much larger than the observed shock width, hence, the shock is interpreted as being collisionless, and of the electrostatic type.

With a similar goal, a completely independent experiment was developed and demonstrated on the Vulcan laser using an ultrahigh intensity, short pulse laser passed through a low density He gas at an intensity of a few x 10^{20} W/cm^2 (Nilson et al. 2009) They interpret their data as a cylindrically diverging, collisionless, electrostatic shock moving at ultrahigh velocity (near-relativistic, at $v_{shk} \sim c/30$). Both of these experiments show considerable potential for studying astrophysical collisionless shocks in the laboratory, and a new effort on the Omega laser and soon on the NIF laser are starting to observe these effects over larger scales and longer time scales (Park et al. 2011).

3. Jets

3.1. Jets in astrophysics

Jets in astrophysics are also a very common phenomena and energy source in the universe. Two examples are shown in Fig. 8. In Fig. 8a, the protostellar jet called Herbig-Haro

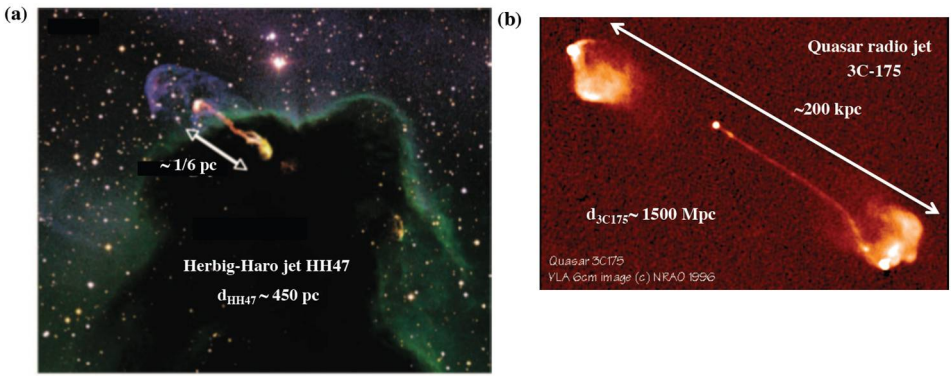

Fig. 8.— Astrophysical jets, (a) within our galaxy, such as protostellar jet HH47 (Reipurth et al. 2001) and (b) external to our galaxy, such as quasar radio jet 3C-175 (Bridle et al. 1994).

47 (ie, HH-47) is shown (Reipurth et al. 2001; Hartigan 1997; Heathcote et al. 1996; Raymond et al. 1994). Protostellar jets are of great interest because they are observed during the star formation process, and are believed to be one mechanism by which the protostar sheds angular momentum. They are generally high Mach number, moving at tens of km/s, and

often are radiatively cooled, depending on their densities. Their spatial extent is typically of order ∼1 light yr (1/3 pc). Extragalactic jets, such as the quasar radio jet 3C-175 shown in Fig. 8b, are of a very different nature. They are highly relativistic, and thought to be composed of relativistic electrons, positrons, and protons (Bridle et al. 1994; Fermini 2007). The quasar radio jet 3C-175 shown in Fig. 8b is categorized as a Fanaroff-Riley class II (FR II) extragalactic jet. The 3C-175 jet, which is located at a distance of ∼1500 Mpc, has a spatial extent of ∼200 kpc. This is more than a factor of ∼10 larger than the entire host galaxy out of which it emanates. The electrons and positrons stream outwards towards the ends or lobes of the jet, and emit synchrotron radiation. These relativistic intergalactic jets are associated with an accreting massive black hole at the center of its galaxy, which serves as the "central engine" energy source. Experimental studies shedding light on either of these two very different types of jets would be very beneficial.

3.2. Hydrodynamic jets in the lab

High Mach number, non-radiative jets have been developed very successfully on the Omega laser over the past decade (Hartigan et al. 2009; Foster et al. 2002, 2005; Coker et al. 2007). An example of a Ti plasma jet launched into a low-Z, low density (∼0.1 g/cm^3) resorcinol-formaldehyde (C_{15} H_{12} O_4) foam of initial density ∼0.1 g/cm^3 foam is shown in Fig. 9a (Hartigan et al. 2009; Coker et al. 2007). At its base, the diameter of the jet, ∼300

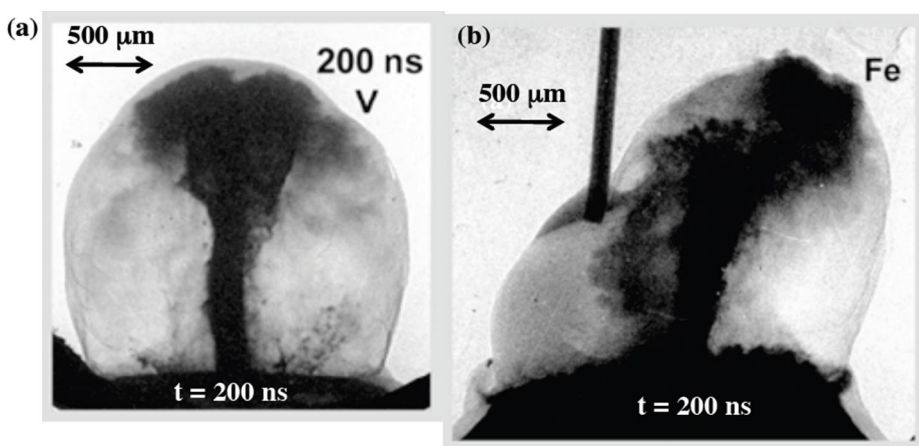

Fig. 9.— Scaled protostellar jet experiment done on the Omega laser, mocking up the dynamics of Herbig-Haro jet HH-110, (a) without any obstruction, and (b) after a glancing impact on a spherical obstruction (Hartigan et al. 2009).

μm, matches the bore of the washer through which it was launched. By the time the side-

on x-ray radiograph is taken, using point projection imaging onto x-ray film, the jet has penetrated ∼2 – 3 mm into the foam, and launched a strong bow shock into the surrounding foam plasma. The head of the jet, or working surface, appears to be starting to become turbulent. The Mach number of the jet is M ∼ 3, and the Reynolds number 10^5 – 10^6. By ∼200 ns, the density ratio between the jet tip and ambient foam is ∼1 – 10, chosen to match the density ratio of overdense protostellar jets, such as HH-110. In comparison experiments, this Ti plasma jet was impacted onto a ∼1 mm diameter solid density CH sphere, causing a distinct and abrupt deflection, as shown in Fig. 9b. This staged impact was an experimental demonstration of what is presumed to be the reason for the abrupt change in direction of the HH-110 protostellar jet. Radiation hydrodynamics modeling of the laser experiment gives reasonably good agreement with the experiment. This supports, then, the hypothesis that the protostellar jet HH-110 has been deflected by impacting a dense cloud or obstruction.

3.3. Radiative jets

A second class of jet experiments on HED experimental facilities has been aimed at producing radiatively cooled jets, motivated again by protostellar jets, and as a fundamental test of radiation-hydrodynamics simulations for astrophysical settings. High Mach number, radiatively cooled jets have been demonstrated on the Nova and Gekko lasers (Farley et al. 1999; Shigemori et al. 2000), as shown in Fig. 10. The technique used was to irradiate at high intensity (10^{14} – 10^{15} W/cm^2) the inner surface of a conical opening in Au or Fe. The high velocity plasma generated converges on axis and jets outwards. The stagnation shock created in this convergence strongly radiatively cools the plasma. These jets successfully demonstrated radiative cooling in a hydrodynamic flow. They were of short duration (∼1 ns), however, and extended distances only of order ∼1 mm. To improve upon this technique, high Mach number jets, M ∼ 20, have been generated and studied on the Magpie Z-pinch facility using conical wire arrays to generate the converging plasma flow. These radiative jets are a factor of at least 10 larger spatially and last a factor of ∼100 longer than the jets created on the Nova and Gekko lasers, as shown in Fig. 11 (Lebedev et al. 2002). By varying the Z of the initial wire array, the degree of radiative cooling can be controlled, as shown in Figs. 11a-c. These jets can also be propagated into an ambient low density plasma, thereby capturing more of the relevant radiative hydrodynamics of scaled protostellar jet dynamics.

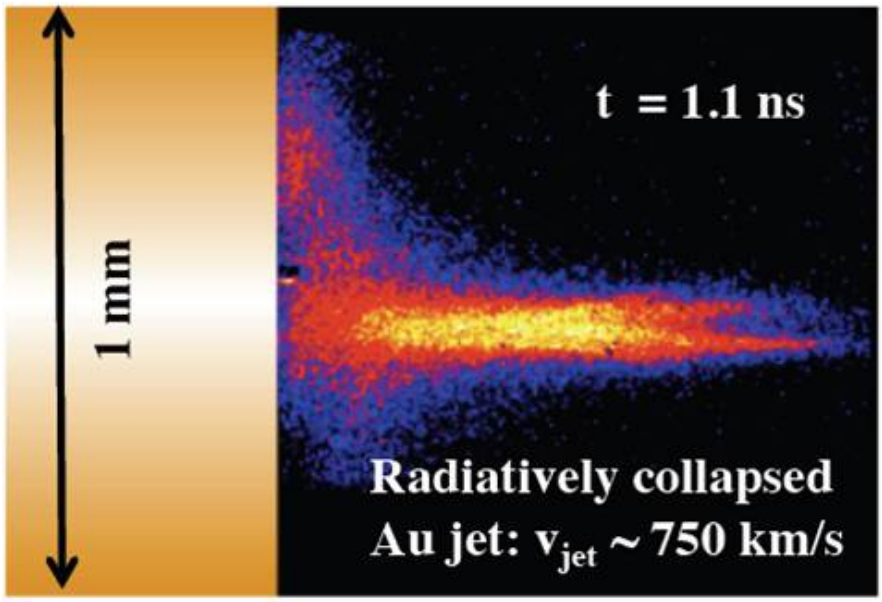

Fig. 10.— First radiatively collapsing jet experiment, done on the Nova laser (Farley et al. 1999).

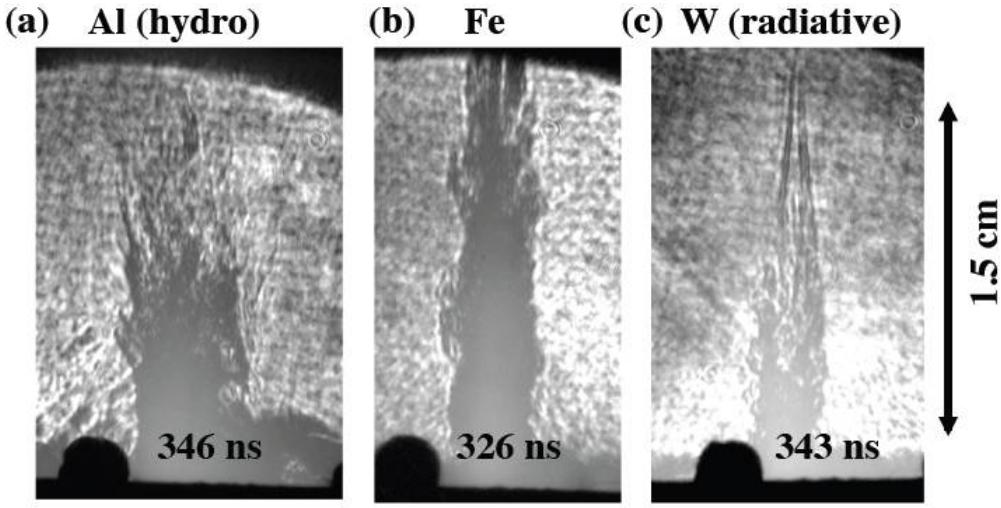

Fig. 11.— A sequence of radiatively collapsing jet experiments done on the Magpie magnetic pinch facility, using (a) Al, (b) Fe, and (c) W conical wires (Lebedev et al. 2002).

3.4. MHD jets

A new configuration at the Magpie Z-pinch facility has allowed "magnetic tower jets" to be launched and studied, using radial wire arrays, and planar radial current flows, as shown

in Figs. 12 and 13 (Ciardi et al. 2007; Lebedev et al. 2005; Suzuki-Vidal 2009). Using a radial

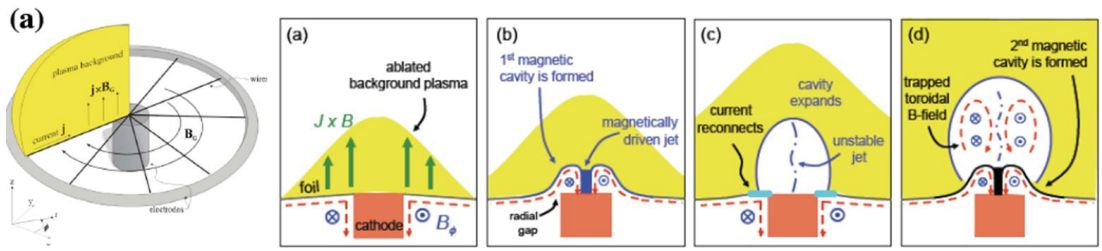

Fig. 12.— Sketches of the experimental configuration at the Magpie magnetic pinch facility for generating magnetic tower experiments. (a) Radial wire configuration. (b) – (e) Time sequence for magnetic tower jets creating episodic jet bursts from a radial planar foil electrode (Lebedev et al. 2005).

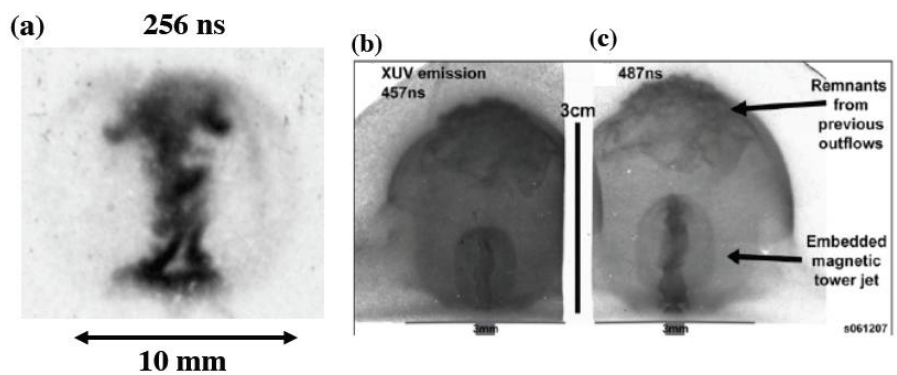

Fig. 13.— Images in emission of experimental magnetic tower jets from the Magpie facility. (a) Jet using radial wire electrodes. (b) Episodic jets using a radial foil electrode, taken in x-ray emission at (b) 457 ns, and (c) 487 ns (Suzuki-Vidal 2009).

wire array (Fig. 12a), the first HED magnetic tower jets were produced (Fig. 13a). Here, the magnetic pressure by the current flow pattern pushes the plasma upwards, launching the MHD jet. By switching to a continuous radial foil electrode (Fig. 13b-e), episodic MHD jets have been created, as shown in Figs. 13b,c. These episodic laboratory MHD jets bear a intriguing resemblance to several protostellar jets that clearly show episodic behavior, such as HH-47 shown in Fig. 8a. The Euler scale transformations for ideal MHD dynamics experiments, as is relevant for these jet experiments, have also been worked out (Ryutov et al. 2001).

On spatial and time scales that are another factor of 10 larger, laboratory MHD jets were launched in much lower density plasma at the Caltech lab-astrophysics experiment, as

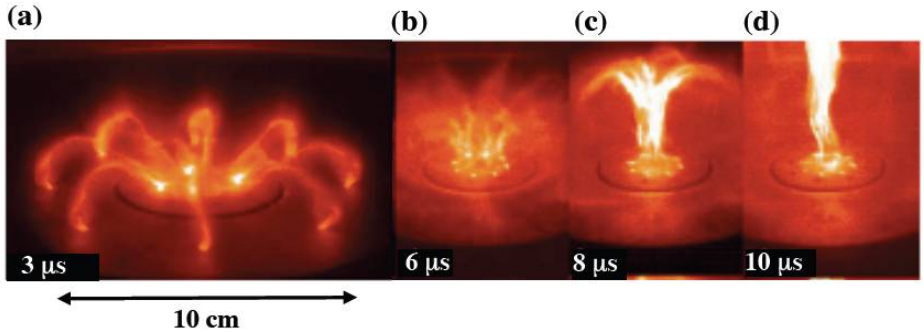

Fig. 14.— Large scale, MHD jets taken at the Caltech lab-astrophysics plasma device. (a) Spider legs starting plasma condition. (b) – (d) evolving MHD jet at 6, 8, and 10 μs (You 2005).

shown in Fig. 14 (You 2005; Bellan 2005, 2009; Hsu & Bellan 2005). Due to the larger scales and optical diagnostics, much more fine detail can be observed and followed as a function of time, elucidating how the plasma jet forms, evolves, and develops instabilities.

3.5. Relativistic jets

Although still in the early stages of development, laboratory astrophysics experiments with relativistic plasmas are being developed on short pulse, ultra-intense lasers. For example, relativistic jets of electrons and positrons have been observed in the laboratory (Chen et al. 2010). Fig. 15a shows the energy spectra of set of different experiments generating jets of positrons and electrons, with the peak energies ranging from 5 – 20 MeV. Fig. 15b shows that the positrons come off in a forward directed cone or jet of $\sim$20° opening half-angle. If relativistic jet experiments can be further developed and enhanced, this may allow laboratory experiments to probe the physics of relativistic extragalactic jets, such as shown in Fig. 8b, and which tie to the physics of accreting massive black holes at galactic centers called Active Galactic Nuclei (AGN) and to accreting stellar mass black holes such as microquasars and gamma ray bursts (Liang et al. 2011). The scale transformation for these collisionless, relativistic plasma flow experiments has also been examined and elucidated (Ryutov 2006).

4. Conclusion and future prospects

Over the past two decades, HEDLA scaled astrophysics experiments have made impressive progress. Scaled experiments measuring turbulent shock driven dynamics are becoming

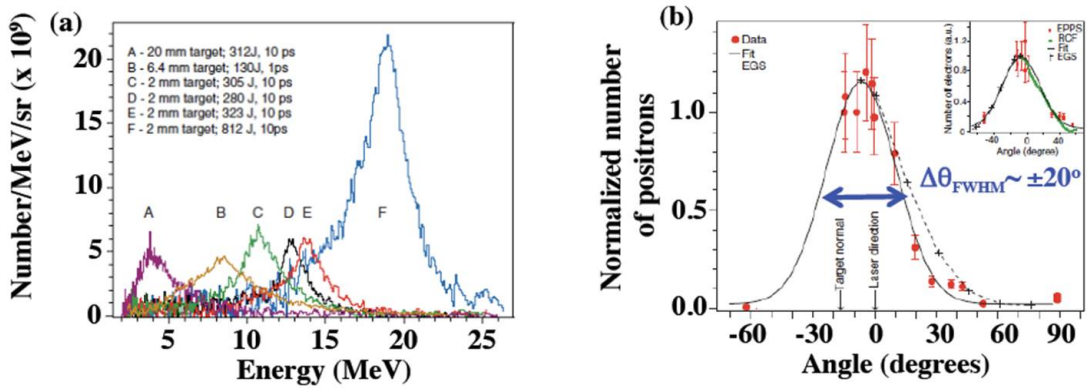

Fig. 15.— Relativistic positron jet (a) energy spectra, and (b) jet opening angle, taken on the Omega-EP laser (Chen et al. 2010).

almost routine. Relevant radiative hydrodynamics, such as radiative shock and radiative jet experiments are now also widely carried out on a whole variety of HED facilities. Scaled MHD experiments on protostellar jets has reached a mature and impressive level. The next new frontier within reach over the next 10 yrs is in the area of relativistic, collisionless plasmas. Also, with the commissioning of the NIF laser (Haynam et al. 2007) at LLNL and ZR at SNLA (Matzen et al. 2005), MJ class experiments are now also possible. When high energy, short pulse, ultra-intense lasers are included into these MJ class facilities, rich new possibilities in the area of laboratory astrophysics will become possible.

REFERENCES

Acero, F., et al., 2010, A&A, 516, A62

Arnett, D., et al., 1989, ARAA, 27, 629

Bellan, P. M., 2005, ApSS, 298, 203

Bellan, P. M., 2009, PoP, 16, 041005

Borkowski et al., 1997, ApJ, 477, 281

Bridle, A. H., et al., 1994, AJ, 108, 766

Chen, H., et al., 2010, PRL, 105, 015003

Chevalier, R., et al., 1992, ApJ, 392, 118

Ciardi, et al, 2007, PoP, 14, 056501

Coker, R. F., et al., 2007, ApSS, 307, 57

Doss, F. W., et al., 2009, PoP, 16, 112705

Doss, F. W., et al., 2011, ApSS, in press

Drake, R. P., 1999, J. Geo. Res., 104, 14,505

Farley, D. R., et al., 1999, PRL, 93, 1982

Fernini, I., 2007, AJ, 134, 158

Foster, J. M., et al., 2002, PoP, 9, 2251

Foster, J. M., et al., 2005, ApJ, 634, L77

France, Science, 329, 1624

Gardner, F. F., et al., 1965, AJ, 70, 754

Hansen, J. F., et al., 2006a, PoP, 13, 112101

Hansen, J. F., et al., 2006b, PoP, 13, 022105

Hansen, J. F., et al., 2007, ApJ, 662, 379

Harding, E. C., et al., 2009, PRL, 103, 045005

Harding, E. C., et al., 2010, PoP, 17, 056310

Hartigan, P., 1997, Accretion Phenomena and Related Outflows, 121, 53

Hartigan, P., et al., 2009, ApJ, 705, 1073

Haynam, C. A., et al., 2007, Appl. Optics, 46, 3276

Heathcote, S., et al., 1996, AJ, 112, 1141 (1996).

HEDLA, 2000, ApJS, 127, 211

HEDLA proceedings, 2005, ApSS, 298, No. 1-2

HEDLA, 2007, ApSS, 307, No. 1-3

HEDLA, 2009, ApSS, 322, No. 1-4

HEDLA, 2011, ApSS, in press

Hsu, S. C. & Bellan, P. M., 2005, PoP, 12, 032103

Hurricane, O. A., et al., 2008, HEDP, 4, 97

Hurricane, O. A., et al., 2009, PoP, 16, 056305

Kane, J., 1997, ApJ, 478, L75

Kifonidis, K., 2003, A&A, 408, 621

Kifonidis, K., 2006, A&A, 453, 661

Klein, R. I., et al., 1994, ApJ, 420, 213

Klein, R. I., et al., 2003, ApJ, 583, 245

Kuramitsu, et al., 2009, ApJ, 707, L137

Kuramitsu, et al., 2011, PRL, 106, 175002

Kuranz, C., et al., 2005, ApSS, 298, 9

Kuranz, C., et al., 2007, ApSS, 307, 115

Lebedev, S., et al., 2002, ApJ, 564, 113

Lebedev, S., et al.,2005, MNRAS, 361, 97

Liang, E., Remington, B. A. & Ryutov, D. D., 2011, Nature Physics, submitted

Matzen, M. K., et al., 2005, PoP, 12, 055503

McCray, R., 1993, ARAA, 31, 175

McCray, R., 2007, AIP 937, 3

Miles, A., et al., 2005, PoP, 12, 056317

Morita et al., 2010, PoP, 17, 122702

Nilson, P. M., et al., 2009, PRL, 103, 255001

Park, H. S., et al., 2011, IFSA-2011, ICHED 2011

Raymond, J. C., et al., 1994, ApJ, 434, 232

Reipurth, B., et al., 2001, ARAA, 39, 403

Reighard, A. B., et al., 2006, PoP, 13, 082901

Reighard, A. B., et al., 2007, PoP, 14, 056504

Remington, B. A., 1997, PoP, 4, 1994

Remington, B. A., 1999, Science, 284, 1488

Remington, B. A., 2000, Phys. Plasmas, 7, 1641

Remington, B. A., 2005, Plasma Phys. Control. Fus., 47, A191

Remington, B. A., et al., 2006, Rev. Mod. Phys., 78, 755

Robey, H. F., et al., 2001, PoP, 8, 2446

Robey, H. F., 2002, PRL, 89, 085001

Ryu, D. & Vishniac, E. T., 1987, ApJ, 313, 820

Ryu, D. & Vishniac, E. T., 1991, ApJ, 368, 411

Ryutov, D., et al., 1999, ApJ, 518, 821

Ryutov, D., et al., 2001, PoP 8, 1804

Ryutov, D., 2006, PPCF, 48, L23

Shigemori, K., et al., 2000, PRE, 62, 8838

Suzuki-Vidal, 2009, ApSS, 322, 19

Vishniac, E. T., 1983, ApJ, 274, 152

Winkler, P., et al., 2003, ApJ, 585, 324

You, S., 2005, PRL, 045002

This preprint was prepared with the AAS LaTeX macros v5.2.

NASA LAW, October 25-28, 2010, Gatlinburg

Non-equilibrium Ionization Diagnostics based on AtomDB

L. Ji, A.R. Foster, R.K. Smith & N.S. Brickhouse

Harvard-Smithsonian Center for Astrophysics, Cambridge, 02138

lji@cfa.harvard.edu

J. Houck

MIT Kavli Institute For Astrophysics & Space Research, Cambridge, MA, 02139

houck@space.mit.edu

ABSTRACT

The new version of the AtomDB atomic database (v2.0) contains ionization and recombination rates enabling modeling of non-equilibrium ionization (NEI) plasmas as well as those in collisional ionization equilibrium (CIE). Here we present a comparison between the new and old (v1.3) versions of AtomDB, demonstrating the importance of the atomic data/processes involved in some typical NEI scenarios of astrophysical interests by various line-ratio diagnostics as well as other measurements such as equivalent widths, cooling curves, and spectra.

1. Introduction

Non-equilibrium ionization (NEI) is an important phenomenon related to many astrophysical processes, such as rapid heating or cooling, where gas may be under-ionized or over-ionized. It is seen at small scales such as the winds of massive stars, accretion flows in X-ray binaries, stellar cluster winds, and shocks in supernova remnants (SNR), as well as at large scales such as galactic superwinds, AGN outflows, and the shock flows in the intergalactic medium.

NEI calculations require both a complete model of atomic processes and a complete database of atomic data. For example, AtomDB v2.0 includes the state-selective dielectronic recombination (DR) and radiative recombination (RR) rates for H-, He- and Li-like ions (see

Foster et al. 2011). As shown in Ji et al. (2006, and reference therein), the cascade of electrons following recombination into highly-excited levels could strongly affect the line emissivities of highly-ionized species in an adiabatic expanding wind. In addition, inner-shell processes are known to be important when modelling SNR, although no substantive database for inner-shell processes is available publicly.

2. Non-equilibrium Ionization Issues

2.1. Time-dependent non-equilibrium Ionization

Time-dependent non-equilibrium ionization is generally used in models of astrophysical phenomena such as shocked gas in solar flares, supernova remnants, and intercluster mediums. In these systems, the dynamical timescale is much shorter than the intrinsic timescales, resulting in a plasma that is either in delayed ionization or delayed recombination, and where ion states are far from CIE. AtomDB v1.3 was designed primarily for equilibrium calculations, but AtomDB v2.0 contains updated atomic data allowing calculations for collisional plasmas both in CIE and NEI.

As an example of one such calculation based on AtomDB v2.0, Figure 1 shows the simulated light curves in the six AIA EUV wavebands for the apex of the single loop of a strong solar flare based on the hydrodynamical simulations by Reeves et al. (2007). The difference between CIE and NEI is easily detectable.

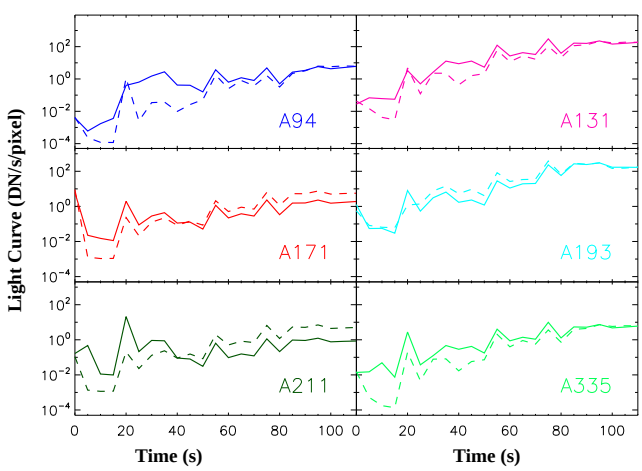

Fig. 1.— Simulated light curves in the six AIA EUV wavebands for the apex of the single loop (see Figure 3 in Reeves et al. 2007 for details of the models): CIE (dash), NEI (solid)

2.2. Radiative/Dielectronic Recombination Cascades

The radiative recombination rate for an ion to the ground state or an excited energy level is typically calculated using Milne's relation combined with the photoionization cross sections (e.g. Ji et al. 2006). The rates are often coarsely calculated and averaged according to the quantum degeneracy of each level. Figure 2 shows that the recombination enhances emission from C V, C VI, O VII, and O VIII in NEI modeling of an adiabatically-expanding stellar wind (for details see Ji et al. 2006).

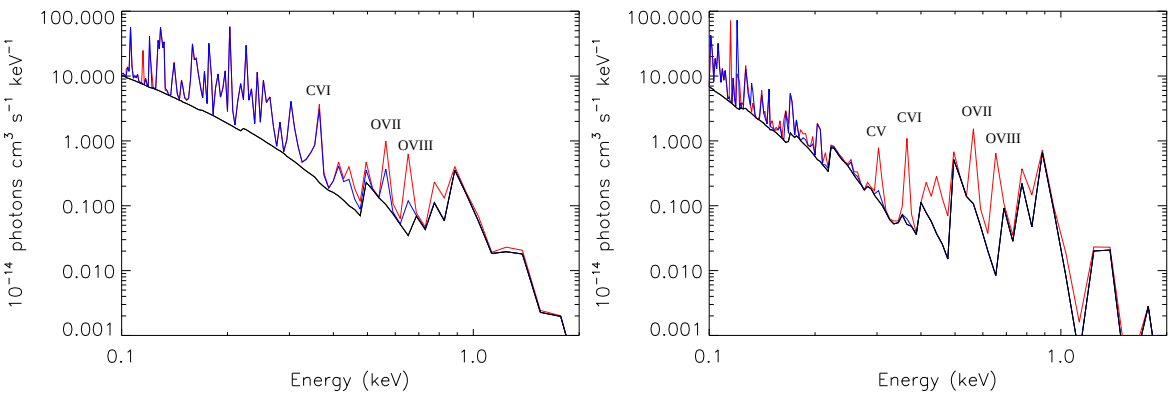

Fig. 2.— Comparison for the spectra with(red) and without(blue) including radiative recombination rates to the excited levels for an adiabatically expanding stellar cluster wind (for details, see text). Black denotes continuum only.

However, Badnell et al. (2003) have recently redone calculations of recombination rates directly in a state-selective calculation that includes both dielectronic and radiative processes using Autostructure (Badnell 1997). These state-selective DR and RR rates are now included in AtomDB v2.0. Successful capture into high-n (> 10) levels above those contained in AtomDB v2.0 have been cascaded down to lower energy levels.

2.3. Inner-shell processes

Also for comparison, we include inner-shell ionization/excitation rates for Li-like ions(G.Y. Liang, private communication). The structure and transition rates were calculated using Autostructure, while the collisional excitation rates were obtained using the Intermediate Coordinate Frame Transformation (ICFT) R-Matrix method (Griffen 1998). We calculate Auger yields separately using the Autostructure code.

Based on the different versions of AtomDB, Figure 3 illustrates line diagnostics of O VII Kα/O VIII Lyα and Si XIII Kα/Si XIV Lyα for the constant temperature, plane-

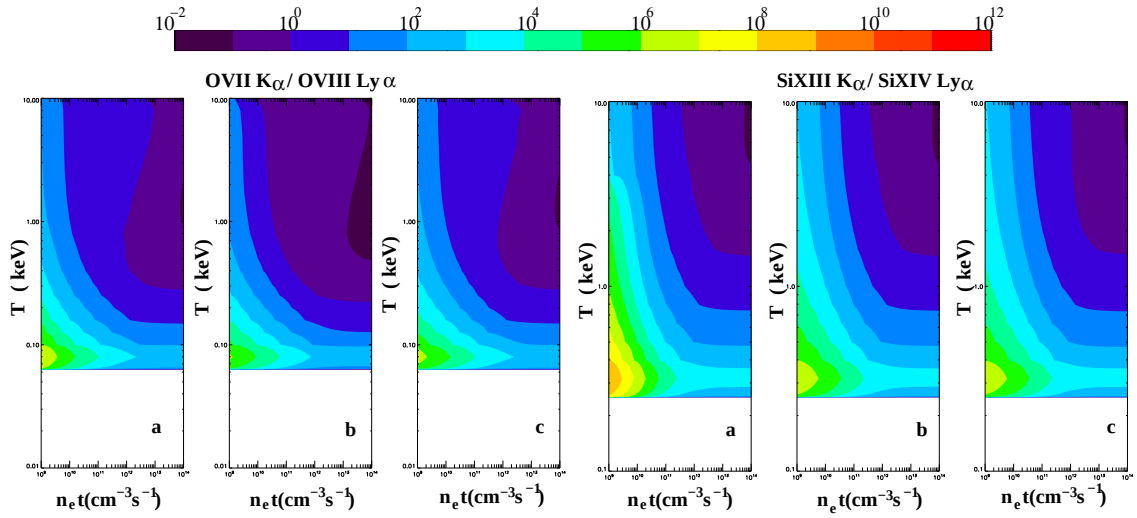

Fig. 3.— Line diagnostics based on vpshock in XSPEC, assuming $[n_e t]_{low} = 0$ based on different versions of AtomDB with (a) and without (b,c) innershell processes: a— upcoming version; b — v2.0; c — v1.3

parallel shock plasma model (vpshock in XSPEC). Note Li-like ions make contributions to the wavelength region of He-like Kα due to inner-shell processes. As expected, such line ratios are enhanced when the temperature is lower and ionization time is shorter. This Li-like data will be incorporated in a future release of AtomDB.

We gratefully acknowledge support for this work form NASA ADP grant NNX09AC71G and from *Chandra* HETG group for database realization in ISIS.

REFERENCES

Badnell, N.R., 1997, JPhB, 30, 1

Badnell, N.R., O'Mullane, M.G., Summers, H.P., et al., 2003, A&A, 406, 1151

Foster, A. R., Smith, R.K., Ji, L. & Brickhouse, N.S., 2011, this proceedings

Griffen J., 1998, Phys. B: At Mol. Opt. Phys. 31, 3713

Ji, L., Wang, Q.D. & Kwan, J., 2006, MNRAS, 372, 497

Reeves, K.K, Warren, H.P. & Forbes, T.G., 2007, ApJ, 668, 1210

This preprint was prepared with the AAS LaTeX macros v5.2.

NASA LAW, October 25-28, 2010, Gatlinburg

AtomDB v2.0: Atomic Data for X-ray Astrophysics

A. R. Foster, R. K. Smith, L. Ji & N. S. Brickhouse
Harvard-Smithsonian Center for Astrophysics, Cambridge, MA 02138
afoster@cfa.harvard.edu

ABSTRACT

A new version of the AtomDB atomic database (version 2.0) has been released and is now available for download from www.atomdb.org. This release is a major upgrade that includes new atomic data for almost every process of every ion in the database, including the addition of many new ions. The changes to the ionization balance and the He-like ion data produce significant changes to several diagnostic line ratios that are used in the plasmas, while also impacting the total radiated power in several temperature ranges.

1. Introduction

Successfully disseminating the results of atomic data producers to the astrophysical (and other) communities which rely on them for spectral analysis is an ongoing project in the scientific community. To successfully analyze an observation, an astrophysicist requires useful tools for converting observed line intensities into plasma conditions and elemental abundances. The raw data (for example, excitation collision cross sections) produced by measurement or calculation in the laboratory astrophysics community requires some post-processing to be in its most useful form for observer to use.

AtomDB (Smith at al. 2001) fulfills this role in two parts. The first is the large database of fundamental atomic data, covering items such as atomic structure, radiative and collisional transition rates, ionization and recombination rates and more for all the astrophysically relevant elements ($Z < 30$). This database is publicly available in FITS format.

The second part is a code for modeling a collisionally-ionized, optically-thin plasma. This converts the fundamental atomic data in the database into line and continuum emissivities for each ion, which are more directly useful in analysis of observations. The results of this code run are released to the public, and have been incorporated into several analysis packages such as Sherpa (Fruscione et al. 2006) and XSPEC (Arnaud 1996). The code will be released in 2011, pending writing of documentation.

2. New data

The last major update to AtomDB was in 2001. We have collected new data from a wide range of sources, incorporating a decade's worth of advances in the laboratory astrophysics field. Collisional excitation data for He- and H-like ions, and for the Fe L-shell ions, have been updated to R-Matrix (Burke & Berrington 1993) calculations from a variety of sources. In addition, we have extended this data to include higher n shells: data in the old version of AtomDB, and the R-Matrix data, usually includes the levels $n \leq 5$. Levels $5 < n \leq 10$ have been included using distorted wave data obtained using the Flexible Atomic Code (Gu 2003) in order to include more lines and cascade effects.

In addition, new ionization and recombination rates from Bryans et al. (2009) have been included, complete with some subsequent updates released after the publication of this data set. These changes significantly alter the ionization balance for some important ions, such as many H- and He-like ions.

State-selective dielectronic and radiative recombination rates for H-, He- and Li-like ions have been included, allowing direct population of excited states during the recombination process as well as capture to high n shells and subsequent cascade. This leads to a modest enhancement of higher-n lines in collisional ionization equilibrium, but a greater effect in non-equilibrium plasmas.

Finally, data for less-highly-ionized ions that generate EUV and longer wavelength lines have been updated using version 6 of the CHIANTI database (Dere et al. 2009).

3. Results

3.1. New lines

The updated H-like data lead to only small changes in line emissivities - the hydrogenic ions are quite well modelled by methods available ten years ago. The addition of the higher n shells does, however, create the possibility of observing more lines. At CCD resolution, these lines would just lead to a modestly skewed line shape towards the high energy side of existing lines. For grating spectroscopy, these lines could be observed in their own right. Figure 1 shows the emissivities of the new lines of Ne X and simulated Chandra HETG spectra for an observation of Capella, in which the high-n lines are clearly visible.

3.2. Cooling Power

The new atomic data have led to several changes in the total radiated power, as is shown in Figure 2. There are four distinct regions where the emission has increased. At $T_e \approx 10^4$ K the enhancement is due to the inclusion of two-photon emission for hydrogen for the first

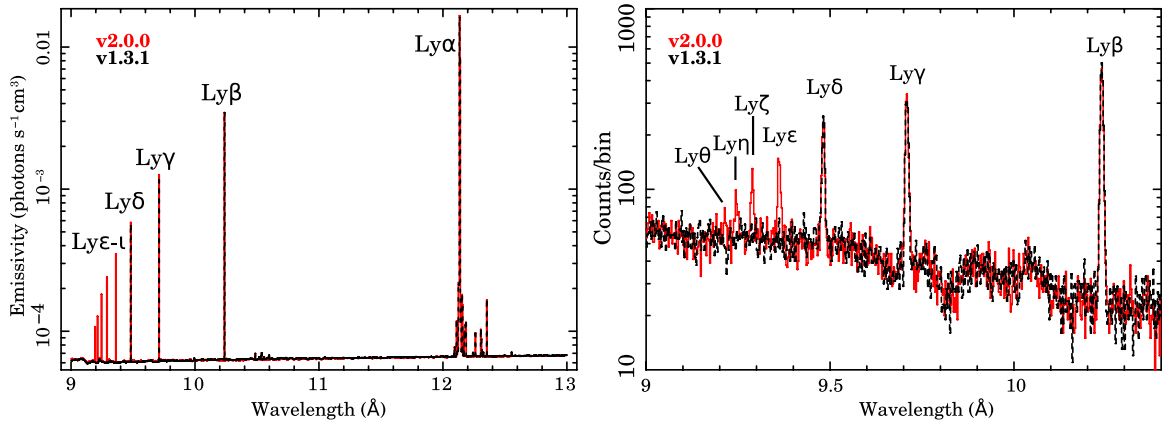

Fig. 1.— *Left:* Emissivities of the Lyman series lines of Ne X at $T_e = 10^7$ K. The new lines from the inclusion of data up to n=10 are apparent. *Right:* The simulated Ne X spectra for a 100ks Chandra HETG observation of a $T_e = 10^7$K plasma.

time. The emission occurs outside the X-ray band and therefore was not a priority in older versions of AtomDB: it is now included for completeness.

At higher temperatures, there are peaks due to the change of ionization balance data. The new dataset has, in general, a higher fraction of less ionized ions at higher temperatures, where they radiate strongly. This results in the $> 10\%$ increases apparent in the higher temperature regions, due to emission from O, Ne and Fe ions respectively (Figure 2).

3.3. Diagnostic Line Ratios

The new data has a significant effect on some individual lines. In particular, the new collisional excitation rates make a significant change to the He-like temperature sensitive line diagnostic, the G ratio (Gabriel & Jordan 1969). The change can be seen in Figure 2. This is a significant change to the observed ratios, and will as a result have a significant effect on plasma temperature estimates. These changes also agree well with the earlier calculations of the Ne IX G ratio by Smith et al. (2009).

4. Conclusion

The fruits of the past ten years of laboratory astrophysics research have been added to AtomDB, ready for access and use by the astrophysical community. Significant changes are apparent in some important line diagnostic ratios. The presence of new data for nearly every single ion, and the significant changes found in some line ratios, show the breadth of laboratory astrophysics program; it also emphasises the need for regular maintenance of

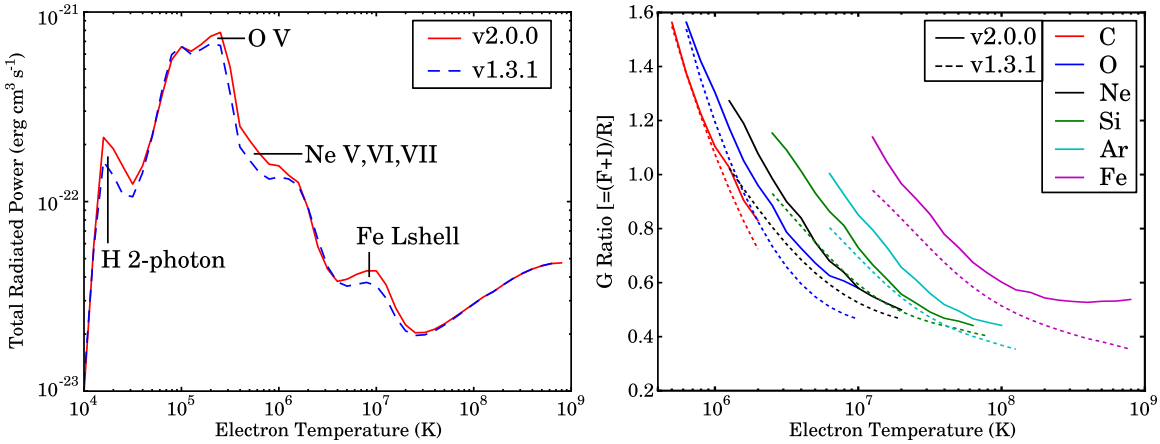

Fig. 2.— Comparisons between the old and new versions of AtomDB. *Left:* The cooling power radiated by a plasma in collisional ionization equilibrium in the 0.01 to 50keV band, assuming solar abundance Arnaud & Raymond (1992). *Right:* The temperature-sensitive G ratio for selected He-like ions.

atomic databases to ensure this data is available to observers in a timely manner.

We gratefully acknowledge support for this work from NASA ADP grant #NNX09AC71G.

REFERENCES

Arnaud, K.A., 1996, Astronomical Data Analysis Software and Systems V, eds. Jacoby G. and Barnes J., 17, ASP Conf. Series volume 101.

Arnaud, M., Raymond, J. C. 1992, ApJ, 398, 394

Bryans, P., Landi, E., Savin, D. W. 2009, ApJ, 691, 1540

Burke, P. G. Berrington, K. 1993, Atomic and Molecular Processes: an R-matrix Approach, Institute of Physics, New York

Dere, K. P. et al. 2009, A&A, 498, 915

Fruscione, A. et al, 2006, Proc. SPIE, Silvia, D. R. & Doxsey, R. E. 6270, 62701V.

Gabriel, A. H., Jordan, C. 1969, MNRAS, 145, 241

Gu, M. 2003 ApJ, 582, 1241

Smith, R. K. Brickhouse, N. S. Liedahl, D. A., Raymond, J. C. 2001, ApJ, 556, L91

Smith, R. K., Chen, G. X., Kirby, K., Brickhouse, N. S. 2009, ApJ, 700, 679

This preprint was prepared with the AAS LaTeX macros v5.2.

NASA LAW, October 25-28, 2010, Gatlinburg

Dielectronic Recombination Calculations for Fe^{15+}

D.-H. Kwon[1] & D. W. Savin

Columbia Astrophysics Laboratory, Columbia University, New York, NY 10027, USA

dk2545@columbia.edu

ABSTRACT

Dielectronic recombination (DR) of Na-like Fe^{15+} forming Mg-like Fe^{14+} via excitation of a $2l$ core electron has been investigated. We find that configuration interaction (CI) between DR resonances with different captured electron principal quantum numbers n can lead to a significant reduction in resonance strengths for $n \geq 5$. Including this form of CI accounts for most of the discrepancy between previous theoretical and experimental results. Here we briefly present our results and discuss their implications for the modeling of cosmic plasmas.

1. Introduction

The physical properties of cosmic sources can be determined using spectral observations coupled with theoretical models. Spectral observations depend on ion and elemental abundances. In order to determine the fractional ionic abundances of the plasma one needs to know the rate coefficients for all relevant ionization and recombination processes. Dielectronic recombination (DR) is the dominant electron-ion recombination process for most ions in cosmic plasmas.

DR is a two-step recombination process which begins when a free electron collides with an ion of charge $q+$ and in initial state i. The incident electron collisionally excites a core electron of the ion with principal quantum number n and is simultaneously captured forming a system of state j. The energy of the intermediate system lies in the continuum and it may autoionize. DR occurs when the state j radiatively decays to a state f emitting a photon.

---

[1]Laboratory for Quantum Optics, Korea Atomic Energy Research Institute, Daejeon 305-600, Republic of Korea.

Here we address a particularly nagging discrepancy between theory and experiment for the relatively simple Na-like Fe^{15+} forming Mg-like Fe^{14+}. Good agreement between experiment and theory has been found for Fe^{15+} DR via $\Delta n_c = 0$ and 1 core excitations of a $3s$ electron (Linkemann et al. 1995; Gorczyca & Badnell 1996; Gu 2004; Altun et al. 2006). For $\Delta n_{\rm c} = 1$ core excitations of $2l$ electron, previous theoretical work has shown the importance of configuration interaction (CI) within a $2s^2 2p^5 3l 3l' nl''$ complex (Gorczyca & Badnell 1996). Including this CI reduced the predicted overall resonance strength. However, all of these theoretical results consider CI only within the same n levels. Such results are still significantly larger than experiment for collision energies over 620 eV.

We have investigated the importance of CI between different n complexes of the captured electron for Fe^{15+} DR via $\Delta n_{\rm c} = 1$ core excitations of $2l$ electron. We use the Flexible Atomic Code (FAC) which is based on a fully relativistic Dirac Hamiltonian equation and utilizes a distorted wave approximation. Here we present some of our results.

2. Theoretical method

We calculated DR using the independent process, isolated resonance (IPIR) approximation. This method treats radiative recombination and DR separately and neglects quantum mechanical interferences between the two and between DR resonances. The energy integrated cross section (i.e., resonance strength) of state j is given by Kilgus et al. (1992) in atomic units as

$$\hat{\sigma}_j = \frac{\pi^2}{E_j} \frac{g_j}{2g_i} \frac{A^a_{ji} \sum_f A^r_{jf}}{\sum_k A^a_{jk} + \sum_f A^r_{jf}}. \tag{1}$$

Here E_j is the resonance energy of the intermediate system, g_i and g_j are statistical weights, A^a_{ji} is the autoionization rate from j to an initial recombining state i, A^a_{jk} is the autoionization rate from j to any state k of A^{q+}, and A^r_{jf} is the radiative decay rate from j to f.

We considered the multiply-excited $2l^7 3l' 3l'' nl'''$ resonance states, thereby including $2s \rightarrow 3l$ promotion; the $2l^8 3l'$, $2l^8 nl'''$, and $2l^7 3l' 3l''$ autoionization decay channels; and the $2l^8 3l' 3l''$ and $2l^8 3l' nl'''$ radiative decay channels. The maximum angular momentum considered was 5. The $n > 6$ $2l^8 3l' nl'''$ levels lie in the continuum and radiative Decays to Autoionizing levels followed by radiative Cascades (DAC) are possible. The branching ratio for the DAC process is given by

$$B_j = \frac{\sum_t A^r_{jt} + \sum_{t'} A^r_{jt'} B_{t'}}{\sum_k A^a_{jk} + \sum_f A^r_{jf}}, \tag{2}$$

where the final states t and t' are below and above the ionization threshold, respectively. $B_{t'}$

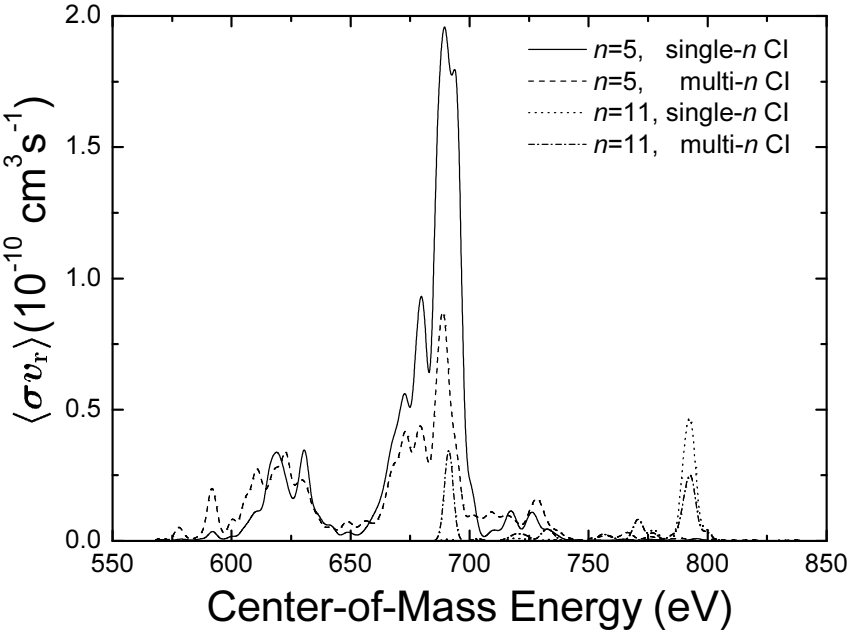

Fig. 1.— DR resonance structure of the $n = 5$ and $n = 11$ resonances for single-n and multi-n CI.

is the branching ratio for radiative stabilization of t' and can be determined by evaluating B_j iteratively.

We performed a large scale CI calculation including all $2l^7 3l' 3l'' nl'''$ complexes from $n = 3$ to 14. This allowed us to consider CI between resonances with different captured electron principal quantum numbers. Radial wave functions were optimized on the $2l^8 3l' 3l''$ configuration. We calculated autoionization and radiative decay rates from the wave functions obtained using this CI mixing.

3. Results

Figure 1 shows a DR resonance spectrum for $n = 5$ and $n = 11$. We plot here the DR cross section σ times the relative collision velocity v_r convolved with the experimental energy distribution of Linkemann et al. (1995) which was $k_B T_\parallel = 2.4$ meV along the beams and $k_B T_\perp = 0.1$ eV perpendicular to the beams. The $n = 5$ resonance spectrum peak is clearly reduced in strength when multi-n CI is considered. This behavior can be explained by configuration mixing of a strong resonance level in single-n CI with weak resonance levels of different n complexes. On the other hand, the weak $n = 11$ resonance level is largely enhanced by CI mixing with the strong $n = 5$ resonance levels. This can be seen around

$\sim$ 680 eV in Figure 1.

Multi-n CI can significantly reduce the theoretical DR resonances strength compared to single-n CI calculations. This brings theory into very good agreement with the experimental results of Linkemann et al. (1995) as is discussed in more detail in Kwon & Savin (in preparation). From our multi-n CI calculations we have derived a Maxwellian rate coefficient $\alpha_{\rm DR}$ needed for plasma modeling. Multi-n CI for $\Delta n_{\rm c} = 1$ core excitation of a $2l$ electron reduces the total Maxwellian rate coefficient by a maximum of about 15% at temperatures where Fe^{15+} forms in collisionally ionized gas.

4. Summary

We have demonstrated the importance of CI between resonances with different captured electron principal quantum numbers n for DR of Na-like Fe^{15+} forming Mg-like Fe^{14+} via $\Delta n_{\rm c} = 1$ core excitation of a $2l$ electron. Multi-n CI significantly reduces the theoretical resonance strengths for capture into $n \geq 5$ levels. This brings theory into very good agreement with experiment and removes a previously existing discrepancy between the two. CI between different n levels reduces the Maxwellian DR rate coefficient by a maximum of about 15% at temperatures where Fe^{15+} forms in collisional ionization equilibrium.

This work was supported in part by the NASA Astronomy and Physics Research and Analysis (APRA) Program.

REFERENCES

Linkemann, J., et al. 1995, Nucl. Instrum. Methods B, 98, 154.

Gorczyca, T., W., & Badnell, N. R. 1996, Phys. Rev. A, 54, 4113.

Gu, M., F. 2004, Astrophys. J. Suppl. Ser, 153, 389.

Altun, Z., et al. 2006, Astron. Astrophys., 447, 1165.

Kilgus, G., et al. 1992, Phys. Rev. A, 46, 5730.

Kwon, D.-H., & Savin, D. W., in preparation.

This preprint was prepared with the AAS LaTeX macros v5.2.

NASA LAW, October 25-28, 2010, Gatlinburg

Recombination and Ionization Measurements at the Heidelberg Heavy Ion Storage Ring TSR

M. Hahn, M. Lestinsky, O. Novotný, & D. W. Savin

Columbia Astrophysics Laboratory, Columbia University, 550 West 120th St. New York, NY 10027 USA.

mhahn@astro.columbia.edu

D. Bernhardt, A. Müller, & S. Schippers

Institut für Atom- und Molekülphysik, Justus-Liebig-Universität Giessen, Leihgesterner Weg 217, 35392 Giessen, Germany.

C. Krantz, M. Grieser, R. Repnow, & A. Wolf

Max-Planck-Institute for Nuclear Physics, Saupfercheckweg 1, 69117 Heidelberg, Germany.

ABSTRACT

Knowledge of the charge state distribution (CSD) of astrophysical plasmas is important for the interpretation of spectroscopic data. To accurately calculate CSDs, reliable rate coefficients are needed for dielectronic recombination (DR), which is the dominant electron-ion recombination mechanism for most ions, and for electron impact ionization (EII). We are carrying out DR and EII measurements of astrophysically important ions using the TSR storage ring at the Max-Plank-Institute for Nuclear Physics in Heidelberg, Germany. Storage ring measurements are largely free of the metastable contamination found in other experimental geometries, resulting in more unambiguous DR and EII reaction rate measurements. The measured data can be used in plasma modelling as well as for benchmarking theoretical atomic calculations.

1. Introduction

Reliable ionization balance calculations are needed to analyze spectra from a wide range of cosmic sources including photoionized objects such as Active Galactic Nuclei and X-ray

binaries and electron ionized objects such as stars, supernovae, galaxies, and clusters of galaxies. In order to calculate the ionization balance, accurate ionization and recombination rate coefficients are needed for all ion charge states of all astrophysically relevant elements, typically taken as hydrogen through zinc.

EII is the main ionization mechanism for collisionally ionized plasmas. There are several channels through which EII can occur. In direct ionization a free electron collides with an ion transferring energy to, and freeing, a bound electron. The most common indirect process is excitation-autoionization (EA) in which an incident electron excites an inner-shell electron forming a doubly-excited state that stabilizes by ejecting an electron.

The main recombination processes for both collisionally ionized and photoionized plasmas are radiative recombination (RR) and dielectronic recombination (DR). In RR a free electron is captured by an ion and the excess energy is released by emitting a photon. DR occurs when a free electron collides with an ion exciting a bound electron and is simultaneously captured. The resulting doubly-excited state lies in the continuum of the recombined system. The excited state may decay by emitting a photon, in which case DR is complete, or it may autoionize leaving the ion in its original charge state. DR is the dominant electron-ion recombination mechanism for most ions.

2. Measurements at TSR

We are carrying out ionization and recombination measurements at the TSR heavy ion storage ring of the Max-Plank-Insitute for Nuclear Physics in Heidelberg, Germany. The ion beam is prepared in a tandem accelerator and injected into TSR (Figure 1). There are separate cold electron beams located in two portions of the ring. These can be merged with the stored ion beam within the ring. Initially the energy of both electron beams is set to a "cooling energy" where the relative velocity between the electrons and ions is zero. Beam-beam collisions reduce the energy spread of (phase space cool) the ions and define the average ion energy. The initial phase lasts several seconds during which metastable levels within the ion beam radiatively decay producing a well defined ground state ion beam.

Measurements are performed by varying the energy of one of the electron beams in small steps while the other provides simultaneous phase space cooling of the stored ions. The ionized and recombined products are separated from the parent ion beam by the first dipole magnet downstream of the interaction region. There they are counted by particle detectors positioned to intersect the product beams. After each measurement step the count rate is measured at a fixed reference energy in order to determine the background count rate

from collisions between the ions and the residual gas.

The largest source of uncertainty comes from the ion current measurement, which is needed to normalize the recombination and ionization count rates and to calculate absolute cross sections and rate coefficients. The 1σ systematic error due to the ion current measurement is about 15%. The uncertainty from counting statistics is typically only a few percent. More details about the experiments can be found in Lestinsky et al. (2009) and Hahn et al. (2010) and in the references listed in each. TSR has been used extensively to study DR of cosmically abundant ions. A recent review of this work has been given by Schippers et al. (2009).

3. Recent Results

DR and EII were recently measured for initially Mg^{7+} ions (Hahn et al. 2010). This ion has a long-lived metastable state with a lifetime of about 3 s, making the storage ring technique necessary in order to measure ground state ions. The DR results are still being prepared for publication.

The EII cross section for Mg^{7+} forming Mg^{8+} over the energy range from 200 to 2000 eV is shown in Figure 1. This energy range includes channels for direct ionization of the $2p$, $2s$, and $1s$ electrons at threshold energies of 265.96 eV, 283.37 eV, and 1587.32 eV, respectively (Ralchenko et al. 2008). It also includes EA from excitation of a $1s$ electron, which can occur at energies above 1291 eV (Safronova & Shlyaptseva 1996). The cross section is compared to a calculation with the Flexible Atomic Code (FAC) reported by Dere (2007) and a calculation using the Los Alamos Atomic Physics Code (Magee et al. 1995). The measured cross section is in agreement with both calculations to within the experimental uncertainties. This is the first experimental measurement of EII for Mg^{7+}.

4. Future Directions

Future potential DR and EII measurements include Fe^{12+} and Fe^{6+}. Additional future EII work could involve measurements in iso-electronic sequences for which no storage ring data exist.

This work was supported in part by the NASA Astronomy and Physics Research and Analysis program.

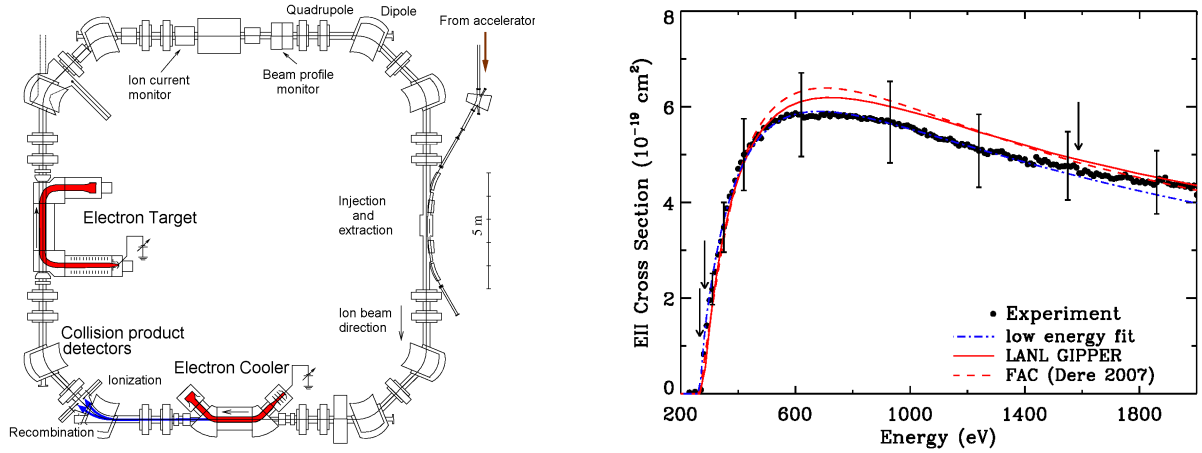

Fig. 1.— (Left) Schematic of the TSR ion storage ring showing the two electron beams. These beams are labeled "Electron Cooler" and "Electron Target", but their roles of continuously cooling the ion beam or serving as a variable energy target are interchangeable. (Right) The EII cross section for Mg^{7+} forming Mg^{8+}. The estimated 1σ experimental uncertainty is illustrated by error bars at selected points. Arrows indicate energy thresholds for the various direct ionization channels ($2p$,$2s$,$1s$). The dot-dashed line shows a fit to the experimental data below 1100 eV using the Lotz formula in order to illustrate the change of shape at high energies that may be caused by EA and direct ionization of a $1s$ electron. Also shown are theoretical results from the LANL Atomic Code and FAC.

REFERENCES

Dere, K. P. 2007, A&A, 466, 771
Hahn, M., et al. 2010, ApJ, 712, 1166
Lestinsky, M., et al. 2009, ApJ, 698, 648
Magee, N. H., et al. 1995, ASP Conf. Ser., 78, 51, http://aphysics2.lanl.gov/tempweb/
Ralchenko, Y., et al. 2008, NIST Atomic Spectra Database, http://physics.nist.gov/asd3
Safronova, U. I., & Shlyaptseva, A. S. 1996, Phys. Scr., 54, 254
Schippers, S., et al. 2009, J. Phys. Conf. Ser., 163, 012001

NASA LAW, October 25-28, 2010, Gatlinburg

New Collisional Ionization Equilibrium Calculations for Optically Thin Plasmas

D. W. Savin, P. Bryans[1], & W. Mitthumsiri[2]

Columbia Astrophysics Laboratory, Columbia University, New York, NY 10027, USA

savin@astro.columbia.edu

N. R. Badnell

Department of Physics, University of Strathclyde, Glasgow, G4 0NG, UK

T. W. Gorczyca

Department of Physics, Western Michigan University, Kalamazoo, MI 49008, USA

J. M. Laming

E. O. Hulburt Center for Space Research, U.S. Naval Research Laboratory, Code 7674L, Washington, DC 20375, USA

ABSTRACT

Reliably interpreting spectra from electron-ionized laboratory and cosmic plasmas requires accurate ionization balance calculations for the plasma in question. However, much of the atomic data needed for these calculations have not been generated using modern theoretical methods and their reliability are often highly suspect. We have carried out state-of-the-art calculations of dielectronic recombination (DR) rate coefficients for the hydrogenic through Mg-like ions of all elements from He to Zn as well as for Al-like to Ar-like ions of Fe. We have also carried out state-of-the-art radiative recombination (RR) rate coefficient calculations for the bare through Na-like ions of all elements from H to Zn. Using

[1]Current address: NASA Goddard Space Flight Center, 8800 Greenbelt Road, Greenbelt, Maryland 20771, USA.

[2]Current address: Department of Physics, Stanford University, Stanford, CA 94305, USA.

our data and the most recently recommended electron impact ionization data, we present improved collisional ionization equilibrium (CIE) calculations. Here, as an example, we present our calculated fractional ionic abundances for iron using these data and compare them with those from the previously recommended CIE calculations.

1. Introduction

Electron ionized plasmas (also called collisionally ionized plasmas) are formed in a diverse variety of objects in the universe. These range from stellar coronae and supernova remnants to the interstellar medium and gas in galaxies or in clusters of galaxies. The physical properties of these sources can be determined using spectral observations coupled with theoretical models. This allows one to infer electron and ion temperatures, densities, emission measure distributions, and ion and elemental abundances. But reliably determining these properties requires accurate fractional abundance calculations for the different ionization stages of the various elements in the plasma (i.e., the ionization balance of the gas).

Since many of the observed sources are not in local thermodynamic equilibrium, in order to determine the ionization balance of the plasma one needs to know the rate coefficients for all the relevant ionization and recombination processes. Often the observed systems are optically-thin, low-density, dust-free, and in steady-state or quasi-steady-state. Under these conditions the effects of any radiation field can be ignored, three-body collisions are unimportant, and the ionization balance of the gas is time-independent. This is commonly called collisional ionization equilibrium (CIE) or sometimes coronal equilibrium.

2. Recent Improvements in Atomic Data

Recently, improved theoretical dielectronic recombination (DR) and radiative recombination (RR) rate coefficients have been published by Badnell et al. (2003), Gu (2003a,b, 2004) and Badnell (2006a,b,c). Data are available for fully-stripped through Mg-like ions of all elements from hydrogen through zinc as well as Al-like through Ar-like for Fe. For electron impact ionization (EII), Dere (2007) has reassessed the ionization database and, using a combination of laboratory measurements and theoretical calculations, has generated recommended EII data for all charge states of all elements from hydrogen through zinc.

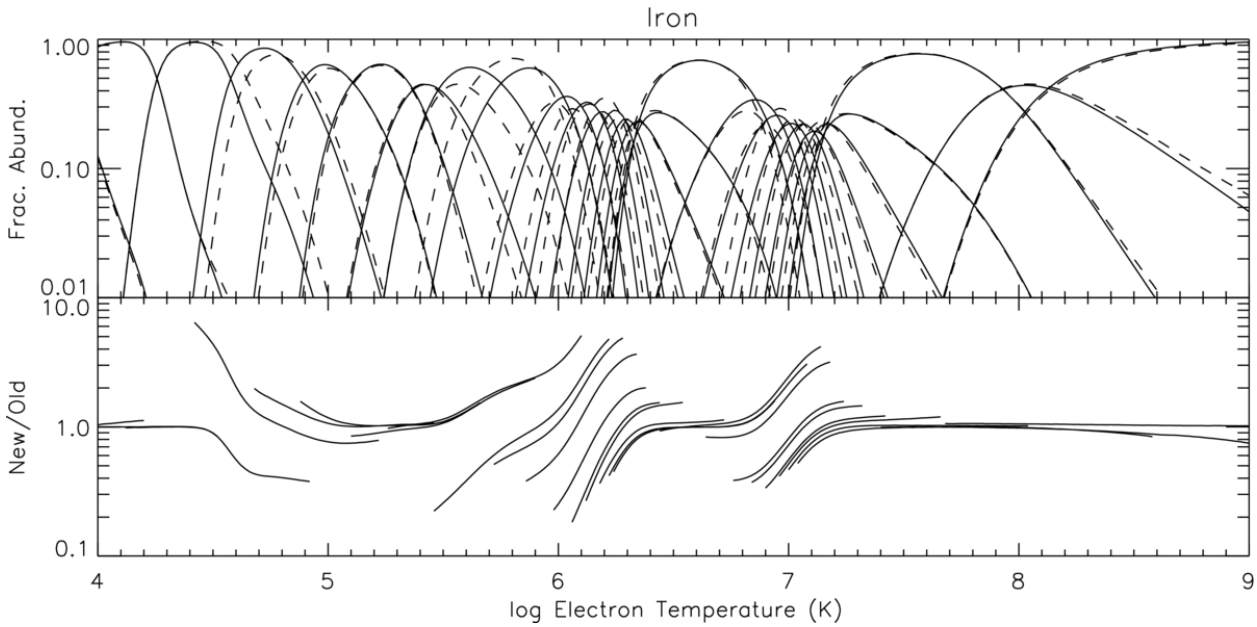

Fig. 1.— Top: CIE fractional abundances for iron from Bryan et al. (2009; solid curves) versus Mazzotta et al. (1998; dashed curves). Bottom: Ratio of the Bryans et al. fractional abundances relative to those of Mazzotta et al.

3. Representative CIE results

These recent improvements to the relevant atomic data have led to a reevaluation of the fractional ionic abundances all elements from hydrogen through zinc (Bryans et al. 2006, 2009). An example of these new CIE results (solid curves) is shown in Figure 1. The previous CIE results are from Mazzotta et al. (1998, dashed curves). Differences of up to factors of ~ 10 are seen.

4. Conclusion

On a regular basis, a number of different groups have evaluated the available atomic data and produced updated CIE calculations (reviewed in Bryans et al. 2006). New DR, RR, and EII data are continually becoming available. Our efforts here are just another step in what promises to be a long line of studies aimed at providing the astrophysics community with the most reliable CIE calculations currently possible.

This work was supported in part by the NASA APRA program.

REFERENCES

Badnell, N. R., O'Mullane, M. G., Summers, H. P., Altun, Z., Bautista, M. A., Colgan, J., Gorczyca, T. W., Mitnik, D. M., Pindzola, M. S., & Zatsarinny, O. 2003, A&A, 406, 1151

Badnell, N. R. 2006a, ApJS, 167, 334

Badnell, N. R. 2006b, http://amdpp.phys.strath.ac.uk/tamoc/DR/

Badnell, N. R. 2006c, http://amdpp.phys.strath.ac.uk/tamoc/RR/

Bryans, P., Badnell, N. R., Gorczyca, T. W., Laming, J. M., Mitthumsiri, W., & Savin, D. W. 2006, ApJS, 167, 343

Bryans, P., Landi, E., & Savin, D. W. 2009, ApJ, 691, 1540

Dere, K. P. 2007, A&A, 466, 771

Gu, M. F. 2003a, ApJ, 589, 1085

Gu, M. F. 2003b, ApJ, 590, 1131

Gu, M. F. 2004, ApJ, 153, 389

Mazzotta, P., Mazzitelli, G., Colafrancesco, S., & Vittorio, N. 1998, A&AS, 133, 403

NASA LAW, October 25-28, 2010, Gatlinburg

Comprehensive Atomic Data Set Relevant To The Nebular Spectral Modeling Of Type Ia Supernovae

D. R. Schultz & Y. Hui

Physics Division, Oak Ridge National Laboratory Bldg. 6010, Oak Ridge, TN 37831, USA

schultzd@ornl.gov, huiy@ornl.gov

ABSTRACT

In order to better explain the observed late-time (or nebular, hereafter) spectra of Type Ia supernovae, we are working on constructing a model which includes the major physical processes involved in the spectral generation, (i.e., the γ-ray energy deposition following the Ni-Co-Fe radioactive decays, the thermal structure and ionization balance determined by various atomic collision channels, and the radiative transport of the final emergent photons). Because the eventual success of the model depends highly on the general availability and accuracy of the atomic data (especially of the iron group elements, such as the radiative transition probabilities and the electron impact excitation/ionization, electron-ion recombination, photoionization, and charge transfer rates) relevant to the calculation of the thermal structure and ionization balance, we have searched, updated and even partly recalculated the data set which was used in our previous work. The ultimate goal is to set up a 3-D synthetic spectral model of the nebular phase in conjunction with the major 3-D explosion simulations of Type Ia supernovae.

1. Introduction

Significant differences exist in explosion models of the energetic disruption of carbon-oxygen-rich white dwarfs through run-away thermonuclear burning – Type Ia supernovae. For example, the fundamental characteristics of the explosion, such as the total energy released, the amount and distribution of radioactive elements synthesized, and the matter spatial asymmetry, are highly dependent on the physical assumptions (e.g., the initial carbon-to-oxygen ratio, the ignition mechanism, and the dimensionality of the model) and on the simulation scheme of the explosion models. In order to discriminate between these models,

we plan to study the spectra of Type Ia supernovae in the nebular phase (typically 100 days and more after reaching its maximum luminosity) based on fully 3-D explosion models chosen to represent varying physical assumptions and levels of numerical sophistication. Given the initial density and velocity distribution of the synthesized matter, we will calculate the energy deposition due to γ-rays and positrons emitted from the radioactive decay of iron-group elements, the thermal balance which determines the temperature profile, the ionization balance and level populations which reflect the non-LTE nature of the moving plasma, and the radiative transfer that dictates the emergent spectrum. To successfully achieve the goal, we need a comprehensive compilation of atomic data set relevant to various collision processes involved in the spectral modeling. A description of this data set is briefly outlined here.

2. Calculation Modules and Data Sources

- γ-ray Energy Deposition: γ-ray photons (through Compton scattering), together with a small amount of positrons (by annihilation with electrons), created from the radioactive decay of ^{56}Ni and ^{56}Co are believed to be the power source for the ejecta at late time after SNe Ia explosions. The γ-ray line list previously used is from Lederer & Shirley (1978) and will be replaced by that from Firestone & Shirley (1996). The collision cross sections are included for channels such as Compton scattering (Klein-Nishina), pair production (Hubbell 1969) and photoelectric absorption (Veigele 1973).

- Thermal and Ionization Balance: The thermal structure of the ejecta is dependent on the balance of the heating and cooling terms of the energy conservation equation, provided that the ejecta reaches a steady state. The calculation of the cooling functions involves the detailed information of the ionization states and level populations of the atoms/ions included. A set of sophisticated rate equations will be solved iteratively with the asymptotic level populations and radiative intensities in order to determine the ionization balance of the medium. The relavant atomic data include:

  - Electron Impact Excitation: Energetic electrons boosted by the γ-ray photons lose energy in exciting the atoms/ions. The collision cross sections previously collected for Fe II (Pradhan & Berrington 1993; Zhang & Pradhan 1995a; Bautista & Pradhan 1996), Fe III (Zhang & Pradhan 1995b; Zhang 1996), Co III (Shaw et al. 1998), Ni II (Bautista & Pradhan 1996), will now be supplemented with new data from Ramsbottom et al. (2002, 2007) and Ramsbottom (2009) for Fe II; McLaughlin (2002) and Bautista (2010) for Fe III; and Bautista (2004) and Cassidy et al. (2010) for Ni II.

- Electron Impact Ionization: Similar energy losing collisions between fast electron and atoms/ions, in which, instead of excitation of the targets, ionization occurs, resulting in an additional slow electron. The collision cross sections were collected from Lennon et al. (1988) and Freund et al. (1990).
- Photoionization: The source of the photons is mostly a combination from photo-deexcitation and electron-ion recombination. The cross sections used for photoionizating collisions for Fe I, II and III are collected from Nahar & Pradhan (1994), Nahar (1996a) and Bautista (1997).
- Electron-Ion Recombination: Electron-ion recombination not only affects the ionization balance of the ejecta, but also provides photons energetic enough to ionize lower-charged ions. The cross sections used for this recombination process are collected from Nahar (1996b, 1997) and Nahar et al. (1997).
- Charge Exchange: The ionization distribution is significantly affected by charge exchange between iron-group ions and the neutral atoms. The rate coefficients for Fe II, III and IV have been collected from Krstić et al. (1998). New data will be calculated to supplement this data set.

• Radiative Transfer: The radiative transfer effects were taken into account by applying the Sobolev escape probability approximation to a homogonously expanding medium. Further improvement includes fully Monte-Carlo treatment of the photon transfer, such as that implemented by Kasen et al. (2006).

This work has been supported by NASA Astrophysical Theory Program Grant NNH10AN40I.

REFERENCES

Bautista, M. A. & Pradhan, A. K. 1996, A&A Suppl. Ser., 115, 551

Bautista, M. A. 1997, A&A Suppl. Ser., 122, 167

Bautista, M. A. 2004, A&A, 420, 763

Bautista, M. A. et al. 2010, ApJ, 718, L189

Cassidy, C. M. et al. 2010, A&A, 513, A55

Firestone, R. B. & Shirley, V. S. 1996, Table of Isotopes, 8ed., New York, Wiley

Freund, R. S. et al. 1990, Phys. Rev. A, 41, 3575

Hubbell, J. H. 1969, NSRDS-NBS 29

Kasen, D. et al. 2006, ApJ, 651, 366

Krstić, P. S. et al 1998, in Stellar Evolution, Stellar Explosions and Galactic Chemical Evolution, 79

Lederer, M. C. & Shirley, V. S. 1978, Table of Isotopes, 7ed., New York, Wiley

Lennon, M. A. et al. 1988, JPCRD, 17, 1285

McLaughlin, B. M. 2002, J. Phys. B, 35, 2755

Nahar, S. N. & Pradhan, A. K.1994, J. Phys. B, 27429

Nahar, S. N. 1996a, Phys. Rev. A, 53, 1545

Nahar, S. N. 1996b, Phys. Rev. A, 53, 2417

Nahar, S. N. 1997, Phys. Rev. A, 55, 1980

Nahar, S. N. et al. 1997, ApJ, 479, 497

Pradhan, A. K. & Berrington, K. A. 1993, J. Phys. B, 26, 157

Ramsbottom, C. A. et al. 2002, J. Phys. B, 35, 3451

Ramsbottom, C. A. et al. 2007, A&A, 475, 765

Ramsbottom, C. A. 2009, Atomic Data and Nuclear Data Tables, 95, 910

Shaw, J. A. et al. 1998, Phys. Rev. A, 58, 2920

Veigele, W. J. 1973, Atomic Data Tables, 5, 51

Zhang, H. L. & Pradhan, A. K. 1995a, A&A, 293, 953

Zhang, H. L. & Pradhan, A. K. 1995b, J. Phys. B, 28, 3403

Zhang, H. L. 1996, A&A Suppl. Ser., 119, 523

This preprint was prepared with the AAS LaTeX macros v5.2.

NASA LAW, October 25-28, 2010, Gatlinburg

Molecular Hydrogen Formation in the Early Universe: New Implications From Laboratory Measurements

K. A. Miller, H. Kreckel[1], H. Bruhns[2], & D. W. Savin

Columbia Astrophysics Laboratory, Columbia University, New York, NY 10027, USA

kmiller@astro.columbia.edu

X. Urbain

Institute for Condensed Matter and Nanosciences, Université Catholique de Louvain, Louvain-la-Neuve B-1348, Belgium

M. Čížek

Department of Mathematics and Physics, Charles University Prague, 180 00 Praha 8 Prague, Czech Republic

S. C. O. Glover

Institut für Theoretische Astrophysik, Zentrum für Astronomie der Universität Heidelberg, 69120 Heidelberg, Germany

ABSTRACT

We have performed the first energy-resolved measurement of the associative detachment (AD) reaction $H^- + H \rightarrow H_2 + e^-$. This reaction is the dominant formation pathway for H_2 during the epoch of first star formation in the early universe. Despite being the most fundamental anion-neutral chemical reaction, experiment and theory have failed to converge in both magnitude and energy dependence. The uncertainty in this rate coefficient severely limits our understanding of the formation of the first stars and protogalaxies.

---

[1]Current address: Department of Chemistry, University of Illinois, Urbana, Il 61801, USA.

[2]Current address: INFICON GmbH, D-50968 Cologne, Germany.

1. Introduction

H_2 cooling of primordial clouds in the early universe led to the formation of protogalaxies and the first stars, commonly called Population III stars. H_2 is formed during this epoch via the associative detachment (AD) reaction

$$H^- + H \rightarrow H_2^- \rightarrow H_2 + e^-. \tag{1}$$

Utilizing a novel merged-beams apparatus that we have developed at Columbia University, we have performed absolute measurements for this reaction. Our work is the first energy-resolved experimental study for this reaction and has been published in Kreckel et al. (2010) and Bruhns et al. (2010).

Prior to our work, there was nearly an order-of-magnitude uncertainty in the rate coefficient for this AD reaction Glover et al. (2006). This uncertainty severely limited our ability to model protogalaxies and metal-free stars forming from initially ionized gas, such as in ionized regions (i.e., H II regions) created by earlier Population III stars (Glover et al. 2006; Glover & Abel 2008; Kreckel et al. 2010). These uncertainties have been greatly reduced by our new experimental results with their uncertainty of ±24%.

2. Experiment

Using a duoplasmatron ion source we create a 10 keV H^- beam which is steered through a floating cell of potential U_f. Inside the floating cell the H^- beam crosses a 1.4 kW, 975 nm diode laser which photodetaches ∼7.4% of the anions, creating an H beam of ∼10 keV. In this way we are able to create merged H^- and H beams. The energy of any H_2 formed is essentially the sum of the H^- and H energies or ∼20 keV. The relative energy E_r between the beams is set by varying U_f. Beam collimation is provided by two circular 5-mm-diameter apertures separated by 280 cm, with one located before the photodetachment chamber and the other after.

The beginning of the interaction region is determined by a "chopper" electrode which can deflect and thereby turn the H^- beam on and off. The H beam is chopped by switching the laser on and off. Chopping both beams out of phase allows us to extract the signal generated in the interaction region from various backgrounds. The end of the interaction region is set by a quadrupole deflector which directs the H^- beam into a Faraday cup. The remaining neutrals enter a He gas cell where about 5% of the H_2 and H are stripped generating H_2^+ and H^+. After this cell the neutrals and ions enter an electrostatic energy analyzer. The analyzer is set to transmit the ∼20 keV H_2^+ ions and discriminate against

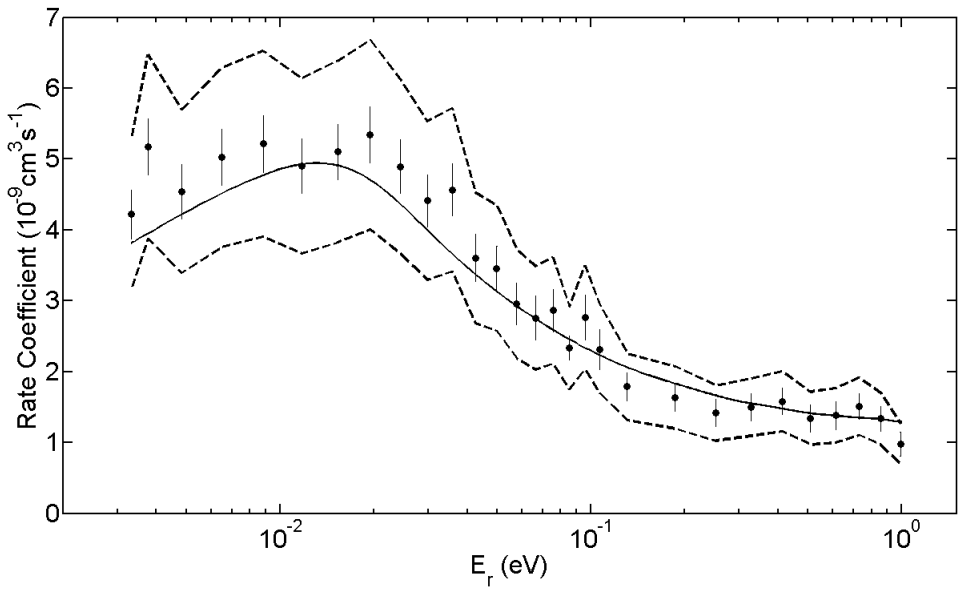

Fig. 1.— Our measured rate coefficient for reaction (1) from Kreckel et al. (2010). The circles show our measurements, the error bars are the 1σ statistical uncertainty, and the dashed lines are the $\pm 1\sigma$ total experimental uncertainty. The solid line is the theory of Čížek et al. (1998).

the ∼10 keV H^+. The transmitted H_2^+ ions are directed onto and counted with a channel electron multiplier.

3. Results

Experimentally, we measure the cross section $\sigma_{\rm AD}$ for reaction (1) times the relative velocity $v_{\rm r}$ between the H^- and H beams convolved with the velocity spread of the experiment. This gives a rate coefficient. Our results as a function of $E_{\rm r}$ are shown in Fig. 1. We find excellent agreement with the theory of Čížek et al. (1998). This is discussed in greater detail in Kreckel et al. (2010) and Bruhns et al. (2010).

To examine the effect of our AD data on primordial star formation, we simulated primordial gas evolving within an initially ionized protogalactic halo Kreckel et al. (2010). Using our results and error bars, the simluations found the uncertainty in the characteristic Population III mass is reduced from more than a factor of twenty to around a factor of two. As a result we are significantly closer to the point where remaining uncertainties in models for protogalaxy and first star formation tell us something about the cosmology and not about

the underlying chemistry.

This was supported in part by the NSF Divisions of Astronomical Sciences and Chemistry.

REFERENCES

Bruhns, H., Kreckel, H., Miller, K. A., Urbain, X., & Savin, D. W., 2010, Phys. Rev. A 82, 042708

Bruhns, H., Kreckel, H., Miller, K. A., Lestinsky, M., Seredyuk, B., Mitthumsiri, W., Schmitt, B. L., Schnell, M., Urbain, X., Rappaport, M. L., Havener, C.C., & Savin, D. W., 2010, Rev. Sci. Instrum. 81, 013112

Čížek, M., Horáček, J., & Domcke, W., 1998, J. Phys. B 31, 2571

Glover, S. C. O., Abel, T., 2008, Mon. Not. R. Astron. Soc. 388, 1627

Glover, S. C. O., Savin, D. W., Jappsen, A.-K., 2006, Astrophys. J. 640, 553

Kreckel, H., Bruhns, H., Čížek, M., Glover, S. C. O., Miller, K. A., Urbain, X., & Savin, D. W., 2010, Science 329, 69

NASA LAW, October 25-28, 2010, Gatlinburg

Theoretical investigation of charge transfer between N^{6+} and H

Y. Wu[1] and P. C. Stancil[1]

Department of Physics and Astronomy and the Center for Simulational Physics, University of Georgia, Athens, Georgia 30602, USA

yongwu@physast.uga.edu, stancil@physast.uga.edu

H. P. Liebermann[2], P. Funke[2], and R. J. Buenker[2],

Fachbereich C-Mathematik und Naturwissenschaften, Bergische Universitat Wuppertal, D-42097 Wuppertal, Germany

D. R. Schultz[3], Y. Hui[3], I. N. Draganic[3], and C. C. Havener[3]

Physics Division, Oak Ridge National Laboratory, Oak Ridge, Tennessee 37831-6373, USA

ABSTRACT

Charge transfer due to collisions of ground state $N^{6+}(1s\ ^2S)$ with atomic hydrogen has been investigated theoretically using the quantum-mechanical molecular-orbital close-coupling method (QMOCC), in which the adiabatic potential and nonadiabatic couplings were obtained with the multi-reference single- and double-excitation configuration interaction approach (MRDCI). Total, $n-$, $l-$, and S-resolved cross sections are obtained for energies between 10 meV/u and 10 keV/u. The QMOCC results are compared to available experimental and theoretical data as well as to new merged-beams measurements and atomic-orbital close-coupling and classical trajectory Monte Carlo calculations. These cross sections, especially state-selective, are necessary parameters in the X-ray emission simulation for heliospheric and Martian exosphere spectra due to $\sim$1 keV/u solar wind ion collisions. In particular, we propose an optimization method for the atomic basis sets used in the MRDCI calculation of the adiabatic potentials and nonadiabatic couplings for highly charged ions. The computational accuracy of the QMOCC charge transfer cross sections is found to be sensitive to the accuracy of the adiabatic potentials and couplings.

1. INTRODUCTION

There has been significant progress (Kallman *et al* 2007, and references therein) in X-ray astrophysics since 2000, including the recognition that charge exchange plays a dominant role in the production of the X-ray and/or EUV radiation observed in the cometary and planetary atmospheres (Krasnopolsky *et al* 2004; Ali *et al* 2005). Here, we apply the QMOCC method to investigate single electron capture process of N^{6+} with atomic hydrogen, in which N^{6+} is one of the primary ions in the solar wind and the product N^{5+} ions plays an important role in solar wind charge exchange X-ray simulations.

2. THEORY AND RESULT

We will not further discuss the MRDCI (Buenker *et al.* 1974; Krebs & Buenker 1995) and QMOCC (Zygelman *et al* 1992) methods here, but just present the technique for optimizing the atomic basis sets used in the MRDCI calculation. In the collision of N^{6+} with H, an election is transferred from the hydrogen atom to the N ion, but into a high Rydberg state with n typically of 4 or 5 and the captured electron is essentially hydrogen-like in character. We have developed a hybrid basis set consisting of two components: i) the standard Dunning neutral N atom basis and ii) a one-electron basis of hydrogen-like orbitals. The latter basis is optimized to reproduce nearly exactly the hydrogen-like Rydberg ion energies.

Table 1: Comparison of relative asymptotic energies of the $[NH]^{6+}$ system between the experimental data (Kelly 1987) and the MRDCI calculation with the optimized Gaussian basis set functions. ΔE is the absolute errors between the calculated and experimental data. Note that the energy unit used here is eV .

States	Exp.	MRDCI	ΔE
1S(1s3s)	496.6807	496.47792	0.20278
1D(1s3d)	497.644	497.44514	0.19886
1Po(1s3p)	497.9689	497.71457	0.25433
1S(1s4s)	521.046	520.83193	0.21407
1D(1s4d)	521.4564	521.23821	0.21819
1Fo(1s4f)	521.4680	521.24417	0.22391
1Po(1s4p)	521.5779	521.36889	0.20901
1S(1s5s)	532.2666	532.05180	0.21480
1D(1s5d)	532.4712	532.24854	0.22266
1G(1s5g)	532.5112	532.26028	0.25092
1F(1s5f)	532.5212	532.26616	0.25504
1Po(1s5p)	532.6472	532.41312	0.23408
Incident	537.1110	536.86982	0.24121

As shown in Table 1, using the MRDCI calculation with the optimized Gaussian basis set functions, the largest discrepancy of the relative asymptotic energies from experimental data for $[NH]^{6+}$ system is about 0.05 eV for those important channels with n of $3, 4$, and 5.

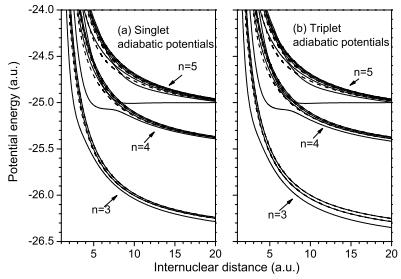

Fig. 1.— Adiabatic potentials of $[NH]^{6+}$ states as a function of internuclear distance.

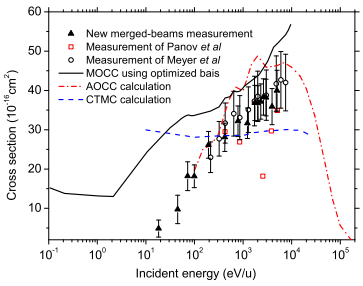

Fig. 2.— Total one electron capture cross section for N^{6+} + H collisions.

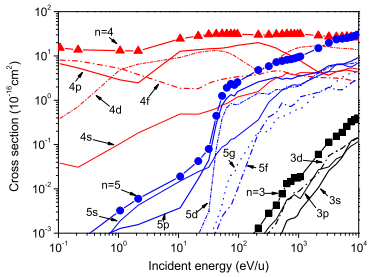

Fig. 3.— QMOCC calculations of state-selective electron capture cross section in the N^{6+} + H collisions .

In figure 1, the adiabatic potential curves are presented, including 13 $^1\Sigma^+$, 13 $^3\Sigma^+$, 9 $^1\Pi$ and 9 $^3\Pi$ states, which are important reaction channels in the charge transfer process investigated. Using the adiabatic potentials and nonadiabatic coupling matrix elements obtained with the MR-DCI approach, the QMOCC method is used to calculate the total and state-selective single-electron capture cross sections for collisions of N^{6+} with atomic hydrogen in the energy region from 0.1 to 10^4 eV/u. The total cross sections are displayed in Figure 2 with available experimental and theoretical data (Panov *et al* 1983; Meyer *et al* 1985). In Figure 3, the present QMOCC calculations of state-selective electron capture cross sections are presented.

3. CONCLUSION

In the present work, single-electron capture processes due to collisions of $N^{6+}(1s\ ^2S)$ ion with atomic hydrogen are investigated using the MOCC, AOCC and CTMC methods. We have developed a hybrid basis set for the MRDCI calculation for highly charged ions and accurate adiabatic potential, nonadiabatic radial and rotational couplings have been obtained. The MOCC total cross sections are compared with the AOCC, CTMC and the merged-beam measurement data.

This work is partial supported by NASA grants NNX09AV46G, NNG09WF24I, and NNH07ZDA001N.

REFERENCES

Kallman, T. R., & Palmeri, P. 2007, Rev. Mod. Phys., 79, 79

Krasnopolsky, V. A., Greenwood, J. B. & Stancil, P. C., 2004 Space Sci. Rev., 113, 271

Ali, R., Neill, P. A., Beiersdorfer, P., *et al*, P. C., 2005 ApJ, 629, L125

Zygelman, B., Cooper, D. L., & Ford, M. J., 1992 Phys. Rev. A 46, 3846

Buenker, R. J. & Peyerimhoff, S. D., 1974 Theoret. Chim. Acta 35, 33; 1975 39, 217

Krebs, S. & Buenker, R. J. 1995 R. J. J. Chem. Phys. 103, 5613

Kelly R. L., 1987 J. Phys. Chem. Ref. Data 16, Suppl. 1, 1

Panov, M. N., Basalaev, A. A., & Lozhkin, K. 0., 1983 Phys. Scr. T3, 124

Meyer, F. W., Howard, A. M., Havener, C. C. *et al*, 1985 Phys. Rev. A 32, 3310

This preprint was prepared with the AAS LaTeX macros v5.2.

NASA LAW, October 25-28, 2010, Gatlinburg

Laboratory Astrophysics Results from the NIST-SAO EBIT Team

J. D. Gillaspy

National Institute of Standards and Technology, Gaithersburg, MD 20899-8421

E. Silver

Harvard-Smithsonian Center for Astrophysics, Cambridge, MD 02138-1500

ABSTRACT

A guide to the laboratory astrophysics papers published by the NIST-SAO EBIT team is presented.

1. Introduction

The Electron Beam Ion Trap (EBIT) at the National Institute of Standards and Technology (NIST) began operating in 1993 and has served a variety of research communities, including those associated with fusion diagnostics, extreme ultraviolet lithography, laboratory astrophysics, and fundamental science (tests of quantum electrodynamics, etc.). A complete list of the associated publications, currently totaling 88, can be found online by searching the Web for the phrase"NIST EBIT bibliography". Below, we provide a guide to the subset of these papers that are relevant to laboratory astrophysics.

2. X-ray microcalorimetry.

In 1999, just before the launch of the Chandra and XMM-Newton space telescopes, the NIST EBIT team and the Smithsonian Astrophysical Observatory (SAO) microcalorimeter team began a collaborative laboratory astrophysics research effort which led to the following publications.

N, O, Ar, and Ne. Our first paper from this collaboration, Silver et al. (2000a), presented spectra from N VI, N VII, O VII, and O VIII in the 0.4 keV to 0.8 keV photon energy range, and Ar XV, Ar XVI, Ar XVII, and Ar XVIII in the 0.25 keV to 3.8 keV photon

energy range. Our second paper, Silver et al. (2000b), added new data for Ne VII, Ne VIII, Ne IX, and Ne X in the 0.8 keV to 1.2 keV photon energy range, and provided fits and line ratios for density diagnostics for both these and our previous data. A later paper, Matranga et al. (2003), presented Ne spectra at 3.56 keV electron beam energy and 0.890 keV to 1.25 keV photon energies, and analyzed this and similar data recorded for a variety of electron beam currents. Line ratios were interpreted in terms of electron density using the HULLAC suite of codes to model the plasma. Tan et al (2005) presents some similar Ar, N, and Ne spectra, sometimes extending to higher photon energies or plotted in higher resolution.

Kr. Kink et al., (2001a) presented a detailed analysis of highly charged Kr ions in the 1.5 keV to 2.4 keV photon energy range. Several pages of tables cataloged and interpreted the spectral lines measured from B-like, C-like, N-like, O-like, F-like, Ne-like, Na-like, Mg-like, and Al-like Kr. Collisional-radiative modeling based on the HULLAC suite of codes was detailed. Predicted density dependences of line ratios were graphed, and charge state distributions were tabulated and compared to fits to the experimental data.

Fe and Ni. Our initial results on the Fe XVII lines in the 0.70 keV to 0.85 keV photon energy range, Laming et al. (2000), are followed by recent results, Gillaspy et al. (2010), which establish consistency between laboratory experiments from two independent groups and theory. With the possible exception of the line at 0.80 keV, which is much weaker than the others, we believe that the Fe XVII lines in this spectral range are now ready for trustworthy application in astrophysical diagnostics. Spectra from higher charge states of Fe (up to XXV) were reported in Takacs et al. (2003), and compared to simulated astrophysical spectra. Higher up the isoelectronic sequence of Ne-like ions, our measurements on Ni XIX, Chen et al., (2006), showed good consistency with measurements from the Livermore EBIT group and with our *ab initio* large-scale relativistic close-coupling calculations.

Xe and W. As a spin-off from our laboratory astrophysics work, the microcalorimeter was also used to obtain spectra of several high-Z elements, including Ni-like Xe, and neighboring charge states, at 1.48 keV and 1.75 keV nominal beam energies, Kink et al. (2001b); this paper also shows an Fe spectrum recorded at 2 keV electron beam energy, not shown in earlier papers, as well as spectra of Ar and Kr in slightly more detail and/or expanded spectral ranges than shown in earlier papers. The microcalorimeter was also used to benchmark collisional-radiative simulations of the x-ray spectra of highly charged tungsten for applications to fusion energy diagnostics, Ralchenko et al. (2006).

3. Photoionization.

We have taken a portable EBIT to the Advanced Photon Source at the Argonne National Laboratory and directed an intense beam of 18 keV photons through a cloud of trapped Ne-like Kr ions (Kr26+), while looking for K-shell x-rays from electrons falling into the photoionized core, Silver et al. (2010). We expect to improve the signal-to-noise ratio in the future by increasing both the ion and photon densities. Earlier related work was done independently by others using lower energy photons (< 1 keV) and extracted ions (see the paper by P. Beiersdorfer in this volume for references). One of us (JDG) also collaborated on absolute cross section measurements using an ECR ion source at the Advanced Photon Source at Berkeley with photon energies around 0.1 keV, Aguilar, et al. (2006).

4. Cometary x-rays (charge exchange).

Beams of highly charged ions were extracted from EBIT and impinged on various gas targets to charge exchange while we recorded the emitted x-ray spectrum. We studied the dependence of the spectra on a variety of factors, such as (1) target gas species having ionization energies that range from 12 eV to 21 eV, using Kr27+ projectiles, Takacs et al. (2007), (2) ion nuclear charge (Z=36, 18, and 10), using fully stripped Kr, Ar, and Ne, Tawara et al. (2006), and (3) a variety of ion charges (q=27 to q=36) for fixed nuclear charge (Z=36), Tawara et al. (2003). Gillaspy et al., (2004) also contains some modeling results not presented elsewhere.

5. Ion-surface interactions.

Recently, researchers in lunar and planetary physics have called for more data on the interaction of highly charged ions with surfaces to facilitate understanding lunar and planetary exospheres (see Killen et al. (2010) and references therein). An ion-surface program was initiated at the NIST EBIT facility in 1994, and has focused on quantifying surface response to highly charged ions using x-ray spectroscopy, Silver et al. (2001), atomic probe microscopy, and electrical measurements (see NIST EBIT online bibliography for more references).

We thank our coauthors on the papers cited above, and NASA (currently supporting us under grant NNX08AK33G).

REFERENCES

Aguilar, A. et al., Phys. Rev. A, 73, 032717.

Chen, G. X., et al. 2006, Phys. Rev. Lett., 97, 143201.

Gillaspy, J. D. et al. 2004, in Atomic Processes in Plasmas, J. S. Cohen et al., Melville: AIP Press, 245.

Gillaspy, J. D., et al. 2010, submitted for publication in Astrophys. J.

Killen, R. M., et al. 2010, Icarus, 209, 75.

Kink, I., et al. 2001a, Phys. Rev. E, 63, 046409.

Kink, I., et al. 2001b, Physica Scripta, T92, 454.

Laming, J. M., et al. 2000, Astrophys. J., 545, L161.

Matranga, M., et al. 2003, Nucl. Instrum. Methods, B205, 244.

Ralchenko, Yu., et al. 2006, Phys. Rev. A, 74,042514.

Silver, E., et al. 2000a, Nucl. Instrum. Methods, A444, 156.

Silver, et al. 2000b, Astrophys. J., 541, 495.

Silver, E., et al. 2001, Photonic, Electronic, and Atomic Collisions (XXII ICPEAC), R. Vane, Princeton: Rinton Press, 312.

Silver, E., et al. 2010/2011, to be published in the Proceedings of the 21st International Conference on the Applications of Accelerators in Research and Industry.

Takacs, E., et al. 1997, Nuc. Instrum. Methods, B124, 431.

Takacs, E., et al. 2003, Nuc. Instrum. Methods, B205, 144.

Takacs, E. et al. 2007, Rad. Phys. Chem., 76, 617.

Tan, J. N., et al. 2005, Physica Scripta, T119,30.

Tawara, H. et al. 2003, Nucl. Instrum. Methods, B205, 605.

Tawara, H. et al. 2006, Phys. Rev. A, 73, 012704.

This preprint was prepared with the AAS LaTeX macros v5.2.

NASA LAW, October 25-28, 2010, Gatlinburg

Atomic Spectroscopic Databases at NIST

J. Reader, A.E. Kramida, & Yu. Ralchenko

National Institute of Standards and Technology, Gaithersburg, MD 20899

j.reader@nist.gov, a.kramida@nist.gov, yuri.ralchenko@nist.gov

ABSTRACT

We present recent work at NIST to develop and maintain databases for spectra, transition probabilities, and energy levels of atoms that are astrophysically important. We also describe our programs to critically compile these data as well as the recently developed plasma population kinetics databases and online collisional-radiative code.

The NIST Physical Measurement Laboratory provides several online atomic spectroscopic databases widely used in astrophysics. The data include wavelengths, energy levels, and oscillator strengths that have been critically evaluated in the NIST Atomic Spectroscopy Data Center. These data are important for line identification, spectra modeling, and other astrophysical research. All databases can be accessed from the NIST Physical Reference Data home page at http://www.nist.gov/pml/data/index.cfm.

Since the last Workshop, the databases were significantly upgraded. The NIST Atomic Spectra Database (ASD) has been upgraded from version 3.0 to 4.0. It now contains detailed information on more than 80,000 energy levels and almost 170,000 spectral lines for ions of 99 elements and 9 isotopes. Support for the isotopes is a new extension that appeared in the ASD v. 4.0. New large sets of data were added for the spectrum lines and energy levels of H, D, T, B, Ne, Na, K, Kr in all ionization stages, Hg I, ^{198}Hg, Fe I-II, and highly-charged ions of W. Transition probabilities for H through B in all ionization stages, C I-II, N I-II, and Fe I-II have been updated.

ASD has been fully integrated with the NIST Atomic Spectra Bibliography Databases, which provide complete references for each datum in ASD. These bibliography databases, in addition to the previously existing ones on Transition Probabilities and Line Broadening, now include the database on Energy Levels. They are implemented in the same relational database management system with ASD. A sophisticated system for automated monitoring of the current literature allows us to update the bibliographies on a daily basis.

Our program to carry out critical compilations of the spectra, transition probabilities, and energy levels of atoms of astrophysical interest also continues actively. A major reassessment of transition probabilities for Fe I and II (J.R. Fuhr & W.L. Wiese (2006)) and an updated compilation of transition probabilities for neutral and singly ionized C and N (W.L. Wiese & J.R. Fuhr (2007)) were recently published. Compilations of transition probabilities of Na, Mg, Al, and Si in all stages (D.E. Kelleher & L.I. Podobedova (2008)) were published in 2008. For wavelengths and energy levels, compilations of H, D, T (A.E. Kramida (2010)), B I (A.E. Kramida & A.N. Ryabtsev (2007)), B III-V (A.E. Kramida et al (2008)), Ne II-III (A.E. Kramida & G. Nave (2006)), Ne VII-VIII (A.E. Kramida & M.-C. Bouchet-Poulizac (2006)), Hg I (E. Saloman (2006)), Fr I (J.E. Sansonetti (2007)), Ga (T. Shirai et al (2007)), Kr (E. Saloman (2007)), Rb (J.E. Sansonetti (2006)), K (J.E. Sansonetti (2008)), and W (A.E. Kramida & T. Shirai (2006,2009)) in all stages of ionization were recently published. All data from these compilations have already been added to ASD. Compilations of Cs spectra in all stages (J.E. Sansonetti (2009)), Sr I (J.E. Sansonetti & G. Nave (2010)), Ar II-XVIII (E. Saloman (2010)) and transition probabilities for all ions of S (L.I. Podobedova et al (2009)) were published and will soon be added to ASD. Similar compilations for Ni I-II, Cr I-II, and Ba III-LVI are currently in progress.

The unified relational database management system used in ASD and in our bibliographic databases allows a high level of data integration and consistency. Its flexible user interface provides convenient access to various parameters. Several features of the ASD interface should be especially valuable for astrophysicists. Among those is the online Saha-Local-Thermodynamic-Equilibrium (LTE) spectrum generation tool, which allows calculation of plasma emission spectra under Saha-LTE conditions for user-defined values of electron density and temperature. The calculated spectrum can also be Doppler-broadened for arbitrary values of ion temperature. This may also be used for simulation of instrumental broadening.

Another feature of the graphical interface is the availability of Grotrian diagrams. These diagrams provide an intuitive visualization of the atomic energy level structure and transitions, as well as direct access to the fundamental atomic data (energy levels, wavelengths, transition probabilities).

Work continues on our bibliographic databases for atomic energy levels, transition probabilities and spectral line broadening. We monitor the current literature on atomic spectroscopy and insert references to new articles once in 3-4 weeks.

We also developed two plasma population kinetics databases that contain benchmark results from the 3rd and 4th Non-LTE Code Comparison Workshops. These databases cover data for such diagnostically important elements as, e.g., carbon, argon and gold. Parameters available for comparisons include mean ion charge, ion populations, synthetic spectra, rates

of collisional and radiative processes, radiative power losses and others.

A fully time-dependent collisional-radiative online code FLYCHK (H.-K. Chung et al (2005)) developed in collaboration with Lawrence Livermore National Laboratory is freely available for simulations at http://nlte.nist.gov/FLY. This code allows fast and reliable calculation of major population kinetics parameters such as ionization distributions, radiative power losses and synthetic spectra. The input parameters may include different types of particle density, arbitrary electron energy distribution function, plasma size, external radiation field and so on. This online code is currently used by almost 400 researchers working in astrophysics, laser-produced plasmas, and z-pinches.

Work on these databases and critical compilations is supported in part by the National Aeronautics and Space Administration and by the Office of Fusion Energy Sciences of the U. S. Department of Energy.

REFERENCES

Chung, H.-K., Chen, M.H., Morgan, W.L, Ralchenko, Yu. & Lee, R.W 2005, High En. Dens. Phys., 1, 3

Fuhr, J.R. & Wiese, W.L. 2006, J. Phys. Chem. Ref. Data, 35, 1669

Kelleher, D.E. & Podobedova, L.I. 2008, J. Phys. Chem. Ref. Data, 37, 267; 37, 709; 37, 1285

Kramida, A.E. 2010, At. Data Nucl. Data Tables 96, 586

Kramida, A.E. et al 2008, Phys. Scr. 78, 025301; 78, 025302

Kramida, A.E. & Ryabtsev, A.N. 2007, Phys. Scr. 76, 544

Kramida, A.E. & Bouchet-Poulizac, M.-C. 2006, Eur. Phys. J. D 38, 265; 39, 173

Kramida, A.E. & Nave, G. 2006, Eur. Phys. J. D 37, 1; 39, 331

Kramida, A.E. & Shirai, T. 2006, J. Phys. Chem. Ref. Data 35, 423; 2009, At. Data Nucl. Data Tables 95, 305

Podobedova, L.I, Kelleher, D.E. & Wiese, W.L. 2009, J. Phys. Chem. Ref. Data, 38, 171

Saloman, E. 2006, J. Phys. Chem. Ref. Data, 37, 267

Saloman, E. 2007, J. Phys. Chem. Ref. Data, 36, 215

Saloman, E. 2010, J. Phys. Chem. Ref. Data, 39, 033101

Sansonetti, J.E. 2006, J. Phys. Chem. Ref. Data, 35, 301

Sansonetti, J.E. 2007, J. Phys. Chem. Ref. Data, 36, 497

Sansonetti, J.E. 2008, J. Phys. Chem. Ref. Data, 37, 7

Sansonetti, J.E. 2009, J. Phys. Chem. Ref. Data, 38, 761

Sansonetti, J.E. & Nave, G. 2010, J. Phys. Chem. Ref. Data, 39, 033103

Shirai, T., Reader, J., Kramida, A.E. & Sugar, J. 2007, J. Phys. Chem. Ref. Data, 36, 509

Wiese, W.L. & Fuhr, J.R. 2007, J. Phys. Chem. Ref. Data, 36, 1287

This preprint was prepared with the AAS LaTeX macros v5.2.

NASA LAW, October 25-28, 2010, Gatlinburg

Laboratory Experiments of Solar Wind Charge Exchange with TMU-ECRIS and TES Micro-calorimeter

H. Akamatsu[1], T. Enoki, K. Henmi, Y. Ishisaki, Y. Ezoe, T. Ohashi, T. Kanda, T. Ishida, H. Tanuma

Department of Physics, Tokyo Metropolitan University, Hachioji, Tokyo, 192-0397, Japan

h_aka@phys.se.tmu.ac.jp

H. Ohashi

Institute for Laser Science, The University of Electro-Communications 1-5-1 Chofugaoka, Chofu-shi, Tokyo 182-8585, Japan

K. Shinozaki

Aerospace Research and Development Directorate, JAXA, Tsukuba, Ibaraki 305-8505, Japan

K. Mitsuda

Institute of Space and Astronautical Science, JAXA, Sagamihara, Kanagawa 252-5210, Japan

ABSTRACT

We are conducting a laboratory experiment to reveal the mechanism of Solar Wind Charge eXchange (SWCX) occurring in space. We employ a high resolution X-ray spectrometer system contained TES (Transition Edge Sensor) X-ray micro-calorimeters, and ECRIS (Electron Cyclotron Resonance Ion Source). Here, we report brief description of this experiment and its current status.

1. Introduction

In X-ray astronomy, it is still a question how diffuse soft X-ray emission shows time variations in a few days (Snowden et al. 1994). A possibility has been proposed that the emission is caused by charge exchange process between the solar wind ion and the interplanetary neutral matter.

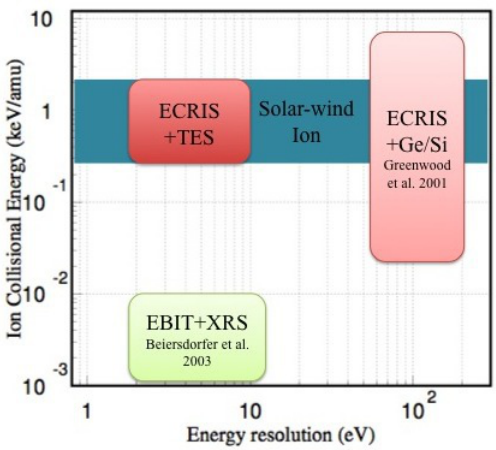

Fig. 1.— The current state of laboratory experiment for SWCX study. The energy of solar wind is around 1 keV. Our target area and previous studies related with SWCX are shown (Greenwood et al. 2001; Beiersdorfer et al. 2003).

Charge exchange process is an interaction between a highly ionized ion (A^{q+}) and a neutral atom (B). An electron is transferred from atom to ion, and goes into a highly excited level. When the electron make transitions to lower levels, the ion produce photon with the energy corresponding to the level difference. However, it is difficult to identify that this emission is truly generated by charge exchange process due to the spectral resolution of current X-ray astronomy satellites($\sim$ FWHM 100 eV).

For proper modeling of X-ray emission from SWCX, we need reliable data about line distribution and cross section of this process. But, there are few data with a few eV resolution under similar condition as the SWCX, regarding collisional energy (0.6-3.0 keV/amu:Fig1) (Greenwood et al. 2001; Beiersdorfer et al. 2003) . To separate individual emission lines of the charge exchange process, the high energy resolution measurement under SWCX condition is strongly required.

2. Our approach

We investigate charge exchange mechanism between solar-wind ion and neutral matter using high resolution TES X-ray micro-calorimeters and TMU-ECRIS(Fig.2). X-ray micro-

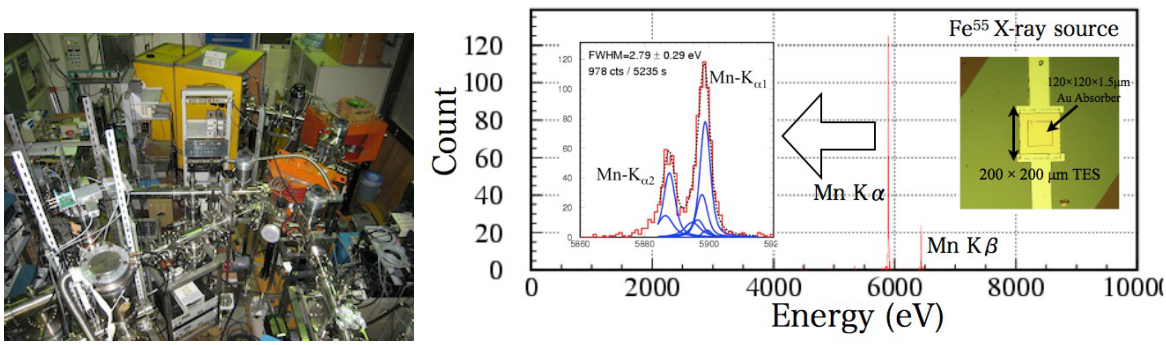

Fig. 2.— Our experimental set up Left: Ion collision facility with TMU-ECRIS. Right: Photo of our TES X-ray micro-calorimeter and energy spectrum of Fe^{55} X-ray source.

calorimeter is an X-ray detector that absorbs X-ray energy with the absorber, and produces signals when TES temperature rise. Micro-calorimeter shows excellent performance at an extremely low temperature below 100 mK. Energy resolution is given by $\Delta E \sim 2.35\sqrt{\frac{k_{\rm B}T^2C}{\alpha}}$. Where, $k_{\rm B}$ is Boltzmann constant, T is a temperature at working point of micro-calorimeter, C is a heat capacity of micro-calorimeter, and α is a temperature sensitivity of thermometer.

TES (Transition Edge Sensor) is a high sensitivity thermometer that works at transition edge of superconductor. TES calorimeters can achieve the energy resolution of 1 eV. Our group produced TES micro-calorimeters through in-house processes, and the sensor show good energy resolution of ΔE=2.8 eV @ 5.9 keV(Akamatsu et al. 2009).

Highly charged ions are produced in the 14.25 GHz electron-cyclotron resonance ion source at Tokyo Metropolitan University (**?**). The ion were extracted with electronic potential of several energy, and selected by a 110° double-focusing dipole magnet, and directed into a collision chamber where the ion intersected an effusive beam of target gas ejected from a micro capillary plate.

Our system (TES micro-calorimeter+ECRIS) will simulate the SWCX process and will measure X-ray with good energy resolution. Then, we can obtain a good laboratory data to understand the SWCX process.

3. Resent result

We measured X-rays from the collision of O^{7+} and O^{8+} ions with neutral He or Hydrogen molecule using a window-less Si(Li) detector. The detector shows an energy resolution of 107 eV @ 1 keV (Kanda et al.). As shown in the Fig. 3, we confirmed emission lines from 2p, 3p, and 4p to 1s transitions of O^{7+}. We analyzed the spectrum by fixing the peak energy of each line using the NIST database and the energy resolution to be 107 eV. The results indicate some difference from the previous work (Greenwood et al. 2001), in point of the intensity ratio of the lines. This might be caused by the correction of X-ray transmission (Tanuma et al. in prep) of the detector windows. To confirm this effect, a new high-resolution measurement will be important.

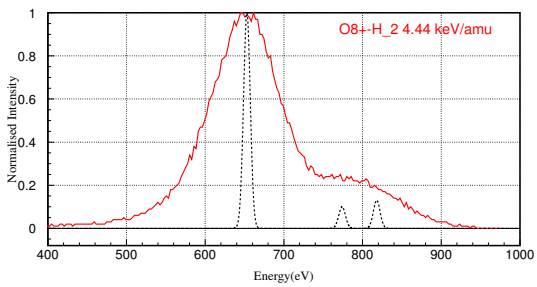

Fig. 3.— Preliminary result obtained by window-less Si(Li) detector. Black dot line show simulation that measured TES calorimeter (ΔE=10 eV).

4. Future prospect

Because the extremely low temperature is necessary for TES, we are developing a double stage Adiabatic Demagnetization refrigerator (dADR). dADR is a quite compact and can be carried to outside experiments. We could cool the double stage ADR down to about 100 mK, and holding time was 2 hours. In parallel with the test with the Si(Li) detector, we are preparing the TES calorimeter and dADR system. For the first step, evaluation of the TES calorimeter installed in the DADR is in progress. We plan to combine dADR system and ECRIS and measure emission lines from SWCX by the next summer.

This work is supported by KAKENHI 21246017, Grant-in-Aid for Scientific Research of JSPS. H.A supported by Grant-in-Aid for JSPS Fellows (22·1582) and the MEXT program "Support Program for Improving Graduate School Education".

REFERENCES

Snowden, S. L. McCammon, D. Burrows, D. N. & Mendenhall, J. A. 1994, ApJ, 424, 714

Greenwood, J. B. Williams, I. D. Smith, S. J. & Chutjian A. 2001, Physica Scripta Volume T, 92, 150

Beiersdorfer P., et al. 2003, Science, 300, 1558

H. Tanuma et al., J. Chin. Chem. Soc., 48 389 (2001).

Akamatsu H. et al. 2009, American Institute of Physics Conference Series, 1185, 195

Kanda T. et al. 2010, HCI Conference, submitted

Tanuma H., et al. in preparation.

This preprint was prepared with the AAS LaTeX macros v5.2.

NASA LAW, October 25-28, 2010, Gatlinburg

Studies of the Spectrum of Chromium for Calibration of STIS and Interpretation of Astrophysical Spectra

Craig J. Sansonetti and Gillian Nave

Atomic Physics Division, National Institute of Standards and Technology, Gaithersburg, MD 20899

craig.sansonetti@nist.gov, gillian.nave@nist.gov

Florian Kerber

European Southern Observatory, Garching, Germany

fkerber@eso.org

ABSTRACT

New observations of the spectrum of Pt/Cr-Ne hollow cathode lamps have been made to provide accurate wavelengths for more than 5000 chromium lines for wavelength calibration of the Space Telescope Imaging Spectrograph. New infrared spectra of chromium hollow cathode lamps will be taken to produce a comprehensive line list for Cr II extending from 1130 Å to 5.5 μm and to increase the accuracy of the Cr II energy level values. Lines of Cr II are prominent in the spectra of many astrophysical objects, especially in chemically peculiar stars, and our results will be significant in interpreting these data.

1. Introduction

The Space Telescope Imaging Spectrograph (STIS) is a high resolution instrument with spectral coverage from the vacuum ultraviolet (VUV) to near infrared (NIR). It is equipped with Pt/Cr-Ne hollow cathode lamps for on-orbit wavelength calibration. The spectrum of Pt-Ne lamps was precisely characterized in work at the National Institute of Standards and Technology (NIST) for calibration of the Goddard High Resolution Spectrograph (GHRS) by Reader et al. (1990). When we began this work, however, no characterization of the Pt/Cr-Ne lamp had been made. Spectral data for Cr I (Kiess 1953) and Cr II (Kiess 1951)

dated from the 1950s. They had an accuracy of only 0.01 Å and did not extend into the VUV or IR. As a consequence, the initial calibration for the STIS high resolution echelle modes was based on Pt alone. This work at NIST was undertaken to provide a more satisfactory list of wavelength standards for STIS.

A second result of our observations was to obtain wavelengths with greatly increased accuracy for many lines of Cr I and Cr II. Lines of these spectra are prominent in many astrophysical objects, but published laboratory data are inadequate to interpret the high quality spectra obtained from instruments such as GHRS and STIS. To address this need we are assembling a comprehensive Cr II line list from our existing measurements and planned new observations in the NIR.

2. Experimental Observations

All of the experimental observations were made using sealed, low-current hollow cathode lamps with MgF_2 windows. The Pt/Cr-Ne lamps were functionally identical to those installed on STIS. To definitively identify which lines in the spectra are attributable to chromium, we also made observations of Cr-Ne hollow cathode lamps.

The spectra were recorded at NIST using two high resolution instruments. The initial observations in the VUV spanned the range 1130 Å to 1827 Å and were recorded using the 10.7 m normal incidence vacuum spectrograph (Sansonetti et al. 2004). The spectra were calibrated using internal standard lines of Pt I and Pt II (Reader et al. 1990). Spectra of both Pt/Cr-Ne and Cr-Ne hollow cathode lamps were recorded in the region from 1552 Å to 7440 Å by using a UV optimized Fourier transform spectrometer (FTS). They were calibrated with internal lines of Pt I and Pt II (Nave & Sansonetti 2004) and the wavelengths have uncertainties ranging from 0.001 Å to 0.0001 Å, depending on the signal-to-noise ratio. About 90% of the lines in the Pt/Cr lamp spectrum in the near UV are due to chromium.

Additional observations of Cr-Ne lamps in the visible and NIR will be made with the NIST 2 m FTS in order to extend the region of observations to 5.5 μm with an accuracy of better than 1 part in 10^7. These new data will allow us to complete a comprehensive chromium line list covering the entire region from 1130 Å to 5.5 μm.

3. Application to Calibration of STIS

For proper calibration of the STIS echelle modes it is necessary to have accurate standards across the entire 2-dimensional detector array. This is particularly important for

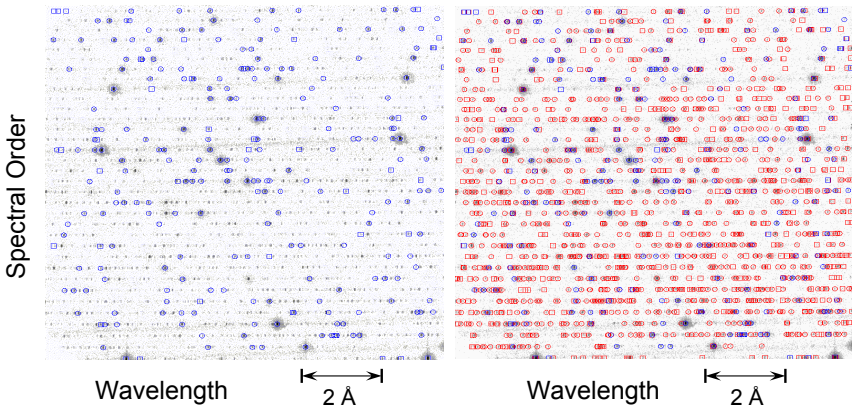

Fig. 1.— STIS spectrum of the Pt/Cr lamp with a central wavelength of 2513 Å. In the left panel Pt provides only 258 lines (marked with blue) for calibration. Including chromium lines (marked with red) increases the number of standards to 1612 for this frame.

dispersion solutions based on polynomial interpolation procedures. For the high-resolution STIS echelle modes the spectral width of each order on the detector may be only a few Å. The impact of including newly measured chromium lines in the wavelength calibration is illustrated in Figure 1. The average number of standards in each spectral order is just eight if only Pt and Ne lines are used. Including lines of Cr I and Cr II increases the number of standards by a factor of more than six. Our new list is also used in conjunction with a physical instrument model developed at the Space Telescope European Coordinating Facility for the STIS Calibration Enhancement effort (Bristow et al. 2005).

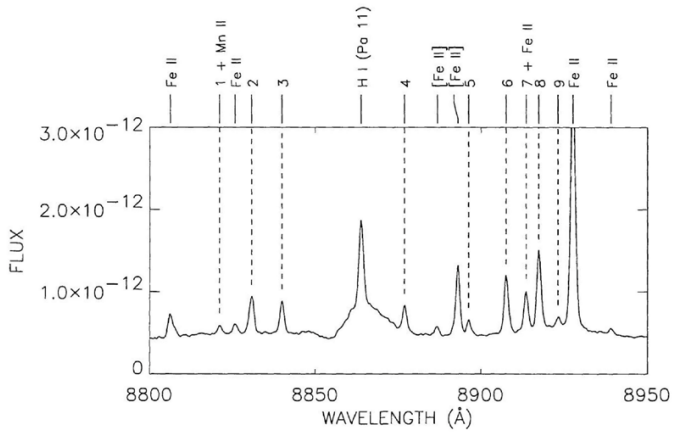

Fig. 2.— The numbered features in this IR spectrum of a Weigelt blob of η Carinae are Cr II fluorescence lines (Zethson et al. 2001). Laboratory wavelengths have not been reported for any of these lines, and there is no line list that includes transitions to the upper levels.

4. Spectrum and Energy Levels of Cr II

Spectral lines of Cr II are prominent in a wide variety of astrophysical objects, but the accuracy of laboratory data is often inadequate to interpret the spectra. An example is shown in Figure 2. The last comprehensive analysis of the spectrum of Cr II (Kiess 1951) includes 99 energy levels and 1843 classified lines with an uncertainty of 0.01 Å. Many additional unpublished levels of uncertain accuracy are included in the NIST Atomic Spectra Database, but for most of them no lines have been published. Our spectra of Cr-Ne hollow cathode lamps contain about 5000 lines from Cr II. We have classified about 4000 of these lines and made an initial re-optimization of about 650 Cr II energy levels. New observations in the IR will extend the line list to cover the entire region 1130 Å to 5.5 μm. We expect these new data will enable the location of additional Cr II levels and the production of globally re-optimized Cr II level values.

Characterization of the Pt/Cr-Ne lamp was supported by the European Space Agency. Analysis of the Cr II spectrum is supported by NASA under contract NNH10AN38I.

REFERENCES

Reader, J., Acquista, N., Sansonetti, C. J. & Sansonetti, J. E. 1990, ApJS, 72, 831

Kiess, C. C. 1953, J. Res. Natl. Bur. Stand. (US), 51, 247

Kiess, C. C. 1951, J. Res. Natl. Bur. Stand. (US), 47, 385

Sansonetti, C. J., Kerber, F., Reader, J., & Rosa, M. R. 2004, ApJS, 153, 555

Nave, G. & Sansonetti, C. J. 2004, J. Opt. Soc. Am. B, 21, 442

Bristow, P., Kerber, F. & Rosa, M. R. 2005, The 2005 HST Calibration Workshop, A. M. Koekemoer, P. Goudfrooij, & L. L. Dressel, Baltimore: Space Telescope Science Institute, 299

Zethson, T., Hartman, H., Johansson, S., Gull, T., Ishibashi, K & Davidson, K., 2001 ASP conference series 242, 97

This preprint was prepared with the AAS LaTeX macros v5.2.

NASA LAW, October 25-28, 2010, Gatlinburg

New atomic data for astrophysics by high-resolution spectroscopy

M. P. Ruffoni, J. C. Pickering, A. P. Thorne, & C. E. Holmes

Department of Physics, Imperial College London, London SW7 2AZ, UK

m.ruffoni@imperial.ac.uk

P. L. Smith

Harvard-Smithsonian Center for Astrophysics, 60 Garden Street, Cambridge, MA 02138, USA

ABSTRACT

We report a summary of recent significant improvements to atomic and molecular data obtained through high resolution Fourier transform spectrometry at Imperial College London. These primarily include wavelengths, energy levels, and oscillator strengths of neutral, singly, and doubly ionised iron-group atoms of astrophysical significance.

1. Introduction

For many years, the Imperial College (IC) laboratory astrophysics team has been working in close collaboration with astronomers and astrophysicists, both within the US and further afield, to provide improvements in the atomic and molecular database. With the constant improvement in spectrographs at both ground-based observatories and on space-borne satellites, the accuracy of the existing database is frequently the limiting factor in spectral analyses. The acquisition of more accurate and complete atomic and molecular data is therefore often a vital prerequisite to interpreting new observations.

Fourier transform (FT) spectrometry is ideal for such work as it combines high resolution, broad spectral range, high absolute wavenumber accuracy and good optical throughput (Pickering 1999). Line wavenumbers are accurate to better than $1 : 10^7$, and the lines observed from broadband spectra may be used for large scale term analyses. This then leads to the identification of new energy levels, improvements in the accuracy of known levels, and

the accurate prediction of lines that may not be observable in the laboratory. If spectra are intensity calibrated, branching ratios of lines from given excited levels may be measured, and when combined with level lifetimes, transition probabilities calculated. Additionally, the high resolution makes it possible to analyze hyperfine structure, which plays an important role in both abundance studies and in the unravelling of blends (Bergemann et al. 2010).

2. Experimental details and wavenumber calibration

IC operates two visible/ultraviolet FT spectrometers (Thorne et al. 1987), one of which is equipped with a MgF_2 beamsplitter to extend its spectral range down to 140 nm (Thorne et al. 1996). Where infrared spectra are required for completeness (such as in term analyses and some branching fraction work), additional spectra have been recorded on the IR FT spectrometer at the National Institute of Standards and Technology (NIST). Neutral and singly ionised spectra are excited in the discharge of a hollow cathode lamp (HCL), typically running in a few mbar of argon or neon and at currents of up to 800 mA. A Penning discharge lamp is also available to excite higher energy levels, or for studies of doubly ionised iron group spectra.

The wavelength scales of FT spectra obtained from an HCL are commonly calibrated against the Ar II standard lines recommended by Learner and Thorne (1988), with the accurate wavenumbers given by Whaling et al. (1995). However, some doubt has existed about their reliability given gas lines are commonly susceptible to wavenumber shifts as a function of lamp running conditions (Learner and Thorne 1988). In a recent study, we therefore verified the reliability of the Ar II standard lines in the ultraviolet against an independent standard created from recently published Mg I and II line wavelengths measured by laser frequency combs (Ruffoni & Pickering 2010). Both showed extremely good agreement within experimental uncertainty, reinforcing previous results that have relied exclusively on the Ar II standards. However, the associated wavelength uncertainties were an average of 2.3 times smaller when using the Mg lines for calibration.

3. Atomic data for studies of variations in fundamental constants

The standard model of particle physics asserts that the fine structure constant, $\alpha = (1/hc)(e^2/4\pi\epsilon_0)$ – and other important constants such as the proton-electron mass ratio, $\mu = m_p/m_e$ – are invariant as a function of time and space. However, other cosmological models (such as superstring theory) contradict this assumption. The most precise method of

searching for variations in α – and measuring any changes, $\Delta\alpha/\alpha$, relative to its modern-day value – is through high resolution spectroscopy of gas cloud absorption lines seen in the spectra of distant quasars (Webb et al. 1999; Murphy et al. 2004, 2008).

However, accurate analysis of the resulting spectra, and thus the detection of any non-zero $\Delta\alpha/\alpha$, is critically dependent on the availability of high-precision laboratory wavelengths for selected transitions seen in quasar spectra (Berengut et al. 2009). These transitions, which are those expected to have the strongest α dependence on their wavelength, reside in the ultraviolet or vacuum ultraviolet in the rest frame. Using our VUV FT spectrometer, we have recently obtained high-precision wavelengths for a pair of important Ti II resonance transitions seen at 191 nm (Ruffoni & Pickering 2010).

Preliminary calculations to assess the impact of these new wavelengths have been performed on a modest set of quasar spectra, which indicated that under some conditions, the inclusion of the 191 nm Ti II lines has little impact on the uncertainty in α, but does change its value by almost 1σ (Webb 2010, private communication).

4. Studies of doubly ionised iron group spectra

The spectra of doubly ionized iron group elements dominate the observed opacity of hot B stars in the ultraviolet, and are ideally suited to measurement on the IC VUV FT spectrometer with a Penning source. We have recently obtained the first accurate reference wavelengths of Cr III (Smillie et al. 2008), improving on previous diffraction grating wavelengths by an order of magnitude. A term analysis of Co III and Fe III is ongoing, with IC visible/ultraviolet spectra supplemented in the vacuum ultraviolet by grating spectra from NIST's NIVS, and in the visible/infrared by NIST FT spectra.

5. Measurement of accurate oscillator strengths (log(gf)s)

Accurate log(gf)s for IR atomic lines can be used to determine stellar physical parameters for cool stars in windows between molecular lines (Lyubchik et al. 2004). We have recently produced new IR log(gf)s for Mn I in collaboration with R. Blackwell-Whitehead at Lund University (Blackwell-Whitehead et al. 2010). Branching fractions for 20 Mn I transitions were measured using FT spectroscopy and placed on an absolute scale using radiative lifetimes. These were then used to determine the manganese abundance in the atmosphere of several late type stars, including the Sun and Arcturus. Further IR measurements are underway to provide new log(gf)s for galactic evolution studies under the APOGEE project.

New 3D non-local thermodynamic equilibrium (NTLE) stellar atmosphere models being used to measure elemental abundances rely on accurate laboratory log (gf)s and knowledge of line broadening effects such as hyperfine structure. A new estimate of solar abundance of Co has recently been made possible by the laboratory study of Co II hyperfine structure (Bergemann et al. 2010). New measurements of Fe II f-values are planned, which are particularly urgent for lines in the visible spectrum (Ryabchikova & Landstreet 2010).

Imperial College would like to thank the UK Science and Technology Facilities Council (STFC) for funding this work.

REFERENCES

Berengut, J. C., Dzuba, V. A., Flambaum, V. V., King, J. A., Kozlov, M. G., Murphy, M. T. & Webb, J. K. 2009, Mem. S. A. It., 80, 795

Bergemann, M., Pickering, J. C., & Gehren, T. 2010, MNRAS, 401, 1334

Blackwell-Whitehead, R., & Bergemann, M. 2007, A&A, 472, L43

Blackwell-Whitehead, R., Pavlenko, Y. V., Nave, G., Pickering, J. C., Jones, H. R. A., Lyubchik, Y., & Nilsson, H. 2010, A&A, in press

Learner, R. C. M. & Thorne, A. P. 1988, J. Opt. Soc. Am. B, 5, 2045

Lyubchik, Y., Jones, H.R.A., Pavlenko, Y.V., Viti, S., Pickering, J.C., Blackwell-Whitehead, R. 2004, A&A, 416, 655

Murphy, M. T., Flambaum, V. V., Webb, J. K., Dzuba, V. V., Prochaska, J. X. & Wolfe, A. M. 2004, Lect. Not. Phys., 648, 131

Murphy, M. T., Webb, J. K. & Flambaum, V. V. 2008, MNRAS, 384, 1053

Pickering, J. C. 1999, Physica Scripta, T83, 27

Ruffoni, M. P., & Pickering, J. C. 2010, ApJ, 725, 424

Ryabchikova, T., & Landstreet, J. 2010, ICAMDATA, A6

Smillie, D. G., Pickering, J. C., & Smith, P. L. 2008, MNRAS, 390, 733

Thorne, A. P., Harris, C. J., Wynne-Jones, I., Learner, R. C. M. & Cox, G. 1988, J. Phys. E, 20, 54

Thorne, A. P. 1996, Physica Scripta, T65, 31

Webb, J. K., Flambaum, V. V., Churchill, C. W., Drinkwater, M. J. & Barrow, J. D. 1999, Phys. Rev. Lett., 82, 884

Whaling, W., Anderson, W. H. C., Carle, M. T., Brault, J. W. & Zarem, H. A. 1995, J. Quant. Spec. Radiat. Transf., 53, 1

This preprint was prepared with the AAS LaTeX macros v5.2.

NASA LAW, October 25-28, 2010, Gatlinburg

A comprehensive analysis of the spectrum of Fe II

Gillian Nave

National Institute of Standards and Technology, Gaithersburg, MD

gnave@nist.gov

ABSTRACT

A new analysis of the laboratory spectrum of Fe II is described. The aim is to produce a comprehensive list of Fe II lines, based on high-resolution grating and Fourier transform spectra, covering wavelengths from 900 Å to 5.5 μm. Particular attention has been paid to the wavelength calibration of the spectra and its relevance to the detection of possible changes in the fine-structure constant in the early Universe.

1. Introduction

In 1978, Sveneric Johansson published a comprehensive analysis of the spectrum of Fe II, consisting of about 3300 lines from 576 energy levels covering wavelengths from 900 Å to 11200 Å (Johansson 1978). Since then, high-resolution Fourier transform (FT) spectrometers at Imperial College, London and the National Solar Observatory, AZ have been used to record spectra of high-current hollow cathode lamps. These measurements have increased the number of lines by a factor of over 5, extended the wavelength measurements up to 5.5 μm, and reduced the wavelength uncertainty by an order of magnitude. Additional grating spectra taken at the National Institute of Standards and Technology (NIST), covered wavelengths from 800 Å to 3250 Å with an uncertainty of about 0.002 Å. The spectra contain over 40 000 spectral lines, roughly 9500 of which were published as a multiplet table for Fe I (Nave et al. 1995). Over 15 000 spectral lines match differences of energy levels in Fe II. The interpretation of Fe II lines in these spectra occupied Sveneric Johansson for the rest of his life, and the number of known Fe II energy levels now exceeds 1000. However, this work remained incomplete when he died in 2008. Almost all of the levels, including the very highest ones observed in the laboratory, give lines in astronomical spectra (Johansson 2009).

I am completing the analysis of laboratory spectra of Fe II that was started with Sveneric Johansson in 1994. The aim is to produce a comprehensive list of Fe II lines based on high-resolution Fourier transform and grating spectra, covering wavelengths from 900 Å to 5.5 μm. Particular attention has been paid to the wavelength calibration of these spectra because of the need for accurate wavelengths for the detection of possible changes in the fine-structure constant during the history of the Universe.

2. Description of Spectra

The laboratory spectra used in this study were obtained using three different instruments: the 1 m FT spectrometer at the National Solar Observatory (NSO), Tucson, Arizona for the region 2000 cm^{-1} to 35 000 cm^{-1} (5 μm to 2857 Å); the vacuum ultraviolet FT spectrometer at Imperial College, London for spectra in the region 33 000 cm^{-1} to 68 000 cm^{-1} (3000 Å to 1470 Å); and the 10.7 m Normal Incidence Vacuum Spectrograph at the NIST for high-resolution grating spectra between 30 770 cm^{-1} and 125 000 cm^{-1} (3250 Å to 800 Å).

The light source used for the FT investigations was a hollow cathode lamp, run with either neon or argon. The lamp was operated at pressures of 500 Pa of Ne or 400 Pa of Ar for the visible and infrared observations, and 300 Pa to 400 Pa of Ne for the ultraviolet observations. The currents ranged from 320 mA to 1.1 A. Both iron-neon and iron-argon hollow cathode lamps were used for the grating observations. The iron-neon hollow cathode was run in continuous mode with currents of 0.6 A to 0.8 A and a gas pressure of 130 Pa. The iron-argon hollow cathode was run in pulsed mode with peak currents of 100 A, pulse width of 70 μs, frequency 100 Hz, and pressure of 30 Pa to 40 Pa. The grating spectra were calibrated from Ritz wavelengths derived from energy levels optimized using the FT spectra.

The wavenumber, integrated intensity, width and lineshape parameters of all lines in the FT spectra were obtained by fitting Voigt profiles using Brault's DECOMP program (Brault & Abrams 1989) or its successor Xgremlin (Nave et al. 1997).

3. Wavelength Calibration

Current interest in detecting possible changes in the fine structure constant, α, during the history of the Universe has put stringent demands on the accuracy of the wavelengths of Fe II lines. Absorption spectra of gas clouds in the line of sight to distant quasars are observed. Since the wavelengths of atomic lines depend with differing sensitivities on the value of α, any differences between the wavelength separation of line pairs in distant gas

clouds and on Earth will indicate that α may have had a different value in the early Universe. The Fe II line at 1608 Å, due to the transition $3d^6(^5D)4p\ a^6D_{9/2} - 3d^5(^6S)4s4p(^3P)\ y^6P_{7/2}$, has been of particular interest because the variation of its wavelength with α has the opposite sign to that of nearby lines (Murphy et al. 2003). In order to use this line to verify previously-reported changes in α, its wavelength is needed to a few parts in 10^8. However, archival spectra show inconsistencies in its wavelength of about 2 parts in 10^7.

All of the FT spectra trace their calibration to 28 Ar II lines and the original calibration used wavenumbers measured by Norlén (1973). The Ar II lines were re-measured by Whaling et al. (1995) using FT spectroscopy with a much smaller uncertainty. Whaling's wavenumbers are systematically higher than Norlén's by 6.7 parts in 10^8.

The wavenumber scale of Fe I and Fe II lines has been re-investigated with new spectra recorded with the NIST 2 m FT spectrometer and by using a re-analysis of archival spectra (Nave & Sansonetti 2010). We verified the wavenumbers of Whaling et al. (1995) and found that wavenumbers in the visible and near infrared regions published in previous papers (e.g. Learner & Thorne (1988)) need to be increased by 6.7 parts in 10^8. In the region below 2860 Å, we found that the wavenumbers in Nave et al. (1991) should be increased by 10.6 parts in 10^8 to correct for an error in the transfer of the wavenumber scale to the ultraviolet. Using this correction, the Fe I and Fe II wavenumbers are consistent with more recent measurements of Fe II lines that were measured simultanously with magnesium lines (Aldenius 2009). The wavenumbers of these magnesium lines have since been confirmed using frequency comb spectroscopy. Using these revisions, we find the wavelength of the $a^6D_{9/2} - y^6P_{7/2}$ line to be 1608.45081(7) Å.

4. Description of linelist

The spectra contain over 15 000 lines of Fe II covering wavelengths from 800 Å to 5.5 μm. Over 1000 levels are known, 250 of which have not been published previously. In comparison, the most comprehensive previous publication of the spectrum of Fe II (Johansson 1978), contains roughly 3300 lines from 576 levels. Many of the new levels have high excitations but still give rise to strong lines in stellar spectra. The wavelength scale has been revised and now has an uncertainty of a few parts in 10^8 in all wavelength regions.

Since roughly a third of the lines in the spectra have more than one possible classification, the first task in preparing a new comprehensive analysis of the Fe II spectrum is to determine the most probable identifications. Accurate energy level values are essential in minimizing the number of spurious classifications. They are derived by optimizing the

fit of the levels to the observed wavenumbers. A preliminary optimization of the levels has decreased their uncertainties from roughly 0.5 cm^{-1} to under 0.01 cm^{-1}. However, a large number of multiply-classified lines remains, and determining the most likely classifications is the major task remaining in the analysis of the data.

This work is partially supported by NASA under the inter-agency agreement NNH10AN38I.

REFERENCES

Aldenius, M. 2009, Phys. Scr, T134, 014008

Brault, J. W., Abrams, M. C. 1989, OSA Technical Digest Series, 6, 110

Johansson, S. 1978, Phys. Scr, 18, 217

Johansson, S. 2009, Phys. Scr, T134, 014013

Learner, R. C. M., Thorne, A. P. 1988 J. Opt. Soc. Am. B 5, 2045

Murphy, M. T., Webb, J. K. , Flambaum, V. V. 2003, MNRAS, 345, 609

Nave, G., Learner, R. C. M., Thorne, A. P., Harris, C. J. 1991, J. Opt. Soc. Am. B 8, 2028

Nave, G., Johansson, S., Learner, R. C. M., Thorne, A. P., Brault, J. W. 1995, ApJS, 94, 221

Nave, G., Sansonetti, C. J., Griesmann, U. 1997, OSA Technical Digest Series, 3, 38

Nave, G., Sansonetti, C. J. 2010 J. Opt. Soc. Am B. (submitted)

Norlén, G. 1973, Phys. Scr, 8, 249

Whaling, W., Anderson,W. H. C., Carle, M. T., Brault, J. W., Zarem, H. A. 1995, J. Quant. Spec. Radiat. Transf., 53, 1

This preprint was prepared with the AAS LaTeX macros v5.2.

NASA LAW, October 25-28, 2010, Gatlinburg

Laboratory Calibration of Density-Dependent Lines in the EUV and Soft X-Ray Regions

J. K. Lepson, P. Beiersdorfer[1], M. F. Gu & P. Desai

Space Sciences Laboratory, University of California, Berkeley, CA 94720

lepson@ssl.berkeley.edu

M. Bitter & L. Roquemore

Princeton Plasma Physics Laboratory, Princeton, NJ, 08543

M. L. Reinke & J. L. Terry

Massachussetts Institute of Technology, Cambridge, MA 02139

ABSTRACT

We analyzed spectral data of Fe XXII and Ar XIV from laboratory sources in which the electron density varies by several orders of magnitude to help benchmark density-sensitive emission lines useful for astrophysics and to test the atomic models underlying the diagnostic line ratios. We found excellent agreement for Fe XXII, but poorer agreement for Ar XIV.

1. Introduction

A number of astrophysically important emission lines are sensitive to electron density in the EUV and soft X-ray regions. Lines from Fe XXII, for example, have been used in recent years as diagnostics of stellar coronae, such as the active variable AB Dor, Capella, and EX Hya (Sanz-Forcada et al. 2003, Mewe et al. 2001, Mauche et al. 2003).

Here we report spectral data of Fe XXII and Ar XIV from laboratory sources in which the electron density is known from either K-shell density diagnostics (for electron beam ion traps) or from non-spectroscopic means (tokamaks), ranging from 5×10^{10} cm^{-3} to 5×10^{14} cm^{-3}. These measurements were used to test the atomic data underlying the density diagnostic line ratios, complementing earlier work (Chen et al. 2004).

[1]Also Physics Division, Lawrence Livermore National Laboratory, Livermore, CA 94550

2. Methods

Spectra from the Livermore electron beam ion trap were taken with a varied-line-spacing flat-field grating spectrometer with a mean spacing of 1200 lines/mm and a CCD detector. Wavelength calibrations were periodically performed with higher orders of the well known K-Shell emission lines of N VI and N VII, commonly referred to as w and Lyman-α, respectively, and with lines of O V and O VI; see Lepson et al. (2002) for further details of spectrometer set-up and data acquisition. The electron density of the EBIT plasma was estimated via the ratio of the density-sensitive 1-2 N VI transition lines known as y and z (Chen et al. 2004).

Further measurements were taken with the same spectrometers, which were installed on the NSTX tokamak and christened "XEUS" for the lower wavelength instrument and "LoWEUS" for the higher wavelength instrument (Lepson et al. 2008, 2010). Wavelength calibrations were performed with higher orders of the C VI Lyman-α and C V w lines, as well as with O V and O VI, as on EBIT. The electron density of the plasma was measured directly with Multi-Point Thomson Scattering.

Measurements on the Alcator C-Mod tokamak at MIT were taken on a 2.2 m Rowland circle grating spectrometer with a micro-channel plate detector. Spectral resolution was lower than on EBIT and NSTX, but had time-resolution of 4–16 ms. Density was also measured with Multi-Point Thomson Scattering.

Observations of Capella (α Aurigae) were taken with the *Chandra X-Ray Observatory*'s Low Energy Transmission Grating Spectrometer. We used the minus order summed from several observations totalling ∼500 ksec.

We used the Flexible Atomic Code (Gu 2003, 2008) to calculate emission strengths of two boron-like line pairs in iron and argon known to be sensitive to the electron density. In iron, we examined the Fe XXII line pair $(2s2p^2)_{3/2} \rightarrow (2s^22p)_{3/2}$ at 114.44 Å and $(2s2p^2)_{1/2} \rightarrow (2s^22p)_{1/2}$ at 117.17 Å, which was also used by Mewe et al. (2001) as part of an analysis of the corona of Capella. For argon we examined the Ar XIV line pair $(2s^22d)_{3/2} \rightarrow (2s^22p)_{1/2}$ at 27.47 Å and the blend $(2s^23d)_{5/2} \rightarrow (2s^22p)_{3/2}$ and $(2s^23d)_{3/2} \rightarrow (2s^22p)_{3/2}$ at 27.63 Å.

3. Results and Discussion

Spectra of Fe XXII are shown in Figures 1 (a) – 1 (d) for EBIT-II, NSTX, and Alcator C-Mod. The change in relative line strength is obvious between the low- and high-density regimes.

Figure 2 shows the line ratio curve of boron-like density-sensitive lines calculated with

the Flexible Atomic Code for Fe XXII (a) and Ar XIV (b) and the ratios measured on EBIT-II, NSTX, and Alcator C-Mod (Chen et al. 2004, Lepson et al. 2010, Reinke et al. 2010). For Fe XXII, excellent agreement is found between theory and tokamak measurements near the high density limit. Agreement at lower density is not as good, but overlaps within the error limits. We are attempting measurements around the critical density of 10^{13} cm^{-3}, where the rate of change is greatest. For Ar XIV, agreement between theory and measurements is rather poor at both low and, especially, high densities, indicating the need for improved atomic models.

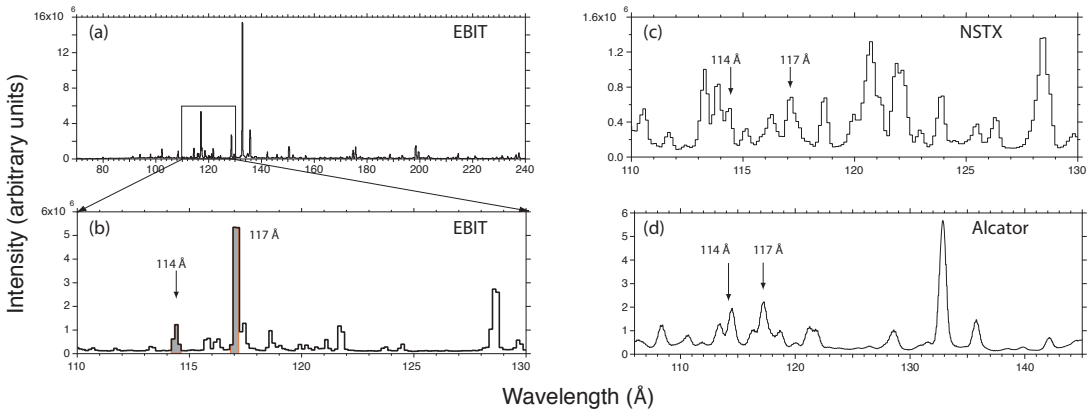

Fig. 1.— Spectra of iron from plasmas of different densities: (a) XEUS spectrometer at EBIT-II, with electron density $\sim 2 \times 10^{11}$ cm^{-3}. (b) inset showing the density-sensitive lines of B-like Fe XXII. (c) LoWEUS spectrometer on NSTX tokamak, where the electron density ranged from 9×10^{13} cm^{-3} to 1×10^{14} cm^{-3}. (d) Spectrum from Alcator C-Mod tokamak, where the electron density ranged from 9×10^{13} cm^{-3} to 5×10^{14} cm^{-3}.

This work was supported by the NASA APRA program and the DOE General Plasma Science program. Part of this work was performed under the auspices of the U S Department of Energy by Lawrence Livermore National Laboratory under Contract DE-AC52-07NA27344 and Princeton Plasma Physics Laboratory under Contract DE-AC02-09CH11466.

REFERENCES

Chen, H., Beiersdorfer, P., Heeter, L. A., Liedahl, D. A., Naranjo-Rivera, K. L., Träbert, E., Gu, M. F., & Lepson, J. K., 2004, ApJ, 611, 598

Gu, M. F., 2003, ApJ, 582, 1241

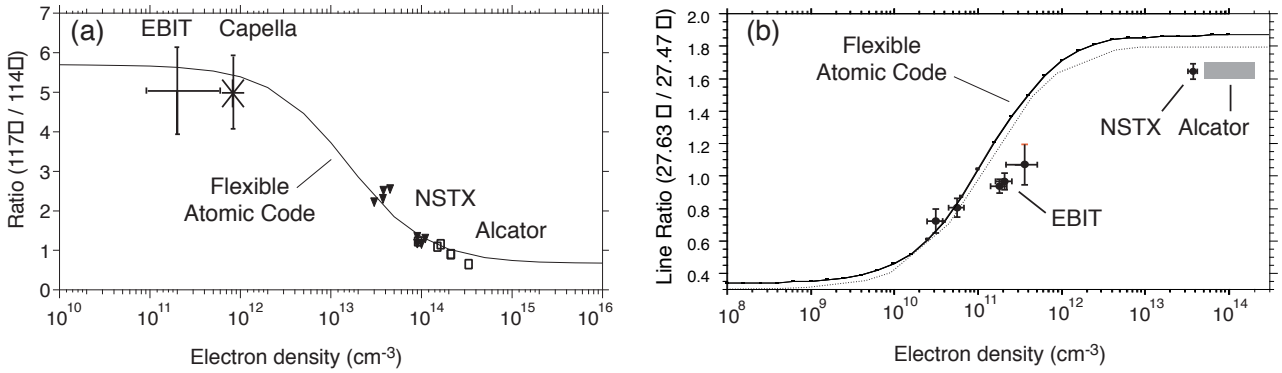

Fig. 2.— Comparison of theory with measurements: (a) Ratio curve calculated for the boron-like Fe XXII line pair 117.17 Å / 114.44 Å. (b) Ratio curve calculated for the boron-like Ar XIV line pair 27.63 Å / 27.47 Å. Solid line is calculated for a Maxwellian distribution with electron energy of 0.3 keV for tokamaks; dotted line is calculated for monoenergetic beam with electron energy of 1.0 keV for EBITs.

Gu, M. F., 2008, Can. J. Phys., 86, 675

Lepson, J. K., Beiersdorfer, P., Brown, G. V., Liedahl, D. A., Utter, S. B., Brickhouse, N. S., Dupree, A. K., Kaastra, J. S., Mewe, R., & Kahn, S. M., 2002, ApJ, 578, 648

Lepson, J. K., Beiersdorfer, P., Bitter, M., & Kahn, S. M., 2008, Can. J. Phys, 86, 175

Lepson, J. K., Beiersdorfer, P., Clementson, J., Gu, M. F., Bitter, M., Roquemore, L., Kaita, R., Cox, P. G., & Safronova, A., 2010, J. Phys. B, 43, 14410

Mauche, C. W., Liedahl, D. A., & Fournier, K. B., 2003, ApJ Lett., 588, L101

Mewe, R., Raassen, A. J. J., Drake, J. J., Kaastra, J. S., van der Meer, R. L. J., & Porquet, D, 2001, A&A, 368, 888

Reinke, M. L., Beiersdorfer, P., Howard, N. T., Magee, E. W., Podpaly, Y., Rice, J. E., & Terry, J. L., 2010, Rev. Sci. Instrum 81, 10D736

Sanz-Forcada, J., Maggio, A., & Micela, G., 2003, A&A, 408, 1087

This preprint was prepared with the AAS LaTeX macros v5.2.

NASA LAW, October 25-28, 2010, Gatlinburg

Towards More Accurate Atomic Oscillator Strengths

W. L. Wiese, J. R. Fuhr, & J. M. Bridges

National Institute of Standards and Technology, Gaithersburg, MD, 20899

wiese@nist.gov, jeffrey.fuhr@nist.gov, bridges@nist.gov

ABSTRACT

Accurate determinations of atomic oscillator strengths have been a problem for a long time. But in recent years considerable progress has been made, especially for weak lines. Atomic structure calculations have become sophisticated as well as efficient, and measurements of emission intensities in combination with cascade-free lifetimes have become an accurate experimental approach. In view of these developments, we have updated and enlarged our compilations of oscillator strengths of some astrophysically important spectra. We have also measured with a refined emission method a number of weak lines of several light-element spectra and found very good agreement with the most advanced calculations.

In the early years, most numerical data were obtained by a variety of experimental methods, including atomic lifetime measurements. But as demands for large amounts of data strongly increased since the 1960s and as powerful computers became widely available, the numerical data generation shifted to theory, especially for the astrophysically very important lighter elements, including the Fe-group. Several advanced atomic structure codes were developed, such as the HFR code, Superstructure, the R-matrix code, CIV 3, MCHF and MCDHF (see, e.g. Hibbert 2000). A principal shortcoming of the calculations has been the impossibility to produce uncertainty estimates of the results, since the calculations are complex and involve many approximations and cut-offs. Advanced calculations of the wave functions for various atomic states have used the concept of expanding them in terms of configuration state functions of the same total angular momentum and parity. This configuration interaction, or multi-configuration, treatment has turned out to be an excellent approximation. However, in early applications the size of the expansions was apparently insufficient. Accurate data were only produced for the strong lines, as shown by many comparisons with experiments. For the weaker lines large scatter in the results between different multi-configuration calculations as well as between the calculations and experimental data was encountered. Two examples are shown in Figs.1 and 2 for the spectra of C I and N II,

where 1993 and 1995 calculations with the CIV 3 code (Hibbert et al.1993, Bell et al. 1995) are compared with 1989 R-Matrix calculations from the OPACITY project (Topbase1989). For the weak lines, apparently considerable cancellation occurred between the positive and negative contributions to the line strength, and the calculations became rather uncertain. On the experimental side, measurements of the signals from weak lines also presented considerable problems and for this reason were often not even undertaken.

Starting about 1995, significant advances toward more accurate oscillator determinations have been made, especially for weaker lines. The most significant progress has come from improvements in sophisticated calculations with the MCHF, MCDHF and CIV 3 codes, and from more extensive tests of their results. Three important assessments have been often performed: 1. The calculated atomic transition energies have been compared with the usually very precisely known experimental energy values. Agreements within small fractions of a percent have been achieved. 2. Also, many numerical calculations have been routinely carried out with both the dipole length and dipole velocity forms of the transition integral. For exact wave functions, these two forms should produce the same oscillator strength, so that the magnitude of the residual difference is used as an indicator of the quality of the results. 3. Convergence studies have been performed for the differences between experimental and calculated energies, for the differences between length and velocity forms and for changes in the oscillator strength itself (always the length value), as more and more interacting configurations were successively added. But the convergence is slow and there is often no monotonic progression. Therefore, extremely large expansions in the wave functions are required to arrive at conditions where further changes become very small. In recent work, tens of thousands of configuration state functions have been used (Froese Fischer and Tachiev 2004, Oliver and Hibbert 2007). Also, it was found that relativistic effects needed to be included, which is usually done with the Breit-Pauli approximation for the light elements.

On the experimental side, considerable improvements have taken place, too. Atomic radiative lifetime measurements with state-selective laser excitation have produced precise values for strong spectral lines and served to provide absolute scales for branching fraction emission measurements for many more lines, including weak transitions. Measurements of line intensities were increasingly done by curve fitting to the line profiles. We have recently made some detailed emission measurements of weak lines of N I, Ne II and Cl I (Bridges and Wiese 2007, 2008, 2010). The observed line profiles were fitted to Voigt profiles, since under our experimental conditions the lines are predominantly pressure broadened, with some Doppler broadening also present. A deconvolution process was employed to distribute the overall observed intensity envelope into the individual lines. Also, filters were used to separate spectral orders and to eliminate continua originating from different wavelength regions. Two graphical comparisons with the most recent calculations illustrate the progress

achieved for the accuracy of atomic oscillator strengths, or transition probabilities (A-values), of weak lines. Figs. 3 and 4 show that the agreement is now almost as good for the weak transitions as for the strong ones.

In view of all this progress, we have in the last five years undertaken new, much expanded and more accurate critical compilations for H, He, Li(Wiese and Fuhr 2009), for C I and C II and N I and N II(Wiese and Fuhr 2007), and for Fe I and Fe II(Fuhr and Wiese 2006). These are now part of the NIST Atomic Spectroscopic Database, Version 4(NIST 2010).

REFERENCES

Bell, K. L., & Stafford, R.P. 1995, Phys. Scr., 52, 240

Bridges, J. M., & Wiese, W.L. 2007, Phys. Rev. A, 76, 022513

Bridges, J. M., & Wiese, W.L. 2008, Phys. Rev. A, 78, 062508

Bridges, J. M., & Wiese, W.L. 2010, Phys. Rev. A, 82, 024502

Froese Fischer, C., & Tachiev, G. 2004, At. Data Nucl. Data Tables, 87, 1

Fuhr, J. R., & Wiese, W. L.. 2006, J. Phys. Chem. Ref. Data, 35, 1669

Hibbert, A. 2000, Atomic and Molecular Data and Their Applications, AIP Conf. Proc., K. A. Berrington & K. L. Bell, Melville, NY: American Institute of Physics, 242-254

Hibbert, A., Biémont, E., Godefroid, M., & Vaeck, N. 1993, Astron. Astrophys., Suppl. Ser., 99, 179

NIST Atomic Spectra Database, Version 4 2010, http://www.nist.gov/pml/data/asd.cfm

O'Brian, T. R., Wickliffe, M. E., Lawler, J. E., Whaling, W., & Brault, J. W. 1991, J. Opt. Soc. Am. B, 8, 1185

Oliver, P. & Hibbert, A. 2007, J. Phys. B, 40,2847

Tachiev, G. I.& Froese Fischer, C. 2002, Astron. Astrophys., 385,716

Topbase database 1989, http://cdsweb.u-strasbg.fr/topbase/topbase.html

Wiese, W. L., & Fuhr, J. R. 2007, J. Phys. Chem. Ref. Data, 36, 1287

Wiese, W. L., & Fuhr, J. R. 2009, J. Phys. Chem. Ref. Data, 38, 565

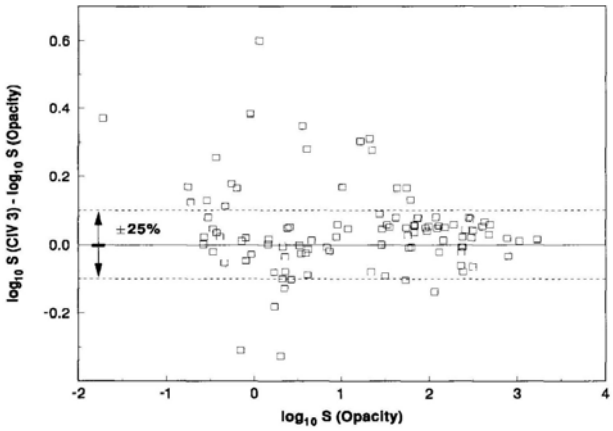

Fig.1. Comparison of multiplet line strengths S from CIV calculations (Bell et al. 1995) with the Opacity project (Topbase 1989) results for C I.

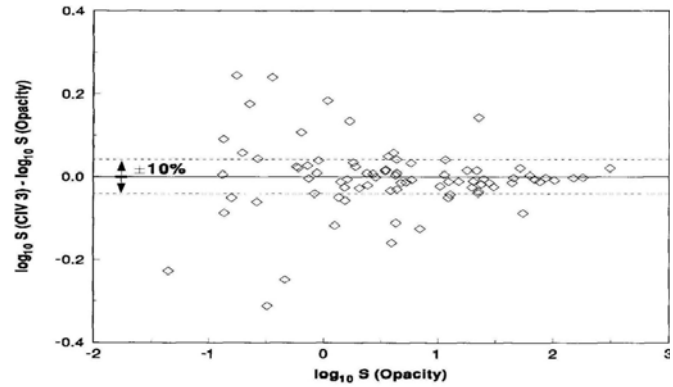

Fig. 2. Comparison of multiplet line strengths S from CIV 3 calculations (Hibbert et al. 1993) with the Opacity project (Topbase 1989) results for N II.

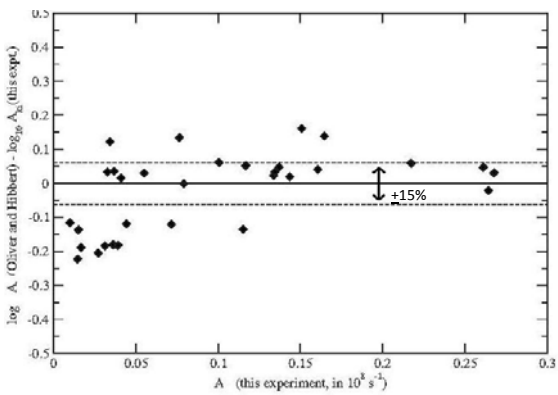

Fig.3 Comparison of CIV 3 calculations (Oliver and Hibbert 2007) with our emission experiment (Bridges and Wiese 2007) for Cl I.

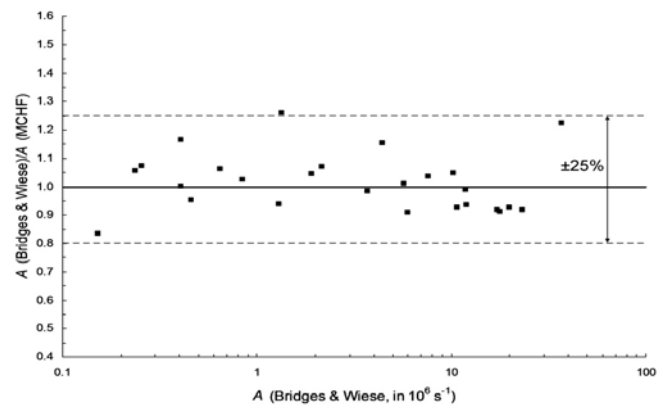

Fig.4 Comparison of MCHF calculations (Tachiev and Froese Fischer 2002) with our emission experiment (Bridges and Wiese 2010) for N I.

This preprint was prepared with the AAS LaTeX macros v5.2.

NASA LAW, October 25-28, 2010, Gatlinburg

Calculation of K-shell Photoabsorption Cross Sections for the Mg Isonuclear Sequence

Sh. A. Abdel Naby,[1] M. F. Hasoglu,[1,2] & T. W. Gorczyca[1]

[1]*Department of Physics, Western Michigan University, Kalamazoo, MI 49008*

[2]*Department of Physics & Astronomy, Georgia State University, Atlanta, Georgia 30303*

shahin.a.abdelnaby@wmich.edu, hasoglu@phy-astr.gsu.edu, gorczyca@wmich.edu

ABSTRACT

We report on K-shell photoabsorption (PA) cross section calculations for magnesium ions using the state-of-the-art R-matrix method. Comparisons with available data are presented and good agreement is obtained. The cross sections for Mg I and Mg II are complicated by the $n = 3$ M-shell occupancy and the multiple Auger decay pathways.

1. Introduction

There is a demand for accurate data for inner shell processes such as excitation and ionization, especially after the huge advances in the spectral resolutions of the launched X-ray telescopes. Such data are used for modeling astrophysical plasmas, interpreting the observed spectra from distant cosmic emitters, and determining the elemental abundances of the interstellar medium (ISM). Spectra of K-shell processes were observed from all ionic stages of the most abundant elements between oxygen and nickel (Paerels & Kahn (2003)).

Previously, our group carried out a series of successful K-shell photoabsorption calculations for argon (Gorczyca & Robicheaux (1999)), oxygen (Gorczyca & McLaughlin (2000)), and neon (Gorczyca (2000)). These calculations were also used to interpret *Chandra* high-resolution spectroscopic observations for oxygen ions (Garcia et al. (2005); Juett et al. (2004)) and neon ions (Juett et al. (2006)). Recently, we have carried out K-shell photoabsorption calculations for carbon ions (Hasoglu et al. (2010)).

2. Methodology

The K-shell photo-excitation of the ground states of Mg ions can be represented as initial $1s \rightarrow np$ photoabsorption followed by two competing decay routes. The first is *participator* Auger decay, in which the valence electron np participates in the autoionization process, with a decay rate that scales as $1/n^3$ and goes to zero near the K-shell threshold. These channels are included in the R-matrix calculations. The second route is *spectator* Auger decay, in which the valence electron np does not participate in the autoionization process, giving instead a decay width that is independent of n. Therefore, it is the dominant decay route as $n \rightarrow \infty$ and guarantees a smooth cross section as the K-shell threshold is approached; above each threshold, K-shell photoionization to the $1s2\ell^q$ states occurs instead.

We use the the R-matrix codes by Berrington et al. (1995), which are modified to account for the spectator Auger broadening via an optical potential approach as described by Gorczyca & Robicheaux (1999). This enhanced R-matrix method is shown to be successful in describing experimental synchrotron measurements for argon (Gorczyca & Robicheaux (1999)), oxygen (Gorczyca & McLaughlin (2000)), and neon (Gorczyca (2000)). The Auger widths for the $1s2\ell^q$ states are computed by applying the Smith time-delay method (Smith (1960)) to the photoabsorption R-matrix calculation of the neighboring $1s^22\ell^{q-1}$ magnesium ion.

3. Results and Discussions

In Figure 1, we present a comparison between our Mg VII K-shell photoabsorption, the results obtained by Witthoeft et al. (2009) using the same Breit Pauli R-matrix (BPRM) method, and the photoionization results of Verner et al. (1993). The lowest $1s \rightarrow np$ photoexcitation obtained from the $1s^22s^22p^2(^3P)$ ground state of Mg VII gives rise to the $1s2s^22p^2np(^3D^o,^3S^o,^3P^o)$ photoexcited states for $n = 2$. The energy positions for the $^3D^o$,$^3S^o$, and $^3P^o$ states are located at $1286.57, 1289.66$, and 1290.63 eV, respectively, while the corresponding energy positions of Witthoeft et al. (2009) are $1288.88, 1291.88$, and 1292.94 eV, respectively, with a difference of up to 2.31 eV. Our binding energy for Mg VII is higher than the one obtained from NIST by 0.26 eV. Our calculated K-shelll photoabsorption cross section in the length and velocity gauges differs by less than 5%.

In Figure 2, we present the K-shell photoabsorption for Mg II and Mg I, respectively. In the case of Mg II, the lowest $h\nu + 1s^22s^22p^63s(^2S) \rightarrow 1s2s^22p^63snp(^2P)$ resonance for $n = 3$ is obtained at 1307.08 eV, while the corresponding value by BPRM of Witthoeft et al. (2009) is 1316.23 eV with a difference of 9.05 eV. As we can see, our results align with the

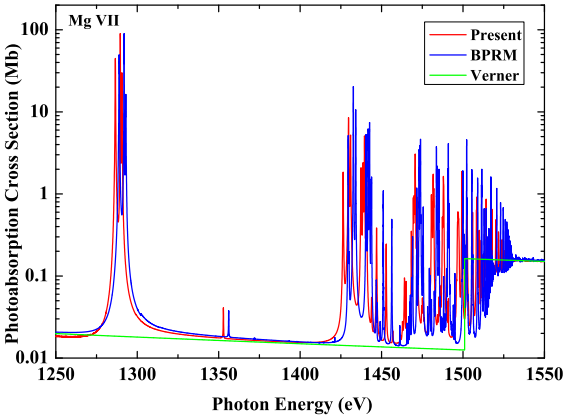

Fig. 1.— A comparison of our calculated Mg VII K-shell photoabsorption cross section, the results obtained by Witthoeft et al. (2009) using the same Breit Pauli R-matrix (BPRM) method, and the photoionization results of Verner et al. (1993).

photoionization results of Verner et al. (1993) above the K-shell threshold. In the case of Mg I, the lowest $h\nu + 1s^2 2s^2 2p^6 3s^2(^1S) \rightarrow 1s2s^2 2p^6 3s^2 np(^1P)$ resonance for $n = 3$ is obtained at 1304 eV.

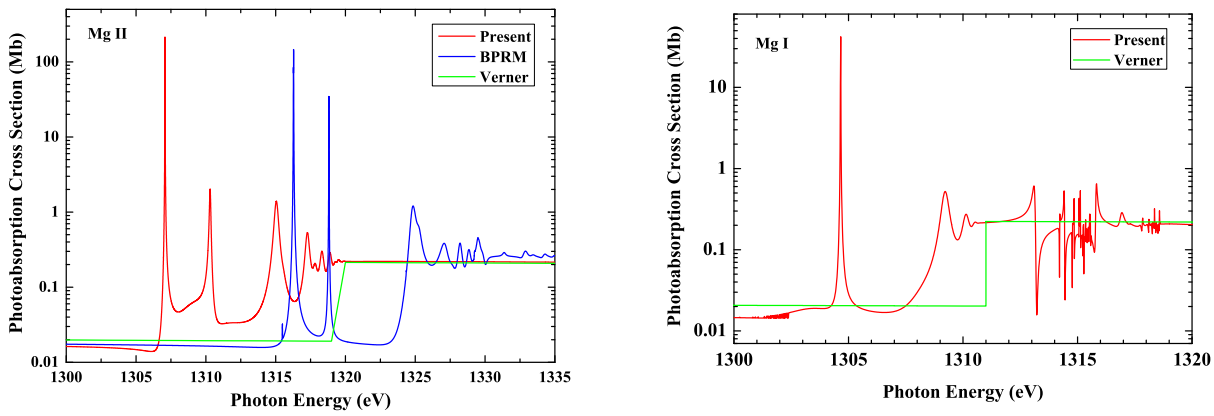

Fig. 2.— Same as Fig. 1 but for Mg II and Mg I ions, respectively.

This work was funded in part by NASA Astronomy and Physics Research and Analysis (APRA) grants.

REFERENCES

Berrington, K. A., Eissner, W., & Norrington, P. H. 1995, Comput. Phys. Commun., 92, 290

Garcia, J., Mendoza, C., Bautista, M. A., Gorczyca, T. W., Kallman, T. R., & Palmeri, P. 2005, ApJS, 158, 68.

Gorczyca, T. W., & Robicheaux, F. 1999, Phys. Rev. A, 60, 1216.

Gorczyca, T. W., & McLaughlin, B. M. 2000, J. Phys. B: At. Mol. Opt. Phys., 33, L859.

Gorczyca, T. W. 2000, Phys. Rev. A, 61, 024702.

Hasoglu, M. F., Abdel-Naby, Sh. A., Gorczyca, T. W., Drake, J. J., & McLaughlin, B. M. 2010, ApJ, 724, 1296.

Juett, A. M., Schulz, N. S., & Chakrabarty, D. 2004, ApJ, 612, 308.

Juett, A. M., Schulz, N. S., Chakrabarty, D., & Gorczyca, T. W. 2006, ApJ, 648, 1066.

Paerels, F. B. S., & Kahn, S. M. 2003, ARA&A, 41, 291.

Smith, F. T. 1960, Phys. Rev., 118, 349.

Verner, D. A., Yakovlev, D. G., Band, I. M., & Trzhaskovskaya, M. B. 1993, At. Data Nucl. Data Tables, 55, 233.

Witthoeft, M. C., Bautista, M. A., Mendoza, C., Kallman, T. R., Palmeri, P., & Quinet, P. 2009, ApJS, 182, 127.

This preprint was prepared with the AAS LaTeX macros v5.2.

NASA LAW, October 25-28, 2010, Gatlinburg

Photoionization of Atoms and Molecules using a Configuration-Average Distorted-Wave Method

M. S. Pindzola, C. P. Ballance, S. D. Loch, & J. A. Ludlow

Department of Physics, Auburn University, Auburn, AL 36849

Pindzola@physics.Auburn.edu

ABSTRACT

A configuration-average distorted-wave method is applied to calculate the photoionization cross section for the outer subshells of the C atom and the C_2 diatomic molecule. Comparisions are made with previous R-matrix and Hartree-Fock distorted-wave calculations.

1. Introduction

Photoionization cross sections for atoms and molecules are needed to better understand the physics and chemistry of the interstellar medium using X-ray absorption spectroscopy (Paerels et al. 2001; Kallman & Bautista 2001). In particular, photoionization cross sections are needed for various charge states of the astrophysically abundant elements from C to Fe. Photoionization cross sections are also needed for diatomic molecules like C_2, O_2, and CO.

A configuration-average distorted-wave method developed for electron collisions with atoms and their ions (Pindzola et al. 1986, 2010a) is applied to calculate photoionization cross sections for the C atom. In addition, a configuration-average distorted-wave method developed for the electron-impact excitation and ionization of diatomic molecules and their ions (Pindzola et al. 2005, 2010b) is applied to calculate photoionization cross sections for the C_2 molecule.

The rest of the article is organized as follows: in Section 2 we review the configuration-average distorted-wave (CADW) method as applied to the photoionization of atoms and molecules, in Section 3 we calculate photoionization cross sections for the C atom and the C_2 diatomic molecule, while in Section 4 we give a brief summary of future plans. Unless otherwise stated, all quantities are given in atomic units.

2. Theory

2.1. Photoionization of Atoms

The photoionization of an atomic configuration has the general form:

$$(n_i l_i)^{w_i} \rightarrow (n_i l_i)^{w_i - 1} k_f l_f \ , \tag{1}$$

where n is the principal quantum number, l is the angular quantum number, w is the occupation number of the subshell, and $\epsilon = \frac{k^2}{2}$ is the electron energy. In the dipole length gauge for the external electromagnetic field, the configuration-average photoionization cross section is given by:

$$\sigma_{ion} = \frac{8\pi\omega}{ck_f} \sum_{l_f} \frac{2w_i \max(l_i, l_f)}{3(4l_i + 2)} [D(n_i l_i \rightarrow k_f l_f)]^2 \ , \tag{2}$$

where ω is the radiation field frequency and c is the speed of light. For $l_i = 0$, $l_f = 1$, while for $l_i \neq 0$, $l_f = l_i \pm 1$. The radial dipole integral is given by:

$$D(n_i l_i \rightarrow k_f l_f) = \int_0^\infty dr P_{k_f l_f}(r) r P_{n_i l_i}(r) \ . \tag{3}$$

The energies and bound radial orbitals, $P_{nl}(r)$, are calculated in the Hartree-Fock relativistic (HFR) approximation (Cowan 1981), which includes the mass velocity and Darwin corrections within modified Hartree-Fock differential equations. The continuum radial orbitals, $P_{kl}(r)$, are calculated by solving a single channel radial Schrodinger equation, where the Hartree local exchange distorting potential is constructed with HFR bound orbitals and the continuum normalization is chosen as one times a sine function.

2.2. Photoionization of Diatomic Molecules

The photoionization of a molecular configuration has the general form:

$$(n_i l_i \lambda_i)^{w_i} \rightarrow (n_i l_i \lambda_i)^{w_i - 1} k_f l_f \lambda_f \ , \tag{4}$$

where n is the principal quantum number, l is the angular quantum number, $\lambda = |m|$ is the magnetic quantum number, w is the occupation number of the subshell, and $\epsilon = \frac{k^2}{2}$ is the electron energy. In the dipole length gauge for the external electromagnetic field, the configuration-average photoionization cross section is given by:

$$\sigma_{ion} = \frac{8\pi\omega}{3ck_f} \sum_{l_f} w_i \left([DC(n_i l_i \lambda_i \rightarrow k_f l_f \lambda_i)]^2 + [DS(n_i l_i \lambda_i \rightarrow k_f l_f \lambda_i)]^2 \right) \tag{5}$$

for $\lambda_i = 0$ and

$$\sigma_{ion} = \frac{8\pi\omega}{3ck_f}\sum_{l_f} w_i([DC(n_il_i\lambda_i \to k_fl_f\lambda_i)]^2 + \frac{1}{2}[DS(n_il_i\lambda_i \to k_fl_f(\lambda_i - 1)]^2 + \frac{1}{2}[DS(n_il_i\lambda_i \to k_fl_f(\lambda_i + 1)]^2) \quad (6)$$

for $\lambda_i \neq 0$, where ω is the radiation field frequency and c is the speed of light. The radial and angular dipole integrals are given by:

$$DC(n_il_i\lambda_i \to k_fl_f\lambda_f) = \int_0^\infty dr \int_0^\pi d\theta P_{k_fl_f\lambda_f}(r,\theta) r\cos\theta P_{n_il_i\lambda_i}(r,\theta) \quad (7)$$

and

$$DS(n_il_i\lambda_i \to k_fl_f\lambda_f) = \int_0^\infty dr \int_0^\pi d\theta P_{k_fl_f\lambda_f}(r,\theta) r\sin\theta P_{n_il_i\lambda_i}(r,\theta) \ . \quad (8)$$

The energies and bound orbitals, $P_{nl\lambda}(r,\theta)$, are calculated in a self-consistent field (SCF) approximation based on a linear combination of Slater type orbitals (Theoretical Chemistry Group 1970). The bound orbitals are then transformed (Morrison 1980) onto a two dimensional (r,θ) numerical lattice. The continuum orbitals, $P_{kl\lambda}(r,\theta)$, are calculated by solving a single channel (r,θ) Schrodinger equation, where the Hartree local exchange distorting potential is constructed from SCF bound orbitals and the continuum normalization is chosen as one times a sine function.

3. Results

The configuration-average distorted-wave method was used to calculate the photoionization cross section for the C atom. The outer subshell transition:

$$1s^22s^22p^2 \to 1s^22s^22pkl \ , \quad (9)$$

has an ionization potential of 10.0 eV. The CADW cross section results are found to be in reasonable agreement with the non-resonant background from an early R-matrix calculation (Taylor & Burke 1976).

The configuration-average distorted-wave method was used to calculate the photoionization cross section for the C_2 molecule at an internuclear separation of $R = 2.35$. The outer subshell transition:

$$1s\sigma^22p\sigma^22s\sigma^23p\sigma^22p\pi^4 \to 1s\sigma^22p\sigma^22s\sigma^23p\sigma^22p\pi^3kl\lambda \ , \quad (10)$$

has an ionization potential of 12.6 eV. The CADW cross section results are found to be in reasonable agreement with previous Hartree-Fock distorted-wave calculations (Padial et al. 1985).

4. Summary

In conclusion, we have carried out configuration-average distorted-wave calculations for the photoionization of the outer subshells of the C atom and the C_2 molecule. The CADW cross section results are found to be in reasonable agreement with previous R-matrix and Hartree-Fock distorted-wave results.

In the future, we plan to publish CADW results for the photoionization of all subshells of the C atom and the C_2 molecule. We then plan to continue calculations for the photoionization of those atoms, molecules, and their ions that are of particular interest for a better understanding of astrophysical observations.

Acknowledgments

This work was supported in part by grants from the US Department of Energy, the US National Science Foundation, and the US National Aeronautics and Space Administration. Computational work was carried out at the National Energy Research Scientific Computing Center in Oakland, California and the National Institute for Computational Sciences in Knoxville, Tennessee.

REFERENCES

Cowan, R. D. 1981, "The Theory of Atomic Structure and Spectra," University of California Press, Bekeley

Kallman, T., & Bautista, M. 2001, Astrophys. J. Suppl. Ser. 133, 221

Morrison, M. A. 1980, Comput. Phys. Commun., 21, 63

Padial, N. T., Collins, L. A., & Schneider, B. I. 1985, Astrophys. J., 298, 369

Paerels, F., Brinkman, A. C., Van der Meer, R. L. J., Kaastra, J. S., Kuulkers, E., Den Boggende, A. J. F., Predehl, R., Drake, J. J., Kahn, S. M., Savin, D. W., & McLaughlin, B. M. 2001, Astrophys. J., 546, 338

Pindzola, M. S., Ballance, C. P., Ludlow, J. A., Loch, S. D., & Griffin, D. C. 2010, J. Phys. B, 43, 025201

Pindzola, M. S., Ballance, C. P., Ludlow, J. A., Loch, S. D., & Colgan, J. P. 2010, J. Phys. B, 43, 065201

Pindzola, M. S., Griffin, D. C., & Bottcher, C. 1986, Atomic Processes in Electron-Ion and Ion-Ion Collisions, Vol. 145 of NATO Advanced Study Institute Series B: Physics, F. Brouillard, Plenum, New York, 75

Pindzola, M. S., Robicheaux, F., Ludlow, J. A., Colgan, J., & Griffin, D. C. 2005, Phys. Rev. A, 72, 012716

Taylor, K. T., & Burke, P. G. 1976, J. Phys. B, 9, L353

Theoretical Chemistry Group 1970, Computer code named ALCHEMY, San Jose, CA: IBM Research Laboratory.

NASA LAW, October 25-28, 2010, Gatlinburg

Dissociative Recombination in an Ion Storage Ring

O. Novotný[1], M. B. Mendes, C. Nordhorn, M. H. Berg, D. Bing, M. W. Froese, C. Krantz, S. Menk, S. Novotny, D. A. Orlov, A. Petrignani, A. Shornikov, J. Stützel, & A. Wolf

Max-Planck-Institut für Kernphysik, D-69117 Heidelberg, Germany

oldrich.novotny@mpi-hd.mpg.de

H. Buhr[2], O. Heber, M. L. Rappaport, & D. Schwalm[2]

Weizmann Institute of Science, Rehovot 76100, Israel

D. W. Savin

Columbia Astrophysics Laboratory, Columbia University, New York, NY 10027, USA

ABSTRACT

The astrophysically important molecular ions $DCND^+$ and D_3O^+ can dissociate upon capture of a free electron, a process known as dissociative recombination (DR). We give here a brief summary of recent experimental studies of the DR of these molecules that have been carried out at the TSR heavy ion storage ring.

1. Introduction

Dissociative recombination (DR) of molecular ions plays a key role in controlling the charge density and composition of the cold interstellar medium (ISM). Experimental DR data and reliable predictions based on a good knowledge of the underlying quantum mechanisms are required in order to understand the ISM chemical network and related processes such as star formation from molecular clouds. The required data does not only include reaction cross sections, but also the chemical composition and excitation states of the neutral products.

---

[1]Present address: Columbia Astrophysics Laboratory, Columbia University, New York, NY 10027, USA

[2]Also at: Max-Planck-Institut für Kernphysik, D-69117 Heidelberg, Germany

DR of molecular ions involves the resonant capture of an incident electron into the potential energy surface of a doubly-excited state of the neutral molecule lying within the Franck-Condon region of the ion (Larsson & Orel 2008). Such states are usually dissociative and their asymptotic energy lies below that of the ion, reflecting the energy gained in binding the free electron. This excess energy is stabilized by dissociation into neutral, often excited fragments. Measurement of the fragment relative kinetic energies provides information on the internal states of both the parent ion and the DR products.

At the TSR heavy ion storage ring in Heidelberg, Germany, we employ a merged beams technique to study DR at low energies (Buhr et al. 2010). The ions discussed are generated in a discharge, accelerated, and injected into the storage ring. With ring pressures of $\sim 10^{-11}$ mbar, the ions can be stored for several tens of seconds. In general, ions with a dipole moment relax vibrationally – although not necessarily rotationally – to the 300 K ambient temperature. An electron beam device provides a beam of electrons with only ~ 1 meV energy spread. At matching beam velocities, elastic collisions of the ions with the low-energy-spread electron beam transfer energy from the recirculating ions to the single pass electrons, thereby reducing the energy-spread of the ions (i.e., translational phase-space cooling). Thus the collision energy resolution of the experiment is defined by that of the electron beam. The electron beam velocity can be detuned from the ion velocity to investigate DR versus collision energy. The neutral DR products are not deflected by the first dipole magnet downstream of the electron beam and hit one of the dedicated DR detectors.

The studies presented here use the recently introduced Energy sensitive MUltistrip detector (EMU), which is capable of simultaneously determining both the positions and masses of all DR products. This allows the DR fragmentation channels to be distinguished on an event-by-event basis. The distribution of the kinetic energy releases (KER) is derived from the position pattern of the fragments. Knowing the basic molecular structure provides the information on the excitation level of the DR products.

2. Dissociative Recombination of D_3O^+

DR of the hydronium ion H_3O^+ is an important process for the production of H, OH and H_2O in diffuse and dense interstellar clouds. Water production is of particular interest as it is an important coolant of the ISM and this cooling contributes to the star formation rate (Neufeld et al. 1995). The branching ratios of the different DR fragmentation channels are critical parameters in modeling these cold environments. Thus, if H_2O+H is the primary channel, water will be the main reservoir of oxygen. If, on the other hand, $OH + H + H$ or $OH+H_2$ are preferred, O_2 will become the dominant oxygen-storing molecule after subsequent reactions of the OH radical.

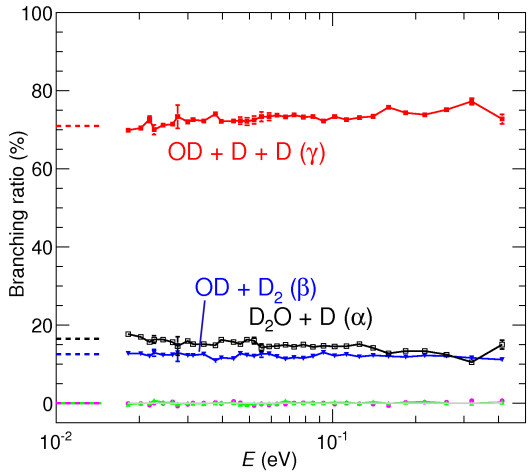

Fig. 1.— Fragmentation branching ratios for the DR of D_3O^+. The branching ratios at near-zero collision energy are marked by dashed lines. Fragmentation channels δ and ϵ are compatible with 0% over the whole energy range. The error bars represent shown only statistical errors. Additional systematic errors can reach up to 5%. Total errors at matched beam velocities are lower than 2%. See Novotný et al. (2010) for more details.

At the TSR we have investigated DR of the deuterated hydronium ion D_3O^+ employing the EMU detector. The following DR fragmentation channels can occur at low collision energies: (α) D_2O+D, (β) $OD+D_2$, (γ) $OD+D+D$, (δ) $O+D_2+D$, and (ϵ) $O+D+D+D$. With the exception for the four-body channel (ϵ), all channels are exothermic and therefore already accessible at matched beam velocities ($E \approx 0$), where the impact energies are only determined by the electron energy spread, corresponding to $\sim$ 1.0 meV. The branching ratios for the collision energy range between 18 meV and 500 meV are plotted in Fig. 1. Only the channels α, β, and γ appear to be relevant at ISM temperatures of $\sim$ 10 K. The prior experimental results of Neau et al. (2000) and Jensen et al. (2000), obtained only at matched beam velocities, are discrepant for the (α) and (γ) channels. Our work supports the results of Neau et al. and yields data for collision energies up to $\sim$ 2 orders of magnitude higher than previous work. Our novel approach of measuring branching ratios using the EMU detector results in a significantly higher precision than was previously achieved. Going from energies of 18 meV to 500 meV, only a marginal increase in the branching ratio of the γ channel and a corresponding decrease in α are observed.

3. Dissociative Recombination of $DCND^+$

Recently we have also investigated $DCND^+$, which is an isotopologue of the astrophysically important ion, $HCNH^+$. For this system, DR at near-zero collision energy has three fragmentation channels (Semaniak et al. 2001). The two isomeric channels HCN/HNC + H are expected to be the main source of HCN and HNC in the cold ISM. Observations show a source-to-source variations in the abundance ratios of these isomers which cannot be explained by astrochemical models (Hirota 1998). Thus knowledge of DR branching ratios of $HCNH^+$ forming HCN/HNC is essential for understanding the chemistry in these environments.

At the TSR we have investigated DR of $DCND^+$ at collision energies $\lesssim 1$ meV using the EMU detector. The channels DNC + D and DCN + D cannot be distinguished through the fragment masses as they are the same for these two outgoing channels. The maximum KER for each channel is predicted to be 5.3 eV and 5.9 eV, respectively. However, the observed KER distribution for these two channels displays a broad distribution with mean value which is about 4.5 eV lower than the maximum expected values. The missing kinetic energy reflects a ro-vibrational excitation of the DCN/DNC molecular products of several eV. The majority of molecules are clearly produced with high internal excitation well above the isomerisation barrier (Bowman et al. 1993). We conclude that the DR process enables both isomers to be formed, with the final yields determined by the relaxation of the dissociated molecular products. Additional studies are needed for obtaining the branching ratios for the combined DR after the relaxation.

This work was supported in part by grants of German-Israeli Foundation for Scientific Research [GIF under contract Nr. I-900-231.7/2005] and by the NASA Astronomy and Physics Research and Analysis Program. D.S. is acknowledging support by the Weizmann Institute through the Josef Meyerhoff programm.

REFERENCES

Bowman, J. M. et al. 1993, J. Chem. Phys., 99, 308-323

Buhr, H. et al. 2010, Phys. Rev. Lett., 105, 103202, and references therein

Hirota, T. & Yamamoto, S. & Mikami, H. & Ohishi 1998, Astrophys. J., 503, 717

Jensen, M. J. et al. 2000, Astrophys. J., 543, 764

Larsson, M., & Orel, A. E. 2008, Dissociative Recombination of Molecular Ions, Cambridge: Cambridge University Press

Neau, A. et al. 2000, J. Chem. Phys., 113, 1762

Novotný, O. et al. 2010, J. Phys. Chem. A, 114, 4870

Neufeld, D. A. & Lepp, A. & Melnick, G. J. 1995, Astrophys. J., Suppl. Ser., 100, 132

Semaniak, J. et al. 2001, Astrophys. J., Suppl. Ser., 135, 275-283

This preprint was prepared with the AAS LaTeX macros v5.2.

NASA LAW, October 25-28, 2010, Gatlinburg

Development of Two Ion Generation Systems at JPL

S. Yu[1], W. W. Chun, J. C. Pearson, B. J. Drouin, T. J. Crawford & H. Gupta

Jet Propulsion Laboratory, California institute of Technology, Pasadena, CA 91109

Shanshan.Yu@JPL.nasa.gov, William.W.Chun@jpl.nasa.gov,
John.C.Pearson@jpl.nasa.gov, Brian.J.Drouin@jpl.nasa.gov,
Timothy.J.Crawford@jpl.nasa.gov, Harshal.Gupta@jpl.nasa.gov

ABSTRACT

Ions play an important role in the interstellar chemistry: ion-neutral reactions accelerate the production of interstellar molecules. Due to their high reactivity, ions typically occur at very low concentration in the laboratory, which makes laboratory detection extremely difficult. Many astronomical spectra are waiting to be interpreted because comparable laboratory data are missing or incomplete. This paper presents a description of two ion generation systems, which were designed for generating different ions with different production chemistry.

1. Introduction

Over 150 molecules have been identified in the interstellar and circumstellar medium, including 21 positive molecular ions: SO^+, SH^+, CO^+, CH^+, CF^+, OH^+, N_2H^+, $H_3{}^+$, H_2D^+, $HD_2{}^+$, HCS^+, HOC^+, HCO^+, H_2Cl^+, H_2O^+, H_3O^+, $HCO_2{}^+$, $HCNH^+$, CH_2D^+, H_3CO^+, HC_3NH^+ and 6 negative molecular ions: CN^-, C_3N^-, C_4H^-, C_5N^-, C_6H^- and C_8H^-. Due to their high reactivity, ions typically occur at very low concentration in the laboratory, which makes laboratory detection extremely difficult. Recently at JPL, an extended negative glow DC discharge system was constructed to effectively generate positive ions based on the following principle: of the eight zones occurring between the cathode and the anode of a DC glow discharge, a high density of positive charges exists in the so called negative glow discharge zone, which is short under regular discharge conditions (Engel 1965); by cooling the discharge and applying a magnetic field, the negative glow zone can be extended to fill almost the entire discharge cell, which greatly enhances the column of positive ions (De Lucia et al 1983). The extended negative glow discharge has been successful in generating protonated species. Protonated species are usually produced in a discharge with excess

hydrogen; the highly reactive H_3^+ is formed and readily donates a proton to a molecule with a higher proton affinity, i.e. $H_3^+ + X \rightarrow XH^+ + H_2$. This chemical mechanism simulates the H_3^+ pathway in the ISM. This paper will present a description of this system and the observed N_2H^+ spectra.

Many simple ions necessary for the interstellar chemical network to function have not yet been observed, e.g. NH^+, NH_2^+, NH_3^+, CH_2^+. These ions are open shell species with unpaired electron(s) and cannot be detected effectively in the extended negative glow discharge, as the applied magnetic field interacts with the unpaired electron (s), resulting in magnetic splittings in the energy levels. A high power radio frequency (RF) AC discharge system is under development at JPL, with the aim to generate these open shell species by stripping electrons off molecules. The RF discharge has been successful in generating open shell species even in highly excited vibrational states (Bustreel et al 1983). The chemical mechanism simulates cosmic rays and photo ionization, i.e., $He^* + X \rightarrow X^+ + e + He$. This paper will present a description of this system as well.

2. Extended negative glow discharge system at JPL

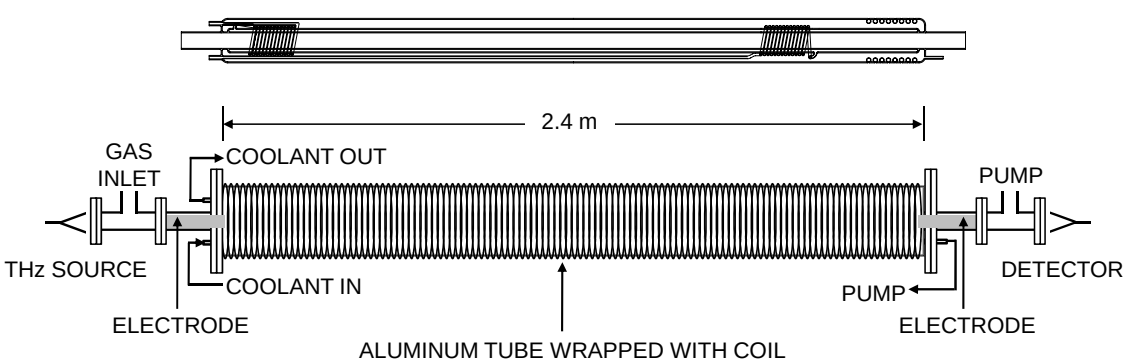

Fig. 1.— The triple-jacketed Pyrex glass cell (top) and the schematic diagram (bottom) of the extended negative glow discharge system.

The main part of the negative glow discharge system is a triple-jacketed Pyrex glass cell, which is placed inside an aluminum house tube (Figure 1). The innermost glass tube (L=2.6 m, OD=41 mm, ID=37 mm) is used to handle gas samples; the middle glass jacket(L= 2.37, OD=57 mm, ID=52 mm) is used to fill coolant for cooling the innermost tube; the outmost glass jacket(L=2.4 m, OD=100 mm, ID=95 mm) is used to pull vacuum and isolate the coolant jacket from the air. The aluminum house tube (L=2.4 m, OD=114 mm, ID=110 mm) is wrapped with a solenoid coil for generating magnetic field. The maximum magnetic field we can achieve is 212 G. An electrode tube (OD=36 mm, ID=34 mm) is inserted 140

mm deep into each end of the innermost tube. Gas inlet and pumping ports are located at each end of the sample cell, and two polyethylene windows are used to seal the cell. In our experiment, absorption spectroscopy is used. The terahetz radiation source passes through the sample cell and is detected with a silicon bolometer cooled to 1.2 K. Figure 2 shows the observed N_2H^+ transition at 558.9 GHz. The signal-to-noise ratio of this line is about 300 and is enhanced by a factor of about 30 by the applied magnetic field. The enhancement is smaller than that of two orders of magnitude reported by De Lucia et al 1983, which is probably due to the fact that we could only cool our cell to 230 K. A new glass cell will be used, which will allow us to cool the cell to liquid nitrogen temperature.

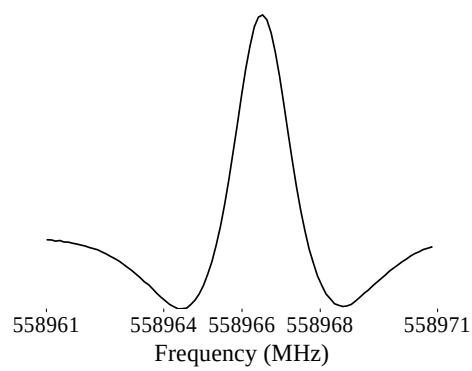

Fig. 2.— The N_2H^+ $N = 6 \leftarrow 5$ transition in the ground state.

3. Radio frequency discharge system at JPL (under development)

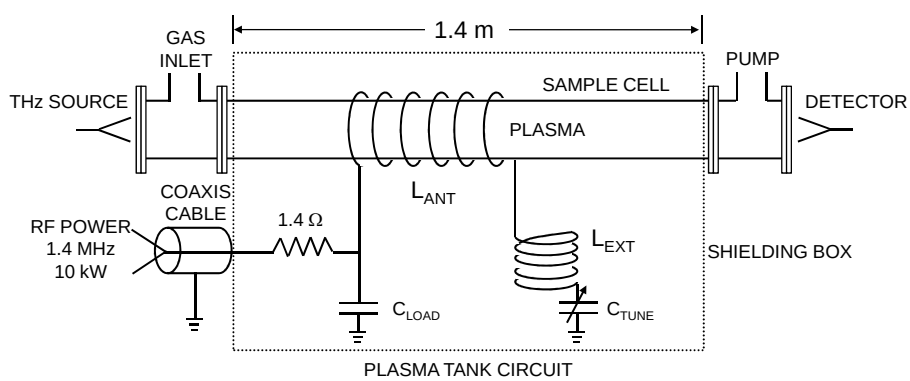

Fig. 3.— Schematic diagram of the RF discharge system.

Figure 3 shows a schematic diagram for the RF discharge system. The plasma tank circuit is the main basis of our ion generation system. It is a high power π network LC parallel resonant circuit encompassing the antenna coil. This antenna coil wraps around

the central part of the sample cell (L=1.5 m, OD=152 mm, ID=135 mm) in series with an external inductor coil. While increasing power to the antenna coil, its inductance (L_{ANT}) decreases as plasma conductor increases shielding to the antenna coil. When the RF tank frequency shifts as such with increasing RF power, the coupling between the RF power and the plasma can be optimized by adjusting the tuning capacitor (C_{TUNE}). External coil inductance (L_{EXT}) is made larger than L_{ANT} to avoid large tank frequency shifts. The RF power source is an AM transmitter at 1.4 MHz frequency with a maximum power of 15 kW.

4. Conclusion

This paper reports two ion generation systems in several stages of development at JPL. A new extended negative glow discharge system has been successfully constructed, with which N_2H^+ has been observed with a significantly enhanced concentration. This system was designed to efficiently generate new protonated species like $CH_3OH_2{}^+$ (protonated methanol). The extended negative glow discharge system is ineffective in forming open-shell species like H_2O^+ and NH^+, as the applied magnetic field interacts with the magnetic field. An RF discharge system was designed to strip electrons off molecules to efficiently generate open-shell ions.

This research was performed at the Jet Propulsion Laboratory, California Institute of Technology under contract with the National Aeronautics and Space Administration. Funding from APRA supported this effort. We would like to thank Professor T. Amano for coming to JPL to help with optimizing the extended negative glow discharge system.

REFERENCES

Engel A.V. 1965, Ionized Gases, 2nd ed. Oxford.

De Lucia, F. C., Herbst E., Plummer, G. M., & Blake G. A. 1983, J. Chem. Phys., 78, 2312.

Bustreel R., Demuynck-Marliere C. Destombes J. L., & Journel G. 1979, Chem. Phys. lett. 67, 178.

This preprint was prepared with the AAS LaTeX macros v5.2.

NASA LAW, October 25-28, 2010, Gatlinburg

Gas-phase Reactions of Carbanions with Atomic Species

Z. Yang, O. Martinez Jr., M. Y. Carpenter, B. Eichelberger, V. M. Bierbaum

Department of Chemistry and Biochemistry, University of Colorado, Boulder, CO 80309

zhibo.yang@colorado.edu, oscar.martinez@colorado.edu,
marshall.carpenter@colorado.edu,bmgpeich@gmail.com,
veronica.bierbaum@colorado.edu

T. P. Snow

Department of Astrophysical and Planetary Sciences, University of Colorado, Boulder, CO 80309

theodore.snow@colorado.edu

ABSTRACT

Six molecular anions have now been detected in the denser regions of the interstellar medium (ISM). Hydrogen, nitrogen, and oxygen atoms are the most abundant atomic species in the ISM, and the chemistry of these atomic species with anions may contribute to molecular synthesis in these clouds. This work is an experimental and computational study of the reactions of organic molecular anions with H, N, and O atoms. The experiments were carried out using the tandem flowing afterglow-selected ion flow tube (FA-SIFT). *Ab initio* theoretical calculations were carried out to explore the reaction mechanisms and investigate the factors influencing reaction efficiencies. The rich chemistry observed provides a greater understanding of the processes that are likely to occur in these interstellar clouds.

1. Introduction

More than 160 molecular species have been detected in the ISM, and among the discovered species, six anions have been detected in the denser regions of the ISM, i.e., HC_n^- (n = 2, 4, and 6) and C_nN^- (n = 1, 3, and 5) (McCarthy et al. 2006; Brünken et al. 2007;

Cernicharo et al. 2007, 2008; Remijan et al. 2007; Thaddeus et al. 2007; Agúndez et al. 2010). Study of anion-atom reactions can enhance our understanding of the negative ion chemistry and chemical transformations, and the corresponding rate constants are crucial for astrochemical modeling to establish the reaction networks among species in the ISM.

2. Experimental

Ions were generated by electron and chemical ionization methods. H atoms were produced by thermal dissociation of H_2, and N and O atoms were generated with a microwave discharge. The reactant ions were mass-selected using a quadrupole mass filter and injected into the reaction flow tube where they were thermalized through collisions with He buffer gas, and allowed to react with the atomic reagent. The rate constants were measured by monitoring the decrease of the reactant-ion signal using a quadrupole mass filter as a function of atom flow. *Ab initio* calculations were performed to support the experimental studies.

3. Results and discussion

The reaction rate constants were determined, and the reaction efficiencies (k_{Exp}/k_{Coll}) were obtained by taking the ratio between the experimental reaction rate constant and the theoretical collision rate constant. The results indicate that the reactions between carbanions and H atoms proceed through an associative detachment pathway, and the reaction efficiencies are largely proportional to reaction exothermicities. As an example, results of deprotonated nitriles (CH_2CN^-, CH_3CHCN^-, and $(CH_3)_2CCN^-$), acetaldehyde ($HC(O)CH_2{}^-$), acetone ($CH_3C(O)CH_2^-$), ethyl acetate ($CH_3CH_2OC(O)CH_2^-$), methanol (CH_3O^-), acetic acid ($CH_3CO_2^-$), and glycine ($NH_2CH_2CO_2^-$) are shown in Fig. 1, in which the logarithms of the reactions efficiencies have an approximately linear relationship to their exothermicities. Other factors influencing reaction efficiencies include the charge density on the reactive site of the anion, the characteristics of the potential energy surfaces along the approach of the reactants, and angular momentum conservation of the anion-H atom collision (Yang et al. 2010c). Studies of nitrogen-containing carbon chain anions (C_nN^- (n = 1 – 6), $C_nN_2^-$ (n = 1, 3, 4, and 5), and $C_nN_3^-$(n = 2 and 4)) were also carried out. Our results indicate C_nN^- and $C_nN_2^-$ are reactive with H atoms, whereas $C_nN_3^-$ (n = 2 and 4) anions are unreactive. These results are interpreted by the corresponding reaction potential surfaces (Yang et al. 2010d).

Experiments and calculations of deprotonated nitriles (CH_2CN^-, CH_3CHCN^-, and

$(CH_3)_2CCN^-$), acetaldehyde ($HC(O)CH_2^-$), and carbon-chain species (C_n^- (n = 2, 4 – 7) and HC_n^- (n = 2, 4, and 6)) with N and O atoms were carried out. The reaction channels include associative detachment and formation of smaller anions by fragmentation. Reaction efficiencies are determined by electronic spin effects; reactions that proceed through spin-forbidden channels are much less efficient than those that proceed through spin-allowed pathways. The semi-quantitative interpretation of the reaction efficiency in terms of spin effects is illustrated in Fig. 2 (Yang et al. 2010a,b).

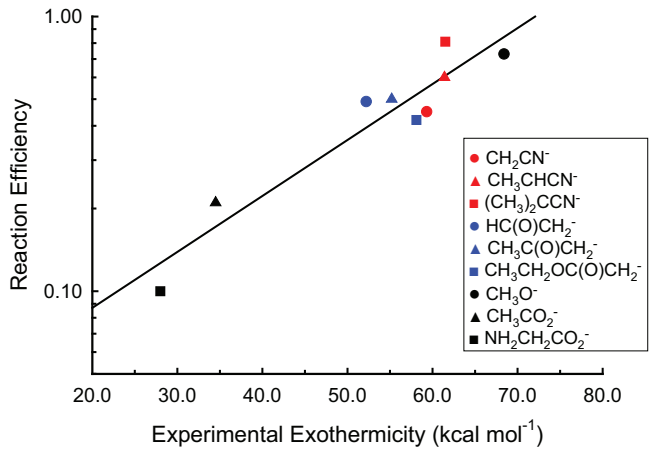

Fig. 1.— The correlation between the logarithm of the reaction efficiency and experimental exothermicity. Symbols in color indicate the anions, and the line indicates the linear regression of all points. Experimental exothermicities were derived from Hess's law.

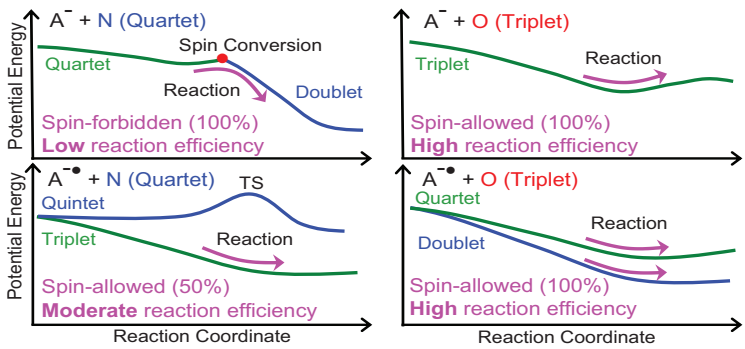

Fig. 2.— The influence of spin effects on the gas-phase reactions of carbanions with N and O atoms.

We gratefully acknowledge financial support from NASA, the NASA Graduate Student Researchers Program (GSRP), and the National Science Foundation (CHE-1012321). This research was supported in part by the National Science Foundation through TeraGrid resources provided by NCSA.

REFERENCES

Agúndez, M., Cernicharo, J., Guélin, M., Kahane, C., Roueff, E., Klos, J., Aoiz, F. J., Lique, F., Marcelino, N., Goicoechea, J. R., González García, M., Gottlieb, C. A., McCarthy, M. C., & Thaddeus, P. 2010, A&A, 517, L2

McCarthy, M. C., Gottlieb, C. A., Gupta, H., & Thaddeus. P. 2006, ApJ, 652, L141

Brünken, S., Gupta, H.; Gottlieb, C. A.; McCarthy, M. C.; & Thaddeus, P. 2007, ApJ., 664, L43

Cernicharo, J., Guélin, M., Agúndez, M., Kawaguchi, K., McCarthy, M., & Thaddeus. P. 2007, A&A, 467, L37

Cernicharo, J., Guélin, M., Agúndez, M., McCarthy, M. C., & Thaddeus, P. 2008, ApJ, 688, L83

Remijan, A. J., Hollis, J. M., Lovas, F. J., Cordiner, M. A., Millar, T. J., Markwick-Kemper, A. J., & Jewell, P. R. 2007, ApJ, 664, L47

Thaddeus, P., Gottlieb, C. A., Gupta, H.; Brünken, S., McCarthy, M. C., Agúndez, M., Guélin, M., & Cernicharo, J. 2007, ApJ, 677, 1132

Yang, Z., Eichelberger, B., Martinez Jr., O., Stepanovic, M., Snow, T. P., & Bierbaum, V. M. 2010a, J. Am. Chem. Soc., 132, 5812

Yang, Z., Snow, T. P., & Bierbaum, V. M. 2010b, Phys. Chem. Chem. Phys., 12, 13091

Yang, Z., Eichelberger, B., Carpenter, M. Y., Martinez Jr., O., Snow, T. P., & Bierbaum, V. M. 2010c, ApJ., 723, 1325

Yang, Z., Martinez Jr., O., Carpenter, M. Y., Snow, T. P., & Bierbaum, V. M. 2010d, ApJ., manuscript in preparation

---

This preprint was prepared with the AAS LaTeX macros v5.2.

NASA LAW, October 25-28, 2010, Gatlinburg

Application of Symmetry-Broken H_2-H_2 Potential Energy Surface to Low Energy *o*-/*p*-H_2+HD Collisions of Astrophysical Interest

Renat A. Sultanov[1] & Dennis Guster

Department of Information Systems & BCRL at SCSU, St. Cloud, MN 56301

rasultanov@stcloudstate.edu, dcguster@stcloudstate.edu

Sadhan K. Adhikari

Instituto de Física Teórica, UNESP − Universidade Estadual Paulista, 01140 São Paulo, SP, Brazil

adhikari@ift.unesp.br

ABSTRACT

A possibility of correct description of non-symmetrical HD+H_2 collision at low temperatures (T≤300 K) is considered by applying symmetrical H_2-H_2 potential energy surface (PES) [Diep, P. & Johnson, K. 2000, J. Chem. Phys. 113, 3480 (DJ PES)]. With the use of a special mathematical transformation technique, which was applied to this surface, and a quantum dynamical method we obtained a quite satisfactory agreement with previous results when another H_2-H_2 PES was used [Boothroyd, A.I. et al. 2002, J. Chem. Phys. 116, 666 (BMKP PES)].

1. Introduction

The possible importance of the HD cooling in ISM was first noted by Dalgarno & McCray (1972). Because of the special properties of HD this molecule is even more effective cooler than H_2. This happens at low temperatures $T \leq 100$ K, where the cooling function of HD becomes ∼15 times larger than the H_2 cooling function, Dalgarno & McCray (1972). At higher temperatures H_2 molecules dominate the heating, however HD molecules dominate

[1]Corresponding author.

the kinetic process at lower temperatures. When H_2 is inefficient, HD becomes important in cooling the primordial gas and the ISM. In order to accurately model the thermal balance and kinetics of ISM one needs accurate state-to-state cross sections and thermal rate constants $k_{vj\to v'j'}(T)$. Theoretical state-resolved treatment requires precise PESs and a reliable dynamical method, Schaefer (1990). On the other hand, measurements of these cross sections is a difficult technical problem. Unfortunately, up to now no reliable experiments are available on HD+H_2, which has important astrophysical applications. Moreover, different calculations with various H_4 PESs showed very different results for thermal rate coefficients.

2. Method & Results

Below we briefly present our method to convert the symmetric DJ H_2-H_2 PES to be suitable for the non-symmetric system HD+H_2. The method is based on a mathematical approach, i.e. a geometrical rotation of the 3D space and the corresponding space-fixed coordinate system $OXYZ$, as shown in Fig. 1. The few-body system (1234), or H-H-H-H, can be characterized by four radius-vectors: $\{\vec{r}_1, \vec{r}_2, \vec{r}_3, \vec{r}_4\}$, or alternatively by so-called three Jacobi vectors: $\{\vec{R}_1, \vec{R}_2, \vec{R}_3\}$. Next, the initial geometry of the system is taken in such a way that the Jacobi vector $\vec{R}_3$ connects the center of masses of the two molecules and is directed over the OZ axis. We can also choose $OXYZ$ in such a manner that the Jacobi vector $\vec{R}_2$ lies in the X-Z plane. Finally, the vector $\vec{R}_1$ can be directed anywhere. Then the spherical coordinates of the Jacobi vectors are: $\vec{R}_1 = (R_1, \theta_1, \phi_{12})$, $\vec{R}_2 = (R_2, \theta_2, 0)$, and $\vec{R}_3 = (R_3, 0, 0)$. Thus the 4-body system H_2-H_2/HD can be fully determined with the use of six variables. However, the DJ PES has been prepared for the rigid monomer model of H_2-H_2, so actually we have only four active variables in this consideration: R_3, θ_1, θ_2, and ϕ_{12}. The surface is a multivariable function of the distance R_3 between two H_2 molecules, two polar angles $\theta_{1(2)}$ and one torsional angle ϕ_{12}. First we start with the original DJ PES. Then we replace one hydrogen atom "H" with a deuterium atom "D". Thus we break the symmetry by shifting the center of mass of one H_2 molecule to another point, that is from O_{H_2} to O_{HD} as shown in Fig. 1, we also need to take into account the difference between the number of rotational states in H_2+H_2 and HD+H_2. The length of the the vector $\vec{x}$ is $x = |\vec{R}_1|/6$. Now we rotate the $OXYZ$ coordinate system around the OY axis in such a way that the new OZ' axis goes through the point O_{HD}. The OY' axis and the old OY axis are parallel, and the angle of this small rotation is η, see Fig. 1. This transformation converts the initial Jacobi vectors in $OXYZ$: $\vec{R}_1 = \{R_1, \theta_1, \phi_{12}\}$, $\vec{R}_2 = \{R_2, \theta_2, 0\}$ and $\vec{R}_3 = \{R_3, 0, 0\}$ to the corresponding Jacobi vectors with new coordinates in the new $O'X'Y'Z'$: $\vec{R}'_1 = \{R'_1, \theta'_1, \phi'_{12}\}$, $\vec{R}'_2 = \{R'_2, \theta'_2, 0\}$ and $\vec{R}'_3 = \{R'_3, 0, 0\}$. As a result of this simple procedure we obtain a new surface, namely: $V_{DJ}^{\mathrm{H_2}}(R_3, \theta_1, \theta_2, \phi_{12}) \to \tilde{V}_{DJ}^{\mathrm{HD}}(R'_3, \theta'_1, \theta'_2, \phi'_{12})$. It is quite obvious, that the rotation does not

affect the coordinate function $V_{l_1,l_2,l}(R_3)$ in the DJ PES. Next, any rotation of the 3D $OXYZ$

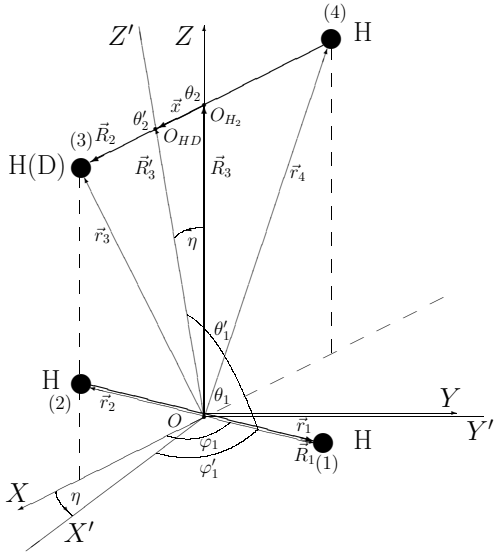

Fig. 1.— HD+H_2 in the framework of two different Cartesian coordinate systems.

coordinate system can be represented by Euler angles, i.e. $\{\alpha, \beta, \gamma\}$. In this paper we choose the following Euler angles: $\{\alpha = 0, \beta = \eta, \gamma = 0\}$. To calculate the rotational angle η in Fig. 1, one can consider the internal triangle $\triangle O_{HD}\ O\ O_{H_2}$. In such a way the rotation of the coordinate system from $OXYZ$ to $O'X'Y'Z'$ makes a corresponding transformation of the coordinates of the atoms in the 4-body system and the distance between two molecules. In the calculation of HD+H_2 with the DJ PES one has to use new coordinates $\theta_1', \theta_2', \phi_{12}', R_3'$. However, the potential has been expressed through the old H_2-H_2 variables, hence it is to be transformed to new variables. In Fig. 2 some of our preliminary results for elastic and rotational transitions in HD+H_2 are presented together with other results, Schaefer (1990).

Sponsors: Office of Sponsored Programs at SCSU & CNPq / FAPESP of Brazil.

REFERENCES

Dalgarno, A. & McCray, R. 1972, Ann. Rev. Astron. Astrophys., 10, 375.

Schaefer, J. 1990, Astron. Astrophys. Suppl. Ser., 85, 1101.

This preprint was prepared with the AAS LaTeX macros v5.2.

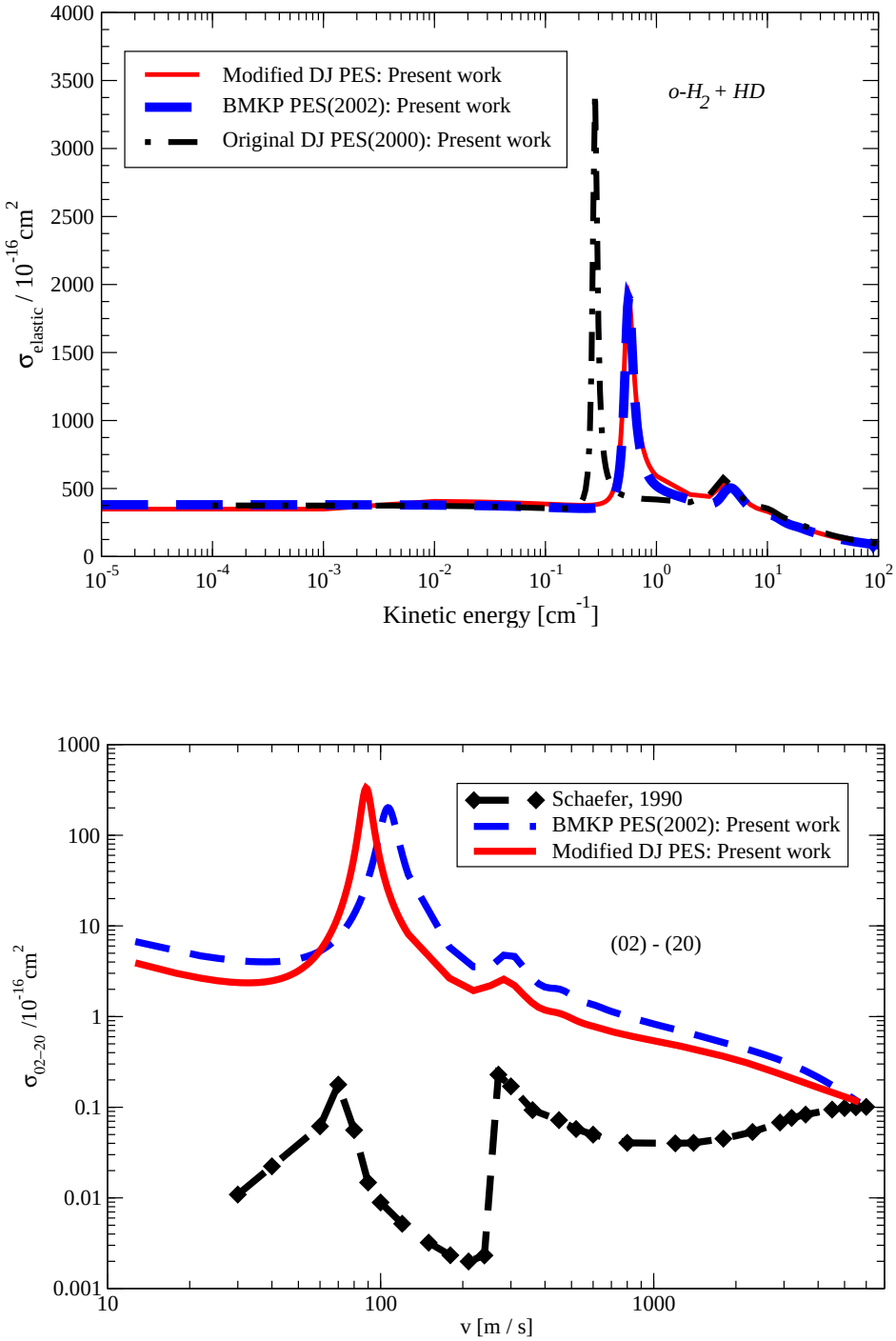

Fig. 2.— Low energy elastic scattering integral cross sections in o-H_2+HD (upper plot) and in rotational energy transfer: $HD(j_1 = 0)+H_2(j_2 = 2) \rightarrow HD(j_1' = 2)+H_2(j_2' = 0)$.

NASA LAW, October 25-28, 2010, Gatlinburg

Rovibrational quenching rate coefficients in collisions of He with HD

J. L. Nolte & P. C. Stancil

Department of Physics and Astronomy and Center for Simulational Physics, University of Georgia, Athens, GA 30602

T.-G. Lee

Allison Physics Lab, Auburn University, Auburn, AL 36849

N. Balakrishnan

Department of Chemistry, University of Nevada-Las Vegas, Las Vegas, NV 89154

R. C. Forrey

Department of Physics, Pennsylvania State University, Berks Campus, Reading, PA 19610

ABSTRACT

HD has been found to play an important role in the cooling of the primordial gas in the formation of the first stars and galaxies. The rate of cooling by HD molecules requires a knowledge of collision rate coeffcients with both H and He. In this study, we present rate coefficients for the He-HD collision system over a range of collision energies from 10^{-5} to 5×10^{3} cm^{-1}, obtained from fully quantum mechanical scattering calculations for initial HD rovibrational states of $j = 0$ and 1 for $v = 0$ to 17. We report our progress in these calculations, presenting rate coefficients for $\Delta v = 0$, -1, and -2 transitions.

1. Introduction

While H_2 has long been know to be the dominant coolant in the formation of the first stars, nevertheless the permanent dipole moment and low rotational constant of the other primary coolant HD mean that, in certain circumstances, HD cooling may dominate over H_2. Because of the smaller rotational energy level spacing and possibility of $\Delta j = \pm1$ transitions,

HD cooling may equal or surpass that of H_2 at high densities and low temperatures (see, e.g. Flower et al. 2000). Several studies over the past decade have investigated the role of HD cooling in various scenarios of star formation; for instance, it was recently shown that, for low mass (10^5 $M_\odot$) primordial halos, HD cooling may surpass the H_2 cooling rate, leading to the formation of relatively low mass stars (McGreer & Bryan 2008).

Detailed knowledge of collision rate coefficients is vital in determining the molecular contribution to the thermal balance, and models of star formation can only be as accurate as the molecular data provided. In this paper, therefore, we report our progress on the calculation of rovibrational de-excitation rate coefficients for the system HD-He, of which the most thorough previous study (Roueff & Zeippen 2000) was limited to only the first few vibrational levels.

2. Results

The inelastic collisional cross sections were obtained by solving the close-coupled scattering equations using the nonreactive scattering program MOLSCAT developed by Hutson & Green (1994) and employing the potential surface developed by Muchnick & Russek (1994). Rate coefficients are presented for Δv=0, -1, and -2 transitions.

Generally, $\Delta v = -1$ transitions dominate over $\Delta v = -2$, with the magnitude of cross section or rate coefficient decreasing with decreasing rotational number at low energy. Figure 1 illustrates this trend in rate coefficients, for $v_i = 10$, $j_i = 1$. In Figure 2 we show rate coefficients for the dominant case of $j_i = 1$, with $\Delta v = 0$, $\Delta j = -1$. In the calculation by Roueff & Zeippen (2000), only the first four vibrational levels and only four collision energies were used. We compare our results for the $v_i = 2$, $j_i = 0$ rovibrational levels in Figure 3. While agreement is good for lower v_f, the results begin to diverge for higher vibrational states, which may be due in part to a large difference in the size of basis sets and potential expansion terms, 90 basis states and 30 potential terms being included in our calculations, compared with 45 states and 15 expansion terms in Roueff & Zeippen (2000).

3. Conclusion

Collisional de-excitation rate coefficients for HD are needed to accurately model its role in cooling the primordial gas. Calculations for the entire range of vibrational states up to $v = 17$ will soon be completed, the results of which will be assembled into an online database of rate coefficients for He-HD collisions.

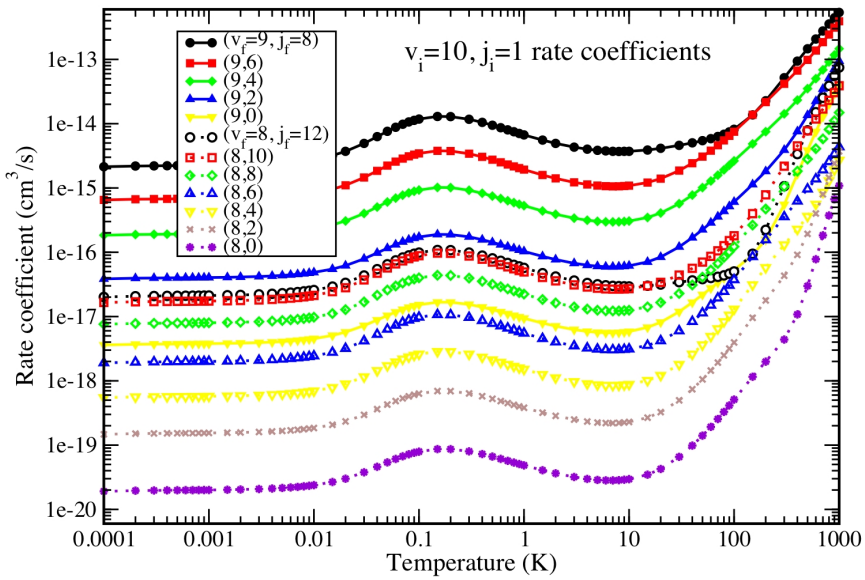

Fig. 1.— Rate coefficients for $v_i = 10$, $j_i = 1$. Only even j_f states are shown for clarity.

This work was supported in part by NASA Grant No. NNG06GJ11G and NSF Grant No. AST-0607733 (JLN and PCS); NSF Grant No. PHY-0855470 (NB); NASA Grant No. NNG05GD81G (TGL); NSF Grant No. PHY-0854838 (RCF).

REFERENCES

Flower, D. R., Le Bourlot, J., Pineau des Forêts, G., & Roueff, E., 2000, MNRAS, 314, 753

McGreer, I. D. & Bryan, G. L., 2008, ApJ, 685, 8

Roueff, E. & Zeippen, C. J., 2000, A&AS, 142, 475

Hutson, J. M. & Green, S., MOLSCAT computer code (distributed by Collaborative Computational Project No. 6 of the United Kingdom Engineering and Physical Sciences Research Council, Swindon, 1994), Version 14.

Muchnick, P., & Russek, A., 1994, J. Chem. Phys., 100, 4336

This preprint was prepared with the AAS LaTeX macros v5.2.

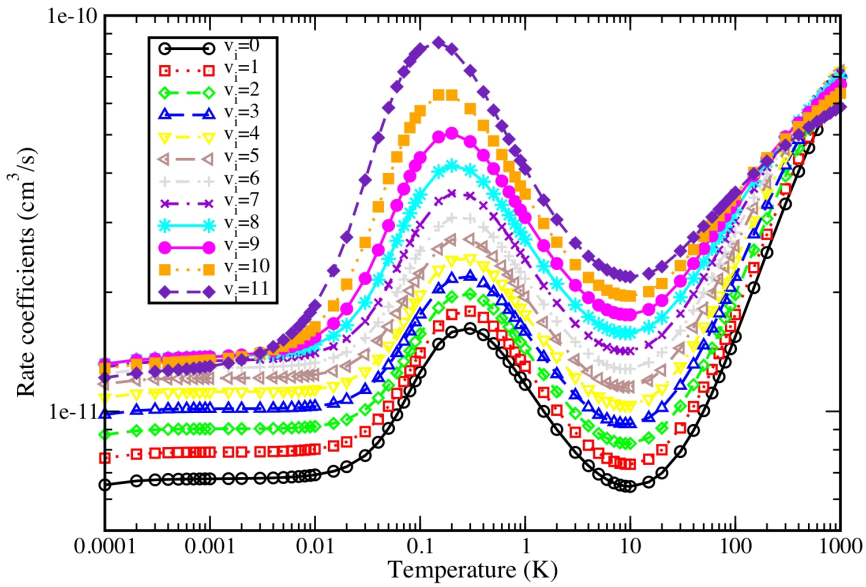

Fig. 2.— $\Delta v = 0$, $\Delta j = -1$ transitions for $j_i = 1$.

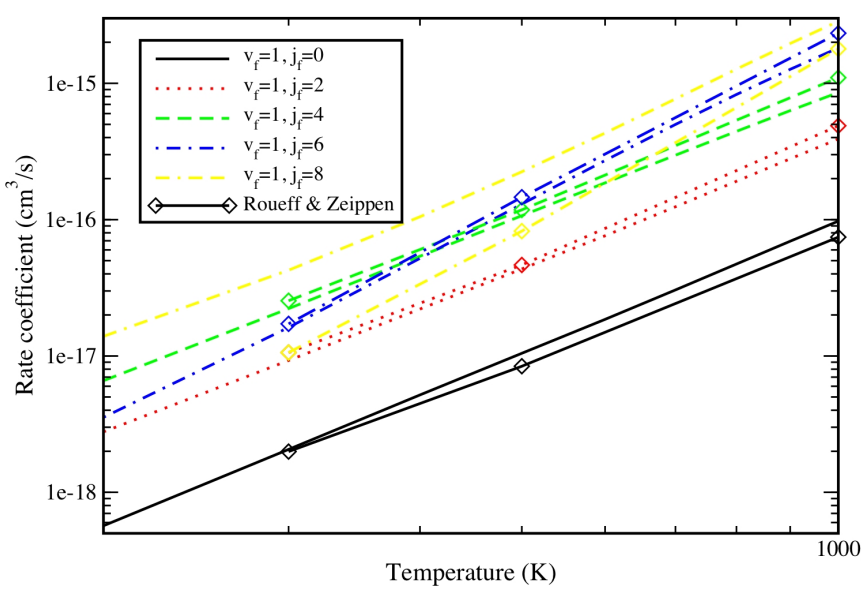

Fig. 3.— Comparison with Roueff & Zeippen (2000) for $v_i = 2$, $j_i = 0$ to $v_f = 1$ transitions.

NASA LAW, October 25-28, 2010, Gatlinburg

The Ion-Induced Charge-Exchange X-ray Emission Of The Jovian Auroras: Magnetospheric Or Solar Wind Origin?

Y. Hui, & D. R. Schultz

Physics Division, Oak Ridge National Laboratory Bldg. 6010, Oak Ridge, TN 37831, USA

huiy@ornl.gov, schultzd@ornl.gov

ABSTRACT

With the newly acquired charge-exchange cross sections for the solar abundant heavy elements (carbon, oxygen and sulfur) colliding with molecular hydrogen in a wide range of energies (0.01 – 50 MeV/u), we are able to construct a more comprehensive model of charge-exchange induced X-ray emission, due to ions precipitating into the Jovian atmosphere near the poles. We use this model to calculate the synthetic spectra of the Jovian polar X-rays and compare them to the observations from both *Chandra* and *XMM-Newton*. Because of the inclusion of carbon ions, in addition to the oxygen and sulfur ions previously considered (Kharchenko et al. 2006, 2008), the model fits to observed data could distinguish hypothetically the origin of the precipitating heavy ions either from Jovian magnetospheric surroundings or the injected solar wind in the polar areas. After comparing to the newly reprocessed *Chandra* observations (Hui et al. 2009), and also reassured by model fitting to the *XMM-Newton* observations (Hui et al. 2010), our model shows a negligible contribution from the carbon ions and therefore suggests that the highly accelerated precipitating ions are of magnetospheric origin.

1. Introduction

The first detection of X-rays from Jupiter was made by the Einstein observatory in the 1980s (Metzger et al. 2010). Since then, it has been clearly shown that the X-ray emission has two distinct components: one from the lower latitudes and the equatorial regions (the so-called disk component) which is attributed to the scattering and fluorescence of solar X-rays in the Jovian atmosphere, and the other from the high latitudes (north and south polar X-ray

auroras) which is thought to be charge exchange (CX) induced X-rays (<2 keV) that arise from energetic heavy ions that precipitate into the Jovian upper atmosphere (Branduardi-Raymont, et al. 2004, 2007; Elsner et al. 2005) (see Hui et al. (2010) and references therein).

Focusing on the soft X-ray emission from the Jovian auroras, the key question to ask is: What is the origin of the precipitating ions at the Jovian poles? Cravens et al. (2003) proposed two possible sources for the heavy ions that lead to the Jovian X-ray auroras: (1) solar wind ions entering into the magnetospheric polar cusps and (2) ambient sulfur and oxygen ions accelerated in the outer magnetosphere by large field-aligned potentials. Previous works (such as Kharchenko et al. (2006, 2008), in which only oxygen and sulfur ions were considered) are insufficient to distinguish between these two ion sources, so we have improved and extended our recent spectral model (Kharchenko et al. 2006, 2008) and added the contribution of carbon ions, the most abundant heavy element in the solar wind after oxygen, in order to make a distinction and seek better constraints on other characteristics such as the ion acceleration mechanism.

2. Method and Results

We developed a series of Monte Carlo simulations (Kharchenko et al. 2008) to treat the ion precipitation and charge exchange collisions during the ions deceleration through the atmosphere, using collision probabilities for the three major channels, and resulting in the CX collision number distribution, $N_{CX}(E, q)$. We calculated, meanwhile, the radiative transition matrices, which describe the pathway from any initial state to any final state of a charge exchange excited ion (Kharchenko et al. 1998; Kharchenko & Dalgarno 2000) and determined the final synthetic spectrum, using state-selective CX cross sections and $N_{CX}(E, q)$, which yielded the synthetic spectrum (see Fig. 1(a) for an example). We then calculated a series of synthetic spectra with a grid of initial ion energies for carbon, oxygen and sulfur, which are bundled in an Xspec (v12) model. By retrieving the high-resolution spectra from *Chandra* and *XMM-Newton*, reprocessing when necessary, we fitted the model to these observed data giving results, for example, such as those in Table 1 and Fig. 1(b).

Our work has compared model fits for both *Chandra* and *XMM-Newton* observations of the Jovian polar aurora, demonstrating from the inferred precipitating ion energies and relative abundances for each spectral observation that they are significantly variable in time (observation date) and space (north and south polar X-ray aurora). The work has also extended our preliminary analysis of only the *Chandra* spectra (Hui et al. 2009), which used the new synthetic spectra model briefly described here, that showed the relatively unimportance of including carbon in the model implying a magnetospheric origin for the ion

precipitation rather than from the solar wind.

Table 1: Spectral fitting of the north and south polar spectra of *Chandra* observations 3726 and 4418 without carbon. All uncertainties are computed with $\Delta\chi^2 = 2.706$, equivalent to 90% confidence for a single parameter. "$*$" in the errors means that the parameter is not bounded in that direction. The superscript outside of the bracket represents the power of 10. See Hui et al. (2009) for descriptions and discussion of the results tabulated here.

OBS ID	$E_{\rm O}$ (MeV/amuu)	$E_{\rm S}$ (MeV/amu)	$A_{\rm S}$	NORM	Red. χ^2 [DOF]
North 3726	$1.48^{+*}_{-0.28}$	$0.81^{+0.48}_{-0.45}$	5^{+243}_{-3}	$(1.06^{+0.52}_{-0.32})^{-6}$	0.64 [13]
North 4418	$2.00^{+*}_{-0.37}$	$0.98^{+0.26}_{-0.42}$	$2.5^{+2.6}_{-1.3}$	$(7.3^{+1.2}_{-0.8})^{-7}$	1.05 [19]
South 3726	$2.00^{+*}_{-0.66}$	$1.52^{+*}_{-0.81}$	$1.5^{+4.3}_{-1.0}$	$(3.3^{+4.4}_{-0.8})^{-7}$	1.29 [6]
South 4418	$2.00^{+*}_{-0.47}$	$0.68^{+0.64}_{-0.24}$	17^{+94}_{-16}	$(4.2^{+1.0}_{-0.6})^{-7}$	1.43 [11]

We gratefully acknowledge our many collaborators on this work: V. Kharchenko (U. Conn. & CfA), A. Dalgarno (Harvard & CfA), P.C. Stancil (U. Georgia), A. Bhardwaj (Vikram Sarabhai Space Center), G. Branduardi-Raymont (U. College London), T. Cravens (U. Kansas), and C. Lisse (APL). This work has been supported by NASA Planetary Atmospheres Program Grant NNH07AF12I.

REFERENCES

Branduardi-Raymont, G. et al. 2004, Astron. Astrophys., 424, 331

Branduardi-Raymont, G. et al. 2007, Astron. Astrophys., 463, 761

Cravens, T. E. et al. 2003, J. Geophys. Res., 108(A12), 1465

Elsner, R. F. et al. 2005, J. Geophys. Res., 110, A01207

Hui, Y.-W., Schultz, D. R., Kharchenko, V., Stancil, P. C., Cravens, T. E., Lisse, C. M. & Dalgarno, A. 2009, Astrophys. J., 702, L158

Hui, Y., Schultz, D. R., Kharchenko, V. A., Bhardwaj, A., Branduardi-Raymont, G., Stancil, P. C., Cravens, T. E., Lisse, C. M. & Dalgarno, A. 2010, J. Geophys. Res., 115, A07102

Kharchenko, V., Liu, W. & Dalgarno, A. 1998, J. Geophys. Res., 103, 26687

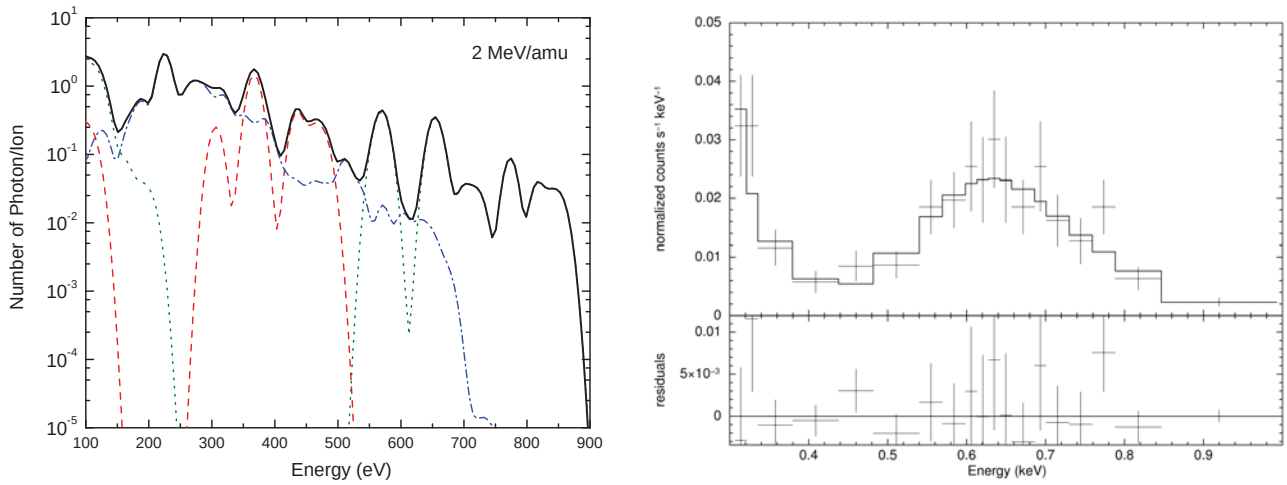

Fig. 1.— (a.) LEFT – Synthetic spectra for $E_{init} = 2$ MeV/amu. The elemental abundances are equal and the initial charge state is one. Contributions from carbon, oxygen, and sulfur are indicated by the red dashed, green dotted, and blue dashed-dotted curves, respectively. The total spectrum is given by the solid black curve. The line width is chosen to be 10 eV. (b.) RIGHT – Fits to the spectrum of the north polar X-ray aurora observed by *chandra* (observation ID 3726) neglecting carbon in the CX model.

Kharchenko, V. & Dalgarno, A. 2000, J. Geophys. Res., 105, 18351

Kharchenko, V., Dalgarno, A., Schultz, D. R. & Stancil, P. C. 2006, Geophys. Res. Lett., 33, L11105

Kharchenko, V., Bhardwaj, A., Dalgarno, A., Schultz, D. R. & Stancil, P. C. 2008, J. Geophys. Res., 113, A08229

Metzger, A. E., et al. 1983, J. Geophys. Res., 88, 7731

This preprint was prepared with the AAS LaTeX macros v5.2.

NASA LAW, October 25-28, 2010, Gatlinburg

Measurement and Calculation of Absolute Charge-Exchange and Electron-Impact Excitation Cross Sections for Highly-Charged Ions

A. Chutjian[1], J. Simčič

Atom. & Molec. Phys. Group,JPL/Caltech, Pasadena CA 91109 USA

I. Čadež

Josef Stefan Inst., 1000 Ljubljana, Slovenia

J. B. Greenwood

Physics Department, Queens University, Belfast BT7 1NN, UK

C. M. Lisse

Space Dept., APL/JHU, Laurel, MD 20732 USA

R. J. Mawhorter

Department of Physics and Astronomy, Pomona College, Claremont, CA 91711 USA

B. V. McKoy, C. Winstead

Department of Chemistry, California Institute of Technology, Pasadena, CA 91125

D. R. Schultz

Physics Division, Oak Ridge National Laboratory, Oak Ridge, TN 37831-6372 USA

S. J. Smith

Physics Department, Indiana Wesleyan University, Marion, IN 46953 USA

S. S. Tayal

Physics Department, Clark Atlanta University, Atlanta, GA 30314 USA

[1]ara.chutjian@jpl.nasa.gov

ABSTRACT

Electron-impact excitation of highly-charged ions (HCIs), and HCI-neutral charge exchange play fundamental roles in planetary and solar/stellar atmospheres. For collisions of solar- and stellar-wind ions with planetary exospheres, comets, and circumstellar clouds, we report absolute cross sections for single, double, triple, and quadruple charge exchange of Fe^{q+} (q=5-13) ions with CO, CO_2, and H_2O at a collision energy of 7q keV (and one pentuple charge exchange cross section in the Fe^{9+}-H_2O collision). Experimental results are compared with new results of the n-electron classical trajectory Monte-Carlo approximation. Also presented are preliminary absolute excitation cross sections in the $3s\ ^2S \rightarrow 3p\ ^2P^o$ transitions in S^{5+} for the Io Torus; and in the $^4S^o_{3/2} \rightarrow {}^2D^o_{3/2,5/2}$ transitions in Fe^{11+} for solar and stellar plasma simulations. Comparisons are made with available results from Distorted Wave and R-Matrix theoretical calculations.

1. Introduction

Progress in detection of solar and stellar X-ray emissions,including interactions involving the solar wind (SW), has allowed one to address the collisions of highly charged ions (HCIs) in solar/stellar atmospheres and in the SW with electrons, planetary exospheres, and comets. For SW collisions the resulting X-rays are produced through charge exchange (CEX) between the SW-HCI and the neutral target. The neutral species are components of planetary exospheres, their moons, and the geocorona; as H and He that stream in from the ISM; and as atoms and molecules that desorb from a comet as it approaches the Sun. The three ingredients required for mapping the X-ray emissions are the SW composition, the neutral target composition, and knowledge of CEX cross sections. Reported herein are measurement of absolute single- and multiple the CEX cross sections. These data are coupled with theoretical calculations in order to corroborate experiment, and to establish trends in charge transfers and autoionizations leading to the final HCI charge states. A dramatic example of X-ray emissions recorded by Chandra at the exosphere of Venus is shown in [Denn (2008)]. There are two sources of X-rays: one is that of strong elastic and fluorescent scattering of solar X-rays. These mask the second source, the weaker line emissions from the SW-CEX process. However, when Venus was viewed during solar minimum the fluorescent scattering component was diminished, and one could observe the weak CEX component. The specie relevant to this study is the tenuous CO_2 atmosphere at altitudes of $\sim$125 km. Another source of X-rays is comet X-ray emissions observed by Chandra at Comet 8P/Tuttle

[Chrst (2010)] as Tuttle approached the Sun. Here, unlike at Venus, the X-rays are entirely SW-CEX in origin: fluorescent scattering is negligible due to the thin comet atmosphere, and CEX dominates by virtue of its larger cross section.

2. Results

In the following are presented a few of many measurements of absolute CEX cross sections relevant to X-ray emissions from planetary, cometary, and interplanetary regions. Experimental absolute cross sections were determined for single and multiple charge exchanges of Fe^{5-13+} ions with CO, CO_2, and H_2O [Sim (2010a,b)]. Shown in Fig. 1 are CEX cross sections for the Fe ions with H_2O in which three electrons are transferred from the target to the Fe projectile. One sees good agreement between the experimental results and results of the n-electron classical trajectory Monte-Carlo (nCTMC) theory that includes Auger and cascade contributions [Sim (2010b)]. For the problems of SW interactions with planetary He and interstellar He^{2+}, shown in Fig. 2 are JPL results for single CEX compared with previous measurements. Care was taken in the measurements to account for the full angular distribution of the outgoing He^{+} ions, as well as to simulate the target He gas density distribution near the entrance and exit apertures of the collision gas cell [Mawh (in prep.)].

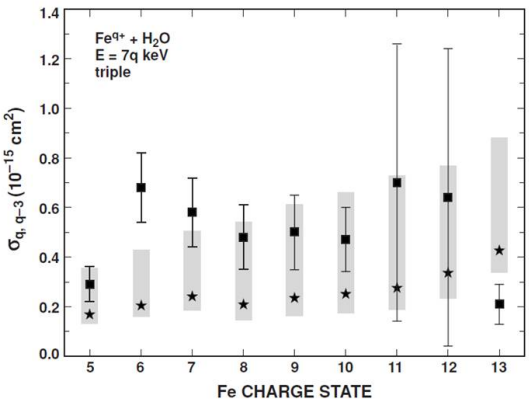

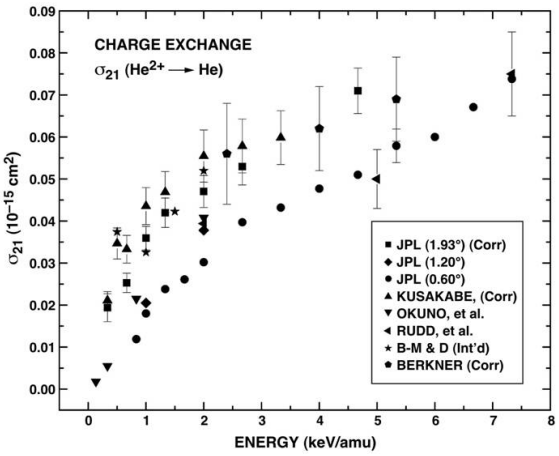

Fig. 1.—: (Left) Results of the nCTMC calculation and radiative/Auger cascade calculation for CEX in Fe^{5-13+} collisions with H_2O (★), compared with the JPL cross sections (■) [Sim (2010b)]. Errors are the maximum estimated uncertainty in the cascade model.

Fig. 2.—: (Right) Absolute CEX cross sections for He^{2+} ions on He. Comparisons are given with other experimental values. Details will be given in [Mawh (in prep.)].

Electron excitation of HCIs and the subsequent plasma-cooling photon radiation are

central to‘ the plasma properties of the solar/stellar atmospheres, and the Io torus. Accurate cross sections are also needed to validate the use of transitions as part of a temperature- or density-sensitive line ratio. Highly-charged S and Fe ions are prominent in many solar/stellar objects. However, only scattered measured data are available on collision strengths for allowed or forbidden transitions. Shown in Fig. 3 are recent JPL results on excitation of the $^2S \rightarrow {}^2P$ transition in S^{5+}, with threshold at 13.2 eV . The results are in good agreement with both a distorted-wave [Flwr (1975)], and an 11-state R-Matrix calculation [Kimr (1998)]. Benchmarking of theory by experiment validates theory so that it can be used to calculate collision strengths that have not been, or are too difficult to measure experimentally.

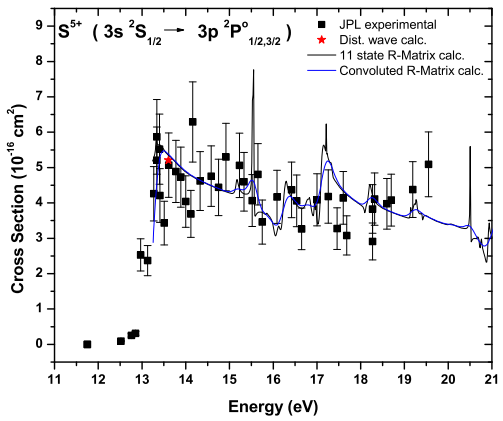

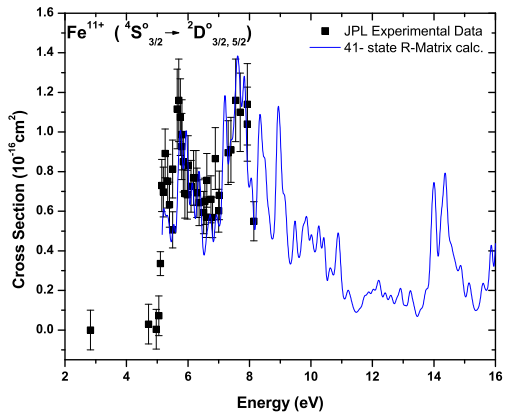

Fig. 3.—: (Left) Preliminary results for absolute excitation cross sections in the $^2S \rightarrow {}^2P$ transition in S^{5+}. Shown are the JPL data (■), results of a distorted-wave calculation (★) [Flwr (1975)], an 11-state R-Matrix calculation (–) [Kimr (1998)], and the 11-state calculation convoluted with a 125 meV electron-energy width of the JPL results (–).

Fig. 4.—: (Right) Preliminary results for cross sections in the $^4S^o \rightarrow {}^2D^o$ transition in Fe^{11+}. Shown are the JPL data (■) and results of a 41-state R-Matrix calculation (–) [Stor (2005)].

The Fe^{11+} ion transitions play a key role in determining the populations of excited levels of the ground configuration through collisional excitation and radiative cascade. Emissions at κ Ceti have been observed by FUSE, magnetic dipole transitions are detected by STIS/HST at the dwarf star ϵ Eri, and transient Fe XII jets have been observed by EIT/SOHO. Shown in Fig. 4 are recent JPL results for excitation of the forbidden $^4S^o \rightarrow {}^2D^o$ transition. Comparison is made with a 41-state R-Matrix calculation. One sees good agreement, especially with the resonance structures at 5.2 eV, 5.5 eV, and 7.5 eV.

This work was supported at JPL/Caltech by NASA through agreement with the Caltech.

REFERENCES

D. J. Christian et al., 2010, Ap. J., Suppl. Ser. 187, 447

K. Dennerl, 2008, Planet. Space Sci. 56, 1414

D. R. Flower & H. Nussbaumer, 1975, A&A 42, 265

E. Kimura et al., 1998, A&A, Suppl. Ser. 132, 99

R. J. Mawhorter et al., Phys. Rev. A (in preparation)

J. Simčič et al., 2010a, Phys. Rev. A 81, 062715

J. Simčič et al., 2010b, Ap. J. 722, 435

P. J. Storey et al., 2005, A&A 433, 717

This preprint was prepared with the AAS LaTeX macros v5.2.

NASA LAW, October 25-28, 2010, Gatlinburg

A novel merged beam apparatus to study the cosmic origins of organic chemistry

M. Garrido, A. P. O'Connor, K. A. Miller, & D. W. Savin

Columbia Astrophysics Laboratory, Nevis Laboratories, Columbia University, Irvington, NY 10533, USA

mgarrido@astro.columbia.edu

X. Urbain

Institute for Condensed Matter and Nanosciences, Université Catholique de Louvain, B-1348, Louvain-la-Neuve, Belgium

ABSTRACT

Reactions of atomic carbon with molecular ions play a critical role for gas phase molecular formation in interstellar clouds. These interactions are the first links in the chain of chemical reactions leading to the synthesis of complex organic species. Much of our knowledge of this process is through spectroscopic observations and theoretical models. However, our understanding of this chemistry is constrained by uncertainties in the underlying reaction rate coefficients. Data from quantum calculations are limited to reactions involving three or fewer atoms. Meanwhile, previous experimental studies have been hampered by the difficulty in generating a sufficiently intense and well characterized neutral carbon beam. To address these issues and to study these reactions experimentally, we are building a novel laboratory device which does not suffer from such limitations.

1. Introduction

The cosmic pathway towards life is thought to begin in molecular clouds when atomic carbon is fixed into molecules (Herbst 1995). These reactions initiate not only the formation of organic molecules in the cosmos, but also provide some of the first threads knitting atoms and molecules into solid material. Such processes are critical for the eventual formation of

planets and may determine a major component of the organic chemistry that is present on their young surfaces.

Space-based observations of molecular lines are used extensively to understand the molecular universe and its role in the chemical pathway towards life. Interpreting spectral observations from these facilities requires the use of sophisticated astrochemical models (Wakelam et al. 2006; Woodall et al. 2007). However, our chemical understanding of the universe is limited to a large degree by uncertainties in the atomic and molecular data used in the astrochemical models.

To address these astrochemical needs we are constructing a novel device to study gas-phase chemical reactions involving neutral atomic C and molecular ions. Our understanding for these reactions is extremely poor. Experimentally this is because of the difficulty in producing a sufficiently intense and well characterized beam of carbon atoms (Savić et al. 2005). Theoretically this is because fully quantum mechanical calculations of chemical reactions for molecular systems with four or more atoms are still not yet computationally feasible (Bettens & Collins 1998).

The initial steps in the carbon chemistry of molecular clouds begin with reactions involving C and C^+. For our proof-of-principle measurement, we propose to study the reaction

$$C + H_3^+ \rightarrow CH^+ + H_2. \tag{1}$$

H_3^+ is ubiquitous in both diffuse and dense molecular clouds (Geballe 2006; McCall 2006), thereby making reaction 1 one of the first steps towards organic chemistry in molecular clouds (e.g., van Dishoeck 1998). No measurements for this reaction exist at temperatures relevant for molecular clouds; and the uncertainty in the rate coefficient is at least a factor of 5 (see Figure 1).

2. Apparatus Description

Using a negative ion sputter source, we will produce a 30 keV C^- beam. We will cross a 2 kW diode laser at 808 nm with the C^- beam at an angle of 2.7° (similar to the arrangement of Kreckel et al. 2010a). The resulting ∼21 cm overlap length will convert ∼10% of the C^- beam into a ground term $C(^3P_J)$ beam. The population of the J levels will mimic that of molecular clouds. The C^- beam will then be electrostatically removed, leaving behind a pure neutral C beam.

We will use a duoplasmatron source to generate a 7.5 keV beam of H_3^+. Initial studies will be carried out using this hot H_3^+ ion source. Future upgrades will replace this with a

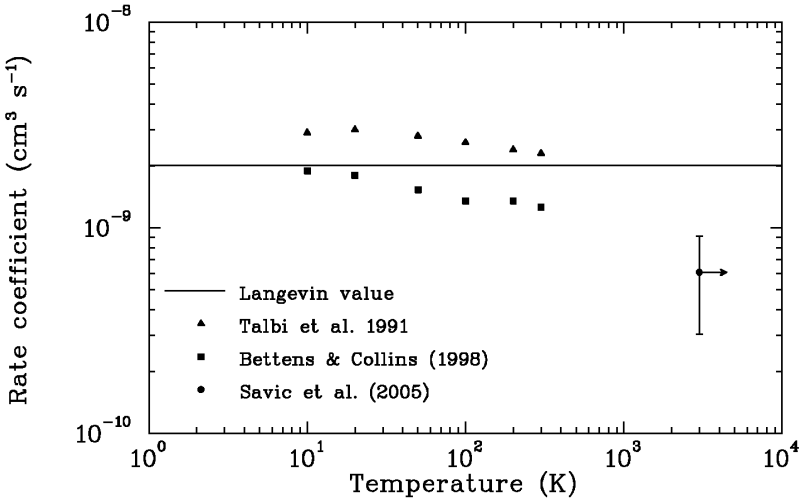

Fig. 1.— Rate coefficients for the reaction 1 showing the Langevin value and the classical trajectory theoretical results of Talbi et al. (1991) and Bettens & Collins (1998). The experimental result from Savić et al. (2005) on D_3^+ has been scaled by the reduced masses of the C/H_3^+ and C/D_3^+ systems.

cold molecular ion source. The H_3^+ beam will be merged electrostatically with the C beam for an interaction length of ∼1 m. Because the beams will co-propagate, we will be able to achieve the low relative collision energies required to study collisions at molecular cloud temperatures.

Chemical reactions will occur throughout the interaction length. Using low density beams and low background pressures ensures that multiple collisions have an insignificant effect on the measured reactions. As a result of using fast beams, the angular spread of the reaction products will be strongly compressed in the forward direction, allowing their 4π detection on a small surface with standard detector technology.

The end of the interaction region will be determined by the first in a series of parallel electrostatic plates, together called a chicane. The first set will be used to demerge the H_3^+ from the heavier C and CH^+ beams. The H_3^+ will be directed into a Faraday cup. The chicane will remerge the CH^+ beam with the C beam. Both beams will then be directed into an electrostatic energy analyzer (similar to that described in Kreckel et al. 2010b). The neutrals will pass through the analyzer and be collected in a calibrated neutral particle current detector. The CH^+ will be directed into a channel electron multiplier with a detection efficiency of nearly 100%. Reactions between the 7.5 keV H_3^+ and 30 keV C will produce 32.5 keV CH^+. Stripping of C off the background gas will produce 30 keV C^+. The energy analyzer will allow us to select against this background, so that it does not swamp the desired

CH^+ signal. Standard beam chopping techniques will be used to collect data and extract the signal from the background.

3. Conclusion

We are developing a unique instrument for studying chemical reactions with atomic C, which will not suffer from the limitations of previous experimental methods. Measuring all the relevant currents, beam shapes, energies, signal counts, and background rates will enable us to determine absolute cross sections. Our innovative apparatus will provide important laboratory data for interpreting molecular cloud spectra in the visible, infrared, and radio regions of the spectrum.

This was supported in part by the NSF Divisions of Astronomical Sciences.

REFERENCES

Bettens, R. P. A., & Collins, M. A. 1998, J. Chem. Phys., 108, 2424. Erratum, 114, 6490

Geballe, T. R. 2006, Phil. Trans. R. Soc. A, 364, 3035

Herbst, E. 1995, Ann. Rev. Astron. Astophys., 46, 27

Kreckel, H., Bruhns, H., Cízek, M., Glover, S. C. O., Miller, K. A., Urbain, X., & Savin, D. W. 2010a, Science, 329, 69

Kreckel, H., Bruhns, H, Miller, K. A., Wåhlin, E., Davis, A., Höckh, S., & Savin, D. W. 2010b, Rev. Sci. Instrum., 81, 063304

McCall, B. J. 2006, Phil. Trans. R. Soc. A, 364, 2953

Savić, I., Čermák, I., & Gerlich, D. 2005, Int. J. Mass Spectrom., 240, 139

Talbi, D., DeFrees, D. J., Egolf, D. A., & Herbst, E. 1991, Astrophys. J., 374, 390

van Dishoeck, E. F. 1998, The Molecular Astrophysics of Stars and Galaxies, T. W. Harquist & D. A. Williams, Oxford: Clarendon Press, 53

Wakelam, V., Herbst, E., & Seleis, F. 2006, Astron. Astrophys., 451, 551

Woodall, J., Agundez, M., Markwick-Kemper, A. J., & Millar, T. J. 2007, Astron. Astrophys., 466, 1197

NASA LAW, October 25-28, 2010, Gatlinburg

Laser Spectroscopy of CH_2^+ and Its Deuterated Species in the Near Infrared

Haiming Wang, Christopher P. Morong, Maria Kleshcheva, & Takeshi Oka

Department of Chemistry, Department of Astronomy & Astrophysics, and the Enrico Fermi Institute, University of Chicago, Chicago, IL 60637

haiming@uchicago.edu, mak@uchicago.edu, cmorong@uchicago.edu, t-oka@uchicago.edu

ABSTRACT

CH_2^+ and its deuterated species are potentially very useful astrophysical probes and are an interesting subject for theoretical studies due to their unique intramolecular dynamics. Using He-dominated (∼10 Torr) liquid-N_2 cooled plasmas containing a small amount (∼0.1 Torr) of reagent gas selected from CH_4, CD_4, CH_2D_2, and a 1:1 mixture of CH_4+CD_4, we have measured the spectra of CH_2^+, CD_2^+ and CHD^+ in the near infrared from 11,000 cm^{-1} to 12,500 cm^{-1} with our Ti:sapphire laser spectrometer that combines velocity modulation and phase modulation with heterodyne detection for near shot-noise-limited sensitivity. Several low-lying rovibrational bands of CD_2^+ and CHD^+ have been measured based on the theoretical predictions by Bunker and colleagues.

1. Introduction

Laboratory spectroscopy of deuterated molecular ions is essential for observing them in interstellar space and thus for understanding interstellar deuterium ion chemistry–a significant area in astrochemistry developed from observations of many highly deuterated species in prestellar cores and protostars in recent years (Roberts et al. (2003)). Aiming at providing approximate rotational constants for laboratory millimeter and submillimeter spectroscopists to measure rotational spectra of deuterated molecular ions and thus to aid radio astronomers in detecting the deuterated species in space, we have been studying the laboratory rovibronic spectra of simple deuterated molecular ions. CH_2^+ is of particular interest as our target ion because it is an intermediate between the observed abundant CH^+ and yet to be observed

but very important CH_3^+ in interstellar chemistry. The well established abundance of CH^+ suggests an abundance of CH_2^+ just like the recently discovered OH^+ and H_2O^+ (Gerin et al. (2010)), although our search for interstellar CH_2^+ based on our infrared (Rosslein et al. (1992)) and near-infrared (Gottfried & Oka (2004)) laboratory spectra has not yet been successful. Like the case of CH_3^+, radio observation of deuterated species may be more realistic than observing the optical spectra. CH_2^+ and its deuterated species are also of special interest for theoretical studies because of their unique intramolecular dynamics, i.e., the Renner-Teller interaction and quasi-linearity (Bunker (2007a)).

2. Experimental

The spectra were recorded in the NIR using a spectrometer based on a Ti:sapphire laser which has been described in detail elsewhere (Gottfried et al. (2003) and Morong et al. (2009)). A combination of frequency modulation via an electro-optic modulator (EOM) at 500 MHz with heterodyne detection, and velocity modulation via an AC discharge at 19 kHz with bidirectional optical multi-passing yields a second derivative Gaussian line shape and allows us to conduct spectroscopy with near shot-noise-limited sensitivity. The AC discharge velocity modulates only the ions and provides charge discrimination, while keeping the neutrals unaffected. For most of the lines it took approximately one hour to scan 5 cm^{-1} to obtain sufficient S/N for a conclusive identification.

To produce the molecular ions, a positive column discharge in a triply jacketed glass tube was used. The innermost tube contains the plasma which is cooled ($T_{rot} \sim 600$ K) by liquid nitrogen contained in the middle jacket. The outer jacket is held under vacuum to provide thermal insulation. By mixing a 10-Torr He buffer and 0.1-Torr reagent gases, and applying a 200-mA (rms) AC current, the desired molecular ions were produced efficiently in the plasma cell. It is believed that meta-stable helium (He^*) which has a long lifetime is the dominant ionization mechanism in our plasmas. The CD_2^+ is formed via He^* Penning ionization of CD_4 via the exothermic reaction $CD_4 + He^* \rightarrow CD_2^+ + He + 2D + e^-$. In reality the other ions, CD_4^+, CD_3^+ are also formed but do not have transitions in the NIR. CD^+ is not formed because the reaction is endothermic.

3. Results and Discussion

The absorption spectra of CH_2^+ and its deuterated species were scanned between 11,000 cm^{-1} and 12,500 cm^{-1}. A typical section of the spectra is shown in Fig. 1.

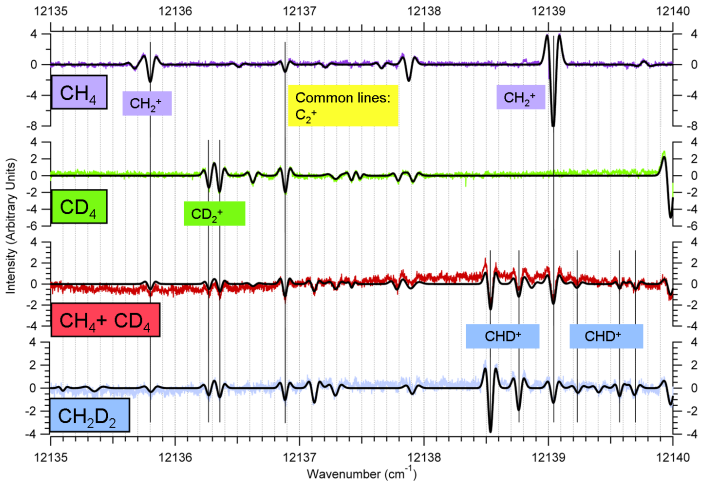

Fig. 1.— Comparison of the scanned spectra with different reagent gases (from top to bottom: CH_4, CD_4, CH_4+CD_4, and CH_2D_2) to discriminate the CD_2^+ and CHD^+ lines against CH_2^+ lines and those of interfering ionic impurities, such as C_2^+.

By comparing the spectrum of deuterated methane with that of normal methane under the same plasma conditions, one can clearly discriminate the CD_2^+ and CHD^+ lines against CH_2^+ lines and those of interfering ionic impurities. The most significant impurity lines are from C_2^+ and this has been confirmed by a comparison with a CO/He plasma which was used to study C_2^+ in the visible region (Tarsitano et al. (2004)). As one can see, the intensities of the signals are comparable between the two lower traces indicating that CHD^+ was successfully created in both the CH_2D_2 and the 1:1 mixture of CH_4 and CD_4. This result resolved a longtime puzzle on the production mechanism of molecular ions, especially for the intensively studied CH_2^+. It clearly shows that the production of CH_2^+ is not a simple one-step Penning dissociative ionization but is a more complicated multiprocess scrambling of protons.

The assignment of the recorded lines is a difficult issue. Unlike the previous work on CH_2^+ in the NIR which had mid-IR data to make lower state combination differences, there is essentially no prior experimental data on CD_2^+ and CHD^+ to compare with to verify the assignments. Furthermore, the Renner-Teller interaction is unpredictable except by detailed *ab initio* theory and we were reliant on the theoretical predictions by Bunker and others to focus our search (Bunker (2007b)). However, the asymmetric rotor spectral pattern, the 2:1 intensity alteration for CD_2^+ due to spin statistics, and combination differences of the observed spectral lines can be employed to assign the rotational structure. Based on these assignments, the ground-state rotational constants and the centrifugal distortion constants can be calculated via a least-squares fit of the combination differences of the P and R

branches of the corresponding transitions.

4. Conclusion

One isolated vibronic band, $\tilde{A}(0,5,0)^1 \leftarrow \tilde{X}(0,0,0)^0$, and two overlapped bands, $\tilde{A}(0,5,0)^0 \leftarrow \tilde{X}(0,0,0)^1$ and $\tilde{A}(0,4,0)^2 \leftarrow \tilde{X}(0,0,0)^1$ bands of CD_2^+ have been identified and analyzed (Wang et al. (2007, 2008)). The $\tilde{A}(0,4,0)^1 \leftarrow \tilde{X}(0,0,0)^0$ band of CHD^+ has been recently measured and is being assigned. The details of the analysis will follow soon in an upcoming paper (Wang et al. (2011)).

This work was supported by NASA Grant No. NMO711043.

REFERENCES

Roberts H., Herbst E., and Millar T. J. 2003, ApJ, 591, L41

Gerin M. et al. 2010, Astronomy & Astrophysics, 518, L110

Rösslein, M., Gabrys, C. M., Jagod, M.-F., and Oka, T. 1992, J. Mol. Spectrosc., 153, 738

Gottfried, J. L., and McCall, B. J., and Oka, T. 2003, J. Chem. Phys., 118, 10890

Gottfried J. L., & Oka, T. 2004, J. Chem. Phys., 121, 11527

Morong, C. P., Gottfried, J. L. and Oka, T. 2009, J. Mol. Spectrosc., 255, 13

Tarsitano, C. G. and Neese, C. F. and Oka, T. 2004, J. Chem. Phys., 121, 6290

Wang H.-M., Morong C. P., and Oka, T. 2007, 2008, 62nd, 63rd OSU International Symposium on Molecular Spectroscopy, MJ02 (2007) and WG04 (2008)

Wang H.-M., Morong C. P., and Oka, T. 2011, to be submitted to Journal of Molecular Spectroscopy

Bunker, P. R., Kraemer, W. P., Yurchenko, S. N., Thiel, W., Neese, C. F., Gottfried, J. L., and Jensen, P. 2007, Mol. Phys., 105, 1369

Bunker, P. R. 2007, private communication.

This preprint was prepared with the AAS LaTeX macros v5.2.

NASA LAW, October 25-28, 2010, Gatlinburg

Spectroscopic line parameters of $^{14}NH_3$ at 1.5 μm

Keeyoon Sung and Linda R. Brown

Science Division, Jet Propulsion Laboratory,
California Institute of Technology, Pasadena, CA 91109

ksung@jpl.nasa.gov, lrbrown@jpl.nasa.gov

ABSTRACT

Ammonia (NH_3) is one of the major opacity sources in the atmosphere of outer planets, low mass brown dwarfs, and possibly extrasolar planets, particularly in the 1.5 μm region (the *H*-band). Spectroscopic information of NH_3 in this region, however, is completely missing in the HITRAN database. In order to remedy deficiency of the spectroscopic data in the 1.5 μm region, we analyze the laboratory spectra recorded with the McMath-Pierce Fourier transform spectrometer (FTS) on Kitt Peak Observatory in Arizona. Preliminary results are discussed for a few lines, which includes their line positions, strengths, lower state energies, and quantum assignments. The full analysis is in progress.

1. Introduction

Ammonia (NH_3), one of the earliest molecules detected in Jupiter (**?**), is ubiquitous in Jovian atmospheres, constituting the major source for opacity. It is also a significant opacity source at 1.5 μm (the *H*-band) for the atmospheres of ultra-cool (T $<\backsim$600 K) brown dwarfs (**?**) and Extrasolar Giant Planets (EGPs, known as 'hot Jupiters'); in these atmospheres, NH_3 is considered to be an important nitrogen (N) carrier. The spectroscopic importance of the NH_3 bands in this region relative to that of three most abundant telluric species (CO_2, H_2O, and CH_4) is illustrated in Fig. 1, where a laboratory spectrum of NH_3 recorded with the McMath-Pierce Fourier transform spectrometer (FTS) on Kitt Peak Observatory is compared with their synthetic spectra at the same conditions. Delorme et al.(2008) pointed out that these bands can be used to characterize low mass brown dwarfs. They reported *H*-band spectrum of four cool brown dwarfs (Fig. 8 in their work) shows variations in the blue side of the *H*-band flux, implying the spectral variation can be used as an indicator of a

Fig. 1.— Laboratory NH_3 spectrum (bottom panel), compared to synthetic CH_4, H_2O and CO_2 in the spectral region of interest in the present study (indicated by dashed lines).

T-Y brown dwarf transition, but confirmation is hindered by the lack of NH_3 line parameters in the region.

As briefly hinted earlier, the spectroscopic information of NH_3 in the 1.5 μm region is completely missing in the HITRAN database (**?**). Only a few experimental measurements, mostly on line positions and strengths, have been reported (**??????**), which cover only less than a quarter of the features observable in a high resolution laboratory spectrum with much worse coverage ($\backsim$10%) on quantum assignments. Therefore, extensive spectroscopic study on NH_3 in this region is urgently needed for accurate interpretation of spectroscopic data of Jovian atmospheres observed by IRIS, NIMS, CIRS, etc. It also supports the photospectrometric observations in the infrared by NIRSPEC, SOFIA, HST, and JWST to come.

2. Analysis of Kitt Peak spectra and Quantum assignment in 1.5 μm region

NH_3 has four infrared active fundamental modes (ν_2, ν_4, ν_1, and ν_3 at 1030, 1690, 3503, and 3591 cm^{-1}, respectively), all of which have inversion doubling, in addition to the usual vibrational degeneracies (for ν_3 and ν_4). Its strong bands, ν_1, ν_3 and $2\nu_4$, dominate the spectrum at 3 μm, while their corresponding overtone and combination bands (e.g., $2\nu_1$, $2\nu_3$, ν_1+ν_3, ν_1+$2\nu_4$ and ν_3+$2\nu_4$) are prominent in the 1.5 μm region. Substantial normal mode-local mode coupling and anharmonic resonances make effective Hamiltonians for the near-IR nearly intractable. More than 43 bands are predicted from 6200 to 7050 cm^{-1}using *ab initio* calculations by Huang et al. (2008). However, refining the potential energy surface for the *ab initio* calculations using laboratory measurements has been hindered by the lack of sufficient intensity data for the near-IR.

In order to provide a complete set of NH_3 spectroscopic information at 1.5 μm, we retrieved line positions, ν (cm^{-1}), and intensities, I (cm^{-1}/(molecule cm^{-2})) from laboratory spectra at various temperatures (200 - 298 K), and determined lower state energies, E$''$(cm^{-1}) by intensity variations at two different temperatures, T and T$_o$

$$\frac{I_\nu(T)}{I_\nu(T_o)} = \frac{Q(T_o)}{Q(T)}\exp[-E''(\frac{1}{kT} - \frac{1}{kT_o})] \quad (1)$$

where Q is partition sum and k is Boltzmann constant. The lower state energy estimates are compared to the *ab initio* calculations (**?**) to obtain new quantum assignments, which are confirmed by combination differences.

3. Preliminary compilation and comparison at 296 K - in Progress

Fig. 2.— Comparison of a measured (solid) and a calculated(dotted) NH_3 spectrum in the 6710 cm^{-1}region at 296 K, 1.90 Torr, 16.4 m path length. Preliminary quantum assignments available are labeled.

We have so far measured 5060 line positions and intensities stronger than 5×10^{-24} cm^{-1}/(molecule cm^{-2}) from 6300 to 7000 cm^{-1}. Less than 10% of these features have quantum assignments. A sample of preliminary results of the line positions and strengths are presented in Fig. 2 with their quantum assignments labeled, showing fairly good agreement between a laboratory spectrum and synthetic one based on our measured linelist. Further refinements on the empirical line parameters and quantum assignments are in progress in collaboration with the *ab initio* calculation groups (*Priv. Comm.* to X. Huang et al. from AMES, NASA and J. Tennyson from Univ. College London, UK).

4. Conclusion

We have measured line positions and strengths of NH_3 transitions in the 1.5 μm region from the laboratory spectra recorded with the McMath-Pierce Fourier transform spectrometer (FTS) on Kitt Peak Observatory in Arizona, which would provide the missing spectroscopic information in the HITRAN 2008 (**?**). Preliminary results for a few lines are presented here, and full analysis is in progress.

The research at the Jet Propulsion Laboratory (JPL), California Institute of Technology has been performed under contracts and grants with National Aeronautics and Space Administration. Copyright 2010 California Institute of Technology. Government sponsorship acknowledged.

REFERENCES

Delorme, P., Delfosse, X., Albert, L., et al. 2008, Astron. Astrophys., 482, 961

Huang, X., Schwenke, D. W., & Lee, T. J. 2008, J. Chem. Phys., 129, 214304

Jia, H., Zhao, W., Cai, T., Chen, W., Zhang, W., & Gao, X. 2009, J. Quant. Spectrosc. Radiat. Transfer, 110, 347

Lees, R. M., Li, L., & Xu, L.-H. 2008, J. Mol. Spectrosc., 251, 241

Leggett, S. K., Marley, M. S., Freedman, R., et al. 2009, Ap. J., 695, 1517

Li, L., Lees, R. M., & Xu, L. -H. 2007, J. Mol. Spectrosc., 243, 219

Lundsberg-Nielsen L., Hegelund F., Nicolaisen, F. M. 1993, J. Mol. Spectrosc., 162, 230

O′Leary, D. M., Orphal, J., Ruth, A. A., et al. 2008, J. Quant. Spectrosc. Radiat. Transfer, 109, 1004

Rothman, L. S., Gordon, I. E., et al. 2009, J. Quant. Spectrosc. Radiat. Transfer, 110, 533

Wildt, R. 1931, Naturwiss, 19, 109

Xu, L.-H., Liu, Z., Yakovlev, I., Tretyakov, M. Y., & Lees, R. M. 2004, Infra. Phys., 45, 31

NASA LAW, October 25-28, 2010, Gatlinburg

Spectroscopy of Astrophysically Significant Carbon Molecules and Ions - The Search for PAHs in Interstellar Spectra

F. Salama[1], G. A. Galazutdinov[2], J. Krełowski[3], L. Biennier[4]

[1]*Space Science Division, NASA Ames Research Center, Moffett Field, CA 94035*
[2]*Instituto de Astronomia, Universidad Catolica del Norte, Antofagasta, Chile*
[3]*Nicolaus Copernicus University, Center for Astronomy, Pl-87-100 Toruń, Poland*
[4]*Institut de Physique de Rennes UMR 6251, Universite Rennes 1, 35042, Rennes, France*

Farid.Salama@nasa.gov, runizag@gmail.com, jacek@astri.uni.torun.pl, ludovic.biennier@univ-rennes1.fr

ABSTRACT

The spectra of several cold, isolated gas–phase PAHs have been measured in the laboratory under unique experimental conditions that mimic the interstellar conditions and are compared with an extensive set of astronomical spectra of reddened, early type stars. This comparison provides – for the first time – accurate upper limits for the abundances of *specific* PAH molecules along *specific* lines-of-sight. Something not attainable from infrared observations alone. The comparison of these unique laboratory data with high resolution, high S/N ratio spectra leads to two major findings: (i) the abundance of the neutral PAHs sampled in this study must be very low in the individual translucent interstellar clouds that were probed in this survey (PAH features remain below the level of detection) and, (ii) neutral PAHs exhibit intrinsic band profiles that are similar to the profile of the narrow diffuse interstellar bands (DIBs) indicating that the carriers of the narrow DIBs must have close molecular structure and characteristics. This study is the first quantitative survey of PAHs in the optical range and it opens the way for unambiguous quantitative searches of PAHs in a variety of interstellar and circumstellar environments. We are now, for *the first time*, in the position to *directly* compare laboratory spectra of PAHs and carbon nanoparticles with astronomical observations. This new phase offers tremendous opportunities for the data analysis of space missions geared toward the detection of large aromatic systems (HST/COS, JWST, SOFIA, Herschel).

1. Introduction, Laboratory Approach, Astronomical Observations & Results

PAHs are a class of very stable organic molecules made only of fused benzenoid rings and hydrogen atoms. Carbon molecules, in their neutral and ionized forms, play an important role in the interstellar medium due to the rich chemistry of carbon and its ability to form a large variety of complex molecular species involving hydrogen – the most abundant element (for a recent review see Salama 2008). PAHs are now thought to be largely responsible for the infrared bands seen in emission in HII regions, planetary and reflection nebulae, and the ISM of the Milky Way and other galaxies (Tielens 2008). PAHs form a link between the gas and the solid phase of interstellar dust and are a key element for the coupling of stellar FUV photons with the interstellar gas. It is becoming important to search for the signature of PAHs in other wavelength windows (UV, visible) to test the predictions of the PAH model that is exclusively based on observations in the IR range that only provide information on chemical group structure and cannot be used to identify *specific* individual PAHs.

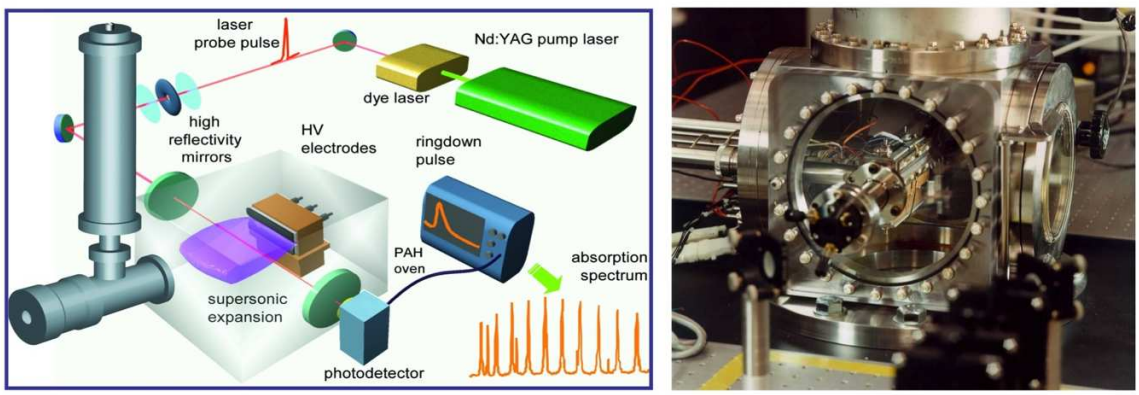

Fig. 1.— *Left*: Configuration of the Laboratory Facility. *Right:* close-up view of the Chamber consisting of a Pulsed Discharge Nozzle (PDN) coupled to a Cavity Ringdown Spectrometer (CRDS) and an orthogonal Reflectron time-of-flight mass spectrometer (ReTOF-MS).

Extensive laboratory studies were performed to measure the UV and visible spectra of neutral and ionized PAHs in media that are astrophysically relevant, i.e., media where the neutral PAH molecules and their ions are free and isolated at low temperature. In these laboratory experiments, the harsh physical conditions reigning in interstellar clouds -low temperature, collisionless, strong UV radiation fields- are simulated by generating molecular beams seeded with PAH molecules (see Fig. 1). Cold, neutral PAH molecules are formed in an isolated environment and probed with high-sensitivity cavity ringdown spectroscopy (CRDS) in the NUV-NIR range. These experiments provide unique information on the spectra of free, cold ($\sim 50-100\ K$) PAH molecules in the gas phase that can now be *directly* compared

to astronomical observations of diffuse and translucent interstellar clouds. An extensive set of *gas–phase* spectra of neutral and ionized PAHs is now available (Salama 2008) making it possible for the *first time* to unambiguously search for the signature of specific PAHs in the diffuse interstellar medium and to test the PAHs as potential DIB carriers (Salama et al. 2010). We've compared the gas-phase laboratory spectra of a set of neutral PAH molecules to an extensive set of high-resolution astronomical data of translucent clouds.

Our laboratory approach, relies on the association of a pulsed discharge slit nozzle (PDN) with ultra-high sensitivity cavity ringdown spectroscopy (CRDS) and is independent of inter- and intra- molecular processes. In brief, a pulsed planar supersonic beam expansion containing the sample seeded in Ar is prepared with a pulsed discharge slit nozzle (PDN). The PDN consists of a heated copper sample reservoir and a 10-cm long by $200 - \mu$m wide slit, which is sealed from inside by a Vespel (Dupont, SP-22 Grade) slit poppet driven by three synchronized pulsed solenoid valves (General Valve Series 9). Two stainless knife-edge electrodes are mounted outside the PDN on each side of the slit. The two electrodes are separated by an even gap of 400 μm and configured as the cathode of a high-voltage pulse generator. The PDN assembly itself is configured as the anode. This design enables the generation of cold atomic and molecular neutrals, ions and radicals in the planar jet expansion. In the experiments described here, the high voltage is applied only for the wavelength calibration, which is achieved by monitoring the Ar* atomic lines generated in the discharge. PAHs samples are solid at room temperature. The PAH vapor pressure is increased by heating a pick-up cell that contains the sample upstream the Argon flow. The supersonic beam expansion containing the carrier gas seeded with the PAH sample ($< 0.1\%$) is probed by cavity ring-down spectroscopy several mm downstream with a sub-ppm absorption sensitivity. The spectra are probed using frequency-doubled output of an Nd: yttrium aluminum garnet (YAG) (Quanta-Ray Lab 150 from Spectra-Physics) pumped dye laser (Quanta-Ray PDL-2 from Spectra-Physics). The ring-down cavity consists of two high-reflectivity (99.999%) concave (6-m curvature radius) mirrors (Los Gatos Research) mounted 55 cm apart. The ringdown signal is collected by a photosensor module (H6780-04 from Hamamatsu) and digitized by a 20-MHz 12-bit acquisition board (Adlink, PCI9812). The data is then processed by a personal computer (PC) program and the cavity losses are extracted. The recent addition of a reflectron time-of-flight mass spectrometer (ReTOF-MS) allows to monitor in situ and in real time the formation of larger particles when the plasma is operated (Ricketts et al. 2010). A sample of the absorption spectra of the cold ($\sim 50 - 100K$) neutral PAH molecules measured with this approach are reported in Figure 2 where they are compared to the high-resolution spectra of diffuse interstellar clouds.

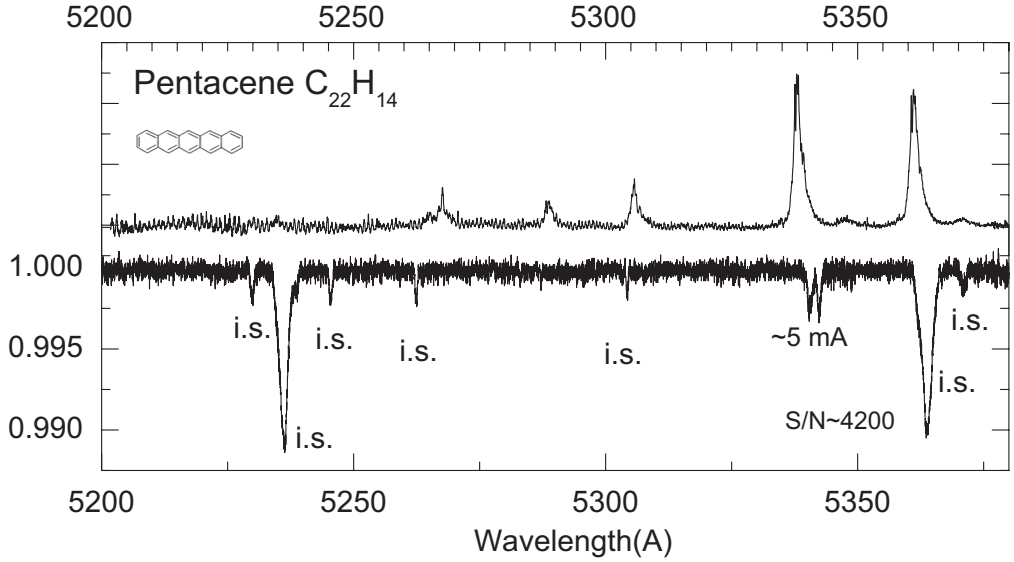

Fig. 2.— Cavity ringdown spectrum of pentacene ($C_{22}H_{14}$) prepared in a cold jet expansion with Ar buffer gas (*top*) is compared to the average spectrum of the program stars (*bottom*).

2. Conclusion

We have compared our recently acquired data on the spectroscopy of free cold PAH molecules in the NUV-to-visual spectral range with an extensive set of astronomical observations taken along the lines-of-sight of selected reddened stars (see Figure 2). The gas-phase laboratory spectra of jet-cooled PAHs, which allow to determine the *intrinsic* band profiles of the cold molecules, show that neutral PAHs exhibit narrow bands (FWHMs are of the order of a few cm^{-1}) with a band profile that is *closely* similar to the profile of the narrower DIBs. The case is strikingly illustrated in the comparison of the 5362.8 Å band of neutral pentacene, ($C_{22}H_{14}$), with the narrow 5363.8 Å DIB detected along the individual lines-of-sight we observed in our survey. The laboratory band exhibits a 1.9$\AA$ FWHM while the DIB feature extracted from the average spectrum shows a 2.1$\AA$ FWHM. Note that the laboratory spectrum of $C_{22}H_{14}$ exhibits another band of comparable strength at 5339.5 Å where only a weaker feature is found in the astronomical spectra ruling the pentacene molecule out as a potential band carrier for the 5363.8$\AA$ DIB.

This survey demonstrates that the direct comparison of the spectra of a sample of 10 neutral PAH molecules measured under relevant astrophysical laboratory conditions (i.e., free, cold molecules) with high S/N astronomical spectra measured along the lines of sight of a set of 15 selected reddened stars does not lead to the identification of DIBs. The stellar spectra do not contain telluric features which could prevent the detection of weak PAH bands.

Accurate upper limits for the abundances of the neutral PAHs population along those lines of sight can be derived from this comparison. We've shown that it is now possible - for the first time- to unambiguously search for the signature of *specific* PAH molecules and ions in space. This information cannot be obtained from IR data alone that is not characteristic enough and can only be retrieved from the UV and optical ranges. This is a requisite for demonstrating the presence of PAHs in the diffuse ISM. A new exciting era opens that will hopefully allow to detect specific PAHs in space and fully test the PAH proposal. The spectrograph used in this project is particularly adapted to this task and will be used to collect an extensive set of high quality spectra of reddened stars. More laboratory measurements of *direct* absorption spectroscopy are also needed to measure the spectra of larger PAH molecules and their ions (both positive and negative) as well as radicals (hydrogenated and dehydrogenated PAHs). A new era begins for the search of complex molecules in space. This new phase offers tremendous opportunities for the data analysis of space missions geared toward the detection of large aromatic systems (HST/COS and JWST).

The authors acknowledge the support of the NASA SMD APRA program.

REFERENCES

Ricketts, C., Contreras, C., Walker, R. & Salama, F. 2010, Int. J. Mass Spectrom., in press, doi:10.1016/j.ijms.2010.11.017

Salama, F. 2008, Organic Matter in Space, Proceedings of the International Astronomical Union, 4, 357, Cambridge University Press, doi: 10.1017/S1743921308021960

Salama, F., Galazutdinov, G., Krełowski J., et al. 2010, ApJ, in press

Tielens, A. 2005, The Physics and Chemistry of the Interstellar Medium, Cambridge Univ Press, Cambridge, UK

This preprint was prepared with the AAS LaTeX macros v5.2.

NASA LAW, October 25-28, 2010, Gatlinburg

High-Resolution Cavity-Enhanced Spectroscopy of Molecular Ion Beams

Manori Perera, Andrew A. Mills, Brian M. Siller, Michael W. Porambo, Kyle N. Crabtree, Carrie A. Kauffman, Holger Kreckel, & Benjamin J. McCall[1]

Department of Chemistry, University of Illinois, Urbana, IL 61801, USA

mperera@illinois.edu, aamills2@illinois.edu, bsiller2@illinois.edu, porambo1@illinois.edu, kcrabtr2@illinois.edu, kauffma2@illinois.edu, hkreckel@illinois.edu, bjmccall@illinois.edu

ABSTRACT

Molecular ions play a pivotal role in the chemistry of the interstellar medium due to their high reactivity even at low temperature. To identify these ions in interstellar space, it is essential to obtain high resolution laboratory spectra of potential interstellar ions for comparison to observational data. At the University of Illinois, we are developing a Sensitive, Cooled, Resolved Ion BEam Spectrometer (SCRIBES) that will allow us to obtain high resolution infrared direct absorption spectra of rotationally cold molecular ions in the absence of neutral molecules. This instrument can overcome many of the problems that arise when using other spectroscopic techniques. It benefits from the high sensitivity of cavity enhanced techniques and accurate laser frequency calibration using a frequency comb. Currently, we are using a cold cathode ion source to produce an N_2^+ test beam that will be studied using SCRIBES.

1. Introduction

More than 150 molecules have been observed in the interstellar medium (ISM) to date. The vast majority of these molecules are formed by ion-neutral reactions at low temperatures and low densities. New telescopes such as Herschel and SOFIA will obtain spectra at previously unavailable frequencies in the sub-mm/far-infrared range with high-resolving power

[1]Department of Astronomy, University of Illinois, Urbana, IL 61801, USA

to study the molecular composition of the universe. This will necessitate extensive laboratory work to identify new molecules or classes of molecules responsible for astronomically observed transitions in these frequency domains.

Compared to neutral molecules, relatively few high resolution spectra of molecular ions have been obtained in the laboratory. This is due to experimental difficulties as, e.g., low number densities, high temperatures in laboratory plasmas, and spectral confusion due to neutral species. In addition to these obstacles in creating and isolating the ions, studying them at THz frequencies is also not a simple task. Although the availability of THz light sources is improving, the experimental difficulties related to their operation are still significant. Alternatively, we can use mid-IR spectroscopy – benefitting from the availability of mid-IR light sources and the accuracy of frequency combs – to indirectly acquire THz spectra by studying combination differences to infer rotational level spacings. In this article, we will discuss the research conducted at the University of Illinois, where we are developing a Sensitive, Cooled, Resolved Ion BEam Spectrometer (SCRIBES) and various high resolution spectroscopic techniques to acquire indirect THz signatures of molecular ions.

2. Instrumentation and Spectroscopy Techniques

An overview of the SCRIBES instrument is shown in Fig. 1. A fast molecular ion beam (4 kV) will be extracted from a supersonic ion source (described in detail by Crabtree et al. (2010)) and guided into the overlap region by dedicated ion optics. In the overlap region the ions will be superimposed with a laser cavity for sensitive absorption techniques. A difference frequency generation laser will be used to produce IR radiation between 2.2 μm and 4.8 μm. For absolute frequency calibration a frequency comb will be coupled to the laser setup, to provide an accuracy that is orders of magnitude better than traditional wavemeter calibration. After the overlap region the ions enter a time-of-flight mass spectrometer (TOF-MS) that will allow for *in situ* characterization of the ion beam. In its final form, the instrument will offer the following advantages over previous techniques: (1) physical separation of ions and neutrals, (2) narrow linewidths due to kinematic compression in a fast ion beam, (3) reduced spectral congestion and low rotational temperatures using a supersonic ion source, and (4) high sensitivity due to modern cavity-enhanced spectroscopy methods.

We are exploring several spectroscopic techniques that can ultimately couple with SCRIBES to produce high resolution absorption spectra such as cavity ringdown spectroscopy (CRDS), cavity enhanced velocity modulation spectroscopy (CEVMS), and noise immune cavity enhanced optical heterodyne molecular spectroscopy (NICE-OHMS). Previous work in our lab has shown the sensitivity of CRDS (by Weaver et al. (2008)) and

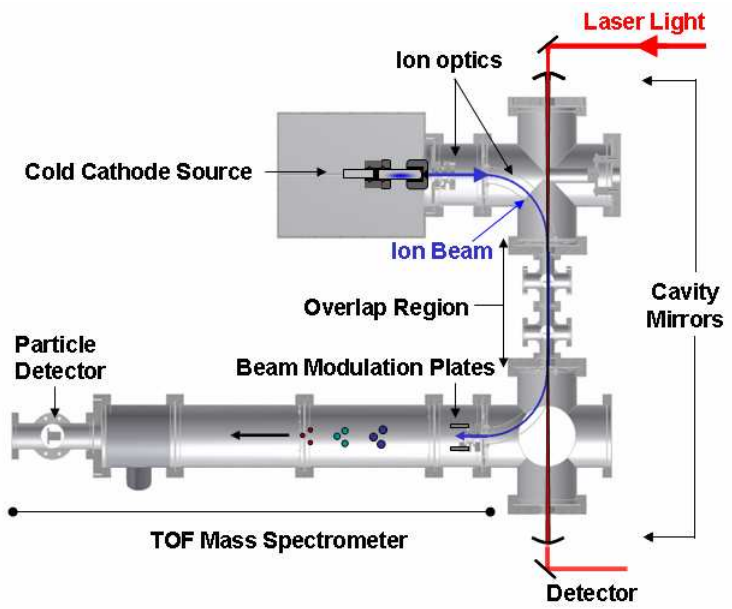

Fig. 1.— A schematic of SCRIBES with a cold cathode ion source.

CEVMS (by Siller et al. (2010) and Mills et al. (2010)) using a N_2^+ plasma in a positive column. Currently, we are studying N_2^+ plasma in a positive column using NICE-OHMS method to understand the signal shape and the sensitivity of the technique. Applying these techniques to a fast ion beam will provide a sufficiently high sensitivity and resolution to enable the use of combination differences to calculate THz transition frequencies (needed for astronomical observations) from our mid-infrared frequencies.

We have also characterized the ion beam properties using the TOF-MS. We found that the beam energy is different from the voltage source reading but has a low energy spread. Also, we found that the ions extracted from the cathode undergo fewer collisions than ions extracted from the anode. We determined this by studying a H_2 plasma and monitoring ions that are produced (see Fig. 2). The H_2^+ signal was reduced under conditions that favored collisions before extraction, because H_2^+ quickly reacts with H_2 to produce H_3^+. Based on these results, it seems critical to extract ions from the anode, in order to ensure that ions extracted from the source are thermalized.

3. Future Outlook

We are currently at the stage of combining SCRIBES with the NICE-OHMS setup to study a beam of N_2^+ ions. After finding the sensitivity and accuracy of our instrument

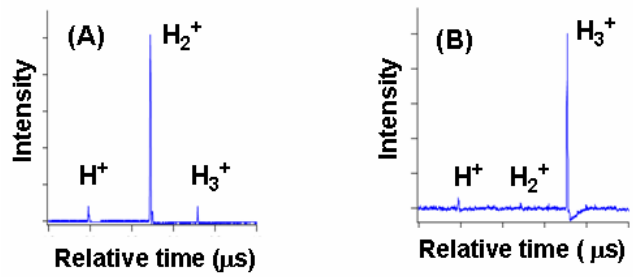

Fig. 2.— Mass spectra taken with a H_2 plasma show ions produced by a plasma with (A) less collisions when extracted from the cathode and (B) more collisions when extracted from the anode.

with the N_2^+ ion beam, we will use the ion HN_2^+, which has been extensively studied in the THz, to validate our procedures for interpreting our ultra precise IR spectra. We will then study known interstellar ions, such as HCS^+, HOC^+, HCO^+, CO^+, and $HCNH^+$ in the mid-IR frequencies. These frequencies then can be used with known microwave frequencies to acquire indirect THz frequencies.

This work is supported in part by the University of Illinois, the National Science Foundation, NASA, the David and Lucile Packard Foundation, the Research Corporation, Air Force Office of Scientific Research, and the Camille and Henry Dreyfus Foundation.

REFERENCES

Crabtree, K. N., Kauffman, C. A., & McCall, B. J. 2010, Rev. Sci. Instrum., 81, 086103

Mills, A. A., Siller, B. M., & McCall, B. J. 2010, Chem. Phys. Lett., 501, 1

Siller, B. M., Mills, A. A., & McCall, B. J. 2010, Opt. Lett., 35, 1266

Widicus Weaver, S. L., Wiczer, M. B., Negru, B., DiGangi, J. P.,Tom, B. A., & McCall, B. J. 2008, J. Mol. Spec., 249, 14

This preprint was prepared with the AAS LaTeX macros v5.2.

NASA LAW, October 25-28, 2010, Gatlinburg

Methanol: The Simplest C_{3V} Internal Rotor and Ubiquitous Interstellar Weed

J. C. Pearson, B. J. Drouin, S. Yu, L. R. Brown, C. S. Brauer, H. Gupta, K. Sung

Jet Propulsion Laboratory, California Institute of Technology, 4800 Oak Grove Dr., Pasadena CA, 91109

John.C.Pearson@jpl.nasa.gov

L.-H. Xu

Center for Laser, Atomic and Molecular Sciences (CLAMS), Department of Physics, University of New Brunswick, PO Box 5050, Saint John, NB, Canada E2L 4L5

S. Wang & E. A. Bergin

Department of Astronomy, University of Michigan, 500 Church Street, Ann Arbor, MI 48109

ABSTRACT

Methanol is the simplest three-fold internal rotor by virtue of the internal rotation of the CH_3 top with respect to the OH frame. Without the internal rotation methanol would be a relatively benign nearly prolate asymmetric top molecule. The internal rotation results in an A-state that acts as an asymmetric top and two symmetric top like E-states. The ground state is best described as rotation problem perturbed by internal rotation, but by the time the second excited torsional state is reached a more apt description would be of a free-rotor perturbed by a rotation problem. *Herschel* observations have detected methanol through at least the second excited torsional state and with $J > 30$ including many levels above the range of transitions included in the latest analysis. A number of new laboratory spectra have made it possible to assess the ability of the ρ-axis method methanol Hamiltonian models to be used in extrapolation. The validity of using the permanent electric dipole moment in calculation of torsional line strengths has also been assessed through FTIR intensities. We report the extension of methanol data to $J = 45$ and $K = 16$ in the lowest 3 torsional states and compare the results with *Herschel* observations.

1. Introduction

The spectrum of methanol has been the subject of many years of spectroscopic investigation both theoretical and experimental. The torsional bands have been extensively characterized in the $0-1258$ cm^{-1} region (Moruzzi et al. 1995). The pure rotation and most of the torsional bands have been modeled using a rho-axis method Hamiltonian to very close to experimental accuracy for many K sub-bands of $v_t = 0, 1, 2$ (Xu et al. 2008). In spite of the successes, there are transitions measured and assigned correctly over 50 years ago that lie above the range of the most recent analyses. Additionally, about half the observed methanol laser lines remain to be assigned. The grand challenge in the study of methanol is to solve the problem of coupling a small amplitude normal vibration to the bath of internal rotation states. In methanol this becomes important in the $\mathrm{C-O}$ stretch state and the third excited torsional state (Pearson et al. 2009). Methanol features a strong dipole moment along both the a- and b-axes (Sastry et al. 1981). The a-axis is nearly aligned with the internal rotation so the torsional effects on the a-moment are small. However, conservation of angular momentum of top relative to frame requires the b-moment to precess opposite the internal rotation. This means that the torsional bands obtain their intensity directly from the permanent electric dipole, primarily along the b-axis making many torsional bands very strong.

2. Laboratory Studies and Astronomical Observations

A program of systematic measurements has been undertaken to support *Herschel*, SOFIA and ALMA observations. To date laboratory spectra covering $8-700, 765-935, 950-1200, 1575-1658, 1680-1900$ and $2480-2770$ GHz has been collected. Rotational bands of $v_t = 0, 1, 2, 3$, and 4 have been assigned in the ground torsional manifold. Pure rotation bands of the C-O stretch and the CH_3 in-plane rock have also been identified. Torsional bands connecting $v_t = 1-0, 2-1$ and $3-2$ have also been identified. The known $K-$sub-bands have been extended to $K = 17$ in the ground and $v_t = 1$ state and to $K = 15$ in the $v_t = 2$ state. The agreement between observed and calculated transitions for $v_t = 0, 1$ is excellent even when extrapolating to higher J quantum numbers. The situation becomes progressively worse in $v_t = 2$ or when extrapolating in the K quantum number. The challenges appear to be in torsional part of the ρ-axis Hamiltonian, which predominately contributes to the K structure in methanol. The role of several significant torsional resonances between $K = 15, 13,$ & 11 in the A-states, $K = 17, 15,$ & $13, K = -17, -15,$ & $-13, K = 14, 12,$ & 10 and $K = -16, -14,$ & -12 E-states for $v_t = 0, 1$ and 2, respectively is suspected to be the cause(Moruzzi et al. 1995; Xu et al. 2008). The details of these interactions were

extrapolated in the previous work resulting in some systematic deviations.

The internal rotation in methanol should result in a three-fold component of the dipole moment, which has only been calculated at a fairly low level of theory (Mekhtiev et al. 1999). The existing dipole moment determination (Sastry et al. 1981) did not provide any insight into the magnitude of the three-fold component. As a result, Fourier Transform spectroscopy was used on the torsional bands of methanol between 300 and 500 cm^{-1}. This investigation illuminated several problems in methanol. The generally accepted partition function (Xu et al. 2004) was found to be too small by a few % when compared to the energy levels calculated by Xu et al. (2008). The intensities of the $v_t = 1$ and 2 bands agreed well with predictions if the *ab initio* three-fold dipole component (Mekhtiev et al. 1999) was included.

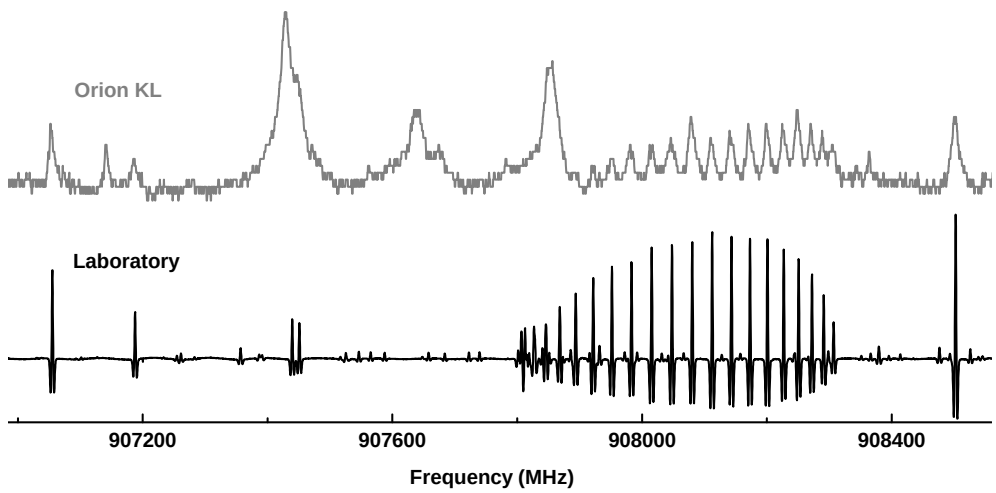

Fig. 1.— $v_t = 2K = 4 - 3$ A-state Q-branch Orion KL (*top*), laboratory (*bottom*).

It was expected that methanol would be abundant in astronomical observations with the *Herschel* Space Observatory. The opacity of the dust in the rich molecular sources at THz frequencies definitely does increase in the $1.4 - 1.9$ THz frequency range; however, methanol remains prominent and the dust never becomes completely optically thick (Bergin et al. 2010). The richness of the methanol spectrum below 1.25 THz is truly impressive. To date transitions of the $v_t = 0, 1$, and 2 states have been observed with J up to 35. The richness of the spectrum quickly becomes an asset in interpretation since any reasonably sized frequency window contains transitions spanning a large range of excitation energy. This allows an enormous amount of source information to be extracted from a rapid observation (Leurini et al. 2004; Wang et al. 2010). Figure 1 shows the $v_t = 2, K = 4 - 3$ A-symmetry Q branch in Orion KL and in the laboratory.

3. Conclusion

The spectrum of methanol is now well characterized in the ground and first excited torsional state to $K = 13$ and $K = 12$, respectively. The second torsional state is well characterized when microwave accuracy transitions connect the K sub-bands to the rest of the energy levels. New data measured here should extend this to $K = 17$ of the ground and first excited torsional state and to $K = 15$ of the second torsional state. The intensities of the rotational and torsional bands are well understood and in good agreement with experimental measurements. The major remaining work is to connect the third and higher excited torsional state to the lower states with microwave accuracy transitions and to fully characterize the low lying $C - O$ stretch and in-plane CH_3 rock small amplitude vibration states.

A portion of this work was performed at the Jet Propulsion Laboratory, California Institute of Technology, under contract with the National Aeronautics and Space Administration. Copyright 2010© California Institute of Technology. All rights reserved. LHX gratefully acknowledges financial support form the Natural Science and Engineering Research Council of Canada.

REFERENCES

Bergin, E. A., et al., 2010, Astron. & Astrophys., 521, L20

Leurini, S., et al., Astron. & Astrophys., 422, 573

Mekhtiev, M.A., Godfrey, P.D., & Hougen, J.T., 1999, J. Mol. Spectrosc., 194, 171

Moruzzi, G., et al., 1995, Microwave Infrared and Laser Transitions of Methanol atlas of assigned lines from 0 to 1258 cm^{-1}, CRC Press: Boca Raton, Florida

Pearson, J. C., Brauer, C. S., Drouin, B. J., & Xu, L.-H., 2009, Can. J. Phys., 87, 449

Sastry, K.V.L.N., Lees, R.M., & Van der Linde, J., 1981, J. Mol. Spectrosc., 88, 228

Wang, S., et al., 2010, Astron. & Astrophys., in press

Xu, L.-H., et al., 2004, J. Mol. Spectrosc., 228, 453

Xu, L.-H., et al. 2008, J. Mol. Spectrosc., 251, 305

This preprint was prepared with the AAS LaTeX macros v5.2.

NASA LAW, October 25-28, 2010, Gatlinburg

Organic Compounds in the $C_3H_6O_3$ Family: Microwave Spectrum of *cis-cis* Dimethyl Carbonate

B. A. McGuire, & S. L. Widicus Weaver[1]

Department of Chemistry, Emory University, Atlanta, GA 30322

bamcgui@emory.edu, susanna.widicus.weaver@emory.edu

F. J. Lovas & D. F. Plusquellic

Optical Technology Division, National Institute of Standards and Technology, Gaithersburg, MD 20899

lovas@nist.gov, david.plusquellic@nist.gov

G. A. Blake

Division of Geological and Planetary Science, California Institute of Technology, Pasadena, CA 91125

gab@gps.caltech.edu

ABSTRACT

A number of recent spectroscopic and observational efforts have focused on simple sugars and sugar alcohols because of their importance in prebiotic astrochemistry. The simplest sugar-related species, glycolaldehyde, has been detected in Sgr B2(N), as have its $C_2H_4O_2$ structural isomers acetic acid and methyl formate. Additional studies of the C_3-sugars with empirical formula $C_3H_6O_3$, glyceraldehyde and dihydroxyacetone, resulted in no clear interstellar detection. Structural isomerism is extensive in interstellar clouds, and there is a high level of correlation between the relative energies of isomers and their relative abundances, with the lowest energy isomers detected in greatest abundance. The detected members of the $C_2H_4O_2$ family, however, defy this trend, having relative

[1]To whom correspondence should be addressed.

abundances of (acetic acid):(glycolaldehyde):(methyl formate) of about 2:1:52, despite acetic acid being the lowest energy isomer. These puzzling abundance ratios and the lack of detection of the $C_3H_6O_3$ sugars gives rise to the question: "Which is the most likely isomer in the $C_3H_6O_3$ family to be detectable in interstellar clouds?" In an attempt to answer this question, we carried out geometry optimization calculations to determine the relative binding energies of the 13 members of the $C_3H_6O_3$ family. Of the four lowest-energy isomers, only lactic acid [$CH_3CH(OH)COOH$] and dimethyl carbonate [$(CH_3)_2CO_3$] are commercially available, and lactic acid has been previously investigated spectroscopically. We have therefore conducted a laboratory study of dimethyl carbonate, measuring its rotational spectrum from 8.4 - 25.3 GHz using a Fourier-Transform microwave spectrometer, and from 227 - 350 GHz using a direct absorption spectrometer. We report on the theoretical calculations performed on the $C_3H_6O_3$ family of isomers, the experimental studies of *cis-cis* dimethyl carbonate, and the implications of these results for interstellar chemistry. The details of this work are also reported in Lovas et al. (2010).

1. Introduction

Several recent spectroscopic and observational efforts focusing on simple sugars have resulted in the detection of the simplest sugar-related species, glycolaldehyde, in Sgr B2(N) as well as its structural isomers, acetic acid and methyl formate. Searches for the more complex C_3-sugars glyceraldehyde and dihydroxyacetone, however, have resulted in no clear interstellar detection [Hollis et al. (2004); Widicus Weaver et al. (2005); Apponi et al. (2006a,b)].

Structural isomerism is extensive in interstellar clouds, and isomer relative abundances typically correlate with their relative energies [Lattelais et al. (2009)]. The $C_2H_4O_2$ family is a notable exception, with relative abundances of (acetic acid):(glycoladehyde):(methyl formate) of about 2:1:52 [Snyder et al. (2002)], despite acetic acid being the lowest in energy. These puzzling trends give rise to the question: "Which is the most likely isomer in the $C_3H_6O_3$ family to be detectable in interstellar space?"

In an attempt to answer this question, we have undertaken electronic structure calculations for the $C_3H_6O_3$ isomers to determine their relative energies, and rotational spectroscopic studies to provide rest frequencies for observational searches.

2. Electronic Structure Calculations

To determine the relative binding energies of the members of the $C_3H_6O_3$ family, starting conformations for each isomer were selected to minimize steric effects and maximize hydrogen bonding. Each functional group was then rotated 360° in 20° increments to find local minima on their potential energy surface. At each minimum, DFT calculations (B3LYP/6-311+G) were performed to determine the lowest energy conformation. The lowest-energy conformer of each isomer was then optimized at the MP2/6-311++G(d,p) level.

Of the four lowest-energy isomers, only lactic acid and dimethyl carbonate are commercially available. As lactic acid has been previously investigated spectroscopically [Pszczolkowski et al. (2005)], dimethyl carbonate was chosen for laboratory study, necessitating additional electronic structure calculations. Three conformations of dimethyl carbonate were optimized at the MP2/aug-cc-pVTZ level to determine the lowest energy conformation and predict spectroscopic parameters. Table 1 gives the rotational constants determined for each conformer.

Table 1: Rotational constants for dimethyl carbonate conformers.

Conformer	A (MHz)	B (MHz)	C (MHz)	Relative Energies (cm^{-1})
cis-cis	10380.4	2389.4	1990.9	0
cis-trans	6528.4	2999.4	2109.7	1108
trans-trans	4397.0	3926.9	2130.7	7539

3. Laboratory Spectroscopy

The microwave spectrum was obtained using a FTMW spectrometer at NIST [Lovas & Suenram (1987); Suenram et al. (1999)]. Splitting arising from the hindered internal rotation of the methyl groups is observed. The spectrum from 227-350 GHz was obtained using a flow-cell spectrometer at Caltech [Widicus et al. (2003)]. The ERHAM program [Groner (1997)] was used to determine molecular parameters for the *cis-cis* conformer.

4. Conclusion

Searches for lactic acid, dihydroxyacetone, and glyceraldehyde in Sgr B2(N) have been unsuccessful. Based on relative energies, the next interstellar search candidates from the

$C_3H_6O_3$ family of isomers should be hydroxymethylacetate or dimethyl carbonate. A laboratory study of hydroxymethylacetate is required to guide these searches. Searches for dimethyl carbonate are now possible, though its relatively small dipole moment, ($\mu = 0.293$ D) will hinder such attempts.

This work was supported in part by the NSF Centers for Chemical Innovation grant No. 0847919, NASA Exobiology and SARA grants Nos. NAG5-11423 and NAG5-13457, the Cherry L. Emerson Center for Scientific Computing at Emory University, and SLWW's startup funds provided by Emory University.

REFERENCES

Lovas, F. J. et al. 2010, J. Mol. Spectrosc., 264, 10

Hollis, J. M. et al. 2004, Astrophys. J. Lett., 610, L21

Widicus Weaver, S. L. et al. 2005, Astrophys. J. Lett., 624, L33

Apponi, A. J. et al. 2006, Astrophys. J. Lett., 643, L29

Apponi, A. J. et al. 2006, in: NASA/CP-2006-214549, 150

Lattelais, M. et al. 2009, Astrophys. J. Lett., 696, L133

Snyder, L. E. et al. 2002, Astrophys. J., 578, 245

Pszczolkowski, L. et al. 2005, J. Mol. Spectrosc., 234, 106

Lovas, F. J. & Suenram, R. D. 1987, J. Chem. Phys., 87, 2010

Suenram, R. D. et al. 1999, Rev. Sci. Instrum., 70, 2127

Widicus, S. L. et al. 2003, J. Mol. Spectrosc., 217, 278

Groner, P. 1997, J. Chem. Phys., 107, 4483

This preprint was prepared with the AAS LaTeX macros v5.2.

NASA LAW, October 25-28, 2010, Gatlinburg

Low Temperature Pressure Broadening of HD

H. Gupta, B. J. Drouin, & J. C. Pearson

Jet Propulsion Laboratory, California Institute of Technology, Pasadena, CA 91109

Harshal.Gupta@jpl.nasa.gov, Brian.J.Drouin@jpl.nasa.gov,
John.C.Pearson@jpl.nasa.gov

ABSTRACT

Hydrogen deuteride (HD), the simplest closed shell molecule with a rotational spectrum, is of astrophysical and cosmological significance. HD is an unambiguous probe of the D/H ratio of the upper atmospheres of the gas giant planets and interstellar molecular clouds; and its formation as well as collisions in the primordial gas could affect critically the initial mass of Population III stars. Accurate spectroscopic and collisional parameters of HD are therefore needed as inputs for astrophysical and cosmological models. Here we report pressure broadening measurements of the $J = 1 - 0$ rotational transition of HD near 2.7 THz at 18 K. From the pressure induced self-shift of HD, the center frequency of the $1 - 0$ transition is determined to better than 25 kHz, improving this determination by nearly an order of magnitude over the previous measurement (Evenson et al. 1988). The work underway to determine pressure broadening parameters of HD by He, normal H_2 and *para*-H_2 is also discussed and the prospects outlined.

1. Introduction

Hydrogen deuteride, HD, is the simplest and most abundant deuterium-bearing molecule in the universe. It has been detected by space-based telescopes in many astronomical sources, including diffuse and dense molecular molecular clouds (Neufeld et al. 2006), star-forming regions (Neufeld et al. 2006), and atmospheres of the gas giant planets (Davis et al. 2006; Lellouch et al. 2001). HD is used as a probe of the D/H ratio in planetary atmospheres; it is also used to determine the deuterium abundance in the interstellar gas and hence the total molecular H_2 abundance of the gas for a given D/H ratio. Sufficiently high HD abundances in the primordial gas are thought to cool the gas efficiently, reducing the initial

masses of Population III stars (Glover & Abel 2008); however, models of star formation require accurate collisional and reaction rates, measurements for which are sparse and of limited quality. Good laboratory data at conditions relevant to astronomical sources, i.e., low temperature and pressure, are therefore required to accurately determine HD abundances in space, as well as to inform astrophysical and cosmological models.

Here we report an improved rest frequency of the $J = 1 - 0$ rotational transition of HD derived from the pressure-induced frequency shift of self-broadened lines of HD at 18 K. We also report on the work underway at the Jet Propulsion Laboratory to characterize the pressure broadening parameters of this fundamental molecule.

2. Experimental

The pressure broadening measurements of HD were done with a slightly modified version of the collisional cooling cell described by (Dick et al. 2006); Figure 1 shows a schematic of this experiment. The cell was cooled to 18 K by a helium cryostat. In the self-broadening experiments, we started with 0.05 Torr of HD in the cell, and added small aliquots of HD to measure self-broadened spectra at total pressures from 0.05 Torr to 10 Torr, approximately. Broadening of HD by He, H_2, and *para*-H_2 was also studied by adding small amounts of the desired gas to 0.5 Torr of HD, to achieve total pressures between 0.5 Torr and 10 Torr.

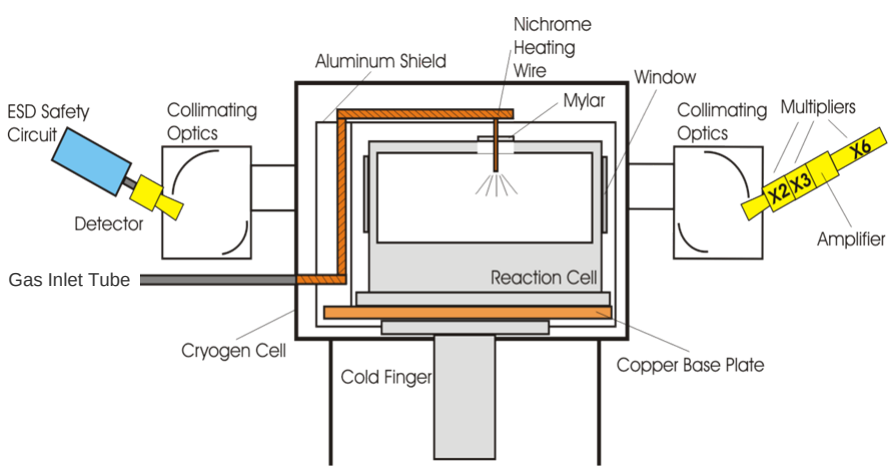

Fig. 1.— Liquid-Helium-cooled cell employed in the present work.

The $J = 1 - 0$ rotational transition of HD near 2.7 THz was probed with radiation generated by multiplying the output of an RF synthesizer 162 times; the power output was $1 - 14$ μW between 2470 and 2750 GHz. Transmission profiles of the lines were detected by a liquid-Helium-cooled Si bolometer, and analyzed using a line shape fitting routine.

3. Results and Discussion

The high signal-to-noise ratio of the $J = 1-0$ line of HD allows a study of the three main effects—pressure broadening, pressure-induced frequency shift, and collisional narrowing—illustrated in Fig. 2. Figure 2(a) shows the transmission profiles of the self-broadened $J = 1-0$ line of HD. Figure 2(b) shows a linear least-squares fit of the center frequencies of these lines as a function of total pressure. The fit yields two quantities: the slope is a measure of the frequency shift per unit pressure, and the intercept is the extrapolated frequency of the line at zero pressure. The rest frequency of 2674986.094(25) MHz determined from the extrapolation is nearly an order of magnitude more accurate than the previous measurement of 2674985.66(15) MHz reported by Evenson et al. (1988), and within one standard deviation of the theoretical value, 2674986.134(240) MHz, predicted by Pachuki & Komasa (2010).

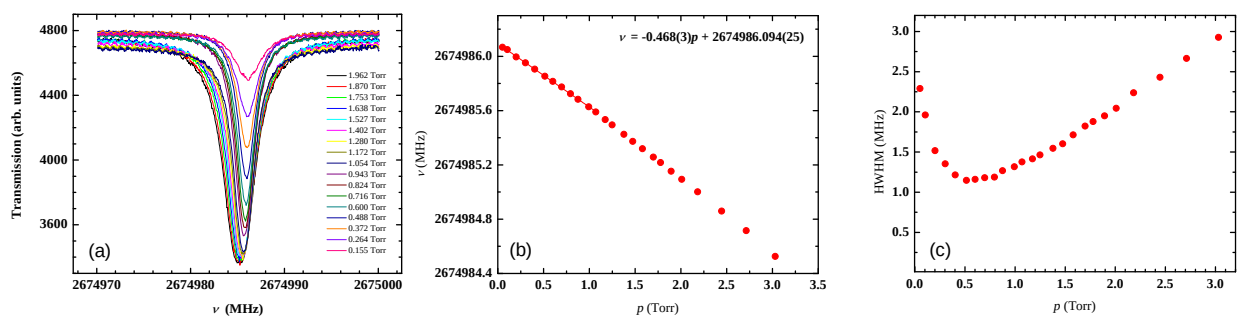

Fig. 2.— Pressure-broadening, frequency shift, and collisional narrowing in HD. (a) Self-broadened profiles of the $J = 1-0$ line of HD; (b) pressure-induced frequency shift and extrapolated center frequency of the $J = 1-0$ transition of HD (only points below ∼1 Torr were fit, as the line gets saturated above this pressure); and (c) the effect of collisional narrowing on the line width. Error bars in (b) and (c) are typically $1-5\%$.

Figure 2(c) shows the effects of collisional narrowing of the self-broadened HD lines. In the absence of narrowing, a plot of the line width as a function of pressure is expected to be a straight line whose intercept is the doppler width. A drastic departure from this behavior is seen in the HD self-broadened spectra, with the half-width at half-maximum reduced significantly from that expected. Although this effect is the strongest for HD−HD collisions, it is also observed in the pressure broadening of HD with H_2 and *para*-H_2 not presented here. A detailed analysis of collisional narrowing in HD, both with itself as well as with other gases, is underway, and will be reported in a forthcoming publication.

4. Conclusions

The pressure broadening measurements of HD reported here were done at 18 K, the lowest temperature accessible to our experiment, and have already yielded a significantly improved estimate of the rest frequency of the $J = 1 - 0$ transition of HD. A thorough characterization of the broadening and collisional parameters of HD will require a study of the temperature dependence of these parameters, with the aim of providing benchmarks for theory, as well as useful quantities for astrophysical and cosmological models. The temperature agility of the present apparatus will allow an extension of the data set to higher temperatures. The high sensitivity of the experiment should enable observation of pressure broadening, pressure-induced frequency shift, as well as collisional narrowing over a wide range of conditions, and would precede experimental studies of state-specific collisional cross-sections. In this regard, the development of a double-resonance experiment is a logical next step, and would be highly desirable.

This work was performed at the Jet Propulsion Laboratory, California Institute of Technology under contract with the National Aeronautics and Space Administration.

REFERENCES

Davis, G. R. et al., 2000, ESA SP-456, 29 and references therein

Dick, M. J., Drouin, B. J., Crawford, T. J., & Pearson, J. C. 2009, J. Quant. Spectr. & Rad. Tran., 110, 628

Evenson, K. M., et al. 1988, Astroph. J., 330, L135

Glover, S. C. O. & Abel T. 2008, MNRAS, 388, 1627

Lellouch, E. et al., 2001, Astron. & Astrophys., 670, 610 and references therein

Neufeld, D. A. et al., 2006 Astroph. J., 647, L33 and references therein

Pachuki, K. & Komasa, J. 2010, Phys. Chem. Chem. Phys., 12, 9188

This preprint was prepared with the AAS LaTeX macros v5.2.

NASA LAW, October 25-28, 2010, Gatlinburg

Infrared Photodissociation Spectroscopy of Cold Carbocations

Michael A. Duncan

Department of Chemistry, University of Georgia, Athens, Georgia 30602, U.S.A.

maduncan@uga.edu

ABSTRACT

Mass-selected infrared photodissociation spectroscopy provides IR spectra for a variety of small carbocations including $C_2H_3^+$, $C_3H_3^+$, $C_3H_5^+$, protonated benzene and protonated naphthalene. Spectra in the frequency range of 600-4500 cm$^-$1 provide the some of the first IR data for these ions and evidence for the presence of co-existing isomeric structures (e.g., $C_3H_3^+$ is present as both cyclopropenyl and propargyl). Protonated naphthalene bands at 6.2, 7.7 and 8.6 microns match prominent features in the UIR spectra.

1. Introduction

Small carbocations are likely constituents in the interstellar medium, and believed to be intermediates in the synthesis of larger molecules such as polycyclic aromatic hydrocarbons (Hartquist & Williams 1998; Tielens 2005). However, their direct spectroscopic detection in space has been problematic because of limited laboratory data. New NASA missions focusing on infrared spectroscopy (Hershel, JWST) need this laboratory data more than ever. It has been known for many years that even the smallest carbocations may have more than one isomeric structure (Holmes et al. 2007). The relative stabilities of different isomers has been investigated extensively with computational chemistry. Unfortunately, experimental measurements of the spectroscopy of carbocations have been limited by the energetic conditions in which they are produced. Hot ions have broad spectra that are difficult to distinguish from neutral precursors present in the same experiment, and also difficult to compare to interstellar spectra measured at low temperature. The low densities of carbocations produced also provide a challenge to experiments. We describe a new pulsed discharge ion source in a supersonic expansion that provides high densities of cold carbocations. These ions are studied with IR photodissociation spectroscopy and computational chemistry, providing isomer-specific infrared signatures.

Previous gas phase spectroscopy measurements on carbocations are extremely limited (Crofton et al. 1989; Gabrys et al. 1995; Huang et al. 2006; Yeh et al. 1989; Boo et al. 1995; Dopfer et al. 2002; Solcà & Dopfer 2002; Lorenz et al. 2002). The available experiments suffer from low sample densities, high ion temperature, or the limited infrared laser tuning ranges available. Nevertheless, significant insights were obtained, including the identification of specific structures for certain ions and evidence for isomers. Laser photodissociation studies are more definitive (Yeh et al. 1989; Boo et al. 1995; Dopfer et al. 2002; Solcà & Dopfer 2002; Lorenz et al. 2002); because ions are mass-selected, there is no overlap with neutral precursor spectra. However, these studies were limited by the infrared lasers available, which until recently covered only the higher frequency C-H stretches. In our new experiments, gas phase ion production is combined with efficient supersonic molecular beam cooling and mass-selection to produce higher densities of cold ions. To cover the full infrared spectral range, we take advantage of new optical parametric oscillator laser sources. These developments allow significant improvements in carbocation spectroscopy. Here, we describe new infrared spectra of $C_2H_3^+$, $C_3H_3^+$, $C_3H_5^+$, protonated benzene and protonated naphthalene.

2. Experimental

Carbocations are produced by a pulsed discharge synchronized with a pulsed-nozzle gas expansion. A General Valve provides gas pulses 250 microseconds in duration containing helium or argon expansion gas with a small partial pressure of a hydrocarbon precursor such as acetylene or ethylene. The discharge pulse lasts 5-10 microseconds and is timed to occur in the middle of the gas pulse. Ions traverse the molecular beam apparatus as a neutral plasma to a differentially pumped chamber downstream, where pulsed acceleration plates extract them into a reflectron time-of-flight mass spectrometer (RTOF). The RTOF mass analyzes and size-selects ions for infrared photodissociation spectroscopy (Duncan 2003). Size selection eliminates neutral precursor signals, but the density remaining is too low for absorption measurements. Photodissociation measurements are problematic because the hydrocarbon bonds energies are higher than the energies of vibrational fundamentals to be probed. To enhance photodissociation, we employ the method of rare gas atom "tagging," in which a mixed complex containing one or more attached argon atoms is produced and mass selected, and infrared excitation leads to elimination of argon (Duncan 2003). Computational studies using density functional theory or MP2 methods examine both the carbocation and its argon complex.

The infrared laser employed is a Nd:YAG (Spectra Physics Pro-230) pumped optical parametric oscillator/amplifier (OPO/OPA) system provided by LaserVision. In its basic configuration with KTP oscillator and KTA amplifier crystals, this laser provides output in

the 2000-4500 cm^{-1} region. An added $AgGaSe_2$ crystal covers the range of 600-2200 cm^{-1}. The linewidth throughout the tuning range is about 1 cm^{-1}.

3. Results and Discussion

$C_2H_3^+$ has two possible low energy structures, including protonated acetylene, with a proton in the symmetric π position on the triple bond, and the vinyl cation, which has the $HCCH_2^+$ structure (Holmes et al. 2007). Computational studies find these to lie within 1-2 kcal/mol of each other. Previous IR absorption spectroscopy by Oka and coworkers studied the C-H stretching region (Crofton et al. 1989; Gabrys et al. 1995), finding evidence for the protonated acetylene structure, although the spectra were complex to assign because of the high temperature of the plasma. A key feature of the protonated acetylene structure not detected previously is the proton stretch vibration, which is predicted to occur near 2200 cm^{-1}. Our IR photodissociation spectra of $C_2H_3^+$-Ar, found an extremely strong resonance at 2217 cm^{-1} (Douberly et al. 2008a). The vinyl cation has no vibrations predicted anywhere near this frequency. This observation therefore confirms that $C_2H_3^+$ has the protonated acetylene structure suggested by theory to be most stable.

$C_3H_3^+$ has isomers corresponding to the cyclopropenyl cation and the propargyl cation, having the linear backbone H-C=C-C^+H_2 (Holmes et al. 2007). The cyclic species is predicted to be more stable, lying 25 kcal/mol lower in energy than propargyl. Previous gas phase measurements by Dopfer and coworkers studied mass-selected photodissociation in the C-H stretching region (Dopfer et al. 2002). The spectra were broad with poor signal levels, but evidence was found for the presence of both isomeric structures. This was surprising because the barrier to interconversion of these isomers is quite high (about 50 kcal/mol) (Holmes et al. 2007). Our new spectrum detects sharp bands throughout the infrared, with a cluster of five bands in the C-H stretching region (Ricks et al. 2010). Because of its high symmetry, the cyclic species should have only one IR-active vibration here, while the propargyl ion should have several. Likewise, propargyl should have several bands in the fingerprint region, with a strong C=C stretch near 2100 cm^{-1}, which we detect at 2077 cm^{-1}. This and other distinctive bands confirm that our spectrum is dominated by the propargyl cation. This makes sense, as the precursor used for this experiment was propargyl bromide. The cyclopropenyl cation should have only one strong IR band in the fingerprint region corresponding to the asymmetric carbon ring deformation. We detect this at 1293 cm^{-1}, but only when the discharge is hot. One of the bands in the C-H stretching region (3182 cm^{-1}) grows in intensity together with this 1293 cm^{-1} band, and is therefore assigned to the asymmetric C-H stretch of the cyclic species. However, none of the band positions in the C-H stretching region agree well with the predictions of theory.

Protonated benzene ($C_6H_7^+$) was determined by Olah and coworkers to have a sigma complex structure, with a CH_2 protonation site (Holmes et al. 2007). The gas phase spectrum was first measured by Dopfer and coworkers in the C-H stretching region (Solcà & Dopfer 2002). Our spectrum covers the full range of the C-H stretches and the fingerprint region (Douberly et al. 2008b). It includes a strong band near 2820 cm^{-1} assigned to the overlapping symmetric and asymmetric stretches of the CH_2 group resulting from sigma bonding of the proton, and another at 1607 cm^{-1} corresponding to the C_3 asymmetric stretch in the back-side of the ring where the charge is delocalized. This latter feature confirms that protonation partially disrupts the aromaticity of the ring system.

The band in the protonated benzene spectrum near 1607 cm^{-1} is quite close to the position of the 6.2 micron band seen in the Unassigned Infrared Bands, or so-called "UIRs" (Tielens 2008). Because of this, and because the UIRs are associated with polycyclic aromatic hydrocarbons (Tielens 2008), we extended these studies to the next-larger PAH system, naphthalene. Neutral and cation forms of PAHs had already been shown to not match the UIR patterns (Tielens 2008), and so we focus on protonated PAHs. The infrared spectrum of protonated naphthalene (Figure 1) has prominent features like those for protonated benzene, but with small spectral shifts (Ricks et al. 2009). We present our spectrum in microns to compare to the UIR bands. The 1607 cm^{-1} band seen for protonated benzene occurs at 1617 cm^{-1} for protonated naphthalene, bringing this into nice agreement with the 6.2 micron UIR band. Surprisingly, two other well-known UIR bands at 7.7 and 8.6 microns are also reproduced in the H^+naphthalene spectrum. Significantly, all of these bands are associated with protonation of the aromatic system. The 6.2 band is the C_3 carbon ring vibration where the charge is delocalized after sigma protonation, the 7.7 micron band is the scissors motion of the CH_2 group resulting from sigma protonation, and the 8.6 micron band is the bend of this same CH_2 group. These same features are expected for larger protonated PAHs, suggesting a compelling explanation for some of the key UIR features.

We gratefully acknowledge support from the National Science Foundation for this work.

REFERENCES

Boo, D. W., Liu, Z. F., Suits, A. G., Tse, J. S., Lee, Y. T. 1995, Science, 269, 57

Crofton, M. W., Jagod, M.-F., Rehfuss, B. D., Oka, T. 1989, J. Chem. Phys., 91, 5139

Dopfer, O., Roth, D., Maier, J. P. 2002, Intl. J. Mass Spectrom., 218, 281

Douberly, G. E., Ricks, A. M., Ticknor, B. W., McKee, W. C., Schleyer, P. v. R., Duncan, M. A. 2008a, J. Phys. Chem. A, 112, 1897

Douberly, G. E., Ricks, A. M., Ticknor, B. W., Schleyer, P. v. R., Duncan, M. A. 2008b, J. Phys. Chem. A, 112, 4869

Duncan, M. A. 2003, Intl. Rev. Phys. Chem., 22, 407

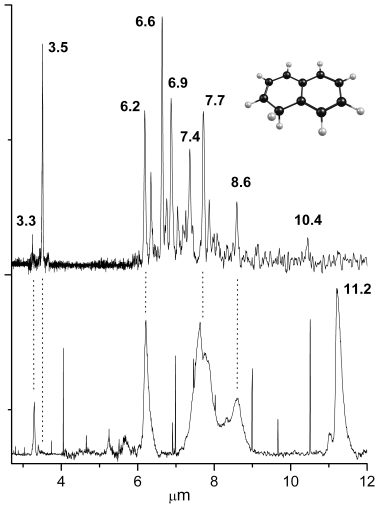

Fig. 1.— The infrared photodissociation spectrum of protonated naphthalene measured with argon tagging (upper trace) compared to the UIR spectra.

Gabrys, C. M., Uy, D., Jagod, M.-F., Oka, T. 1995, J. Phys. Chem., 99, 15611

Hartquist, T. W., Williams, D. A., eds. 1998, *The Molecular Astrophysics of Stars and Galaxys*, Oxford Science Publications, Clarendon Press, Oxford, U.K.

Holmes, J. L., Aubry, C., Mayer, P. M. 2007, *Assigning Structures to Ions in Mass Spectrometry*, CRC Press, Boca Raton, Florida

Huang, X., McCoy, A. B., Bowman, J. M., Johnson, L. M., Savage, C., Dong, F., Nesbitt, D. J. 2006, Science, 311, 60

Lorenz, U. J., Solcà, N., Lemaire, J., Maître, P., Dopfer, O. 2007, Angew. Chem. Int. Ed., 46, 6714

Ricks, A. M., Douberly, G. E., Duncan, M. A. 2009, Astrophys. J., 702, 301

Ricks, A. M., Douberly, G. E., Schleyer, P. v. R., Duncan, M. A. 2010, J. Chem. Phys., 132, 051101

Solcà, N., Dopfer, O. 2002, Angew. Chem. Int. Ed., 41, 3628

Tielens, A. G. G. M. 2005, *The Physics and Chemistry of the Interstellar Medium*, Cambridge University Press, Cambridge, U. K.

Tielens, A. G. G. M. 2008, Ann. Rev. Astron. Astrophys., 46, 289

Yeh, L. I., Price, J. M., Lee, Y. T., 1989, J. Am. Chem. Soc., 111, 5597

NASA LAW, October 25-28, 2010, Gatlinburg

Oscillator Strengths and Predissociation Rates of CO Rydberg Bands: Initial Results from Measurements at the SOLEIL Synchrotron

S.R. Federman, & Y. Sheffer[1]

Department of Physics and Astronomy, Univ. of Toledo, Toledo, OH 43606

steven.federman@utoledo.edu, ysheffer@astro.umd.edu

M. Eidelsberg, J.L. Lemaire, & F. Rostas

LERMA UMR8112 du CNRS et l'Observatoire de Paris, Meudon, France

michele.eidelsberg@obspm.fr, jean-louis.lemaire@obspm.fr, francois.rostas@obspm.fr

G. Stark

Department of Physics, Wellesley College, Wellesley, MA 02481

gstark@wellesley.edu

J.-H. Fillion

Laboratoire de Physique Moléculaire pour l'Atmosphère et l'Astrophysique, UPMC, Univ. Paris 06, UMR7092, LPMAA, F-75005, Paris, France

jean-hugues.fillion@upmc.fr

J.R. Lyons

Inst. of Geophysics and Planetary Physics, UCLA, Los Angeles, CA 90095

jimlyons@ucla.edu

P.L. Smith

Center for Astrophysics, Cambridge, MA 024138

plsmith44@gmail.com

B.R. Lewis, & A.N. Heays

Research School of Physics and Engineering, Australian National Univ., Canberra, Australian Capital Territory 0200, Australia

brenton.lewis@anu.edu.au, alan.heays@anu.edu.au

N. de Oliveira, & M. Roudjane[2]

Société Civile Synchrotron Soleil, Orme des Merisiers St AUBIN BP 48, 91192 GIF sur Yvette CEDEX, FRANCE

nelson.de.oliveira@synchrotron-soleil.fr, rmo233@uky.edu

ABSTRACT

CO is used as a probe of astrophysical environments ranging from planetary atmospheres and comets to interstellar clouds, the environment of the early Solar Nebula, and the envelopes surrounding stars near the end of their lives. One of the processes controlling the CO abundance and the ratio of its isotopologues is photodissociation. Accurate oscillator strengths and predissociation rates for Rydberg transitions are needed for modeling this process. We present initial results of a survey to obtain the necessary data for transitions in $^{12}C^{16}O$, $^{13}C^{16}O$, $^{13}C^{18}O$, and $^{12}C^{18}O$. Absorption spectra between 900 and 1200 Å were acquired at the DESIRS beam-line on the SOLEIL synchrotron. A VUV Fourier Transform Spectrometer provided a resolving power of about 300,000; this greatly aided our ability to disentangle absorption arising from overlapping bands. The spectra were analyzed with codes developed independently at Meudon, Toledo, and Canberra. Non-linear least-squares fitting procedures were used to determine optimum values of line and band oscillator strengths and predissociation line widths. We will compare our results to previous ones and will describe future directions for this effort.

---

[1]Currently at the Univ. of Maryland.

[2]Currently at the Univ. of Kentucky.

1. Introduction

Models of astronomical environments containing CO require accurate molecular data when trying to reproduce observations. Rydberg transitions are particularly important for CO photodissociation (e.g., van Dishoeck & Black 1988). Our group has been active producers of the necessary data on electronic transitions, mainly oscillator strengths, for over 20 years. Stark et al. (1999) obtained band oscillator strengths (f-values) for B-X (0,0) and (1,0) (hereafter, B00 and B10) via laser absorption. Federman et al. (2001) obtained f-values for B00, B10, C00, C10, and E00 from measurements at the Synchrotron Radiation Center at the Univ. of Wisconsin. The results for the relatively weak B00 and B10 bands showed excellent agreement. Sheffer et al. (2003) detected interstellar Rydberg bands in spectra acquired with the *Far Ultraviolet Spectroscopic Explorer*, confirming the results of Federman et al. for the C00, C10, and E00 bands. Furthermore, Sheffer et al. also derived f-values for bands that lead to CO photodissociation according to the models, such as those of van Dishoeck & Black (1988), (i.e., E10, K00, L′10, W10, W20, W30, and I′00). Using the SuperACO synchrotron in Orsay, France, Eidelsberg et al. (2004b) obtained results for K00, L00, and L′10, while Eidelsberg et al. (2006) provided results on E10, B60, and W00 through W30. The latter study yielded predissociation widths as well. These two studies confirmed the f-values derived by Sheffer et al. for the $^{12}C^{16}O$ isotopologue. Eidelsberg et al. (2004b, 2006) also presented results for the $^{13}C^{16}O$ and $^{13}C^{18}O$ isotopologues.

2. Experiment

The high-resolution DESIRS beamline at the SOLEIL synchrotron was recently commissioned. The Fourier Transform Spectrometer can provide unprecedented spectral resolution, $\lambda/\Delta\lambda \approx$ 1,000,000, at far ultraviolet wavelengths [de Oliveira et al. (2009)]. The FTS is based on wave front division instead of amplitude division and relies on a modified bimirror configuration requiring only flat mirrors. The path difference is scanned through the translation of one reflector. The bandpass is set by an undulator and is typically 50 Å between 900 and 1100 Å.

Data were acquired at several pressures for each wavelength region. The typical values were 10 to 50 mTorr within the capillary of the differentially pumped sample chamber. It is important to know the column of gas as accurately as possible. The CO column is derived from fitting absorption from the B00 and B10 bands. In the past, we used the E00 and W00 bands, but subsequent analysis of SOLEIL spectra revealed the presence of perturbations in E00 and W00. In addition, W00 is too strong for accurate determinations of gas columns. All syntheses are based on adopting a sinc function for the instrumental line width.

3. Results

Among the transitions of interest are a series of bands between 930 and 936 Å. For $^{12}C^{16}O$, there are interactions involving the Rydberg levels 4pπ(2), II $^1\Pi$, 4pσ(2), 5pπ(0), 5pσ(0), and I $^1\Pi$. The band nomenclature is from Eidelsberg et al. (2004a). Our preliminary results are for a single pressure. The f-value obtained for the transition to 4pπ(2) agrees well with earlier experimental efforts (Eidelsberg et al. 1991; Stark et al. 1991; Yoshino et al. 1995). While summed f-values for complexes, and sub-complexes, are consistent across studies, our experiments now resolve individual bands for the first time. In the earlier studies, the blends involving II $^1\Pi$, 4pσ(2), and 5pπ(0) on the one hand, and 5pσ(0) and I $^1\Pi$ on the other, could not be distinguished.

The ultimate goal of our set of CO experiments is to provide the data needed in photochemical models. We are currently deriving oscillator strengths and predissociation rates for the W–X series of bands for each isotopologue. We will then turn our attention to the interacting bands near 930 Å, followed by the first high-resolution study of the interacting bands of the complex 6pσ + 6pπ(0) near 915 Å. Once the models incorporate the extensive set of molecular data, we can look forward to improved understanding of the environments probed by CO.

This research was supported by funds from NASA (grants NNG 06-GC70G and NNX10AD80G to the Univ. of Toledo and NNX09AC56G to Wellesley) and CNRS.

REFERENCES

de Oliveira, N., Joyeux, D., Phalippou, D., Rodier, J. C., Polack, F., Vervloet, M., & Nahon, L. 2009, Rev. Sci. Instru., 80, 043101

Eidelberg et al. 2004a, J. Chem. Phys., 121, 292

Eidelsberg, M., Lemaire, J. L., Fillion, J.-H., Rostas, F., Federman, S. R., Sheffer, Y., 2004b, A&A, 424, 355

Eidelsberg, M., Sheffer, Y., Federman, S. R., Lemaire, J. L., Fillion, J.-H., Rostas, F., & Ruiz, J. 2006, ApJ, 647, 1543

Eidelsberg, M., Viala, Y., Rostas, F., & Benayoun, J. J. 1991, A&AS, 90, 231

Federman, S. R., Fritts, M., Cheng, S., Menningen, K. M., Knauth, David C., & Fulk, K. 2001, ApJS, 134, 133

Sheffer, Y., Federman, S. R., & Andersson, B.-G. 2003, ApJ, 597, L29

Stark, G., Lewis, B. R., Gibson, S. T., & England, J. P. 1999, ApJ, 520, 732

Stark, G., Yoshino, K., Smith, Peter L., Ito, K., & Parkinson, W. H. 1991, ApJ, 369, 574

van Dishoeck, E. F., & Black, J. H. 1988, ApJ 334, 771

Yoshino, K., Stark, G., Esmond, J. R., Smith, P. L., Ito, K., & Matsui, T. 1995, ApJ, 438, 1013 (Y95)

NASA LAW, October 25-28, 2010, Gatlinburg

Construction of a High-Resolution Terahertz Cavity Ringdown Spectrometer

P. Brandon Carroll, Brett A. McGuire, & Susanna L. Widicus Weaver[1]

Department of Chemistry, Emory University, Atlanta, GA 30322

pbcarro@emory.edu, brett.mcguire@emory.edu, susanna.widicus.weaver@emory.edu

ABSTRACT

Two NASA far-infrared observatories, the Herschel Space Observatory and the Stratospheric Observatory for Infrared Astronomy (SOFIA), have undertaken their science missions in the past year. These observatories are set to provide an unprecedented amount of astronomical data in the relatively unexplored far-IR, or terahertz (THz), spectral window. However, the corresponding laboratory spectra needed to interpret these observations remain largely unavailable. Acquisition of such spectra is hindered by the limitations of current-generation laboratory spectrometers at these frequencies. Spectral data for transient species that are thought to play important roles in interstellar chemistry are particularly difficult to acquire without a high-sensitivity, high-resolution spectroscopic technique that goes beyond the standard direct absorption spectrometer. We are developing a THz cavity ringdown spectrometer coupled with a supersonic expansion to aid in the laboratory characterization of unstable molecules that are of astronomical importance. We will report on the performance of our benchtop prototype instrument, as well as our progress toward development of a full THz cavity ringdown spectroscopy (THz-CRDS) system for the study of transient astrochemical molecules.

1. Introduction

Many transient molecules such as ions and radicals are thought to be key intermediates in interstellar chemistry, yet the spectroscopic information needed to identify and characterize

[1]Department of Chemistry, Emory University, 1515 Dickey Dr. Atlanta, GA 30322

these species through astronomical observations is either limited in coverage or nonexistent. This is mainly due to the unstable nature of these molecules and the challenging methods required for their production. Because transient molecules are produced in such low yield and often have very weak signals, their laboratory spectroscopic study requires a technique with very high sensitivity. Although techniques are available in the microwave and infrared ranges that offer high sensitivity, the sensitivity of THz spectrometers has lagged behind those at shorter and longer wavelengths.

The most common technique used in the THz spectral window is direct absorption spectroscopy, where the sensitivity is limited by the pathlength of the radiation through the sample. Long pathlength spectrometers and multi-pass configurations can improve the sensitivity, but are ultimately limited by signal attenuation. This results in a minimum detectable absorption coefficient, α_{min}, of $\sim 10^{-5}$ cm^{-1}, well above that required for the detection of many transient species. The case of protonated methanol ($CH_3OH_2^+$), a key gas-phase reaction intermediate in interstellar chemistry, can be used to illustrate the current sensitivity limitations. The estimated production efficiency of this ion in a plasma discharge source ($\leq 10^{-6}$) coupled with the predicted rotational spectral line strengths based on electronic structure calculations [Woon (2007)] indicate that $\alpha_{min} \leq 10^{-9}$ cm^{-1} is required for its laboratory study. There is no spectroscopic technique currently available in the THz range that provides this level of sensitivity.

Cavity ringdown spectroscopy (CRDS) is a highly sensitive technique commonly used in the infrared and optical regimes that provides $\alpha_{min} \leq 10^{-10}$ cm^{-1} [Berden et al. (2000)]. This technique is currently limited to frequencies >30 THz, well above the frequency coverage of the Herschel observatory and most SOFIA instruments. This frequency limit arises from a lack of suitable high-reflectivity mirrors [Schiwon et al. (2002), Du Bosq et al. (2004)]. An alternative to traditional systems that use dielectric mirrors is an optical cavity formed with wire grid polarizers rotated 90° from their normal orientation as proposed by Braakman et al. (2006). Wire grid polarizers offer extremely high reflectivity (R≥99.9%) in the THz region, and maintain this reflectivity across wide spectral ranges. The losses in a cavity formed from two wire grid polarizers are due almost entirely to transmission, making them extremely well-suited for implementation in THz-CRDS.

2. Cavity Design and Performance

We are developing a continuous wave (cw) THz-CRDS instrument based on a previous cavity design utilizing wire grid polarizers [Braakman et al. (2006)]. The cavity layout is shown in Figure 1. The cavity consists of of a photolithographically etched gold polarizer

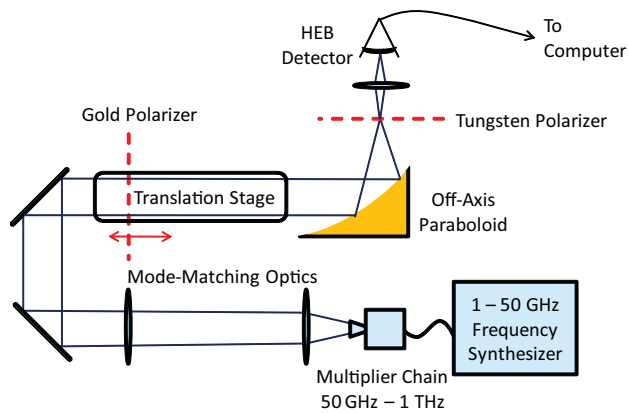

Fig. 1.— Schematic diagram for the THz-CRDS benchtop instrument.

mounted on a translation stage and a free-standing tungsten wire polarizer. These polarizers are arranged in an off-axis configuration with a 90° off-axis parabolic mirror serving as a focusing element within the cavity. The light source is a 1 - 50 GHz frequency synthesizer coupled with a multiplier chain that produces output frequencies from 50 GHz - 1 THz. The output of the multiplier is collimated using mode-matching optics, and is coupled into the cavity through the gold polarizer. The output of the cavity is then detected through the tungsten polarizer by a hot electron bolometer. The use of slightly transmissive polarizers in an off-axis configuration circumvents the need for beam splitters, thus avoiding the attenuation and back reflection issues faced by earlier designs [Braakman et al. (2006); Meshkov & De Lucia (2005)].

Cavity mode spectra have now been acquired that demonstrate the cavity performance. A representative spectrum acquired by scanning the input frequency while holding the cavity length constant is shown in Figure 2. Sharp peaks, arising solely from the fundamental cavity mode are observed with a spacing of 445 MHz and a width of $\delta\nu \approx 1.7$ MHz, corresponding to

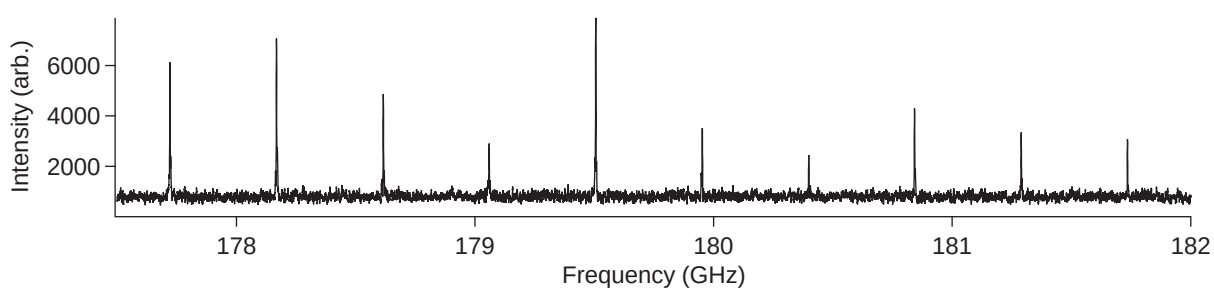

Fig. 2.— Cavity mode spectrum taken by varying the input frequency while holding the cavity length constant.

a cavity reflectivity of R $\approx$ 98.8%. A translation stage has now been incorporated to move the gold polarizer, enabling acquisition while scanning the cavity length and holding the input frequency constant, as is the typical acquisition mode for cw-CRDS. Neither polarizer used in our current setup is of the quality required to achieve $\alpha_{min} \leq 10^{-9}$ cm^{-1}. However, this equipment was loaned to our group by our collaborators for the purpose of developing a proof-of-concept benchtop instrument.

3. Conclusion and Future Work

A proof-of-concept cw-THz-CRDS instrument that uses wire grid polarizers to form the cavity has now been demonstrated. We plan to next incorporate higher reflectivity polarizers to form a higher quality cavity and increase the sensitivity of the instrument. We will then move the instrument from the benchtop to a vacuum chamber, where an ion source will be incorporated. This instrument will provide the sensitivity required for spectroscopic studies of transient molecules such as radicals and ions that are important in interstellar chemistry in the wavelength range covered by the Herschel and SOFIA observatories.

This work was supported by the startup funds of SLWW provided by Emory University. We thank Geoffrey Blake for the loan of the tungsten polarizer, and Kenneth Wood and QMC Instruments, Ltd., for the loan of the gold polarizer.

REFERENCES

Berden, G., Peeters, R., & Meijer, G. 2000, Int. Reviews in Physical Chemistry, 19, 565

Braakman, R., Kelly, M. J., Cossel, K., & Blake, G. A. 2006, 61st Ohio State University International Symposium on Molecular Spectroscopy, WI03

Du Bosq, T. W., Muravjov, A. V., & Peale, R. E. 2004, Proc. SPIE, 5411, 167

Meshkov, A. I. & De Lucia, F. C. 2005, Rev. Sci. Instrum. 76, 083103

Schiwon, R., Schwaab, G., Bründermann, E., & Havenith, M. 2002, Appl. Phys. Lett. 73, 259

Woon D. 2007, 62nd Ohio State University International Symposium on Molecular Spectroscopy, TI10

NASA LAW, October 25-28, 2010, Gatlinburg

Construction of Spectroscopically Accurate IR Linelists for NH_3 and CO_2

Xinchuan Huang[1], David W. Schwenke[2], & Timothy J. Lee[3]

NASA Ames Research Center, Moffett Field, CA 94035

Xinchuan.Huang-1@nasa.gov, David.W.Schwenke@nasa.gov, Timothy.J.Lee@nasa.gov

ABSTRACT

The strategy of using the best theory together with high-resolution experiment was applied to NH_3 and CO_2: that is, refine a highly accurate ab initio PES with the most reliable HITRAN or pure experimental data. With 0.01 - 0.02 cm^{-1} accuracy, our calculations are clearly far beyond simply reproducing experimental data, but are also capable of revealing many deficiencies in the current experimental analysis of the various isotopologues, as well as provide reliable predictions with similar accuracy.

1. Introduction

The lack of accurate spectral opacity data for important molecules in astrophysical environments has limited our ability to fully analyze the huge amount of astronomical data from space missions and earth-based observations. In 1997, the "best theory + high-resolution experimental data" strategy was first adopted by one of us (DWS) to generate a highly accurate IR line list for water and its isotopologues((Pattridge&Schwenke,1997)). The linelist has greatly enhanced experimentalists' ability to analyze and model water spectra under extreme conditions. Recently, this strategy has been extended from water(H_2O) to Ammonia (NH_3) [see (Huang,Schwenke&Lee,2008) and (Huang,Schwenke&Lee,2010) and Carbon Dioxide(CO_2) (Huang,Schwenke&Lee,2010)]. This is a progress summary including the unprecedented accuracies obtained in these studies.

---

[1]SETI Institute, 189 Bernardo Ave.,Mountain View, CA 94043

[2]MS T27B-1, NASA Ames Research Center, Moffett Field, CA, 94035

[3]MS 245-1, NASA Ames Research Center, Moffett Field, CA, 94035

2. Short Summary of Strategy and Technical Aspects

A high-quality, purely ab initio global potential energy surface (PES) was refined with the most reliable high-resolution experimental data from the HITRAN data base. Full-dimensional, exact quantum rovibrational calculations are run using the refined PES to get highly accurate energy levels, line positions, and wavefunctions, followed by calculation of IR intensities with a high-quality dipole moment surface. For NH_3, both the Diagonal Born-Oppenheimer Correction and non-adiabatic corrections have been incorporated into the refinement to achieve 0.01-0.02 cm^{-1} accuracy on the HSL-2 PES. For CO_2, a QZ level PES was chosen to refine since that PES showed the most promise. Non-adiabatic corrections have not yet been included. See Refs. 1-2 for more details.

3. Results and Findings

Ammonia: How to Achieve σ_{rms} =0.01-0.02 cm^{-1} Accuracy? See Fig.1

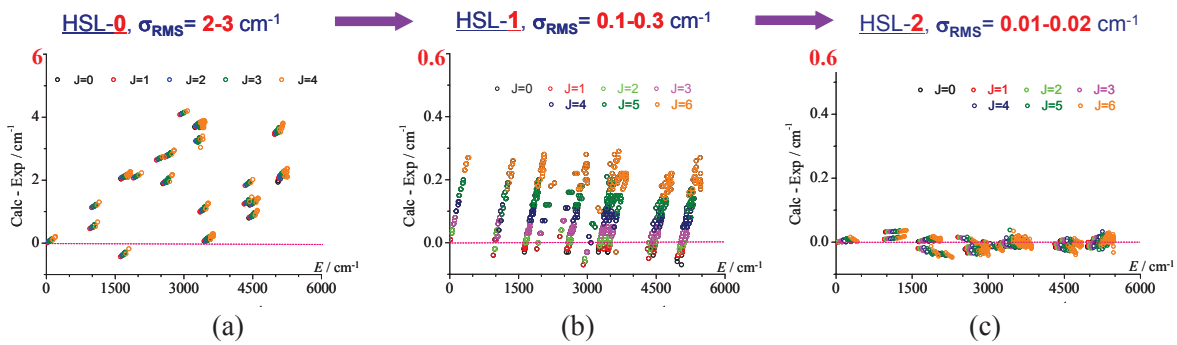

Fig. 1.— Two orders of magnitude RMS error reduction from the purely ab initio HSL-0 to HSL-1 to the latest HSL-2. From left to right, a), b), and c) are for HSL-0/1/2, respectively.

(1) New assignments are proposed for a few $\nu_3 + \nu_4$ transitions and/or levels.
(2) HITRAN models of the $2\nu_4$ bands are identified as UNRELIABLE. New assignments are suggested for new or missing $2\nu_4$ levels and the strong mixing between the $2\nu_4$ and $2\nu 2 + \nu_4$ bands is identified as the source of the difficulties in the experimental modeling of $2\nu_4$.
(3) New bands found in existing HITRAN data: ν_2+ν_4, (ν_3+ν_4)-A'/A", ν_1+2ν_2, and 2ν_2+2ν_4.
(4) $4\nu_2$ band analysis confirms the prediction reliability & accuracy that HSL-2 yields.
(5) IR energy level lists are available for other bands missing from HITRAN(<5100 cm^{-1})
(6) For $^{15}NH_3$, similar agreement for the available HITRAN levels or transitions is achieved. The ^{15}N isotopic effects are presented for all J=0-6 levels of 13 HITRAN bands.
(7) For $^{14}ND_3$, we can easily reproduce the pure rotational inversion spectra line frequencies

with an accuracy similar to that found for $^{14}NH_3$. However, it is not possible to reproduce the four pairs of inversion-splitting vibrational fundamentals with ALL deviations $< 0.05 cm^{-1}$ simultaneously. We will re-visit the $^{14}ND_3$ ν_2/ν_4 bands.

Table 1: Number of J=0-6/7-12 IR levels and σ_{rms} for 13 $^{14}NH_3$ bands in HITRAN.(cm^{-1})

J	IR	HITRAN	Missing	$\sigma(s/a)$	$\sigma(\Delta)$
0-6	1030	1005	25	0.015	0.011
7	315	294	21	0.020	0.014
8	357	328	29	0.023	0.015
10	441	341	100	<0.039	<0.029
12	525	274	251	<0.043	<0.032

Carbon Dioxide: Highly Accurate PES and Primitive IR LineList. See Fig.2

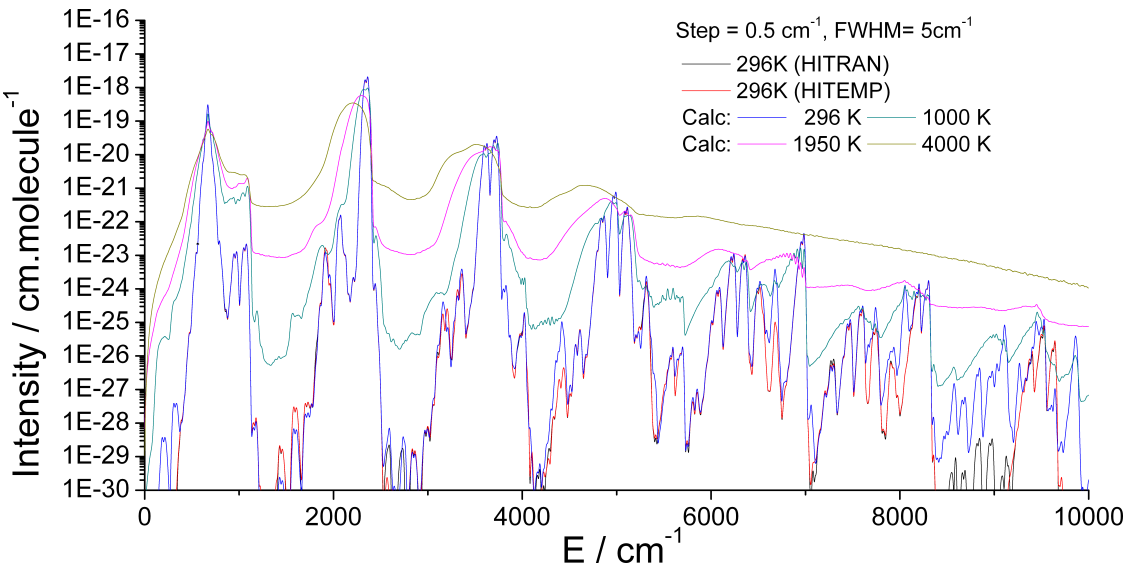

Fig. 2.— Simulated IR spectra at 296K,1000K,1950K,and 4000K, generated in this work, and compared with HITEMP/HITRAN spectra.

(1) For refinement involving J>15-20, purely experimental data must be used! (HITRAN models contain too much contamination)
(2) Very consistent σ_{rms}=0.01-0.02 cm^{-1} for ALL purely experimentally determined energy levels (J=0-117, E=0-14,320 cm^{-1}).
(3) The refined PES (HSL-1 for CO_2) has excellent extrapolation properties, it can be used to

search and assign new bands of minor CO_2 isotopologues, as well as to verify/check current models. For example, 0.00-0.03 cm^{-1} accuracy is obtained for the 626/636 isotopologue band origins, while very consistent 0.03-0.10 cm^{-1} deviations are obtained for band origins of all other isotopologues. In addition, new bands have been identified for 636/727, and unreliable band origins have been found for 626/727/638.
(4) Using our initial IR linelist, simulated spectra have been generated at 296K, 1000K, 1950K, and 4000K. They compare well with HITRAN2008 and HITEMP2010. Measured IR intensities of >80% experimental transitions have been reproduced with 5-10% deviations.
(5) High temperature IR simulations at 1000K and 2350K have shown that the reliability and accuracy of our Ames Linelist for $^{12}CO_2$ is nearly identical to the CDSD database.

4. Conclusion

The accuracy of our work has gone far beyond simply reproducing experimental data; we can now provide very solid analysis and predictions to help experimentalists in future lab or astronomical data analysis. The present work represents a very significant advance in the state of our knowledge of the spectroscopy of NH_3 and CO_2. Further improvments are feasible for both line position and intensities, and will be reported in due course.

We gratefully acknowledge the financial support from the NASA grant 08-APRA08-0050, the NASA Spitzer GO Program (Cycle 4, AR-4 PID 40645), and the Venus Express Supporting Investigator Program. X.H. acknowledges financial support by NASA Post-Doctoral Fellowship (2006-2009) and NASA/SETI Institute Cooperative Agreement NNX09AI49A. For the CO_2 work, we also deeply thank Dr. Sergey Tashkun for sharing the most reliable experimental data collection.

REFERENCES

Partridge, H. & Schwenke, D. W. 1997, J. Chem. Phys. 106, 4618

Huang, X., Schwenke, D. W., & Lee, T. J. 2008, J. Chem. Phys. 129, 214304

Huang, X., Schwenke, D. W., & Lee, T. J. 2010, J. Chem. Phys., submitted.

This preprint was prepared with the AAS LaTeX macros v5.2.

NASA LAW, October 25-28, 2010, Gatlinburg

Excited states and the completeness of astrophysical catalogs

S. M. Fortman, I. R. Medvedev, C. F. Neese, & F. C. De Lucia

Department of Physics, Ohio State University, Columbus, OH 43210

fortman@mps.ohio-state.edu, medvedev@mps.ohio-state.edu, cfneese@mps.ohio-state.edu, fcd@mps.ohio-state.edu

ABSTRACT

Calculations based on quantum mechanical (QM) models have successfully provided the laboratory basis for astrophysical observations. However, many unidentified spectral features remain and new telescopes will probe hotter regions with higher sensitivity. As a consequence, spectra in highly perturbed, difficult to analyze excited vibrational states will become more important. Here we discuss the completeness of catalogs based on QM calculations by comparing them with experimental observations for eight astrophysical weeds. It is shown that the difficulty of analysis of these excited states leads to substantial catalog incompleteness. Strategies for analysis, dissemination, and use of these new experimental results are discussed.

1. Introduction

We have developed a solution to the quantum mechanical (QM) catalog completeness problem that is based on intensity calibrated spectra taken at many temperatures, coupled with an analysis technique which makes it possible to calculate the usual parameters of the standard catalog - the spectral line strengths and lower state energies - without QM analysis. Fortman et al. (2010) Medvedev & De Lucia (2007)

2. Experimental Results - The Incompleteness of Catalogs

A comparison between the QM catalog and experimental results are shown for eight of the most common astrophysical weeds in Fig. 1.

Fig. 1.— An intensity sorted comparison between the catalog (red) and experimental (black) results. The horizontal red line is at the intensity ratio predicted from the lowest vibrational state that is missing from the QM catalog.

These plots show that the QM catalogs are massively incomplete. There are many strong lines that are not included. Conversely, many weak lines are included - not because they are important, but rather because they are easy to calculate. As a numerical example, in the 210 - 270 GHz region only 317 of the 3096 strongest lines in the experimental spectrum of ethyl cyanide are in the QM catalogs, while 936 of the lines in the QM catalogs are not among the 3096 strongest experimental lines. Based on this missing states analysis, Fig. 2 shows the ratio between the first line not included in the QM catalogs and the strongest line in the 210 - 270 GHz spectral region plotted as a function of temperature for each species. As expected, at low temperature, the QM catalogs are complete. However, in the 300 - 500 K region lines that are as strong as 50 percent of the strongest lines are missing.

The difficulty of obtaining these lines via QM analyses is highlighted by the fact that 40 different vibrational states - typically highly mixed and perturbed, contribute to the experimental results for ethyl cyanide shown in Figs 1 and 2.

Fig. 2.— The strongest missing line as a fraction of the strongest ground state line.

3. Catalog Results and Dissemination

In addition to the usual astrophysical catalog results, we also have developed a numerical frequency point-by-point approach which uses a similar fitting procedure on frequency points rather than lines. This is especially useful for blends and congested spectral regions. For a particularly congested and hard to model spectral region of ethyl cyanide, Fig. 3 shows a comparison of a single experimental scan (the green line), a spectrum calculated from the experimental catalog lines (the blue line), the frequency point-by-point fit (the black line), and the QM catalog (the red vertical lines). There are several points to notice: (1) Only a few of these lines are in the QM catalog and weaker lines are included in the QM catalog than some lines that are missed by the QM catalog, (2) Because of blends, some of the lines in the spectrum calculated from a convolution of the experimental catalog and the experimental

Doppler linewidth are too narrow, and (3) The point-by-point fit does a good job in dealing with the blends and overlaps. In addition, because the point-by-point fit is effectively an average over 400 lines, both the noise and baseline problems are significantly reduced from that of single experimental scans.

4. Summary

The experimental catalog summarized here is an attractive and accurate solution to an otherwise intractable problem, the massive incompleteness of catalogs based on QM calculations.

Fig. 3.— A comparison between an experimental scan (green), a simulation based on the experimental catalog (blue), a simulation based on the point-by-point fit (black), and the QM catalog (vertical red lines).

This work was supported by NASA.

REFERENCES

Fortman, S. M., Medvedev, I. R., Neese, C. F. & De Lucia, F. C. 2010, Ap. J., 714, 476

Medvedev, I. R. & De Lucia, F. C. 2007, Ap. J., 621, 656

NASA LAW, October 25-28, 2010, Gatlinburg

Ground Control Monitoring for the Organics Experiment on the EXPOSE-R Facility on the International Space Station

K. L. Bryson[1,2], F. Salama[2], P. Ehrenfreund[3], A. J. Ricco[2], Z. Peeters[4], B. Foing[5], E. Jessberger[6], F. Robert[7], & M. Mumma[8]

[1]*Bay Area Environmental Research Institute, Moffett Field, CA 94035*
[2]*NASA Ames Research Center, Moffett Field, CA*
[3]*Leiden Institute of Chemistry, The Netherlands*
[4]*Dept. of Terrestrial Magnetism, Carnegie Institute of Washington, Washington, DC*
[5]*ESA-SCI-S, The Netherlands*
[6]*University of Müenster, Germany*
[7]*LEME, France*
[8]*NASA Goddard Space Flight Center, Greenbelt, Maryland, 20771*

kathryn.bryson@nasa.gov, farid.salama@nasa.gov, p.ehrenfreund@chem.leidenuniv.nl

ABSTRACT

The *Organics* experiment is integrated into the multi-user facility EXPOSE-R mounted on the International Space Station (ISS). In this experiment organic samples of astronomical interest are exposed for a long duration to the space environment and will remain 24 months on-board the ISS before they are returned to Earth in March 2011. The radiation dose that is collected by the samples during flight exceeds the limits of simulations in the laboratory and the results will greatly enhance our knowledge on the evolution of large molecules in space environments. We describe the experimental components that are being used on the ISS for the exposure experiments and in the laboratory for ground-control measurements and present spectra measured in the UV-Vis range monitoring the ground control samples.

1. Introduction

Aromatic networks are likely the most abundant organic material in space. Specifically, PAHs and fullerenes have been identified in meteorites (Sephton et al 1998) and are

thought to be among the carriers for numerous astronomical absorption and emission features (Mathis, J.S. 1994; Salama et al 1996; Allamandola et al 1999; Tielens 2008). Recently, the fullerenes C_{60} and C_{70} neutral molecules have been discovered in the young planetary nebula Tc 1 (Cami et al 2010). PAHs and fullerenes seem widely distributed in space and to obtain knowledge on the stability of these molecules is crucial to enhance our understanding about the evolution of organics in space. Thin films of selected PAHs and fullerenes are being subjected to the low Earth orbit environment as part of the *Organics* experiment on EXPOSE-R onboard the ISS. The *Organics* experiment will monitor the chemical evolution, survival, destruction, and chemical modification of the samples in the space environment.

2. EXPOSE-R facility

EXPOSE-R is a multi-user facility attached to an external platform at the outer hull of the Service Module of the Russian Segment of the International Space Station (RS-ISS). The external platform, called URM-D, provides mechanical, electrical and data interfaces. EXPOSE-R accommodates 10 biological and biochemical experiments, which are mounted in three removable trays (see Fig. 1). EXPOSE-R allows defined long-term and/or short-term exposure of experiments to solar UV under vacuum or controlled atmosphere.

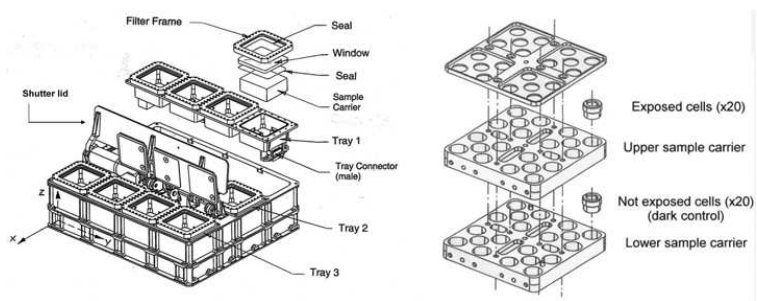

Fig. 1.— The EXPOSE facility is made of 3 trays into which 4 square sample carriers are fitted (left). For the *Organics* experiment, each sample carrier is designed for up to 20 cells (right).

EXPOSE-R with its experiment trays launched on flight 31P on November 26, 2008 with an unmanned PROGRESS cargo ship on a SOYUZ launcher from Baikonur, Kazakhstan. After a storage period inside the RS-ISS, it was mounted to the external URM-D by EVA on March 10, 2009 to start the exposure of the experiments to the space environment. All trays carry dark samples that are shielded from the UV photons and enable us to discriminate between the effects of exposure to photons and cosmic rays. Space exposure is planned for a period of at least 18 months, which will provide ∼2000 h effective exposure. The trays will be recovered by EVA in early spring 2011 and returned to Earth.

3. *Organics* experiment

The *Organics* experiment on EXPOSE-R consists of 12 PAHs (see Table 1) and the fullerenes C_{60}, C_{70}, and a $C_{60}/C_{70}/C_{84}$ mixture. The goal is to test the stability of such compounds when exposed to space conditions. PAH molecules such as those in Table 1 are expected to reside in the interstellar medium. It was our goal to identify the most stable PAH and fullerene species to gain insights into PAH chemistry. The PAH samples selected include a few small PAHs (e.g. tetracene) as well as large PAHs of catacondensed and pericondensed structure that were specially synthesized for this space experiment (at high purity: 99.9 %). Some of the PAHs and C_{60} have previously flown on the Organics experiment on BIOPAN V (Ehrenfreund et al. 2007), which had 58 h exposure with effective solar pointing.

Table 1: PAHs selected for the Organics experiment on EXPOSE-R.

PAH (formula)	Structure
Chrysene ($C_{18}H_{12}$)	4 ring, catacondensed
Triphenylene ($C_{18}H_{12}$)	4 ring, catacondensed
Tetracene ($C_{18}H_{12}$)	4 ring, catacondensed
Perylene ($C_{20}H_{12}$)	5 ring, pericondensed
Coronene ($C_{24}H_{12}$)	7 ring, pericondensed
Diphenantrho[9,10-b:910-d]thiophene ($C_{28}H_{16}S$)	7 ring, catacondensed
Ovalene ($C_{32}H_{14}$)	10 ring, pericondensed
Dinaphtho[8,1,2-abc:2,1,8-klm]coronene ($C_{36}H_{16}$)	11 ring, pericondensed
Circobiphenyl ($C_{38}H_{16}$)	12 ring, pericondensed
Dibenzo[jk,ab]octacene ($C_{40}H_{22}$)	10 ring, pericondensed
Tetrabenzo[de,no,st,cd]heptacene ($C_{42}H_{22}$)	11 ring, pericondensed
Dicoronylene ($C_{48}H_{20}$)	15 ring, pericondensed

The samples were deposited as thin (∼few hundred nm) films by sublimation onto MgF_2 windows to allow efficient penetration of UV photons (Ehrenfreund et al. 2007). The samples were analyzed before exposure to the space environment with UV-VIS and IR spectroscopy. The same analyses will also be performed after space exposure. 70 flight samples are being exposed on the EXPOSE-R facility.

4. Ground control measurements

Eight sample carriers remained on Earth. Two of these samples carriers are being ground truth monitored through UV-VIS spectroscopy every three months in the Astrophysics and Astrochemistry Laboratory at NASA Ames Research Center (Fig. 2). The samples are stored in a dark desiccator between measurements. Figure 3 shows the first and last UV-VIS

absorption spectra collected of the ground sample tetracene ($C_{18}H_{12}$) and its stability over 1.5 years.

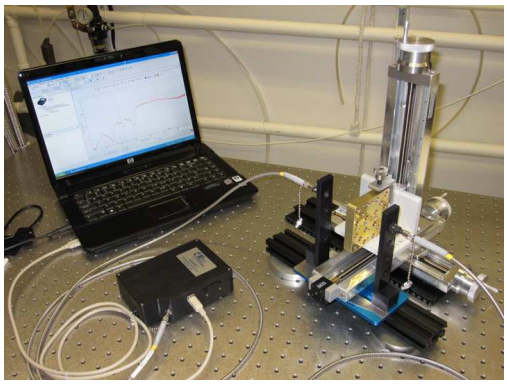

Fig. 2.— Ocean Optics HR4000 UV/VIS Spectrometer with x-y-z slide assembly in the Astrophysics and Astrochemistry Laboratory at NASA Ames setup for ground truth monitoring.

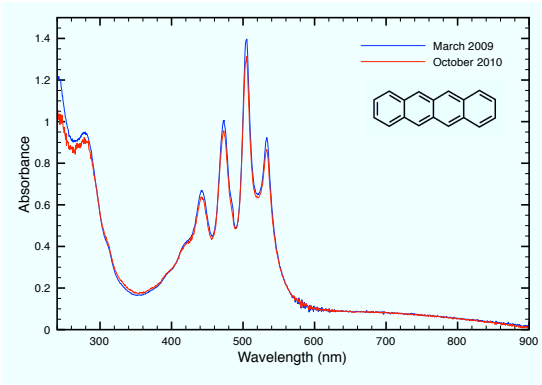

Fig. 3.— The ground control monitoring UV-Vis spectra of a thin film of the PAH tetracene sublimed onto MgF_2, displaying a strong band system around 500 nm.

The *Organics* experiment monitors the chemical evolution, survival, destruction and chemical modification of PAHs and fullerenes in space environment. From the results we shall determine constraints on the photochemistry of these compounds in the interstellar medium. Since PAHs are also present in meteorites, the obtained data are also relevant for the reconstruction of events in the early Solar System.

The authors acknowledge the support of the NASA SMD APRA program.

REFERENCES

Allamandola, L.J., Hudgins, D.M., & Sandford, S.A. 1999, Astrophys. J. 511, 115
Cami, J., Bernard-Salas, J., Peeters, E., & Malek, 2010, Science, 329, 1180
Ehrenfreund, P. et al. 2007, PSS, 55, 383
Mathis, J.S. 1994, Ap. J., 422, 176
Salama, F. et al. 1996, Ap. J., 458, 621
Sephton MA, Pillinger CT, & Gilmour I. 1998, Geochim. Cosmochim. Acta. 62, 1821
Tielens, A.G.G.M. 2008. Annu. Rev. Astron. Astrophys. 46, 289

This preprint was prepared with the AAS LaTeX macros v5.2.

NASA LAW, October 25-28, 2010, Gatlinburg

The OPASI-T Project: Investigating Optical Properties of Astronomical Silicates with Infrared Techniques

R. E. Kinzer, Jr.[1], S. Rinehart[1], D. Benford[1], E. Dwek[1], R. Henry[2], J. Nuth[3], R. Silverberg[1], E. Wollack[1]

NASA Goddard Space Flight Center, Greenbelt, MD 20771

stephen.a.rinehart@nasa.gov, raymond.e.kinzer@nasa.gov

ABSTRACT

Astronomical dust is observed in a variety of astrophysical environments and plays an important role in radiative processes and chemical evolution in the galaxy. Depending upon the environment, dust can be either carbon-rich or oxygen-rich (silicate grains). Both astronomical observations and ground-based data show that the optical properties of silicates can change dramatically with the crystallinity of the material, and recent laboratory research provides evidence that the optical properties of silicate dust vary as a function of temperature as well. Therefore, correct interpretation of a vast array of astronomical data relies on the understanding of the properties of silicate dust as functions of wavelength, temperature, and crystallinity. The OPASI-T (Optical Properties of Astronomical Silicates with Infrared Techniques) project addresses the need for high quality optical characterization of metal-enriched silicate condensates using a variety of techniques. A combination of both new and established experiments are used to measure the extinction, reflection, and emission properties of amorphous silicates across the infrared (near infrared to millimeter wavelengths), providing a comprehensive data set characterizing the optical parameters of dust samples. We present room temperature transmission measurements of iron silicate dust analogues and the experimental apparatus to be used to investigate and characterize additional metal-silicate materials.

[1]NASA Goddard Space Flight Center, Code 665, Greenbelt, MD 20771

[2]NASA Goddard Space Flight Center, Code 551, Greenbelt, MD 20771

[3]NASA Goddard Space Flight Center, Code 691, Greenbelt, MD 20771

1. Introduction

Astronomical dust is found in many environments. It forms in the outflows from stars and enters the interstellar medium, becoming an important component of the interstellar clouds from which stars form. Dust can be found in the disks surrounding young stars, where it can coalesce to form planetesimals and ultimately planets like Earth. The amount of order in silicates varies. The high temperatures, oxidizing atmosphere, and cooling processes of terrestrial environments produce crystalline structures (olivine, pyroxene, quartz), in whcich metal cations neutralize the charge of silicon tetrahedra, and melts, a mixture of unaligned crystalline structures with randomly distributed metal cations. In most astrophysical settings, silicates take less ordered structures. Chaotic condensates lack silicate tetrahedra, appearing like a "frozen" gas state, and are typically under-oxygenated with relatively high metal abundance. Neutral metal atoms and adsorbed water can be found on the surface or under layers as the grain grows. If these grains are then exposed to high temperatures ($\geq$1000 K), they can anneal, becoming increasingly ordered. Annealing of such chaotic condensates proceeds through a set of distinct steps towards crystallinity (Hallenbeck 2002) and implies that if the temperature history of the grains is known, their crystallinity (and, therefore, their infrared emission spectrum) can be predicted.

2. Overview of the OPASI-T Project

OPASI-T uses multiple techniques and apparatus to provide spectral data of silicates for a wide range of frequencies and temperatures (Kinzer 2010). Pe-exisintg experimental methods include extinction measurements [using Bruker IFS113v and IFS125HR Fourier transform spectrometers (FTS)] and waveguide measurements for extinction data at long wavelengths. New experimental techniques and instrumentation include a reflectometer, with an integrating sphere (using FTS) emissivitometer, using the integrating sphere operated at 4.2 K with a bolometer detector. From these measurements, we will then calculate the dielectric constants of the materials as a function of sample temperature (at various cryogenic temperatures) and annealing or crystallinity.

2.1. Condensate Sample Production

An apparatus for producing dust samples analogous to astronomical dust has been developed and demonstrated at Goddard (Nuth 2002). 10 nm scale smoke particles are produced by combusting hydrogen gas containing small amounts of silane, iron pentacarbonyl,

and metal vapor (e.g. Mg, Fe). Condensates are rapidly quenched and are collected on an aluminum substrate downstream of the furnace at temperatures below 350 K.

3. Preliminary Measurements of Iron Silicates

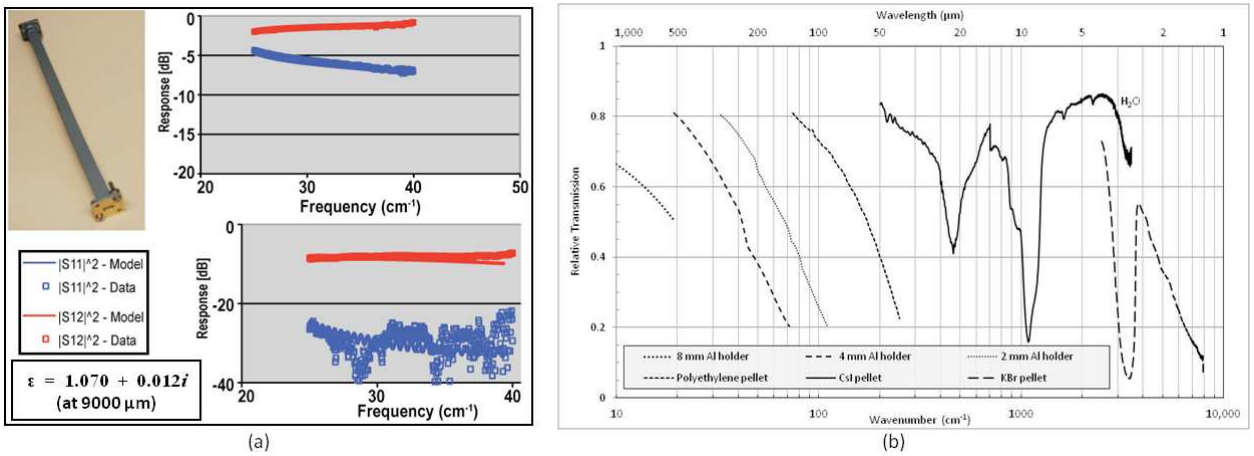

Fig. 1.— (a) Waveguide shim (upper left) and data with the measured dielectric constant at 9000 μm and (b) FTS extinction data for iron silicate powder.

Waveguide (WG) measurements are built upon previous experience with measurements and modeling of WG resonators. A WG shim is loaded with sample material forming a Fabry-Perot resonator within the WG. Using WG resonators packed with an iron rich silicate sample, we are able to derive the complex dielectric constant at submillimeter and millimeter wavelengths. The upper right panel of Fig.1(a) shows measurements taken for sample materials embedded in a plastic matrix. The lower right panel shows measurements for material loosely packed into the WG. Models fit the data well; these models combined with knowledge of the filling factor of the material, allow accurate derivation of the dielectric constants. The calculated dielectric constant is shown at bottom-left.

Extinction measurements using Bruker FTS systems (IFS 113v and 125HR) have been made to assess appropriate sample holder designs and sample thicknesses. Two basic methods of encapsulating the dust sample have been developed: 1) Aluminum Holders (2, 4, 8 mm thickness, etc.) for $\lambda \geq 100$ μm and 2) Dust + Substrates (polyethylene, CsI, KBr) for Far-, Mid-, Near-IR. Transmission as a function of crystallinity (annealing) and as a function of various temperatures (5-300 K) will be measured using an Oxford Optistat dynamic continuous flow cyrostat. Figure 1(b) shows preliminary transmission spectra (10-10,000 cm^{-1}) using various sample holders. Water is present at $\sim$ 3 μm, and bands at $\sim$10 and $\sim$20 μm

commonly attributed to silicates are observed (CsI substrate).

4. Current and Future Work

Construction of the integrating sphere apparatus is complete and currently being tested. Investigation of sample substrates and holders for transmission measurements is effectively complete, and we are currently preparing for measurements of silicate samples (not metal-enriched) that will be used to test and calibrate our apparatus.

In future work, iron silicate and magnesium silicate samples will be investigated and optical constants will be calculated for varying sample temperatures and crystallinities. We intend to continue this research program to investigate the optical properties of carbonaceous materials which play a vital role in astrophysical processes (similar to silicates). We will produce a variety of carbon dust samples that can be characterized by existing OPASI-T apparatus.

This material is based upon work supported by the National Aeronautics and Space Administration through the ROSES/APRA program and by a research appointment (Kinzer) to the NASA Postdoctoral Program at GSFC administered by Oak Ridge Associated Universities (ORAU).

REFERENCES

Hallenbeck, S.L., Nuth, J.A. III, & Nelson, R. 2002, ApJ , 535, 247

Kinzer, R. E., Jr., Rinehart, S., Benford, D., Dwek, E., Henry, R., Nuth, J., Silverberg, R., Wheeler, C., & Wollack, E. 2010, Proceedings of SPIE Astronomical Instrumentation, 7741, 774128-1

Nuth, J. A. III, & Rietmeijer, F. J. M., & Hill, H. G. M. 2002, Meteoritics & Planetary Science, 37, 1579

This preprint was prepared with the AAS LaTeX macros v5.2.

NASA LAW, October 25-28, 2010, Gatlinburg

Laboratory Studies of the Formation and Destruction Processes of Carbonaceous Interstellar Dust

C. S. Contreras, C. L. Ricketts, & F. Salama

Space Science Division, NASA Ames Research Center, Moffett Field, CA 94035

cesar.contreras@nasa.gov, claire.l.ricketts@nasa.gov, farid.salama@nasa.gov

ABSTRACT

Dust analogs formed in a plasma from hydrocarbon and PAH precursors are characterized and monitored *in situ* with high-sensitivity spectroscopy and mass spectrometry techniques using the new facility that we have developed to simulate interstellar and circumstellar processes. From these measurements we derive the size and the structure of dust particles, as well as a better understanding of the growth and destruction processes of extraterrestrial dust.

1. Introduction

The study of the formation, growth and destruction mechanisms of cosmic dust grains is essential for a correct understanding of the physical and chemical evolution of the interstellar medium (ISM). Dust particles span a continuous size distribution from large molecules to μm-sized particles and influence the evolution of the ISM through the energy and ionization balance and the chemical composition of molecular clouds (Tielens (2005)). Carbon particles are thought to be primarily formed in the outflow of carbon stars, through a combustion-like process where small carbon chains (e.g., acetylene) form polycyclic aromatic hydrocarbons (PAHs) that nucleate into larger-size PAHs and, ultimately, into nanoparticles (Pascoli & Polleux (2000)). Although a large amount of laboratory data exists on the formation and the properties of solid dust analogs and in particular of Si-based materials (e.g., Michael, Joseph & Lilleleht (2003)), very little is known, about the specific properties (structure, size and spectral signatures) and the formation mechanisms of the key intermediate range of the size distribution (nanoparticles) of cosmic dust. The scarcity of relevant laboratory data on the transition from gas-phase molecules to solid grains is due to the difficulty of forming and isolating these large species and in tracking their evolutionary path under astrophysically realistic laboratory conditions. Here we describe new laboratory studies that have been performed to address this key issue and discuss the preliminary results and their implications.

2. Experimental

The Cosmic Dust Simulation Chamber (CDSC) was recently set up in our laboratory for the study of cosmic analogs (Figure 1a). The CDSC has been previously used to obtain the first electronic spectra of PAHs under conditions that realistically simulate astrophysical environments (Salama (2008)). It combines three complementary techniques: Cavity Ring Down Spectroscopy (CRDS), Pulsed Discharge Nozzle (PDN) Expansion and Reflectron Time-of-Flight Mass Spectrometry (ReTOF-MS) providing both spectroscopic and ion mass information for the identification of the molecules and particles that are formed in the plasma source. The PDN allows the study of molecules, ions and particles isolated in the gas phase. The species are generated in the hot, confined, plasma from carbonaceous precursors and are suddenly frozen by the expansion providing a very efficient cooling over short distances (a few mm). The current geometry of the PDN leads to a residence time of a few microseconds for the particles in the active region of the discharge. The plasma expansion generated by the PDN is well characterized (Remy, Biennier & Salama (2003); Broks et al. (2005)) and is probed by CRDS several mm downstream with a sub-ppm to ppm sensitivity. CRDS is based on a Nd:YAG pumped tunable pulsed dye laser for the injection of UV-visible photons into a high-finesse cavity (Biennier et al. (2003); Tan & Salama (2005)). For the ReTOF-MS, in order to collect and analyze the ions formed in PDN plasma, a portion of the expansion is skimmed through a 2 mm orifice which is attached to a long tube that leads to a second aperture of 2 mm. The second aperture is polarized ($-30V$) in order to attract the positive ions from the plasma. A repelling pulse of $+200V$ is applied when the positively-charged ions have arrived in the extraction region; the ions are steered orthogonally to their original flight path, to minimize noise, and guided into the free flight tube of the ReTOF-MS. The ion pulse is then back reflected with the Reflectron optics toward the MCP detector. The ions are dispersed in time according to their velocity (proportional to their mass-to-charge ratio, m/z) so the discrete packets of different m/z ions are detected (Ricketts et al. (2010)).

The laboratory species that are generated in the expanding discharge plasma experience a strong temperature gradient that ranges from a few thousand degrees Kelvin to 100 K over a short distance ($1.5-2.5$ mm) from the edge of the plasma chamber to the probing zone where the particles are detected (Remy, Biennier & Salama (2003); Broks et al. (2005); Biennier, Benidar & Salama (2006)). Plasma discharges were conducted with small hydrocarbons, methane, ethane, ethylene, and acetylene representative of the alkane, alkene, and alkyne groups, respectively. The formation of larger molecules and carbon grains was probed by the addition of small PAH precursors (naphthalene, 1-methylnaphthalene, acenaphthene) into the hydrocarbon-seeded argon gas mixture. In all experiments, gases are seeded into argon and expanded through the PDN. Solid and liquid PAH samples are held in the bottom

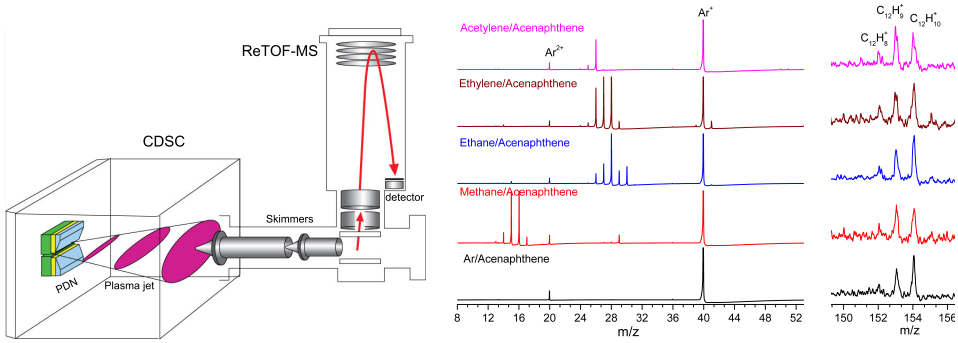

(a) (b)

Fig. 1.—: a) The Cosmic Dust Simulation Chamber (CDSC) consists of a Pulsed Discharge Nozzle coupled to both a Cavity Ring Down spectrometer and to an orthogonal, Reflectron time-of-flight mass spectrometer. b) Representative argon plasma discharges seeded with hydrocarbons and the PAH acenaphthene.

reservoir of the PDN and are heated to increase their vapor pressure. In typical experiments, the high voltage discharge is 300 μs long and is applied within a gas pulse that lasts 1.2 ms. The ReTOF-MS extraction pulse event is timed to coincide with the discharge and the time it takes the ions to reach the mass spectrometer. The extraction pulse occurred 200 μs after the discharge starts.

3. Preliminary Results

Linear Hydrocarbon Precursors: In the case of methane, a 1-C alkane, carbon build up leads to structures with 2, 3 and 4 carbons, as is shown in Figure 1b. The highest mass ion detected is $C_4H_6^+$. Dehydrogenation (from CH_3 to bare C) is also observed. Carbon build up is also observed in the case of ethane, a 2-C atom alkane, with structures with 2, 3 and 4 carbons. The highest mass ion detected is $C_4H_7^+$. Dehydrogenation (from C_2H_5 to C_2) as well as fragmentation into 1-C structures is observed. These results seem to indicate that the 1-C alkane precursor (CH_4) exhibits a higher reactivity. Ethylene and acetylene, both unsaturated hydrocarbons, show greater reactivity and propensity to form larger mass ions than ethane. In the case of ethylene, structures up to 5-C atoms are detected and the highest mass ion being $C_5H_9^+$. In the case of acetylene, structures up to 6-C atoms are found with the highest mass ion detected is $C_6H_5^+$. It should be noted that acetylene is routinely stored in acetone and that some of the peaks in the mass spectrum (e.g. 58 and 59 m/z) could be due to oxygen containing hydrocarbons (acetone and protonated acetone ions, respectively). The lower reactivity of the alkane, results in lower mass ions formed in the plasma discharge.

Polycyclic Aromatic Hydrocarbons: As a basis for the study of the formation of larger PAHs, plasma discharge experiments with the precursors naphthalene ($C_{10}H_8$), methylnaphthalene ($C_{11}H_{10}$) and acenaphthene ($C_{12}H_{10}$) were performed. While no ions with a higher m/z than the PAH precursors were detected in these preliminary runs, a fragmentation pattern was observed to be distinct for each PAH molecule. For example, in the case of naphthalene, the formation of the $C_8H_6^+$ ion corresponds to a loss of C_2H_2 from the precursor. The detection of the $C_4H_4^+$ and its dehydrogenated ions ($C_4H_3^+$, $C_4H_2^+$) demonstrates the loss of C_6H_x fragments, C_6H_4, C_6H_5, and C_6H_6, respectively. The hydrogen loss observed for naphthalene seems to occur in a sequential manner, since both the $C_{10}H_7^+$ and $C_{10}H_6^+$ ions are observed. In the case of 1-methylnaphthalene, the fragmentation process seems to be distinct to that of naphthalene. There is a single H loss ($C_{11}H_9^+$, 141 m/z), and instead of a sequential loss of hydrogen, no peak is observed at 140 m/z. A corresponding fragment ion ($C_9H_7^+$) is observed at 115 m/z, which is a total loss of C_2H_3. In the acenaphthene spectrum, two clear, sequential hydrogen losses are observed. One possible explanation for this observation is that the hydrogen loss most likely occur at the two adjacent, saturated carbons, thereby forming a double bond between them, with no other fragment ions detected.

Plasma experiments with both hydrocarbons and PAHs seeded in Argon indicate minimal reactivity between the two carbon containing species. A notable exception is the formation of the doubly-charged $C_2H_3^{2+}$ ion (13.5 m/z), which only appears in experiments with mixed precursors. With a few exceptions, most of the peaks that are detected in this case follow the trend found for the hydrocarbon-only experiments, with similar relative peaks intensities. Follow-up studies are on-going to identify the processes responsible for the formation of doubly charged ions.

4. Conclusion

These preliminary experiments demonstrate that adding a ReTOF-MS to the Cosmic Dust Simulation Chamber constitutes a powerful tool to probe the formation and fragmentation processes of laboratory analogs of interstellar and circumstellar dust. Experiments with hydrocarbon molecule precursors indicate fragmentation and the formation of larger species through chain growth in all the cases probed so far. The PAHs naphthalene and acenaphthene show subsequent hydrogen loss, with naphthalene dissociating into smaller hydrocarbon fragments. There are indicators that multiply-charged ions are being produced in the plasma discharge as indicated by the detection of the $C_2H_3^{2+}$ and $C_2H_5^{2+}$ ions. These observations seem to point to the fact that the presence of the PAHs may facilitate the formation of the doubly-charged species between ions and neutrals from the hydrocarbon gas.

Additonal experiments are being performed to further explore these reactions.

This research was supported by the NASA SMD APRA Program. C. Contreras and C. Ricketts hold NPP fellowships at NASA-Ames. The authors wish to acknowledge fruitful discussions with L. Biennier and the outstanding technical support of R. Walker.

REFERENCES

Tielens, A. 2005, The Physics and Chemistry of the Interstellar Medium, Cambridge Univ Press, Cambridge, UK

Pascoli, G. & Polleux, A. 2000, A&A 359, 799

Michael, B., Joseph III, A., & Lilleleht, L. 2003, ApJ 590, 579

Salama, F. 2008, Organic Matter in Space, IAU Proceedings, Kwok & S. Sandford, Cambridge University Press, p. 357, and references therein

Remy, J., Biennier, L., & Salama, F. 2003, Plasma Sources Sci. Technol. 12, 295

Broks, B., Brok, W., Remy, J., van der Mullen, J., Benidar, A., Biennier, L., & Salama, F. 2005, Physical Review E 71(3), 36409

Biennier, L., Salama, F., Allamandola, L., & Scherer, J. 2003, J. Chem. Phys. 118, 7863

Tan, X. & Salama, F. 2005, J. Chem. Phys. 122, 084318

Ricketts, C., Contreras, C., Walker, R. & Salama, F. 2010, Int. J. Mass Spectrom., in press

Biennier, L., Benidar, A., & Salama, F. 2006, Chem. Phys. 326(2-3), 445

This preprint was prepared with the AAS LaTeX macros v5.2.

NASA LAW, October 25-28, 2010, Gatlinburg

Formation of Polyatomic Molecules on a Dust-Grain Analogue Using Superthermal H and O Atoms: Relevance to Discovery of Circumstellar H_2O by Herschel

S. M. Madzunkov[1], A. Chutjian, M. R. Darrach & J. A. MacAskill

Atom. & Molec. Phys. Group, JPL/Caltech, Pasadena CA 91109 USA

P. Ehrenfreund

Leiden Institute of Chemistry, 2300 RA Leiden, The Netherlands

G. Vidali

Physics Department, Syracuse University, Syracuse, NY 13244 USA

ABSTRACT

Carbon dioxide (CO_2), formaldehyde (H_2CO), methanol (CH_3OH), ethanol (CH_3CH_2OH), and formic acid (HCOOH) have been formed in separate measurements involving collisions of superthermal beams of H(^{2}S) atoms and O(^{3}P) atoms with CO and CH_4 molecules adsorbed on a gold surface at 4.8K. The collision products are detected using temperature-programmed desorption and mass spectrometry. Identification of the species is made through use of the Metropolis random-walk algorithm as constrained by the fractionation patterns. The relevance of this work to the recent discovery of H_2O at the star IRC+10216 by PACS-SPIRE/Herschel will be discussed in terms of the grain-mediated reaction O(^{3}P, 1-5 eV) + $H_{2(grain)} \rightarrow H_2O_{(grain)}$, in which the O(^{3}P) arises from stellar UV photodissociation.

1. Introduction

Dust plays an indispensable role in the chemical evolution of protostellar regions from the catalytic production of molecular hydrogen to the formation of organics (H_2CO, CH_3OH,

[1]stojan.madzunkov@jpl.nasa.gov

CH_3CH_2OH, CN-, sulfur-bonded species, etc.) critical to the origin(s) of life. Organic species found in cometary bodies appear to trace their origin, in part, to the presolar nebula. The lack of experimental and theoretical data on dust-catalyzed chemistry is only recently being addressed through observations, laboratory studies, and detailed simulation to understand the chemical evolution of the molecular cloud core from the early stages of star formation to the development of the circumstellar/protoplanetary disk [Ehr (2000); Char (2008)]. The role of the abundant ground-state, superthermal atoms such as H(^{2}S) and O(^{3}P) in molecular formation on grains is only recently being addressed through laboratory studies [Madz (2006, 2009, 2010a)]. There are a number of sources of superthermal projectiles in astrophysical bodies. Some examples are: (1) an H-atom [O-atom] accelerated in a C-shock to 10 km s^{-1} will provide 0.52 eV [8.3 eV] kinetic energy towards an atom-grain collision to open reaction channels that are thermally closed. Corresponding energies in a more energetic J-shock at 35 km s^{-1} will be H (6.4 eV) and O (102 eV). (2) Superthermal atoms are produced in circumstellar clouds and in the atmospheres of the outer planets by stellar/solar UV photodissociation of abundant species such as H_2, CO, SiO, NH_3, CH_4, and H_2O. (3) Charged, icy grains are accelerated by local electric fields, leading to energetic collisions with ambient atoms. (4) Fast atomic ions that have charge-exchanged with gas-phase neutral species will become fast atomic neutrals. (5) A comet traversing a molecular cloud at 20 km s^{-1} presents a ram energy of the order of 2.1 eV (H atoms) to 33 eV (O atoms). Hence the ram direction of a comet would be a nursery for molecular synthesis through superthermal-atom chemistry. A recent example of circumstellar molecule formation is the discovery of water in the carbon-rich star CW Leonis [Hersch (2010)]. Detection was made at three infrared wavelengths by Herschel's PACS and SPIRE instruments. The presence of water is explained by penetrating UV light from surrounding stars photodissociating abundant species such as CO and SiO, leading to superthermal O(^{3}P) atoms that then participate in further reactions, including atom-grain reactions with adsorbed H_2 to form H_2O.

The JPL/Caltech Fast-Atom Facility has been described previously [Madz (2006, 2009, 2010a); Chut (1996)]. Briefly, magnetically-confined electrons are accelerated to 5.0 eV and dissociatively attach to a beam of CO to form C+O$^-$ (^{2}P) [Chut (1996)]. The magnetically-confined negative ions and electrons are separated by a trochoidal monochromator. The ions are then accelerated to the desired final energy, after which they are photodetached using the 514.5 nm green line from an argon-ion laser. From detachment energetics the resulting fast O atoms are left exclusively in the ground ^{3}P state. The target consists of a gold substrate cooled to 8K upon which is adsorbed the neutral species. After exposure to the fast-atom beam for approximately 1h, the target is heated *via* temperature-programmed desorption (TPD) with detection of the fractionation patterns by mass hopping through pre-programmed mass peaks in the interval 2-46 Da. Conversion of the TPD mass spectra

to atomic/molecular species spectra is through a novel random-walk (RW) method [Madz (2010a,b)]. Presented in the following are some of the results of the superthermal reactions on frozen ices. Shown in Fig. 1 is production of CO_2 in the reaction $O(^3P)+ CO_{(grain)} \rightarrow CO_{2(grain)}$. This is the first demonstration of the formation of a polyatomic molecule on a surface under fast-atom collision conditions [Madz (2006)]. One see abundant CO_2 formation at all O-atom energies in the range 2-14 eV. These results may explain the large abundance of CO_2 found on icy mantles in isolated, dark clouds [Dart (2005)]. A series of measurements

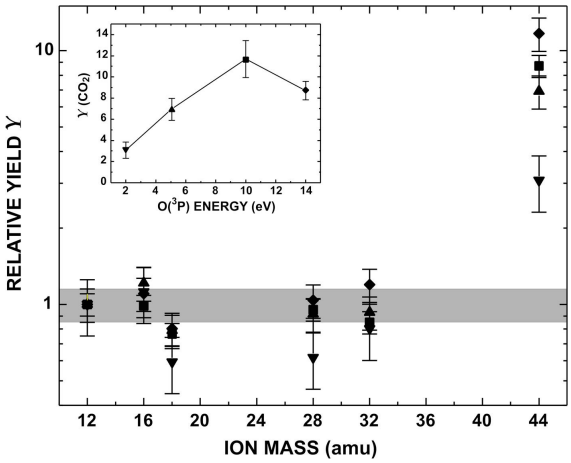

Fig. 1.— Relative production yields $\boldsymbol{Y}$ of the species ^{12}C, ^{16}O, $^{18}H_2O$, ^{28}CO, $^{32}O_2$, and $^{44}CO_2$ at 2eV (▼), 5eV (▲), 10eV (■), and 14eV (♦) [Madz (2006)]. Note the significant production of $^{44}CO_2$. The shaded region with 30% error band denotes the region of no effect by the presence of O-atoms. The insert is the relative excitation function for the CO_2 production, peaking at an $O(^3P)$ energy of 10 eV.

was carried out in which a CO/CH_4 mixed ice was used as the target, and $O(^3P)$ atoms as the projectile. Results are shown in Fig. 2. Here, one see production of the species CO_2, CH_3OH, CH_3CH_2OH and HCOOH at 9 eV atom energy [Madz (2010a)]. Conversion of the superimposed fractionation patterns to species identifications was made using the RW method. Finally, shown in Fig. 3 is the relative production yield of CO_2 and H_2CO formed in the reaction of $H(^2S$, 3eV) with CO_{grain}. A possible formation mechanism for H_2CO is through two H-atom additions to CO to form HCO then H_2CO. Formation of CO_2 may proceed through oxidation of CO by intermediate OH radicals formed from H-atom reaction with H_2O present in the CO ice [Madz (2009)]. Coming full circle, work is in progress to study the CW Leonis phenomena of the detection of circumstellar water. The *Occam's Razor* approach would be to study the simple reaction O (^3P, <5 eV) + $H_{2(grain)} \rightarrow H_2O_{(grain)}$. Measurements would be needed to show that this channel is open under circumstellar-like conditions, together with the absolute yield needed to assess its significance at CW Leonis.

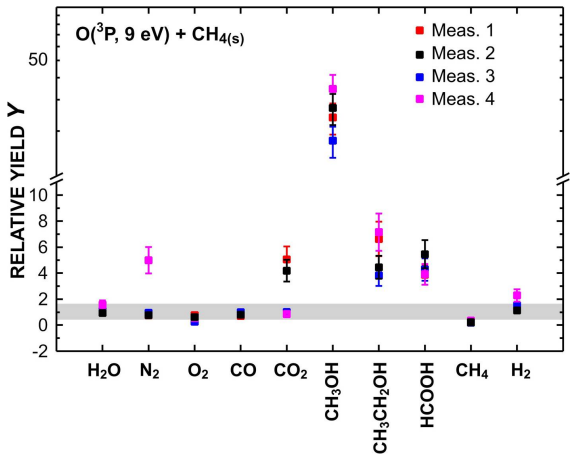

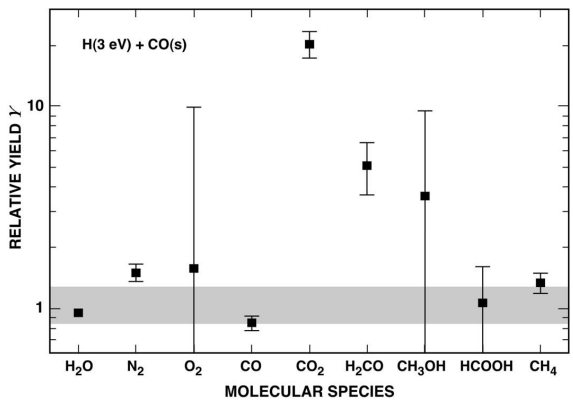

Fig. 2.— (Left) Relative yields of CO_2, CH_3OH, CH_3CH_2OH and HCOOH produced in the reaction of O(^{3}P, 9 eV) atoms with a CH_4/CO ice [Madz (2010a)]. Reaction scenarios are given in [Madz (2010a)].

Fig. 3.— (Right) Relative production yields $\boldsymbol{Y}$ for various molecular species in the reactions H(^{2}S, 3eV) + $H_2O/CO_{(grain)}$ [Madz (2009)]. Enhancement of CO_2 and H_2CO production is seen. Reaction scenarios are given in [Madz (2009)].

This work is presently in progress.

This work was supported at JPL/Caltech by NASA through agreement with the Caltech.

REFERENCES

S. B. Charnley & S. D. Rodgers, 2008, Space Sci. Revs. 138, 59

A. Chutjian & O. J. Orient, in *Atomic, Molecular and Optical Physics: Atoms and Molecules (Experimental Methods in the Physical Sciences,* Vol. 29B) (ed. F. B. Dunning and R. G. Hulet, Academic Press, San Diego 1996).

E. Dartois, K. Pontoppidan, W.-F Thi & G. M. Muñoz Caro, 2005, A&A 444, L57

P. Ehrenfreund & S. B. Charnley, 2000, Annu. Rev. Astron. Astrophys. 38, 427

Herschel, see: http://sci.esa.int/science-e/www/object/index.cfm?fobjectid=47649

S. M. Madzunkov et al., 2006, Phys. Rev. A 73, 020901(R)

S. M. Madzunkov, et al., 2009, Ap. J. 697, 801 *[Due to typographical error note that the reaction product of Reaction (4) should be $H_2(s)$, and not $H_2O(s)$.]*

S. M. Madzunkov, J. A. MacAskill & A. Chutjian, 2010a, Ap. J. 712, 194

S. M. Madzunkov et al., 2010b, Astron. Soc. Pacific Conf. Series, in press

This preprint was prepared with the AAS LaTeX macros v5.2.

NASA LAW, October 25-28, 2010, Gatlinburg

Methanol photodissociation and its effect on complex chemistry in the interstellar medium

J. C. Laas, & S. L. Widicus Weaver[1]

Department of Chemistry, Emory University, Atlanta, GA 30322

jlaas@emory.edu, swidicu@emory.edu

R. T. Garrod

Department of Astronomy, Cornell University, Ithaca, NY 14853

rgarrod@astro.cornell.edu

E. Herbst

Departments of Physics, Chemistry and Astronomy, The Ohio State University, Columbus, OH 43210

herbst@mps.ohio-state.edu

ABSTRACT

A variety of complex organic molecules have been detected in the interstellar medium, but the chemical pathways to these molecules are not well-understood. Grain surface chemistry plays an important role in their formation, where radical-radical combination reactions on ice surfaces can efficiently form these molecules during star formation. One major source of radicals that ultimately react to form complex organics is thought to be methanol photodissociation. However, the branching ratios for this process are not well-characterized. To this end, we are conducting laboratory measurements of methanol photodissociation via quantitative terahertz (THz) spectroscopy. We have also used chemical modeling to test the influence of these branching ratios on the formation of complex organics in interstellar environments.

[1]Author to whom correspondence should be sent.

1. Introduction

Modeling of grain surface chemistry by Garrod, Widicus Weaver & Herbst (2008) (hereafter referred to as GWWH08) illustrates the importance of radical-radical addition reactions for the formation of complex organic molecules (COMs). However, the quantitative laboratory data necessary to improve the accuracy of the models and our understanding of astrochemical systems are lacking. Examination of the chemical pathways leading to the formation of these radicals and the effects of these pathways on COM formation is essential.

An intriguing case study is the methanol photodissociation mechanism, which occurs in the gas phase and in the condensed state (i.e. grain surfaces or ice matrices) and is induced either by interstellar or cosmic ray-induced photons. The three primary radical products for methanol photodissociation shown in Equations 1a-1c are methyl (CH_3), hydroxymethyl (CH_2OH) and methoxy (CH_3O):

$$\mathrm{CH_3OH} + \mathrm{h}\nu \rightarrow \mathrm{CH_3} + \mathrm{OH}, \tag{1a}$$

$$\rightarrow \mathrm{CH_2OH} + \mathrm{H}, \tag{1b}$$

$$\rightarrow \mathrm{CH_3O} + \mathrm{H}. \tag{1c}$$

Because of the high fractional abundance of methanol in astrochemical environments, its photodissociation is a primary source for each of these radicals in interstellar chemistry, which can react with other radicals to form a wide variety of COMs, many of which are of prebiotic interest.

2. Gas-Grain Astrochemical Modeling

We've used the OSU gas/grain code from GWWH08 to test various sets of methanol photodissociation branching ratios to determine their influence on COM abundances (Laas et al. 2010). The three sets of branching ratios used each emphasized one of the three radical pathways at 90%, with each of the two complementary pathways set to 5%. A recent ice study (Öberg et al. 2009) determines the grain-surface product branching percentages for 1a:1b:1c to be 14:73:13, so that the hydroxymethyl channel dominates. These trials were also compared to the branching ratios used in GWWH08 (1a:1b:1c = 60:20:20), which are labeled as "standard" in Figure 1. Changes in the gas-phase branching ratios were found to have negligible influence on COM abundances, whereas changes in the grain-surface branching ratios have significant influence on the COM abundances. The branching ratios favoring the CH_3O channel were found to best match the observed abundances of COMs in Sgr B2(N).

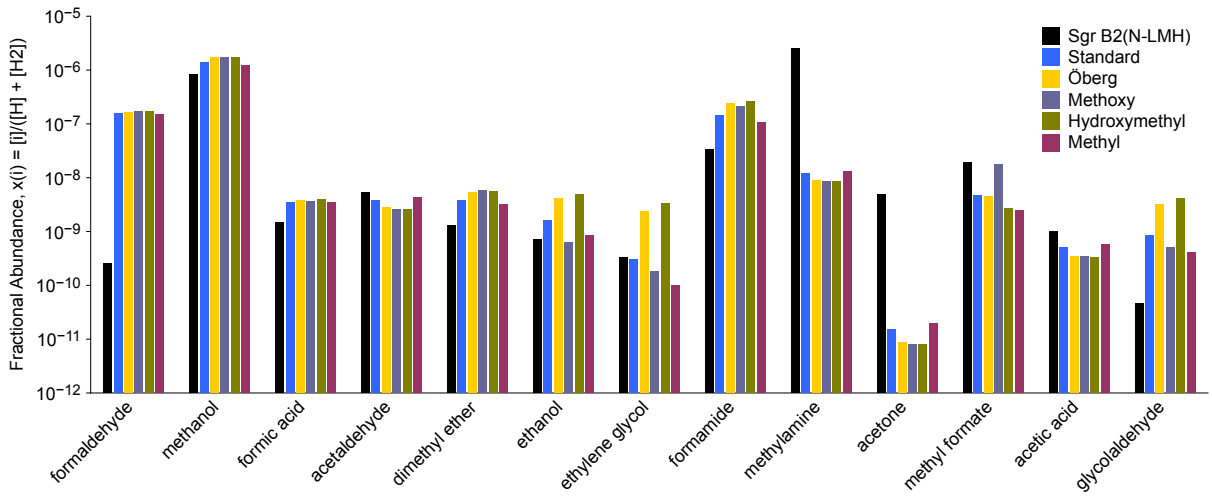

Fig. 1.— Observed and predicted peak abundances for a high-mass hot core.

3. Laboratory Measurements

The branching ratios for gas-phase methanol photodissociation have not been quantitatively determined in the laboratory. Hagege et al. (1968) used an indirect method utilizing chemical scavengers and determined the methoxy/hydroxymethyl channel to be the dominant pathway at λ=184 nm. However, this method could not differentiate between the two radical products.

For more accurate modeling, strict constraints on the branching ratios must be obtained across all relevant UV bands. To this end, we are using a submillimeter spectrometer combined with a photolysis setup to monitor the gas-phase photodissociation products directly. This will allow us to extract quantitative branching ratio information. In this setup, the methanol photolysis occurs in the throat of a supersonic expansion. The cooled and stabilized photolysis products are then monitored spectroscopically in the expansion (see Figure 2). Initial tests indicate sufficient methanol photodissociation efficiency to enable future investigation of the photodissociation branching ratios.

4. Conclusion

Astrochemical modeling has been used to test the influence of methanol photodissociation branching ratios on COM abundances. The grain surface photodissociation branching ratios were found to influence the relative abundances of COMs, but more observational information is essential for comparison. Further laboratory work is underway to quantify

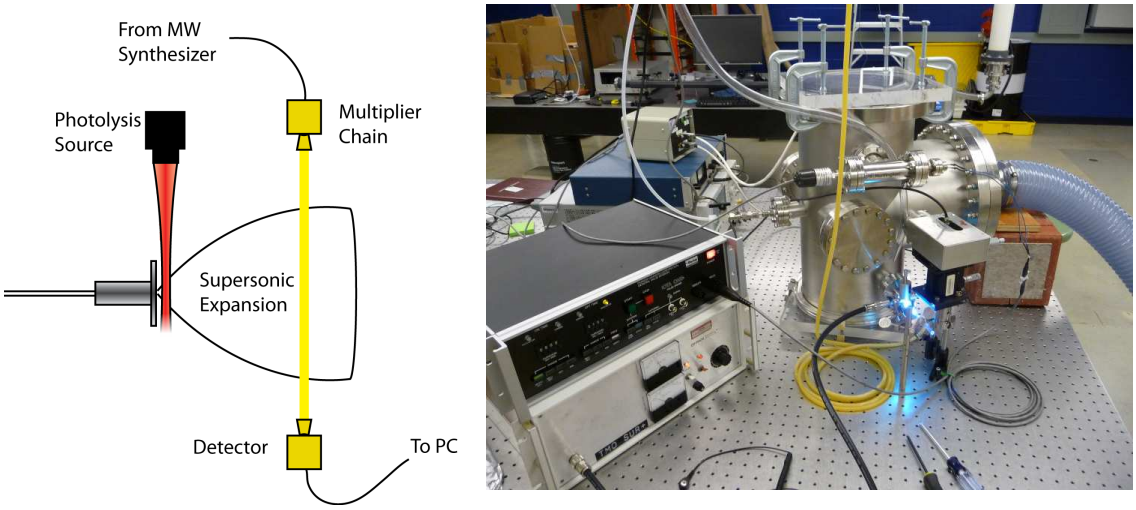

Fig. 2.— Cartoon diagram (left) and laboratory realization (right) of the experimental setup used to measure photodissociation branching ratios.

the methanol photodissociation branching ratios to enable more realistic chemical modeling of interstellar organic chemistry.

Support for this work was provided in part by National Science Foundation Center for Chemical Innovation grant CHE-0847919. JCL was also supported by SLWW's startup funds, provided by Emory University. EH acknowledges the National Science Foundation for the support of his program in astrochemistry. We would like to acknowledge George Hassel for his assistance with the gas/grain code. We would also like to thank Karin Öberg for discussions concerning her experimental studies of methanol ice photodissociation.

REFERENCES

Garrod, R. T., Widicus Weaver, S. L., & Herbst, E. 2008, ApJ, 682, 283

Hagege, J., Roberge, P. C., Vermeil, C. 1968, Trans. Faraday Soc., 64, 3288

Laas, J., Garrod, R. T., Herbst, E., & Widicus Weaver, S. L. 2010, ApJ, accepted

Öberg, K. I., Garrod, R. T., van Dishoeck, E. F., & Linnartz, H. 2009, A&A, 504, 891

This preprint was prepared with the AAS LaTeX macros v5.2.

NASA LAW, October 25-28, 2010, Gatlinburg

Icy photochemical origins of interstellar complex organics

Karin I. Öberg[1]

Harvard-Smithsonian CfA, 60 Garden St, Cambridge, MA, USA

koberg@cfa.harvard.edu

Robin T. Garrod

Department of Astronomy, Cornell University, Ithaca, NY, USA

Ewine F. van Dishoeck[2] and Harold Linnartz[1]

Leiden Observatory, Leiden University, Leiden, The Netherlands

ABSTRACT

Complex organic molecules have been detected with space- and ground-based telescopes toward low- and high-mass star-forming regions, demonstrating the existence of efficient astrophysical pathways to chemical complexity. Understanding the origins of these species are crucial to use them as tracers of physical environments, to predict the prebiotic evolution during star- and planet-formation, and to plan future observations with e.g. JWST. Many complex organics form on interstellar grains, in ices that evolve with their environment and finally evaporate as the grains are heated by new-born stars or by shocks. This ice evolution has been explored through a combination of Spitzer spectra of ices, laboratory simulations of UV induced ice photochemistry, and millimeter observations tracing complex ice evaporation. The experiments show that UV irradiation of protostellar ices is efficient enough to explain the complex molecule observations in so called protostellar 'hot cores'. Moreover, the experiments predict that before the onset of thermal evaporation close to the protostar, small fractions of the complex ice will continuously evaporate non-thermally due to photodesorption, resulting in gas-phase fingerprints of the ice composition as it evolves. Some of the proposed chemical scenarios can be tested by current facilities, while others require more detailed experiments as well as access to upcoming NASA missions.

---

[1]Sackler Laboratory for Astrophysics, Leiden University, Leiden, The Netherlands

[2]Max-Planck Institute für Extraterrestrische Physik, Garching, Germany

1. Introduction

Star formation begins with the collapse of an interstellar cloud core to form a protostar, which grows from infall of envelope material and later through an accretion disk, where planets may form. This physical evolution from cores to (extra)solar systems is accompanied by a chemical evolution, which will affect planet and comet compositions. Much of this chemical evolution takes place on interstellar grain surfaces, in icy mantles. Simple ices, up to CH_3OH have been detected directly, but much more complex molecules are associated with ice evaporation in hot cores during the protostellar phase and in outflows (Herbst & van Dishoeck 2009, for a review). Commonly-suggested formation routes for the detected molecules include various gas-phase reactions starting with thermally evaporated CH_3OH ice, atom-addition reactions on dust grains, and UV- and cosmic ray-induced chemistry in the icy grain mantles that form during the pre-stellar stages. The focus is currently on an ice formation pathway (e.g. Garrod et al. 2008) because of the failures of gas phase chemistry to explain the observed abundances of some of the most common complex molecules toward low-mass protostars, especially $HCOOCH_3$. The aim of this proceeding is to summarize recent advances in our understanding of the chemical evolution from simple to complex ices – through ice surveys, laboratory ice experiments and millimeter observations of non-thermal ice desorption – and to outline expected discoveries with JWST and Herschel and the laboratory needs to interpret them.

2. A Spitzer ice survey toward protostars

The high sensitivity of the *Spitzer Space Telescope* made it possible to observe ices at 5–30 μm toward 50 low-mass protostars within the *c2d* program (Boogert et al. 2008; Pontoppidan et al. 2008; Öberg et al. 2008; Bottinelli et al. 2010), providing an unprecedented sample size. With aid of laboratory spectra of pure and mixed ices, ice features belonging to H_2O, CO, CO_2, CH_4, NH_3 and CH_3OH have been identified and their abundances and the abundances of CO and CO_2 in different ice layers have been quantified. Combining the information in the survey, ice formation can generally be divided into early hydrogenation of atoms in clouds resulting in a H_2O-dominated ice, which is fast compared to cloud core formation time scales, later CO-freeze-out dependent formation pathways in the pre-stellar core, resulting in a CO-dominated ice where CH_3OH form through hydrogenation of CO, and finally thermal and possibly UV processing in the protostellar envelope. This entails that the CO:CH_3OH ice photochemistry can be simulated separately from the chemistry in the H_2O-rich ice layer.

3. Ice photochemistry experiments on CH_3OH ices

Guided by the *Spitxer* ice survey and models by Garrod et al. (2008), where CH_3OH is the major precursor of the complex molecules observed in hot cores, we ran a series of ice photochemistry experiments on pure CH_3OH ice and CO:CH_3OH ice mixtures (Öberg et al. 2009a). The ices were irradiated with a broad-band UV hydrogen microwave-discharge lamp under ultra-high vacuum conditions, at 20–70 K, and then heated to 200 K. The reaction products were identified by reflection-absorption infrared spectroscopy (RAIRS) and temperature programmed desorption (TPD), and through the observed spectroscopic effects of isotopic substitution and the chemical effects of CO and CH_4 to the ice compared to pure CH_3OH experiments. Complex organics were readily formed in all experiments, both during irradiation and during the slow warm-up of the ices after the UV lamp was turned off. C_2H_6, CH_3CHO, CH_3CH_2OH, CH_3OCH_3, $HCOOCH_3$, $HOCH_2CHO$ and $(CH_2OH)_2$ were all detected in at least one experiment and their relative abundances were used to estimate photodissociation branching ratios of CH_3OH ice. The relative abundances of photoproducts depend on the UV fluence, the ice temperature, and whether pure CH_3OH ice or CH_3OH:CO ice mixtures are used. Important for the following section $HCOOCH_3$ and $HOCH_2CHO$ are only clearly detected following irradiation of CO-rich ices and in these experiments $HCOOCH_3$ is the dominant product at low temperatures (CH_3CHO probably forms abundantly as well, but its production could not be quantified in the CO-rich experiments).

4. Millimeter observations of CH_3OH ice photochemistry products

Informed by the ice chemistry experiments, and previous UV photodesorption results (Öberg et al. 2009b) we proposed a search for CH_3OH:CO ice chemistry products (i.e. CH_3CHO and $HCOOCH_3$) in the vicinity of the CH_3OH-ice-rich protostar B1-b (Öberg et al. 2010). We first mapped the B1-b region in CH_3OH gas using the IRAM 30m telescope to identify locations of efficient non-thermal ice desorption and found an abundance peak of quiescent, cold CH_3OH gas on the side of a cold core facing a protostar with an outflow cavity. We had thus identified a position with cold CH_3OH and CO ice probably exposed to UV radiation, which according to the experiments should result in both efficient production of HCO-bearing complex molecules and photodesorption of a fraction of the ice chemistry products. New observations did indeed reveal cold $HCOOCH_3$ and CH_3CHO gas at abundances with respect to CH_3OH of $\sim$2.3% and 1.1%, respectively. This confirms the predictions of the existence of efficient cold ice (below 25 K, the sublimation point of CO) formation pathways of complex molecules followed by non-thermal desorption through e.g. UV photons traveling through outflow cavities.

5. Future mission needs and opportunities

Herschel observations have revealed a wealth of sub-millimeter lines due to warm organic gas (e.g. Crockett et al. 2010). Interpreting these observations relies on that gas and ice formation pathways can be disentangled. However, quantitative data on gas phase complex-molecule-formation reactions are few and quantitative ice chemistry data is rarer still. Optimizing the science output of *Herschel* and of SOFIA requires both new experiments and the development of model frameworks that translate the laboratory data into astrochemical predictions.

With the James Webb Space Telescope direct observations of complex ices toward solar-type protostars may become possible; *Spitzer* could not address this question because of its low sensitivity. Direct ice observations would put direct constraints on the ice chemical evolution. Interpreting these ice spectra requires an update of the current ice data bases so that complex molecules in different ice matrices can be identified.

This work was supported by NASA through a Hubble Fellowship grant, awarded by STScI. Astrochemistry in Leiden is supported by a SPINOZA grant of NWO and NOVA.

REFERENCES

Boogert, A. C. A., Pontoppidan, K. M., Knez, C., et al. 2008, ApJ, 678, 985
Bottinelli, S., Adwin Boogert, A. C., Bouwman, J., et al. 2010, ApJ, 718, 1100
Crockett, N. R., Bergin, E. A., Wang, S., et al. 2010, A&A, 521, L21+
Garrod, R. T., Weaver, S. L. W., & Herbst, E. 2008, ApJ, 682, 283
Herbst, E. & van Dishoeck, E. F. 2009, ARA&A, 47, 427
Öberg, K. I., Boogert, A. C. A., Pontoppidan, K. M., et al. 2008, ApJ, 678, 1032
Öberg, K. I., Bottinelli, S., Jørgensen, J. K., & van Dishoeck, E. F. 2010, ApJ, 716, 825
Öberg, K. I., Garrod, R. T., van Dishoeck, E. F., & Linnartz, H. 2009a, A&A, 504, 891
Öberg, K. I., Linnartz, H., Visser, R., & van Dishoeck, E. F. 2009b, ApJ, 693, 1209
Pontoppidan, K. M., Boogert, A. C. A., Fraser, H. J., et al. 2008, ApJ, 678, 1005

NASA LAW, October 25-28, 2010, Gatlinburg

Magnetic Reconnection in High-Energy-Density Plasma Experiments

W. Fox, A. Bhattacharjee, & K. Germaschewski

Space Science Center, University of New Hampshire, Durham, NH 03824

william.fox@unh.edu

ABSTRACT

Recent experiments have observed magnetic reconnection in high-energy-density (HED), laser-produced plasma bubbles, with reconnection rates observed to be much higher than can be explained by classical theory. This is a novel regime for magnetic reconnection study, characterized by extremely high magnetic fields (∼MG), high plasma beta, and strong, supersonic plasma inflow. Understanding reconnection in these experiments can provide a new test of reconnection theories and identify ways in which these HED experiments can serve as a new tool for laboratory astrophysics. Work to-date with collisionless particle-in-cell simulations identifies two key ingredients, simultaneously present for the first time, for explaining the fast reconnection rates: two-fluid reconnection mediated by collisionless effects, and strong flux-pileup of the inflowing magnetic field.

1. Introduction

Magnetic reconnection, a fundamental process in magnetized plasmas, allows magnetic fields to relax topologically and gain accessibility to states of lower energy [Yamada et al. (2010); Biskamp (2000)]. The energy thus liberated can produce heat, flows, and can enable the acceleration of a large number of particles to high energies. Magnetic reconnection is ubiquitous in laboratory (including fusion) devices as well as space and astrophysical plasmas. It is widely believed to play a central role in phenomena as diverse as sawtooth crashes in fusion plasmas [Hastie (1997)], magnetospheric substorms [Angelopoulos et al. (2008)], and solar flares [Masuda et al. (1994)]. Magnetic reconnection is an excellent example of a problem where earthbound *dynamical laboratory astrophysics* experiments elucidate the

fundamental physics behind astrophysical observations. Theory and computation must also play a role, based on the complexity of the problem and difficulty scaling all the dimensionless parameters from experiments to their astrophysics counterparts.

Recently, magnetic reconnection has been observed in high-energy-density (HED) laser-produced plasmas [Nilson et al. (2006); Li et al. (2007)], in the presence of extremely high magnetic fields, opening up yet another regime of great interest to laboratory and plasma astrophysics. HED plasma bubbles are created by focusing terawatt (TW)-class lasers ($\sim$kJ/ns) down to sub-millimeter-scale spots on a plastic or metal foil. The foil is ionized into hemispherical bubbles that expand supersonically off the surface of the foil. Each bubble is found to self-generate a strong magnetic field of order megagauss (MG), which forms a toroidal ribbon wrapping around the bubble. If multiple bubbles are created at small separation, the bubbles expand into one another, and the opposing magnetic fields are squeezed together and seen to reconnect.

These laser-driven experiments are complementary in many ways to traditional reconnection laboratory experiments based on magnetized discharge plasmas [reviewed by Yamada et al. (2010)]. The diagnostics employed, such as proton radiography, generate magnetic field maps of the entire experiment geometry, so that the global topology is apparent. Very high plasma β is attained (typically at least 5–10), as is an extremely strong reconnection drive (which results from the laser-powered bubble expansion), such that the reconnection inflows are comparable or larger than the sound speed and Alfvén speeds. The bubbles are also found to be in an MHD-like regime, where the bubble is larger than fundamental plasma length scales such as the ion skin-depth ($d_i = c/\omega_{pi}$, where ω_{pi} is the ion plasma frequency).

To date, only very basic theory has been put forward toward understanding reconnection in the laser-driven experiments. Both Li et al. (2007) and Nilson et al. (2008) found that their observed rates were substantially faster than allowed by Sweet-Parker reconnection theory. This is perhaps not surprising, since this has generally been found to be the case in most reconnection experiments not completely dominated by collisions. Going beyond the classical Sweet-Parker model, Nilson et al. (2008) suggest anomalous resistivity, and Willingale et al. (2010) suggest that Hall reconnection may play a role.

Our work to date [Fox et al. (2010)] has used collisionless particle-in-cell (PIC) simulations to study reconnection between expanding plasma bubbles, with parameters and geometry relevant to the bubble experiments. We find that reconnection can be explained as a combination of two effects: (1) a strong pile-up of magnetic flux [Biskamp (1986)] at the shoulder of the current sheet, caused by the sonic inflow and corresponding ram pressure that drives substantial compression of the plasma and magnetic field between the two bubbles, and (2) the intervention of collisionless effects (Hall current and electron pressure

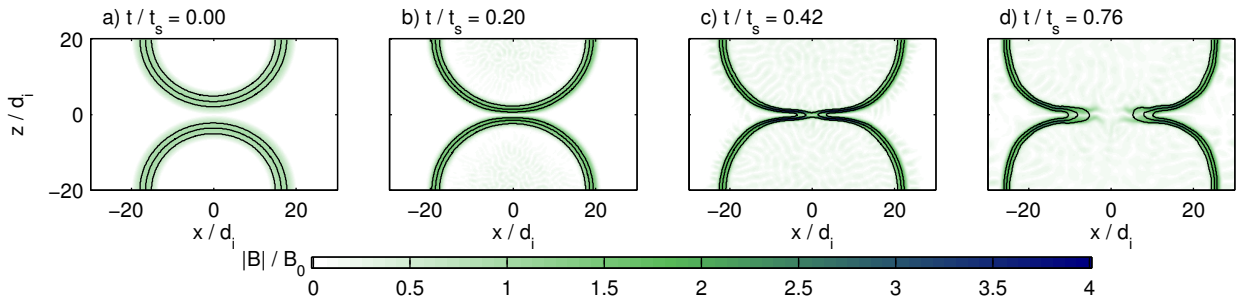

Fig. 1.— Evolution of $|B|$ and contours of magnetic flux during the simulation.

tensor) when the current sheet width falls below the ion skin depth [Ma and Bhattacharjee (1996)]. To our knowledge, these laser-driven experiments are the first in which flux pile-up as well as collisionless effects play important roles.

Figure 1 presents the evolution of the magnetic field in one simulation. We adopt an initial condition corresponding to a time about halfway through the experiments, after the bubbles have expanded and generated their magnetic ribbons, but before the pair of bubbles has begun to interact. We then model the subsequent expansion and interaction of the plasma bubbles. Here we choose parameters relevant to the Rutherford experiments [Nilson et al. (2006)]: bubble size $L_n = 20d_i$, the ratio of background to peak bubble density of $n_b/n_0 = 0.1$, initial magnetic ribbon width $L_B = L_n/6$, plasma $\beta_{e0} = 2\mu_0 n_0 T_{e0}/B_0^2 = 8$, and peak expansion velocity $V_0 = 3(T_{e0}/m_i)^{1/2}$. We choose the PIC parameters $M_i/m_e = 100$, $T_{i0} = T_{e0} = 0.02 m_e c^2$, and an initial 100 particles per cell. Simulations were conducted with the relativistic, electromagnetic, explicit PIC code PSC [Ruhl (2006)].

The image backgrounds show $|B|$, over which are plotted contours of the magnetic flux Ψ, which gives the field lines. Panel (a) shows the initial condition. The next three panels show the evolution, with time scaled in units of the dynamical time $t_s = L_n/V_0$. As the bubbles interact, a reconnection x-line forms at the leading point of tangency between the bubbles. Near $t/t_s = 0.42$, the reconnection is about half complete, and the reconnection rate is near its maximum. Notice the strong pileup of flux upstream of the reconnection region. In contrast to reconnection considered in other contexts, here the strong inflows have sufficient force to compress the flux in the current sheet by a ratio of about 4. The flux pileup raises the relevant Alfvén speed, allowing reconnection to occur within one dynamical time, rather than a time which scales with the nominal Alfvén time. Indeed, with a suite of simulations, it is found that the reconnection time does not depend on the initial magnetic field strength in this strongly-driven, flux-pileup regime. This scaling is consistent with the extremely fast experimentally observed reconnection rate.

To conclude, magnetic reconnection remains an important, unsolved problem for astrophysics, space plasma physics, and fusion research, for which dynamical laboratory astrophysics experiments will play a crucial role. Interesting new experiments have recently been conducted on inertial fusion laser facilities, observing magnetic reconnection in HED laser-produced plasma bubbles. We have made progress on understanding reconnection in the strongly-driven regime relevant to these experiments using PIC simulations, with an ultimate goal of turning these first experiments into quantitative tools to test reconnection theories.

This work was supported in part by the DOE Center for Magnetic Self-Organization and DOE Center for Integrated Computation and Analysis of Reconnection and Turbulence.

REFERENCES

M. Yamada, R. Kulsrud, and H. Ji, Rev. Mod. Phys. **82**, 603 (2010).

D. Biskamp, *Magnetic Reconnection in Plasmas* (Cambridge University Press, Cambridge, 2000).

R. J. Hastie, Astrophys. Space Sci. **256**, 177 (1997).

V. Angelopoulos, J. P. McFadden, D. Larson, et al., Science **321**, 931 (2008).

S. Masuda, T. Kosugi, H. Hara,et al. Nature **371**, 495 (1994).

P. M. Nilson, L. Willingale, M. C. Kaluza, et al., Phys. Rev. Lett. **97**, 255001 (2006).

C. K. Li, F. H. Séguin, J. A. Frenje, et al., Phys. Rev. Lett. **99**, 055001 (2007).

P. M. Nilson, L. Willingale, M. C. Kaluza, et al., Phys. Plasmas **15**, 092701 (2008).

L. Willingale, P. M. Nilson, M. C. Kaluza, et al., Phys. Plasmas **17**, 043104 (2010).

W. Fox, A. Bhattacharjee, K. Germaschewski, submitted to Phys. Rev. Lett. (2010).

D. Biskamp, Phys. Fluids **29**, 1520 (1986).

Z. W. Ma and A. Bhattacharjee, Geophys. Res. Lett. **23**, 1673 (1996).

H. Ruhl, in *Introduction to Computational Methods in Many-Body Physics*, edited by M. Bonitz and D. Semkat (Rinton Press, 2006), chap. 2.

NASA LAW, October 25-28, 2010, Gatlinburg

Plasma Streaming Across Magnetic Field

R. Presura, C. Plechaty, S. Stein, D. Martinez, & S. Neff*

Nevada Terawatt Facility, University of Nevada, Reno, NV 89506

presura@physics.unr.edu

ABSTRACT

In a variety of instances, including supernova explosions and the interaction of stellar winds with planetary magnetospheres, plasma acceleration by magnetic fields produces instabilities at the plasma-field boundary, which affect the plasma dynamics and lead, in extreme cases, to plasma penetration across the field. Experiments focused on plasma-field interactions actuated the Rayleigh-Taylor instability (RTI) in several distinct regimes including the common magneto-RTI ($k\rho \ll 1$) and the large-Larmor-radius-RTI ($k\rho \gg 1$), k being the wavenumber and ρ the ion Larmor radius. The RTI evolution in the nonlinear stage led to plasma streaming across the magnetic field over several ion Larmor radii, by $\boldsymbol{E}\times\boldsymbol{B}$ drift.

1. Introduction

Rayleigh-Taylor instabilities (RTI) growing at dynamic interfaces between plasma flows and magnetic fields lead to the interpenetration of the two media. Several astrophysical and space physics phenomena have prompted controlled laboratory investigations of this instability. These include supernova explosions, the solar wind interaction with the earth's magnetic field at the magnetopause, and Ba releases in the magnetotail. Most experiments produced a plasma flow by laser ablation (generally not magnetized), which interacted with an external magnetic field or magnetized ambient plasma. Two types of RTI were observed in the sub-Alfvénic expansions created: for collisionless plasma the lower hybrid drift instability (Okada (1981), Zakharov (1986)), and for collisional plasma the large-Larmor radius RTI (Ripin (1987), Dimonte (1991), Kasperczuk (1999)), although some uncertainties remain in the interpretation of those results. In this paper we present a related experiment that allows significant parameter variation so that different RTI varieties can be controllably actuated.

---

*Currently at the Technical University Darmstadt, Germany

2. Experimental Study of Flute Instabilities

A flexible experimental setup was developed to investigate the instability development in the interaction region of a plasma flow with an external magnetic field (Presura (2005)). Explosive plasma flows were produced by laser ablation of low-Z solid targets with irradiance 10^{12} - 10^{17} W/cm^2. Ambient fields with strength up to 60 T, azimuthal symmetry, and $1/r$ radial dependence were generated in vacuum by driving a 0.6 MA current through a cylindrical conductor. All plasma-magnetic field interaction experiments were performed in vacuum (p $\leq$ 2 mPa), therefore the plasma expansion speed remained lower than the Alfvén speed. The instabilities studied developed from random perturbations in the target surface and the laser beam wavefront. A typical experimental configuration is shown in Figure 1. The main observables are related to the evolution of the plasma density distribution and the magnetic field strength at the plasma-field boundary. Space- and time-resolved measurements of the plasma density were based on pulsed laser refractometry (interferometry and schlieren imaging). The magnetic field strength was estimated from current measurements.

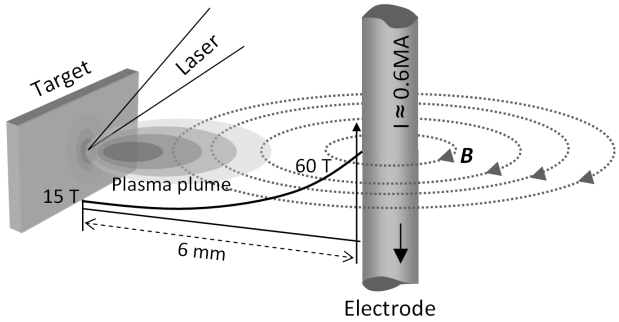

Fig. 1.— Typical experimental set-up. The magnetic field configuration and the ablation plasma expansion are shown.

Two main types of plasma flow conditions were included in the study: quasi-isothermal and quasi-adiabatic expansion. The latter produced relatively lower temperature and higher density plasma in the region of interaction with the magnetic field. Flute instabilities were actuated in both situations and they evolved in different regimes, as expected. A laser pulse with energy 5 J and 6 ns duration was used to produce the quasi-isothermally expanding plasma (Presura (2005)). At best focus, the laser intensity on target was $\approx 10^{13}$ W/cm^2. Without a magnetic field, the plasma plume expanded quasi-hemispherically, elongated in direction normal to the target. In the presence of an external magnetic field (6.5 T at the target surface), a diamagnetic cavity formed, surrounded by a higher density shell, where the field decelerated the plasma (Horton (2007)). The boundary assumed a flute structure (Figure 2). The plasma parameters pointed to the Large-Larmor-Radius RTI, for

which $k\rho \gg 1$, where k is the wavenumber and ρ is the ion Larmor radius. In a different

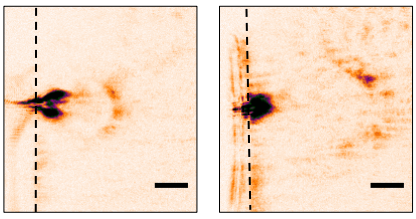

Fig. 2.— Schlieren images recorded in the plane perpendicular to the magnetic field at 4 ns and 12 ns after the ablation laser pulse. The dashed line indicates the target surface and the horizontal bar is 1 mm long in Figures 2-4.

experiment, the plasma expansion was examined for several gyro-periods by using a 2 J, 5 ps, $\approx 10^{15}$ W/cm^2 laser pulse (Plechaty (2009)). The instability continued to grow, maintaining the flute structure (Figure 3). For this case, $k\rho \ll 1$, identifying the magneto-RTI. Using a

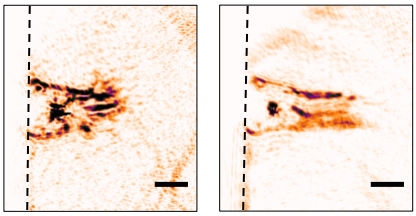

Fig. 3.— Schlieren images recorded in plane perpendicular to the magnetic field at 14 ns and 21 ns after the ablation laser pulse. The magnetic field at the target surface was 10 T.

10 J, 1 ps, 10^{17} W/cm^2 laser pulse and 8 T field at the target surface (Plechaty (2009)), the expansion was examined for longer expansion time (in units of inverse gyro-frequency). Eventually a single flute dominated and it streamed across the magnetic field over many ion Larmor radii with unchanged velocity, via $\boldsymbol{E}\times\boldsymbol{B}$ drift (Figure 4).

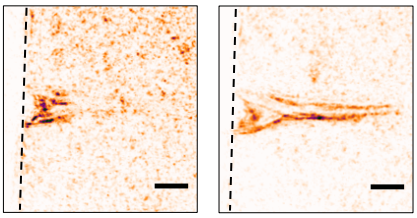

Fig. 4.— Schlieren images recorded in the plane perpendicular to the magnetic field at 6 ns and 21 ns after the ablation laser pulse.

3. Discussion and Conclusion

Experiments with explosive plasma expansion in external magnetic field actuated the magneto-RTI and the large-Larmor-radius-RTI. Charge separation due to the plasma-field interaction led to plasma penetration across the field by $\boldsymbol{E}\times\boldsymbol{B}$ drift. Low-beta plasma propagated over distances much larger than the ion Larmor radius. In our and previous experiments, 2D flute-type instabilities formed, in which the RT spikes are plasma sheets, because the magnetic field is strong enough to mitigate the perturbation growth in the plane of the field. In nature, the RT structures are often 3D. For instance, in plerions (*e.g.* the Crab Nebula) the pulsar wind accelerates the ejecta shell and filaments form at the interface, that have been identified by Hester (1996) as magneto-RTI based on 2D MHD simulations by Jun (1995). Scaled experiments require magnetic field tens of times lower, close to the critical value. The instability growth will be significantly reduced, so the experiment has to be designed to maintain the plasma flow over multiple e-folding times of the instability.

The authors acknowledge experimental support and useful discussions with Y. Sentoku, A. Esaulov, V. Sotnikov, V. Ivanov, Y. Stepanenko, P. Wiewior, and A. Astanovitskiy. This work was supported by the DOE/NNSA under UNR grant DE-FC52-06NA27616.

REFERENCES

Hester, J. J. *et al.* 1996, Ap. J., 456, 225

Horton, W. *et al.* 2007, Adv. Space Res., 39, 358

Jun, R. *et al.* 1995, Ap. J., 453, 332

Okada, S. *et al.* 1981, Jap. J. Appl. Phys., 20, 157; Zakharov , Yu. P. *et al.* 1986, Sov. J. Plasma Phys., 12, 674

Plechaty, C. *et al.* 2009, Astrophys. Space Sci., 322, 195

Plechaty, C. *et al.* 2010, High Energy Density Physics, 6, 258

Presura, R. *et al.* 2005, Astrophys. Space Sci., 298, 299

Ripin, B. H. *et al.* 1987, Phys. Rev. Lett., 59, 2299; Dimonte, G. *et al.* 1991, Phys. Rev. Lett., 67, 1775; Kasperczuk *et al.* 1999, Laser & Particle Beams, 17, 537

This preprint was prepared with the AAS LaTeX macros v5.2.

NASA LAW, October 25-28, 2010, Gatlinburg

Laboratory Dynamo Experiments

M. D. Nornberg[a] & C. B. Forest[a] & B. P. Brown[b] & E. G. Zweibel[b] & J. B. Wallace[a] & M. Clark[a] & E. J. Spence[c] & N. Z. Taylor[a] & E. J. Kaplan[a] & K. Rahbarnia[a]

Center for Magnetic Self-Organization in Laboratory and Astrophysical Plasmas

mdnornberg@wisc.edu, cbforest@wisc.edu

ABSTRACT

The basic physics of a dynamo have been addressed utilizing magnetohydrodynamic (MHD) simulations and liquid metal experiments to determine the requirements for the excitation, sustainment, and saturation of magnetic fields generated from turbulent flows. The more challenging problem of addressing plasma physics effects will require experiments with unmagnetized plasmas. An experimental facility utilizing cusp field confinement to produce a hot, steady-state unmagnetized plasma would provide the necessary conditions for studying effects beyond MHD (such as two-fluid and kinetic effects) in a turbulent dynamo.

1. Introduction

Even with 400 years of recorded sunspot observations our understanding of solar variability and the process of magnetic field generation causing it is insufficient to provide accurate forecasts of stellar activity except through empirical trends (Hathaway et al. 1994). The need for accurate forecasting of solar activity becomes more acute as modern society becomes more dependent on satellite based communication and navigation[1]. It is also integral to our understanding of climate variability and the search for habitable planets.

---

[a]Department of Physics, University of Wisconsin-Madison, Madison WI 53706

[b]Department of Astronomy, University of Wisconsin-Madison, Madison WI 53706

[c]Princeton Plasma Physics Laboratory, Princeton, NJ 08648

[1]See *e.g.* NASA's Living with a Star Program

Establishing models for planetary, stellar, and galactic dynamos is exceedingly difficult due to the disparity in scales and dimensionless parameters between laboratory experiments, numerical simulations, and astrophysical objects (Charbonneau 2005). Validation of turbulence models and numerical codes by observation is hindered by the inability of codes to access astrophysically relevant Reynolds numbers (Brown et al. 2010). Simulation of the sun requires either resolution beyond current computing capabilities or validated sub-grid MHD turbulence models which currently lack an experimental benchmark. Without validated simulations, one is unable to judge the validity of various stellar dynamo models. Heliophysics related NASA missions including SDO, Hinode, STEREO, SOHO, and the upcoming NSF ground-based ATST are motivated by questions arising from the processes of magnetic field generation, flux tube buoyancy, and magnetic reconnection. A flexible laboratory facility that can replicate these processes will provide strong constraints on observational interpretation and the required benchmark for turbulence models.

2. Liquid Metal Experiments

Liquid metal experiments have begun to probe the dynamics of magnetic field generation in the MHD limit. Successful dynamo experiments have required strict control of boundary conditions either through the use of flow control devices such as pipes and baffles (Gailitis et al. 2002) or ferritic materials (Verhille et al. 2010). Experiments in unconstrained two-vortex flows have shown strongly enhanced resistivity due to a turbulence induced emf (Spence et al. 2006). Stabilization of the flows with baffles has significantly reduced the turbulent emf and increased the effective magnetic Reynolds number of the flow as evidenced by the flux compression of an axial applied magnetic field, toroidal field amplification through the Ω-effect, and increasing decay times of an applied field.

3. The Need for a Plasma Dynamo Experiment

Despite these advances, liquid metal experiments provide limited insight into the dynamo process. Most critically, the threshold for achieving a dynamo in the laboratory is only marginally satisfied by liquid metal experiments necessitating very contrived flow geometries and boundary conditions. Liquid metals are limited to $Rm \sim 10$—100 whereas a hot laboratory plasma on the other hand is highly conducting and can achieve $Rm \sim 10^3$.

Liquid metals also have a fixed relationship between magnetic and viscous diffusivity with low magnetic Prandtl numbers $Pm \sim 10^{-5}$. In contrast, simulations are typically

limited to $Pm \sim 1$ to fully resolve the turbulence. Astrophysical dynamos range from very low Pm to very high and so a plasma experiment is attractive in that the magnetic and viscous diffusivities are decoupled and can be altered by varying the ion mass, density, and temperature of the plasma to match those of simulations for validation.

Finally, aside from planetary cores, astrophysical dynamos are typically in plasmas with varying collisionality necessitating the understanding of two-fluid and kinetic effects present in weakly collisional plasmas.

4. Capabilities of the Madison Plasma Dynamo Experiment

To produce a plasma with sufficiently high Rm for a dynamo requires good thermal confinement to produce a hot plasma. This confinement will be provided in the Madison Plasma Dynamo Experiment by a series of strong cusp fields localized at the edge of the plasma (Spence et al. 2009). Rings of NdFeB permanent magnets with alternating polarity are placed along in inner walls of a 3 m diameter stainless steel spherical vacuum vessel (see Fig. 1). The plasma is produced by either heating a negatively biased lanthanum hexaboride filament or by electron cyclotron heating. The edge cusp confinement field also provides a means of driving flow in the plasma. A series of biased electrodes placed in the strong magnetic field can drive an $E \times B$ flow in the edge plasma which is viscously coupled to the unmagnetized core plasma. The confinement strategy, plasma sources, and electrode flow drive have all been demonstrated on a smaller prototype device.

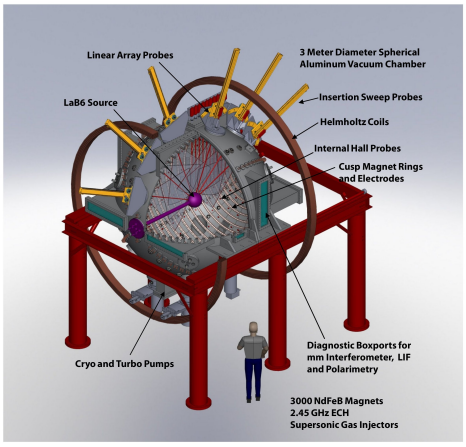

plasma radius	1.5	m
density	10^{17}—10^{19}	m^{-3}
electron temperature	10—30	eV
ion temperature	0.5—2	eV
peak flow speed	~ 10	km/s
ion species	H, He, Ne, Ar	
Rm	10—10^3	
Re	1—10^4	
Pm	10^{-3}—10^3	

Fig. 1.— The Madison Plasma Dynamo Experiment will provide a flexible facility for studying flow driven instabilities in unmagnetized plasmas.

Another advantage of a plasma experiment is the access to more extensive diagnostics.

Examples being implemented on the prototype experiment include an interferometer and polarimeter for density and magnetic field measurements, laser induced fluorescence for flow and ion temperature measurements, fast framing cameras with gas puff imaging to observe coherent structures, and an array of magnetic sensors and probes for measuring the local magnetic field, density, and electron temperature.

A number of experiments to probe basic astrophysical processes using this new facility have been proposed[2] such as studying large and small scale dynamos varying between laminar and turbulent flows, buoyancy driven stratified convection and magnetic buoyancy instabilities, flow-driven plasma turbulence in near-equipartition which can impact a model magnetosphere, magnetic field line stretching with flow-driven reconnection, and instabilities in collisionless plasmas. These basic physics experiments will create the benchmarks necessary for validating heliospheric codes used to model our sun and forecast solar activity.

The MPDX facility is being constructed through funds from the NSF Major Research Instrumentation program and the University of Wisconsin-Madison. Further support was provided by the CMSO.

REFERENCES

Brown, B., Forest, C., Nornberg, M., Zweibel, E., Cattaneo, F., & Cowley, S. 2010, An Experimental Plasma Dynamo Program for Investigations of Fundamental Processes in Heliophysics, White paper, 2012 Heliophysics Decadal Survey

Charbonneau, P. 2005, Living Rev. Solar Phys., 2, cited on December 15, 2010

Gailitis, A., Lielausis, O., Platacis, E., Gerbeth, G., & Stefani, F. 2002, Rev. Mod. Phys., 74

Hathaway, D., Wilson, R., & Reichmann, E. 1994, Solar Physics, 151, 177

Spence, E. J., Nornberg, M. D., Jacobson, C. M., Kendrick, R. D., & Forest, C. B. 2006, Phys. Rev. Lett., 96, 055002

Spence, E. J., Reuter, K., & Forest, C. B. 2009, Astrophys. J., 700

Verhille, G., Plihon, N., Bourgoin, M., Odier, P., & Pinton, J.-F. 2010, New J. Phys., 12

[2]See the planning workshop website at http://cmso.info/html/meetings/wi_dec09.htm

NASA LAW, October 25-28, 2010, Gatlinburg

LASSIE: Laboratory Astrochemical Surface Science In Europe

M. P. Collings[1**]

Principal Investigators: M.R.S. McCoustra[1*], W.A. Brown[10], D. Chakarov[8], H.M. Cuppen[7], D. Field[2], T.A. Field[12], H.J. Fraser[13], Th. Henning[5], L. Hornekær[2], C. Jäger[5], J.L. Lemaire[3], G. Leto[6], H. Linnartz[7], N.J. Mason[11], T.J. Millar[12], G. Nyman[9], M.E. Palumbo[6], M.J. Paterson[1], S.D. Price[10], E.F. van Dishoeck[7], S. Viti[10], H. Zacharias[4]

www.lassie-itn.eu

ABSTRACT

The LASSIE network is a consortium of 13 institutions and 7 commercial associates that brings together leading European researchers in observational, experimental and computational surface and solid state astrochemistry, with experts in public engagement and industrial partners developing relevant laboratory instrumentation and computational software. It is funded under the European Commission's Seventh Framework Programme as a Marie Curie Initial Training Network (ITN), and seeks to address the key issue of the interaction of the astronomical gas phase with the dust that pervades the Universe. It supports 28 early stage (postgraduate level) researcher and 4 experienced (first postdoctoral level) researcher positions, and provides for extensive training and outreach activities over a four year duration.

[*]Project Coordinator: m.r.s.mccoustra@hw.ac.uk

[**]Network Manager: lassie@hw.ac.uk

[1]Heriot-Watt University, Edinburgh, UK (HWU); [2]Aarhus University, Denmark (AU); [3]Observatoire de Paris et Université de Cergy-Pontoise, France (OBSParis); [4]Westfälische Wilhelms-Universität Münster, Germany (UM); [5]Max Planck Institüt fur Astronomie, Heidelberg & Friedrich Schiller University, Jena, Germany (MPG); [6]Istituto Nazionale di Astrofisica - Osservatorio Astrofisico di Catania, Italy (INAF); [7]Leiden Observatory, Leiden University, Netherlands (LUO); [8]Chalmers University of Technology and University, Gothenburg, Sweden (Chalmers); [9]University of Gothenburg, Sweden (UGot); [10]University College London, UK (UCL); [11]The Open University, Milton Keynes, UK (OU); [12]Queens University Belfast, UK (QUB); [13]University of Strathclyde, Glasgow, UK (SU)

1. Introduction

In recent years the European Research Area (ERA) has made an investment in sophisticated observational platforms approaching many billions of Euros. To support this investment, it is essential that experimental and theoretical astrophysics continue to receive financial backing, within research programs that are integrated with observational investigations. The future development of astrochemistry is dependent on researchers who can communicate across these interdisciplinary boundaries. However, within Europe the field lacks a clear identity, with young researchers entering it tending to have experience in only one of the traditional subjects of astronomy, physics and chemistry.

To address this problem, the LASSIE project was created under the European Commission's 7th Framework Programme as a Marie Curie Initial Training Network. It aims to create an integrated training programme within a research led environment, with a goal of establishing world leading astrochemistry in support of the major investment by the ERA in observational astronomy and space exploration. The resources of leading astrochemistry groups within the thirteen European institutions of the authors have been combined with the resources of six industrial partners - Gridcore AB, Hiden Analytical Ltd, Kore Technology Ltd, HITEC2000, Quantel SA, SPECS GmbH - and an outreach consultancy partner - Graphic Science. LASSIE has grown out of the Astrosurf Network (2004-2007), which provided a forum for discussion by UK researchers with interests in surface astrochemistry, and has expanded its function to create an intergrated European research consortium. It operates in parallel with COST Action CM0805 - 'The Chemical Cosmos', a pan-European network which provides support for conferences, summer schools and short term scientific collaborations.

2. Research Programme

The LASSIE network's research programme recognises the crucial role that dust grains play in the chemical evolution of the universe and the importance of the gas-grain interaction to the understanding of this role. It has been divided into 5 themes:

The formation and destruction of interstellar dust: Mechanisms for the formation and condensation of grains; the release of energy into translation, vibration and rotation of product molecules during heterogeneous chemistry on grain surfaces; rates of molecule formation during heterogeneous chemistry on grain surfaces; morphology of reactively formed ice mantles; spectroscopy of reactively formed ice mantles.

Physical Processes in and on Icy Grains: Thermal, photon, electron and ion desorption

of simple ices, complex ice mixtures and clathrates; thermal, photon, electron and ion induced morphology changes in simple ices, complex ice mixtures and clathrates.

Chemical Transformations in and on Icy Grains: Chemical changes in icy mantles irradiated with electrons, ions or photons at a range of wavelengths; chemical changes of icy mantles following atom, radical or thermal molecular ion bombardment.

Modelling the Gas-Grain Interaction: Models of amorphous ices and dust grains; calculating IR and UV spectra of water and adsorbates in crystalline and amorphous ices; modelling the dynamics of photon driven processes in amorphous ices; modelling the formation of H_2 and small molecules on dust and ice surfaces; calculating diffusion rates of atoms and molecules on ice surfaces; modelling coupled grain growth and chemistry under interstellar conditions; simulating the growth of and evolution of water ice under interstellar conditions.

Observations and Astronomical Models Involving Dust and Ices: Large and small scale mapping of H_2 and deuterated species; an inventory of ices in different environments (Spitzer); constraints on ice formation through ice mapping (AKARI); the formation and life cycle of water through gas to solid phase (Herschel), the formation and composition of carbonaceous and silicate grains in disks and envelopes; high spatial resolution IR spectroscopy of PDRs; modelling gas-grain chemistry in hot cores and disks.

These themes address the key questions in modern solid state and surface astrochemistry identified by the investigators and their colleagues across the ERA. Research is each theme is distributed across the network, with most institutions contributing to multiple themes.

3. Training Programme

The principal goal of LASSIE is to provide a comprehensive and coherent training package that will produce researchers with well rounded skills in astrochemistry. As not all researchers will wish to pursue a career in academia, the training program must provide a portfolio of transferable and complementary personal, technical and business skills in addition to research specific observational, experimental and computational proficiency, analytical and problem solving abilities, and leadership and teamwork capabilities. The training program will be implemented via a range of methods.

Local Training: 'Training by research' will form the basis of each researchers training portfolio. However, existing training courses and monitoring systems in place at each institution will be taken advantage of. Importantly, we will endeavour to make each institutions

resources available across the network.

Secondments: researchers will undertake research placements (1∼3 months) hosted by commercial partners and other academic partners within the network. These placements are designed to give researchers experience with at least one additional scientific technique not available at their host institution, and some insight into the application of their scientific skill in a commercial environment.

Workshops and Conferences: training best carried out at a network level will be provided in three Summer Schools, with themes of Observational Astrochemistry, Surface and Solid State Astrochemistry and State-of-the-Art Astrochemistry, and other network wide training events. ESRs and ERs will attend and present research results at annual student-centred meetings and biannual network conferences held in collaboration with Astrosurf and COST (Action CM0805 Working Group 2) meetings. They will also be encouraged to make presentations at major international astrochemistry conferences.

Supervisory Skills: Each ER appointment is to a different research theme. To encourage the development of their supervisory skills each ER will be given some supervisory responsibility across the whole network to the ESRs appointed within their research theme.

4. Outreach

Public engagement is an aspect of the scientific process that is often neglected, but will form an important component of the LASSIE network's operation. Researchers will be given training in public engagement, provided by the outreach consultancy partner. They will also have the opportunity to take part in public engagement events, both at a network (European) and institutional (national or local) level, some of which may be linked to the International Year of Chemistry in 2011.

It is recognised that for the network to maintain an impact beyond its four year funding period, long term collaborations both amongst network partners and between network members and external collaborators must be established. With this mind in, LASSIE will operate in an outward looking manner, with external participants welcomed at network funded conferences and events.

LASSIE is supported by the European Commission's 7th Framework Programme under Grant Agreement Number 238258.

Appendix

Agenda: The 2010 NASA Laboratory Astrophysics Workshop

Park Vista Hotel, Gatlinburg, Tennessee, USA
October 25-28, 2010

Monday, October 25

4:00 – 7:00 pm Workshop registration, Lower Lobby

Tuesday, October 26

I. Workshop Introduction

8:00 – 8:30 am Continental breakfast, Prefunction Hall

8:30 – 8:45 *Welcoming remarks* – David Schultz, Daniel Wolf Savin

Chair – Daniel Wolf Savin

8:45 – 9:15 *Workshop goals and objectives* – Douglas Hudgins

II. Astro2010 Decadal Survey and Science Frontier Panel Reports

9:15 – 10:00 *The Astro2010 decadal survey: What does it say about laboratory astrophysics?* – Dan McCammon

10:00 – 10:30 Coffee break, Prefunction Hall

Chair – Hashima Hasan

10:30 – 11:00 *Cosmology and fundamental physics: Laboratory astrophysics needs of NASA astrophysics missions* – Wick Haxton
11:00 – 11:30 *Planetary systems and star formatio*n – Hector Arce
11:30 – 12:00 *Laboratory astrophysics in the stars and stellar evolution Astro 2010 Panel* – Marc Pinsonneault

12:00 – 1:30 Lunch, Ballroom 2

Chair – Douglas Hudgins

1:30 – 2:00 *Galactic neighborhood and laboratory astrophysics* – Daniel Wang
2:00 – 2:30 *Galaxies Across Cosmic Time* – Andrew Baker

III. Current and Future NASA Missions

2:30 – 3:00 *Herschel, SOFIA, and laboratory data* – John Pearson

3:00 – 3:30 Coffee Break, Prefunction Hall

Chair – Caroline Kilbourne

3:30 – 4:00 *The James Webb Space Telescope: Mission overview and status* – Matt Greenhouse

4:00 – 4:30 *The Hubble Space Telescope: UV, visible, and near-infrared pursuits* – Jennifer Wiseman

4:30 – 5:00 *Laboratory astrophysics needs for current and future X-ray missions* – Randall Smith

5:00 – 6:30 Posters and Reception, Ballroom 1

Wednesday, October 27

IV. Laboratory Astrophysics: Atoms

8:00 – 8:30 am Continental breakfast, Prefunction Hall

Chair – Steve Federman

8:30 – 9:00 *Atomic data from the ultraviolet to the infrared* – Glenn Wahlgren

9:00 – 9:30 *Review of laboratory astrophysics in support of X-ray astronomy* – Peter Beiersdorfer

9:30 – 10:00 *Low-energy electron-ion and ion-atom collisions: Progress and needs for modeling of future NASA astrophysics observations*– Phillip Stancil

10:00 – 10:30 Coffee break, Prefunction Hall

Chair – Susanna Widicus Weaver

10:30 – 11:00 *High-energy electron-ion and photon-ion collisions: Status and challenges* – Tim Kallman

V. Laboratory Astrophysics: Molecules

11:00 – 11:30 *Vibrations and high-frequency rotations: Supporting current and future space missions in the laboratory* – Michael McCarthy

11:30 – 12:00 *Spectroscopic databases for astronomical applications* – Linda Brown

12:00 – 1:30 Lunch, Ballroom 2

Chair – Lou Allamandola

1:30 – 2:00 *Molecular processes in the gas phase and on dust* – Eric Herbst

VI. Laboratory Astrophysics: Dust

2:00 – 2:30 *Laboratory spectroscopy of astrophysically-relevant materials: Developing dust as a diagnostic* – Stephen Rinehart

2:30 – 3:00 *Formation of molecules on stardust: What we know and what we don't know, but should* – Gianfranco Vidali

3:00 – 3:30 Coffee break, Prefunction Hall

VII. Laboratory Astrophysics: Ices

Chair – Karin Oberg

3:30 – 4:00 *Laboratory spectroscopy of ices of astrophysical interest* – Marla Moore

4:00 – 4:30 *The origins and evolution of molecules in icy solids* – Reggie Hudson

VIII. Laboratory Astrophysics: Plasmas

Chair – Martin Laming

4:30 – 5:00 *Laboratory study of plasma processes of astrophysical interests: Magnetic reconnection, angular momentum transport, and dynamos* – Hantao Ji

5:00 – 5:30 *High energy density laboratory astrophysics (HEDLA): Shocks, jets, and other extreme dynamics* – Bruce Remington

5:30 – 7:00 Posters and Reception, Ballroom 1

<u>Thursday, October 28</u>

IX. Laboratory Astrophysics Working Groups

8:00 – 8:30 am Continental breakfast, Prefunction Hall

9:00 – 12:00 *Break-out sessions for working groups*
(with coffee break 10:00-10:30, Prefunction Hall)
Atomic astrophysics working group
(led by Daniel Wolf Savin and David Schultz), Garden View B

	Molecular astrophysics working group (led by Steve Federman and Susanna Widicus Weaver), Garden View C *Dust and ices astrophysics working group* (led by Lou Allamandola and Karin Oberg), Garden View D *Plasma astrophysics working group* (led by Martin Laming), Garden View E
12:00 – 1:30	Lunch, Ballroom 2
1:30 – 1:45	*Atomic astrophysics working group report* – Daniel Wolf Savin and David Schultz
1:45 – 2:00	*Molecular astrophysics working group report* – Steve Federman and Susanna Widicus Weaver
2:00 – 2:15	*Dust and ices astrophysics working group report* – Lou Allamandola and Karin Oberg
2:15 – 2:30	*Plasma astrophysics working group report* – Martin Laming
2:30 – 3:00	Coffee break, Prefunction Hall
3:00 – 3:15	*Plenary discussion*
3:15 – 3:30	*Final remarks, adjourn workshop*
3:30 – 5:30	Scientific Organizing Committee executive session

List of Participants

Hiroki Akamatsu
Tokyo Metropolitan University
Department of Physics
Minami-Osawa 1-1
Tokyo, Hachioji 192-0397
Japan
h_aka@phys.metro-u.ac.jp

Lou Allamandola
NASA Ames Research Center
M/S 245-6
Moffett Field, CA 94035-1000
Louis.J.Allamandola@nasa.gov

Hector Arce
Yale University
Department of Astronomy
260 Whitney Avenue
New Haven, CT 06511
hector.arce@yale.edu

Bernhard Bach
University of Nevada, Reno
Mail Stop 372
Reno, NV 89557
bbac2@unr.edu

Andrew Baker
Rutgers, The State University
of New Jersey
Department of Physics and Astronomy
136 Frelinghuysen Road
Piscataway, NJ 08854-8019
ajbaker@physics.rutgers.edu

Connor Ballance
Auburn University
206 Allison Lab
Auburn, AL 36849
ballacp@auburn.edu

Mark Bannister
Oak Ridge National Laboratory
Physics Division, Bldg. 6010
P.O. Box 2008
Oak Ridge, TN 37831-6372
bannisterme@ornl.gov

Peter Beiersdorfer
Lawrence Livermore National
Laboratory
7000 East Avenue, L260
Livermore, CA 94550
beiersdorfer@llnl.gov

Nancy Brickhouse
Harvard-Smithsonian Center
for Astrophysics
60 Garden Street, MS 15
Cambridge, MA 02138
nbrickhouse@cfa.harvard.edu

Linda Brown
Jet Propulsion Laboratory
Mail Stop 183-601
4800 Oak Grove Dr.
Pasadena, CA 91109
linda.r.brown@jpl.nasa.gov

Anthony Calamai
Appalachian State University
201 IG Greer Hall/401 Academy St.
Boone, NC 28608
daycl@appstate.edu;
calamaiag@appstate.edu

Brandon Carroll
Emory University
Department of Chemistry
1515 Dickey Drive
Atlanta, GA 30322
susanna.widicus.weaver@emory.edu

Ara Chutjian
Jet Propulsion Laboratory and
California Institute of Technology
4800 Oak Grove Drive
Pasadena, CA 91109
ara.chutjian@jpl.nasa.gov

Mark Collings
Heriot-Watt University
Department of Chemistry
School of Engineering and
Physical Sciences
Edinburgh, Scotland EH14 4AS
United Kingdom
m.p.collings@hw.ac.uk

Cesar Contreras
NASA Ames Research Center
Mail Stop 245-6, Bldg. 245, Rm. 309
P.O. Box 1
Moffett Field, CA 94035-0001
cesar.contreras@nasa.gov

Paul Cooper
George Mason University
Department of Chemistry and
Biochemistry
4400 University Dr MS# 3E2
Fairfax, VA 22030
pcooper6@gmu.edu

John Curry
National Institute of Standards
and Technology
100 Bureau Drive MS8422
Gaithersburg, MD 20899
larmitage@nist.gov

Frank De Lucia
Ohio State University
191 W. Woodruff Avenue
Columbus, OH 43210
fcd@mps.ohio-state.edu

Bruno deHarak
Illinois Wesleyan University
P.O. Box 2900
Bloomington, IL 61702-2900
bdeharak@iwu.edu

Ilija Draganic
Oak Ridge National Laboratory
Physics Division, Bldg. 6010
P.O. Box 2008
Oak Ridge, TN 37831
draganicin@ornl.gov

Michael Duncan
University of Georgia
Department of Chemistry
Athens, GA 30602-2556
maduncan@uga.edu

Steven Federman
University of Toledo
Department of Physics and Astronomy
MS 111
Toledo, OH 43606
steven.federman@utoledo.edu

Zineb Felfli
Clark Atlanta University
J.P. Brawley Drive at Fair St., SW
Atlanta , GA 30314
zfelfli@cau.edu

Vanessa Fivet
Western Michigan University
Physics Department
1903 W. Michigan Avenue
Kalamazoo, MI 49008
vanessa.fivet@wmich.edu

Adam Foster
Smithsonian Astrophysical Observatory
60 Garden Street, MS 67
Cambridge, MA 02144
afoster@cfa.harvard.edu

William Fox
Space Science Center
University of New Hampshire
Morse Hall, 8 College Road
University of New Hampshire
Durham, NH 03824
william.fox@unh.edu

Mauricio Garrido
Columbia University
136 South Broadway, Nevis Labs
Irvington, NY 10533
mgarrido@astro.columbia.edu

John Gillaspy
National Institute of Standards
and Technology
100 Bureau Drive
Gaithersburg, MD 20899
john.gillaspy@nist.gov

Tom Gorczyca
Western Michigan University
1903 West Michigan Ave.
Kalamazoo, MI 49008-5252
gorczyca@wmich.edu

Matthew Greenhouse
NASA Goddard Space Flight Center
Building 29 Room 200G
Greenbelt, MD 20771
matt.greenhouse@nasa.gov

Harshal Gupta
Jet Propulsion Laboratory
California Institute of Technology
4800 Oak Grove Drive, MS 264-782
Pasadena, CA 91106
Harshal.Gupta@jpl.nasa.gov

Michael Hahn
Columbia University
550 West 120th Street, MC 5247
New York, NY 10027
mhahn@astro.columbia.edu

Hashima Hasan
NASA Headquarters
300 E Street SW
Washington, DC 20546
hhasan@nasa.gov

Muhammet Hasoglu
Georgia State University
29 Peachtree Center Avenue
Science Annex, Suite 400
Atlanta, GA 30303
mhasoglu@gsu.edu

Charles Havener
Oak Ridge National Laboratory
Physics Division, Bldg. 6010
P.O. Box 2008
Oak Ridge, TN 37831-6372
havenercc@ornl.gov

Wick Haxton
University of California, Berkeley
and Lawrence Berkeley Laboratory
431 Old LeConte Hall MC 7300
Berkeley, CA 94720-7300
haxton@berkeley.edu

Eric Herbst
The Ohio State University
Department of Physics
191 West Woodruff Avenue
Columbus, OH 43210
ericherb@gmail.com

Douglas Hudgins
NASA Headquarters
17625 Marsh Harbor Ln.
Dumfries, VA 22026
Douglas.M.Hudgins@nasa.gov

Reggie Hudson
NASA Goddard Space Flight Center
8800 Greenbelt Rd.,CODE 691.0
Greenbelt, MD 20771
reggie.l.hudson@nasa.gov

Yawei Hui
Oak Ridge National Laboratory
Physics Division, Bldg. 6010
P.O. Box 2008
Oak Ridge, TN 37831-6372
huiy@ornl.gov

Hantao Ji
Princeton Plasma Physics Laboratory
PO Box 451
Princeton, NJ 08543
hji@pppl.gov

Li Ji
Smithsonian Astrophysical Observatory
60 Garden Street
Cambridge, MA 02139
lji@cfa.harvard.edu

Jelle Kaastra
SRON
Netherlands Institute for Space Research
Sorbonnelaan 2, Utrecht
Utrecht 3584 CA
Netherlands
j.kaastra@sron.nl

Timothy Kallman
NASA Goddard Space Flight Center
Code 662, X-ray Astrophysics Laboratory
Greenbelt, MD 30771
timothy.r.kallman@nasa.gov

Duck-Hee Kwon
Columbia Astrophsics Laboratory
Columbia University
550 West 120th Street
New York, NY 10027
dk2545@columbia.edu

Jacob Laas
Department of Chemistry
Emory University
1515 Dickey Dr.
Atlanta, GA 30322
susanna.widicus.weaver@emory.edu

Timothy Lee
NASA Ames Research Center
Mail Stop 245-1
Moffett Field, CA 94035
timothy.j.lee@nasa.gov

Jaan Lepson
Space Sciences Laboratory
7 Gauss Way
Berkeley, CA 94720
lepson@ssl.berkeley.edu

Stojan Madzunkov
Jet Propulsion Laboratory
4800 Oak Grove Drive
Pasadena, CA 91109
stojan.madzunkov@jpl.nasa.gov

Steven Manson
Georgia State University
Department of Physics & Astronomy
Atlanta, GA 30030
smanson@gsu.edu

Dan McCammon
University of Wisconsin
Physics Dept., 1150 University Avenue
Madison, WI 53706
mccammon@physics.wisc.edu

Michael McCarthy
Harvard-Smithsonian Center for Astrophysics
60 Garden Street
Cambridge, MA 02138
mccarthy@cfa.harvard.edu

Brett McGuire
Emory University
Department of Chemistry
1515 Dickey Drive
Atlanta, GA 30322
susanna.widicus.weaver@emory.edu

Alan McLoughlin
Queen's University Belfast
143a Lisburn Road
Belfast, United Kingdom BT97AG
macalan@gmail.com

Kenneth Miller
Columbia University
550 West 120th Street
New York, NY 10027
kmiller@astro.columbia.edu

Marla Moore
NASA/Goddard Space Flight Center
Astrochemistry Laboratory
Greenbelt, MD 20771
marla.h.moore@nasa.gov

Alfred Msezane
Clark Atlanta University
Department of Physics/CTSPS
Atlanta, GA 30314
amsezane@cau.edu

Gillian Nave
National Institute of Standards
and Technology
100 Bureau Drive MS8422
Gaithersburg, MD 20899
gillian.nave@nist.gov

Jeff Nolte
University of Georgia
131 Soule Street
Athens, GA 30605
jeffreyn@uga.edu

Mark Nornberg
University of Wisconsin-Madison
150 University Avenue
Madison, WI 53706
mdnornberg@wisc.edu

Oldrich Novotny
Columbia Astrophysical Laboratory
550 West 120th Street, MC 5247
New York, NY 10027
oldrich.novotny@mpi-hd.mpg.de

Aodh O'Connor
Columbia Astrophysics Laboratory
Nevis Labs, 136 S. Broadway
Irvington, NY 10533
aodh@astro.columbia.edu

Karin Oberg
Harvard-Smithsonian Center
for Astrophysics
60 Garden Street, MS 42
Cambridge, MA 02138
koberg@cfa.harvard.edu

Hye-Sook Park
Lawrence Livermore National
Laboratory
7000 East Avenue, L-481
Livermore, CA 94550
park1@llnl.gov

John Pearson
Jet Propulsion Laboratory
California Institute of Technology
4800 Oak Grove Dr.
Pasadena, CA 91109
John.C.Pearson@jpl.nasa.gov

Manori Perera
University of Illinois at
Urbana-Champaign
170 RAL, 600 S. Mathews Avenue
Urbana, IL 61801
mperera@uiuc.edu

Thushara Perera
Illinois Wesleyan University
1312 Park Street
Bloomington, IL 61821
tperera@iwu.edu

Michael Pindzola
Auburn University
Department of Physics
Auburn, AL 36849
pindzola@physics.auburn.edu

Marc Pinsonneault
Ohio State University
Dept. of Astronomy
140 W. 18th Avenue
Columbus, OH 43210
pinsonneault.1@osu.edu

Nick Pope
Appalachian State University
201 IG Greer Hall/ 401 Academy St.
Boone, NC 28608
popenc@appstate.edu;
daycl@appstate.edu

Radu Presura
University of Nevada, Reno
MS 372
Reno, NV 89557
presura@unr.edu

Joseph Reader
National Institute of Standards
and Technology
100 Bureau Drive, MS 8422
Gaithersburg, MD 20899
joseph.reader@nist.gov

Bruce Remington
Lawrence Livermore National
Laboratory
7000 East Avenue, L-481
Livermore, CA 94550
remington2@llnl.gov

Stephen Rinehart
NASA Goddard Space Flight Center
Code 665
Greenbelt, MD 20771
Stephen.A.Rinehart@nasa.gov

Matthew Ruffoni
Imperial College London
Blackett Laboratory
Imperial College London
London SW7 2AZ
United Kingdom
m.ruffoni@imperial.ac.uk

Farid Salama
NASA Ames Research Center
Space Science & Astrobiology
Division, MS 245-6
Moffett Field, CA 94035-1000
Farid.Salama@nasa.gov

Wilton Sanders
NASA Headquarters
300 E Street SW
Washington, DC 20546
Wilton.T.Sanders@nasa.gov

Craig Sansonetti
National Institute of Standards
and Technology
100 Bureau Dr MS8422
Gaithersburg, MD 20899
craig.sansonetti@nist.gov

Daniel Wolf Savin
Columbia Astrophysics Laboratory
550 West 120th Street, MC 5247
New York, NY 10027
savin@astro.columbia.edu

David R. Schultz
Oak Ridge National Laboratory
Physics Division, Bldg. 6010
P.O. Box 2008
Oak Ridge, TN 37831-6372
schultzd@ornl.gov

Jurij Simcic
Jet Propulsion Laboratory
4800 Oak Grove Drive
Pasadena, CA 91109
jurij.simcic@jpl.nasa.gov

Randall K Smith
Smithsonian Astrophysical Observatory
60 Garden Street
Cambridge, MA 02138
rsmith@cfa.harvard.edu

Phillip C. Stancil
University of Georgia
Department of Physics and Astronomy
Athens, GA 30602-2451
stancil@physast.uga.edu

Renat Sultanov
St. Cloud State University (SCSU)
BCRL at SCSU
720-4th Ave. So.
Centennial Hall, 367B
St. Cloud, MN 56301
rasultanov@stcloudstate.edu

Randy Vane
Oak Ridge National Laboratory
Physics Division, Bldg. 6010
P. O. Box 2008
Oak Ridge, TN 37831-6372
vanecr@ornl.gov

Gianfranco Vidali
Syracuse University
201 Physics Bldg.
Syracuse, NY 13244-1130
gvidali@syr.edu

Glenn Wahlgren
The Catholic University of America
Department of Physics
620 Michigan Avenue, NE
Washington, DC 20064
Glenn.M.Wahlgren@nasa.gov

Haiming Wang
The University of Chicago
Department of Chemistry
5735 S. Ellis Avenue
Chicago, IL 60637
haiming@uchicago.edu

Q. Daniel Wang
University of Massachusetts
Astronomy Department
619-E, LGRT
710 N. Pleasant Street
Amherst, MA 01003
wqd@astro.umass.edu

Susanna L. Widicus Weaver
Emory University
Department of Chemistry
1515 Dickey Drive
Atlanta, GA 30322
susanna.widicus.weaver@emory.edu

Wolfgang L. Wiese
National Institute of Standards
and Technology
100 Bureau Drive
Gaithersburg, MD 20899 8420
Wiese@nist.gov

Jennifer Wiseman
NASA Goddard Space Flight Center
Code 667, NASA GSFC
Greenbelt, MD 20771
jennifer.wiseman@nasa.gov

Michael Witthoeft
NASA/Goddard Space Flight Center
Mail Code 662
Greenbelt, MD 20771
michael.c.witthoeft@nasa.gov

Yong Wu
University of Georgia
113 College Station Rd., Apt. L303
Athens, GA 30605
yongwu@hal.physast.uga.edu

Zhibo Yang
University of Colorado, Boulder
215 UCB
Boulder, CO 80309
zhibo.yang@colorado.edu

Shanshan Yu
Jet Propulsion Laboratory
4800 Oak Grove Drive
Pasadena, CA 91101
shanshan.yu@jpl.nasa.gov

Hsiao-Ling Zhou
Georgia State University
Department of Physics & Astronomy
Atlanta, GA 30303
zhou@phy-astr.gsu.edu

Index of Authors

Adhikari, S., C-22
Akamatsu, H., C-11
Allamandola, L., W-1
Arce, H., I-3

Badnell, N., C-5
Baker, A., I-6
Balakrishnan, N., C-23
Ballance, C., C-18
Beiersdorfer, P., I-12, C-15
Benford, D., C-40
Berg, M., C-19
Bergin, E., C-31
Bernhardt, D., C-4
Bhattacharjee, A., C-45
Biennier, L., C-29
Bierbaum, V., C-21
Bing, D., C-19
Bitter, M., C-15
Blake, G., C-32
Brickhouse, N., W-1, I-10, C-1, C-2
Bridges, J., C-16
Brown, B., C-47
Brown, L., I-16, C-28, C-31
Brauer, C., C-31
Bruhns, H., C-7
Bryans, P., C-5
Bryson, K., C-39
Buenker, R., C-8
Buhr, H., C-19

Cadez, I., C-25
Carpenter, M., C-21
Carroll, P.B., C-36
Chun, W., C-20
Chutjian, A., C-25, C-42
Ĉižek, M., C-7
Clark, M., C-47
Collings, M., C-48
Contreras, C., C-41
Crabtree, K., C-30
Crawford, T., C-20

Darrach, M., C-42
De Lucia, F., C-38
de Oliveira, N., C-35
Desai, P., C-15
Draganic, I., C-8
Drouin, B., C-20, C-31, C-33
Duncan, M., C-34
Dwek, E., C-40

Ehrenfreund, P., C-39, C-42
Eichelberger, B., C-21
Eidelsberg, M., C-35
Enoki, T., C-11
Ezoe, Y., C-11

Federman, S., W-1, C-35
Fillion, J-H., C-35
Foing, B., C-39
Forest, C., C-47
Forrey, R., C-23
Fortman, S., C-38
Foster, A., C-2, I-10, C-1
Fox, W., C-45
Froese, M., C-19
Funke, P., C-8
Fuhr, J., C-16

Galazutdinov, G., C-29
Garrido, M., C-26
Garrod, R., C-43, C-44
Germaschewski, K., C-45
Gillaspy, J., C-9
Glover, S., C-7
Goldsmith, P., W-1
Gorczyca, T., C-5, C-17
Greenhouse, M., I-8
Greenwood, J., C-25
Grieser, M., C-4
Gu, M., C-15
Gupta, H., C-20, C-31, C-33
Guster, D., C-22

Hahn, M., C-4
Hasoglu, M., C-17
Havener, C., C-8
Haxton, W., I-2
Heays, A., C-35

Heber, O., C-19
Henmi, K., C-11
Henry, R., C-40
Herbst, E., I-17, C-43
Holmes, C., C-13
Houck, J., C-1
Huang, X., C-37
Hudson, R., I-21, I-20
Hui, Y., C-24, C-6, C-8

Ishida, T., C-11
Ishisaki, Y., C-11

Jessberger, E., C-39
Ji, H., W-1, I-22
Ji, L., C-1, I-10, C-2

Kallman, T., I-14
Kanda, T., C-11
Kaplan, E., C-47
Kauffman, C., C-30
Kerber, F., C-12
Kilbourne, C., W-1
Kinzer, R., C-40
Kleshcheva, M., C-27
Kramida, A., C-10
Krantz, C., C-4, C-19
Kreckel, H., C-7, C-30
Krelowski, J., C-29
Kwon, D-H., C-3

Laas, J., C-43
Laming, J., C-5
Lee, T., C-37
Lee, T-G., C-23
Lemaire, J., C-35
Lepson, J., C-15
Lestinsky, M., C-4
Lewis, B., C-35
Liebermann, H., C-8
Linnartz, H., C-44
Lisse, C., C-25
Loch, S., C-18
Lovas, F., C-32
Ludlow, J., C-18
Lyons, J., C-35

MacAskill, J., C-42
Madzunkov, S., C-42
Martinez, D., C-46
Martinez, O., C-21
Mawhorter, R., C-25
McCall, B., C-30
McCammon, D., I-1
McCarthy, M., I-15
McGuire, B., C-32, C-36
McKoy, B., C-25
Medvedev, I., C-38
Mendes, M., C-19
Menk, S., C-19
Miller, K., C-7, C-26
Mills, A., C-30
Mitthumsiri, W., C-5
Mitsuda, K., C-11
Moore, M., I-20, I-21
Morong, P., C-27
Müller, A., C-4
Mumma, M., C-39

Naby, S., C-17
Nave, G., C-14, C-12
Neese, C., C-38
Neff, S., C-46
Nolte, J., C-23
Nordhorn, C., C-19
Nornberg, M., C-47
Novotný, O., C-19, C-4
Novotny, S., C-19
Nuth, J., C-40

O'Connor, A., C-26
Oka, T., C-27
Oberg, K., W-1, C-44
Ohashi, H., C-11
Ohashi, T., C-11
Orlov, D., C-19

Park, H-S., I-23
Pearson, J., I-7, C-31, C-20, C-33
Peeters, Z., C-39
Perera, M., C-30
Petrignani, A., C-19
Pickering, J., C-13
Pindzola, M., C-18

Pinsonneault, M., I-4
Plechaty, C., C-46
Plusquellic, D., C-32
Porambo, M., C-30
Presura, R., C-46

Rahbarnia, K., C-47
Ralchenko, Y., C-10
Rappaport, M., C-19
Reader, J., C-10
Reinke, M., C-15
Remington, B., W-1, I-23
Repnow, R., C-4
Ricco, A., C-39
Ricketts, C., C-41
Rinehart, S., I-18, C-40
Robert, F., C-39
Roquemore, L., C-15
Rostas, F., C-35
Roudjane, M., C-35
Ruffoni, M., C-13

Salama, F., W-1, C-29, C-39, C-41
Sansonetti, C., C-12
Savin, D., W-1, C-5, C-3, C-4, C-7, C-19, C-26
Schippers, S., C-4
Schultz, D., W-1, C-6, C-8, C-24, C-25
Schwalm, D., C-19
Schwenke, D., C-37
Sheffer, Y., C-35
Shinozaki, K., C-11
Shornikov, A., C-19
Siller, B., C-30
Silver, E., C-9
Silverberg, R., C-40
Simčič, J., C-25
Smith, P., C-13, C-35
Smith, R., I-10, C-1, C-2
Smith, S., C-25
Snow, T., C-21
Spence, E., C-47
Stancil, P., I-13, C-8, C-23
Stark, G., C-35
Stein, S., C-46
Stützel, J., C-19
Sultanov, R., C-22
Sung, K., C-28, C-31

Tanuma, H., C-11
Tayal, S., C-25
Taylor, N., C-47
Terry, J., C-15
Thorne, A., C-13

Urbain, X., C-7, C-26

van Dishoeck, E., C-44
Vidali, G., I-19, C-42

Wahlgren, G., I-11
Wallace, J., C-47
Wang, H., C-27
Wang, Q.D., I-5
Wang, S., C-31
Widcus Weaver, S., W-1, C-32, C-36, C-43
Wiese, W., C-16
Winstead, C., C-25
Wiseman, J., I-9
Witthoeft, M., I-14
Wolf, A., C-4, C-19
Wollack, E., C-40
Wu, Y., C-8

Xu, L-H., C-31

Yang, Z., C-21
Yu, S., C-20, C-31

Ziurys, L., W-1
Zweibel, E., C-47